DE GRUYTER

ZEITSCHRIFT FÜR KRISTALLOGRAPHIE SUPPLEMENT

29TH ANNUAL CONFERENCE OF THE GERMAN CRYSTALLOGRAPHIC SOCIETY

MARCH 15-18, 2021
HAMBURG, GERMANY

ABSTRACTS

2021 · NUMBER 41

29th Annual Conference of the German Crystallographic Society

Zeitschrift für Kristallographie Supplement

2021 Number 41

29th Annual Conference of the German Crystallographic Society

March 15–18, 2021,
Hamburg, Germany (video conference)

Abstracts

DE GRUYTER

ISBN 978-3-11-074007-3
e-ISBN (PDF) 978-3-11-074017-2
e-ISBN (EPUB) 978-3-11-074022-6
ISSN 0930-486X

Library of Congress Control Number: 2021935289

Bibliographic information published by the Deutsche Nationalbibliothek
The Deutsche Nationalbibliothek lists this publication in the Deutsche Nationalbibliografie; detailed bibliographic data are available on the Internet at http://dnb.dnb.de.

Printing and binding: Frantz X. Stückle Druck und Verlag e.K., Ettenheim

www.degruyter.com

Table of Contents

Plenary talks

Fascinating structures of magnetic materials

M. Holynska[1]

[1] Philipps University Marburg and European Space Research and Technology Centre

Magnetic materials, in particular molecular magnets, can display remarkable, aesthetically pleasing and elegant structures, although most promising properties have been detected in simple mononuclear compounds [1]. The highly interdisciplinary field of molecular magnetism has been defined by Oliver Kahn as study of "magnetic properties of isolated molecules and/or assemblies of molecules" [2]. Applications of molecular magnets are foreseen in high-density data storage and quantum computing. The latter might be significant not only for on-ground, but also for space applications (e.g. satellite quantum communications).

Crystal structures of molecular magnets, although not fully representative of the targeted applications, play an important role in resolution of magnetostructural correlations [3]. These correlations may be retrieved via special setups, such as high-pressure crystallography [4]. For polynuclear metal complexes (Figure 1) often problems with diffraction data quality and solvent disorder are faced [5].

References

[1] A. Castro-Alvarez et al., "High performance single-molecule magnets, Orbach or Raman relaxation suppression?", *Inorg. Chem. Front.*, vol. 7, pp. 2478, 2020.

[2] O. Kahn, Molecular Magnetism, VCH, 1993.

[3] C. J. Milios et al., "Hexanuclear manganese(III) single-molecule magnets", *Angew. Chem.*, vol. 43, pp. 210, 2004.

[4] A. M. Thiel et al., "High-Pressure Crystallography as a Guide in the Design of Single-Molecule Magnets", *Inorg. Chem.*, vol. 59, pp. 1682–1691, 2020.

[5] A. J. Tasiopoulos et al., "Giant Single-Molecule Magnets: A Mn84 Torus and Its Supramolecular Nanotubes", *Angew. Chem. Int. Ed.*, vol. 43, pp. 2117 –2121, 2004.

[6] M. Holynska et al., "[MnIII6O3Ln2] single-molecule magnets: Increasing the energy barrier above 100 K", *Chem. Eur. J.*, vol. 35, pp. 9605–9610, 2011.

[7] M. Holynska et al., "A Defect Supertetrahedron Naphthoxime-Based [Mn9(III)] Single-Molecule Magnet", *Inorg. Chem.* vol. 52, no. 13, pp. 7317–7319, 2013.

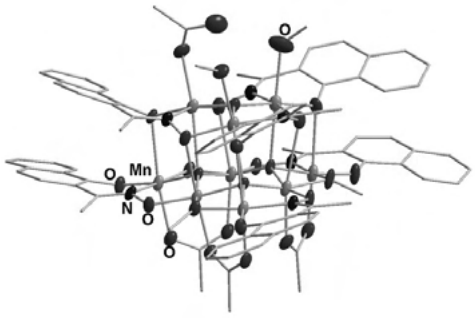

Figure 1

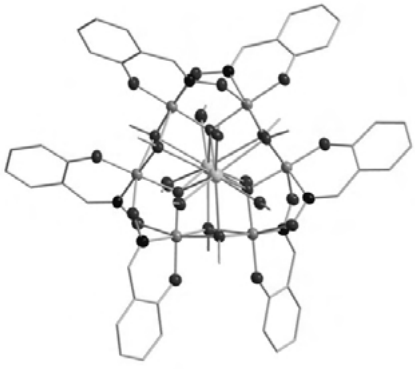

Figure 2

Exploring the Complex Structural Landscape and Potential Applications of Rare-Earth Metal–Organic Frameworks

A. J. Howarth[1], V. Quezada-Novoa[2], P. R. Donnarumma[2], H. M. Titi[3]

[1] Concordia University, Montreal

[2] Department of Chemistry and Biochemistry, Concordia University

[3] Department of Chemistry, McGill University

Metal–organic frameworks (MOFs) are structurally diverse, porous materials comprised of metal nodes bridged by organic linkers. [1] Through careful choice of nodes and linkers, the chemical and physical properties of MOFs can be elegantly tuned and materials with very high surface area and porosity can be obtained. As a consequence, MOFs have been explored for many potential applications including, but not limited to, gas storage and release, chemical separations, catalysis, drug

delivery, light harvesting and energy conversion, and the detoxification of hazardous analytes. [2] In addition to these promising potential applications, MOFs offer an interesting platform for studying fundamental concepts in inorganic materials chemistry. We are particularly interested in the study of MOFs comprised of rare-earth (RE) elements, [3] in part, because of the high and variable coordination number of these elements, which allows several unique and intricate MOF topologies to be designed and synthesized. Furthermore, RE-MOFs can be produced with diverse optical and electronic properties dictated by the 4f electron configurations of the RE-elements. In this presentation, RE-MOFs are explored from design and synthesis, to potential application.

References

[1] B. F. Hoskins and R. Robson, "Infinite polymeric frameworks consisting of three dimensionally linked rod-like segments", *J. Am. Chem. Soc.*, vol. 111, pp. 5962–5964, 1989); O. M. Yaghi and H. Li, Hydrothermal Synthesis of a Metal-Organic Framework Containing Large Rectangular Channels, *J. Am. Chem. Soc.*, vol. 117, pp. 10401–10402, 1995.

[2] A. J. Howarth, Y. Liu, P. Li, Z. Li, T. C. Wang, J. T. Hupp and O. K. Farha, "Chemical, thermal and mechanical stabilities of metal–organic frameworks", *Nat. Rev. Mater.*, vol. 1, pp. 15018, 2016.

[3] F. Saraci, V. Quezada-Novoa, P. R. Donnarumma, "Rare-earth metal–organic frameworks: from structure to applications", *Chem. Soc. Rev.*, vol. 49, pp. 7949–7977, 2020.

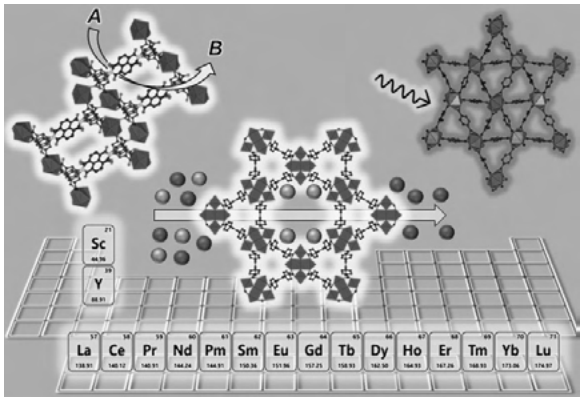

Figure 1

3D Pair Distribution Function Analysis in Materials Science

B. Iversen[1]

[1] Aarhus University, Aarhus, Denmark

X-ray diffraction from powders and single crystals has for decades been the key analytical tool in materials science. Bragg intensities provide information about the average crystals structure, but often it disorder and specific local structure that control key material properties. For 1D data there has been an immense growth in combined analysis of Bragg and diffuse scattering using the Pair Distribution Function (PDF), and in our group we frequently use 1D PDF analysis to study nanocrystal nucleation in solvothermal processes [1] or thin films [2], or to analyse materials under operating conditions [3]. For single crystals, diffuse scattering studies have a long history with elaborate analysis in reciprocal space, but direct space analysis of the 3D-PDF is still in its infancy. We have used 3D-PDF analysis to study the crystal structures of high performance thermoelectric materials Cu2Se (Fig 1) [4], PbTe [5], and 19-e half-heusler Nb1-xCoSb [6], where the true local structure is essential for understanding the unique properties. For frustrated magnetic materials direct space analysis of diffuse magnetic scattering provides a new route to magnetic structures [7].

References

[1] N. L. N. Broge et al., "Auto-catalytic formation of high entropy alloy nanoparticles", *Angew. Chem. Intl. Ed.*, vol. 59, pp. 21920-21924, 2020.

[2] M. Roelsgaard et al., "Time-Resolved Surface Pair Distribution Functions during Deposition by RF Magnetron Sputtering", *IUCrJ*, vol. 6, pp. 299–304, 2019.

[3] L. R. Jørgensen et al., "Operando X-ray scattering study of thermoelectric β-Zn4Sb3", *IUCrJ*, vol. 7, pp. 100-104, 2020.

[4] N. Roth et al., "Solving the disordered structure of β-Cu2-xSe using the three-dimensional difference pair distribution function", *Acta Crystallogr. Sect. A*, vol. 75, pp. 465–473, 2019.

[5] K. A. U. Holm et al., "Temperature Dependence of Dynamic Dipole Formation in PbTe", *Phys. Rev. B*, vol. 102, pp. 024112, 2020.

[6] N. Roth et al., "A simple model for vacancy order and disorder in defective half-Heusler systems", *IUCrJ*, vol. 7, pp. 673-680, 2020.

[7] N. Roth et al., "Model-free reconstruction of magnetic correlations in frustrated magnets", *IUCrJ*, vol. 5, pp. 410–416, 2018.

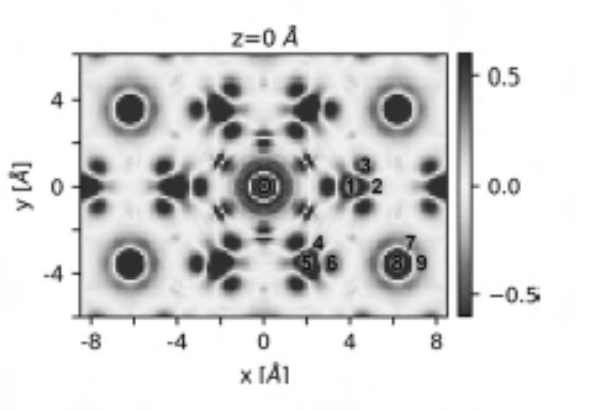

Figure 1

Massive X-ray screening against SARS-CoV-2 main protease

A. Meents[1], P. Reinke[1], S. Günther[1]

[1] Deutsches Elektronen-Synchrotron - DESY, Hamburg, Germany

As a response to the SARS-CoV-2 pandemic we have set up a large consortium of more than one hundred scientist centered at DESY in Hamburg in order to find suitable drug candidates. In contrast to common screening techniques such as biochemical activity-based assays or X-ray fragment screening, here we employed massive X-ray crystallographic screening of two drug-repurposing libraries against the SARS-CoV-2 main protease (Mpro) as initial target. In total co-crystallization experiments of 5953 individual drugs with Mpro were setup and datasets from more than 8000 crystals were collected at the PETRA III MX beamlines. Our screening effort resulted in the identification of 37 compounds binding to Mpro. Secondary screening of these hits in a cell-based viral infection assay carried out at the Bernhard Nocht-Institute revealed antiviral activity in combination with low cytotoxicity for six compounds, which have not yet been reported as inhibitors of SARS-CoV-2. While four of these inhibitors bind to the catalytic site of the enzyme, the remaining two bind to a previously undescibed allosteric site within the dimerization domain [1]. For the two most promising compounds from our screen, Calpeptin and Pelitinib, we have intiated further preclinical testing.

References

[1] S. Günther, P. Y. A. Reinke, et al., *bioRxiv*, doi:10.1101/2020.11.12.378422, 2020.

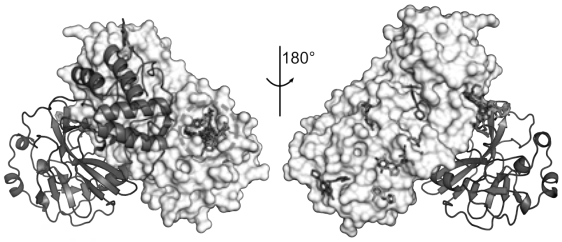

Figure 1

Time-resolved diffraction experiments at an X-ray free electron laser reveal ultrafast structural changes within a photosynthetic reaction centre

R. Neutze[1]

[1] Univ. Gothenburg, Gothenburg, Sweden

X-ray free electron lasers (XFEL) have facilitated the development of time-resolved serial femtosecond crystallography (TR-SFX) approaches to study protein structural changes [1]. This method relies upon the continuous replacement of microcrystals using micro-jet (or other) technologies and has many advantages relative to traditional time-resolved Laue diffraction methods using synchrotron radiation [2]. Photosynthetic reaction centres are integral membrane proteins which harvest the energy content of sunlight in order to power the movement of electrons. We collected TR-SFX data at the LCLS in order to observe light induced structural changes in a bacterial photosynthetic reaction centre. Our observations revealed how the light-induced movement of electrons induced a complementary structural response of the protein which stabilized the charge-separated state [3].

References

[1] Tenboer, J., et al. "Time-resolved serial crystallography captures high-resolution intermediates of photoactive yellow protein" *Science*, vol. 346, pp. 1242-1246, 2014.

[2] A. Wöhri et al., "Light-induced structural changes in a photosynthetic reaction center caught by Laue diffraction", *Science*, vol. 328, pp. 630-633, 2010.

[3] R. Dods et al., "Ultrafast structural changes within a photosynthetic reaction centre", *Nature*, vol. 589, pp. 310-314, 2021.

Atomic resolution structure determination by cryo-EM – where are the limits?

H. Stark[1], K. M. Yip[2], N. Fischer[2], E. Pakina[2], A. Chari[2]

[1] MPI Göttingen

[2] Max-Planck-Institute für biophysikalische Chemie, Göttingen

Single particle cryo electron microscopy (cryo-EM) has developed into a powerful technique to determine 3D structures of large macromolecular complexes. Due to improvements in instrumentation and computational image analysis, the number of high-resolution structures is steadily increasing. The method cannot only be used to determine high-resolution structures but also to study the dynamic behavior of macromolecular complexes and thus represents a very complementary method to X-ray crystallography. Furthermore, the maximum attainable resolution by cryo-EM has constantly improved in recent years. Most of the high-resolution structures are still in the 3 Angstrom resolution regime but some have even crossed the 2 Angstrom barrier. We have recently installed a new prototype electron microscope which is equipped with a monochromator and a next-generation spherical aberration corrector. This microscope is optically superior to the currently commercially available instruments and can therefore be used to test the resolution limits in cryo-EM. We have used the test specimen apoferritin to determine its structure at 1.25 Angstrom resolution [1] which is sufficient to visualize for the first time individual atoms clearly separated in the density map (Figure 1). Recently, we managed to use this microscope not only to improve the resolution of the very stable and rigid protein apoferritin. We also obtained significant improvement in resolution for other more dynamic macromolecular complexes for which one could have expected that the microscope itself may not be a major resolution limiting factor.

References

[1] Yip et al., "Atomic resolution protein structure determination by cryo-EM", *Nature*, vol. 587, pp. 157–161, 2020.

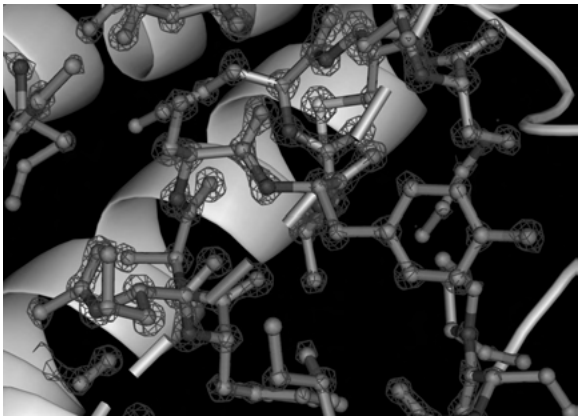

Figure 1

Research activities at the HZB-MX beamlines directed towards fighting SARS-CoV-2

M. S. Weiss[1], T. Barthel[1], C. Feiler[1], R. Foerster[1], C. Gless[1], T. Hauss[1], M. Hellmig[1], F. Lennartz[1], U. Müller[1], M. Steffien[1], H. Taberman[1], J. Wollenhaupt[1]

[1] Macromolecular Crystallography, Helmholtz-Zentrum Berlin

Since the worldwide outbreak of the Covid-19 pandemic in early 2020, researchers in many different parts of the world have started activities directed towards a better understanding of the SARS-CoV-2 virus life cycle or even towards medical treatment of Covid-19. Large-scale research facilities such as for instance synchrotron radiation facilities are playing a particularly important role in this respect by providing state-of-the-art Macromolecular crystallography (MX) facilities. MX has been instrumental in deciphering the first atomic resolution structure of the SARS-CoV-2 main protease (Figure 1) [1]. Several other viral protein structures have been determined following that [2]. Furthermore, owing to the manifold developments of MX towards automation and the concomitant increase in throughput, MX has also been employed as a primary screening technique for finding new substances, which might be active against SARS-CoV-2. In the presentation several user and in-house projects will be highlighted, which are directed towards this goal.

References

[1] L. Zhang, et al., "Crystal structure of SARS-CoV-2 main protease provides a basis for design of improved α-ketoamide inhibitors", *Science*, vol. 368, pp. 409–412, 2020.

[2] M. Scudellari, "The sprint to solve coronavirus protein structures - and disarm them with drugs", *Nature*, vol. 581, pp. 252–255, 2020.

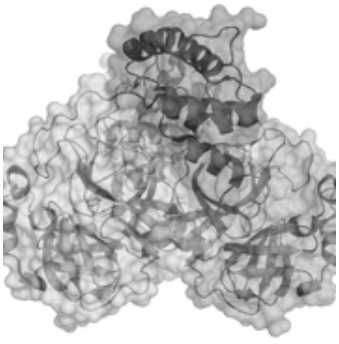

Figure 1

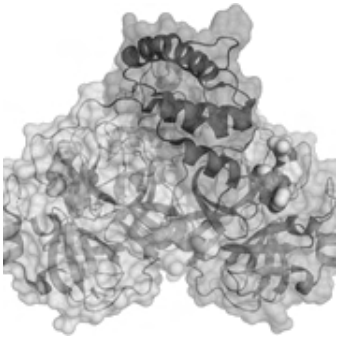

Figure 2

Max von Laue Talk:
Self-organization of biomolecular building blocks and inorganic nanoparticles into biohybrid nanomaterials

T. Beck[1,2]

[1] University of Hamburg, Institute of Physical Chemistry, Grindelallee 117, Hamburg, Germany

[2] The Hamburg Centre for Ultrafast Imaging, Hamburg, Germany

Self-organization is a key tool for the construction of functional nanomaterials. We have recently established a novel method for the self-organization of biomolecular building blocks and nanoparticles. Here, protein containers, engineered with opposite surface charge, are used as an atomically precise ligand shell for the assembly of inorganic nanoparticles.[1] The assembly of these protein-nanoparticle composites yields highly ordered nanoparticle superlattices with unprecedented precision (Fig. 1A). The structure of the protein scaffold can be tuned with external stimuli such as metal ion concentration.[2] Importantly, these composite materials show catalytic activity inside the porous material.[3] Along these lines, the protein containers used as a scaffold offer a viable route towards renewable materials.[4]

For the formation of these biohybrid materials, the inorganic cargo has to be synthesized or encapsulated into the protein containers. Here, we demonstrate that the highly specific cargo-loading mechanism of the bacterial nanocompartment encapsulin can be employed for encapsulation of artificial cargo such as inorganic nanoparticles.[5] For this purpose, gold nanoparticles were decorated with cargo-loading peptides. By lock-and-key interaction between the peptides and the peptide-binding pockets on the inner container surface, the nanoparticles are encapsulated with extremely high efficiency (Fig. 1B). Importantly, the container does not change, as shown by electron microscopy. Most notably, the supramolecular peptide binding is independent from external factors such as ionic strength.[5] Cargo-loading peptides may serve as generally applicable tool for efficient and specific encapsulation of cargo molecules into a protein compartment. Moreover, these nanoparticle protein-container composites are suitable for applications as building blocks in materials, exploiting the plasmonic properties of gold nanoparticles for light manipulation or sensing.

References

[1] M. Künzle, T. Eckert, T. Beck, *J. Am. Chem. Soc.*, vol. 138, pp. 12731-12734, 2016.

[2] M. Künzle, T. Eckert, T. Beck, *Inorg. Chem.*, vol. 57, pp. 13431-13436, 2018.

[3] M. Lach, M. Künzle, T. Beck, *Chem. Eur. J.*, vol. 23, pp. 17482-17486, 2017.

[4] a) M. Künzle, M. Lach, T. Beck, *Dalton Transactions*, vol. 47, pp. 10382-10387, 2018; b) M. Lach, M. Künzle, T. Beck, *Biochemistry*, vol. 58, pp. 140, 2019.

[5] M. Künzle, J. Mangler, M. Lach, T. Beck, *Nanoscale*, vol. 10, pp. 22917-22926, 2018.

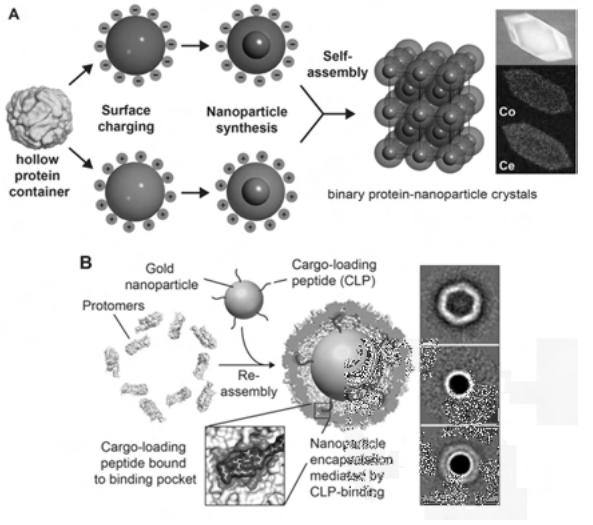

Figure 1 A) General strategy for the assembly of binary protein-nanoparticle crystals based on charged protein containers. B) Efficient encapsulation of functionalized gold nanoparticles into the encapsulin protein container. Right panel: TEM class averages of empty containers, gold nanoparticles and encapsulated gold nanoparticles.

Max von Laue Talk: From the perturbation of crystal symmetry towards functionality

M. Zschornak[1]

[1] TU Bergakademie Freiberg, Freiberg, Germany

The formation of crystals and symmetry on the atomic scale has persistently attracted scientists through the ages. The structural symmetry itself depends in this respect subtly on boundary conditions such as defects or external physical fields. In particular sensitive details in the electronic structure determine the nature of a vast diversity of symmetry-related phenomena – among them piezoelectricity, pyroelectricity, and ferroelectricity. Owing to their versatile orbital character, especially transition metal oxides span the range of ionic, covalent and metallic bonding and thus offer both local and highly dispersive degrees of freedom.

In the talk, crystalline symmetry reductions due to structural defects and external electric fields will be discussed, exemplarily for the perovskite $SrTiO_3$. To gain a thorough physical understanding of the underlying processes, interactions and dynamics, details of the local atomic and electronic structure are accessed by means of experimental Resonant X-ray Scattering methods as well as electronic structure modeling. Based on the variability of X-ray photon energy at synchrotrons, new respective approaches are presented with unique capabilities to increase the contrast for the characterization of subtle structure deviations and a positional precision below the picometer.

Talks

Advanced Instrumentation

The New PHOTON III Detector with Photon Counting in Mixed-Mode Detection

M. Adam[1], T. Stuerzer[1], M. Ruf[2], J. Kaercher[2], A. Abboud[1]
[1] MA: Bruker AXS GmbH, Karlsruhe, Germany
[2] MA: Bruker AXS, LLC; Madison WI, USA

The best crystal structures for publication require X-ray detectors with high signal-to-noise ratios and accurate intensities. The new PHOTON III detector family matches these requirements perfectly, offering mixed mode detection for the first time. Mixed mode detection simultaneously combines photon counting and integration, providing data of ultimate quality for both strong and weak reflections. Conventional photon counting detectors, like HPC or HPADs, suffer from poor linearity and count rate limitations for strong reflections, significantly degrading data quality. The mixed mode PHOTON III detector eliminates all detector noise, delivering the highest linearity and guaranteeing the highest quality data for the most challenging samples. The PHOTON III is available in three different sizes to ensure the best performance for your application needs. Users admire the detectors' ultimate sensitivity over a wide energy range (from In-Kα to Ga-Kα), low point-spread, and parallax-free diffraction data. The PHOTON III also features high-energy event discrimination (HEED) that eliminates ubiquitous cosmic radiation artefacts making it the best detector ever developed.

Details on the function principle of the PHOTON III detector and latest application examples will be discussed.

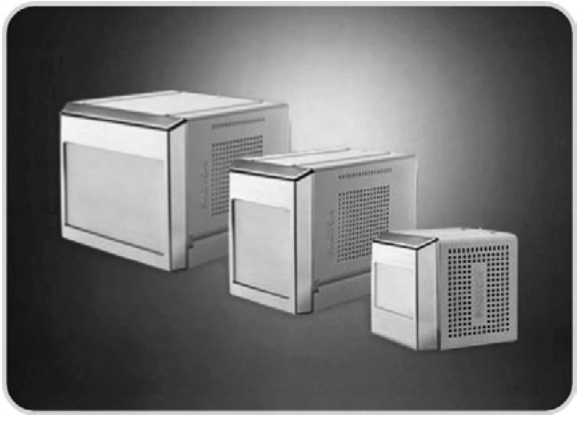

Figure 1

First user experiments of the PERCIVAL soft X-ray imager

J. Correa Magdalena[1], A. Marras[2], C. Wunderer[2], H. Graafsma[2], K. Bagschik[3], M. v. Zimmermann[4], T. Nicholls[5], H. Hyun[6], S. Rah[6], R. Pan[2], B. Keitel[2], V. Vardanyan[2], F. Krivan[2], S. Gang[2], M. Ruiz-Lopez[2], R. Battistelli[7], B. Pfau[8], F. Buettner[7], A. Dawiec[9], F. Orsini[9], K. Kharitonov[2], M. Mehrjoo[2], E. Plönjes[2], K. Kim[7], N. Tartoni[14], V. Felk[2], I. Shevyakov[2], M. Zimmer[2], N. Guerrini[5], S. Lange[2], R. Menk[11], B. Marsch[15], M. Hoesch[2], W. Nichols[10], A. Greer[10], G. Cautero[11], U. Pedersen[10]
[1] DESY, Photon Science, FS-DS (Detector Systems), Hamburg, Germany
[2] DESY, Notkestr. 85, 22607 Hamburg, Germany
[3] DESY, Photon Science, FS-PE (Experiment Support PETRY III), Hamburg, Germany
[4] DESY, HASYLAB, Hamburg, Germany
[5] STFC Rutherford Appleton Laboratory, Didcot, United Kingdom
[6] Pohang Accelerator Laboratory, Pohang, South Korea
[7] Helmholtz-Zentrum Berlin, Berlin, Germany
[8] Max-Born-Institut, Max-Born-Straße 2 A, 12489 Berlin, Germany
[9] Synchrotron SOLEIL, Saint-Aubin, France
[10] Diamond Light Source, Didcot, United Kingdom
[11] Elettra Synchrotron Trieste, Basovizza, Italy

The PERCIVAL detector, a CMOS imager specifically designed for the soft X-ray regime, has served in 2020 its two first user experiments, both at a Synchrotron Radiation source (SR) and also at a Free Electron Laser (FEL). Here, we report some preliminary results of both experiments as well as future plans.

The first experiment, in collaboration with groups at the HZB and MBI, used the P04 XUV beamline at PETRA-III to perform holography imaging of topological materials (in particular skyrmions) at an energy or 780eV. The second experiment, in collaboration used the FL24 at FLASH-2 to performed ptychography imaging of plasma treated surfaces at an energy range between 92 and 462eV. Both experiments benefited from a very large dynamic range, thanks to the PERCIVAL auto-adaptative gain switching.

With its 4 x 4 cm^2 active area, extendable to 8 x 8 cm^2 in clover-leaf like configurations, and its 2 Megapixels, 27 μm size, PERCIVAL can provide images with high spatial resolution. Moreover, its fast readout, wil be capable of speeds up to 300 frames per second. A dynamic range from 14e- to 3.5 Me- is to be expected. The development, jointly carried by 5 light sources (DESY,

PAL, Elettra, DLS and SOLEIL) and RAL/STFC, will enable increased science yield from today's FEL and synchrotron light sources in the soft X-ray regime.

Clamp cells for high pressure neutron scattering at low temperatures and high magnetic fields at the MLZ

A. Eich[1], K. Friese[1], M. Hölzle[1], Y. Su[1], T. Müller[1], V. Hutanu[1,2], M. K. B. Poli[2], R. Georgii[3], L. Beddrich[3], M. Meven[2], A. Grzechnik[2]

[1] Forschungszentrum Jülich, JCNS-MLZ, Garching, Germany

[2] RWTH Aachen University, Institute of Crystallography, Aachen, Germany

[3] Heinz Maier-Leibnitz Zentrum, Garching, Germany

To study the effect of high pressure on any sample property, suitable pressure devices are a fundamental requirement. Their design has to be tailored to the experimental demands regarding the intended pressure, the employed instrumentation and the expected scientific results. Our work presents the development of high pressure cells for neutron scattering on polycrystalline and single-crystalline samples at low temperatures and with applied magnetic fields.

One of the most common devices for high-pressure neutron experiments is the clamp cell [1], where the pressure is applied ex situ and which can be used independently in various setups. Our cell design [2] has been specifically developed for neutron scattering experiments at low temperatures in the closed-cycle cryostats on the instruments DNS (diffuse scattering neutron spectrometer), MIRA (cold three axes spectrometer), and POLI (polarized hot neutron diffractometer) at the Heinz Maier-Leibnitz Zentrum (MLZ) in Garching, Germany. The compact monobloc cell has been produced in two variants, the CuBe alloy and NiCrAl "Russian Alloy", working up to about 1.1 GPa and 1.5 GPa, respectively. The low paramagnetic moment of both alloys allows also measurements of magnetic properties.

First tests of the cell with neutron radiation were performed to calibrate the load/pressure-curve of the CuBe cell (up to 1.15 GPa), to estimate its neutron absorption and background, and to measure magnetic reflections. In addition, the thermal response in the instrument cryostat was measured and the experimental findings were complemented by simulations.

Ultimately, these cells are intended as standard cells for high pressure measurements on different instruments at MLZ suitable for all available magnets and cryostats down to 1.5 K. Further tests under various conditions (temperature, pressure, magnetic field) as well as simulations are planned for both cells. The results will help both to establish the present cells and to optimise the design of subsequent cells to achieve higher pressures, to fit into smaller cryostats and to enable neutron-independent pressure calibration.

Acknowledgement

This work was supported by the Bundesministerium für Bildung und Forschung (BMBF) [grant number 05K19PA2] and by the Deutsche Forschungsgemeinschaft (DFG) [grant number GE971/5-2].

References

[1] Klotz, S., *Techniques in High Pressure Neutron Scattering*, Boca Raton, USA: CRC Press, 2013.

[2] Eich, A. *et al.*, *High Press. Res. Advance*, 2020, doi: 10.1080/08957959.2020.1841759.

New polarized neutron diffraction setup for precise investigations of magnetic structures up to 8 T at the MLZ

V. Hutanu[1], H. Thoma[2], H. Deng[1,2], G. Brandl[2], A. Weber[2], V. Rubanskiy[2], J. Peters[3], W. Luberstetter[1,2], T. Krist[4], G. Roth[1], L. Peters[1], T. Brückel[2]

[1] RWTH Aachen University, Institute of Crystallography, Aachen, Germany

[2] Forschungszentrum Jülich, JCNS outstation @ MLZ Garching, Garching, Germany

[3] TU Munich, FRM II, Munich, Germany

[4] NOB Berlin GmbH, Berlin, Germany

Polarized neutron diffraction (PND) is a powerful method for investigating magnetic structures. It gives unique access to contributions from nuclear and magnetic scattering, their interference terms, and their magnetic chirality, and permits to distinct between them. In contrast to non-polarized neutron diffraction, where the scattered intensity depends on the square of the magnetic structure factor, PND has a linear nuclear–magnetic interference term as part of the scattered intensity. This increases the precision in the determination of the ordered magnetic moment by at least one order of magnitude. Recently, a first PND setup using a compact high Tc superconducting magnet and a 3He spin filter polarizer has been successfully implemented [1,2] on the hot neutrons single crystal diffractometer POLI at Maier-Leibnitz Zentrum (MLZ) in Garching b. München. Although this setup performs well and first scientific output from the measurements performed using it starts to appear [3], it suffers from the relatively low maximal available field of only 2.2 T. For studying many modern-topic (e.g quantum, topologic order, complex frustrated, etc.) magnetic materials with

small ordered magnetic moment, the field-limit of about 2 T is insufficient in order to produce significant measurable signal, even for PND. To overcome this limitation, a new 8 T split-coil superconducting magnet has been procured and implemented for measurements on POLI. Although, this new magnet is actively shielded, reducing the stray field by an order of magnitude compared to the classical design, its fringe fields are still too large to be used with the sensitive 3He polarizer of the previous setup. To overcome this issue, a new large-beam-cross-section solid-state supermirror bender (SB) polarizer has been developed for POLI. It was realized by a Fe/Si multilayer coating on both sides of the thin Si wafers (m=3) by the NOB company. An additional Gd oxide layer is deposited on the convex side of each wafer to absorb the neutrons with the wrong polarization. An existing shielded Mezei-type flipper is used between the magnet and SB. A dedicated guide field construction was numerically simulated, optimized and built to link the magnetic field of the SB to the flipper and to the stray field of the magnet. The neutron beam path between the monochromator drum to the sample magnet is shown in the Fig. 1. The new setup was successfully tested using a 3He spin filter as analyzer at low fields ($<$ 1 T), and a high quality Cu2MnAl single-crystal at high fields ($>$ 2T). An almost loss-free spin transport within the instrument for the complete field range of the new magnet was achieved. A high polarization efficiency of above 99% even for short wavelength neutrons could be experimentally reached using the new solid-state bender (Fig.2). The new high–field PND setup is now available for precise magnetic structure investigations on POLI for the internal and external user communities.

References

[1] H. Thoma, H. Deng, G. Roth, V. Hutanu, "Setup for polarized neutron diffraction using a high-Tc superconducting magnet on the instrument POLI at MLZ and its applications", *J. Phys.: Conf. Ser.*, vol. 1316, 2019, Art. no. 012016.

[2] H. Thoma, W. Luberstetter, J. Peters & V. Hutanu, "Polarised neutron diffraction using novel high-Tc superconducting magnet on single crystal diffractometer POLI at MLZ," *J. Appl. Cryst.*, vol. 51, pp. 17–26, 2018.

[3] J. Jeong, B. Lenz, A. Gukasov *et al.*, "Magnetization density distribution of Sr2IrO4: Deviation from a local jeff = 1/2 picture," *Phys. Rev. Lett.*, vol. 125, 2020, Art. no. 097202.

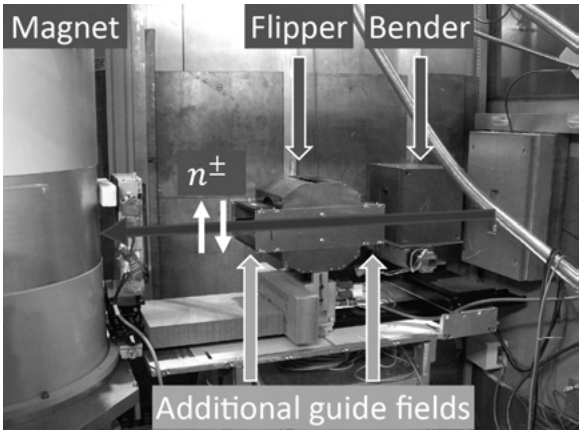

Figure 1

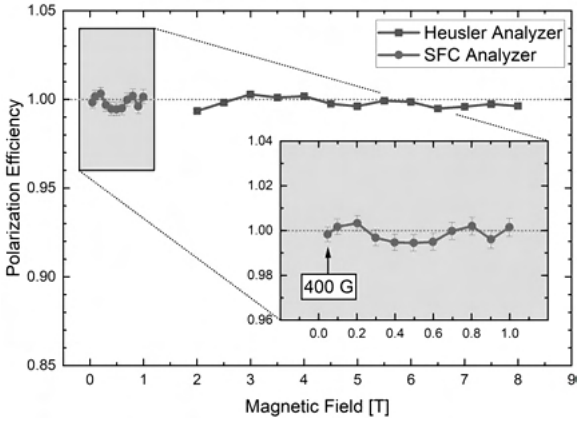

Figure 2

Single Crystal Diffraction Experiments under High Pressure with Hot Neutrons at MLZ

M. Meven[1], A. Grzechnik[1], V. Hutanu[1], K. Friese[2], A. Eich[3], G. Roth[1]

[1] Institute of Crystallography, RWTH Aachen University, Aachen, Germany

[2] Jülich Centre for Neutron Science at Heinz Maier-Leibnitz Zentrum, Forschungszentrum Jülich GmbH, Garching, Germany

[3] Jülich Centre for Neutron Science–2/Peter Grünberg-Institute–4, Forschungszentrum Jülich GmbH, 52425 Jülich, Germany

Due to their specific peculiarities neutrons are a very useful probe for structural studies on various hot topics related to physics, chemistry and mineralogy. The neutron single crystal diffractometer HEiDi at the Heinz Maier-Leibnitz Zentrum (MLZ) offers high flux, high resolution and large q range, low absorption and high sensitivity for light elements. These properties apply in a similar way to its polarized sister diffractometer POLI, which is optimized for magnetic structure determinations.

In 2016 a project was launched in order to allow studies on tiny samples < 1 mm^3 and to develop new pressure cells for HEiDi which can be combined with its existing low temperature equipment in order to study structural properties down to temperatures below 10 K, e.g. MnFe4Si3 compounds and their magnetic features [1]. As part of this project (funded by the BMBF, No. 05K16PA3), various neutron-optical components (Cu220-monochromator, solid state collimators, neutron guides) were developed and optimized in order to generate a sufficiently high flux density at the sample location at the wavelength $\lambda = 0.87$ Å. Very tiny single crystal samples (< 0.1 mm^3) were successfully studied using various newly developed diamond anvil cells up to several GPa, either with a panoramic pressure cell in combination with low temperatures [2] or in a transmission pressure cell, which allows simultaneous studies of the same sample using neutron, synchrotron as well as laboratory x-ray sources [3].

This project is now followed up by a second one (BMBF No. 05K19PA2) focusing on further improving the high pressure capabilities on HEiDi and POLI (including the installation of a 2-dimensional detector) and the development of optimized pressure cells for further instruments at the MLZ, namely POLI, DNS and MIRA (see contribution by A. Eich).

References

[1] A. Grzechnik et al., "Single-Crystal Neutron Diffraction in Diamond Anvil Cells with Hot Neutrons", *J. Appl. Cryst.*, vol. 51, pp. 351-356, 2018.

[2] A. Eich et al., "Magnetocaloric Mn_5Si_3 and $MnFe_4Si_3$ at variable pressure and temperature",*Mater. Res. Express*, vol. 6, pp. 096118, 2019.

[3] A. Grzechnik et al., "Combined X-ray and neutron single-crystal diffraction in diamond anvil cells", *J. Appl. Cryst.*, vol. 53(1), pp. 1 - 6, 2020.

Neutron protein crystallography at the Heinz Maier-Leibnitz Zentrum (MLZ): New developments and recent application examples

T. E. Schrader[1], A. Ostermann[2], M. Monkenbusch[3], B. Laatsch[4], W. Petry [2], D. Richter[3]

[1] 1Forschungszentrum Jülich GmbH, Jülich Centre for Neutron Science (JCNS) at Heinz Maier-Leibnitz Zentrum (MLZ), Lichtenbergstr.1, 85747 Garching, Germany

[2] 2Heinz Maier-Leibnitz Zentrum (MLZ), Technische Universität München

[3] Forschungszentrum Jülich GmbH, Institute for Complex Systems ICS

[4] Forschungszentrum Jülich GmbH, Engineering and Technology (ZEA-1)

The neutron single crystal diffractometer BIODIFF at the research reactor Heinz Maier-Leibnitz (FRM II) is especially designed to collect data from crystals with large unit cells. The main field of application is the structural analysis of proteins, especially the determination of hydrogen atom positions. BIODIFF is a joint project of the Jülich Centre for Neutron Science (JCNS) and the FRM II. BIODIFF is designed as a monochromatic instrument with a narrow wavelength spread of less than 3 %. To cover a large solid angle the main detector of BIODIFF consists of a neutron imaging plate in a cylindrical geometry with online read-out capability.

BIODFF is equipped with a standard Oxford Cryosystem "Cryostream 700+" which allows measurements at 100 K. A new kappa goniometer head was added recently. This allows an automated tilting of the crystal in order to increase the completeness of the data set when recording another set of frames in the tilted geometry. Typical scientific questions addressed are the determination of protonation states of amino acid side chains in proteins and the characterization of the hydrogen bonding networks between the protein active centre and an inhibitor or substrate.

Picking out some recent highlights from measurements at BIODIFF it will be shown how the method of neutron protein crystallography could be used to answer mechanistic questions in enzymatic processes or help to improve inhibitor fragment screening. New developments at the instrument will also be presented: A new collimation for the primary beam should lead to a reduction in background. It should also make it easier to align the neutron beam with the centre of the neutron imaging plate detector. Furthermore, a new single crystal x-ray diffractometer has been installed in the new MLZ lab building. It features a Molybdenum and a Copper Microfocus x-ray source and a 150° (2) x-ray detector. It also features also an Oxford Cryosystems 800 series Cryostream for sample temperatures between 80-400K. This x-ray diffractometer can be used to record an x-ray data set of the protein crystal after having been measured at the BIODIFF instrument. It may also be used to pre-scan the diffraction quality of the crystals the user brings for neutron beam times at MLZ instruments.

Diffractometer portfolio at FRM II neutron source: status and perspectives

A. Senyshyn[1]

[1] Heinz Maier-Leibnitz Zentrum (MLZ)

In the meantime the diffraction activities form the major portion of research at each large scale facility. Diffraction at neutron sources is exploring the full range of unique neutron properties (sensitivity to isotopes and magnetic subsystems, nuclear scattering form-factors independent on Q etc) and provides structural information complementary to X-ray or electron diffraction. Despite the different underlying physics supplementing the interaction of neutrons and photons with the matter, the ways of the data A wealth of neutron diffraction instrumentation as a probe of long-range atomic and magnetic orders from single crystal and powder samples at a variety of environmental conditions is available at MLZ, namely high-resolution and engineering diffractometers SPODI and STRESS-SPEC; hot, thermal and cold (macromolecular) single crystal diffractometers HEIDI, RESI and BioDIFF; diffuse instrument DNS and a pool of triple axis spectrometers. A number of new instrumental developments (POWTEX, SAPHIR, ERWIN) as well as new life project for FIREPOD (E9) are on their way to strengthen diffraction at MLZ even further.

There is a broad spectrum of structure-related scientific activities at MLZ e.g. (i) electrochemical energy storage systems and related materials; (ii) modern ferroelectrics; (iii) multiferroic materials and interrelation of the ferroic degrees of freedom; (iv) new generation engineering and shape memory alloys; (v) biological macromolecules; (vi) rock-forming minerals and glasses. In the current contribution an overview of the diffraction instrumentation at FRM II neutron source will be presented along with the future prospects and running developments.

Giant supramolecules meet synchrotron radiation: Experience with DESY P11 and P24 beamlines

A. Virovets[1], E. Peresypkina[1], M. Scheer[1]

[1] University of Regensburg, Regensburg, Germany

During last decades we have been using organometallic *cyclo*-Pn complexes (n = 4, 5) as building blocks for the rational design of giant supramolecules, up to 4.6 nm in size [1-4]. The supramolecules consisting of hundreds of atoms frequently demonstrate weak scattering power due to the severe crystallographic disorder. In many cases, the use the high-flux synchrotron sources becomes the only remedy.

The samples of organometallic supramolecules must be permanently protected from oxygen to avoid the oxidation of *cyclo*-Pn fragments. Any traces of water in the organic solvents also should be avoided. Therefore, the proper sample handling requires a vacuum-argon line (Schlenk line) that protects the sample from air during the extraction of the portion of crystals for the diffraction study. Within the long-term project II-20180597 with DESY (Hamburg, Germany) we have installed such line in the sample preparation lab of P24 beamline.

To obtain quality data at dmin $>$ 1 Å for giant supramolecules we developed optimal strategies to perform the single-crystal diffraction experiments at both P11 and P24 beamlines. For P11 beamline, the most critical is to choose radiation energy as a compromise between dmin and quantum efficiency (QE) of a PILATUS 6M detector. Higher energies improves the resolution by the cost of significantly lower QE.

The optics at the P24 beamline allows using hard X-ray radiation with E up to 44 keV. It helps in reducing the absorption and radiation damage in Ag and Ta-containing crystals. Helium open-flow cryostat provides temperature down to 10 K.

Optimization of the experimental strategy allowed us to obtain high-quality diffraction data even from weakly scattering crystals (Fig. 1) and to investigate such subtle structural effects as superstructural ordering.

This work was supported by the German Research Foundation (DFG) within the project Sche 384/44-1.

References

[1] E. Peresypkina, C. Heindl, A. Virovets, M. Scheer, *Structure and Bonding*, vol. 174, p. 321, 2016.

[2] H. Brake, E. Peresypkina, C. Heindl, *et al.*, *Chem. Sci.*, vol. 10, p. 2940, 2019.

[3] E. Peresypkina, M. Bielmeier, A. Virovets, M. Scheer, *Chem. Sci.*, vol. 11, p. 9067, 2020.

[4] J. Schiller, A.V. Virovets, E. Peresypkina, M. Scheer, *Angew. Chem. Int. Ed.*, vol. 59, p. 13647, 2020.

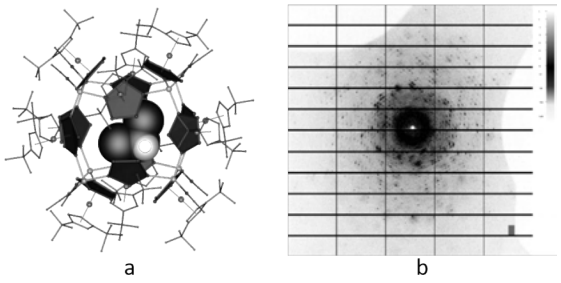

Figure 1 a) Giant cationic supramolecule [(Cp''Fe(η5-P5)12(CuNCCH3)8]8+ with an external diameter of 2.5 nm [4]. Hydrogen atoms are omitted for clarity; b) the diffraction pattern from the single crystal at P11 beamline (E = 18 keV, 0.1° scan)

Bio-crystallography

EasyAccess Frame - sliding puzzle inspired tool for eased crystal handling

T. Barthel[1], F. U. Huschmann[1], D. Wallacher[1], C. Feiler[1], G. Klebe[2], J. Wollenhaupt[1], M. Weiss[1]

[1] Helmholtz-Zentrum Berlin, Macromolecular Crystallography, Albert-Einstein-Straße 15, 12489 Berlin, Germany

[2] Philipps-University Marburg, Marburg, Germany

The experimental workflow of macromolecular crystallography has been improved enormously in the last two decades, especially regarding speed and throughput. One step of this workflow, namely the manipulation and harvesting of crystals, remains labour- and time-intense even though considerable efforts have been applied. In order to tackle this bottleneck, we developed a novel, low-cost device that acts as a lid for 96-well crystallization plates. It includes 96 movable parts that allow access to the individual experiment and simultaneously minimize the evaporation of the other experiments. Primary results show the successful evaporation minimization of many typical crystallization cocktails for up to six hours. The device, named EasyAccess Frame, avoids any sealing by foil and unsealing of individual wells in the process and thus facilitates easy crystal manipulation and harvesting. Therefore, the device increases throughput and is useful for a range of macromolecular crystallography experiments, especially screening campaigns. The device is successfully being used in crystallographic fragment screening campaigns at HZB and significantly reduces time and effort necessary for the crystal handling involved.

References

[1] Barthel T., Huschmann F. U., Wallacher D., Feiler C. G., Klebe G., Weiss M. S., Wollenhaupt J., "Facilitated crystal handling using a simple device for evaporation reduction in microtiter plates," *J. Appl. Cryst.*, accepted for publication, 2021.

Molecular mechanisms of the bacterial DEAH/RHA NTPase HrpA and its role in antibiotics susceptibility

L. Grass[1], J. Wollenhaupt[1], T. Barthel[1], B. Loll[1], M. C. Wahl[1]

[1] Laboratory of Structural Biochemistry, Freie Universität Berlin, Berlin, Germany.

Many bacteria harbor RNA-dependent nucleoside-triphosphatases of the DEAH/RHA family [1], whose molecular mechanisms and cellular functions are poorly understood [2]. Here, we show that the Escherichia coli DEAH/RHA protein, HrpA, is an ATP-dependent 3'-to-5' RNA helicase, and that the RNA helicase activity of HrpA influences bacterial survival under antibiotics treatment. Limited proteolysis, crystal structure analysis and functional assays showed that HrpA contains an N-terminal DEAH/RHA helicase cassette preceded by a unique N-terminal domain and followed by a large C-terminal region that modulates the helicase activity. Structures of an expanded HrpA helicase cassette in the apo and RNA-bound states revealed ratchet-like domain movements upon RNA engagement much more pronounced than hitherto observed in related eukaryotic DEAH/RHA enzymes (Fig. 1). Consistent with similar conformational changes supporting RNA translocation, structure-based functional analyses delineated transient inter-domain contact sites that support substrate loading and unwinding. Analogous dynamic intramolecular contacts are not possible in the related, but helicase-inactive, RNA-dependent nucleoside-triphosphatase, HrpB [3,4]. Our results indicate that HrpA may be an interesting target to interfere with bacterial tolerance toward certain antibiotics and suggest possible interfering strategies.

References

[1] Khemici, V. & Linder, P., "RNA helicases in bacteria," *Curr. Opin. Microbiol.*, vol. 30, pp. 58–66, 2016.

[2] Redder, P., Hausmann, S., Khemici, V., Yasrebi, H. & Linder, P., "Bacterial versatility requires DEAD-box RNA helicases," *FEMS Microbiol. Rev.*, vol. 39, pp. 392–412, 2015.

[3] Pietrzyk-Brzezinska, A. J. *et al.*, "Crystal Structure of the Escherichia coli DExH-Box NTPase HrpB," *Structure*, vol. 26, pp. 1462-1473.e4, 2018.

[4] Xin, B.-G., Chen, W.-F., Rety, S., Dai, Y.-X. & Xi, X.-G., "Crystal structure of Escherichia coli DEAH/RHA helicase HrpB," *Biochem. Biophys. Res. Commun.*, vol. 504, pp. 334–339, 2018.

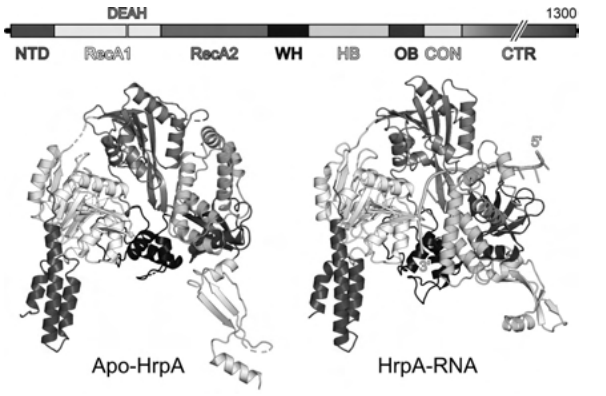

Figure 1 Top, Domain composition of the E. coli DEAH/RHA-type RNA helicase, HrpA. NTD, N-terminal domain; RecA1/2, RecA-like domains; WH, winged-helix domain; HB, helical bundle ("ratchet") domain; OB, oligonucleotide/oligosaccharide-binding domain; CON, connector domain; CTR, C-terminal region. Bottom, comparison of the crystal structures of the expanded helicase cassette of E. coli HrpA in the apo (left) and RNA-bound (right) states.

Massive X-ray screening against SARS-CoV-2 main protease

S. Guenther[1], P. Reinke[2], A. Meents[2]

[1] DESY, Photon Science, FS-BMX, Hamburg, Germany

[2] DESY, Notkestr. 85, 22607 Hamburg, Germany

Contributed on behalf of the Hamburg SARS-CoV-2 X-ray screening initiative

As a response to the current SARS-CoV-2 pandemic we have set up a large consortium of more than one hundred scientist centered around DESY in Hamburg. In contrast to common screening techniques such as biochemical activity-based assays or X-ray fragment screening, here we employed massive X-ray crystallographic screening of two drug-repurposing libraries against SARS-CoV-2 main protease (MPro) of SARS-CoV-2 as initial target. Already in March 2020 co-crystallization experiments of 5953 individual drugs with MPro were setup. In April data from more than 8000 of these crystals were collected at the PETRA III MX beamlines. In the following weeks a data analysis pipeline for fully automatic data processing and subsequent structure refinement followed by ligand identification by pan-dataset density analysis (PanDDA) was established. Our screening effort resulted in the identification of 37 compounds binding to MPro. Secondary screening of these hits in a cell-based virus-infection assay revealed antiviral activity in combination with low cytotoxicity for six compounds which have not yet been reported as inhibitors of SARS-CoV-2. While four of these inhibitors bind to the catalytic site of the enzyme, the remaining two bind to an allosteric site within the dimerization domain [1].

To our knowledge, this is the first time X-ray crystallography has been used as a primary screen for drug discovery while using drug-like molecules rather than smaller fragments. The platform developed for this project is currently being further extended and optimized and will be available for future drug discovery efforts.

References

[1] S. Günther, P. Y. A. Reinke, *et al.*, *bioRxiv*, in press, doi:10.1101/2020.11.12.378422.

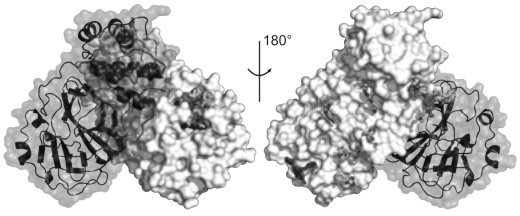

Figure 1 SARS-CoV-2 MPro dimer with hits derived from X-ray screening of drug repurposing libraries. Drug binding (stick representation) is observed across the complete MPro dimer. One MPro monomer with bound drugs is shown in white surface representation. The other monomer is shown as mixed cartoon/surface representation.

The Corona-year 2020 at Biodiffraction Beamline P11

J. Hakanpaeae[1], S. Saouane[2], E. Crosas[3], J. Meyer[3], B. Kistner[3], A. Henkel[4], S. Chatziefthymiou[5], G. Pompidor[3]

[1] DESY, Photon Science, FS-PETRA-D, P11 Beamline, Hamburg, Germany

[2] DESY, Photon Science, FS-PS (FS-Photon Science), Hamburg, Germany

[3] DESY, Notkestr. 85, 22607 Hamburg, Germany

[4] University of Lübeck, Lübeck, Germany

[5] DESY, Photon Science, FS-PE (Experiment Support PETRA III), Hamburg, Germany

Beamline P11 at PETRA III in Hamburg is a versatile instrument for macromolecular crystallography (1). During 'the Corona-year' 2020 we operated in very exceptional conditions. Here we describe DESY responses to the pandemic situation, such as the fast-track access to the beamline, exceptional user regulations and remote access.

To date, 35 PDB depositions have arisen from P11 related to Covid-19 by our fast-track, proposal and priority access users (2-5). Additionally, P11 participates to three DESY Strategic Fund projects relating to Covid-19 research: 1) Inhibitor screening and structural characterization of virulence factors from SARS-CoV-2, 2) Multidimensional serial crystallography of Sars-CoV-2 proteins to unravel structure and dynamics of function and inhibition and 3) Automated X-ray crystallography compound screening pipeline at DESY.

In spite of the restricted user operations, the beamline had a very busy user run and the scarce commissioning time was used to employ our new Eiger2 X 16M. We successfully employed the detector for serial data collections. Dedicated nodes in our central computational cluster Maxwell will be at the disposal of our users for processing (and autoprocessing) their Eiger data next year. Inspired by the properties of our new detector, we started to streamline the serial crystallography methods available at the beamline and to integrate both the data collection and the data processing more tightly into the beamline environment.

References

[1] Burkhardt *et al.*, *Eur. Phys. J. Plus*, vol. 131, 2016, Art. no. 56.

[2] Zhang *et al.*, *Science*, vol. 368, pp. 409-412, 2020.

[3] Günter *et al.*, *BioRxiv*, 2020, doi.:10.1101/2020.05.02.043554.

[4] Rut *et al.*, *Nat. Chem. Biol.*, 2020, doi:10.1038/s41589-020-00689-z.

[5] Oerlemans *et al.*, *RSC Med. Chem.*, 2021, DOI: 10.1039/D0MD00367K.

Crystal structure of bacterial cytotoxic necrotizing factor CNFy reveals molecular building blocks for intoxication

P. Chaoprasid[1], P. Lukat[2], S. Mühlen[1], T. Heidler[3], E.-M. Gazdag[2], S. Dong[2], W. Bi[4], C. Rüter[1], M. Kirchenwitz[5], A. Steffen[5], L. Jänsch[6], T. E. Stradal[5], P. Dersch[1], W. Blankenfeldt[2]

[1] University of Münster, Institute of Infectiology, Center for Molecular Biology of Inflammation (ZMBE), Münster, Germany

[2] Helmholtz Centre for Infection Research, Structure and Function of Proteins, Braunschweig, Germany

[3] Helmholtz Centre for Infection Research, Molecular Structural Biology, Braunschweig, Germany

[4] Helmholtz Centre for Infection Research, Cellular Proteomics, Braunschweig, Germany

[5] Helmholtz Centre for Infection Research, Cell Biology, Braunschweig, Germany

[6] Helmholtz Centre for Infection Research, Cellular Proteomics, Braunschweig, Germany

Cytotoxic Necrotizing Factors (CNFs) are single-chain AB-toxins and important virulence factors in pathogens such as uropathogenic *E. coli* (UPEC) or enteropathogenic *Yersinia* species. Their cytotoxic effect is based on the constitutive activation of small GTPases (Rho family) by deamidation of a glutamine residue in the switch II region, leading to cytoskeletal alterations and finally death of the host cell. Several steps are required for the toxin to fulfill its task, such as receptor binding, endocytosis and yet unknown structural changes in the B-part in order to translocate the catalytically active, toxic A-part through the endosomal membrane into the cytosol. So far, a crystal structure that could provide insight into these processes is still lacking.

Here we report on the crystal structure of full-length CNFy from *Yersinia pseudotuberculosis* at a resolution of 2.7 Å. The structure was solved by molecular replacement with the existing model of the C-terminal catalytic domain and the structure of the B-part, where the phases of the latter were obtained by single anomalous dispersion experiments in advance. The full-length AB-toxin comprises 1014 amino acid residues. While the two C-terminal domains (485 residues) are forming the A-part, the N-terminal B-part (529 residues) is consisting of 3 individual domains, of which all possess novel folds. From cell-biology experiments, the receptor-binding and translocation functions could be assigned to the first three domains although their mechanism(s) and the receptor of the host cell remain still unknown. The fourth domain shows structural similarity to ADP-ribosyl transferases but no similar function in CNFy could yet be detected.

Additionally, we also determined the structure of the two-domain A-part - as it should be released into the cytoplasm - alone (1.8 Å). The two domains show a different orientation towards each other than in the structure of the full-length toxin, which could hint towards activation of the catalytic domain upon release of the A-part.

Our first crystal structure of a full-length CNF-toxin lays the groundwork for further studies of the complex mechanism of this important bacterial virulence factor. CNF-toxins might not only be promising targets for future development of anti-infective drugs, the B-part might even have the potential to be exploited as delivery vehicle for large and complex drugs.

Facilities for Macromolecular Crystallography at the HZB

U. Müller[1], T. Barthel[2], C. Feiler[3], R. Förster[4], C. Gless[1], T. Hauß[3], M. Hellmig[4], F. Lennartz[3], M. Steffien[1], H. Taberman[1], J. Wollenhaupt[3], M. Weiss[4]

[1] Helmholtz-Zentrum Berlin für Materialien und Energie, Berlin, Germany

[2] Laboratory of Structural Biochemistry, Institute of Chemistry and Biochemistry, Freie Universität Berlin, Berlin, Germany

[3] Helmholtz-Zentrum Berlin, Berlin, Germany

[4] Helmholtz-Zentrum Berlin, Macromolecular Crystallography, Berlin, Germany

The Macromolecular Crystallography (MX) group at the Helmholtz-Zentrum Berlin (HZB) has been in operation since 2003. Since then, three state-of-the-art synchrotron beam lines (BL14.1-3) for MX have been built up on a 7T-wavelength shifter source [1-3]. Currently, the three beam lines represent the most productive MX-stations in Germany, with more than 3500 PDB depositions (Status 12/2020). BLs14.1 and 14.2 are energy tuneable in the range 5.5-15.5 keV, while beam line 14.3 is a fixed-energy side station operated at 13.8 keV. All three beam lines are equipped with state-of-the-art detectors: BL14.1 with a PILATUS3S 6M detector, BL14.2 with a PILATUS3S 2M and BL14.3 with a PILATUS 6M detector. BL14.1 and BL14.2 are in regular user operation providing close to 200 beam days per year and about 600 user shifts to approximately 100 research groups across Europe. Recently, remote beamline operation has been started successfully at BL14.1. BL14.3 is been equipped with a MD2 micro-diffractometer, a HC1 crystal dehydration device and a REX nozzle changer making it suitable for room temperature experiments. Additional user facilities include office space adjacent to the beam lines, a sample preparation laboratory, a biology laboratory (safety level 1) and high-end computing resources. Within this presentation a summary on the experimental possibilities of the beam lines and the ancillary equipment provided to the user community will be given.

References

[1] Heinemann U., Büssow K., Mueller, U. & Umbach, P., *Acc. Chem. Res.*, vol. 36, pp. 157–163, 2003.

[2] U. Mueller, N. Darowski, M. R. Fuchs, R. Förster, M. Hellmig, K. S. Paithankar, S. Pühringer, M. Steffien, G.Zocher & M. S. Weiss, *J. Synchr. Rad.*, vol. 19, pp. 442–449, 2012.

[3] Mueller, U., Forster, R., Hellmig, M., Huschmann, F. U., Kastner, A., Malecki, P., Puhringer, S., Rower, M., Sparta, K., Steffien, M., Uhlein, M. & Weiss, M. S., *Eur. Phys. J. Plus*, vol. 130, pp. 141–150, 2015.

Structure of SARS-CoV-2 papain-like protease PLpro reveals a framework for antiviral inhibitor design

V. Srinivasan[1], N. Werner[1], S. Falke[1], H. Brognaro[1], S. Günther[2], P. Y. A. Reinke[2], C. Ehrt[3], M. Rarey[3], A. Meents[2], C. Betzel[1,4]

[1] Universität Hamburg, Department of Chemistry, Institute of Biochemistry and Molecular Biology and Laboratory for Structural Biology of Infection and Inflammation, c/o DESY, 22607 Hamburg, Germany

[2] Center for Free-Electron Laser Science, DESY, Notkestrasse 85, 22607 Hamburg, Germany

[3] Universität Hamburg, Center for Bioinformatics, Bundesstr. 43, 20146 Hamburg, Germany

[4] Hamburg Centre for Ultrafast Imaging (CUI), Universität Hamburg, Luruper Chaussee 149, 22761, Hamburg, Germany.

The severe acute respiratory syndrome coronavirus 2 (SARS-CoV-2) papain-like protease (PLpro) is essential for the virus replication. PLpro has the additional function of removing ubiquitin and ISG15 (Interferon-stimulated gene 15) from host-cell proteins to aid coronaviruses in their evasion of the host innate immune responses. PLpro is thus an excellent drug target for a two-fold strategy to develop antiviral compounds that both inhibit viral replication and strengthen the immune response of the host. To provide a structural framework for efficient screening of inhibitor compounds, we expressed, purified and crystallized PLpro (Fig.1). The crystals are stable, reproducible, have a high solvent content of 66% suitable for soaking experiments and diffract to a high resolution of 1.5Å (Fig.2). Bioinformatics analysis of the active site based on the PLpro crystal structure coordinates showed interestingly high similarities to the proteasome and we screened 37 proteosome inhibitors by soaking and co-crystallization experiments. The PLpro crystals complexed with these compounds diffracted in the resolution

range of 1.5Å-2.5Å and structural efforts to identify new antiviral compounds to combat the coronavirus spread will be presented.

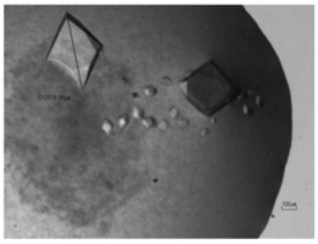

Figure 1 Trigonal PLpro crystals with cell dimensions $a = 82.03$, $b = 82.03$, $c = 134.45$, $\alpha = 90°$, $\beta = 90°$, $\gamma = 120°$.

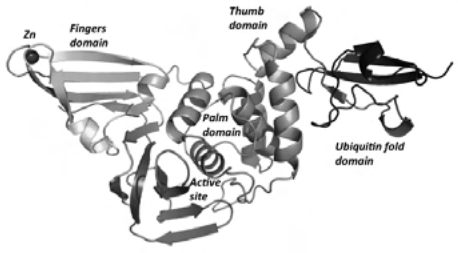

Figure 2 X-ray crystal ctructure of PLpro illustrating the four domains and the active site. The Zinc ion is represented as a magenta sphere.

The Coronavirus Structural Taskforce

A. Thorn[1]

[1] Universität Hamburg

The Coronavirus Structural Task Force [1] was an ad hoc collaboration of mostly junior researchers across nine time zones, brought together by the desire to fight the pandemic.

Most of us are crystallographic methods developers and as early as February 2020, we started evaluating the structures of macromolecules in SARS-CoV and later SARS-CoV-2 as they became available from the Protein Data Bank. We found that many could be improved. A website (www.insidecorona.net) and a database containing the evaluations and revised models were set up to aid in-silico drug discovery and other downstream research. Newly deposited structures are analysed as they come out by a bespoke structure evaluation/comparison pipeline. In addition, many individual structures were revised manually, atom-by-atom. In order to spread knowledge about the structural biology of the virus, we also reviewed the literature, putting the molecular models into a larger context for the rapidly growing community of researchers - drug developers, bioinformaticians, crystallographers - tackling the COVID-19 pandemic. We established a large network of COVID-19 related research, and forged friendships and collaborations across national boundaries.

As public outreach is so important right now, we also refine structures live on Twitch, write articles and offer a 3D printable virus model for schools.

References

[1] Croll, T., Diederichs, K., Fischer, F., Fyfe, C., Gao, Y., Horrell, S., Joseph, A. P., Kandler, L., Kippes, O., Kirsten, F., Müller, K., Nolte, K., Payne, A., Reeves, M. G., Richardson, J., Santoni, G., Stäb, S., Tronrud, D., Williams, C. & Thorn, A. *BioRxiv*, doi:10.1101/2020.10.07.307546, 2020.

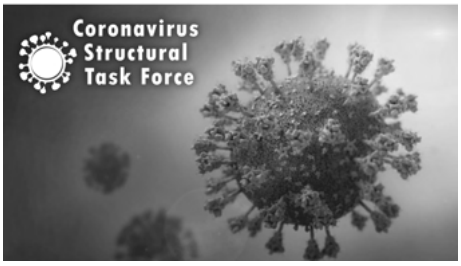

Figure 1

Disordered Materials, complex crystal structures and aperiodic crystals, diffuse scattering and 3D-PDF

Surface modifications of ion- irradiated diamonds

K. Bunk[1], W. Morgenroth[2], I. Alencar[3], F. Bertram[4], C. Schmidt[5], P. Gruszka[1], C. Trautmann[6], B. Winkler[1]

[1] Goethe University Frankfurt, Frankfurt, Germany

[2] University of Potsdam, Potsdam, Germany

[3] Federal University of Santa Catarina, Florianópolis, Brazil

[4] Deutsche Elektronen Synchrotron (DESY) (FS-PET-D Fachgruppe P08), Hamburg, Germany

[5] GFZ German Research Center for Geosciences, Potsdam, Germany

[6] GSI Helmholtz Centre for Heavy Ion Research and Technical University of Darmstadt, Darmstadt, Germany

Ion- irradiation is an established technology to change properties of diamonds in a controlled way [1] and has been studied as a function of ion species, energy and fluence for many years [2-4]. However, little is known regarding surface effects for irradiations with high energy ions which penetrate deep into the diamond. Irradiation experiments were carried out on various synthetic dia-

mond samples using 14 MeV Au6+ ions and a maximal fluence of 2.4 ×1015 ions/cm2. The penetration depth of such ions in diamond is about 1.7 μm [5]. The surface of the samples was characterized by atomic force microscopy (AFM), Raman spectroscopy and X-ray reflectometry (XRR).

Due to the irradiation, the formerly transparent samples darkened, which suggests partial amorphisation of the material. Raman spectroscopy revealed significant changes in the lattice dynamics and the formation of sp3 bonded amorphous carbon (Fig. 1). XRR experiments performed at beamline P08 @ PETRA III (Hamburg, Germany) revealed the formation of modified layers near the sample surface (Fig. 2). AFM provided information on changes of the surface topography including increased roughness and swelling. The surface roughness deduced from XRR data compared to AFM results will be discussed for the different diamond materials.

References

[1] R. Kalish, Semiconductors and Semimetals, 76, (2003), 145–181.

[2] R. Kalish and S. Prawer, Nuclear Instruments and Methods in Physics Research Section B: Beam Interactions with Materials and Atoms 106, (1995), 429.

[3] J. F. Prins, Materials Science Reports 7, (1992), 275.

[4] B. A. Fairchild, S. Rubanov, D. W. Lau, M. Robinson, I. Suarez-Martinez, N. Marks, A. D. Greentree, D. McCulloch, and S. Prawer, Advanced Materials 24, (2012), 2024.

[5] J. F. Ziegler, M. D. Ziegler, and J. P. Biersack, Nuclear Instruments and Methods in Physics Research Section B: Beam Interactions with Materials and Atoms 268, (2010), 1818-1823.

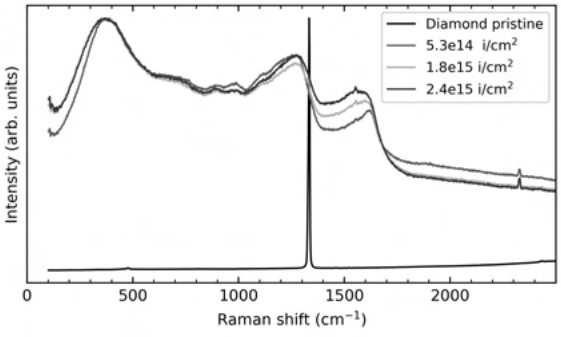

Figure 1 Raman spectra of pristine (black lines) and irradiated (colored lines) diamonds for a single crystal diamond sample irradiated with 14 MeV Au-ions of different fluences.

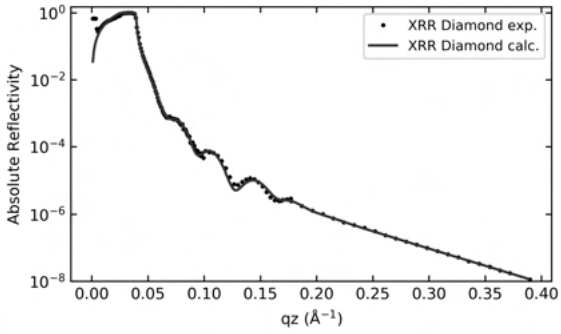

Figure 2 XRR curves for the experimental (black lines) and calculated (red lines) data of a single crystal diamond sample irradiated with 14 MeV Au-ions of fluence 2.4 × 10^{15} ions/cm^2.

Direct lock-in transition in 4-biphenylcarboxy substituted L-phenylalaninate crystals

S. Dey[1], S. Sasmal[2], D. Haldar[2]

[1] Institute of Crystallography, RWTH Aachen University, Aachen, Germany

[2] Department of Chemical Sciences, Indian Institute of Science Education and Research (IISER) Kolkata, Department of Chemical Sciences, Indian Institute of Science Education and Research (IISER) Kolkata Mohanpur, India

Protection of amino acids is an essential aspect for peptide synthesis.[1] Recently, crystals of 4-biphenylcarboxy substituted *L*-serine, *L*-tyrosine, *L*-alanine, *L*-leucine and *L*-phenylalanine methyl esters have been demonstrated to possess diverse supramolecular assembly governed by C–H···π and π···π interactions between biphenyl fragments and intermolecular N–H···O interactions between the amide O=C–N–H groups.[2,3] Amongst them, 4-biphenylcarxy-*L*-phenylalaninate is elusive because it crystallizes in monoclinic space group symmetry P21 within a pseudo-orthorhombic lattice[3] [a = 5.0748(2) Å, b = 8.7658(3) Å, c = 42.4828(13) Å, β = 90.038(3)°] at ambient conditions (phase **I**). The crystal comprises of two independent molecules (Z' = 2) with disparate molecular torsion and the monoclinic distortion is retained up to its melting temperature.

Temperature dependent single crystal X-ray diffraction experiments revealed a reversible structural phase transition at Tc ≈ 124 K upon cooling. Below Tc (phase **II**), satellite reflections in addition to main reflections were observed. **q** remains invariant as function of temperature that can be indexed with a modulation wave vector, $\mathbf{q} = (\frac{1}{2}, 0, \frac{1}{2})$ with respect to the basic monoclinic lattice. The crystal structure is described as a (3+1)D commensurately modulated structure in superspace group

P21(σ10σ3)0 ($\sigma_1 = 1/2$, $\sigma_3 = 1/2$). The equivalent 3D superstructure [space group monoclinic (b–unique) B21] comprises of four independent molecules in the asymmetric unit.

Here we present the phase relations between **I** and **II**. The phase transition at Tc is primarily characterized by evolution of torsional modulation within the biphenyl fragments that are unequal for the two independent molecules. The origin of the torsional modulation is argued to lie in the competition between possible steric hindrance between the ortho-hydrogens of the biphenyl fragment that favors torsion and intermolecular C–H$\cdots\pi$ interactions that favors planar biphenyl moiety. Stabilized by weak C–H$\cdots$O hydrogen bonds, short H–C$\cdots$C–H interactions involving the biphenyl fragment suppresses the torsion for one independent molecule while longer H–C$\cdots$C–H contacts allows larger torsional amplitude for the other.

References:

[1] Isidro-Llobet, A.; Alvarez, M. and Albericio, F. (2009) *Chem. Rev.* **109**, 2455–2504.
[2] Sasmal, S.; Podder, D.; Debnath, M.; Nandi, S. K. and Haldar, D. (2019) *ChemistrySelect* **4**, 10302–10306.
[3] Sasmal, S.; Nandi, S. K.; Kumar, S. and Haldar, D. (2019) *ChemistrySelect* **4**, 11172–11176.

Three-Dimensional Mapping of Diffuse Scattering of Perfect Si

O. Ivashko[1], A. Sarma[2], A.-C. Dippel[1], M. v. Zimmermann[3], O. Gutowski[2]
[1] DESY, FS-PETRA-D (FS-PET-D Fachgruppe P07211), Hamburg, Germany
[2] DESY, Hamburg, Germany
[3] HASYLAB at DESY, Hamburg, Germany

Single crystals often present disorder in their structure due to dopant substitution/intercalation or as an intrinsic instability of the compound. In many cases the disorder-to-order balance is responsible for key properties of the material. For example it can account for low thermal conductivity in PbTe or for the superconducting transition temperature in Sr2RuO4 where the highest Tc is obtained in disorder-free samples.

Here we present the three-dimensional mapping technique of diffuse scattering. At the Broad-Band Diffraction Swedish Material Science beamline (P21.1) at PETRA III synchrotron radiation source, total scattering measurements are possible thanks to the combination of high energy x-rays (100 keV) and large area detectors. Diffraction signal is acquired at high repetition rate allowing to operate with high incident photon flux. This is essential since the signal contains both the high intensity Bragg reflections, related to the average crystal structure, and the low intensity diffuse scattering signal accounting for the disorder. The acquired data are reconstructed in the hkl space and can be converted into the real space by Fourier transformation obtaining the three dimensional pair distribution function (3D-PDF) [1-3]. This technique is presented with the results obtained on perfect Si crystal as a standard. It is shown that 3D-PDF is sensitive to minor imperfections and/or impurities in the material.

References

[1] P. Schaub, T. Weber and W. Steurer, *Philosophical Magazine*, vol. 87, pp. 2781–2787, 2007
[2] T. Weber and A. Simonov, *Z. Kristallogr.*, vol. 227, pp. 238–247, 2012
[3] N. Roth et al., *IUCrJ*, vol. 5, pp. 410–416, 2018

Information Theory and Crystallography – a Fruitful Combination for Assessing Crystal Structure Complexity?

G. Kieslich[1]
[1] Technical University of Munich, Department of Chemistry, Munich, Germany

What is the complexity of a crystal structure? The definition of complexity is a challenging and similarly fascinating subject, touching different scientific disciplines such as economy, informatics, biology, math, and chemistry amongst others. Instead of defining complexity per sé, it is in practice easier to ask which system is more complex, showing that the challenge of defining complexity is closely related to the identification of an appropriate scale to measure complexity. In this contribution, the Shannon entropy is used as measuring system as defined by information theory, providing us with a framework to differentiate between the complexity of crystal structures as initially introduced by S. Krivovichev.[1]

In my presentation I discuss the opportunities and challenges that come with an information theory-based analysis of crystal structures as measure for complexity. I show that comparisons between Shannon entropy, crystal structure complexity and configurational entropy can be drawn,[2] opening intriguing opportunities for the systematic assessment of configurational entropy of crystal structures with implications in the areas of crystal growth and chemical bond theory.[3] Finally, and following on from recent developments in the field where theory development is in the centre, I introduce *crystIT* (crystallography & Information Theory),[4] a

python-based open-access program.[5] *crystIT* calculates various information measures based on a ∗.cif file as input, providing an easy-to-use platform for an information theory-based crystal structure analysis.

References

[1] S. Krivovichev, *Angew. Chem. Int. Ed.*, vol. 53, p. 654, 2014.
[2] S. Krivovichev, *Acta. Cryst. B*, vol. 72, p. 274, 2016.
[3] E. S. Harper, G. v. Anders, S. C. Glotzer, *Proc. Acad. Nat. Sci.*, vol. 116, p. 16703, 2019.
[4] C. Kaußler, G. Kieslich, *J. Appl. Cryst.*, accepted for publication, 2021.
[5] http://www.github.com/GKieslich/crystIT/

Tunable bonding in the incipient metal thermoelectric GeTe

S. Kimber[1], J. Zhang[2], Y. Cheng[3], D. Abernath[3], T. Ramirez-Cuesta[3], J. Hudspeth[4], Z.-Z. Luo[5], M. Kanatzidis[5], S. Billinge[6], T. Chatterji[7]
[1] University of Burgundy - Franche-Comté, Besancon, France
[2] Brookhaven National Laboratory, Upton (NY), USA
[3] Oak Ridge National Laboratory, Oak Ridge (TN), USA
[4] ESRF, Grenoble, France
[5] Northwestern University, Evanston (IL), USA
[6] Columbia University, New York (NY), USA
[7] Institut Laue-Langevin, Grenoble, France

The group IV-VI chalcogenides have important thermoelectric applications. GeTe has emerged as a promising non-toxic candidate, especially when the high-temperature cubic phase is suppressed to room temperature. However, even the mechanism of phase transition is disputed, as is the presence of disorder. Here we combine ab initio MD with synchrotron X-ray and dynamic neutron pair distribution function (PDF) analysis. We show that previous reports of disorder and symmetry breaking are entirely due to highly damped and anharmonic phonons. As predicted by metavalent bonding theories, this arises due to a softening in local bonding on heating, which strengthens long-range <100>c correlations. This picture is consistent with reported changes in resistivity and dielectric constant, and shown to be ubiquitously present in other polarisable binary chalcogenides and hR6 structured elements. Our results unify the results of local probes and spectroscopy as applied to binary chalcogenides, and should inspire a re-examination of other highly anharmonic energy materials such as hybrid perovskites and 'rattling' thermoelectrics.

The complexity of magnetic spin orders and dynamically disordered hydrogen bond networks in a hureaulite-type oxyhydroxide, Mn5[(PO4)2(PO3OH)2](HOH)4

S. Part[1]
[1] Ludwig-Maximilians-Universität München, the Department of Earth and Environmental Sciences, München, Germany

Pentamers of transition metal octahedra and double semi-helical chains of hydrogen bonds frame hureaulite-type oxyhydroxides (C2/c; a = 11.5 Å, b = 9.1 Å, c = 9.5 Å, beta = 96.4°) highly interesting for rich magnetic spin orders and polaron-dependent charge transport phenomena. Neutron powder diffraction data of its manganese end-member agree with that the magnetic lattice retains the (1a x 1b x1c) unit cell below the Curie temperature 7.2 K down up to 2 K, but magnetic moments of Mn2+ within MnO6 pentamers oriented predominantly parallel to the crystallographic b axis vividly change on to the (a-c) plane at lowered temperatures. The respective ferrimagnetic order corresponds to the magnetic space group C2/c at 6.5 K (Figure 1a) and C2'/c' at 3.4 K (Figure 1b). This reflects complicated discontinuity curves of AC magnetic susceptibility. Another phase transition occurs around at 2 K, where the magnetic spins are incommensurately modulated with a propagation vector (0.545(2), 0, 0). We present here subtle details of a complex evolution of magnetic spin orders of the title compound along with briefing quasi- and inelastic neutron scattering studies to demonstrate mechanism for the ease with protonic superconductivity.

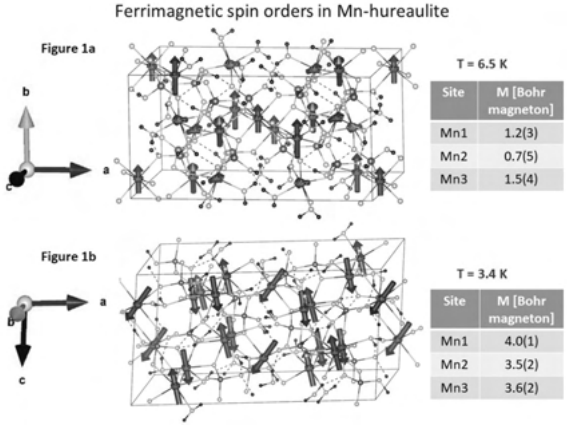

Figure 1

Single-crystal-to-single-crystal phase transitions of commensurately modulated sodium saccharinate 1.875-hydrate

T. Rekis[1], A. M. Schaller[1], S. R. Kotla[1], A. Schönleber[1], L. Noohinejad[2], M. Tolkiehn[2], C. Paulmann[2], S. van Smaalen[1]
[1] University of Bayreuth, Bayreuth, Germany
[2] DESY, Notkestr. 85, 22607 Hamburg, Germany

This contribution reports reversible, single-crystal-to-single-crystal phase transitions of commensurately modulated sodium saccharinate 1.875-hydrate [Na(sac)(15/8)H_2O]. The phases were studied in the temperature range 298 to 20 K. They exhibit complex disordered states. An unusual reentrant disorder has been discovered upon cooling through a phase transition at 120 K. The disordered region involves three sodium cations, four water molecules and one saccharinate anion. At room temperature, the structure is an eightfold superstructure that can be described by the superspace group $C2/c(0b0)s0$ with $\mathbf{q} = (0, 3/4, 0)$. It demonstrates maximum disorder with the disordered chemical entities having slightly different but close to 0.50:0.50 disorder component ratios. Upon cooling, the crystal tends to an ordered state, smoothly reaching a unified disorder component ratio of around 0.90:0.10 for each of the entities. Between 130 and 120 K a phase transition occurs involving a sudden increase of the disorder towards the disorder component ratio 0.65:0.35. Meanwhile, the space group and general organization of the structure are retained. Between 60 and 40 K there is another phase transition leading to a twinned triclinic phase. After heating the crystal back to room temperature its structure is the same as before cooling, indicating a complete reversibility of the phase transitions.

The application of mean field theory to single crystal diffuse scattering

E. Schmidt[1], A. L. Goodwin[1], J. Bulled[1]
[1] University of Oxford

Correlated disorder in crystalline materials gives rise to single crystal diffuse scattering. While the average structure determination via Bragg data analysis is considered a standard procedure, disorder analysis is thought of as a lengthy and complicated process. We present a mean field approximation to model single crystal diffuse scattering in molecular materials from a simple pair-interaction Hamiltonian.

Mean filed theory is a self-consistent field theory, which is widely used in statistical physics to model high-dimensional random systems. It has proven a valuable tool in the analysis of magnetic diffuse scattering data [1]. Here, the formalism is applied to describe orientationally disordered molecular crystals.

We present a computational study based on the mean field model suggested by Naya [2] and proof its applicability to strongly correlated disorder, where the local building block geometry dictates allowed and prohibited local configurations. The system that will be analysed in detail is a two-dimensional analogue the mercury diammonium halide $Hg(NH_3)_2Cl_2$ as depicted in the Figure [3].

We compare the results of the diffuse scattering analysis using the mean field model as introduced by Naya [2] to the results of RMC modelling and ΔPDF models based on a Warren-Cowley short range order parameter refinement (see Figure). Finally, the stability of the mean field analysis on limited data availability is demonstrated: Diffraction experiments under pressure or electric field yield a limited reciprocal space coverage. Here, we demonstrate the robustness of the proposed method against incomplete data sets.

References

[1] Paddison, J. A. textitet al., *Phys. Rev. Lett.*, vol. 11, no. 26, Jun. 2013, Art. no. 267207.
[2] Naya, S., *J. Phys. Soc. Jpn.*, vol. 37, no. 2, pp. 340–347, Aug. 1974.
[3] Lipscomb, W., *Anal. Chem.*, vol. 25, no. 5, pp. 737–739, May 1953.

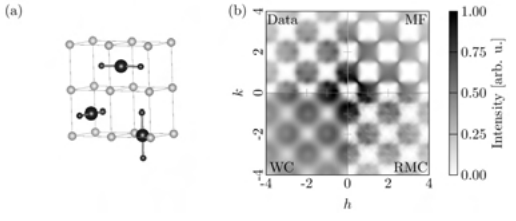

Figure 1 (a) Disordered structure of mercury diammonium halide $Hg(NH_3)_2Cl_2$ [3]. Hg in black, N in blue, Cl in light green. H atoms were omitted for clarity. The Hg is disordered over the face centres of the cubic unit cell. The ammonia groups occupy the centre of the shown cell, while the Cl is placed on the corner of the unit cell.
(b) X-ray diffuse scattering for the two-dimensional model system. Due to the fourfold symmetry of the average structure, one quadrant of the hk-layer is sufficient to represent the full data. Upper left corner: data as calculated from a model structure that fulfils the local rules; upper right corner: mean field refinement; bottom right corner: RMC refinement; bottom left corner: Warren-Cowley short range order analysis.

First order CDW phase transitions in R2Ir3Si5 (R = Ho, Er, Lu)

S. van Smaalen[1], S. Ramakrishnan[1], A. Schönleber[1], J. Bao[1], C. Eisele[1], S. R. Kotla[1], A. M. Schaller[1], T. Rekis[1], N. van Well[2], B. Bag[3], A. Thamizhavel[3], S. Ramakrishnan[3], D. Pal[4], N. S. Sangeetha[4], L. Noohinejad[5], M. Tolkiehn[5], C. Paulmann[5]

[1] University of Bayreuth, Laboratory of Crystallography, Bayreuth, Germany

[2] Ludwig Maximilians University of Munich, Department for Earth- and Environmental Sciences, Crystallography Section, Munich, Germany

[3] Tata Institute of Fundamental Research, Department of Condensed Matter Physics and Materials Science, Mumbai, India

[4] Indian Institute of Technology, Department of Physics, Indian Institute of Technology, Guwahati, India

[5] DESY, Notkestr. 85, 22607 Hamburg, Germany

$R_2Ir_3Si_5$ (R = Ho, Er, Lu) crystallize in the $U_2Co_3Si_5$ structure type at room temperature (orthorhombic space group Ibam) [1]. Upon cooling they undergo first-order charge-density-wave (CDW) phase transitions, as evidenced by anomalies with hysteresis in the temperature dependencies of the electrical resistivity (ρ), specific heat (C_p), magnetic susceptibility (χ), Seebeck coefficient (S) and thermal conductivity (κ) [1-4]. The CDW character of the low-temperature phases is corroborated by the appearance of satellite reflections at q = (0.2495, 0.4973, 0.2483) in diffraction experiments [4,5]. Single-crystal x-ray diffraction has revealed that the incommensurate CDW is accompanied by a strong monoclinic lattice distortion, while the symmetry of the CDW phase is reduced to triclinic. Here, we discuss the microscopic mechanism of CDW formation on the basis of a superspace analysis of single-crystal x-ray diffraction data [4].

Acknowledgement

Single-crystal X-ray diffraction data were collected at Beamline P24 of PETRA-III at DESY, Hamburg, Germany.

References

[1] Y. Singh, D. Pal, S. Ramakrishnan, A. M. Awasthi and S. K. Malik, *Phys. Rev. B*, vol. 71, 2005, Art. no. 045109.

[2] Y. K. Kuo, K. M. Sivakumar, T. H. Su and C. S. Lue, *Phys. Rev. B*, vol. 74, 2006, Art. no. 045115.

[3] N. S. Sangeetha, A. Thamizhavel, C. V. Tomy, S. Basu, A. M. Awasthi, P. Rajak, S. Bhattacharyya, S. Ramakrishnan and D. Pal, *Phys. Rev. B*, vol. 91, 2015, Art. no. 205131.

[4] S. Ramakrishnan, A. Schonleber, T. Rekis, N. van Well, L. Noohinejad, S. van Smaalen, M. Tolkiehn, C. Paulmann, B. Bag, A. Thamizhavel, D. Pal and S. Ramakrishnan, *Phys. Rev. B*, vol. 101, 2020, Art. no. 060101(R).

[5] M. H. Lee, C. H. Chen, M. -W. Chu, C. S. Lue and Y. K. Kuo, *Phys. Rev. B*, vol. 83, 2011, Art. no. 155121.

Electron diffraction and electron microscopy

Three-dimensional electron diffraction for structure and property analysis of metal-organic framework nanocrystals

Z. Huang[1]

[1] Stockholm University, Stockholm, Sweden

Metal-organic frameworks (MOFs) or porous coordination polymers (PCPs) are known for their versatile combination of inorganic building units and organic linkers, which offers immerse opportunities in a wide range of applications. Such applications are often designed by considering the inherent properties of MOFs, which in turn are governed by the crystal structures. Therefore, development of new structural characterization techniques parallels discovery of new materials.

Although single crystal X-ray diffraction (SCXRD) is the most practiced and routine method for structure determination, the acquisition of adequate data quality from weakly scattering nano- and submicro-sized crystals remains a challenge for this technique. While powder X-ray diffraction (PXRD) is more suitable technique for handling small crystals, structure determination of MOFs in particular can be challenging due to severe peak overlap as a consequence of large unit cell parameters, complexity of the structures themselves, as well as phase mixtures.

Three-dimensional electron diffraction (3DED) techniques have shown to be powerful for structural determination of 'intractable' crystals that are too small for SCXRD analysis. These techniques benefit from the strong Coulomb interaction between electrons and matter. Compared to X-ray, electrons generate much higher signal-to-noise ratios, even when the volume of the crystals are 6 or 7 orders of magnitude smaller. I will discuss applying 3DED in revealing the unique properties of MOFs for photo- and electrocatalysis. I will first present it on investigating heteroatom distribution in a photoactive MOF1. Further example will be given by applying 3DED on the study of the electrocatalyst PCN-226, where the spacing between active-sites are found crucial for its activity2. Last, I will demonstrate

3DED as a high throughput single crystal approach that can accelerate the discovery of new materials, especially in a phase mixture of nanocrystals, which makes the structure determination inaccessible to other characterization techniques. I believe 3DED as a significant development for the community of MOFs, where it allows to obtain accurate atomic information from nanocrystals, and can thus avoid the slow and arduous process of crystal growth.

References

[1] Yuan, S.; Qin, J.-S.; Xu, H.-Q.; Su, J.; Rossi, D.; Chen, Y.; Zhang, L.; Lollar, C.; Wang, Q.; Jiang, H.-L.; Son, D. H.; Xu, H.; Huang, Z.; Zou, X.; Zhou, H.-C. ACS Cent. Sci. 2018, 4 (1), 105–111.

[2] Cichocka, M. O.; Liang, Z.; Feng, D.; Back, S.; Siahrostami, S.; Wang, X.; Samperisi, L.; Sun, Y.; Xu, H.; Hedin, N.; Zheng, H.; Zou, X.; Zhou, H.-C.; Huang, Z. J. Am. Chem. Soc. 2020, 142, 15386-15395.

Exomorphism of jacobsite precipitates in bixbyite single crystals from the Thomas Range in Utah

J. Peter[1], M. Trapp[1], S. Lauterbach[1], P. Gollé-Leidreiter[1], U. Kolb[2], H.-J. Kleebe[1]

[1] Technical University of Darmstadt, Institute of Applied Geosciences, Working Group: Geomaterialscience, Schnittspahnstr. 9, 64287 Darmstadt, Germany

[2] Johannes Gutenberg University Mainz, Institute of Physical Chemistry, Centre for High Resolution Electron Microscopy (EMC-M), Duesbergweg 10-14, 55128 Mainz, Germany

Naturally occurring single crystals of bixbyite, (Fe,Mn)2O3, from the Thomas Mountain Range in Utah, USA were studied via (scanning) transmission electron microscopy (S)TEM. With up to 5 cm edge length, these mineral specimens are the largest bixbyite crystals found worldwide. Their hexahedral shapes are often modified by 211 facets at the corners and small 211 truncations along their cube edges. Characteristic lamellar defects running parallel to the 100 planes can be observed via TEM imaging, which are, according to EDS analyses, attributed to the tetragonal manganese silicate braunite, Mn7[SiO12]. In the present study, electron nano-diffraction and atomic resolution (S)TEM were employed to verify the presence of braunite lamellae and to investigate their orientation relationship with bixbyite. The analysis confirmed an epitaxial intergrowth of both phases, with their main axes being parallel and the unique c axis of braunite always aligned perpendicularly to the lamellar plane. Moreover, small rectangular shaped precipitates, which had been, due to their almost identical chemical composition, previously interpreted as small bixbyite inclusions within the host crystal, were often observed in contact with the braunite lamellae. Electron nano-diffraction and atomic resolution (S)TEM imaging revealed these crystallites not to be bixbyite but jacobsite, a cubic iron-manganese spinel with the stoichiometric formula MnFe2O4, whose occurrence in this unique context had not been reported before. Moreover, due to the higher temperatures needed for spinel crystallization, the occurrence of jacobsite may serve as a geo-thermometer. (S)TEM in conjunction with automated crystal orientation mapping (ACOM)-TEM showed that no orientation relationship exists between the jacobsite inclusions and the bixbyite/braunite matrix. Nevertheless, their characteristic rectangular shape is typically aligned concordantly with the (001) plane of the braunite lamellae. The resulting crystal shape of jacobsite is determined by the presence of the braunite lamellae, while the respective crystallites maintain their freedom of rotation. To the authors' knowledge, this is a novel observation of exomorphosis of jacobsite, i.e. the change in habitus of the spinel crystallites due to external conditions. Note that the term exomorphosis is used here in the mineralogical sense in contrast to the often used petrological aspect. Based on the TEM results, the formation of the jacobsite precipitates is discussed and a growth model suggested.

Electron diffraction and nanocrystallography: A device dedicated to the crystallography community

G. Santiso-Quinones[1], G. Steinfeld[1], E. Hovestreydt[1]

[1] Eldico Scientific AG, Villigen, Switzerland

After the Science nomination for "Breakthrough of the year 2018"[1,2], 3D-Electron Diffraction (3D-ED) using the continuous rotation method and X-ray crystallographic software, is gaining a lot of attention. In the past years many achievements using electron diffraction techniques have been made in the fields of organic and inorganic molecules, polymorphism, material sciences, geological sciences, natural products, energetic materials, bio-molecules and many others [2,3]. Such experiments are done in a (modified)-Electron Microscope. Though the realization of such experiments still requires plenty of expertise and efforts and it cannot be applied on daily bases by everyone. Pioneers in the field of Electron Diffraction [4], all agree that a dedicated device for the realization of such experiments would be of great advantage to the crystallographic community. Though such a device doesn't exists (up to now) at all. Therefore, it is a necessity that such a device could be made available for the realization

of this exciting field of nano-crystallography. Here will present a new device which is dedicated exclusively for such purposes. The device, an Electron Diffractometer, is built and optimized for electron diffraction experiments. Furthermore, it uses exclusively the crystallographic approach (continuous rotation method) and crystallographic software. Experimental examples carried out in this device will be showcased too.

References

[1] R. F. Service. "Molecular structures made simple." sciencemag.com.
https://vis.sciencemag.org/breakthrough2018/finalists/#rapid-structure
[2] a) T. Gruene *et al.*, *Angew. Chem. Int. Ed.*, vol. 57, pp. 16313–16317, 2018. b) C. G. Jones *et al.*, *ACS Cent. Sci.*, vol. 4, pp. 1587–1592, 2018.
[3] a) P. Brázda *et al.*, *Science*, vol. 364, pp. 667–669, 2019. **b)** R. Bücker *et al.*, *Nat. Commun.*, vol. 11, p. 996, 2020. c) E. T. Broadhurst *et al.*, *IUCrJ*, vol. 7, pp. 5–9, 2020.
[4] S. Parsons, T. Grüne, M. Gemmi, U. Kolb, among others, private communication.

Energy materials: batteries, photovoltaics, etc.

Solid-solution modelling using first-principles methods: Case studies for $(Cu,Ag)_2ZnSnSe_4$ and (FA,Cs)PbI_3

D. Fritsch[1], S. Schorr[1]
[1] Helmholtz-Zentrum Berlin, Berlin, Germany

Our quest to find new materials to be utilised in technological applications leads us more and more towards solid solutions between different materials. These solid solutions allow for the fine-tuning of desired material properties, but also pose additional problems in experimental characterisation and theoretical modelling. While we're able to deal with fractional occupancies of Wyckoff positions in experimental investigations, this is not the case for theoretical materials modelling based on density functional theory, and we have to resort to additional methods to properly model the structural, electronic, and optical properties of solid solutions.

Here, we're using first-principles calculations based on density functional theory to shed some light into the structure-property relations in the $(Cu,Ag)_2ZnSnSe_4$ and (FA,Cs)PbI_3 solid solutions (FA: formamidinium). While $(Cu,Ag)_2ZnSnSe_4$ only requires the mixing over different Wyckoff positions, in (FA,Cs)PbI_3 we additionally have to account for the rotations of the FA cation. For both systems, in order to simulate the different concentrations within the solid solution, we're employing a supercell approach. All our structure models are geometry optimised employing the recently developed SCAN exchange and correlation functional. In order to obtain more reliable electronic and optical properties, selected optimised structures are subjected to one-shot calculations employing the more accurate hybrid functional HSE06.

Acknowledgement
This work made use of computational resources provided by the North-German Supercomputing Alliance (HLRN).

Tuning the structural and electronic properties of strontium titanite thin films by Ni doping

Z. Jansa[1], P. Šutta[1], F. Alarab[1,2], L. Prušáková[1], B. Leikert[3], R. Claessen[3], C. Richter[2], K. Hricoviny[2], J. Minár[1]
[1] New Technologies Research Centre, University of West Bohemia, Pilsen, Czech Republic
[2] LPMS, CY Cergy Paris Université, Neuville-sur-Oise, France
[3] Physikalisches Institut und Röntgen Center for Complex Materials (RCCM), Universität Würzburg, Germany

We report the fabrication of SrTiO3 thin films doped by Ni and its influence on the electronic structure. The SrTiO3 thin films were deposited by magnetron sputtering which is suitable for mass-production of samples adapted for nanoelectronic applications. The structure of the STO:Ni was investigated by XRD phase analysis. We evaluated the influence of Ni on crystallinity, the size of coherent diffract areas, and micro-stress in the lattice of STO as a function of Ni concentration[1]. The second part of the presentation deals with the study of the electronic band structure of STO films doped with Ni, high-quality ordered pristine and SrTiO3:Nix films with x=0.06 and 0.12 were prepared by pulsed laser deposition. Electronic band structure calculations for the ground state, as well as one-step model photoemission calculations performed by using the Korringa-Kohn-Rostoker Greens's function method, predicted the formation of localized 3d-impurity bands in the bandgap of SrTiO3 close to the valence band maxima. The measured valence bands at the resonance Ni2p excitation and band dispersion are in agreement with theory [2].

References

[1] Z. Jansa, L. Prusakova, F. Alarab, P. Sutta; Structural analysis of Ni-doped SrTiO3: XRD study, AIP Conference Proceedings 2131(1):020022, July 2019

[2] F. Alarab, K. Hricovini, B. Leikert, L. Nicolai, M. Fanciulli, O. Heckmann, Ch. Richter, L. Prušáková, Z. Jansa, P. Šutta, J. Rault, P. Lefevre, M. Muntwiller, R. Claessen, and J. Minár; Photoemission study on pristine and Ni-doped SrTiO3 thin films, Materials Science, arXiv:2011.12684, November 2020

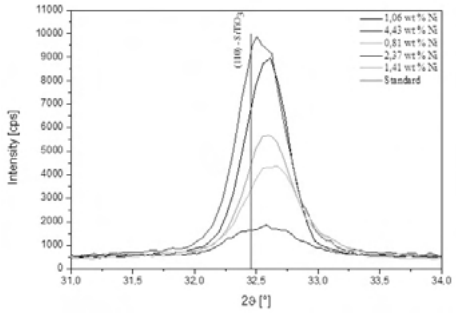

Figure 1

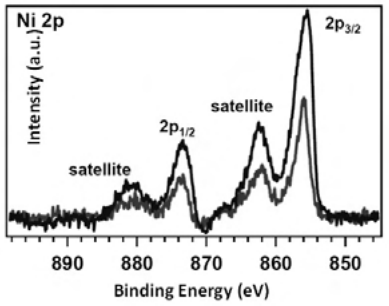

Figure 2

2D layered perovskite micro-crystalline films as efficient X-Ray dosimeters

F. Lédée[1], M. Verdi[1], L. Basiricò[1], C. Andrea[1], B. Fraboni[1]
[1] University of Bologna, Department of Physics and Astronomy (DIFA), Bologna, Italy

Hybrid halide perovskites are a new class of solution-processed semiconductors that combine low-temperature (<100 °C) synthesis, high charge carrier diffusion length and low defect density. The past few years, hybrid halide perovskites such as $CH_3NH_3PbI_3$ have shown promising results for the detection of high-energy ionizing radiation (X- and Gamma-rays).[1] Their large-scale commercialization is however hindered by their poor stability, owing to the volatility of the small organic cation $CH_3NH_3^+$.

2D layered hybrid halide perovskites ($R - NH_3)_2PbX_4$ (R = organic chain, X = Cl^-, Br^-, I^-) have recently shown an increasing interest in the fields of solar cells and LEDs. This sub-class of perovskite crystallizes in a natural, self-assembled quantum well structure and possess several interesting features, among which a much better stability than their 3D counterparts.[2,3] We will present in this work the first solid-state ionizing radiation detector based on a 2D layered hybrid perovskite. This material can be deposited from solution in the form of micro-crystalline thin films that display a single crystalline orientation. We will expose the direct integration of this material onto a pre-patterned flexible substrate and demonstrate the effective detection of X-Rays with sensitivity values as high as 757 uC.Gy-1.cm-2 and a Limit of Detection (LoD) of 8 nGy.s-1, which is among the lowest reported value for solid-state detectors. 2D perovskites offers the prospects of flexible solid-state detectors capable of working at low radiation flux for real-time X-Ray dosimetry.

References

[1] L. Basiricò, S. P. Senanayak, A. Ciavatti, M. Abdi-Jalebi, B. Fraboni and H. Sirringhaus, Adv. Funct. Mater., 2019, 9.
[2] D. B. Mitzi, Journal of the Chemical Society, Dalton Transactions, 2001, 0, 1–12.
[3] J. V. Passarelli, D. J. Fairfield, N. A. Sather, M. P. Hendricks, H. Sai, C. L. Stern and S. I. Stupp, J. Am. Chem. Soc., 2018, 140, 7313–7323.

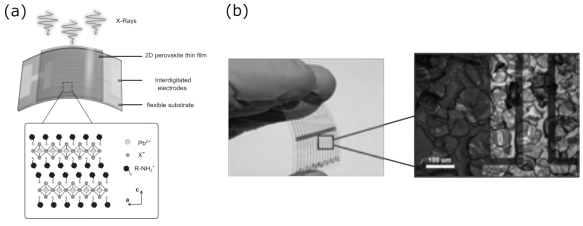

Figure 1 (a) Schematic of the device structure. Bottom: graphical representation of the $(R - NH_3)_2PbX_4$ crystal structure projected along the direction ⟨010⟩ showing the stacking of the 2D layers. (b) Photograph (left) and microscope image (right) showing the crystal grains morphology close to the pixel area.

Oxygen release from nanoporous perovskite oxides and its effect on thermal catalysis applications

S. Mascotto[1], E. Poffe[1], H. Kaper[2], B. Ehrhardt[1], L. Gigli[3], L. Nodari[4], S. Gross[5]
[1] University of Hamburg, Hamburg, Germany
[2] CNRS/Saint-Gobain CREE, Cavaillon, France
[3] Elettra-Sincrotrone, Trieste, Italy
[4] ICMATE-CNR, Padua, Italy
[5] University of Padua, Italy

The oxygen mobility and exchange are fundamental properties of perovskite oxides which regulate their application in catalysis, sensing, energy conversion and information technology [1]. The increasing need of sustainable catalytic materials has driven the development of nanoporous perovskite structures with improved surface reactivity [2,3]. Although it is intuitive that enhanced specific surface area (SSA) might improve the catalytic activity, it is not clear yet how this increase influences oxygen release and mobility in nanostructured grains and what is its effect on catalysis.

In the present paper, we investigate the role of porosity on the oxygen release of mesoporous perovskite oxides and demonstrate how the combination of these two parameters affects methane and carbon monoxide oxidation. We prepared mesoporous SrTi0.65Fe0.35O3-δ perovksites with SSA ranging from 45 to 80 m2/g via a template-free approach [2]. Combining thermal analyses with in situ synchrotron X-ray diffraction under Ar-atmosphere we showed that the material with least porosity does not release surficial oxygen species as the more porous counterparts. Instead much larger desorption of lattice oxygen is observed, as result of the larger lattice strain and higher Fe(IV) concentration.

This had significant effects on the catalytic performance of the materials. For low-temperature reactions as the CO oxidation the highly porous perovskite shows better performance due to the higher SSA and larger surface defect concentration. In case of high temperature reactions as methane combustion, the contribution of lattice oxygen is more relevant and the least porous material achieves the same performance as the high porous systems.

Hence, even though nanoporosity is usually considered beneficial for catalysis applications, mere maximization of the SSA is not necessarily of help and oxygen defect location (surface, bulk) and concentration need to be taken into account for the design of nanostructured catalysts.

References

[1] Y. Cao, M. J. Gadre, A. T. Ngo, S. B. Adler, Dane D. Morgan, *Nat. Commun.*, vol. 10, p. 1346, 2019.

[2] B. Kayaalp, S. Lee, K. Klauke, S. Jongsu, L. Nodari, A. Kornowski, W. Jung, S. Mascotto, *Appl. Catal. B Environ.*, vol. 245, pp. 536–545, 2019.

[3] B. Kayaalp, S. Lee, L. Nodari, J. Seo, S. Kim, W. Jung, S. Mascotto, *ACS Appl. Nano Mater.*, vol. 3, pp. 11352–11362, 2020, doi: 10.1021/acsanm.0c02456.

Study on the anharmonicity of the lead-halide bond and effective pair potentials of chlorine-substituted $CH_3NH_3PbI_3$

G. Schuck[1], D. M. Többens[1], D. Wallacher[1], N. Grimm[1], S. Schorr[1,2]

[1] Helmholtz-Zentrum Berlin für Materialien und Energie, Hahn-Meitner-Platz 1, 14109 Berlin, Germany

[2] Institut für Geologische Wissenschaften, Freie Universität Berlin, Malteserstr. 74, 12249 Berlin, Germany

Research interest has increasingly focused on hybrid perovskites $MABX_3$ like $[CH_3NH_3]^+$ (MA), B = Pb and X = I or Cl as a future photovoltaic material. There is a strong demand to better understand the possible impact of various entropy contributions (stochastic structural fluctuations, anharmonicity and lattice softness) on the optoelectronic properties of halide perovskite materials and devices [1]. There are essentially two sources of dynamic disorder in halide perovskites. One is the motion of the organic cations. FTIR [2] and quasi-elastic neutron scattering (QENS) [2] studies showed that chlorine substitution has a large influence on the rotational dynamics of the MA molecule in $MAPbI_{3-x}Cl_x$ perovskites [3] since the chlorine substitution leads to a weakening of the hydrogen bridge bonds (these bonds connect the MA molecules with the $[PbX_6]^-$ octahedra host structure) [3]. Another source of dynamic disorder is the anharmonic motion of the halide atom. The analysis of the Pb L3-edge EXAFS Debye-Waller factor of chlorine-substituted $MAPbI_3$ allows a direct determination of the influence of chlorine substitution on the anharmonicity of the lead-halide bond. This allows quantitative statements to be made about the effective pair potentials of the bond. The experimentally determined potential parameters can then be compared with computational results obtained, for example, from ab initio molecular dynamics simulations.

References

[1] Katan, C. et al, *Nature Materials*, vol. 17, pp. 377, 2018.

[2] G. Schuck, et. al., *J. Phys. Chem. C*, vol. 122, pp. 5227, 2018.

[3] G. Schuck, et. al., *J. Phys. Chem. C*, vol. 123, pp. 11436, 2019.

A solid-state chemistry approach for bulk $ZnSnN_2$ at ambient pressure

Z. Wang[1,2], J. Breternitz[1], S. Schorr[1,2]

[1] Helmholtz-Zentrum Berlin für Materialien und Energie, Hahn-Meitner-Platz 1, 14109 Berlin, Germany

[2] Free University of Berlin, Department Geosciences, Malteserstraße 74-100, 12249 Berlin, Germany

$ZnSnN_2$ is an earth-abundant semiconductor with a predicted direct bandgap between 1.12-2.09 eV, based on DFT calculations.[1] Thus, it has been considered as a potential absorber material for solar cells. Recently, a numerical device simulation based on reported experimental material properties found a theoretical maximum efficiency of $\eta \approx 22\%$ of for a $ZnSnN_2$ based solar cell.[2]

Still, the fundamental study of structural properties of $ZnSnN_2$ is essential to facilitate the development of high-efficiency solar cells. Well crystallised bulk $ZnSnN_2$ is key to an in-depth study on its material properties, while thin-film $ZnSnN_2$ may hinder advanced studies due to preferred orientation and low crystallinity. However, the narrow stability region of $ZnSnN_2$ due to the small decomposition energy,[3] and the low decomposition temperature of $ZnSnN_2$ [4] hamper the preparation of bulk $ZnSnN_2$.

In this work, we report a convenient pathway to obtain well-crystallised bulk zinc tin oxide nitrides as approximant towards $ZnSnN_2$ at ambient pressure and open the door to investigate structure-property relationships based on bulk samples. We achieved zinc tin oxide nitrides ($Zn_{1+x}Sn_{1-x}N_{2-2x}O_{2x}$) in the form of well-crystallised powder through a solid-state reaction route. This method further allows advanced characterisations that require bulk material and/or well-crystallised samples. We performed XRD experiments and interconnected it with a chemical analysis (XRF) to investigate the chemical composition and structural properties of the synthesised material. Using Raman spectroscopy, we compared the synthesised compound with reported $ZnSnN_2$ thin films.[5] The optical bandgap value of our powder material is in the range of the values reported by thin-film $ZnSnN_2$.[6] By correlating the synthesis conditions with the structural properties of the synthesised $Zn_{1+x}Sn_{1-x}N_{2-2x}O_{2x}$, we are now able to optimise the synthesis route. This will allow us to reduce the oxygen content in the material in a controlled way to obtain bulk $ZnSnN_2$ and tailor the materials properties.

References

[1] N. Feldberg, J. Aldous, W. Linhart, L. Phillips, K. Durose, P. Stampe, R. Kennedy, D. Scanlon, G. Vardar and R. Field III, *Appl. Phys. Lett.*, vol. 103, 2013, Art. no. 042109.

[2] A. Laidouci, A. Aissat and J. Vilcot, *Sol Energy*, vol. 211, pp. 237–243, 2020.

[3] S. Chen, P. Narang, H. A. Atwater and L. W. Wang, *Adv. Mater.*, vol. 26, pp. 311–315, 2014.

[4] F. Kawamura, N. Yamada, M. Imai and T. Taniguchi, *Cryst. Res. Technol.*, vol. 51, pp. 220–224, 2016.

[5] P. C. Quayle, G. T. Junno, K. He, E. W. Blanton, J. Shan and K. Kash, *Phys. Status Solidi B*, vol. 254, 2017, Art. no. 1600718.

[6] T. D. Veal, N. Feldberg, N. F. Quackenbush, W. M. Linhart, D. O. Scanlon, L. F. Piper and S. M. Durbin, *Adv. Energy Mater.*, vol. 5, 2015, Art. no. 1501462.

Extreme/non-ambient conditions

Amorphous–amorphous transition in SnI_4 reexamined

K. Fuchizaki[1]

[1] Ehime University, Matsuyama 790-8577, Japan

The pressure-induced solid-state amorphization found in 1985 [1] set off a series of subsequent researches on polyamorphism in SnI_4. The discovery of another amorphous state [2], called Am-II to Am-I previously identified, on decompression became a breakthrough in solving the puzzle.

Later, a consistent thermodynamic argument has been given for the observed polyamorphic behaviors [3]. However, the following questions remain unanswered: The ambient crystalline phase CP-I never transforms into Am-II, which appears only on Am-I decompression. Nonetheless, CP-I can directly transform to Am-I on *recompression* skipping CP-II [4], the high-pressure modification of CP-I.

We reexamined the Am-I-to-Am-II process conducting high-pressure synchrotron x-ray diffraction studies with a diamond anvil cell [5]. Detailed analysis of the structural evolution revealed that the association of molecules, which are entirely dissociated, starts at around 14 GPa on decompression. About 30% of isolated Sn atoms suddenly complete the molecular formation at the Am-I-to-Am-II transition at 3.3 GPa, associated with an abrupt drop of

density. Thus, the molecules formed recover their original symmetry of T_d at the transition, implying the strong coupling between the global order parameter of density and the local symmetry.

Because the centers (Sn atoms) were distributed everywhere in Am-I, formed molecules' resulting location is not necessarily energetically optimized, leaving uniform distribution of shorter (2.64 Å) van der Waals I_2 bonds, which play as *defects*. The open questions are then understandable in terms of the defects. Crystallization of Am-II to CP-I could be a defect extinction process, but the reverse process would hardly occur. It seems impossible to remove the whole defects in recovering CP-I, and the residual defects prevent defective CP-I from reordering to CP-II, which may require highly ordered stacking of Sn layers [6].

References

[1] Y. Fujii *et al.*, *J. Phys. C*, vol. 18, p. 789, 1985.
[2] N. Hamaya *et al.*, *Phys. Rev. Lett.*, vol. 79, p. 4597, 1997.
[3] K. Fuchizaki *et al.*, *J. Chem. Phys.*, vol. 135, 2011, Art. no. 091101.
[4] B. Grocholski *et al.*, *Phys. Rev. B*, vol. 81, 2010, Art. no. 094101.
[5] K. Fuchizaki *et al.*, *J. Phys.: Condens. Matter*, submitted for publication.
[6] H. Naruta *et al.*, *J. Phys.: Condens. Matter*, vol. 32, 2019, Art. no. 055401.

Probing ultrafast laser plasma processes inside solids with resonant small-angle X-ray scattering

L. Gaus[1]
[1] HZDR, Drezden, Germany

The development of second-generation short-pulse laser-driven radiation sources requires a mature understanding of the relativistic laser-plasma processes such as heating and transport of relativistic electrons as well as the development of plasma instabilities. Accessing these dynamic effects occurring on femtosecond and nanometer scales experimentally is very difficult but it is crucial to understand the behavior of matter under the extreme conditions, which follow the interaction of solids with ultra-intense laser irradiation.

In a first experiment in 2014 at the Matter of Extreme Conditions facility at LCLS we demonstrated that Small Angle X-ray Scattering (SAXS) of femtosecond x-ray free electron laser pulses is able to make these fundamental processes accessible on the relevant time and length scales in direct in-situ pump-probe experiments [Kluge et al., Phys. Rev. X 8, 031068 (2018)]. Here we report on a follow-up experiment with significantly higher pump intensity reaching the relativistic intensity domain, improved targetry, XFEL shaping, and particle diagnostics. We give an overview of the new capabilities in combining a full suite of particle and radiation diagnostics and SAXS. In particular, probing at resonant x-ray energies has shown to give new insight into the ionization process, plasma opacity and density by studying asymmetries in SAXS patterns from nanostructured grating targets [Gaus et al., arXiv: 2012.07922 (under review)].

High Pressure Single-Crystal X-Ray Diffraction Investigation of Nitrosonium Nitrate: Solving a 55 Years Old Enigma

D. Laniel[1], B. Winkler[2], E. Koemets[1], T. Fedotenko[1], S. Chariton[3], V. Milman[4], K. Glazyrin[5], V. Prakapenka[3], L. Dubrovinsky[1], N. Dubrovinskaia[1]
[1] University of Bayreuth, Bayreuth, Germany
[2] Goethe-University Frankfurt, Frankfurt, Germany
[3] University of Chicago, Chicago, USA
[4] Dassault Systèmes BIOVIA
[5] DESY, Photon Science, FS-PE (Experiment Support PETRA III), Hamburg, Germany

The study of the behavior of matter at extreme pressure conditions is essential to deepen our understanding of the pressure dependence of interatomic interactions and to benchmark theoretical models. Simple molecular systems at high densities are well known to exhibit a transformation towards polymeric (*e.g.* N_2,[1,2] CO,[3] CO_2,[4,5] C_2H_2[6]) or metallic (*e.g.* O_2,[7] H_2[8,9]) states as a mechanism to redistribute their electron density. In contrast, nitrogen-oxygen systems (N_2O, N_2O_4, N_2-O_2 mixtures) are hypothesized to instead exploit a third avenue, ionization, and are presumed to form nitrosonium nitrate ($NO^+NO_3^-$).[10,11] Despite its first solid state synthesis in 1965[12] and an impressive number of subsequent in-situ high pressure powder X-ray diffraction studies as well as theoretical calculations,[10,11,13−−19] the crystal structure of nitrosonium nitrate remains controversial.

Here, we present experimental investigations on nitrosonium nitrate between 3 and 55 GPa employing synchrotron single-crystal X-ray diffraction applied to polycrystalline samples (sc-XRDp)—a novel technique developed by our group. Through these measurements, a full structural solution of $NO^+NO_3^-$ was obtained. Its structure is shown in Fig. 1. Chemical peculiarities of this compound were unveiled, namely the striking presence of a positively charged oxygen atom in the NO^+ ion deduced from crystal-chemical principles. Accompanying

theoretical calculations validated the positively charged nature of the oxygen atom in the NO^+ ion and established the experimentally determined structure as the most thermodynamically stable among those previously proposed.

This study unambiguously authenticates the unorthodox preference of nitrogen and oxygen to form an ionic compound to redistribute its pressure-induced increase in electron density. Moreover, it highlights the importance of a high accuracy characterization techniques, such as sc-XRDp, as an essential method that is key to expose the crystal chemical and physico-chemical singularities indigenous to high pressure research.

References

[1] M. I. Eremets, A. G. Gavriliuk, I. A. Trojan, D. A. Dzivenko, R. Boehler, *Nat. Mater.*, vol. 3, pp. 558–563, 2004.

[2] D. Laniel, B. Winkler, T. Fedotenko, A. Pakhomova, S. Chariton, V. Milman, V. Prakapenka, L. Dubrovinsky, N. Dubrovinskaia, *Phys. Rev. Lett.*, vol. 124, 2020, Art. no. 216001.

[3] W. J. Evans, M. J. Lipp, C. S. Yoo, H. Cynn, J. L. Herberg, R. S. Maxwell, M. F. Nicol, *Chem. Mater.*, vol. 18, pp. 2520–2531, 2006.

[4] K. F. Dziubek, M. Ende, D. Scelta, R. Bini, M. Mezouar, G. Garbarino, R. Miletich, *Nat. Commun.*, vol. 9, pp. 5–10, 2018.

[5] F. Datchi, V. M. Giordano, P. Munsch, A. M. Saitta, *Phys. Rev. Lett.*, vol. 103, 2009, Art. No. 185701.

[6] C. C. Trout, J. V. Badding, *J. Phys. Chem. A*, vol. 104, pp. 8142–8145, 2000.

[7] G. Weck, P. Loubeyre, R. LeToullec, *Phys. Rev. Lett.*, vol. 88, 2002, Art. no. 035504.

[8] P. Loubeyre, F. Occelli, P. Dumas, *Nature*, vol. 577, pp. 631–635, 2020.

[9] E. Wigner, H. B. Huntington, *J. Chem. Phys.*, vol. 3, pp. 764–770, 1935.

[10] M. Somayazulu, A. Madduri, A. F. Goncharov, O. Tschauner, P. F. McMillan, H. Mao, R. J. Hemley, *Phys. Rev. Lett.*, vol. 87, 2001, Art. no. 135504.

[11] S. F. Agnew, B. I. Swanson, L. H. Jones, R. L. Mills, D. Schiferl, *J. Phys. Chem.*, vol. 87, pp. 5065–5068, 1983.

[12] L. Parts, J. T. Miller, *J. Chem. Phys.*, vol. 43, pp. 136–139, 1965.

[13] S. F. Agnew, B. I. Swanson, L. H. Jones, R. L. Mills, *J. Phys. Chem.*, vol. 89, pp. 1678–1682, 1985.

[14] Y. Meng, R. B. Von Dreele, B. H. Toby, P. Chow, M. Y. Hu, G. Shen, H. K. Mao, *Phys. Rev. B - Condens. Matter Mater. Phys.*, vol. 74, 2006, Art. no. 214107.

[15] C. S. Yoo, V. Iota, H. Cynn, M. Nicol, J. H. Park, T. Le Bihan, M. Mezouar, *J. Phys. Chem. B*, vol. 107, pp. 5922–5925, 2003.

[16] A. Y. Kuznetsov, L. Dubrovinsky, A. Kurnosov, M. M. Lucchese, W. Crichton, C. A. Achete, *Adv. Phys. Chem.*, vol. 2009, pp. 1–11, 2008.

[17] Y. Song, M. Somayazulu, H. Mao, R. J. Hemley, D. R. Herschbach, *J. Chem. Phys.*, vol. 118, pp. 8350–8356, 2003.

[18] Y. Song, R. J. Hemley, Z. Liu, M. Somayazulu, H. Mao, D. R. Herschbach, *J. Chem. Phys.*, vol. 119, pp. 2232–2240, 2003.

[19] D. Sihachakr, P. Loubeyre, *Phys. Rev. B*, vol. 74, 2006, Art. no. 064113.

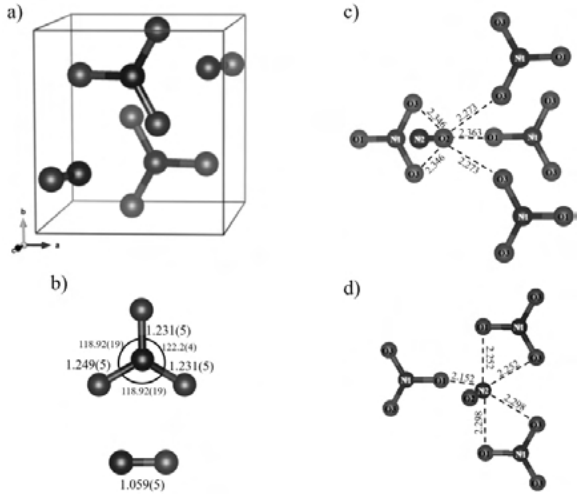

Figure 1 a) Monoclinic unit cell of $NO^+NO_3^-$ at 37 GPa. b) Representation of the trigonal planar nitrate (top) and linear nitrosonium (bottom) ions. c-d) Environment of the O2 and N2 atoms forming the NO^+ cation: both N2 and O2 atoms are five-fold coordinated by negatively-charged oxygen atoms from the $NO^+NO_3^-$ anions. When shown, bond lengths and bond angles are given in Angstroms (Å) and degrees (°), respectively.

Dedicated X-ray diffraction setup for diamond anvil cell studies at European X-ray free electron laser

C. Prescher[1], H.-P. Liermann[2], Z. Konopkova[3], K. Appel[3], R. Husband[4], J. Mainberger[5], H. Damker[6], P. Talkovski[6], M. Röper[4], A. Berghäuser[7], C. Strohm[5], C. Baehtz[7], U. Zastrau[3], . EuXFEL Community Proposal #2292

[1] Universität Freiburg, Freiberg, Germany

[2] DESY, FS-PE (Experimentebetreuung PETRA III), Hamburg, Germany

[3] European XFEL, HED, Schenefeld, Germany

[4] DESY-HiBEF, Hamburg, Germany

[5] DESY, Hamburg, Germany

[6] DESY-ZM1, Hamburg, Germany

[7] Helmholtz-Zentrum Dresden-Rossendorf, Germany

Scientific advances are often enabled by either new emerging techniques or a previously unconsidered combination of existing methods. Particularly synchrotron X-ray diffraction (XRD) has led to large advances in our understanding of materials under high pressure and temperature conditions. Especially its combination with diamond anvil cells (DAC) has been very fruitful and, therefore, almost every 3rd generation synchrotron source in the world has now one or several beamlines dedicated to high pressure DAC research.

On the other hand, in the regime of X-ray free-electron lasers (XFEL), which provide previously unprecedented brightness in a single X-ray pulse, high-pressure and temperature XRD experiments as of today are mainly conducted with a combination of laser driven shock. The absence of DAC research at these facilities is mainly due to a combination of two factors: either the XFEL sources provide only a relatively low photon energy (<11 keV) leading to strong absorption of the X-rays in the diamond anvils as well as a small angular XRD coverage; or if the pulse energy is high enough (e.g. SACLA up to 25 keV on the fundamental) repetition rate on the order of only 10 to 120 Hz is not fast enough to provide significant advantage over 3rd generation synchrotron sources for time-resolved studies, such as the dynamic piezo-driven DAC.

The European XFEL (EuXFEL) in Schenefeld, Germany, is now capable of providing X-ray photons with energies up to 25 keV and a repetition rate of 4.5 Mhz and thus, facilitates the opportunity of combining DAC-XRD experiments with the unique properties of XFEL radiation sources.

Here we want to present the new DAC setup dedicated to XRD studies at the high energy density (HED) instrument of the EuXFEL. This setup has been provided through the Helmholtz International Beamline for Extreme Fields (HiBEF) user consortium and is situated in the interaction chamber 2 of the HED instrument. Currently, two sample platforms are available in the vacuum chamber: the first is a combination of standard or membrane DACs, for use with time resolved optical spectroscopy as well as pulsed laser heating, and the second provides capabilities and space for dynamic DACs with ultrafast piezo driven compression drivers.

The primary goal of both setups is to utilize the high brightness of the EuXFEL source, which permits good quality XRD images, comparable to several seconds of exposure in a 3rd generation synchrotron, even from a single X-ray pulse. The EuXFEL provides bursts of X-ray pulses within a so-called pulse-train with a frequency of 4.5 MHz, equating to 220 ns between each pulse. In combination with an AGIPD detector currently commissioned at the instrument, images will be collected with 4.5 MHz, facilitating the study of physical phenomena by XRD with a unique time resolution.

In the standard DAC setup, the thermal response due to single laser heating pulses or heating by intense X-ray pulses can be investigated by a combination of spectroradiometric measurements (utilizing a streak camera) and XRD on a submicrosecond timescale without the need of collecting multiple iterations in a pump-probe experiment, as performed previously at 3rd generation synchrotron facilities. The dynamic DAC setup enables the study of materials under fast compression and closes the strain rate gap between these type of experiments at synchrotron facilities and shock compression experiments further.

First experiments utilizing the standard DAC setup have been conducted during a community assisted commissioning beamtime in October 2019 (Proposal number 2292, PI R.S. McWilliams). Many exciting new results have been obtained, but also challenges arising from the nature of an XFEL source have been identified.

We will present the setup, its capabilities and some of the first interesting results in this contribution.

Acknowledgment

The authors are indebted to the HiBEF UC for the provision of instrumentation and Staff that enabled this experiment. We acknowledge European XFEL in Schenefeld, Germany, for provision of X-ray free-electron laser beamtime at Scientific Instrument HED (High Energy Density Science) and would like to thank the staff for their assistance.

The low-dimensional magnetic van der Waals compound FeOCl at extreme conditions: pressure and temperature induced phase transitions and structural evolution

A. M. Schaller[1], M. Bykov[2], E. Bykova[2], K. Glazyrin[3], S. van Smaalen[1]

[1] University of Bayreuth, Laboratory of Crystallography, Bayreuth, Germany

[2] Carnegie Institution for Science, Earth & Planets Laboratory, Washington DC, USA

[3] DESY, Photon Science, FS-PE (Experiment Support PETRA III), Hamburg, Germany

FeOCl features a simple structure built from Fe-O double layers stacked along the c-axis and separated through bi-layers of chlorine; the latter are bonded through weak van der Waals forces. On cooling, an orthorhombic-to-monoclinic lattice distortion occurs at $T_N = 81$ K [1] which removes the geometric frustration of magnetic order of Fe^{3+} moments, as it exists on the orthorhombic lattice [1,2]. This allows antiferromagnetic order to develop [1,2]. The quasi-two-dimensional magnetic character of FeOCl stems from the unpaired 3d electrons (Fe^{3+} with $3d^5$ electronic state), which results in strong intra- and interchain exchange interactions in the ab-plane of the structure [2,3]. (Quasi-)hydrostatic pressure, applied within a diamond anvil cell (DAC) up to ≈ 38 GPa, provides a way of modifying the interlayer van der Waals gap and more importantly, through geometrical modifications of the $FeCl_2O_4$ octahedra, a way to modify and tune the magnetic exchange interactions. These experiments have been carried out above and below the Néel temperature, which allows us to investigate the interplay of magnetic order and pressure-induced structural changes in FeOCl. Here we present one of the essential steps in this project: a detailed analysis of the pressure and temperature dependent structural evolution of FeOCl, as investigated by high-pressure low-temperature single crystal X-ray diffraction at beamline P02.2/PETRA III (Hamburg, Germany). This includes the phase transitions and an in-depth analysis of bond lengths and -angles, which sheds light on the magneto-elastic interplay in this compound. This may further contribute to the understanding of the mechanisms in exotic strongly correlated systems in general and low dimensional magnetic compounds in particular.

References

[1] Zhang *et al.*, *Phys. Rev. B*, vol. 86, no. 13, Oct. 2012, Art. no. 134428.

[2] Angelkort *et al.*, *Phys. Rev. B*, vol. 80, no. 14, Oct. 2009, Art. no. 144416.

[3] Glawion *et al.*., *Phys. Rev. B*, vol. 80, no. 15, Oct. 2009, Art. no. 155119.

Experimental Charge Densities of Minerals under Pressure

K. Wozniak[1]

[1] University of Warsaw, Warsaw, Poland

This is quite a paradox that a century after introduction of the spherical Independent Atom Model (IAM, 1914 [1]), 99.7% of all ca. 1.5mln known crystal structures, including almost all structures of minerals, have been refined using IAM which suffers from severe methodological deficiencies. Far better results can be obtained when new approaches of quantum crystallography ustilising aspherical atomic factors are applied.

A short beam wavelength (0.4Å) and a special type of Diamond Anvil Cell (DAC) with large opening angle allow us to collect data with extremaly high resolution and 100% completeness up to as high resolution as ca. 0.4 Å.

We will present details of aspherical Hansen-Coppens pseudoatom refinement of electron density which we applied in multipole modeling [2] of electron density in crystals of minerals including minerals under pressure. We have successfully refined quantitative experimental electron densities for crystals of several minerals such as fluorite, grossular and hsianghualite and others. We will present the most interesting results such as onset of F...F interactions (charge-shift bonding) in fluorite [3] and flow of charge among ions in the structure of hsianghualite, Ca3Li2(Be3Si3O12)F2, under pressure. Up to our best knowledge, these are the very first successful experimental determinations of quantitative charge density distributions in mineral crystals under high pressure. They allow for quantitative characterisation of electron density in crystals of minerals including studies of changes of electron density under pressure.

Such studies open a new field of mineralogical subatomic investigations (at the level of changes of electron density properties) of different mineralogical processes in the Earth mantle by simulating them in DAC in laboratory conditions.

Acknowledgement

KW acknowledges a financial support within the Polish National Science Centre (NCN) OPUS17 grant number DEC-2019/33/ B/ST10/02671.

References

[1] Compton, A.H., *Nature.*, vol. 95, pp. 343–344, 1915.

[2] Hansen, N. K., & Coppens, P., *Acta Cryst. A*, vol. 34, pp. 909–921, 1978.

[3] Stachowicz, M., Malinska, M., Parafiniuk, J., &Woźniak, K., *Acta Cryst. B*, vol. 73, pp. 643–653, 2017.

[4] Gajda, R., Stachowicz, M., Makal, A., Sutuła, S., Parafiniuk, J., Fertey, P., & Wozniak, K., *IUCRJ*, vol. 7, no. 3, pp. 383–392, 2020.

Framework structures: MOFs, COFs, etc.

High-Throughput Electron Diffraction Reveals a Hidden Novel Metal-Organic Framework

M. Ge[1], X. Zou[1], Z. Huang[1]

[1] Stockholm University, Stockholm, Sweden

Metal-organic frameworks (MOFs) are known for their versatile combination of inorganic building units and organic linkers, which offers immense opportunities in a wide range of applications. However, many MOFs are typically synthesized as multiphasic polycrystalline powders, which are challenging for studies by X-ray diffraction. Therefore, developing new structural characterization techniques is highly desired in order to accelerate discoveries of new materials. Here, we report a high-throughput approach for structural analysis of MOF nano- and sub-microcrystals by three-dimensional electron diffraction (3DED). A new zeolitic-imidazolate framework (ZIF), denoted ZIF-EC1, was first discovered in a trace amount during the study of a known ZIF-CO3-1 material by 3DED. The structures of both ZIFs were solved and refined using 3DED data. ZIF-EC1 has a dense 3D framework structure, which is built by linking mono- and bi-nuclear Zn clusters and 2-methylimidazolates (mIm-). The discovery of this new MOF highlights the power of 3DED in developing new materials and their applications.

Water cluster structure in the MOF CAU-10-H: A powder diffraction perspective

G. Nenert[1], S. Canossa[2], D. Rega[3], M. van der Veen[3]

[1] Malvern Panalytical, Malvern, United Kingdom

[2] University of Antwerpen, Department of Physics, Groenenborgerlaan 171, 2020 Antwerpen, Belgium

[3] TU Delft, Catalysis Engineering, Department of Chemical Engineering, Delft, the Netherlands

Several metal-organic frameworks (MOF) excel in harvesting water from the air or as heat pumps as they show a steep step in the water isotherm at 10-30 RH%c [1]. Yet, a precise understanding of the water structure within the confined space of such MOF is still lacking. Here, we unravel the structural properties of CAU-10-H under various water content. We show that the water content can be tuned using the relative humidity, temperature and history of the sample. Previous studies have shown a structural phase transition from hydrated (non-centrosymmetric structure) to dry (centrosymmetric structure) [2]. Here in this contribution, we show that high resolution powder diffraction can allow to locate water molecules and the existence of various states of hydrated phases including centrosymmetric one.

This study besides bringing further insight into the water clusters present in this MOF enlights also the powerfulness of powder diffraction in the study of MOF materials.

References

[1] Wentao Xu, Omar M. Yaghi, *ACS Cent. Sci.*, vol. 6, no. 8, pp. 1348–1354, 2020.

[2] Dominik Fröhlich *et al.*, *J. Mater. Chem. A*, vol. 4, pp. 11859–11869, 2016.

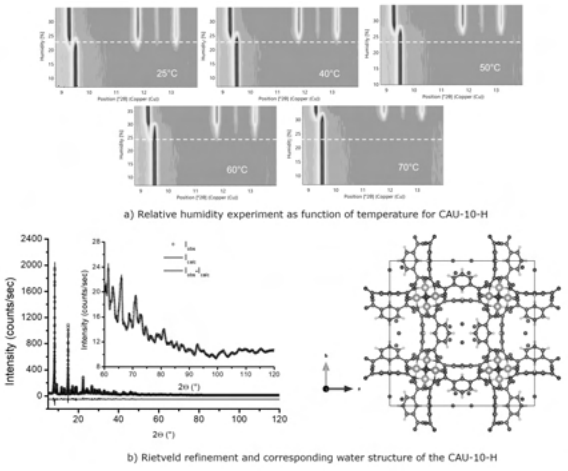

Figure 1

Discontinuous three-component self-assembly: A leap from simple polymers to 3D networks of spherical host-guest assemblies

E. Peresypkina[1], K. Grill[1], B. Hiltl[1], A. Virovets[1], M. Scheer[1]
[1] University of Regensburg, Regensburg, Germany

In the artificial self-assembling systems based on metal atoms and spacing ligands small variations of reagents, stoichiometry, solvents or concentration may cause drastic changes in the structure of the resulting supramolecular architectures [1,2]. Methodologically based rational supramolecular design requires the systematic study of the effects of variation of one of the parameters when other controllable synthetic conditions are kept as close as possible.

Having experience in using pentaphosphaferrocenes [CpRFe(η5-P5)] (CpR = η5-C5R5, R = Me, CH2Ph) as building blocks to construct coordination polymers and giant supramolecules via coordination of the cyclo-P5 ligand to coinage metal cations [3,4], we systematically investigated how the direction of one-pot self-assembly reaction of [Cp*Fe(η5-P5)] (A) with AgSbF6 and flexible aliphatic dinitriles NC(CH2)xCN (DNx) [5] depends on the length of the aliphatic chains in a range x = 1 – 10. We found that this reaction can lead to two distinct types of the products, namely, 1D–3D simple coordination polymers (CPs), or 3D supramolecular coordination polymers (SCPs), where huge polycationic nano-sized supramolecules are linked by the DNx spacers into 3D networks (Fig.). The value of x = 7 marks the borderline: for x < 7 the self-assembly leads to various 1D–3D CPs, while at x = 7 the system discontinuously switches to 3D SCP (SbF6)@[(A)9Ag11(DN7)6](SbF6)10 with huge, supramolecules of ø2.21 nm in size as nodes. For x = 8 – 10 the self-assembly leads to 3D SCPs (A)@[(A)12Ag12(DNx)6](SbF6)12 with spherical cationic supramolecules of 2.40 – 2.44 nm in size acting as nodes. The SCPs specifically encapsulate guests, SbF6- anion or A, inside the nodes, while the voids between the nodes in the 3D network are filled with solvent molecules and SbF6- counterions. All products are characterized by NMR spectroscopy, MS spectrometry and single-crystal X-ray diffraction at 10-90 K.

The research was partly performed at P11 and P24 beamlines on PETRA III at DESY. This work was supported by the German Research Foundation (DFG) within the project Sche 384/44-1.

References

[1] T. Schnitzer, G. Vantomme, *ACS Cent. Sci.*, vol. 6, p. 2060, 2020.
[2] Y. Sun, C. Chen, P. J. Stang, *Acc. Chem. Res.*, vol. 52, p. 802, 2019.
[3] E. Peresypkina, C. Heindl, A. Virovets, M. Scheer, *Structure and Bonding*, vol. 174, p. 321, 2016.
[4] J. Schiller, A. V. Virovets, E. Peresypkina, M. Scheer, *Angew. Chem. Int. Ed.*, vol. 59, p. 13647, 2020.
[5] E. Peresypkina, M. Bielmeier, A. Virovets, M. Scheer, *Chem. Sci.*, vol. 11, pp. 9067–9071, 2020.

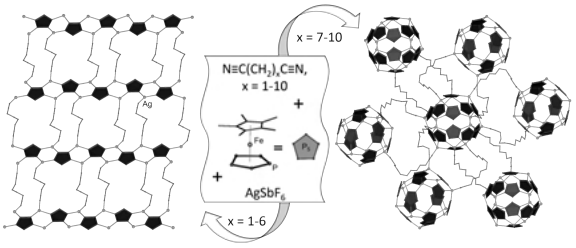

Figure 1

Tracking nerve-agent simulant decomposition in UiO-67 using in situ total scattering pair distribution function analysis

M. Terban[1], S. Ghose[2], A. Plonka[3], D. Troya[4], P. Juhás[5], R. Dinnebier[1], J. Mahle[6], W. Gordon[6], A. Frenkel[3,7]
[1] Max Planck Institute for Solid State Research, Heisenbergstr. 1, 70569 Stuttgart, Germany
[2] Brookhaven National Laboratory, National Synchrotron Light Source II, Upton, New York, NY 11973, USA
[3] Stony Brook University, Department of Materials Science and Chemical Engineering, Stony Brook, New York, NY 11794, USA
[4] Virginia Tech, Department of Chemistry, Blacksburg, VA 24061, USA
[5] Brookhaven National Laboratory, Computational Science Initiative, Upton, New York, NY 11973, USA
[6] Aberdeen Proving Ground, U.S. Army Combat Capabilities Development Command Chemical Biological Center, Aberdeen, Maryland, MD 21010, USA
[7] Brookhaven National Laboratory, Chemistry Division, Upton, New York, NY 11973, USA

The ability to selectively take up and store gases is one of the promising properties of metal–organic frameworks (MOFs) already implemented for industrial applications. Judicious choice of secondary building units can allow for further catalyzing reactions with stored content; for example, much research is currently pursuing their use for fil-

tration of chemical warfare agents. Recently, the Zr-based MOF UiO-67 was shown to effectively adsorb and decompose the nerve-agent simulant, dimethyl methylphosphonate (DMMP).

Various methods are available for probing the gas sorption and reaction pathway, but quantitative structural information on the localized binding is difficult to obtain. A better understanding of the binding behavior is necessary to improve the performance of these MOFs for chemical agent neutralization. Here, we demonstrate the quantitative tracking of both framework and binding component structures using in situ X-ray total scattering measurements of UiO-67 under DMMP exposure, pair distribution function analysis, and theoretical calculations. The adsorption and desorption of DMMP within the pores, association with linker-deficient Zr6 cores, and decomposition to irreversibly bound methyl methylphosphonate were directly observed and analyzed with atomic resolution.

Going forward, wider access to powerful synchrotron beamlines and robust in situ capabilities will allow for comprehensive investigations into the structural implications of the full processing procedure from activation to adsorption, reaction, and re-activation. The procedures developed in this study could help guide further investigations into processes in other MOF/functional systems.

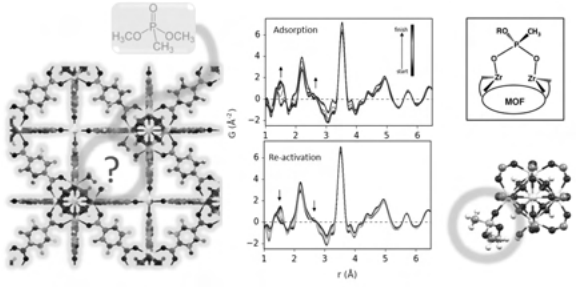

Figure 1

Inorganic crystal structures

High-pressure synthesis of novel yttrium nitride, Y5N14, at 50 GPa

A. Aslandukov[1], A. Aslandukova[1], D. Laniel[1], T. Fedotenko[1], L. Yuan[2], G. Steinle-Neumann[2], K. Glazyrin[3], L. Dubrovinsky[2], N. Dubrovinskaia[1]

[1] University of Bayreuth, Bayreuth, Germany

[2] University of Bayreuth, Bayerisches Geoinstitut, Bayreuth, Germany

[3] DESY, Photon Science, FS-PE (PETRA III Experiment Support), Hamburg, Germany

Homonuclear dinitrogen anions are common intermediates in biological and organometallic synthetic chemistry, and play an important role in the processes of nitrogen reduction to ammonia. In extended solid-state compounds, nitrogen is typically present in the form of a nitride anion N3- and does not form catenated polyanions. However at high-pressure conditions MN2 dinitride compounds of alkali-earth metals (M = Ca, Sr, Ba), transition metals (M=Ti, Cr, Fe, Co, Ni, Cu, Ru, Rh, Pd, Re, Os, Ir, Pt) and rare earth metal (M = La) were obtained. In MN2 compounds, metals usually possess their common oxidation states, while the dinitrogen anion formally accommodates from 1 to 4 electrons. The degree of charge transfer from the metal to the nitrogen dimers significantly affects the properties of the materials (e.g. MN2 (M = Pt, Ir, Os, Ti) pernitrides with [N2]4- units are much less compressible than MN2 (M = Cr, Fe, Co, Ni, Ru, Rh) with [N2]3- units). In this study yttrium and molecular nitrogen were compressed to 50 GPa and laser heated above 2000 K. Under these conditions, synchrotron single-crystal X-ray diffraction from multigrain samples revealed the formation of a new tetragonal yttrium nitride phase with the unusual Y5N14 composition (Fig. 1a). All nitrogen atoms form dimers, but strikingly there are three different types of nitrogen dimers in the structure with 1.24 Å, 1.28 Å and 1.36 Å nitrogen-nitrogen bond length (Fig. 1b). The bond length correlates with the multiplicity of the nitrogen-nitrogen bond and charge state of the nitrogen dimers. Our detailed analysis shows that there are six [N=N]2- dimers and one [N- N]3- dimer per Y5N14 formula unit, which corresponds to the typical Y3+ oxidation state for all yttrium atoms. Ab-initio calculations confirm that this structure is dynamically stable at such pressure. Although [N2]2- and [N2]3- ions are known in the structures of other dinitrides, Y5N14 is the first example of the presence of two different types

of charged nitrogen dimers in the same structure, which indicates more complex chemical processes of dense dinitrides formation under high pressure.

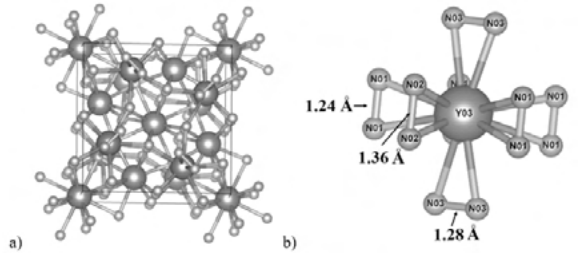

Figure 1 a) Structure of the novel Y5N14 phase and b) different dinitrogen anions in the Y03 atom coordination environment.

Novel high-pressure yttrium carbide, HP-Y4C5.

A. Aslandukova[1], L. Yuan[1], D. Laniel[1], A. Aslandukov[1], S. Khandarkhaeva[2], T. Fedotenko[1], G. Steinle-Neumann[3], N. Dubrovinskaia[1], L. Dubrovinsky[3], K. Glazyrin[4]

[1] University of Bayreuth, Bayreuth, Germany

[2] DESY, Photon Science, FS-PS (FS-Photon Science), Hamburg, Germany

[3] University of Bayreuth, Bayerisches Geoinstitut, Bayreuth, Germany

[4] DESY, Photon Science, FS-PE (PETRA III Experiment Support), Hamburg, Germany

Transition-metal carbides exhibit high melting points, high hardness, and metallic conductivity that make these materials attractive candidates for different technological applications and for material science studies. Carbon has the capability of forming various bonding states affecting the structures and properties of transition metal carbides. High pressure can be used to alter bonding patterns, leading to new compounds with unusual bonding states and properties. The yttrium carbide family shows a large variety of possible phases at ambient pressure with different stoichiometry (e.g., Y2C, Y4C5, Y3C4, Y2C3, Y4C7, YC2). Here, we report results on the synthesis and characterization of a previously unknown high-pressure yttrium carbide, HP-Y4C5, which displays very unusual crystal chemistry. The HP-Y4C5 phase was synthesized by the chemical reaction of pure metallic yttrium and paraffin oil at P 44 GPa and T 1500 K in a laser-heated diamond anvil cell, and was characterized by synchrotron single-crystal X-ray diffraction and Raman spectroscopy. On decompression, diffraction lines of HP-Y4C5 were traced down to at least 16(2) GPa, and the characteristic Raman modes of the phase were observed to 2 GPa. The HP-Y4C5 phase crystallizes in the orthorhombic system (space group Cmce, Z = 16) with the unit cell parameters a = 12.1834(8) Å, b = 7.6592(4) Å and c = 8.8584(11) Å at 44 GPa (Fig. 1). Notable structural elements of HP-Y4C5 are [C2] dumbbells and [C3] trimers. While the first coordination sphere Y-C distances (2.24-2.69 Å) are typical for yttrium carbides, the C-C distances in the [C2] dimers (1.40(2) Å) and the [C3] trimers (1.43(1) Å) are unusual: they are significantly larger than expected for double-bonded carbon atoms (1.33 Å) and much shorter than for single-bonded (1.54 Å). Phonon dispersion calculations show that HP-Y4C5 is dynamically stable at 44 GPa. The electron localization function (ELF) demonstrates strong covalent bonding between carbon atoms within the carbon dumbbells and trimers, and covalent bonds between Y and C. According to our analysis of the charge distribution in the ionic approximation, the HP-Y4C5 phase contains the anions [C2]5- and [C3]6-, with a bond order of 1.5 in both cases. The calculated electronic density of states shows that yttrium carbide HP-Y4C5 is metallic and that the main contribution at the Fermi level comes from Y 4d and C 2p states.

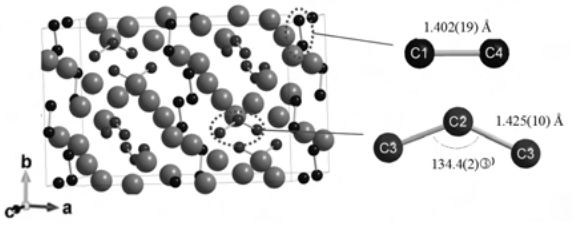

Figure 1 Crystal structure of Y4C5 at 44 GPa. The grey, blue and red spheres represent yttrium and carbon atoms in dimers and trimers, respectively. The [C2]5- and [C3]6- species with their bond lengths and angles are indicated on the right side.

Charge density wave order in Pr2Ru3Ge5

J.-K. Bao[1], Y. Li[2], S. Ramakrishnan[1], S. R. Kotla[1], C. Eisele[1], D. Y. Chung[3], C. Paulmann[4], L. Noohinejad[4], M. Tolkiehn[4], Z.-A. Xu[2], M. Kanatzidis[5], S. van Smaalen[1]

[1] University of Bayreuth, Laboratory of Crystallography, Bayreuth, Germany

[2] Zhejiang University, Department of Physics, Zhejiang Province Key Laboratory of Quantum Technology and Device, Hangzhou, China

[3] Argonne National Laboratory, Materials Science Division, Lemont, IL 60439, USA

[4] DESY, Notkestr. 85, 22607, Hamburg, Germany

[5] Northwestern University, Evanston, IL 60208, USA

The charge density wave (CDW) is a collective phenomenon where electrons at the Fermi level form a density wave with an additional periodicity as compared to the atomic lattice. $RE_2Ru_3Ge_5$ (RE = Pr, Sm, Dy) crystallize in the $Sc_2Fe_3Si_5$-type structure (space group $P4/nmc$). They show peculiar CDW-induced lattice modulations in a certain temperature range below which those modulations disappear.[1] Compared to $Sm_2Ru_3Ge_5$, $Pr_2Ru_3Ge_5$ has a higher transition temperature and no detailed structure refinements have been reported for the modulated phase for this compound. In this presentation, we will show that $Pr_2Ru_3Ge_5$ exhibits phase transitions at around 200 K from specific heat and transport property measurements. Satellite peaks have been observed in x-ray diffraction with a modulation wave vector q = (0.18,±0.18, 0). Unanticipatedly, satellite peaks disappear below 180 K. The modulated crystal structure of the CDW phase of $Pr_2Ru_3Ge_5$ will be presented on the basis of the superspace method.

References

[1] Bugaris, D. E *et al.*, "Charge Density Wave in the New Polymorphs of $RE_2Ru_3Ge_5$ (RE = Pr, Sm, Dy)," *J. Am. Chem. Soc.*, vol. 139, no. 11, pp. 4130–4143, 2017.

Structural investigations of mixed anionic rare-earth and transition metals selenide oxides using synchrotron radiation

D. C. Benndorf[1]

[1] Leipzig University, Leipzig, Germany

The simultaneous reaction of oxygen, its heavier homologs, and metals usually lead to the formation of substances characterized by the presence of covalent O-Ch (Ch = S, Se) bonds within complex anions like sulfates or selenides. Examples for compounds containing both, O^{2-} and Ch^{2-} without any attractive interaction between these species are far less known. Only a few examples for chalcogenide oxides of transition (T) and rare-earth metals (RE) are described in the literature so far, though exhibiting a relatively high variety in composition and crystal structures.

Salt-flux assisted reactions of rare-earth metals and their oxides, transition metals and selenium lead to the discovery of the mixed anionic selenide oxides $RE_2ZrSe_2O_3$ (RE = Ce-Nd, Sm) and $Ce_7TiSe_5O_7$. All these substances appear as thin needle-like crystals with diameters of 5 μm and less which are extraordinarily sensitive to mechanical stress. Consequently, structure determination had to be realized using synchrotron radiation. First investigations of $Ce_7TiSe_5O_7$ were carried out at the ESRF, beamline ID11, using micro-focused synchrotron radiation. Small crystals were pre-selected and pre-characterized using transmission electron microscopy including EDX spectroscopy [1]. The substance crystallizes with the $La_7VSe_5O_7$ structure type [2], space group $Cmcm$, suggesting the presence of Ti^{3+} cations.

The first Zr containing selenide oxides $RE_2ZrSe_2O_3$ (= 2 $RE^{3+}Zr^{4+}2Se^{2-}3O^{2-}$) were investigated at PETRA III, beamline P24, and the ESRF, beamline ID11. The compounds were found to crystallize with their own structure type, space group $C\ 2/m$, characterized by the presence of large cavities extended along [010] formed by Se atoms (see Fig. 1).

References

[1] F. Fahrnbauer, T. Rosenthal, T. Schmutzler, G. Wagner, G. B. M. Vaughan, J. P. Wright, O. Oeckler, *Angew. Chem. Int. Ed.*, vol. 54, pp. 10020–10023, 2015.

[2] S. Peschke, L. Gamperl, V. Weippert, D. Johrendt, *Dalton Trans.*, vol. 46, pp. 6230–6243, 2017.

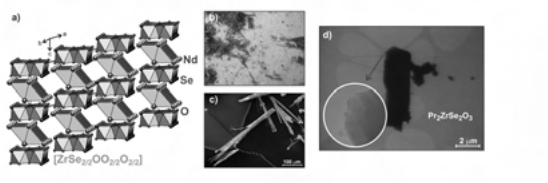

Figure 1 a-c) Crystal structure, bulk material, and SEM-SE image of $Nd_2ZrSe_2O_3$. d) TEM-BF image of the $Pr_2ZrSe_2O_3$ single-crystal investigated at ERSF, beamline ID11. The crystal part used for structure determination is emphasized.

Crystal Structures and Anisotropic Expansion of Coordination Compounds from the Mg(SCN)2 · x H2O/THF System

S. Bette[1], M. Joos[1], M. Conrad[2], R. Merkle[1], T. Schleid[2], J. Maier[1], R. Dinnebier[1]

[1] Max Planck Institute for Solid State Research, Germany

[2] University of Stuttgart, Institute for Inorganic Chemistry, Stuttgart, Germany

Magnesium halides and pseudo-halides are essential compounds for many applications ranging from biochemistry to construction and building materials. These phases exhibit a great variety of chemical and structural properties and hence, were extensively studied. However, in the row of magnesium pseudo-halides, i.e. cyanides, cyanates etc., the thiocyanates were often overseen and are therefore still only poorly characterized.

Mg(SCN)2 · x H2O/THF coordination compounds were synthesized, characterized, their crystal structures solved ab initio from X-ray powder diffraction (XRPD) data and their thermal expansion properties investigated by temperature dependent in situ XRPD.

The recrystallization of Mg(SCN)2 · 4 H2O in THF yields the novel compounds Mg(SCN)2 · 2 (H2O, THF) and α-Mg(SCN)2 · 4 THF. By heating, α-Mg(SCN)2 · 4 THF undergoes a phase transition into β-Mg(SCN)2 · 4 THF that is associated with an increasing disorder of the THF molecules. Finally, two THF molecules are released, which leads to the formation of Mg(SCN)2 · 2 THF. The investigated compounds show a remarkable anisotropic thermal expansion and the growing disorder of THF molecules has a major impact on the expansion properties.

The coordination chemistry of Mg(SCN)2 turned out to be rich and has the potential to go beyond H2O and THF as ligands. An expansion towards other metals like nickel, cobalt or iron appears to be very feasible.

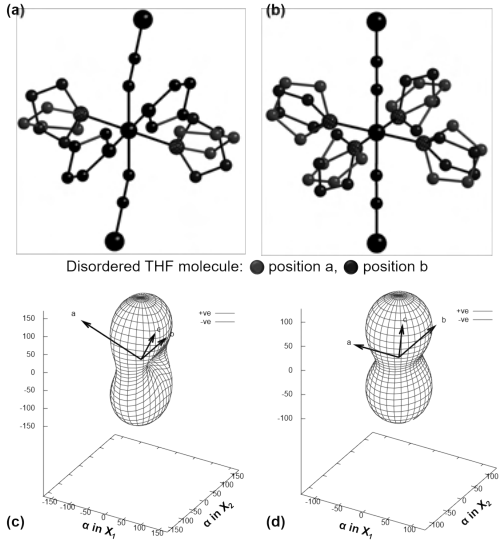

Figure 1 Octahedral coordination of Mg2+ with SCN- and THF for a) α-Mg(SCN)2 · 4 THF; b); β-Mg(SCN)2 · 4 THF, Plots showing the variation of the thermal expansion coefficient α with the principal directions X1, X2 and X3 of c) α-Mg(SCN)2 · 4 THF, d) β-Mg(SCN)2 · 4 THF.

The lanthanoid olxoantimonate(III) bromides $Ln\mathbf{Sb_2O_4Br}$ (Ln = Eu – Tb): Synthesis, crystal structure and luminescence

F. C. Goerigk[1], T. Schleid[1], V. Paterlini[2], A.-V. Mudring[2]

[1] University of Stuttgart, Institute for Inorganic Chemistry, Pfaffenwaldring 55, 70569 Stuttgart, Germany

[2] Stockholm University, Department of Materials and Environmental Chemistry, Arrhenius Laboratory, Stockholm, Sweden

Pale yellow crystals of $Ln\mathrm{Sb_2O_4Br}$ (Ln = Eu – Tb) were synthesized via high temperature solid-state reactions from antimony sesquioxide, the respective lanthanoid sesquioxides and tribromides. Single-crystal X-ray diffraction studies revealed a layered structure in the monoclinic space group $P2_1/c$. In contrast to hitherto reported quaternary lanthanoid(III) halide oxoantimonates(III) [1], in $Ln\mathrm{Sb_2O_4Br}$ the lanthanoid(III) cations are exclusively coordinated by oxygen atoms in the shape of square hemiprisms. These $[Ln\mathrm{O_8}]^{13-}$ polyhedra form layers parallel to the (100) plane by sharing common edges as shown in Figure 1. All antimony(III) cations are coordinated by three oxygen atoms forming ψ^1-tetrahedral $[\mathrm{SbO_3}]^{3-}$ units, which have oxygen atoms in common building up meandering strands along [001] (Figure 2) according to 1D-$[\mathrm{SbO}^{v}_{2/2}\mathrm{O}^{t}_{1/1}]^{-}$– ($v$ = vertex-sharing, t = terminal). The bromide anions are located between two layers of these parallel running oxoantimonate(III) strands and have no bonding contacts with the Ln^{3+} cations. Since Sb^{3+} is known to be an efficient sensitizer for Ln^{3+} emission, photoluminescence studies were carried out to characterize the optical properties and assess their suitability as light phosphors. Indeed, for both, $\mathrm{GdSb_2O_4Br}$ and $\mathrm{TbSb_2O_4Br}$ doped with about 1.0 – 1.5 at-% Eu^{3+} efficient sensitization of the Eu^{3+} emission could be detected. The resulting luminescence properties of both doped and undoped $\mathrm{GdSb_2O_4Br}$ and $\mathrm{TbSb_2O_4Br}$ are summarized in Figure 3. For $\mathrm{TbSb_2O_4Br}$, in addition, a remarkably high energy transfer from Tb^{3+} to Eu^{3+} could be detected that leads to a substantially increased Eu^{3+} emission intensity, rendering it an efficient red light emitting material [2].

References

[1] F. C. Goerigk, Th. Schleid, *Z. Anorg. Allg. Chem.*, vol. 645, pp. 1079–1084, 2019.

[2] F. C. Goerigk, V. Paterlini, K. V. Dorn, A.-V. Mudring, Th. Schleid, *Crystals*, vol. 10, pp. 1089–1111, 2020.

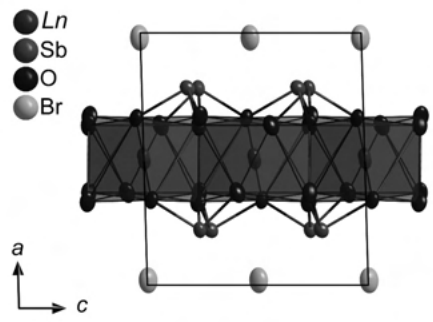

Figure 1 Section of the crystal structure of the $Ln Sb_2O_4Br$ series (*Ln*=Eu-Tb) viewed along [010] emphasizing the unit-cell edges and $[LnO_8]^{13-}$ polyhedra (dark red) utilizing the refined anisotropic displacement parameters with an ellipsoidal probability of 95%.

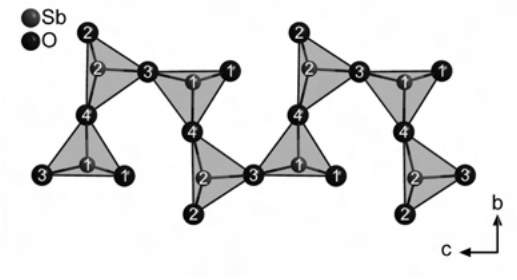

Figure 2 Meandering 1D-$[SbO^{v}_{2/2}O^{t}_{1/1}]^{-}$ chain of vertex-connected $[SbO_3]^{3-}$ ψ^1 - tetrahedra running along [001] in the crystal structure of the $LnSb_2O_4Br$ series (*Ln*=Eu-Tb).

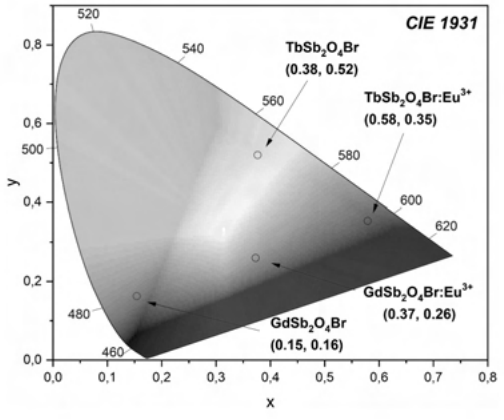

Figure 3 Commission internationale de l'éclairage (CIE) diagram (CIE 1931) for $TbSb_3O_4Br:Eu^{3+}$, $GdSb_3O_4Br$ and $GdSb_3O_4Br:Eu^{3+}$ at λ_{ex} = 257 nm.

A mineral with new loop-branched sechser single chains Khurayyimite Ca7Zn4(Si2O7)2(OH)10·4H2O

B. Krüger[1], I. O. Galuskina[2], E. Galuskin[2], Y. Vapnik[3], M. Murashko[4]

[1] University of Innsbruck, Institute of Mineralogy and Petrography, Innsbruck, Austria

[2] University of Silesia, Faculty of Earth Sciences, Będzińska 60, 41-200 Sosnowiec, Poland

[3] Ben-Gurion University of the Negev, POB 653, Beer-Sheva 84105, Israel

[4] Saint Petersburg State University, Faculty of Geology, 7-9sp Universitetskaya nab., 199034 St Petersburg, Russia

The mineral khurayyimite Caenter code here $Zn_4(Si_2O_7)_2(OH)_{10}·4H_2O$, (IMA 2018-140) was found in small cavities in altered spurrite marbles, in the northern part of the Siwaqa pyrometamorphic rock area, Central Jordan. It is a low-temperature, hydrothermal mineral and it forms at a temperature of ca. 100 °C. It builds nearly 50 μm white or colourless, platy crystals arranged in up to 200-300 μm big spherulitic aggregates.

Single-crystal X-ray diffraction experiments at ambient conditions were performed at the X06DA beamline at the Swiss Light Source (Paul Scherrer Institute, Villigen, Switzerland). Khurayyimite crystallises in space group P21/*c*, with unit cell parameters (a=11.2450(8), b=9.0963(5), c=14.0679(10)Å, β = 113.237(8)°, V = 1322.25(17)Å^3 and Z = 2. The average structure was solved using direct methods. All H-sites are located by difference Fourier analysis. The resulting structure model was refined up to R1= 0.02. The crystal structure of khurayyimite consists of sheets perpendicular to a. Each sheet is built by very unusual loop-branched sechser single chains $\{1B,1^1_\infty\}[^6Zn_4Si_4O_{21}]$. Voids between chains are filled by blocks of five Ca-octahedra and two CaO_7 polyhedra with additional OH groups and water molecules.

The loop-branched *sechser* single chains $\{1B,1^1_\infty\}[^6Zn_4Si_4O_{21}]$ are made of dimers of Si_2O_7 and two types of $ZnO_2(OH)_2$ tetrahedra connected by corners. Loops of the chain contain three tetrahedra, analogous to *dreier* ring. Strong repulsive forces between the tetrahedra in *dreier* ring are pressing connecting O atoms as far as possible forming equilateral triangle with longer ZnO_4 edge (≈ 3.176 Å) and two shorter two SiO_4 edges (≈ 2.67). These repulsive forces are, according to [1], a possible reason for why such loops have not been observed more frequent.

Different combinations of chains and frameworks made of ZnO_4 and SiO_4 tetrahedra are known. In $ZnSiO_3$ [2], with Zn atoms in six and four-fold coordination, two pyroxene-like chains running along the c-direction are branched with two ZnO_4 tetrahedra forming four-membered loops. The crystal structure of the LT and HT forms of $BaZn_2Si_2O_7$ [3] exhibit a disilicate group Si_2O_7 linked via corners with ZnO_4 tetrahedra in a three-dimensional framework. In such a manner are created six member rings ($2\times Si_2O_7$, $2\times ZnO_4$), four member-rings ($2\times SiO_4$, $2\times ZnO_4$) and three-membered rings ($1\times SiO_4$, $2\times ZnO_4$). Still, three-membered loops, made of Si_2O_7 and ZnO_4, like in khurayyimite, have not been observed yet.

References

[1] Libau, F., *Structural Chemistry of Silicates*. Berlin, Heidelberg, Germany: Springer-Verlag Berlin Heidelberg, 1985.

[2] Morimoto, N., Nakajima, Y., Syono, S., Akimoto, S. and Matsui, Y., "Crystal structure of pyroxene-type $ZnSiO_3$ and $ZnMgSi_2O_6$," *Acta Cryst. B*, vol. 31, pp. 1041–1049, 1975.

[3] Lin, J.H., Lu, G.X., Du, J., Su, M.Z., Loong, C.-K. and Richardson, J.W., "Phase transition and crystal structures of $BaZn_2Si_2O7$," *J. Phys. Chem. Solids*, vol. 60, no. 7, pp. 975–983, 1999.

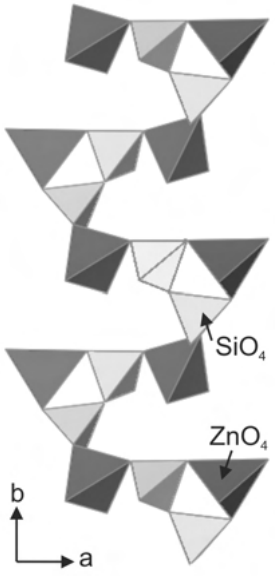

Figure 1

The telluridogallates REGaTe2 (RE = La – Nd)

T. Lindemann[1], O. Oeckler[1]

[1] Leipzig University, Faculty of Chemistry and Mineralogy, Institute of Mineralogy, Crystallography and Materials Science, Leipzig, Germany

New telluridogallates(I) $REGaTe_2$ (RE = La – Nd, space group $Pmc2_1$) were obtained from the elements. Chemical bonding and charge distribution are not trivial. Bond valence sums suggest an electron-precise description according to $RE^{III}Ga^{I}Te_2^{-II}$, and the coordination of gallium(I) is pyramidal as expected for a lone-pair atom. In contrast, known telluridogallates(III) such as $CuGaTe_2$ [1] and $AgGaTe_2$ [2] typically contain $[GaTe_4]$ tetrahedra. $REGaTe_2$ are a rare example of compounds with exclusively monovalent Ga atoms, probably the first one without organic residues. A short Nd-Ga distance of 3.13 Å is a possible indication of an interaction of the lone pair of Ga(I) with the Nd atoms. This is stronger than, for example, $NdGaSb_2$ (Nd-Ga distance 3.35 Å),[3] which has a different structure and bonding situation. Similar Nd-Ga distances are observed in intermetallic phases such as NdGa [4] or NdGaRh [5], so that a description as an oxidized intermetallic phase may also be considered. A formal consideration in the framework of the Zintl concept would assume a mixed chain-like $[Ga^{(-2)}Te^{(0)}Te^{(-1)}]^{3-}$-polyanion. It is consistent with all descriptions that the distances of 2.67 Å to the terminal Te atom are shorter than those to Te atoms bridging along the chain (2.95 Å). Interactions between the polyanionic chains appear negligible. The Nd atoms are located in single-capped trigonal prisms of Te atoms, with Ga atoms forming two additional caps.

References

[1] T. Plirdpring, K. Kurosaki, A. Kosuga, T. Day, S. Firdosy, V. Ravi, G. J. Snyder, A. Harnwunggmoung, T. Sugahara, Y. Ohishi, *Adv. Mater.*, vol. 24, pp. 3622, 2012.

[2] S. Chatraphorn, T. Panmatarite, S. Pramatus, A. Prichavudhi, R. Kritayakirana, J.-O. Berananda, V. Sayakanit, J. C. Woolley, *J. Appl. Phys.*, vol. 57, pp. 1791, 1985.

[3] A. M. Mills, A. Mar, *J. Am. Chem. Soc.*, vol. 123, pp. 1151, 2001.

[4] S.P. Yatsenko, A. A. Semyannikov, B. G. Semenov, K. A. Chuntonov, *J. Less-Common Met.*, vol. 64, pp. 185, 1979.

[5] F. Hulliger, *J. Alloys Compd.*, vol. 239, pp. 131, 1996.

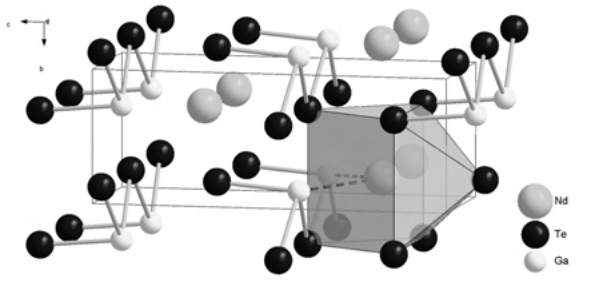

Figure 1 Unit cell of $NdGaTe_2$ in which the polyanionic substructure has been highlighted. The Nd-Ga contacts are shown by dashed "bonds".

Structural variations in RETe1.875–δ – distorted Te nets and chemical bonding

H. Poddig[1], T. Doert[1]
[1] Technical University of Dresden, Helmholtzstr. 10, 01069 Dresden, Germany

The structures of the rare earth metal polychalcogenides $REX_{2-\delta}$ (X = S, Se, Te; $0 \leq \delta \leq 0.2$) share a common motive of alternating stacks of a puckered [REX] double layer and planar [X] layer, which are structurally related to the ZrSSi type. This class of compounds adopts different (super)structures, according to the chalcogen defects in their planar layers. The deficient sulfides and selenides are dominated by X^{2-} and X_2^{2-}-anions, whereas a tendency to form larger anionic entities has been observed for the tellurides.[1–3] Crystals of $RE\mathrm{Te}_{1.875-\delta}$ (RE = Ce, Pr, Sm, Gd; $0.005 \leq \delta \leq 0.02$) have been grown by chemical transport reactions utilizing iodine and alkali halide flux reactions. All compounds crystallize in an orthorhombic unit cell, resembling a 3×4×2 supercell of the basic ZrSSi cell, with cell dimensions of about $a \approx 13.2(2)$, $b \approx 17.6(2)$ and $c \approx 18.0(2)$. Structure solution and subsequent refinement has been performed in space group *Amm2* (No. 38), in accordance with the structures of the related sulfides and selenides.[1] The generalized motif of all compounds resembles well the motif of the $GdSe_{1.875}$ type structure, as two stacks of a puckered [RE Te] and a planar [Te] layer are observed for all structures. Minor structural variations, i.e. slightly shifted atoms or additional vacancies, are observed for individual compounds within the planar [Te] layer, hinting towards marginally different ordered motifs, which can be understood as a result of structural frustration. The structural variety of the planar layer also manifests itself in a growing number of reflections violating the A-centering condition. Quantum mechanical calculations based on DFT theory have been performed to investigate the bonding situation inside the planar [Te] layer by using the real space indicator ELI-D. The results justify the description of small anionic fragments constituting the [Te] layers, but also indicate long range order within a characteristic eight-membered Te ring. Unlike for the sulfides and selenides, these calculations suggest formally a Te_8^{8-} anion, as bonding interactions are expected between all neighboring atoms of the ring.

References

[1] T. Doert, C. J. Müller, in *Reference Module in Chemistry, Molecular Sciences and Chemical Engineering*, Elsevier, 2016.
[2] H. Poddig, T. Donath, P. Gebauer, K. Finzel, M. Kohout, Y. Wu, P. Schmidt, T. Doert, *Z. Anorg. Allg. Chem.*, vol. 644, pp. 1886–1896, 2018.
[3] K. Stöwe, *Z. Kristallogr. - Cryst. Mater.*, vol. 216, pp. 215–224, 2001.

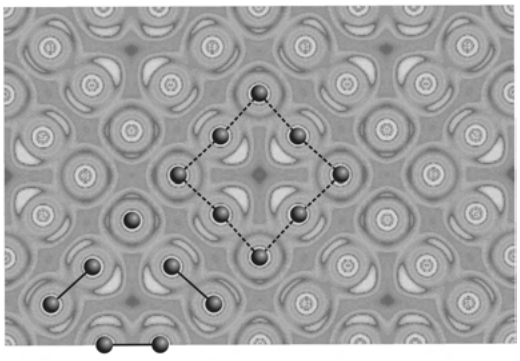

Figure 1

Luminescent nitridoalumooxophosphates by high-pressure/high-temperature synthesis

M. Pointner[1], O. Oeckler[2], W. Schnick[1]
[1] Ludwig Maximilian University of Munich, Munich, Germany
[2] Leipzig University, Leipzig, Germany

Intriguing properties of mixed nitride networks have led to a range of viable applications. Nitrido(litho)aluminates, e.g. $Sr[LiAl_3N_4]:Eu^{2+}$ and $Sr_2[MgAl_5N_7]:Eu^{2+}$, are an important part of developments in the lightening industry due to their chemical and thermal stability and luminescence.[1, 2] Likewise, nitridosilicophosphates and nitridophosphates contain rare structural motifs.[3, 4, 5] Dense frameworks and luminescence properties that may improve the quality of specialized light-emitting diodes (LEDs) are highly sensitive to the valence state, coordination spheres, site symmetry of atoms and the concentration of activator ions. Therefore, understanding relationships between luminescent properties and crystal structures is crucial. In investigating the nitride

network of nitridoalumo(oxo)phosphates, we combine these characteristics and properties and aimed at luminescent properties like low thermal quenching and a narrow emission due to the structural relationship to nitrido(litho)aluminates. $Sr_2Al_{10}P_8N_{20}O_{4.034}F_{5.094}:Eu^{2+}$ was obtained from $Sr(N_3)_2$, $SrCO_3$, P_3N_5, AlN, EuF_3 and the mineralizer NH_4F by mineralizer-assisted high-temperature high-pressure (HT/HP) synthesis (1400 °C, 5 GPa) with a Walker-type module.[6] The structure was elucidated by SCXRD (single-crystal X-ray diffraction, R1 = 0.0142, wR2 = 0.0327). BVS (bond valence sum) and CHARDI (charge-distribution) calculations indicate mixed anionic positions. The new nitridoalumofluoridooxophosphate crystallizes in space group I-4m2 [a = 11.17902(8), c = 5.1484(1) Å]. TEM SAED (transmission electron microscopy selected area electron diffraction) patterns confirmed the metric and TEM and SEM (scanning transmission electron) EDX (energy dispersive X-ray) coincide with the element ratio obtained by SCXRD. $Sr_2Al_{10}P_8N_{20}O_{4.034}F_{5.094}:Eu^{2+}$ shows a broadband emission with a maximum at 450 nm and a fwhm (full width at half maximum) of 108 nm (5315.0 cm^{-1}). It contains chains of face-sharing $Sr(N/O/F)_{12}$ cuboctahedra, supertetrahedra-like elements composed of ten edge-sharing $Al(N/O/F)_6$ octahedra where Al is positioned on three different crystallographic sites. A three-dimensional network is built by twofold and threefold vertex-sharing PN_4 tetrahedra.

References

[1] M. Zeuner, S. Pagano, W. Schnick, *Angew. Chem.-Int. Ed.*, vol. 50, p. 7754, 2011.
[2] P. Wagatha, V. Weiler, P. J. Schmidt, W. Schnick, *Chem. Mater.*, vol. 30, p. 1755, 2018.
[3] S. Vogel, A. T. Buda, W. Schnick, *Angew. Chem.-Int. Ed.*, vol. 58, p. 3398, 2019.
[4] S. Vogel, M. Bykov, E. Bykova, S. Wendl, S. D. Kloß, A. Pakhomova, S. Chariton, E. Koemets, N.Dubrovinskaia, L. Dubrovinsky, W. Schnick, *Angew. Chem.-Int. Ed.*, vol. 58, p. 9060, 2019.
[5] S. D. Kloß, W. Schnick, *Angew. Chem.-Int. Ed.*, vol. 58, p. 7933, 2019.
[6] S. Merlino, C. Biagioni, E. Bonaccorsi, N. V. Chukanov, I. V. Pekov, S. V. Krivovichev, V. N. Yakovenchuk, T. Armbruster, *Mineral. Mag.*, vol. 79, p. 145, 2015.

Crystal structure, complex phase diagram and re-entrant phase transition in NaSrPO4

M. Schreyer[1], G. Nenert[1]
[1] Malvern Panalytical, Malvern, United Kingdom

The crystal chemistry of AIBIIXO4 (AI = Alkali ion, BII = alkali-earth ion, X = P, V, As) is very rich and has been widely investigated, particularly the phosphate family [1]. In recent years, we have been investigated the crystal structures [2,3] and magnetic properties of some compositions within the AIBIIXO4 series [4]. However, despite its simple chemistry NaSrPO4 has never been reported so far. Here, we present the synthesis, crystal structure and phase transitions of this phosphate. Surprisingly, this material exhibits a complex structure (31 atoms in the asymmetric unit-cell, Z = 10) at room temperature characterized by a strongly under bonded Na atom. This under-bonded atom is responsible for the complex and rich phase diagram as function of temperature as illustrated in Figure 1. NaSrPO4 exhibits 4 phase transitions between room temperature and 750°C. Besides its rich phase diagram, NaSrPO4 exhibits a re-entrant phase transition slightly below 600°C before to reach a hexagonal paraelastic phase at high temperature. In addition, we show that the sequence of phase transitions is strongly driven by the history of the sample and several phases can be quenched at room temperature.

References

[1] V. A. Isupov, Ferroelectrics, 274(1), 203–283 (2002)
[2] G. Nénert, P. O'Meara, T. Degen, Phys Chem Minerals 44, 455–463 (2017)
[3] G. Nénert, Z. Kristallogr.; 232(10), 669–674 (2017)
[4] G. Nénert, et al., Inorg. Chem., 52, 9627-9635 (2013).

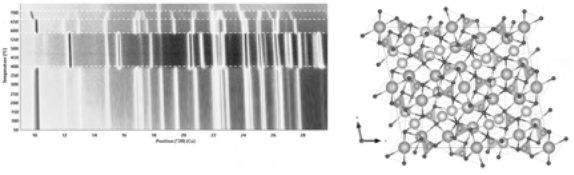

Figure 1 (Left) Temperature phase diagram of NaSrPO4and (right) the crystal structure of the α re-entrant polymorph.

Disorder in layered tellurides Tt1Pn2Te4 (Tt = Ge, Sn, Pb; Pn = As, Sb, Bi)

L. Staab[1], L. Eisenburger[2], S. Geisler[1], O. Oeckler[1]
[1] Universität Leipzig, Leipzig, Germany
[2] LMU München, Munich, Germany

The crystal structure of the mineral tetradymite Bi2S2Te has inspired discussions about its details for a long time.[1,2] Variations of this structure led to a large family of chalcogenides composed of slabs with alternating cation and anion layers stacked in rocksalt-type fashion, which show characteristic van der Waals gaps between anion layers.[3] These compounds are of interest not only for their exact crystal structures but also for their thermoelectric properties and their high likelihood of being topologically non-trivial systems insulators.[4,5] The rhombohedral compounds Tt1Pn2Te4 (*Tt* = Ge, Sn, Pb; *Pn* = As, Sb, Bi) feature septuple layers, in which the multiplicity of Wyckoff positions would allow complete cation ordering, which has been postulated in some cases.[6] However, more detailed studies based on single-crystal diffraction data almost always revealed cation disorder.[7] In the case of small scattering contrast, resonant X-ray diffraction corroborated the disorder.[8] Here we present a systematic investigation of these compounds with high-quality single crystal diffraction data collected with synchrotron radiation in order to establish exact site occupancy factors. As diffraction data cannot exclude short-range ordering, Z-contrast imaging by STEM-HAADF was used as a local probe, complemented by EDX spectroscopy with atomic resolution. All of these data confirm the cation disorder and could not even demonstrate short-range ordering. The disorder observed might be explained as an interplay between charge balance at the vdW-gap and octahedron size mismatch in the layer.

References

[1] Harker, D. *Z. Kristallogr.*, vol. 89, pp. 175-181, 1934.
[2] Pauling, L. *Am. Mineral.*, vol. 60, pp. 994-997, 1975.
[3] Cook, N. J.; Ciobanu, C. L.; Stanley, C. J.; Paar, W. H.; Sundbald, K. *Can. Mineral.*, vol. 45, pp. 417-435, 2007.
[4] Grauer, D. C.; Hor, Y. S.; Williams, A. J.; Cava, R. J. *Mater. Res. Bull.*, vol. 44, pp. 1926–1929, 2009.
[5] Silkin, I. V.; Menshchikova, T. V.; Otrokov, M. M.; Eremeev, S. V.; Koroteev, Yu. M.; Vergniory, M. G.; Kuznetsov, V. M.; Chulkov, E. V. *JETP Letters.*, vol. 96, pp. 322-325, 2012.
[6] Shu, H. W.; Jauilmes, S.; Flahaut, *J. Solid State Chem.*, vol. 74, pp. 277-28, 1988.
[7] Karpinsky, O. G.; Shelimova, L. E.; Kretova, M. A.; Fleurial. J. P. *J. Alloys Compd.*, vol. 268, pp. 112-117, 1998.
[8] Oeckler, O.; Schneider, M. M.; Fahrnbauer, F.; Vaughan, G. *Solid State Sci.*, vol. 13, pp. 1157-1161, 2011.

Inorganic functional materials

Bandgap tuning in ZnGeN2: Effective cation disorder control through oxygen incorporation.

Z. Wang[1], J. Breternitz[1], S. Schorr[1]
[1] Helmholtz-Zentrum Berlin für Materialien und Energie, Hahn-Meitner Platz 1, 14109 Berlin, Germany

Growing concern over resource availability and toxicity are leading to a paradigm shift towards truly sustainable materials for photovoltaics. Zn-group IV-nitrides are one potential class of materials fulfilling these criteria, which adopt a wurtzite-type derived structure. The ternary nitrides were postulated to allow a unique bandgap tuning mechanism through cation disorder [1] in addition to cation alloying. Fully ordered structure $ZnGeN_2$ crystallises in a ß-$NaFeO_2$ type structure in a subgroup of the wurtzite type. Interestingly, incorporating oxygen into $ZnGeN_2$ also introduces an increased degree of disorder in the material [2].

We present a detailed study of the degree of cation disorder in oxygen containing $Zn_{1-x}GeN_2O_x$ that is revealed through neutron powder diffraction. Studying samples with a variable degree of oxygen allows us to conclude on the role of oxygen and further comparing different samples of nominally similar composition allows to decorrelate the oxygen effect from intrinsic cation disorder. We will combine our results with optoelectronic and chemical properties of the materials and finally aim to answer the question, whether cation disorder exists independently of oxygen incorporation or is fundamentally linked to it.

References

[1] A.D. Martinez, A.N. Fioretti, E.S. Toberer, A.C. Tamboli, *J. Mater. Chem. A*, vol. 5, p. 11418, 2017.
[2] J. Breternitz, Z.Y. Wang, A. Glibo, A. Franz, M. Tovar, S. Berendts, M. Lerch, S. Schorr, *Phys. Status Solidi A*, vol. 216, 2019, Art. no. 1800885.

Structure-ammonia sensing property correlation in Sn1-xVxO2 mesoporous nanoparticles

N. Chakraborty[1], A. Sanyal[1], S. Das[1], D. Saha[1], S. K. Medda[1], S. Mondal[1]

[1] CSIR Central Glass & Ceramic Research Institute, Kolkata, India

Doping is a well-known method for improving gas sensing responses by metal oxide based functional materials.[1] And the plausible explanations provided in justification of using a specific dopant have been changes in material crystallinity, particle size, morphology and so on; but these ideas alone aren't able to clearly highlight the fundamental changes and intricacies of a system that exhibits improved performance by virtue of doping.[2] In this context, we have tried to analyze improved ammonia sensing responses by vanadium doped tin oxide nano-particles of formula Sn1-xVxO2 with respect to crystal structure and surface structural aspects.[3] While the doped samples showed a nearly four-fold improved response as compared to pure SnO2, the sample Sn0.696V0.304O2 showed 1.2 times improved response than Sn0.857V0.343O2. Structural analyses by Rietveld refinement[4] revealed reduction of unit cell volume in doped samples, leading to generation of surface active sites up to 1019/mm3 of doped sample, explaining improved response by increase in surface interaction. Surface structure analyses by XPS reveal presence of 1.2 times excess surface positive charge in Sn0.857V0.343O2 as compared to Sn0.696V0.304O2. Considering the concept of charge immobilization by surface electronic states in the former, the variable sensing responses amidst the doped samples can be explained. The specific role of vanadium ion in improving ammonia sensing responses by pure SnO2 has been delineated.

References

[1] Morrison, S. R., "Mechanism of Semiconductor Gas Sensor Operation," *Sensors and Actuators*, vol. 11, pp. 283–287, 1987.

[2] Mirzaei, A., Lee, J. H., Majhi, S. M., Weber, M., Bechelany, M., Kim, H. W., Kim, S. S., "Resistive gas sensors based on metal-oxide nanowires," *J. Appl. Phys.*, vol. 126, 2019, Art. no. 241102.

[3] Rietveld, M. H., "A profile refinement method for nuclear and magnetic structures," *J. Appl. Crystallogr.*, vol. 2, pp. 65–71, 1969.

[4] N. Chakraborty, A. Sanyal, S. Das, D. Saha, S. K. Medda and S. Mondal, "Ammonia Sensing by Sn1-xVxO2 Mesoporous Nanoparticles," *ACS Appl. Nano Mater.*, vol. 3, no. 8, pp. 7572–7579, 2020.

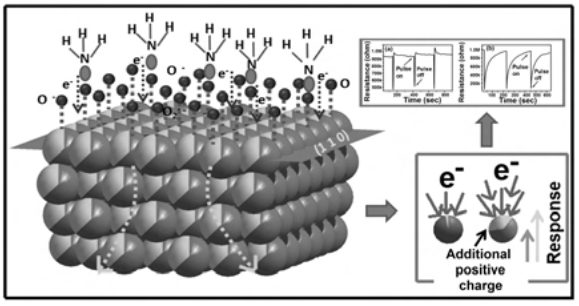

Figure 1

Dynamic disorder of fluoride anions in all-silica zeolites: Enhancing understanding with DFT-based molecular dynamics simulations

M. Fischer[1]

[1] University of Bremen, Faculty of Geosciences, Klagenfurter Straße 2-4, 28359 Bremen, germany

The "fluoride route", synthesis in the presence of fluoride anions, has been established as a versatile strategy for the synthesis of all-silica zeolites. Experimental investigations of as-synthesised zeolites using diffraction and NMR methods have shown that the fluoride anions are often located in small cages and bonded to one Si atom at a cage corner, with dynamic or static disorder occurring in some, but not all systems.[1] It has also been observed that the dynamic disorder can be modulated through a variation of the organic structure-directing agent (OSDA) used in the zeolite synthesis.[2] As relatively little is known about the underlying factors determining the preferred fluoride location(s) in a given cage and the dynamic behaviour, the present work employs a combination of density functional theory (DFT) calculations and DFT-based ab-initio molecular dynamics (AIMD) simulations to contribute to the understanding of these systems.

A systematic comparison of different fluoride positions in four all-silica zeolites with different topologies (IFR, NON, STF, STT) shows excellent agreement with experiment for all systems except STF. A remarkable result is obtained for STT, where the DFT calculations predict three distinct sites to be very close in energy, in perfect correspondence with the experimentally observed disorder over these sites. The AIMD simulations do not only reproduce the dynamic disorder of fluoride anions in IFR and STT, and its absence at room temperature in NON and STF, but also allow to develop an explanation for the qualitative differences between these systems. The role of the OSDA in influencing the dynamics of the fluoride anions is investigated for MFI-type Silicalite-1. AIMD simulations for Silicalite-1 models containing

different alkylammonium OSDAs show that the introduction of asymmetric organic cations with one short alkyl chain leads to a strong reduction of the fluoride mobility, agreeing with experimental observations. Further analysis shows that the heterogeneous charge distribution of these OSDAs, together with their restricted freedom of movement in the channels, enhances electrostatic interactions with the fluoride anions, reducing the dynamic motion.[3] While the primary aim of the present work is an improved fundamental understanding, similar computational approaches may, in the future, be exploited to aid the targeted synthesis of zeolites in fluoride-containing media.

Acknowledgement
Funding by the Deutsche Forschungsgemeinschaft (DFG project no. 389577027) is gratefully acknowledged.

References

[1] D. S. Wragg, R. E. Morris, A. W. Burton, *Chem. Mater.*, vol. 20, no. 4, pp. 1561–1570, Feb. 2008.
[2] S. L. Brace, P. Wormald, R. J. Darton, *Phys. Chem. Chem. Phys.*, vol. 17, no. 18, pp. 11950–11953, May 2015.
[3] M. Fischer, *J. Phys. Chem. C*, vol. 124, no. 10, pp. 5690–5701, Mar. 2020.

Ab initio structure determination of two new titanium phosphates synthesized via molten salt synthesis.

H. Petersen[1], N. Stegmann[1], M. Fischer[2], B. Zibrowius[1], W. Schmidt[1], M. Etter[3], C. Weidenthaler[1]
[1] Max-Planck-Institut für Kohlenforschung, Heterogeneous Catalysis , Kaiser-Wilhelm-Platz 1, 45470 Mülheim, Germany
[2] University of Bremen, Crystallography/Geosciences, Klagenfurter Straße, 28359 Bremen, Germany
[3] DESY, Notkestraße 85, 22607 Hamburg, Germany

The class of transition metal phosphates (TMPs) shows a wide range of chemical compositions, variations of valence states and respective crystal structures. Among TMPs, $VO(P_2O_7)$ and $LiFePO_4$ are of special interest as the only commercially used heterogeneous catalyst for the selective oxidation of butane to maleic anhydride [1] and cathode material in rechargeable batteries [2]. Due to their structural features, TMP are considered as proton exchange-membranes in fuels cells, working in the intermediate-temperature range [2, 3]. We report on the successful ab initio structure determination of two novel titanium pyrophosphates, $NH_4Ti(III)P_2O_7$ and $Ti(IV)P_2O_7$, from X-ray powder diffraction data. Both compounds were synthesized via a new molten salt synthesis route. The low symmetry space groups $P2_1/c$ ($NH_4TiP_2O_7$) and $P\bar{1}$ (TiP_2O_7) complicate the structure determination, making the combination of spectroscopic, diffraction and computation techniques mandatory. In $NH_4TiP_2O_7$, titanium ions (Ti^{3+}) occupy the TiO_6 polyhedron, coordinated by five pyrophosphate groups, one as a bi-dentate ligand. This secondary coordination causes the formation of one-dimensional six-membered ring channels with a diameter d_{max} of 514(2) pm, stabilized by ammonium ions. Annealing $NH_4TiP_2O_7$ in inert atmospheres results in the formation of the new TiP_2O_7, showing a similar framework consisting of $[P_2O_7]^{4-}$ units and TiO_6 octahedra as well as an empty one-dimensional channel (d_{max} = 628(1) pm). The *in situ* X-ray diffraction study of the transformation of $NH_4TiP_2O_7$ to TiP_2O_7 reveals a two-step mechanism, the decomposition of ammonium ions coupled with the oxidation of Ti^{3+} to Ti^{4+} and a subsequent structural relaxation.

References

[1] Hutchings, G.J., "Vanadium phosphate: a new look at the active components of catalysts for the oxidation of butane to maliec anhydirde," *J. Mater. Chem.*, vol. 14, pp. 3385–3395, 2014.
[2] Jin, Y., Y. Shen, and T. Hibino, "Proton conduction in metal pyrophosphates (MP_2O_7) at intermediate temperatures," *J. Mater. Chem.*, vol. 20, pp. 6214–6217, 2010.
[3] Nalini, V., M.H. Sørby, K. Amezawa, R. Haugsrud, H. Fjellvåg, and T. Norby, "Structure, Water Uptake, and Electrical Conductivity of TiP_2O_7," *J. Am. Ceram. Soc.*, vol. 94, no. 5, pp. 1514–1522, 2011.

Termo- and Photo-induced Spin Crossover in a novel 2x2 iron (II) Grid. Crystallography and Photocrystallography studies

J. Velazquez Garcia[1], K. Basuroy[1], J. Wong[2], D. Storozhuk[1], S. Saouane[3], R. Henning[4], S. Techert[1]
[1] DESY, Photon Science, Structural Dynamics in Chemical Systems, Notkestraße 85, Hamburg, 22607, Germany
[2] Georg-August University of Göttingen, Institut for Inorganic Chemistry, Tammannstraße 4, Göttingen, 37077, Germany
[3] DESY, Photon Science, PETRA III, P11 Beamline, Notkestraße 85, Hamburg, 22607, Germany
[4] University of Chicago, Argonne National Laboratory, Center for Advanced Radiation Sources, 9700 South Cass Ave, Lemont, Illinois 90439, USA

We studied the thermo- and photo-induced phase transition between low spin (LS) and high spin (HS) states of the 2x2 grid-like iron complex: [Fe4L4](BF4)4·C2H3N (FE4), L=4-methyl-3,5-Bis6(2,2′-dipyridyl)pyrazole in

solid state, by using X-ray diffraction techniques. The structural analysis of the coordination geometry of the two crystallographically independent metal atoms at different temperatures demonstrates that the formation of the thermo-induced HS in one atom affects the coordination geometry of the other. The analysis of the photo-induced HS over time do not only exhibit similar structural reorganization as the thermo-induced HS state but also a relaxation from HS to LS in less than one nanosecond. The understanding of photo-switching dynamics and its relation with the thermo-induced HS under systems with strong short-range elastic coupling between small set of metal ions, such as the FE4 system, could allow for new mechanism of energy redistribution after photoexcitation and therefore, the design of new storage and processing devices.

Analyzing Order of Light Anions in LiLa2NH2O by Neutron and X-Ray Powder Diffraction and Spectroscopy

N. Zapp[1], D. Sheptyakov[2], M. Bertmer[1], H. Kohlmann[1]
[1] Leipzig University, Leipzig, Germany
[2] Paul Scherrer Institute, Villigen, Switzerland

Heteroanionic hydrides are an emerging class of compounds with representatives showing hydride ion conductivity [1] or catalytic activity [2]. Their properties are fundamentally linked to their anionic substructure; for example, might a difference between ordered and disordered anions change their behavior from a conducting to an isolating behavior [3].

From the solid-state reaction of Li_2O, LaN and LaH_3, we obtained the new nitride hydride oxide $LiLa_2NH_2O$ as a black powder. It crystallizes in the K_2NiF_4 structure type ($I4/mmm$, a = 3.65431(6) Å, c = 13.3570(3) Å) and can be described as an aliovalent substitution product ($2\ O^{2-} \rightarrow N^{3-} + H^-$) of the hydride ion conductor $LiLa_2HO_3$ [1]. The analysis of the anion substructure demanded the combination of different methods. We therefore performed neutron powder diffraction measurements on both hydride $LiLa_2NH_2O$ and deuteride $LiLa_2ND_2O$ (coherent scattering lengths b_c(H) = -3.7 fm, b_c(D) = 6.7 fm) in addition to powder X-ray diffraction and nuclear magnetic resonance spectroscopic analysis.

H/D and N/O show a separation on two crystallographic sites 4*d* and 4*e* with only slight but significant mixing. Additionally, both sites are significantly underoccupied, resulting in a charge imbalanced composition. H/D occupies favorably the Li-rich site 4*d*, while N and O share the La-rich 4*e* position (Figure 1). Both sites are coordinated in a distorted octahedral fashion with Li situated on opposite vertices of the H-rich polyhedron with short Li-H distances (1.83 Å; LiH: 2.04 Å).

References

[1] G. Kobayashi *et al.*, *Science* **2016**, *351*, 1314-7.
[2] M. Kitano *et al.*, *J. Am. Chem. Soc.* **2019**, *141*, 20344-53.
[3] H. Nawaz *et al.*, *Chem. Commun.* **2020**, *56*, 10373-6.

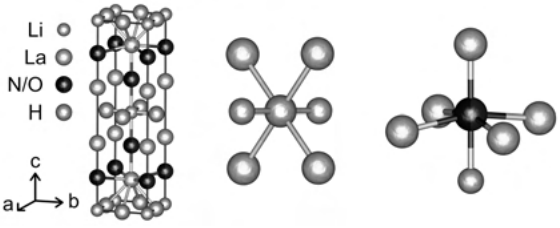

Figure 1

In situ / in operando studies

Insitu X-ray analysis of misfit strain and curvature of bent polytypic InxGa1-xAs/GaAs core/shell nanowires

M. Al-Humaidi[1], J. Feigl[2], J. Jakob[2], P. Schroth[2], A. AlHassan[1], A. Davtyan[1], J. Herranz[3], A. Tahraoui[3], D. Novikov[4], T. Baumbach[2], L. Geelhaar[3], U. Pietsch[1]
[1] Solid State Physics, University of Siegen, Siegen, Germany
[2] Institute for Photon Science and Synchrotron Radiation, Karlsruhe Institute of Technology, Karlsruhe, Germany
[3] Paul Drude Institut für Festkorperelektronik, Leibniz Institut im Forschungsverbund Berlin, Berlin, Germany
[4] DESY, HASYLAB, Hamburg, Germany

Misfit strain in crystalline core-shell nanowires can be elastically released by nanowire curvature in case of inhomogeneous shell growth around the nanowires [1]. In this work, we performed time-resolved in-situ XRD investigations of the evolution of GaAs nanowires bending during the asymmetric growth of InxGa1-xAs shell without substrate rotation. By means of micro X-ray beam at beamline P23 and P09 at PETRA-III at DESY and a portable molecular beam epitaxy chamber (pMBE) [2], this study gives insight into the temporal development of the bending as well as the strain in the core-shell nanowire. In particular, different bending directions of nanowires grown on Si with native oxide and thermal oxide were observed and the demonstration of the nanowire curvature as function of shell thickness showed nonlinear dependency.

References
[1] Lewis R B, Corfdir P, Küpers H, Flissikowski T, Brandt O and Geelhaar L 2018, Nano Lett. 18 2343–50
[2] Slobodskyy T, Schroth P, Grigoriev D, Minkevich A A, Hu D Z, Schaadt D M and Baumbach T 2012, Review of Scientific Instruments vol 83

Observing the oxidation of platinum under operando electrochemical conditions

L. Jacobse[1], R. Schuster[2], X. Deng[1], S. Dolling[1], T. Weber[3], H. Over[3], J. Libuda[2], V. Vonk[1], A. Stierle[1]
[1] Deutsches Elektronen-Synchrotron (DESY), FS-NL (Nanolab), Hamburg, Germany
[2] Interface Research and Catalysis, Friedrich-Alexander-Universität Erlangen-Nürnberg, Erlangen, Germany
[3] Physikalisch-Chemisches Institut and Zentrum für Materialforschung, Justus Liebig University, Giessen, Germany

Platinum electrocatalyst degradation forms a large barrier for the wide-spread application of electrolysers and fuel cells, which are crucial for a sustainable energy society. A detailed understanding of the catalyst surface structure during the chemical reaction is required to design more stable catalysts. We have developed a Rotating Disk Electrode (RDE) setup that enables a structural characterization by synchrotron High-Energy Surface X-Ray Diffraction (HE-SXRD) experiments while maintaining well-defined diffusion conditions and high catalytic reaction rates (current densities). With this setup we followed the oxidation of Pt(111) and Pt(100) model electrodes, from the Place-Exchange surface oxidation occurring around 1.1 V until the formation of a (bulk) oxide at potentials relevant for the oxygen evolution reaction. In contrast with heterogenous oxidation experiments, no ordered oxide structures are observed.

Tracking the facet-resolved strain state of a PtRh nanoparticle under catalytic reaction conditions

Y. Y. Kim[1], T. F. Keller[1], T. J. Goncalves[3], M. Abuin[1], H. Runge[1], L. Gelisio[1], J. Carnis[1], V. Vonk[1], P. N. Plessow[2], I. Vartaniants[1], A. Stierle[1]
[1] Deutsches Elektronen-Synchrotron (DESY), Hamburg, Germany
[2] Institute of Catalysis Research and Technology, Karlsruhe Institute of Technology, D-76344 Eggenstein-Leopoldshafen, Germany

Oxide-supported nanoparticles are important heterogeneous catalysts. The nanoparticles shapes and type of facets are decisive for the catalyst activity and lifetime. During a catalytic reaction, the nanoparticle may be subject to shape changes, and segregation in alloys may adjust the termination of the surface to a changing gas environment.

Here we report on the evolution of the 3D strain state in a single alloy PtRh nanoparticle operando followed by coherent X-ray diffraction imaging (CXDI). At a temperature of T=700 K the nanoparticle environment was switched between the gas compositions (I) inert Ar, (II) CO+Ar, (III) CO+O_2+Ar and (IV) CO+Ar resembling different adsorption and catalytic reaction scenarios on the nanoparticle surface.

$SrTiO_3$ supported nanoparticles were grown by co-deposition of Pt and Rh and annealed in UHV to induce the equilibrium shape. A single nanoparticle was pre-selected in an SEM and subsequently, hierarchical Pt fiducial markers were deposited in the vicinity of the selected nanoparticle and used to re-locate the same particle in the X-ray beam.

The nanoparticle exhibited solely low index <100> and <111> type facet surfaces, intriguingly showing distinct, facet-family specific strain states. Under the catalytic reaction condition (III) we observed significant strain relaxations for all facets accompanied with a preferential segregation of Rh to the nanoparticle surface, in line with density functional theory calculations (DFT). The Rh enrichment on the facets turned out to be non-reversible under the subsequent CO reduction condition (IV) as compared to the identical previous gas condition (II).

Tracking the dynamics of facet-specific structural reorganizations of the nanoparticle is one key for the future design of heterogeneous catalysts with optimized efficiency and selectivity.

Crystallization pathway control of $Bi_2Fe_4O_9$ studied by in situ Pair Distribution Function analysis

A. Kirsch[1], N. Lefeld[2], M. Gogolin[2], S. Banerjee[3], K. Jensen[1]
[1] University of Copenhagen, 2100 Copenhagen, Denmark
[2] Universität Bremen, Bremen, Germany
[3] PETRA III, Deutsches Elektronen-Synchrotron (DESY), Hamburg, Germany

The targeted control of particle/crystallite size, crystallinity, and polymorphism is of crucial importance for many functional materials, in particular quantum materials[1]. They are frequently synthesized by the facile sol-gel method which in a broader sense can be described as the conversion of molecular precursors in solution into inorganic solids via hydrolysis, condensation, and aggregation[2]. The synthesis of pure nanocrystalline samples, however, can be very difficult if various stable and metastable phases exist often leading to co-crystallization. In this study, we use *in situ* total scattering and Pair Distribution Function (PDF) analysis to follow the

transformation of molecular precursors into multiferroic $Bi_2Fe_4O_9$ with a second-scale time resolution. The precursors were synthesized by the sol-gel process using the respective metal nitrates and meso-erythritol as the complexing agent. We show how the crystallization pathways and kinetics of the target compound can dramatically be changed by variation of the synthesis medium and ratio of metal nitrate to the complexing agent and relate this to the precursor structure. As an example, using small amounts of complexing agent leads to a crystalline precursor which first gets amorphous at 613 K, crystallizes into $BiFeO_3$ at 706 K, and subsequently transforms into $Bi_2Fe_4O_9$ at 815 K. On the other hand, bigger amounts of complexing agent produce an amorphous precursor which directly crystallizes into $Bi_2Fe_4O_9$ at 762 K. Using PDF we reveal the importance of the initial gel structure in the overall crystallization behaviour of the system.

References

[1] Samarth, N. *Nat. Mater.*, 2017, 16, 1068.
[2] Niederberger, *M. Acc. Chem. Res.*, 2007, 40, 793.

Stabilization mechanisms of pure tetragonal zirconia nanocrystallites using an original supercritical-based synthesis route

G. Philippot[1], A. Auxemery[2], D. Testemale[3], B. Iversen[4], C. Aymonier[2]

[1] University of Bordeaux, Bordeaux, France

[2] CNRS, ICMCB, Pessac, France

[3] Institut Neel, Grenoble, France

[4] Aarhus University, Aarhus, Denmark

Zirconium dioxide (ZrO2) has been of major industrial and scientific interest over the past decades for its wide range of applications, in particular thanks to its catalytic properties. Regardless the multiple synthesis routes employed, undoped bulk ZrO2 is stabilized in the monoclinic structure (m-ZrO2) at ambient temperature and atmospheric pressure. However, these last years, studies showed that it was also possible to stabilize pure t-ZrO2 without cationic substitution. To do so, three main effects are identified in the literature: (i) the presence of oxygen vacancies, (ii) the existence of structural similarities, and (iii) the size effect, with the existence of a critical size below which pure t-ZrO2 is formed.

In this presentation we will introduce the synthesis of quasi pure t-ZrO2 nanocrystals in supercritical fluids using borderline nonhydrolytic sol-gel (B.N.H.S.G.) conditions. The term borderline is used to express the nuance from nonhydrolytic sol-gel (N.H.S.G.) reactions when small amounts of water molecules are generated in situ from solvent (alcohols) decomposition to trigger hydrolysis/condensation. This amount of water being controlled, the reaction kinetics can be tuned and slow down. This enabled us to performed in situ total scattering measurements in order to catch the various stages of the nanocrystal formation upon various conditions (temperature, nature of the alcohols and presence of surfactants). These observations where combined to various ex situ characterizations (Raman, PDF, EXAFS, HR-TEM, XRD, etc.) to discuss the existence of a critical size below which pure t-ZrO2 is formed, as reported in literature and propose a formation mechanism in this specific synthesis route.

Selective in-situ exsolution of catalytically active metals from doped perovskites during methane dry reforming

F. Schrenk[1], L. Lindenthal[1], D. Hedda[1], R. Rameshan[1], C. Rameshan[1]

[1] TU Wien, Institute of Materials Chemistry, Vienna, Austria

Perovskite type oxides, doped with catalytically active metals, have shown great potential to catalyse MDR (Methane Dry Reforming) [1]. These materials can undergo exsolution, the formation of metallic nanoparticles on the surface, of B-site elements if reducing conditions are applied [2]. These exsolved nanoparticles are leading to an increase in catalytic activity. A Ni-doped perovskite (Nd0.6Ca0.4Fe0.97Ni0.03O3) and a Co-doped perovskite (Nd0.6Ca0.4Fe0.9Co0.1O3) were investigated in MDR conditions with a CH4 excess of 2:1 over CO2. To investigate the changes the catalyst undergoes during the reaction *in situ* NAP XPS (Near Ambient Pressure X-ray Photoelectron Spectroscopy) as well as *in situ* XRD (X-Ray Diffraction) experiments were performed. The XRD data showed the formation of a bcc phase at higher temperatures which cannot be assigned to Fe or the dopant (Ni/Co) due to the bad signal to noise ratio (Figure 1). The XPS data reveals that Ni is exsolving before Fe, as the Ni2p signal is shifting from the oxidized state into a metallic state between 600 °C and 650 °C and the Fe2p signal does not show a metallic component even at 700 °C, as seen in Figure 2. For the Co-doped catalyst, the formation of a metallic Co component was observed while no metallic Fe was detected.

References

[1] D. Pakhare and J. Spivey, "A review of dry (CO2) reforming of methane over noble metal catalysts," *Chem. Soc. Rev.*, vol. 43, no. 22, pp. 7813-7837, Nov. 2014, doi: 10.1039/c3cs60395d.

[2] L. Lindenthal et al., "Modifying the Surface Structure of Perovskite-Based Catalysts by Nanoparticle Exsolution," *Catalysts*, vol. 10, no. 3, Mar. 2020, Art no. 268, doi: 10.3390/catal10030268.

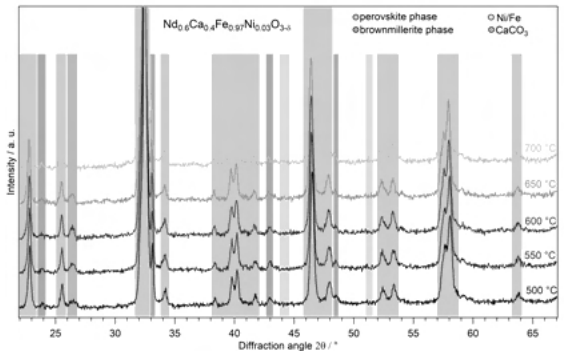

Figure 1 In-situ XRD diffractograms of the Ni-doped catalyst with a CH4:CO2 ratio of 2:1 and temperature steps from 500 °C to 700 °C. The phases observed could be assigned to a perovskite phase (blue) as well as a brownmillerite phase with ordered oxygen vacancies (grey) during all temperatures. Forming at higher temperatures a CaCO3 (violet) and a bcc Phase, stemming ether from Ni or Fe (green), could be detected.

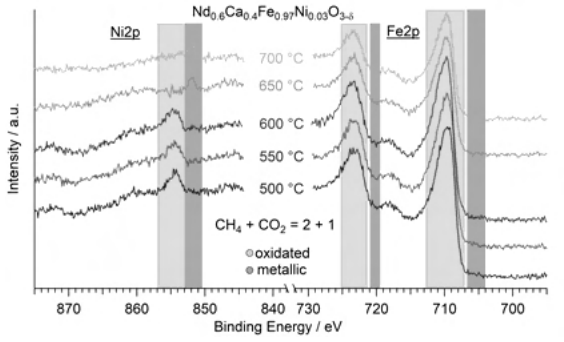

Figure 2 Comparison of the Fe2p and Ni2p transitions in the in-situ NAP XPS experiment of the Ni-doped catalyst. The sample was oxidized at 1 mbar O2 before the reaction, afterwards an atmosphere of 1 mbar CH4 and CO2 in a ratio of 2:1 was set and temperature steps between 500 °C and 700 °C were performed. A metallic component (blue) is forming between 600°C and 650 °C for Ni, whereas the Fe transition does not so such a component even at 700 °C.

Homoepitaxial growth of magnetite (Fe_3O_4) (001)

S. Tober[1], M. Creutzburg[1], B. Arndt[2], S. Chung[1], L. Jacobse[1], A. Vlad[3], A. Resta[3], H. Noei[1], V. Vonk[1], A. Stierle[1]
[1] Deutsches Elektronen-Synchrotron (DESY), FS-NL (Nanolab), Hamburg, Germany
[2] DESY, Hamburg, Germany
[3] Synchrotron SOLEIL, Synchrotron SOLEIL, Saint-Aubin, Essonne, France

The performance of magnetite-based devices and catalysts crucially depends on their surface structure and stoichiometry [1]. While annealing in ultra high vacuum and the adsorption of small molecules (partially) lift the subsurface cation vacancy reconstruction on Fe_3O_4 (001) surfaces [3,4,5], annealing under oxidising conditions results in the growth of new Fe_3O_4 layers involving near-surface cation transport [6].

To study the influence of O_2 pressure on cation transport in the Fe_3O_4 near-surface region, the homoepitaxial growth of Fe_3O_4 by molecular beam epitaxy was observed in-situ by surface X-ray diffraction (SXRD) at different pressures and growth rates.

Details about the grown structures and the growth process obtained from crystal truncation rods and X-ray intensity growth oscillations will be complemented by low energy electron diffraction and X-ray reflectivity data. These results will be presented in relation with their implications for cation transport in Fe_3O_4 [7].

References

[1] Parkinson, G., Surf. Sc. Rep. 71, 272 (2016)
[2] Bliem, R. et al., Science 346, 1215 (2014)
[3] Arndt, B. et al., Chem. Comm. 1, 92 (2019)
[4] Arndt, B. et al., Surf. Sci. 653, 76 (2016)
[5] Arndt, B. et al., PCCP 22, 8336 (2020);
[6] Nie, S. et al., J. Am. Chem. Soc. 135, 10091 (2013),
[7] Dieckmann, R. et al., Ber. Bunsenges. Phys. Chem. 81, 344 (1977)

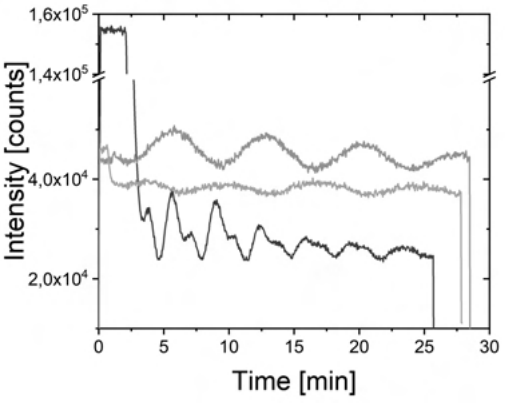

Figure 1. Growth oscillations observed by SXRD at (4 0 1.97) (blue), (4 0 1) (green) and (2 2 0.97) (yellow) indicating a layer by layer growth of half unit cells. Growth at 4×10^{-6} mbar O_2 and a flux of 30 nA.

Understanding thermal exfoliation of h-BN using in situ X-ray diffraction

Z. Yan[1], A. Abdelkader[2], W. Mirihanage[1]

[1] University of Manchester, Manchester M13 9PL, United Kingdom

[2] Bournemouth University, Poole BH12 5BB, United Kingdom

2D materials are considered as unique class of modern materials. Understanding the mechanisms behind the exfoliation processes enables us to significantly enhance processing potential of 2D materials. In-situ synchrotron X-ray characterization is employed to study the temporal changes of hexagonal-boron nitride (h-BN) while its initial processing from bulk 3D crystalline material towards its 2D counterpart. In situ X-ray powder diffraction (XPDF) experiment is conducted with thermal cycle that heating bulk h-BN up to 1273 K and subsequent cooling. The results show a linear expansion in c-axis direction of h-BN crystals as commonly understanding, however a contraction behaviour in a-axis direction is observed up to around 750 K during heating process, followed by an expansion behaviour when temperature over 750 K. Characterization particularly indicates structural changes of long-range order favourable for exfoliation between the range of 750 K to 950 K. With the consideration of thermal oxidation studies also, a hypothesis of thermal assisted exfoliation with oxygen interstitial and substitution of nitrogen at high temperature is proposed through our studies to drive the exfoliation mechanisms.

Micro and nano-crystalline materials

Morphology and growth behavior of Cu nanoparticles on the vicinal ZnO(10-14) surface

R. Gleissner[1], H. Noei[1], V. Vonk[1], S. Chung[1], G. Semione Dalla Lana[1], E. E. Beck[1], G. Gizer[2], A. Stierle[1]

[1] DESY, Photon Science, FS-NL (Nanolab), Hamburg, Germany

[2] Helmholtz-Zentrum Geesthacht, Hamburg, Germany

The ZnO(10-14) surface raised recent scientific interest for its outstanding stability despite its high indexed orientation, which results in a stepped mixed-terminated surface.[1] In this study, copper nanoparticles were grown via physical vapor deposition onto a ZnO(10-14) single crystalline surface and the structure and morphology was investigated using low energy electron diffraction, high energy grazing incidence x-ray diffraction, scanning electron microscopy and scanning tunneling microscopy.

Caused by anisotropic diffusion, elongated Cu particles are formed parallel to the surface steps of the substrate. They show a unique tilt of their (111) planes parallel to the (0001) terraces of the vicinal surface. This causes the generation of large, high indexed Cu facets in which their atomic steps could act as reaction sites in catalytic reactions such as methanol synthesis and CO2 activation.

Self assembled monolayer of silica nanoparticles with improved order by drop casting

A. Qdemat[1], E. Kentzinger[2], J. Buitenhuis[2], U. Rücker[2], M. Ganeva[3], T. Brückel[2]

[1] Forschungszentrum Jülich, Jülich Centre for Neutron Science JCNS and Peter Grünberg Institut PGI Quantum Materials and Collective Phenomena, Jülich, Germany

[2] Forschungszentrum Jülich, Institute of Biomacromolecular Systems and Processes (IBI-4), Jülich, Germany

[3] Forschungszentrum Jülich, JCNS outstation @ MLZ Garching, Garching, Germany

Assembly of NPs into large-area monolayers on a solid substrate is fundamentallyinteresting due to their unique optical and electronic properties. Furthermore, they have an impact on the creation of next-generation materials design [1] and for new devices that require monolayers with ordered structure over large areas formed with a simple method at low cost to meet the growing industrial needs. But controlling the deposition on a substrate to obtain two-dimensional and three-dimensional nanoparticle arrays is a complex process, and it occurs under specific conditions.

In this contribution, we report on the formation of large area, self assembled, highly ordered monolayers of stearyl alcohol grafted silica nanospheres of 50 nm diameter on a silicon substrate based on the drop-casting method. Our novel approach to achieve improved order uses stearyl alcohol as an assistant by adding it to the colloidal NanoParticle (NP) dispersion from which the monolayers are formed. Additionally, a heat treatment step is added, to melt the stearyl alcohol in the monolayer and thereby give the particles more time to further selfassemble, leading to additional improvement in the monolayer quality. The formation of the monolayers is significantly affected by the concentration of the NPs and the stearyl alcohol, the volume of the drop as well as the time of the heat treatment. A high surface coverage and uniform monolayer film of SiO2 NPs is achieved by appropriate control of the abovementioned preparation parameters. Structural characterization of the obtained SiO2 NP monolayer was done locally by Scanning Elec-

tron Microscopy (SEM), and globally by X-ray reflectivity (XRR) and grazing incidence small-angle X-ray scattering (GISAXS), where the data was reproduced by simulation within the Distorted Wave Born Approximation (DWBA) [2]. In conclusion, our modified drop-casting method is a simple, inexpensive method, which provides highly ordered self-assembled monolayers of silica particles, if combined with a compatible additive and a heat treatment step. This method might be more general and applicable to improve the ordering between different particles in monolayers as well as multilayers after finding an appropriate additive [3].

References

[1] M. A. Boles, M. Engel and D. V. Talapin, *Chem. Rev.*, vol. 116, pp. 11220–11289, 2016.
[2] G. Pospelov, W. Van Herck, J. Burle, J. M. Carmona Loaiza, C. Durniak, J. M. Fisher, M. Ganeva, D. Yurov and J. Wuttke, *J. Appl. Crystallogr.*, vol. 53, pp. 1600–5767, 2020.
[3] A. Qdemat, E. Kentzinger, J. Buitenhuis, U. Rücker, M. Ganeva and T. Brückel, *RSC Adv.*, vol. 10, pp. 18339–18347, 2020.

Crystal structure and lattice dynamics of endotaxial $FeSi_2$ nanowires

J. Kalt[1], M. Sternik[2], B. Krause[1], I. Sergueev[3], M. Mikolasek[4], D. G. Merkel[5], D. Bessas[4], O. Sikora[2], T. Vitova[1], J. Göttlicher[1], R. Steininger[1], P. Jochym[2], A. Ptok[2], O. Leupold[3], H.-C. Wille[6], A. Chumakov[4], P. Piekarz[2], K. Parlinski[2], T. Baumbach[1], S. Stankov[1]
[1] Karlsruhe Institute of Technology, Karlsruhe Germany
[2] Polish Academy of Sciences, Poland
[3] Deutsches Elektronen-Synchrotron, Hamburg Germany
[4] ESRF – The European Synchrotron, Grenoble France
[5] Hungarian Academy of Sciences, Hungary
[6] XFEL-User (XFEL-User), Hamburg,Germany

Metallic silicides constitute an important part of current microelectronics, serving as Schottky barriers and ohmic contacts, gate electrodes, local interconnects, and diffusion barriers [1–3]. Silicide nanowires, self-organized on the Si(110) surface, are considered as building blocks of future nanoelectronics and have been intensively investigated [4]. However, the reports about their crystal structure remain contradictory, spanning cubic (s or γ) [5–7] and tetragonal (α) [8] phases. Furthermore, in nanostructures the lattice vibrational waves (phonons) deviate drastically from those in bulk crystals, giving rise to anomalies in thermodynamic, elastic, electronic, and magnetic properties. Hence, a thorough understanding of the physical properties of these materials requires a comprehensive investigation of the crystal structure and lattice dynamics as a function of the nanowire size.

Using extended x-ray absorption fine structure (EXAFS) spectroscopy and nuclear inelastic scattering (NIS) we performed a systematic study of the crystal structure and the lattice dynamics of endotaxial $FeSi_2$ nanowires, which are in-plane embedded into the Si(110) surface. The EXAFS results unveiled the formation of the metastable, surface-stabilized α phase. The Fe-partial phonon density of states, obtained by the NIS experiment, exhibits a broadening of the spectral features with decreasing nanowire width and a pronounced vibrational anisotropy that originates from the specific orientation of the tetragonal α-$FeSi_2$ unit cell on the Si(110) surface. The results from first-principles calculations are fully consistent with the experimental observations [9].

References

[1] S.P. Murarka, Intermetallics 3, 173 (1995).
[2] L. J. Chen, Silicide Technology for Integrated Circuits (Institution of Electrical Engineers, London, 2004).
[3] L.J. Chen, JOM 57, 24 (2005).
[4] P.A. Bennett et al., Thin Solid Films 519, 8434 (2011).
[5] S. Liang et al., Appl. Phys. Lett. 88, 113111 (2006).
[6] S. Liang et al., J. Cryst. Growth 295, 166 (2006).
[7] D. Das et al., Appl. Phys. Lett. 105, 191606 (2014).
[8] Z.-Q. Zou et al., Appl. Surf. Sci. 399, 200 (2017).
[9] J. Kalt et al., Phys. Rev. B 102, 195414 (2020).

Scattering is a powerful tool to follow nucleation and growth of minerals from solutions

T. Stawski[1], A. E. S. Van Driessche[2]
[1] Federeal Institute for Material Research and Testing, Berlin, Germany
[2] Grenoble Alpes University, University Savoie Mont Blanc, CNRS, IRD, IFSTTAR, ISTerre, 38000 Grenoble, France

In recent years, we have come to appreciate the astounding intricacy of the formation process of minerals from ions in aqueous solutions. The original 'textbook' image of these phenomena, stemming from the adaptation of classical nucleation and growth theories, has increased in complexity due to the discovery of a variety of precursor and intermediate species [e.g. 1], including solute clusters (e.g. prenucleation clusters, PNCs), liquid(-like) phases, as well as amorphous and nanocrystalline solids etc. In general, these precursor or intermediate species constitute different, often short-lived, points along the pathway from dissolved ions to the final solids (typically crystals in

this context). In this regard synchrotron-based scattering (SAXS/WAXS/HEXD) appears to be the perfect tool to follow in situ and in a time-resolved manner the crystallization pathways because of the temporal and spatial length scales that can be directly accessed with these techniques. Here, we show how we used scattering to probe the crystallization mechanisms of calcium sulfate. CaSO4 minerals (i.e. gypsum, anhydrite and bassanite) are widespread in natural and industrial environments. During the last several years, a number of studies have revealed indeed that nucleation in the CaSO4-H2O system is non-classical. Our SAXS data demonstrate that gypsum precipitation, involves formation and aggregation of sub-3 nm primary species. These species constitute building blocks of an amorphous precursor phase [2]. Further, we show how in situ high-energy X-ray diffraction experiments and molecular dynamics (MD) simulations can be combined to derive the atomic structure of the primary CaSO4 clusters seen at small-angles [3]. We fitted several plausible structures to the derived pair distribution functions and explored their dynamic properties using unbiased MD simulations based on polarizable force fields. Finally, based on combined SAXS/WAXS, broad-q-range measurements, we show that the process of formation of bassanite, a less hydrated form of CaSO4, is very similar to the formation of gypsum: it also involves the aggregation of small primary species into larger disordered aggregates [4]. Based on these recent insights we formulated a tentative general model for calcium sulfate precipitation from solution. This model involves primary species that are formed through the assembly of multiple Ca2+ and SO42- ions into nanoclusters. These nanoclusters assemble into poorly ordered (i.e. amorphous) hydrated aggregates, which in turn undergo ordering into coherent crystalline units of either gypsum or bassanite (and possibly anhydrite). Determination of the structure and (meta)stability of the primary species is important from both a fundamental, e.g. establishing a general non-classical nucleation model, and applied perspective; e.g. allow for an improved design of additives for greater control of the nucleation pathway.

References

[1] J.J. De Yoreo, P.U.P.A. Gilbert, N.A.J.M. Sommerdijk, R. L. Penn, S. Whitelam, D. Joester, H. Zhang, J. D. Rimer, A. Navrotsky, J. F. Banfield *et al.*, *Science*, vol. 349, 2015, Art. no. aaa6760.

[2] T.M. Stawski, A.E.S. van Driessche, M. Ossorio, J. Diego Rodriguez-Blanco, R. Besselink, L.G. Benning, *Nat. Commun.*, vol. 7, p. 11177, 2016.

[3] T.M. Stawski, A.E.S. Van Driessche, R. Besselink, E.H. Byrne, P. Raiteri, J.D. Gale, L.G. Benning, *J. Phys. Chem. C*, vol. 123, no. 37, 2019.

[4] T.M. Stawski, R. Besselink, K. Chatzipanagis, J. Ho¨velmann, L.G. Benning, A.E.S. Van Driessche, *J. Phys. Chem. C*, vol. 124, no. 15, 2020.

Organic and metal-organic crystal structures

Lattice energies of all known Crystal Structures

D. W. Hofmann[1], L. Kuleshova[1]

[1] CRS4, Pula, Italy

We calculated the Gibb's energy of all known organic and organometallic crystal structures at ambient conditions with FlexCryst [1]. Firstly, the implemented data mining force field was validated for the experimental lattice energies of the reference structures. Secondly, the force field was used for the minimization of 100 structures and the error in density and energy was examined. Finally, the Gibb's energy was calculated for all structures. After applying different filters and cleanser did remain 247 344 crystal structures.

In our analysis of the results we concentrated on crystal structures with a Gibbs energy above zero. Obviously these structures violates the second law of thermodynamics. A visualization of the intermolecular interactions did allow us to indicate poor intermolecular potentials and faulty crystal structures. The condition is fulfilled in 96.7 % of structures.

The data mining force field is integrated in the FlexCryst program suite and we tested it crystal structure prediction and in combination with XPRD for crystal structure determination. Since the obtained energies are Gibb's energies, the energies can be used to predict reactions at ambient conditions, for instance solubility [2], co-crystal formation [3], or polymorphism.

References

[1] Hofmann, Detlef WM., "Data mining in organic crystallography," in *Data Mining in Crystallography*, Berlin, Heidelberg, Germany: Springer, 2009, pp. 89–134.

[2] Hofmann, Detlef Walter Maria, and Ludmila Kuleshova, "New similarity index for crystal structure determination from X-ray powder diagrams," *J. Appl. Crystallogr*, vol. 38, no. 6, pp. 861–866, 2005.

[3] Stepanovs, Dmitrijs *et al.*, "Cocrystals of pentoxifylline: In silico and experimental screening," *Cryst. Growth Des.*, vol. 15, no. 8, pp. 3652–3660, 2015.

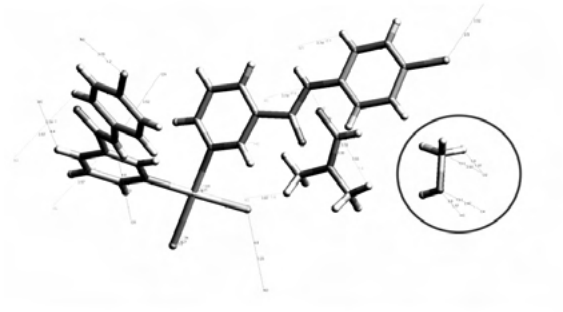

Figure 1 The hydrate of the ruthenium complex (CSD reference code: AMUPUU) show strong repulsive interactions between two water molecules. It indicates that water should be placed different in the correct structure.

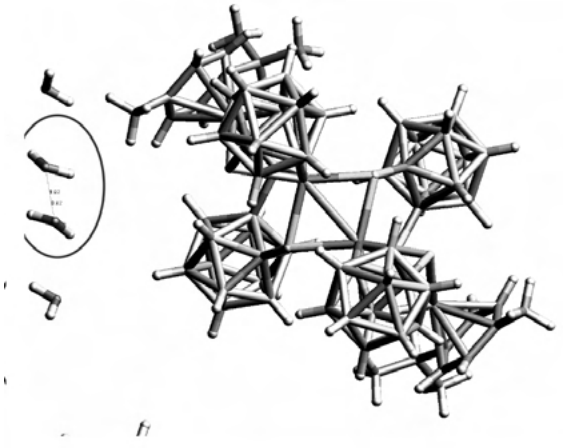

Figure 2 The co-crystal (CSD reference code: ALARAH) of a platinum complex with methanol show strong repulsive interactions between methanol and it image. It indicates that methanol should be placed different in the correct structure.

Chaperone Compounds for Co-crystallization of Organics

T. Stuerzer[1], M. Adam[1], W. Frey[1], F. Krupp[1], F. Rami[1], C. Richert[1]

[1] MA: Bruker AXS GmbH, Karlsruhe, Germany

Modern instrumentation and processing techniques for single crystal X-ray diffraction enable high-quality 3D structure analysis – including absolute structure determination – often in less than an hour, faster and more comprehensively than many spectroscopic methods can even start to achieve. However, large numbers of small or highly flexible organic molecules remain intractable to even the most sophisticated crystallization methods. Our new set of chemical chaperones for co-crystallization [1] offers a new alternative to other methods, such as the crystal-sponge approach [2], [3], can significantly increase the probability of successful crystallization and provides faster access to the absolute 3D structure of an organic analyte:

- The chaperone method is fast and easy to use
- Structures in hours rather than weeks
- Small quantities of analyte required
- Excellent quality crystals
- 88% diffraction-quality crystals from a 52 organic compounds test screen
- The chaperone compounds are highly stable
- 100% analyte occupancy in the crystal guarantees reliable determination of the absolute configuration.

We will discuss and demonstrate the features in detail along the diastereomers of Limonene including a demonstration of the crystal growth.

References

[1] Richert *et al.*, *Angew. Chem. Int. Ed.*, vol. 59, pp. 15875–15879, 2020, doi: 10.1002/anie.202004992.

[2] Fujita *et al.*, *IUCrJ*, vol. 3, pp. 139–151, 2016, doi: 10.1107/S2052252515024379.

[3] Clardy *et al.*, *Acta Cryst. A*, vol. 71, pp. 46–58, 2015, doi: 10.1107/S2053273314019573.

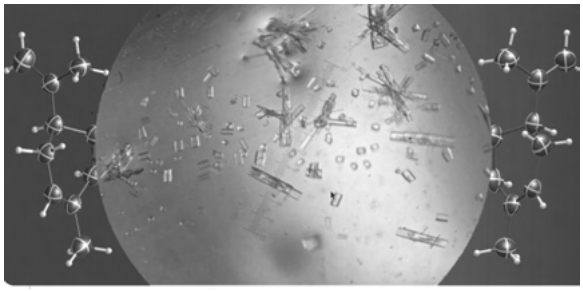

Figure 1

Quantum crystallography

Relativistic Hirshfeld atom refinement of an organo-gold(I) compound

S. Pawlędzio[1], M. Malinska[1], M. Woińska[1], J. Wojciechowski[2], L. A. Malaspina[3], F. Kleemiss[3], S. Grabowsky[3], K. Woźniak[1]

[1] Biological and Chemical Research Centre, Department of Chemistry, University of Warsaw, Warsaw, Poland

[2] Rigaku Europe SE, Neu-Isenburg, Germany
[3] University of Bern, Department of Chemistry and Biochemistry, Bern, Switzerland

During the last 50 years, relativistic quantum chemistry has undergone significant developments and methodological progress. Nowadays, it is well-known that a relativistic quantum formalism is necessary for the study of compounds with heavy elements [1-3].

Within last years it has appeared that quantum crystallography is a very prospective method of refinement of crystal structures. It relies on the high-resolution and high-quality XRD data to describe crystal structure in unprecedented details [4-5]. Intensities of the diffracted beam are affected not only by relativistic effects but also by many other effects such as absorption [6], anharmonic motion [7], anomalous dispersion [8], and others effects which significantly influence electron density distribution in the crystal and, in consequence, derived properties.

In this study, we validated relativistic Hirshfeld atom refinement (HAR) [9] as implemented in Tonto [10] by performing refinement of experimental high-resolution X-ray diffraction data for an organo-gold(I) compound. The influence of relativistic effects on statistical parameters, geometries and electron density properties was analyzed and compared to the influence of electron correlation and anharmonic atomic motions.

Acknowledgement
Support of this work by the National Science Centre, Poland through grant PRELUDIUM no. UMO-2018/31/N/ST4/02141 is gratefully acknowledged. The experiment was carried out at the Spring-8 with the approval of the Japan Synchrotron Radiation research Institute (Proposal Number 2019A1069).

References

[1] I. P. Grant, Advances in Physics, 1970, 19, 747–811.
[2] J. P. Desclaux, Atomic Data and Nuclear Data Tables, 1973, 12, 311–406.
[3] T. Ziegler, J. G. Snijders and E. J. Baerends, The Journal of Chemical Physics, 1998, 74, 1271.
[4] L. J. Farrugia, C. Evans, D. Lentz and M. Roemer, Journal of the American Chemical Society, 2009, 131, 1251–1268.
[5] T. S. Koritsanszky and P. Coppens, Chem. Rev., 2001, 101, 1583–1628.
[6] J. Als-Nielsen and D. McMorrow, in Elements of Modern X-ray Physics, John Wiley & Sons, Ltd, 2011, pp. 1–28.
[7] R. Herbst-Irmer, J. Henn, J. J. Holstein, C. B. Hübschle, B. Dittrich, D. Stern, D. Kratzert and D. Stalke, The Journal of Physical Chemistry A, 2013, 117, 633–641.
[8] S. Caticha-Ellis, Anomalous dispersion of x-rays in crystallography, University College Cardiff Press, Cardiff, Wales, 1981.
[9] L. Bučinský, D. Jayatilaka and S. Grabowsky, The Journal of Physical Chemistry A, 2016, 120, 6650–6669.
[10] D. Jayatilaka and D. J. Grimwood, Acta Crystallographica Section A, 2001, 57, 76–86.

Spectroscopy

MagStREXS: A crystallograhic software for magnetic structure determination from resonant magnetic X-ray diffraction data

P. J. Bereciartua[1], J. Rodríguez-Carvajal[2], S. Francoual[1]
[1] DESY, Photon Science, FS-PETRA-S, Beamline P09, Hamburg, Germany
[2] Institut Laue-Langevin, Grenoble, France

Resonant X-ray elastic scattering (REXS) is a unique element, site, and valence specific probe to study the charge, spin and orbital degrees of freedom and multipole orders in solids and thin films [1,2]. This technique, which combines X-ray diffraction with X-ray absorption spectroscopy, has been successful in unraveling different order parameters and solving magnetic structures.

REXS is complementary to neutron techniques for magnetic structure determination. Several situations make it essential: when the magnetic species involved present a neutron absorption cross-section too large, like Eu, Dy, Gd... [3], when the magnetic moments cannot be determined unambiguously with neutron experiments [4], or when more than one magnetic species is involved.

Different types of data can be collected during a REXS experiments: intensities of a set of magnetic reflections, full linear polarization analysis of a specific magnetic reflection, or its azimuthal dependence. The analysis of these data is highly complex and no crystallographic software has been developed yet to enable users to solve magnetic structures from a REXS experiment.

MagStREXS is a crystallographic software dedicated to the determination of **Mag**-netic **St**-ructures through **R**-esonant **E**-lastic **X**-ray **S**-cattering and the preparation of magnetic diffraction experiments. It is under development since mid-2017 at beamline P09 [5] at PETRA III

at DESY and based on CrysFML, a library developed to facilitate the creation of crystallographic software that includes some resources especially oriented to deal with magnetic structures.

Hereby, we will present an overview of MagStREXS, its current status and some of the magnetic structures which have already been solved with it in the field of highly correlated systems.

References

[1] J. P. Hill and D. F. Mc Morrow, *Acta Cryst. A*, vol. 52, pp. 236–244, 1996.

[2] Y. Murakami and S. Ishihara, *Resonant X-Ray Scattering in Correlated Systems* in Springer Tracts in Modern Physics, vol. 269, Berlin, Heidelberg, Germany: Springer, 2017.

[3] T. Kurumaji *et al.*, "Skyrmion lattice with a giant topological Hall effect in a frustrated triangular-lattice magnet," *Science*, vol. 365, pp. 914–918, 2019.

[4] J. Sears *et al.*, "Ferromagnetic Kitaev interaction and the origin of large magnetic anisotropy in α-$RuCl_3$," *Nature Physics*, vol. 16, pp. 837–840, 2020.

[5] J. Strempfer, S. Francoual, *et al.*, *Synchrotron Rad.*, vol. 20, pp. 541–549, 2013.

An Anomalous Diffraction study of $Cu_2Zn(Ge,Si)Se_4$

D. M. Többens[1], G. Gurieva[1], S. Niedenzu[1], S. Schorr[1]

[1] Helmholtz-Zentrum Berlin (HZB), Hahn-Meitner-Platz 1, 14109 Berlin, Germany

While the silicon-rich members of the series $Cu_2Zn(Ge,Si)Se_4$ crystallize in wurtz-kesterite type structure [1], germanium-rich samples adopt a tetrahedral structure of the kesterite type [2]. Identification of the silicon site is straightforward from regular X-ray diffraction, as Si^{4+} is a light element and has less electrons than the other cations. However, Cu^{1+}, Zn^{2+}, and Ge^{4+} are all isoelectronic and have very similar form factors. The kesterite type of the cation distribution has been established by neutron diffraction [2].

We now applied anomalous X-ray diffraction to this system, using Rietveld refinement and Multiple Edge Anomalous Diffraction (MEAD) [1] with data taken at the K-absorption edges of Cu, Zn, and Ge. These energies are accessible at beamline KMC-2, BESSY II, Berlin [3]. In contrast to previous studies, where Sn^{4+} was the M(IV) species in the structure [1], in $Cu_2ZnGeSe_4$ all cations have very similar scattering power under normal conditions. This results in superstructure peaks (with respect to the cubic ZnS parent structure) that are very weak. For Rietveld analysis this is a drawback, as the optimization will be dominated by the main peaks of the parent structure. In MEAD, however, it increases the effect of the changing scattering power close the absorption edges. As a result, not only are Kesterite and Stannite types clearly distinguishable at the Cu-K edge (figure 1), also the Cu/Zn ordering within the Kesterite structure is clearly detectable and quantifiable at the Zn-K edge. The structure of the MEAD spectrum at the Ge-K edge was found to be very sensitive to the presence of vacancies at the Ge 2*b* site of the structure at the Si-free composition. Within the compositional range, Si^{4+} has very similar influence.

References

[1] D. M. Többens *et al.*, "Cation distribution in $Cu_2ZnSnSe_4$, Cu_2FeSnS_4 and $Cu_2ZnSiSe_4$ by multiple-edge anomalous diffraction," *Acta Crystallographica B*, vol. 76, pp. 1027–1035, 2020.

[2] G. Gurieva *et al.*, "Cu-Zn disorder in $Cu_2ZnGeSe_4$. A complementary neutron diffraction and Raman spectroscopy study," *Journal of Physics and Chemistry of Solids*, vol. 99, pp. 100–104, 2016.

[3] Helmholtz-Zentrum Berlin für Materialien und Energie, "KMC-2: an X-ray beamline with dedicated diffraction and XAS endstations at BESSY II," *Journal of large-scale research facilities*, vol. 2, 2016, Art. no. A49.

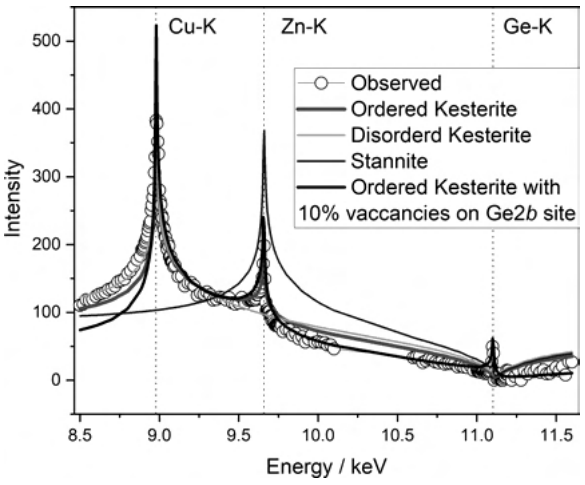

Figure 1 Observed and simulated MEAD spectra of Bragg peak 011 of $Cu_{2.03}Zn_{1.060}Ge_{0.947}Se_4$. The structure is highly ordered Kesterite. The peak at the Ge-edge indicates $\leq$10% vacancies at the Ge 2b site.

Analysis of potentially Ferroelectric Strontium Titanate Thin Films with Resonant X-ray Diffraction and Density Functional Theory

M. Nentwich[1], C. Richter[2], M. Zschornak[3], T. Weigel[2], D. C. Meyer[3], D. Novikov[1]
[1] P23 Beamline, PETRA-III, DESY, Hamburg, Germany
[2] Leibniz Institut für Kristallzüchtung, Berlin, Germany
[3] TU Bergakademie Freiberg

Ferroelectric materials possess a spontaneous polarisation that can be electrically switched between different orientations. Compared to ferromagnetics, the domain walls are small, allowing memory cells of higher storage density. Thin films of ferroelectric materials allow to increase the storage density even further. Exemplarily, incipient ferroelectricity is found in strontium titanate SrTiO3 (STO) at a low transition temperature. This ferroelectricity can be stabilized by a variety of external factors such as doping, strain, electric field, isotope substitution etc., even up to room temperature.

Recently, we studied the effect of the electroformation of STO and the accompanied creation of the *migration-induced field-stabilized polar* (MFP) phase [1] extensively, *i.e.* with the newly developed approach of *Resonantly Suppressed Diffraction* (RSD) [2] at Beamline P23 of PETRA III. Because of the breakdown of Friedel's law under resonant conditions, RSD can be used to obtain information about the polarization state of polar materials, namely by monitoring the Bragg intensity while scanning the energy of the incident beam through the absorption edge of strontium.

Here, we transferred this methodology to ferroelectric STO thin films and measured the energy dependent intensities for different Bragg reflections. As underlying structure model, we combined the structure of the low temperature antiferrodistortive (AFD) phase and of a generalized MFP phase. The resulting structure is ferroelectric and rather unknown within the perovskites. The energy dependent intensities of the chosen reflections of simulated data were fitted against the experimental values. Additionally, we performed *Density Functional Theory* (DFT) calculations to determine the atomic displacements from the lattice parameters at the different low temperatures. The results show that the major structural components within those STO thin films are the AFD displacements, while the MFP displacements are negligible.

References

[1] J. Hanzig, M. Zschornak, F. Hanzig, E. Mehner, H. Stöcker, B. Abendroth, C. Röder, A. Talkenberger, G. Schreiber, D. Rafaja, S. Gemming, D. C. Meyer: Migration-induced field-stabilized polar phase in strontium titanate single crystals at room temperature, Physical Review B 88, 024104 (2013).
[2] C. Richter, M. Zschornak, D. Novikov, E. Mehner, M. Nentwich, J. Hanzig, S. Gorfman, D. C. Meyer: Picometer polar displacements in strontium titanate determined by a new approach of resonant x-ray diffraction, Nature Communications 9, 178 (2018).

Young crystallographers: Lightning talks

A Crystallographic and Spectroscopic Investigation of Photo-Induced Electron Transfer in Pyrene-(CH2)2-N,N'-Dimethylaniline: Time-Resolved Studies in Solutions and Polymorphic Crystals.

K. Basuroy[1], J. D. J. Velazquez-Garcia[1], D. Storozhuk[1], D. Gosztola[1], S. Thekku Veedu[1], S. Techert[1]
[1] DESY, Hamburg, Germany

Photo-induced electron transfer reactions are crucial for many of the biological and chemical reactions that occur in nature. According to Marcus and others, electronic coupling between an electron donor and acceptor must be nonzero, for a successful electron transfer reaction. [1] Several studies are performed in order to have a better understanding of the photoinduced intramolecular electron transfer, in terms of the rate of transfer and the overall geometry of the donor-bridge-acceptor (D-B-A) system.[2] Pyrene and its derivatives, owing to their high quantum efficiency, high fluorescence lifetimes, prone to form excimers or exciplex in high concentrations and highly sensitive nature of their photophysical properties to microenvironmental changes, are considered extremely useful for photoinduced electron transfer studies.[3] We have designed a mono-substituted pyrene derivative, pyrene-(CH2)2-N, N'-dimethylaniline, where dimethylaniline (DMA) (electron donor) is connected to pyrene (electron acceptor, in this case) through alkane chain. The distance between the donor and acceptor in this molecule is expected to be suitable for electron transfer by tunneling mechanism. A serendipitous occurrence of two polymorphic crystals from two separate batches of crystallization setup, while dissolved in ethanol, provided us a unique opportunity to study these two conformational polymorphs, A and B. While, in A crystal

structure pyrene and dimethylaniline are in axial orientation (P-1) with respect to each other, in B they are equatorial (P21/n). Studies on photo-induced intramolecular electron transfer has revealed the importance of conformational parameters of the molecules such as rotation around bonds that affects the distance and relative orientation of donor and acceptor which in turn can proved to be quite decisive in the photo-physical properties of charge transfer states. [4] We have performed time-resolved Laue diffraction experiments with these two polymorphic crystal forms in the ns time domain. Apart from steady-state spectroscopy, we have also measured ultrafast transient absorption with the solution, at different concentrations. A thorough crystallographic and spectroscopic investigation of this particular system, especially with the polymorphic crystals have allowed us to understand the important aspects of photo-induced electron transfer.

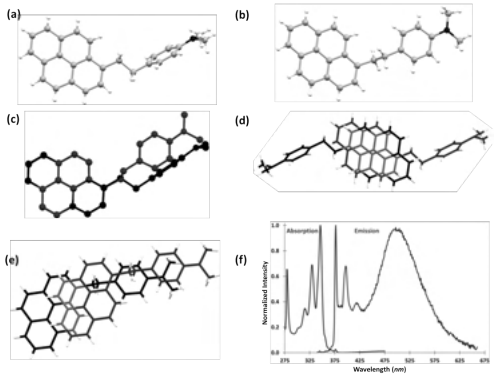

Figure 1 Conformation of molecules in single crystals, a) PyDMA1 and b) PyDMA2. c) Molecular superposition of PyDMA1 (black) and PyDMA2 (red) on pyrene ring with RMSD=0.0427Å. The extent of overlap between the pyrene rings belong to the symmetry related/unit translated molecules in PyDMA1/PyDMA2 in single crystals are 67% and 17%, respectively. f) Absorption (blue) and emission (red) spectra of PyDMA1, in toluene, at 0.1mM concentration.

References

[1] Jortner, J; Bixon, M. Electron Transfer-From Isolated Molecules to Biomolecules, Part 1 and Part 2; John Wiley & Sons, Inc: New York, 1999.

[2] a) Paddon-Row, M. N. Acc. Chem. Res. 1994, 27, 18. b) M. D. Newton, Chem. Rev., 1991, 91, 767.

[3] Stockmann,A; Kurzawa, J.; Fritz, N.; Acar, N.; Schneider, S.; Daub, J.; Engl, R. and Clark. T. J. Phys. Chem. A 2002, 106, 7958.

[4] a) Bleisteiner, B.; Marian, Th.; Schneider, S.; Brouwer, A. M.; Verhoeven, J. W. Phys. Chem. Chem. Phys. 2001, 3, 2070.

b) Verhoeven, J. W.; Wegewijs, B.; Scherer, T.; Rettschnik, R. P. H.; Warman, J. M.; Jäger, W.; Schneider, S. J. Phys. Org. Chem. 1996, 9, 387.

(c) Wegewijs, B.; Ng, A. K. F.; Verhoeven, J. W. Recl. TraV. Chim. Pays-Bas 1995, 114, 6. (d) Jäger, W.; Schneider, S.; Lauteslager, X. Y.; Verhoeven, J. W. J. Phys. Chem. 1996, 100, 8118.

(e) Lauteslager, X. Y.; van Stokkum, I. H. M.; van Ramesdonk, H. J.; Brouwer, A. M.; Verhoeven, J. W. J. Phys. Chem. 1999, 103, 653. (f) Jäger, W.; Schneider, S.; Verhoeven, J. W. Chem. Phys. Lett. 1997, 270, 50.

How Occupancy Disorder Impacts Magnetism in Topological Insulators

L. Folkers[1], A. Isaeva[1]

[1] Technische Universität Dresden, Dresden, Germany

Magnetic topological insulators (MTIs) are a hot topic of materials science, promising future availability of spintronics with low energy consumption, quantum computing and phenomena like the Quantized Anomalous Hall Effect (QAHE) [1-2]. MTIs are chemically and structurally akin to the original non-magnetic topological insulators. Of those, the tetradymites Bi2Te3 and Sb2Te3 have recently proven to allow the introduction of a third magnetic element resulting in magnetically active, topologically non-trivial compounds. A magnetic element can be incorporated either via substitution on the Bi/Sb position in (Bi, Sb)2Te3, or by adding a third element which introduces a new crystallographic site, resulting for example in (MnBi2Te4)(Bi2Te3)m (m = 0, 1, 2). (Bi, Sb)2Te3 itself and all members of its family exhibit the rhombohedral R -3 m 1 space group (No. 166) [2]. Therein interchanging sheets of (Bi, Sb) and Te build (Bi, Sb)2Te3 quintuple layers and Mn, (Bi, Sb) and Te build septuple layers with the central sheet being Mn (Wyckoff position 3a). Situated between the respective layers is a Van der Waals gap (Fig. 1) and depending on m, various stacking orders can be observed. Our group was the first to successfully grow single crystals, and conduct an in depth study of the physical properties of MnBi2Te4, the m = 0 member of the above discussed MTI family [4-5]. Single crystal diffraction experiments reported in

that study showed intermixing of Mn and Bi and since then several studies have reported intermixing of the two elements (MnBi2.14Te3.96 [6], Mn1.01Bi1.99Te4 and Mn0.98Bi2.05Te4 [7]). While a lot of attention has been given to MnBi2Te4 and its higher order relatives, MnSb2Te4 proved to be synthetically achievable too. Similar to MnBi2Te4, MnSb2Te4 features intermixing of Mn and Sb (Mn0.852Sb2.296Te4 [8]). For MnSb2Te4, a recent study by Murakami et al. uncovers the impact of finding a certain amount of the magnetic Mn on the position of the non-magnetic Sb [9]. According to their discoveries, this changes the magnetic order from antiferromagnetic to ferrimagnetic. These compounds are known to react sensitively to synthesis procedure and tempering history. Hence, our studies aim at understanding the greater connection between synthesis aspects and the resulting structural and physical properties. More precisely we studied MnBi2Te4 and MnSb2Te4 containing various amounts of Mn and other analogues of these systems.

References

[1] Y. Ando, *Journal of the Physical Society of Japan*, (2013), *82*, 102001.
[2] I. I. Klimovskikh, M. M. Otrokov, D. Estyunin, et al., *Quantum Materials*, (2020), *54*.
[3] Y. Feutelais, B. Legendre, N. Rodier, V. Agafonov, *Materials Research Bulletin*, (1993), *28*, 591-596
[4] A. Zeugner, F. Nietschke, A. U. B. Wolter, et al., *Chemistry of Materials*, (2019), *31*, 2795-2806.
[5] M. M. Otrokov, I. I. Klimovskikh, H. Bentmann, et al., *Nature*, (2019), *576*, 416-422.
[6] H. Li, S. Liu, C. Liu, et al., *Physical Chemistry Chemical Physics*, (2020), *22*, 556-563.
[7] M.-H. Du, J. Yan, V. R. Cooper, M. Eisenbach, *Advanced Functional Materials*, (2020), 2006516.
[8] L. Zhou, Z. Tan, D. Yan, et al., *Physical Review B*, (2020), *102*, 85114.
[9] T. Murakami, Y. Nambu, T. Koretsune, et al., *Physical Review B*, (2019), *100*, 195103.

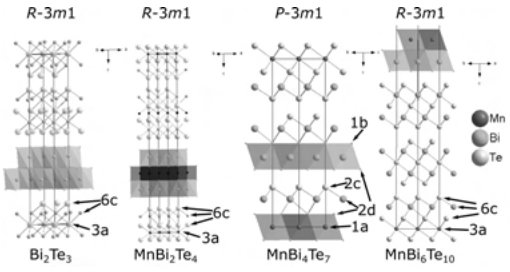

Figure 1 The structure of Bi2Te3 [3] and the stacking variants (MnBi2Te4)(Bi2Te3)m (m = 0 - 2). For clarity, only 1/3 of the unit cell of MnBi6Te10 is displayed.

MOFs of a O,P,N heterotritopic Ligand – One reaction, two networks – A topological analysis

H. Gildenast[1], U. Englert[1]
[1] RWTH Aachen University, Institute of Inorganic Chemistry, Aachen, Germany

The field of metal-organic frameworks (MOFs) is dominated by the chemistry of oxygen and nitrogen donor based ligands [1]. Next to no work revolves around polytopic ligands containing phosphorus donors.

The usage of phosphorus widens the horizon of MOF chemistry. It may broaden the structural variety, enable new applications and stabilize metal cations in low oxidation states that were previously inaccessible to MOF chemists.

The ligand 4-(3-(4-(diphenylphosphino)phenyl)-3-oxopropanoyl)benzonitrile is a prototype for the combination of the three donor atoms O, P and N. It combines a chelating beta-diketone as the oxygen donor, a nitrile representing the nitrogen donors and a triarylphosphine as a phosphorus based ligand functionality.

Using a stepwise approach we were able to synthesize a cationic heterobimetallic Fe^{III}/Ag^{I} MOF with Fe^{III} bound to the oxygen donors and Ag^{I} bound to the P and N donors. The network can emerge in 2 different topologies while the chemical connectivity remains unchanged. Type **A** corresponds to the rtl network type [2], Type **B** has not been observed yet. Both have a three dimensional pore system. The pores are large enough so a sphere with a diameter of 4 Å could move through them along all low-indexed directions.

References

[1] F. Almeida Paz, *Chem. Soc. Rev.*, vol. 41, p. 1088, 2012.
[2] M. O'Keeffe *et al.*, *Acc. Chem. Res.*, vol. 41, p. 1782, 2008.

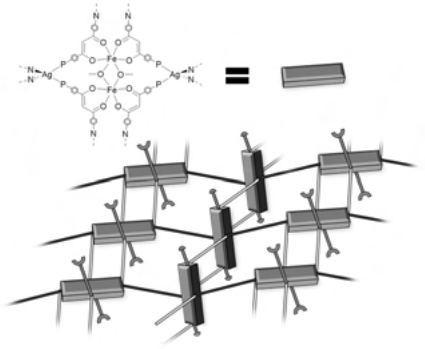

Figure 1

Coordination Polymers featuring Dibenzoyltartaric and Ditoluoyltartaric Acid: A different approach to a popular compound.

M. Kremer[1], U. Englert[1]

[1] RWTH Aachen University, Institute of Inorganic Chemistry, Aachen, Germany

The two tartaric acid derivatives dibenzoyltartaric acid (DBTA) and di-*para*-toluoyltartaric acid (DPTTA) are common compounds in organic chemistry and pharmaceutical science, where they mostly function as derivatisation agents or as chiral templates. There are currently about 250 crystal structures featuring either of the acids deposited in the CCDC [1]. While the compounds are decent chelating ligands with the ability to extend bridges to neighbouring metal centres to form coordination polymers, they are hardly used in this capacity. Less than 40 structures featuring both carboxylato groups connected to a metal are deposited in the CCDC currently.

Our work focusses on the synthesis of coordination polymers with dicarboxylic acids, including tartaric acid and the titular derivatives thereof [2,3]. During these experiments, several new compounds featuring DBTA or DPTTA were synthesised, crystallized, and characterized. In this presentation we showcase several of these compounds, discuss structural similarities and differences as well as the influence of different metals, coligands or stereoisomers on the resulting structures.

References

[1] C. R. Groom, I. J. Bruno, M. P. Lightfoot and S. C. Ward, *Acta Cryst. B*, vol. 72, pp. 171-179, 2016, DOI: 10.1107/S2052520616003954.

[2] M. Kremer, J. van Leusen, U. Englert, *Crystals*, vol. 10, 2020, DOI: 10.3390/cryst10060485.

[3] M. Kremer, Dissertation, RWTH Aachen, Germany, 2020.

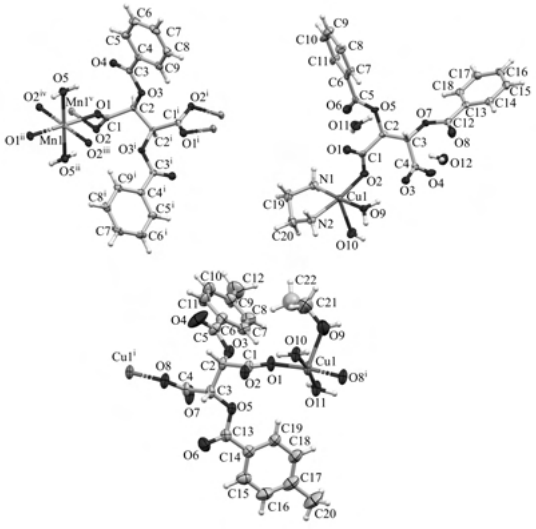

Figure 1

Encapsulation of inorganic nanoparticles into novel T. maritima encapsulin variants

M. Rütten[1], T. Beck[1]

[1] University of Hamburg, Department of Chemistry, Institute of Physical Chemistry, Hamburg, Germany

Supported by an established synthetic strategy towards optical materials protein containers and nanoparticles are used. With protein containers as building blocks, nanoparticles will be assembled with high precision into mesoscale materials with optical properties that emerge from interactions between the components. Along the recent advances in computational redesign of protein containers, it is now possible to combine these results with nanoparticle synthesis and protein crystallography. An innovative design approach with two oppositely charged protein containers as building blocks, a new type of protein-based material will be realized (Figure 1). Surface charged protein containers can be combined with inorganic compounds to unite biological features with the chemical and physical properties of abiotic materials. In particular, protein containers, with their inherent ability to encapsulate cargo molecules, are perfect platforms for the generation of multifunctional assemblies.[1, 2] Gold nanoparticles can be decorated with a small number of encapsulin cargo-loading peptides to fill protein containers. By lock-and-key interaction between the peptides and the peptide-binding pockets on the inner container surface (Figure 2), the nanoparticles will be encapsulated with high efficiency.[3] Typically encapsulin bears a flavin that is attached to the outer surface. The flavin leads to a yellow coloured solution and its presence on the protein surface might be problematic

for future applications or in crystallization. Based on the latest cryo-EM data it was possible to remove the flavin.[4] Crystalline materials are produced, which is crucial for future applications. Because the protein scaffold is independent of the nanoparticle cargo, this modular approach will enable tuning of the optical properties by choice of nanoparticle content, assembly type and protein container type. For further future applications, surface charged protein containers will be used as sustainable building blocks for bioinorganic nanomaterials.[5]

References

[1] M. Künzle, T. Eckert, T. Beck, *J. Am. Chem. Soc.*, vol. 138, p. 12731, 2016.
[2] M. Lach, M. Künzle, T. Beck, *Chem. Eur. J.*, vol. 23, p. 17482, 2017.
[3] M. Künzle, J. Mangler, M. Lach, T. Beck, *Nanoscale*, vol. 10, pp. 22917–22926, 2018.
[4] D. Diaz *et al.*, *bioRxiv*, preprint, 2020.
[5] M. Lach, M. Künzle, T. Beck, *Biochemistry*, vol. 58, pp. 140–141, 2019.

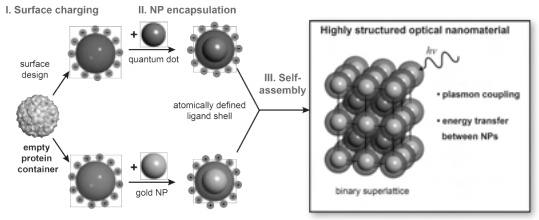

Figure 1 Strategy overview for the synthesis of highly structured optical nanomaterial.

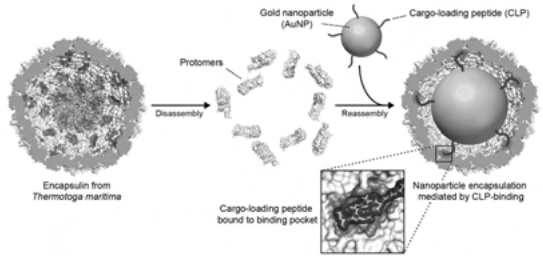

Figure 2 Gold nanoparticle encapsulation via cargo-loading peptide into T. maritima encapsulin.

A One-Dimensional Heterobimetallic Fe(III)/Hg(II) Coordination Polymer Linked by a Ditopic Pyrazole Substituted Acetylacetone

S. van Terwingen[1], B. Ebel[1], U. Englert[1]
[1] RWTH Aachen University, Institute of Inorganic Chemistry, Aachen, Germany

Due to their vast applications monometallic coordination polymers (CPs) have increasingly attracted the interest of various fields over the last years.[1] We focus on using heterofunctional ligands to synthesize heterobimetallic CPs, combining the properties of two metals in one homogenous material.[2] Our stepwise approach includes the synthesis of a metalloligand and, afterwards, its crosslinking using a second metal cation. Herein we present this approach for the ligand (3-(1,3,5-trimethyl-4-1H-pyrazolyl)acetylacetone (HacacMePz) with its heterobimetallic coordination polymer containing Fe(III) and Hg(II).

The CP crystallizes as an acetonitrile solvate in the triclinic space group $P\bar{1}$ with $Z = 2$. The [Fe(acacMePz)$_3$] metalloligands are linked by $Hg_2(\mu_2\text{-}Cl)Cl_3$ moieties. While the coordination sphere around the Fe(III) ion is a rather regular octahedron, the two symmetry inequivalent Hg(II) ions adopt distorted tetrahedral coordination environments (τ_4 = 0.82, 0.76).[3] Interestingly, only one chlorido ligand is bridging and the other three are bound to one Hg(II) ion. This connectivity leads to an one-dimensional CP with a ladder-like structure as seen in Figure 1. The polymer expands in [1 -1 1] direction without any meaningful interactions between adjacent chains.

References

[1] S. R. Batten, S. M. Neville, D. R. Turner, *Coordination Polymers: Design, Analysis and Application*, Cambridge: RSC Publishing, 2009.
[2] M. Kremer, U. Englert, *Z. Kristallogr.*, vol. 233, pp. 437-452, 2018.
[3] A. W. Addison, T. N. Rao, *J. Chem. Soc., Dalton Trans.*, vol. 1984, pp. 1349-1356, 1984.

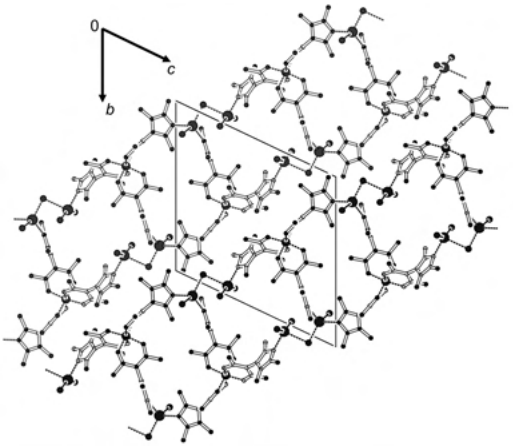

Figure 1

Poster

Bio-crystallography

High-resolution crystal structure and biochemical characterization of a GH11 endoxylanase from Nectria haematococca

H. Andaleeb[1], C. Betzel[1], H. Brognaro[1], S. Falke[1], N. Ullah[1], M. Perbandt[1]

[1] Institute of Biochemistry and Molecular Biology, Laboratory for Structural Biology of Infection and Inflammation, University of Hamburg,, DESY, Hamburg, Germany

Biofuels are one of the important and renewable energy sources, obtained from lignocellulosic waste materials by utilizing special enzymatic cocktails (1). Biofuels can replace fossil fuels to a large extend and in parallel reduce carbon dioxide emission and global warming. Xylanases play crucial role in the hemicellulose biodegradation within the industrial biofuel preparation processes and are in focus of structure-function analyses for many years (2). In this context we anlaysed a xylanase from *Nectria haematococca* (NhGH11) and solved the three-dimensional structure to atomic 1.0 Å resolution. At this resolution the positions of hydrogen atoms in the active site cleft could be identified. Data obtained highlight the potential of NhGH11 to be applied in industrial biomass degradation processes, in which the catalysis of xylan biopolymers can produce sustainable chemicals and bio-based commercial eco-friendly materials. Functional and structural details will be presented.

References

[1] Raud, M., Kikas, T., Sippula, O., & Shurpali, N. J. (2019). Renewable and Sustainable Energy Reviews, 111, 44-56.

[2] Paës, G., Berrin, J. G., & Beaugrand, J. (2012). Biotechnology advances, 30(3), 564-592.

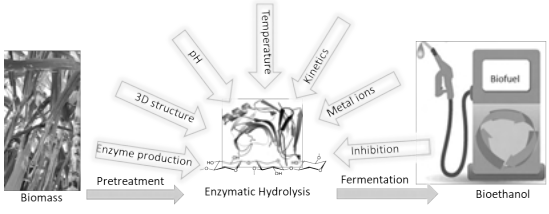

Figure 1 Graphical abstract, presenting a summary of the structural and biochemical analysis of NhGH11.

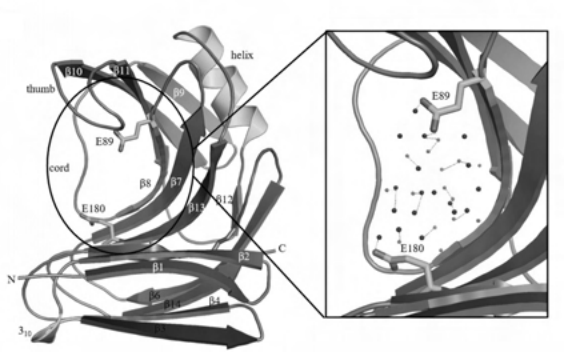

Figure 2 Cartoon plot of NhGH11 with catalytic active residues are shown in sticks. A zoom of the active site region is shown (right figure), with catalytic residues surrounded by solvent molecules in the active site cavity.

XDSAPP3 – the new graphical user interface for the convenient processing of diffraction data using XDS

T. Hauß[1], K. Röwer[1], U. Mueller[1], M. S. Weiss[1]

[1] Helmholtz-Zentrum Berlin, Macromolecular Crystallography, Berlin, Germany

For many years, XDSAPP [1] is a well-known program to (semi-) automatically process diffraction data using XDS [2]. Here, the new version XDSAPP3 is presented, with improvements in the graphical user interface (GUI) as well as in the underlying Python code. The main motivations for the upgrade of XDSAPP were the nowadays widespread use of Dectris EIGER detectors and the phasing out of the Qt 4 framework, with the last release already in 2011, and Python 2.7, its end-of life was finally reached in 2020. XDSAPP3 is written in Python 3 and utilizes the PyQt 5 framework for the GUI and the matplotlib library. EIGER detectors are now supported by using the generate_XDS.INP script [3] in combination with the XDS plugins dectris-neggia [4] from Dectris or durin-plugin [5] from Diamond. Various important statistics generated from the XDS output files are presented in 2-D plots for the convenient inspection of the results. In the command-line version, a multi-dataset mode is implemented for batch processing of multiple datasets. If used on the beam-line, it will process new incoming data as soon as available. XDSAPP3 has been tested on various Linux distributions, like RHEL 6,7 , openSUSE 15, centOS 6, and Kubuntu 20, as well as macOS 10.13 High Sierra through 11.1 Big Sur. The development team may be contacted at xdsapp@helmholtz-berlin.de.

References

[1] Sparta, K., Krug, M., Heinemann, U., Mueller, U., Weiss, M. S., *J. Appl. Cryst.*, vol. 49, pp. 1085-1092, 2016.
[2] Kabsch, W., *Acta Cryst. D*, vol. 66, pp. 125-132, 2010.
[3] Diederichs, K.,
https://strucbio.biologie.uni-konstanz.de/xdswiki/
/index.php/Generate_XDS.INP
[4] https://www.dectris.com
[5] https://github.com/DiamondLightSource/durin

Low dose measurements for spatially resolved anomalous dispersion refinement

F. Lennartz[1], J.-H. Jeoung[2], H. Dobbek[2], M. Weiss[1]

[1] Helmholtz-Zentrum Berlin, Departement of Photon Science, Macromolecular Crystallography, Albert-Einstein-Straße 15, 12489 Berlin, Germany

[2] Humboldt University of Berlin, Berlin, Germany

Spatially resolved anomalous dispersion (SpReAD) refinement is a method to analyse the oxidation states of individual protein-bound metals and is based on collecting several x-ray diffraction datasets across an x-ray absorption edge. Such an approach can expose crystals to relatively high total dose of radiation. This can result in radiation damage, including reduction of metals.

Here, we have conducted experiments for SpReAD analysis on HZB MX beamline 14.1. To analyse the effect of dose on the result of the experiments, we have tested different transmission settings to vary the total dose per experiment and test whether data collected at low transmission are suitable for SpReAD refinement.

High-pressure macromolecular crystallography

J. Lieske[1], S. Saouane[2], S. Guenther[3], P. Reinke[4], T. Pakendorf[2], B. Reime[2], E. Crosas[4], J. Hakanpaeae[2], H. Chapman[1], A. Meents[3]

[1] FS-CFEL-1 (CFEL-Coherent X-Ray Imaging), Hamburg, Germany

[2] FS-PETRA-D (FS-PET-D Fachgruppe P11), Hamburg, Germany

[3] FS-BMX (FS-CFEL-1 Fachgruppe BMX), Hamburg, Germany

Pressure and temperature are physical parameters that define the free energy landscape of proteins and hence their conformational space. Studying the influence of these thermodynamic parameters on the structure and function of proteins provides the basis for understanding fundamental principles of biological processes, ranging from enzymatic reaction mechanisms to protein folding. Whereas experiments performed at varying temperatures using diverse methods are straight-forward and well-established, experiments at elevated or changing pressures are still technically challenging. Current crystallographic methods to obtain high-resolution structural data of proteins at high pressure involve the usage of diamond anvil cells (DAC) that were originally designed for geological science purposes and are suboptimal for fragile protein crystals. In order to overcome practical challenges of the DAC, we developed a new cell for high-pressure macromolecular crystallography using a fixed target-approach combined with the application of thin-walled sapphire and gaseous helium as pressurizing medium. Pressure levels can be freely adjusted between 0.1 and 120 MPa. We will present the experimental setup and first results obtained at beamline P11 of the PETRA III storage ring at DESY.

Structure based identification of Bortezomib and Ixazomib as new lead compounds for the development of novel boron-based ß-lactamase inhibitors

A. Prester[1], N. Werner[2], H. Rohde[1], M. Perbandt[3], C. Betzel[2]

[1] Universitätsklinikum Hamburg-Eppendorf, Institut für Mikrobiologie, Hamburg, Germany

[2] Universität Hamburg, Institut für Biochemie und Molekularbiologie, Hamburg, Germany

[3] UNI/CUI (The Hamburg Centre for Ultrafast Imaging), Hamburg, Germany

In recent years the efficacy of traditional ß-lactam antibiotics against Gram-negative bacteria has declined dramatically, mainly due to their ability to express multiple ß-lactamases that are not inhibited anymore by first-generation ß-lactam inhibitors (BLIs), such as clavulanic acid, tazobactam, and sulbactam [1]. Substantial efforts have been made to develop new families of BLIs that are also effective against many medical problematic β-lactamases. Diazabicyclooctane derivatives (DBOs), such as Avibactam and Relebactam, were the first group of these new non-ß-lactam BLIs, which form a relatively hydrolytically stable acyl enzyme-type complex [2]. However, a novel approach for the development of BLIs is represented by boronate-based compounds, such as Vaborbactam and Taniborbactam [3]. The ability of boron to adopt a tetrahedral geometry allows to effectively mimic tetrahedral transition state analogs during hydrolytic reactions, making it one of the most useful elements in synthetic organic chemistry. In the field of protease inhibitors, boronate-based inhibitors, such as Bortezomib and Ixazomib were already designed and developed with applications in cancer therapy and are ap-

proved drugs for approx. 10 years. As serine β-lactamases and serine proteases share similarities in their mechanism of action, we analysed structural and biochemical features of β-lactamase inhibition, by utilizing these protease inhibitors in terms of a repurposing approach and targeted the ß-lactamase enzyme CTX-M-14 from K. pneumoniae, the most widely distributed extended-spectrum ß-lactamase (ESBL). We will describe and present details for the crystal structures in complex with Bortezomib and Ixazomib, shown on the left. β-lactamase CTX-M-14, in green with covalently bound protease inhibitor Ixazomib in purple. Results obtained prove that both can be not only utilized as proteasome inhibitors, but moreover as ß-lactamase-inhibitors. The dual inhibition mode provides new insights into the catalytic mechanism of inhibition and may guide new strategies for repurposing of known boron-based proteasome inhibitors to antibiotic active drugs.

References

[1] Vena, A., N. Castaldo, and M. Bassetti, The role of new beta-lactamase inhibitors in gram-negative infections. Curr Opin Infect Dis, 2019. 32(6): p. 638-646.
[2] Ehmann, D.E., et al., Avibactam is a covalent, reversible, non-beta-lactam beta-lactamase inhibitor. Proc Natl Acad Sci U S A, 2012. 109(29): p. 11663-8.
[3] Hamrick, J.C., et al., VNRX-5133 (Taniborbactam), a broad-spectrum inhibitor of serine- and metallo-beta-lactamases, restores activity of cefepime in Enterobacterales and Pseudomonas aeruginosa. Antimicrob Agents Chemother, 2019.

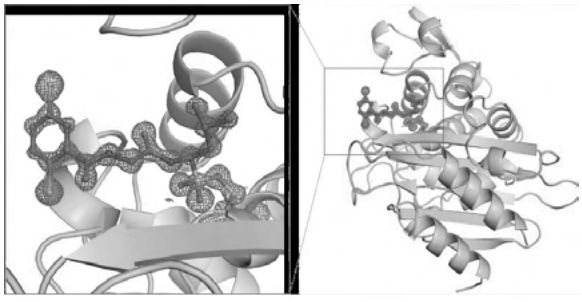

Figure 1

Structural characterization of ClpP and PBPs from Staphylococcus epidermidis - central and vital enzymes in bacterial virulence, stress survival and antibiotic resistance

M. Schwinzer[1], B. Alves França[1], M. Perbandt[1], C. Betzel[1]
[1] University of Hamburg, Institute of Biochemistry and Molecular Biology, Hamburg, Germany

Staphylococcus epidermidis (*Se*) is known to be a highly abundant bacterium on human skin. Although *Se* is usually not pathogenic under normal conditions, immunocompromised patients are at risk of acquiring persistent nosocomial infections caused by the aforementioned organism [1]. In this context, we performed structure-function analysis of two key bacterial enzymes, in terms of drug discovery investigations, known as penicillin-binding proteins (PBPs) and a distinct caseinolytic protease P (ClpP). PBPs are essential for the synthesis and the integrity of the bacterial cell wall. They exhibit a transpeptidase domain, a C-terminal head sub-domain and a N-terminal domain, including a membrane-anchor [2]. Moreover, ClpP is a barrel-like tetradecameric hydrolase composed by two-stacked heptameric rings and 14 identical proteolytic sites. That protein is one of the major intracellular enzymatic gears in protein turnover, in heat and oxidative stress control, and in the transcription of virulence factors [3]. Thus, meticulous studies on PBP and ClpP structures and their non-enzymatic modulators are relevant for the development of novel strategies that aim to reduce bacterial virulence. Further details about initial structural and functional investigations, including structures solved and refined so far to 2.2 Å and 1.9 Å for PBP and ClpP respectively, will be reported.

References

[1] Büttner H, Mack D, Rohde H., et al. Structural basis of Staphylococcus epidermidis biofilm formation: mechanisms and molecular interactions. Front Cell Infect Microbiol., 5, 5(14), pp. 1-14, 2015.
[2] H. Yoshida, F. Kawai, E. Obayashi, S., et al. Crystal Structures of Penicillin-Binding Protein 3 (PBP3) from Methicillin-Resistant Staphylococcus aureus in the Apo and Cefotaxime-Bound Forms, Journal of Molecular Biology, 423(3), pp. 351-364 2012.
[3] Bhandari, V.; Wong, K. S.; Zhou, J. L.; et al. The Role of ClpP Protease in Bacterial Pathogenesis and Human Dieases. ACS Chem, Biol., 13, pp. 1413-1425, 2018.

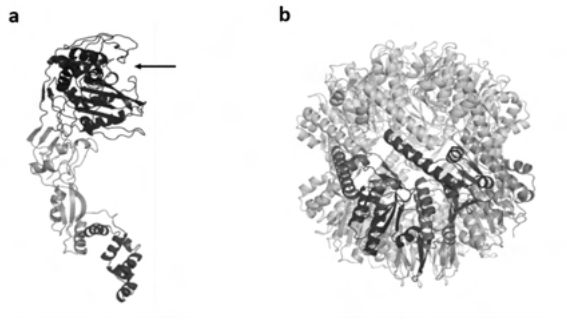

Figure 1 Initial structure of a. PBP: N-terminal domain (orange), head sub-domain (red) and the catalytic center indicated (black arrow) within the transpeptidase domain (blue); and b. ClpP: two-stacked heptameric rings (green and multi colored). Monomeric subunits are displayed in different colors (lower ring). Each domain contains the same internalized proteolytic site with a Ser-His-Asp triad.

Crystallographic fragment screening workflow at HZB

J. Wollenhaupt[1], T. Barthel[1], G. Lima[2], A. Metz[3], D. Wallacher[1], E. Jagudin[2], T. Hauß[1], C. Feiler[1], A. Heine[3], G. Klebe[3], M. Weiss[1]

[1] Helmholtz-Zentrum Berlin, Berlin, Germany

[2] MAX IV Laboratory, Lund, Sweden

[3] Philipps-University Marburg, Marburg, Germany

The only method utilized routinely to discover starting points for ligand development that at the same time delivers detailed 3D-information for downstream ligand optimization is macromolecular crystallography. Typically, small organic compounds, called fragments, are screened against an optimized crystal system of a target protein, and detected by electron density differences compared to the apo protein, i.e. the protein structure without fragments present. This technique, crystallographic fragment screening (CFS), is widely established now in academia and indispensable in the pharmaceutic industry. However, its routine use requires specialized workflows including suitable fragment libraries, dedicated beamlines able to handle large amounts of samples and largely automated software solutions for concise analysis of the results.

At Helmholtz-Zentrum Berlin, we provide the full workflow as well as practical guidance for our users conducting CFS campaigns. We prepared the 96-membered F2X-Entry Screen, an efficient and CFS-focused fragment library, as ready-to-use plates with dried-in compounds that can be used with or without DMSO present in the soaking experiment. In addition, special tools like the EasyAccess Frame, an evaporation protection device for crystallization plates, speed up the crystal handling. The HZB beamlines BL 14.1 and BL 14.2 are both equipped with state-of-the-art photon-counting detectors as well as with robotic sample changers, enabling enhanced throughput. Processing of the data is achieved via FragMAXapp, a user friendly, browser-controlled tool employed at several CFS facilities that manages in and output of many processing, refinement and hit identification software pipelines that are routinely used for CFS nowadays.

Taken together, HZB provides a workflow for routine crystallographic screening experiments via fragments. The intertwined workflow components and gathered expertise increase the chances for successful identification of fragments as starting points for the development of potent ligand molecules.

References

[1] Wollenhaupt, J. *et al.*, "F2X-Universal and F2X-Entry: Structurally Diverse Compound Libraries for Crystallographic Fragment Screening," *Structure*, vol. 28, pp. 694–706.e5, 2020.

[2] Barthel, T. *et al.*, "Facilitated crystal handling using a simple device for evaporation reduction in microtiter plates," *J. Appl. Cryst.*, accepted for publication, 2021.

[3] Lima, G. M. A. *et al.*, "FragMAXapp: Crystallographic Fragment Screening Data Analysis and Project Management System," article in revision, 2021.

[4] Schiebel, J. *et al.*, "High-Throughput Crystallography: Reliable and Efficient Identification of Fragment Hits," *Structure*, vol. 24, pp. 1398–1409, 2016.

Disordered Materials, complex crystal structures and aperiodic crystals, diffuse scattering and 3D-PDF

The incommensurate structure of the binary thallides A_4Tl_{13} (A = Rb, Cs).The solution of an old problem.

B. Lehmann[1], C. Röhr[1]

[1] Institut für Anorganische und Analytische Chemie, Universität Freiburg, Freiburg

In the course of our studies on alkali trielides with mixed triel positions (Ga/In) [1] and (In/Tl), analysis of the binary phase diagrams Rb-Tl and Cs-Tl [2] show incongruent melting behaviour at the composition A Tl $_3$ (A = Rb, Cs). A complete structural description of those phases has not been published to this day, even though *Corbett* and *Dong* [3] were able to determine the composition 'A_4Tl_{13}', as well as one of the structural elements of

those phases. In our work, due to the incongruent melting behaviour, the alkali poorer composition A Tl_4 was chosen for the synthesis of the two isotypic title compounds. X-Ray single crystal data were used to solve the structure.

The main reflections of the modulated structure were indexed with a C-centered orthorhombic lattice. The basic structure was solved in the space group *Cmca* using the *charge-flipping* method (Basic structure of Rb_4Tl_{13}: *Cmca*, $Z = 1$, $a = 545.75(3)$, $b = 3909.95(20)$, $c = 2148.90(11)$ pm). All satellite reflections could be indexed with a primitive orthorhombic lattice and the q-vector $\boldsymbol{q}$ = (0 0 0.2996(1)), allowing the refinement of the (3+1) D modulated structure. The model was obtained by $k2$ symmetry reduction from *Cmca* to *Pbcm* (Rb_4Tl_{13}: *Pbcm*(0 0 γ)s00, $\boldsymbol{q}$ =(0 0 0.2996(1)), $Z = 1$, $a = 3907.80(20)$, $b = 2147.61(11)$, $c = 545.63(3)$ pm, $R1$=0.083, $R1_{\mathrm{mr}}$=0.063, $R1_{\mathrm{sr}+-(1)} = 0.168$). The structure exhibits as one structural element isolated chains of interpenetrating icosahedra

(Fig. 1b). These chains are coordinated by cations only. They are embedded between complex 2D thallide layers (Fig. 1a), similar to those observed in the structure of K_6Tl_{17} [4]. Both positions in the centre of the chains as well as two atoms in the layer exhibit a strong positional modulation, which is refined using the *saw-tooth* function (Fig. 2). The positions of the remaining atoms affected by this modulation can be refined using harmonic modulation functions. The modulation is probably caused by the size of the thallium atoms, which are too large to fit into the structure in a way compatible with the periodicity of the lattice.

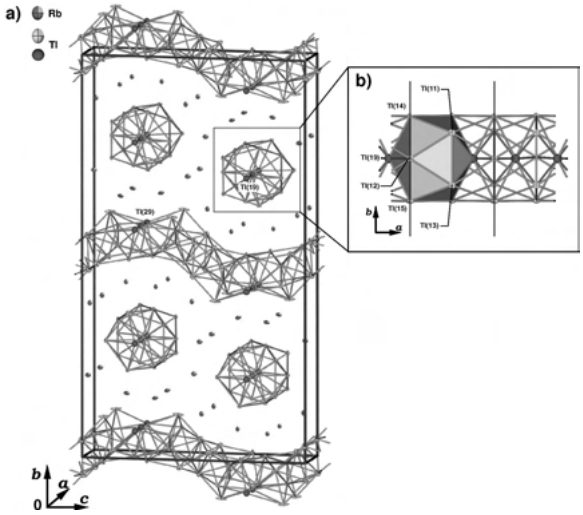

Figure 1 a) Unit cell of the basic structre of Rb_4Tl_{13}. The thallium atoms refined with a saw-tooth function in the final model (Tl(19) and Tl(29)) are represented as blue spheres. All remaining atomic positions are shown as red (Rubidium) resp. green (Thallium) ellipsoids (Probability: 90%). b) Detailed view of one chain of interpenetrating icosahedra with 90% probability ellipsoids and atomic labels from the model of the basic structure (projection along [001]).

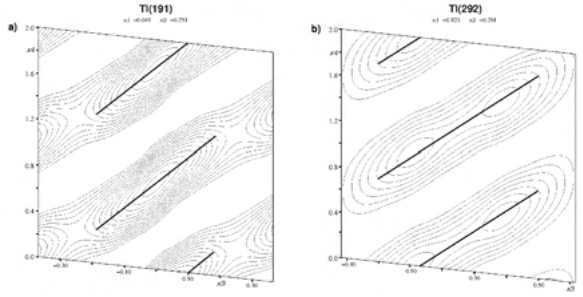

Figure 2 De Wolff's sections from the final structure of Rb_4Tl_{13}. a) $x3$-$x4$-section at the Tl(191) site. b) $x3$-$x4$-section at the Tl(292) site (Contour lines at intervals of 30 e^- x $10^{-6}pm^{-3}$).The difference between the atomic labels of the final and the basic structure (Fig.1) results from the symmetry reduction from *Cmca* to *Pbcm*. The Tl(19) site splits up to Tl(191) and Tl(192) and the Tl(29) site splits up to Tl(291) and Tl(292).

References

[1] M. Falk, C. Röhr, *Z. Kristallogr.* **234**, 623-646 (2019).
[2] T. Massalski, H. Okamoto, and P. R. Subramanian, editors. *Binary Alloy Phases Diagramms*, 2nd Edition, ASM International (1990).
[3] Z. Dong, J. D. Corbett, *Inorg. Chem.* **35**, 1444-1450 (1996).
[4] S. Kaskel, Z. Dong, M. T. Klem, J. D. Corbett, *Inorg. Chem.* **42**, 1835-1841 (2003).

Energy materials: batteries, photovoltaics, etc.

Evaluation of oxygen delivery from nanoporous perovskite solid solutions with in situ XRD and TG-MS

B. Ehrhardt[1], S. Mascotto[1], L. Gigli[2], N.-F. Meyer[1]

[1] University of Hamburg, Department of Chemistry, Hamburg, Germany

[2] Elettra-Sincrotrone Trieste S.C.p.A.„ Strada Statale 14, 34149 Basovizza, Trieste, Italy

Perovskite solid solutions are versatile materials, which are widely used especially in heterogeneous catalysis [1]. Their performance is determined by the materials'defect chemistry, charge charrier transport properties and surface area. Hence, nanoporous perovskites, due to their large surface and thus higher reactive area, are well suited for the use in Solid Oxide Fuel Cells (SOFC), solar-to-fuel processes, the oxidation of n-alkanes and the soot combustion in diesel exhaust gases. All these applications need oxygen as reactive species, so they are all strongly influenced by the oxygen release and transport property of a catalyst or substrate material [1-4].

In order to be able to tailor the perovskites for the above applications, we wanted to understand the influence of the porosity and surface area on oxygen delivery and transport in nanoporous perovskite solid solutions of cubic SrTiO3 with lanthanum and manganese which partly replaced strontium and titanium, respectively (space group $Pm\bar{3}m$). Samples were prepared using a modified Pechini synthesis with surface areas ranging from 5 m^2/g to 150 m^2/g [5]. Structural and morphological characterization of the samples were carried out via x-ray diffraction (XRD), electron microscopy and nitrogen physisorption. Oxygen delivery was quantified via thermogravimetric (TG) measurements coupled with mass spectrometry (MS) as well as in situ high temperature synchrotron radiation x-ray diffraction with temperatures up to 1223 K. Subsequent Rietveld refinement was used to determine the site occupation of oxygen at varying temperatures.

The highest oxygen release rates were found in the perovskite sample with higher porosity. All TG measurement showed three gradients at different temperatures during heating under low oxygen partial pressure, which we contribute to different oxygen species that where released from different sites of the perovskite lattice [6]. The measurements from the in situ x-ray diffraction supported the results from the TG-MS experiments well.

References

[1] Zhou X. *et al.*, *RSC Advances.*, pp. 118–131, 2014.

[2] A. H. McDaniel *et al.*, *Energy Environ. Sci.*, pp. 2424–2428, 2013.

[3] B. Kayaalp *et al.*, *Applied Catalysis B: Environmental.*, pp. 536-545, 2019.

[4] A. Kotarba *et al.*, *Applied Catalysis B: Environmental.*, pp. 169-175, 2011.

[5] B. E. Kayaalp *et al.*, *RSC Advances.*, pp. 90401–90409, 2016.

[6] N. A. Merino *et al.*, *Journal of Catalysis.*, pp. 232–244, 2005.

Cu/Zn disorder in Cu2ZnSn(SxSe1-x)4 monograins: the result of "ordering" procedure

G. Gurieva[1], A. Franz[2], S. Levcenko[2], K. Muska[2], K. Ernits[2], S. Schorr[3]

[1] Helmholtz Zentrum Berlin, Berlin, Germany

[2] Freie Universität Berlin, Department Geosciences, Berlin, Germany

[3] Helmholtz-Zentrum Berlin für Materialien und Energie, Berlin, Germany

Kesterite-type based thin film solar cell technologies are mainly based on polycrystalline absorber layers. A promising low cost alternative technology uses Cu2ZnSn(S,Se)4 (CZTSSe) monograins (single crystals of 50-100 μm size) which are fixed in a polymer matrix to form a flexible solar cell [1]. It is agreed in literature that large band tailing observed in Cu-based kesterite-type semiconductors causes voltage losses limiting the efficiency of kesterite-based devices. The Cu/Zn disorder (CuZn and ZnCu anti-sites in Cu-Zn planes at z=$\frac{1}{4}$ and $\frac{3}{4}$), which is always present in these compounds [2], is discussed as a possible reason for band tailing. The experimental determination of the order parameter Q which is a quantitative measure of the degree of Cu/Zn disorder [3] requires a differentiation between the isoelectronic cations Cu+ and Zn2+. An in depth analysis of neutron diffraction data provides information on the cation distribution in the crystal structure allowing the determination of type and concentration of intrinsic point defects including a distinction between Cu and Zn [2]. On the other hand neutron diffraction requires large sample volumes, thus kesterite monograins offer the unique possibility to correlate structural disorder in kesterite-type absorbers with device performance parameters. We will present a detailed structural investigation of the effect of the disordering procedure and the long low temperature – "ordering" annealing on the Cu/Zn disorder and optical properties of the CZTSSe monograins will be presented.

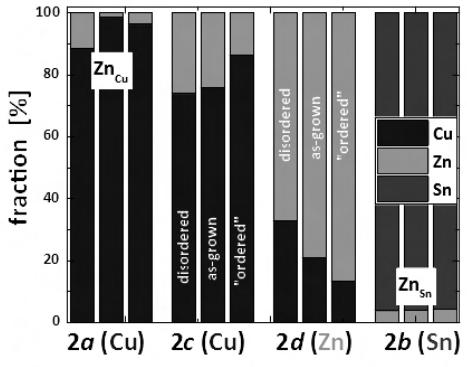

Figure 1

Proton motions in hydrogen bonds of hureaulite-type phosphatic oxyhydroxides

A. Hartl[1], S. Park[1], F. Juranyi[2], M. Krack[2], D. Cheptiakov[2], M. Appel[3], C. Paulmann[4], A. Arauzo[5], P. Lunkenheimer[6]
[1] Ludwig-Maximilians-Universität München, Germany
[2] Paul Scherrer Institut, Villigen, Switzerland
[3] Institut Laue-Langevin, Grenoble, France
[4] DESY, Hamburg, Germany
[5] Universidad de Zaragoza, Zaragoza, Spain
[6] Universität Augsburg, Augsburg, Germany

The peculiar hydrogen arrangement in the hureaulite-type manganese endmember $(Mn_5[(PO_4)_2(PO_3OH)_2](HOH)_4)$ comprises semihelical hydrogen bond chains along porous channels as well as framework HOH ligands in small cages. Results from extensive, complementary studies are presented to show (1) the time and length scales of local and long-range proton dynamics in the title compound and (2) contribute to the basic understanding of proton transport in confinement.

Diffuse difference Fourier maps around those hydrogen bond chains evaluated with X-ray single crystal and high-resolution neutron powder diffraction data adumbrate strong protonic disorder above 250 K together with fast rotating framework polyhedra. This temperature coincides with the onset of DC conductivity as probed by broadband dielectric spectroscopy. Neutron time-of-flight and backscattering spectroscopy revealed proton motions above room temperature with an activation energy of 0.39(1) eV and relaxation time of 11(2) ps. With a combined quasielastic neutron scattering data treatment, alongside geometrical considerations and ab initio molecular dynamics studies, these local motions were assigned to the rotations of HOH groups within the hydrogen bond chains. The vibrational density of states, collected with inelastic neutron scattering, was compared with experimentally obtained infrared and Raman spectra as well as simulated spectra based on electronic structure calculations.

As a result, we could elucidate lattice-dynamic-induced proton motions over the hydrogen bond network in this phosphatic oxyhydroxide. Such proton-phonon coupling is of great interest in the search for superprotonic conductors.

Dynamics of the Lithium-Distribution in commercial LFP|C lithium-ion batteries under charge/discharge

D. Petz[1], V. Baran[2], M. Mühlbauer[3], A. Schökel[4], M. Hofmann[5], P. Müller-Buschbaum[1], A. Senyshyn[5]
[1] Technical University of Munich, Munich, Germany
[2] DESY, Photon Science, FS-PS (FS-Photon Science), Hamburg, Germany
[3] Karlsruhe Institute of Technology (KIT), Karslruhe, Germany
[4] DESY, Notkestr. 85, 22607 Hamburg, Germany
[5] Heinz Maier-Leibnitz Zentrum (MLZ), Garching, Germany

Operation of typical lithium-ion battery is supplemented by the continuous mass transfer, which affects the ionic transport through the electrodes and electrolyte. Ionic transfer is defined by different factors like electrode dimensions and geometry, current density, temperature, pressure, reaction rate etc. All these properties are not necessarily uniformly distributed and, therefore, can affect heterogeneities in lithium concentrations in the cell electrodes [1, 2].

Typically, the lithium distribution in the graphite anode was probed at cells in fully charged and well equilibrated state, leaving the evolution of lithium distribution under real cell charging unclear.

In the current work, the lithium-ion distribution in a graphite anode and a lithium-iron-phosphate cathode were studied using a combination of spatially-resolved neutron-powder diffraction (anode) and X-ray powder diffraction (cathode) during the cell charge/discharge. It will be shown, that different inhomogeneities occur on different length scale still complementing each other.

References

[1] Senyshyn, A. *et al.*, "Homogeneity of lithium distribution in cylinder-type Li-ion batteries," *Scientific Reports*, vol. 5, no. 1, p. 18380, 2015.

[2] Petz, D. *et al.*, "Heterogeneity of Graphite Lithiation in State-of-the-Art Cylinder-Type Li-Ion Cells," *Batteries & Supercaps*, in print.

Extreme/non-ambient conditions

Squeezing the most data out of your high-pressure experiment

J. Graf[1], T. Stürzer[2], P. Dera[3], M. Ruf[4]

[1] Incoatec GmbH, Geesthacht, Germany

[2] Bruker AXS GmbH, Karlsruhe, Germany

[3] University of Hawaii, 2500 Campus Rd, Honolulu, HI 96822, USA

[4] Bruker AXS Inc, Madison, WI, USA

Within the last decade high pressure studies have received significant increase of interest. Present typical applications range from the investigation of high-pressure polymorphism of solid-state organics as part of the pharmaceutical drug development to the study of rocks and minerals with an applied pressure of up to 50 GPa.

A major challenge in the field of high pressure crystallography is the acquisition of data of sufficient quality and completeness for a successful structure determination. This presentation will be reviewing recent advances in hardware development, such as X-ray sources with radiation harder than Mo-Kα, and highlight the latest improvements in software, which help in tackling the problems with data acquisitions in high-pressure experiments.

Using a Bruker D8 VENTURE system, we will be demonstrating the advanced hardware capabilities and processing methods based on selected data, including data from the Indium METALJET X-ray source. Further, we will be showing how to increase the completeness of high-pressure experiments by mounting multiple samples in a diamond anvil cell and measuring and processing data concurrently.

The high flexibility of the D8 VENTURE can be further expanded by adding enhanced features typically only available at synchrotron facilities, e.g. for studying tiny mineral crystals enclosed in diamond anvil cells. These features include highly accurate, motorized sample positioning and the ability to monitor the intensity of the X-ray beam passing through the diamond anvil cell, as well as an extension for online pressure measurements based on ruby fluorescence. This makes the D8 VENTURE system "a little synchrotron at home".

Framework structures: MOFs, COFs, etc.

Elucidating the structural evolution of a highly porous responsive metal-organic framework (DUT-49(M)) upon guests desorption by time-resolved in-situ powder X-ray diffraction

V. Bon[1], B. Garai[1], F. Walenszus[1], A. Khadiev[2], D. Novikov[2], S. Kaskel[1]

[1] Technical University of Dresden, Dresden, Germany

[2] DESY, Photon Science, PETRA III, P23 Beamline, Hamburg, Germany

Metal-organic frameworks (MOFs) are 3-dimensional architectures constructed via the coordination of metal ions or cluster as nodes and organic linkers as struts, resulting in crystallographically well-defined porosity.[1] After removing the guest molecules from the pores, record values of surface area and pore volumes can be reached.

A unique type of adsorption-induced phenomenon has been discovered in the hierarchical mesoporous Cu2(BBCDC) framework, further denoted as DUT-49(Cu).[2] The MOF is constructed from the coordination of tetratropic carbazole-based linker with Cu-Cu paddlewheel, forming three distinct types of pores: cuboctahedral MOPs with 10 Å in diameter, interconnected by edges via biphenyl moieties and form additional tetrahedral (17 Å) and octahedral (24 Å) cages.[3] The framework can be desolvated by exchange with supercritical CO2 without losing crystallinity. Variation in the metal centres of M-M paddle-wheel SBU results in the formation of isostructural DUT-49(M) [DUT-49(M); M= Ni, Mn, Fe, Co, Zn, Cd] frameworks. However, the porosity of the framework was found to be different for each of the structures. All attempts to regain the structure by resolvation at elevated temperatures were unsuccessful and only only DUT-49(Cu) and DUT-49(Ni) retain the structural integrity after the supercritical drying procedure. Thus, herein, we aimed to study the detailed structural transformations that are possibly occurring during the removal of the subcritical fluid from the framework by time-resolved synchrotron PXRD at P23 beamline aiming to access the structural pathways of the framework collapse [4].

References

[1] a) S. Kitagawa, R. Kitaura, S.-i. Noro, *Angew. Chem., Int. Ed.* vol. 43, pp. 2334-2375, 2004; b) M. Eddaoudi, D. B. Moler, H. Li, B. Chen, T. M. Reineke, M. O'Keeffe, O. M. Yaghi, *Acc. Chem. Res.*, vol. 34, pp. 319-330, 2001; c) S. R. Batten, N. R. Champness, X.-M. Chen, J. Garcia-

Martinez, S. Kitagawa, L. Öhrström, M. O'Keeffe, M. P. Suh, J. Reedijk, *Cryst. Eng. Comm.*, vol. 14, pp. 3001-3004, 2012; d) H. Furukawa, N. Ko, Y. B. Go, N. Aratani, S. B. Choi, E. Choi, A. Ö. Yazaydin, R. Q. Snurr, M. O'Keeffe, J. Kim, O. M. Yaghi, *Science*, vol. 329, pp. 424, 2010.

[2] S. Krause, V. Bon, I. Senkovska, U. Stoeck, D. Wallacher, D. M. Többens, S. Zander, R. S. Pillai, G. Maurin, F.-X. Coudert, S. Kaskel, *Nature*, vol. 532, pp. 532, 348-352, 2016.

[3] U. Stoeck, S. Krause, V. Bon, I. Senkovska, S. Kaskel, *Chem. Commun.*, vol. 48, pp. 10841-10843, 2012.

[4] B. Garai, V. Bon, F. Walenszus, A. Khadiev, D. V. Novikov, S. Kaskel, *Cryst. Growth Des.*, vol. 21, 2020, DOI: 10.1021/acs.cgd.0c01080.

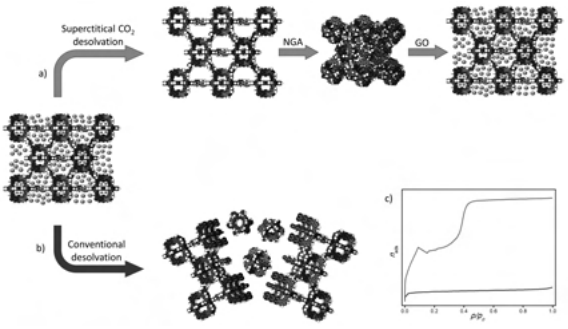

Figure 1 Strucutral transformation of DUT-49(Cu) MOF during solvent removal through (a) supercritical CO2 activation approach to retain the highly porous (op) phase that can undergo further structural transition during gas adsorption process; and (b) conventional activation approach. (c) Typical adsorption isotherm from op phase of the framework (green line) and amorphous phase (red line).

A new type of hydrous layer silicates and zeolites obtained by 3D electron diffraction

Y. Krysiak[1], B. Marler[2], L. Palatinus[3], U. Kolb[4]

[1] Institute of Inorganic Chemistry, Leibniz University Hannover, Hannover, Germany

[2] Departure of Geology, Mineralogy and Geophysics, Ruhr University Bochum, Bochum Germany

[3] Department of Structure Analysis, Institute of Physics of the Czech Academy of Sciences, Prague, Czech Republic

[4] Centre for High Resolution Electron Microscopy, Johannes Gutenberg University Mainz, Mainz Germany

The structure elucidation of zeolites and their related hydrous layer silicates (HLS) is an important aspect in the extensive investigation of structure, synthesis and function of these materials to identify potential applications. The hydrothermal synthesis usually results in crystals that are too small for conventional single crystal X-ray diffraction experiments. Furthermore, the structure determination is even more complicated due to the presence of diffuse scattering, which originates from stacking disorder of the weakly bonded silica layers.

Complete structural models based on the real and average structure of different HLS resp. zeolite samples (RUB-5, RUB-6 and RUB-11) were developed with high-resolution transmission electron microscopy (HRTEM) and 3D electron diffraction (3D ED).

The complex structures of RUB-5, RUB-6 and RUB-11 could be solved ab initio even though strong diffuse scattering with pseudo-tetragonal symmetry was present. The structures of RUB-5 and layer silicate RUB-6 contain the same dense layer-like building units (LLBU). In the case of RUB-5, these building units are interconnected via additional SiO4/2 tetrahedra, giving rise to a framework structure with a two-dimensional pore system consisting of intersecting 8-ring channels. RUB-5 and RUB-11 which are structurally related can be described as pure silica "zeolites" with high framework densities of 22.0 and 21.2 silicon atoms per 1000 $Å^3$.[1]

The frameworks of RUB-5 and RUB-11 are unique and represent two new silica polymorphs. In addition to the comprehensive structural descriptions, the extracted diffuse scattering was used to show that the formation of RUB-5 and RUB-6 occurs through a similar intermediate step.

Acknowledgement

This research was supported by the Czech Science Foundation (project No. 19-08032S).

References

[1] Y. Krysiak, B. Marler, B. Barton, S. Plana-Ruiz, H. Gies, R. B. Neder, U. Kolb, *IUCrJ*, vol. 7, 2020, DOI 10.1107/S2052252520003991.

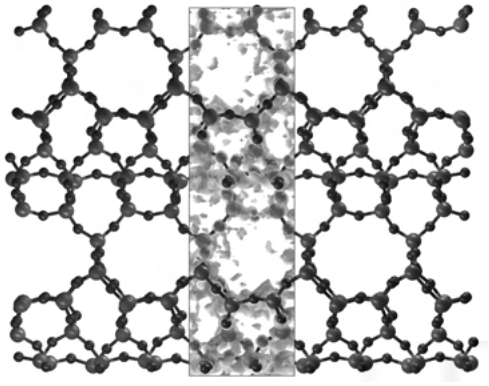

Figure 1 Potential map of structure solution of RUB-11 combined with structure model projected down [100].

Tuning the high-pressure phase behaviour of ultra-compressible zeolitic imidazolate frameworks – From discontinuous to continuous pore closure by linker substitution

J. Song[1], R. Pallach[1], S. Henke[1]

[1] Technical University of Dortmund, Faculty of Chemistry and Chemical Biology, Anorganic Chemistry, Otto-Hahn-Straße 6, 44227 Dortmund, Germany

Zeolitic imidazolate frameworks (ZIFs), a very important subfamily of metal-organic frameworks (MOFs), are constructed from tetrahedrally coordinated M2+ (Zn2+ or Co2+) ions, which are interlinked by imidazolate linkers[1]. Recently, we discovered that the prototypical ZIF-4 (chemical composition M(im)2, im– = imidazolate) undergoes a phase transition from an open pore (op) to a closed pore (cp) phase under hydrostatic pressure[2]. Here we further present the high-pressure (HP) behaviour of a series of isostructural ZIF-4 derivatives, named ZIF-62, with the general chemical composition M(im)2-x(bim)x (bim– = benzimidazolate, $0.02 < x < 0.35$). The ZIF-62 materials crystallize in the space group Pbca and feature the same network topology (cag) as the original ZIF-4, however, some of the im– linkers are substituted by the bulkier bim– linkers. HP-PXRD experiments were performed at beamline I15 of Diamond Light Source in the pressure range from ambient up to 4000 bar using silicon oil as a non-penetrating pressure transmitting medium and a hydraulic pressure cell[3]. Under hydrostatic pressure, all ZIF-62 derivatives reversibly contract from the op to the cp phase only by rotations about the imidazolate-metal bonds (Fig. 1). Crystal symmetry and network topology are preserved. With increasing bim— concentration, the threshold pressure for the op-cp phase transition increases from 700 bar to 1300 bar and the overall volume contraction across the transition decreases from 25% to 17% of the initial volume. Most importantly, the 1st order (discontinuous) transition transfers to a 2nd order (continuous) transition for $x > 0.30$. Thus, the void space and pore openings of ZIF-62 can be tuned continuously by the application of mechanical pressure – a unique feature which might be useful for adjusting and enhancing the gas separation performance of these flexible MOFs.

References

[1] a) J. H. Lee, S. Jeoung, Y. G. Chung, H. R. Moon, *Coord. Chem. Rev.*, vol. 389, p. 161, June 2019. b) J.-P. Zhang, Y.-B. Zhang, J.-B. Lin, X.-M. Chen, *Chem. Rev.*, vol. 112. p. 1001, Feb. 2012.

[2] S. Henke, M. T. Wharmby, G. Kieslich, I. Hante, A. Schneemann, Y. Wu, D. Daisenberger, A. K. Cheetham, *Chem. Sci.*, vol. 9, p. 1654, Feb. 2018.

[3] N. J. Brooks, B. L. L. E. Gauthe, N. J. Terrill, S. E. Rogers, R. H. Templer, O. Ces, J. M. Seddon, *Rev. Sci. Instrum.*, vol. 81, no. 6, May 2010, Art. no. 64103.

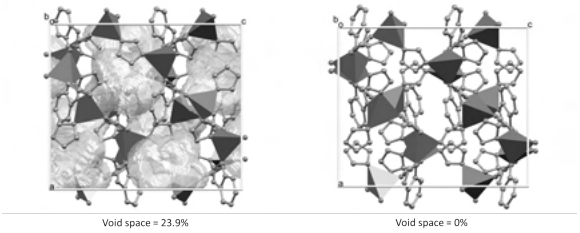

Figure 1 Structural models of ZIF-62 with the composition Zn(im)1.65(bim)0.35 at ambient pressure (left) and 4000 bar (right). The void space available for CO2 molecules (kinetic diameter = 3.30 Å) is shown in gold.

Inorganic crystal structures

$Mn(H_2O)_6[B_{10}Cl_{10}] \cdot 2.5\ H_2O$: Synthesis and Crystal Structure

K. U. Bareiß[1], F. B. Goerigk[1], T. Schleid[1]

[1] University of Stuttgart, Institute for Inorganic Chemistry, Pfaffenwaldring 55, 70569 Stuttgart, Germany

The previously reported crystal structure of $Tl_2[B_{10}Cl_{10}] \cdot 2\ H_2O$ [1] led to the preparation of further hydrated salts with perchlorinated B_{10}-cluster analogues, such as $Mg(H_2O)_6[B_{10}Cl_{10}] \cdot 2.5\ H_2O$ [2]. We now present the synthesis and structural characterization of $Mn(H_2O)_6[B_{10}Cl_{10}] \cdot 2.5\ H_2O$ (CSD-2052005) crystallizing isotypically with $Mg(H_2O)_6[B_{10}Cl_{10}] \cdot 2.5\ H_2O$ and $Co(H_2O)_6[B_{10}Cl_{10}] \cdot 2.5\ H_2O$ [2] in the triclinic space group $P\bar{1}$ with $a = 1172.06(3)$ pm, $b = 1237.42(3)$ pm, $c = 1752.73(4)$ pm, $\alpha = 84.409(2)^\circ$, $\beta = 88.942(2)^\circ$ and $\gamma = 88.694(2)^\circ$ for $Z = 4$. The $[B_{10}Cl_{10}]^{2-}$-cluster anions feature typical B−−B bond lengths of 167 – 169 pm to the caps and 181 – 185 pm inside the square antiprisms as well as B−−Cl distances from 178 to 181 pm. The four crystallographically different Mn^{2+} cations at special sites (1*a*, 1*b*, 1*e* and 1*h*) are coordinated by six water molecules each, of which always three are crystal-

lographically unique. The Mn−−O distances within the $[Mn(H_2O)_6]^{2+}$ octahedra reach from 213 to 222 pm and therefore are significantly longer than in the Mg- and Co-analogues, which show average distances of 207 (Mg) and 209 pm (Co) [2]. These distances perfectly fit the M−−O distance trends in the $M(H_2O)_6[B_{10}H_{10}] \cdot 2\ H_2O$ series (M = Mn – Ni and Zn) crystallizing in the monoclinic space group $C2/c$ [3]. The $[Mn(H_2O)_6]^{2+}$ octahedra in $Mn(H_2O)_6[B_{10}Cl_{10}] \cdot 2.5\ H_2O$ are connected through five crystallographically different interstitial water molecules, revealing O···O distances from 274 to 285 pm, which may be discussed as O−−H···O hydrogen bridges. The water bridged $[Mn(H_2O)_6]^{2+}$ octahedra build up a three-dimensional network of linked chains along [110], [1$\bar{1}$0] and [001] with interstices filled up with the bicapped square antiprismatic $[B_{10}Cl_{10}]^{2-}$ anions.

In order to prepare $Mn(H_2O)_6[B_{10}Cl_{10}] \cdot 2.5\ H_2O$ solid manganese(II) carbonate ($Mn[CO_3]$) was neutralized by an aqueous acidic solution of $(H_3O)_2[B_{10}Cl_{10}]$. The reaction mixture was filtrated and the pale pink solution slowly evaporated isothermally to obtain almost colorless crystals of $Mn(H_2O)_6[B_{10}Cl_{10}] \cdot 2.5\ H_2O$ from the mother liquor.

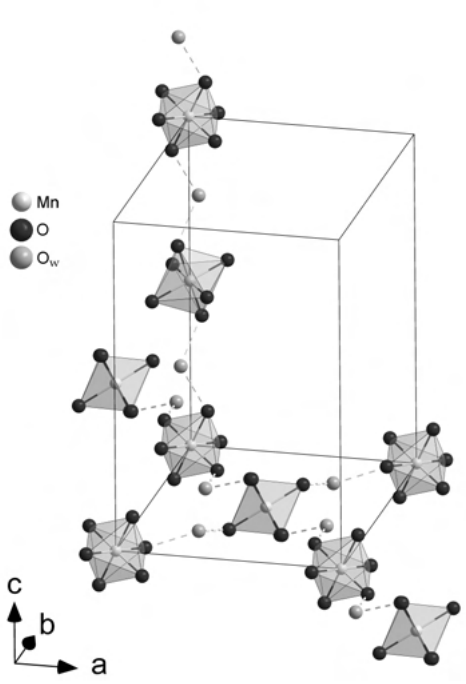

Figure 1 Extended unit cell of $Mn(H_2O)_6[B_{10}Cl_{10}] \cdot 2.5\ H_2O$ as viewed along [001] (*left*) and [100] (*right*).

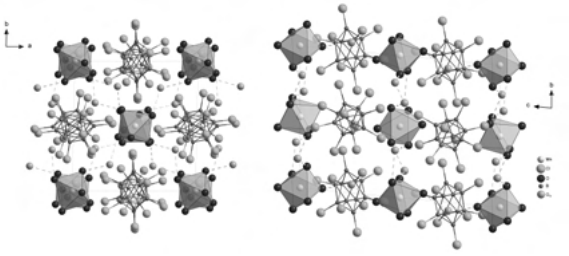

Figure 2 Simplified network $^3_\infty[[Mn(H_2O)_6](H_2O)_{6/2}]^{2+}$ of water-bridged $[Mn(H_2O)_6]^{2+}$ octahedra in $Mn(H_2O)_6[B_{10}Cl_{10}] \cdot 2.5\ H_2O$.

References

[1] K. U. Bareiß, Th. Schleid, in *Joint Polish-German Crytallographic Meeting, February 24–27, 2020, Wroclaw, Poland,* Berlin, Germany, Boston, USA: De Gruyter, 2020, pp. 64–64.

[2] F. M. Kleeberg, Doctoral Dissertation, University of Stuttgart, Germany, 2017.

[3] L. W. Zimmermann, Th. Schleid, *Z. Kristallogr.*, vol. 228, no. 10, pp. 558–564, Oct. 2013.

Group-Subgroup Relationships in Wurtzite-related Nitrides

J. Breternitz[1,2], S. Schorr[1]

[1] Helmholtz-Zentrum Berlin für Materialien und Energie, Hahn-Meitner Platz 1, 14109 Berlin, Germany

[2] University of Potsdam, Potsdam, Germany

A vast number of materials crystallise in the wurtzite-type structure or one of its subgroups. A prominent class of materials that crystallises in this structural family are wurtzite- and wurzite-related nitrides, some of which are, for instance, hopeful solar absorber materials. The different cation orderings and structural distortions in this class of materials open a rich variety of different crystal

structures in subgroups of the wurtzite-type structure. We establish a structural-systematic to this class of materials, which culminates in the establishment of a Bärnighausen tree. [1]

In a second part, we illustrate the practical use of this structural-systematic work on the example of $Zn(IV)N_2$ materials (IV = Ge, Sn). Those materials crystallise either in the wurtzite aristotype structure [2] where the Zn^{2+} and IV^{4+} cations are disordered, or in the ß-$NaFeO_2$-type structure, where the cations are ordered.[3] Furthermore, a third potential structure in the wurtzite subgroup $Pmc2_1$ was proposed that has a nominally higher symmetry than the ß-$NaFeO_2$-type structuer in space group $Pna2_1$.[4] We demonstrate why this alternative in space group $Pmc2_1$ is unlikely to form, due to the symmetry arrangement in this space group.

References

[1] J. Breternitz, S. Schorr, *Acta Crystallogr. A*, to be published.
[2] J. Breternitz, Z. Y. Wang, A. Glibo, A. Franz, M. Tovar, S. Berendts, M. Lerch and S. Schorr, *Phys. Status Solidi (a)*, vol. 216, 2019, Art. no. 1800885.
[3] E. W. Blanton, K. He, J. Shan, K. Kash, *J. Cryst. Growth*, vol. 461, pp. 38–45, 2017.
[4] P. C. Quayle, *Acta Crystallogr. A*, vol. 76, pp. 410–420, 2020.

Crystal-structure determination of hydrothermally produced nanocrystalline synthetic bastnaesite-type NdF[CO_3]

C. Buyer[1], T. Schleid[1]
[1] University of Stuttgart, Institute for Inorganic Chemistry, Stuttgart, Germany

In 1930 *Oftedal* reported the crystal structure of the mineral bastnaesite $REF[CO_3]$ (RE = La – Nd) in the hexagonal space group $P\bar{6}2m$ with a = 709.4(7) pm, c = 485.9(4) pm for Z = 3 [1]. In 1931 he did a correction of his 1930s result and found the space group $P\bar{6}2c$ with a = 709.4(7) pm, c = 971.8(8) pm for Z = 6 [2]. The most abundant rare-earth metal ore mineral is bastnaesite [3]. An Eu^{3+}-doped version of $LaF[CO_3]$ shows luminescence and after thermal decomposition trimorphic LaFO (or LaFO:Eu^{3+}) is obtained [4, 5]. While *Jansen et al.* [6] synthesized bastnaesites by adding aqueous HF to a dispersion of $Ce_2O[CO_3]_2 \cdot 4\,H_2O$ in water under a CO_2 atmosphere, *Janka* and *Schleid* [4] added a solution of $Na[HCO_3]$ and NaF dropwisely to a stirred solution of $La[NO_3]_3 \cdot 6\,H_2O$. Now we synthesized $NdF[CO_3]$ by adding a hot solution of NaF and $Na_2[CO_3]$ fast to a hot solution of $Nd[NO_3]_3 \cdot 6\,H_2O$. After that, we washed the resulting pale bluish violet, insoluble fine powder to remove the soluble by-products with water and dried it at 110 °C. About 150 mg of that powder was heated up to 200 °C for 5 days with about 5 ml water in a teflon autoclave. An X-ray diffraction powder pattern (Figure 1, top) was measured with Cu-Kα radiation on a STADI-P device and Rietveld refinement with the Fullprof program was used for the crystal structure refinement. Our obtained compound $NdF[CO_3]$ (CSD-2053207) crystallizes in the hexagonal space group $P\bar{6}2c$ (no. 190) with a = 707.48(1) pm, c = 973.45(2) pm for Z = 6. The atomic parameters are given in Figure 1 (bottom). The average crystallite size was calculated to be about 30 nm by using *Scherrer* equation. Figure 2 is showing a unit cell of $NdF[CO_3]$ with alternating layers of Nd^{3+}/F^- and $[CO_3]^{2-}$ ions (d(Nd—F) = 239 – 248 pm (3×), d(Nd—O) = 249 – 268 pm (6×) + 304 pm (2×), C.N.(Nd^{3+}) = 9 + 2, d(C—O) = 139 – 152 pm).

References

[1] I. Oftedal, *Z. Kristallogr.*, vol. 72, pp. 239–248, 1930.
[2] I. Oftedal, *Z. Kristallogr.*, vol. 78, pp. 462–469, 1931.
[3] Y. Ni, J. M. Hughes, A. N. Mariano, *Am. Mineral.*, vol. 78, pp. 415–418, 1993.
[4] O. Janka, Th. Schleid, *Eur. J. Inorg. Chem.*, vol. 2009, pp. 357–362, 2009.
[5] C. Buyer, J. Cybinska, E. Zych, Th. Schleid, *in preparation*, 2021
[6] G. J. Jansen, G. B. Magin, B. Levin, *Am. Mineral.*, vol. 44, pp. 180–181, 1959.

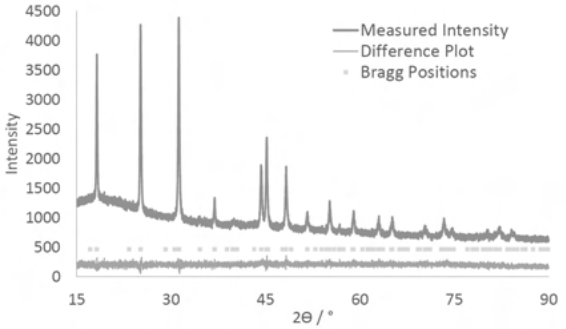

Atom	Wyckoff Site	Symmetry	x/a	y/b	z/c
Nd	6g	.2.	0.3375(9)	0	0
F1	2a	32.	0	0	0
F2	4f	3..	1/3	2/3	0.082(3)
C	6h	m..	0.201(6)	0.267(7)	1/4
O1	6h	m..	0.250(5)	0.005(7)	1/4
O2	12i	1	0.371(6)	0.311(7)	0.1405(11)

Figure 1 Rietveld structure refinement of $NdF[CO_3]$ with bastnaesite-type structure (top) and atomic parameters (bottom).

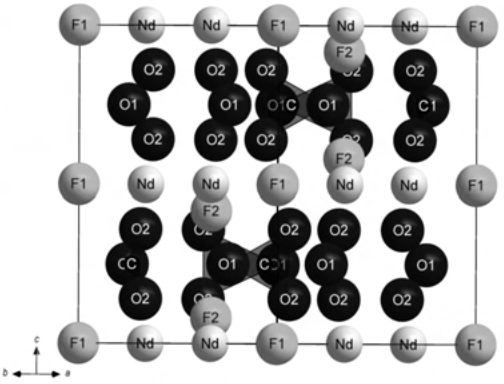

Figure 2 Hexagonal unit cell of $NdF[CO_3]$ as viewed along [110].

Single crystals of orthorhombic BaTa2O6: Serendipitous formation and rational structure determination

M. Conrad[1], T. Schleid[1]

[1] University of Stuttgart, Institute for Inorganic Chemistry, Stuttgart, Germany

The trimorphism of $BaTa_2O_6$ was first described in 1967 by Layden, who grew crystals of an orthorhombic low-temperature and a hexagonal high-temperature modification, along with powder samples of tetragonal $BaTa_2O_6$, which is stable in between [1]. However, he was just able to propose a structure model for hexagonal $BaTa_2O_6$ based on powder X-ray diffraction data in 1968 [2]. Almost half a decade later, in 2007 *Mumme* et al. [3] could collect single-crystal data and determined the structure of hexagonal $BaTa_2O_6$. The structures of the other polymorphs remained elusive until today, which is why the synthesis and characterization of orthorhombic $BaTa_2O_6$ is described here and now.

During an attempt to prepare mixed-anionic barium meta-perrhenates by arc melting equimolar amounts of barium fluoride (BaF_2) and anhydrous barium meta-perrhenate ($Ba[ReO_4]_2$) in an open tantalum crucible using a high-frequency furnace, few single crystals of orthorhombic $BaTa_2O_6$ were obtained after cooling the reaction mixture from roughly 2600 K to room temperature.

Orthorhombic $BaTa_2O_6$ crystallizes in the space group *Cmcm* with lattice parameters of a = 768.96(4) pm, b = 1233.25(7) pm and c = 1032.98(6) pm for Z = 8 (CSD 1897796) matching well with the cell parameters previously reported by *Layden* in 1967 (a = 767 pm, b = 1026 pm, c = 1233 pm) [1].

The crystal structure contains crystallographically unique Ta^{5+} cations octahedrally surrounded by six oxygen atoms (d(Ta–O) = 194 – 204 pm) along with two distinct Ba^{2+} cations in tenfold and twelvefold coordination of oxygen atoms (d(Ba–O) = 275 – 318 pm). Strands of alternatively corner- and edge-sharing $[TaO_6]^{7--}$ octahedra propagate along [010] (Figure 1, *left*), becoming interconnected by a single common oxygen vertex per polyhedron to form corrugated layers parallel to the (001) plane (Figure 1, *right*). These layers are connected in the [001] direction at every second octahedron leading to a three-dimensional network 3D-$[Ta_2O_6]^{2--}$ with Ba^{2+} cations in its voids (Figure 2).

References

[1] G. K. Layden, *Mater. Res. Bull.*, vol. 2, no. 5, pp. 533–539, May 1967.

[2] G. K. Layden, *Mater. Res. Bull.*, vol. 3, no. 4, pp. 349–359, Apr. 1968.

[3] W. G. Mumme, I. E. Grey, R. S. Roth, T. A. Vanderah, *J. Solid State Chem.*, vol. 180, no. 9, pp. 2429–2436, Sep. 2007.

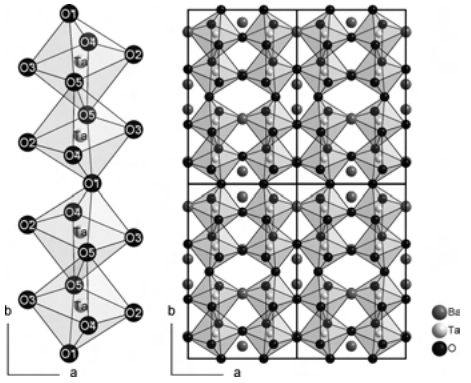

Figure 1 Chains of corner- and edge-sharing $[TaO_6]^{7--}$ octahedra running along [010] (*left*) and corrugated layers of these vertex-connected chains parallel to the (001) plane (*right*) in $BaTa_2O_6$.

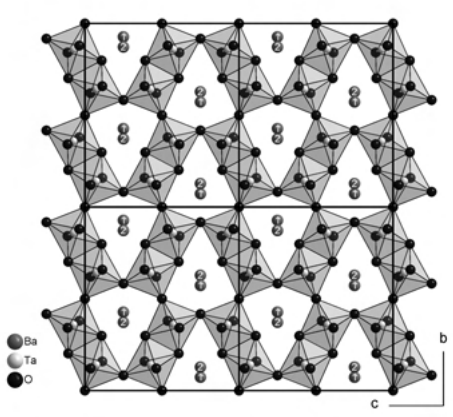

Figure 2 View at the network of interconnected $[TaO_6]^{7--}$ octahedra in $BaTa_2O_6$ along [100] with two kinds of Ba^{2+} cations in the voids.

Synthesis, Crystal Structure and Magnetic Properties of $Gd_2Se[SiO_4]$

P. Djendjur[1], B. Blaschkowski[1], T. Schleid[1]

[1] University of Stuttgart, Institute for Inorganic Chemistry, Stuttgart, Germany

Solid-state syntheses in glassy silica ampoules including elemental rare-earth metals sometimes yield unwanted by-products, such as multinary oxosilicates due to uncontrolled reactions with the container material. An attempt to synthesize Gd_2O_2Se in fused silica vessels furnished colorless, plate-shaped crystals of the title compound, which has structurally not yet been described based on single-crystal X-ray diffraction data in literature. Many other representatives of this substance class of lanthanoid selenide oxosilicates $Ln_2Se[SiO_4]$ (Ln = La, Ce, Nd, Sm, Eu, Tb – Er) have been well characterized throughout the years, however [1–7].

The oxidation of gadolinium metal with selenium dioxide in a molar ratio of 2:1 designed to produce Gd_2O_2Se with caesium chloride as flux led to the formation of $Gd_2Se[SiO_4]$ after some reaction with the SiO_2 container material. This gadolinium selenide *ortho*-oxosilicate crystallizes orthorhombically in the space group *Pbcm* (no. 57) with the lattice parameters a = 607.48(5) pm, b = 702.85(6) pm and c = 1086.74(9) pm for Z = 4 (CSD-2053795).

This structure exhibits two crystallographically distinct Gd^{3+} cations, which feature an (8+1)-membered coordination sphere for $(Gd1)^{3+}$ (6 O and 2+1 Se, d(Gd–O) = 242 – 254 pm, d(Gd–Se) = 291 – 352 pm) and an (8+2)-membered coordination sphere for $(Gd2)^{3+}$ (6 O and 2+2 Se, d(Gd–O) = 239 – 243 pm, d(Gd–Se) = 308 – 376 pm), respectively (Figure 1). Thereby, this structure exhibits Se^{2--} centered $(Gd^{3+})_7$ polyhedra (capped trigonal prisms) connected via corners, edges and faces to form a three-dimensional network $^3_\infty\{[Se(Gd1)_{3/3}(Gd2)_{4/4}]^{4+}\}$ with empty voids apt to be filled with tetrahedral $[SiO_4]^{4--}$ anions (d(Si–O) = 163 – 165 pm) for charge compensation (Figure 2).

Magnetic susceptibility measurements for a bunch of selected crystals of $Gd_2Se[SiO_4]$ show a magnetic moment of μ_{exp} = 7.92 μ_B, which corresponds well to the expected value of μ_{eff} = 7.94 μ_B [8]. The θ value of –7.2 K in the *Curie-Weiss* equation suggests a certain tendency to antiferromagnetic ordering at very low temperatures (Figure 3).

References

[1] T. D. Brennan, J. A. Ibers, *Acta Crystallogr. C*, vol. 47, pp. 1062–1064, 1991.

[2] B. Deng, J. Yao, J. A. Ibers, *Acta Crystallogr. C*, vol. 60, pp. i110–i112, 2004.

[3] M. Grupe, W. Urland, *Z. Naturforsch.*, vol. 45 b, pp. 465–468, 1990.

[4] H. Person, M. Grupe, W. Urland, *Z. Anorg. Allg. Chem.*, vol. 626, pp. 280–283, 2000.

[5] D. D. Zimmermann, Th. Schleid, *Z. Kristallogr./Suppl.*, vol. 36, pp. 88–88, 2016.

[6] I. Ijjaali, K. Mitchell, J. A. Ibers, *Z. Kristallogr. – NCS*, vol. 217, pp. 157–158, 2002.

[7] K. Stöwe, *Z. Naturforsch.*, vol. 49 b, pp. 733–740, 1994.

[8] A. Weiss, H. Witte, *Magnetochemie*, 1. ed, Weinheim, Germany: Verlag Chemie GmbH, 1973, pp. 187–189.

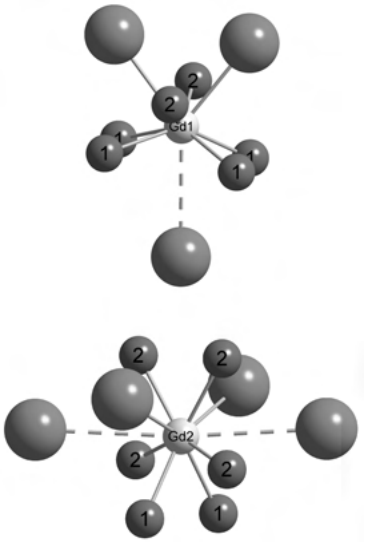

Figure 1 Coordination polyhedra of $(Gd1)^{3+}$ *(top)* and $(Gd2)^{3+}$ *(bottom)* in $Gd_2Se[SiO_4]$.

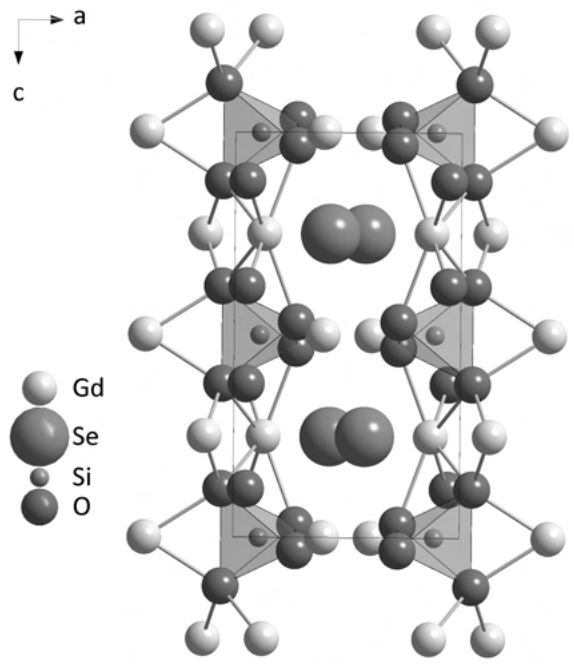

Figure 2 Extended unit cell of $Gd_2Se[SiO_4]$ as viewed along [010].

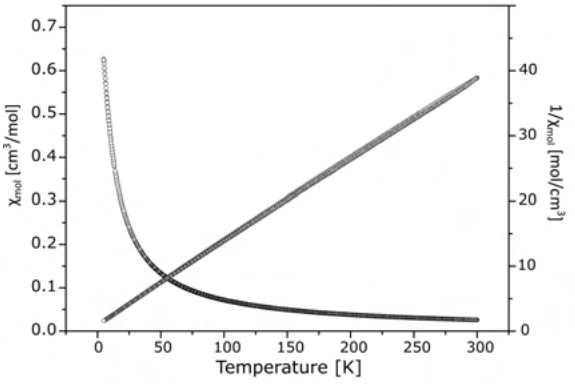

Figure 3 Molar *(black)* and inverse molar susceptibility (red) of $Gd_2Se[SiO_4]$

.

High-Pressure Hydrothermal Synthesis and Single Crystal X-Ray Structure Determination of K_2TmF_5

F. C. Goerigk[1], T. Schleid[1]

[1] University of Stuttgart, Institute of Inorganic Chemistry, Stuttgart, Germany

Prism-shaped single crystals of K_2TmF_5 could be obtained via hydrothermal synthesis from Tm_2O_3, TmF_3 and KF performed in a gold capsule filled with about 20 vol-% H_2O to provide suitable conditions for aiming at TmOF as target product. The sealed capsule was placed in a water-filled autoclave and kept at 300 °C and 75 bar pressure four five days. Single crystal X-ray diffraction revealed an orthorhombic unit cell (a = 1080.58(9) pm, b = 723.45(6) pm, c = 660.12(5) pm) for K_2TmF_5 in the space group *Pnma*.

The crystal structure of K_2TmF_5 features a crystallographically unique position for the Tm^{3+} cations with a coordination number of seven and interatomic $Tm^{3+} - -F^-$ distances of 218 – 227 pm. The edge-connected $[TmF_7]^{4--}$ polyhedra build up strands along the b-axis according to 1D-$[Tm(F1,2,3)^t_{3/1}(F4)^e_{4/2}]^{2--}$, which are bundled like a hexagonal rod packing (Figure 1). The potassium cations also occupy only one single position with a coordination number of eight *plus* one and bond lenghts of $d(K^+ - -F^- -)$ = 264 – 289 pm *plus* 334 pm. The $[KF_{8+1}]^{8--}$ polyhedra are – in contrast – connected via common edges in all spatial dimensions, but link the 1D-$[Tm(F1,2,3)^t_{3/1}(F4)^e_{4/2}]^{2--}$ chains as shown in Figure 2.

In hitherto research, the hydrothermal synthesis of K_2TmF_5 was published for the first time in 1990, but no crystallographic details such as a possible space group or atomic positions were given [1]. Other compounds concerning the K–Ln–F systems, such as K_2SmF_5 (1973) or K_2ErF_5 (1982), have been described using the non-centrosymmetric space group $Pna2_1$ [2, 3]. Single crystal structure solution and refinement calculations in this space group led to a *Flack-x* parameter of 0.45(7), so furthermore no obvious reason resulting in a loss of inversion symmetry could be identified. Hence, the centrosymmetric crystal structure description in space group *Pnma* was concluded to be the most appropriate one for the representatives of the K_2LnF_5 series, just like already described correctly by *Güde* and *Hebecker* for K_2GdF_5 in 1985 [4].

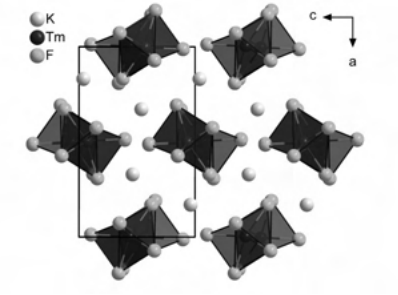

Figure 1 Section of the crystal structure in the centrosymmetric space group *Pmma* showing chains of edge-connected $[TmF_7]^{4-}$ polyhedra bundled like a hexagonal rod packing. The unit cell edges are emphasized as black lines.

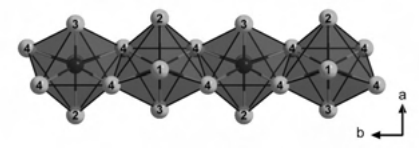

Figure 2 Strands of edge-connected $[TmF_7]^{4-}$ polyhedra according to 1D-$[Tm(F1,2,3)^{t}_{3/1}(F4)^{e}_{4/2}]^{2-}$ propagating along the *b*-axis in the crystal structure of K_2TmF_5.

Li2EuGd4O8: A New Lithium Lanthanoid Oxide with Orange-Yellow Luminescence

J.-L. Hoslauer[1], T. Schleid[1]

[1] University of Stuttgart, Institute for Inorganic Chemistry, Stuttgart, Germany

Orange-red needles of monoclinic $Li_2EuGd_4O_8$ were found in synthesis experiments using Gd_2O_3, $EuBr_2$ and LiH in silica-jacketed, arc-welded niobium capsules at 750 °C. These air- and water-stable crystals show a strong orange-yellow luminescence under ultraviolet light. The novel compound may further exhibit interesting magnetic properties, such as ferromagnetism like already reported for the analogous all-europium derivative $Li_2Eu_5O_8$ [1].

In 1973 *Bärnighausen*, *Schuster* and *Vogt* presented the lithium europium oxides $Li_2Eu_5O_8$, as well as $Li_2SrEu_4O_8$ and $Li_2BaEu_4O_8$ [2]. While their synthesis for the mixed-valent europium representative $Li_2Eu_5O_8$ used a combination of EuO, EuOCl and LiH, we could find similar dark red crystals using Eu_2O_3, $EuBr_3$ and LiH. Although $Li_2Eu_5O_8$ does not exhibit any luminescence under UV light, it shows an interesting ferromagnetic behavior that can described using a linear *Heisenberg* chain model, as reported by *Nyokong* and *Greedan* in 1981 [1].

It was therefore of particular interest to also synthesize the corresponding compound $Li_2EuGd_4O_8$ with an increased overall magnetic moment due to the presence of now five 4 f^7 configurated lanthanoid cations (one Eu^{2+} and four Gd^{3+}). Much to our surprise orange-red needles of $Li_2EuGd_4O_8$ showed a strong orange-yellow luminescence under UV light ($\lambda = 254$ nm). The Eu:Gd ratio was further confirmed by *EDXS* measurements, using three needles that gave Eu:Gd compositions around 1:3.8. An analogous *in-situ* reduction of $EuBr_3$ to $EuBr_2$ using an excess of LiH however did not lead to the formation of the title compound.

$Li_2EuGd_4O_8$ crystallizes in the monoclinic space group $C2/m$ and its crystal structure was refined from powder X-ray diffraction data ($\lambda = 71.07$ pm, Mo-Kα_1) using the *Rietveld* method (Tables 1 and 2). In this structure (Figure 1), the Eu^{2+} cations reside in a cubic arrangement $[EuO_8]^{14-}$ of eight oxide anions (d(Eu-O) = 275 – 284 pm). Both crystallographically distinguishable Gd^{3+} cations are surrounded by seven oxide anions capped trigonal prisms $[GdO_7]^{11-}$ d(Gd-O) = 223 – 250 pm). The Li^+ cations serve as centers of $[LiO_4]^{7-}$ tetrahedra (d(Li-O) = 187 – 207 pm) , while the oxide anions find themselves in three different octahedra $[(O1)Gd_3Eu_2Li]^{12+}$,$[(O2)Gd_4Li_2]^{12+}$ and $[(O3)Gd_3Eu_2Li]^{12+}$ as well as in a $[(O4)Gd_4]^{10+}$ tetrahedron. The $Eu^{2+}\cdots Eu^{2+}$ distances of 353 pm resemble those found for other europium(II) oxides that show ferromagnetic coupling like EuO (364 pm) [4] or Eu_3O_4 (350 pm) [5].

References

[1] T. Nyokong, J. E. Greedan, *Inorg. Chem.*, vol. 21, pp. 398–401, 1982.

[2] H. Bärnighausen, R. Schuster, K. Vogt, in *Proceedings of the 10th Rare Earth Research Conference*, Carefree (AZ), USA, 1973.

[3] H. Bommer, *Z. Anorg. Allg. Chem.*, vol. 241, pp. 273–280, 1939.

[4] H. A. Eick, N. C. Bänzinger, L. Eyring, *J. Am. Chem. Soc.*, vol.78, pp. 5147–5149, 1956.

[5] R. C. Rau, in *Proceedings of the 3rd Conference on Rare Earth Research*, Clearwater (FL), USA, 1963.

Table 1. Crystallographic data and structure refinement for $Li_2EuGd_4O_8$ from powder X-ray diffraction data.

Empirical formula	$Li_2EuGd_4O_8$
Space group	$C2/m$ (no. 12)
a / pm	1333.64(6)
b / pm	352.62(2)
c / pm	963.28(4)
β / °	119.648(1)
Z	2
ρ_{calc} / g·cm^{-3}	7.782
V_m / cm^3·mol^{-1}	118.55(2)
Diffractometer	Stadi-P (STOE & Cie), Mo-Kα_1
F(000)	778
Range in h,k,l	0–26, 0–7, ±19
R_p, R_{wp}	0.089, 0.121
R_{exp}	0.064
Goodness of Fit	1.876

Table 2. Atomic positions and *Wyckoff* sites in the asymmetric unit of $Li_2EuGd_4O_8$.

Atom	Site	x/a	y/b	z/c
Li	4*i*	0.309*	0	0.738*
Eu	2*a*	0	0	0
Gd1	4*i*	0.1102(2)	0	0.4392(2)
Gd2	4*i*	0.3377(2)	0	0.1870(2)
O1	4*i*	0.458*	0	0.758*
O2	4*i*	0.264*	0	0.381*
O3	4*i*	0.315*	0	0.936*
O4	4*i*	0.082*	0	0.656*

* The positions of the lithium and oxide ions are taken from the published data of $Li_2Eu_2O_5$ [2] and were not further refined.

Figure 1

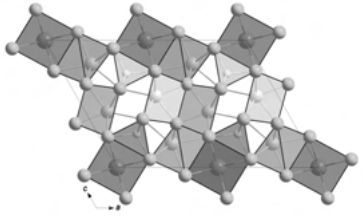

Figure 2 Unit cell of $Li_2EuGd_4O_8$ as viewed along [010] with emphasized oxygen polyhedra around Eu^{2+}, Gd^{3+} and Li^+. The Eu^{2+} cations are displayed in orange, the Gd^{3+} cations in grey, the Li^+ cations in yellow and the O^{2-} anions in blue.

Hydrothermal crystallization in phosphate systems with alkaline and transition metals

E. Kochetkova[1]

[1] Lomonosov Moscow State University, Moscow, Russia

The synthesis was carried out in multicomponent phosphate systems in hydrothermal conditions (T = 280 ° C and P = 100 bar) containing transition metal ions (Mn2+, Ni2+, Co2+), alkali ions (Li+, K+), aluminum ion (Al3+).

The crystallization products were examined under a binocular microscope and separated into phases according to morphological features. To determine the chemical composition of the synthesized phases, a semi-quantitative X-ray spectral analysis was performed on a scanning electron microscope. X-ray diffraction of powder and single-crystal samples was used to determine the symmetry and the unit cell parameters of the compounds. Based on the achieved data, the phases were identified using the ICSD crystal structure database.

As a result of 9 experiments, analogs of minerals such as the Co-analogue of the triphilin-lithiophilite series LiCoPO4, synthetic lithiophosphate Li3PO4, pechkaite Mn5(PO4)3Cl and berlinite AlPO4 were identified. Also in the experiments were obtained KNiPO4·H2O, a phase of mixed composition Mn2(PxV1-x)(VyP1-y)O7, as well as (Mn, Co)6(PO4)4·H2O and KAlPO4OH (Al-analog of KTP).

In one of the experiments in a system containing manganese(II) chloride, potassium pyrophosphate, aluminum oxide and water, two new compounds KMnAl2(PO4)3(H2O)2 and K2Mn3(H2O)2[P2O7] were obtained. Their crystal structures were established as a result of an X-ray diffraction (Xcalibur-S-CCD diffractometer) study based on a single-crystal experimental material. The crystal structures was solved by direct methods and refined by full-matrix leastsquares method using the program SHELX [1,2]. These results were published [3].

References

[1] Sheldrick G.M., "SHELXT – Integrated space-group and crystal structure determination," *Acta Crystallogr. Sect. A*, vol. 71, pp. 3–8, 2015.

[2] Sheldrick G.M., "Crystal structure refinement with SHELXL," *Acta Crystallogr. Sect. C*, vol. 71, pp. 3–8, 2015.

[3] Kiriukhina G. V., Yakubovich O. V., Shvanskaya L. V., Kochetkova E. M., Dimitrova O. V.,. Volkov A. S and Simonov S. V., "Novel K/Mn phosphate hydrates, K2Mn3(H2O)2[P2O7]2 and KMn(H2O)2[Al2(PO4)3]: hydrothermal synthesis and crystal chemistry," *Acta Crystallogr. Sect. C*, vol. 76, pp. 302–310, 2020.

Crystal Structure of a new ternary phase in the system Ba-Mg-Zn

K. Köhler[1], C. Röhr[1]

[1] Albert-Ludwigs-Universität Freiburg, Institut für Anorganische und Analytische Chemie, Freiburg, Germany

Magnesium-containing alloys of the heavier alkaline earth metals Ca and Sr with Zn have been investigated for their mechanical stability combined with low weight and toxicological safety, among other applications, as biodegradable materials [1-3]. The obtained ternary phases exhibit a variety of different crystal structures [1,2,4]. Now the Ba-Mg-Zn ternary system has also been systematically investigated for the presence of analogous phases.

The synthesis was carried out by melting reaction from the elements, which were weighed under argon and sealed in a tantalum tube. The sample was heated up to 900°C and cooled with a rate of 20 K/h. The crystal structure of the new ternary phase was determined by means of single-crystal X-ray data. The intermetallic phase $Ba_6Mg_xZn_{11-x}$ [$x = 2.80(1)$, $R\bar{3}m$, $a = 1011.96(8)$ pm, $c = 1703.6(2)$ pm, $Z = 3$] crystallizes in a new $AM_{\sim 2}$ type structure (s. Fig. 1). The structure consists of one A and three M layers. Six A atoms join, to form an empty octahedral cluster, and the M atoms form corner-linked [M_{11}] dumbbells. The complete structure can be described by a string of these polyhedra along [001] direction (s. Fig. 2). Ba occupies the A positions, $M(1)$ is a pure zinc layer. The remaining atomic positions $M(2)$ and $M(3)$ are occupied by zinc and magnesium satistically (49 at.-% and 67 at.-% Mg at $M(2)$ and $M(3)$, respectively).

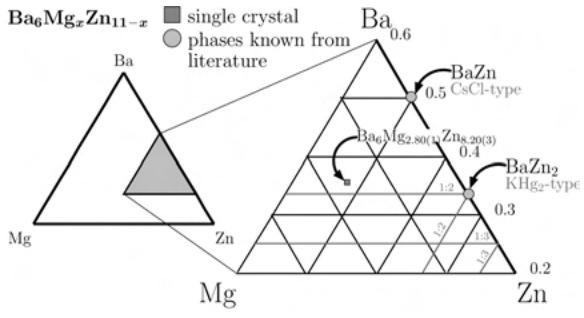

Figure 1 Section of the ternary composition chart of the Ba-Mg-Zn system (the compounds known from literature marked in gray, the composition of the single crystal is in dark blue).

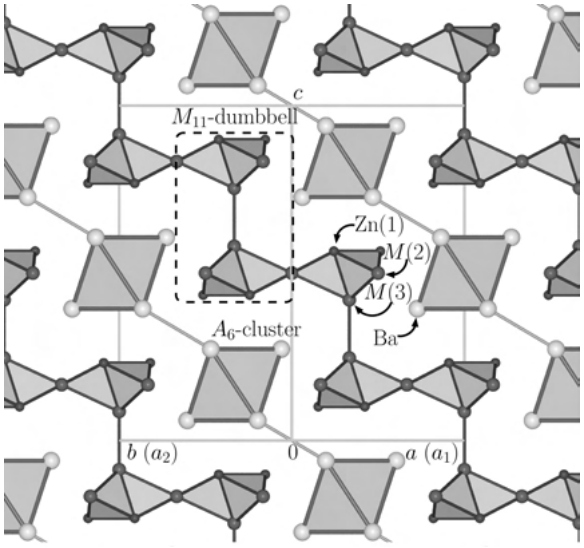

Figure 2 Section [polyhedral layer of the (110) plane] of the crystal structure of $Ba_6Mg_{2.80(1)}Zn_{8.20(3)}$ (red/magenta/gold spheres: Zn/M/Ba atoms , | :A_6 - M_{11} : | along [001] direction).

$K_3Lu_7Se_{12}$: The first potassium lanthanoid selenide with $Cs_3Y_7Se_{12}$-type crystal structure

P. L. Lange[1], A. Friedly[1], B. M. Schulz[1], T. Schleid[1]

[1] University Stuttgart, Institute of Inorganic Chemistry, Solid-State Chemistry, Stuttgart, Germany

In the late 1990s years the first ternary compounds with the composition $A_3RE_7Ch_{12}$ were identified (A = Rb and Cs, RE = Y and Yb) for the examples of $Rb_3Yb_7Se_{12}$ [1] and $Cs_3Y_7Se_{12}$ [2, 3]. Today selenides with the formula $Cs_3RE_7Se_{12}$ are known for RE = Sm, Gd – Tm [4–7] and tellurides $Cs_3Ln_7Te_{12}$ with Ln = Sm, Gd, Tb [8]. Other examples are $K_3Er_7S_{12}$ and $Rb_3Er_7S_{12}$ [9] among the sulfides as well as $Rb_3Dy_7Se_{12}$ [10]. They all crystallize in the orthorhombic space group *Pnnm* in a channel-providing defect Z-type structure of the sesquiselenides (*e.g.* Lu_2Se_3: orthorhombic, *Fddd*; $d(Lu^{3+}–Se^{2--}) = 279 – 286$ pm [11]) according to 3D-$[Lu_7Se_{12}]^{3--}$ filled with A^+ cations. As easily can be seen there is no combination with K^+, Ln^{3+} and Se^{2--} ions so far.

Single crystals of $K_3Lu_7Se_{12}$ were now obtained from the reaction of lutetium powder (Lu), red phosphorus (P), selenium (Se) and potassium chloride (KCl) mixed in a molar ratio of 1:1:4:1 designed to yield $KLu[P_2Se_6]$ in analogy to $KDy[P_2Se_6]$ [12]. The mixture was filled into an evacuated silica glass ampoule and heated to 950 °C for 48 h. The temperature was held for 144 h and subsequently the ampoule was cooled down to 350 °C within 36 h. $K_3Lu_7Se_{12}$ occurs as orange-colored needle-shaped single crystals and crystallizes with the lattice parameters a = 1227.96(8) pm, b = 2561.03(17) pm and c = 407.82(3) pm for Z = 2. Its crystal structure (CSD-2052785) displays a three-dimensional network of vertex- and edge-sharing $[LuSe_6]^{9-}$ octahedra ($d(Lu^{3+}–Se^{2--}) = 277 – 294$ pm). In this way channels along [001] are created and occupied by K^+ cations (Figure 1). To ensure electroneutrality and a reasonable distance between two $(K2)^+$ cations (d(K2···K2) = 237 pm) the K2 position must be half occupied, which is confirmed by the results of the structure refinement.The $K^+–Se^{2--}$ distances within the resulting (capped) trigonal prisms (Figure 2) range from 322 to 372 pm and agree well with those in *anti*-CaF_2-type K_2Se ($d(K^+–Se^{2--})$ = 333 pm for C.N. = 4) [13].

References

[1] S.-J. Kim, S.-J. Park, H. Yun, J. Do, *Inorg. Chem.*, vol. 35, no. 18, pp. 5283–5289, Aug. 1996.

[2] M. Folchnandt, Th. Schleid, *Z. Kristallogr./Suppl.*, vol. 11, p. 80, 1996.

[3] M. Folchnandt, Th. Schleid, *Z. Anorg. Allg. Chem.*, vol. 623, no. 10, pp. 1501–1502, Oct. 1997.

[4] M. Folchnandt, Th. Schleid, *Z. Kristallogr./Suppl.*, vol. 12, p. 125, 1997.

[5] M. Folchnandt, Th. Schleid, *Z. Anorg. Allg. Chem.*, vol. 624, no. 10, pp. 1595–1600, Oct. 1998.

[6] C. Schneck, A. Elbe, C. M. Schurz, Th. Schleid, *Acta Crystallogr. E*, vol. 68, no. 1, i2 , Jan. 2012.

[7] A. H. Geyer, A. Elbe, Th. Schleid, in *26th Annual Conference of the German Crystallographic Society, March 5–8, 2018, Essen, Germany*, Berlin, Germany, Boston, USA: De Gruyter, 2018, p. 99.

[8] O. Tougaît, H. Noël, J. A. Ibers, *Solid State Sci.*, vol. 3, no. 4, pp. 513-518, May 2001.

[9] F. Lissner, I. Hartenbach, Th. Schleid, *Z. Anorg. Allg. Chem.*, vol. 628, no. 7, pp. 1552–1555, Jul. 2002.

[10] M. Folchnandt, Th. Schleid, *Z. Kristallogr. NCS*, vol. 215, no. 1, p. 9, 2000.
[11] M. Folchnandt, C. Schneck, Th. Schleid, *Z. Anorg. Allg. Chem.*, vol. 630, no. 1, pp. 149–155, Jan. 2004.
[12] B. M. Schulz, Doctoral Dissertation, University Stuttgart, Germany, 2021.
[13] E. Zintl, A. Harder, B. Dauth, *Z. Elektrochem.*, vol. 40, no. 8, pp. 588–593, Aug. 1934.

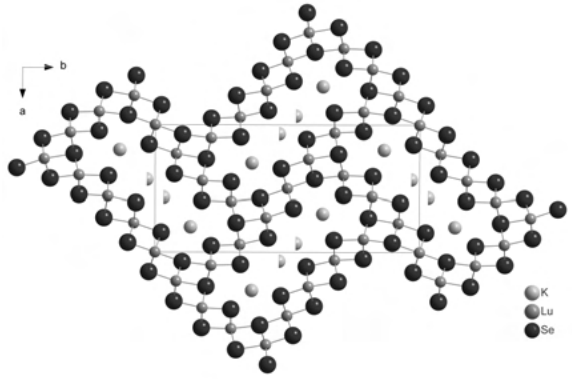

Figure 1 Extended unit cell of $K_3Lu_7Se_{12}$ as viewed along [001]. The lutetium-selenium sublattice consists of vertex- and edge-shared $[LuSe_6]^{9-}$ octahedra, while the empty channels are occupied with potassium cations.

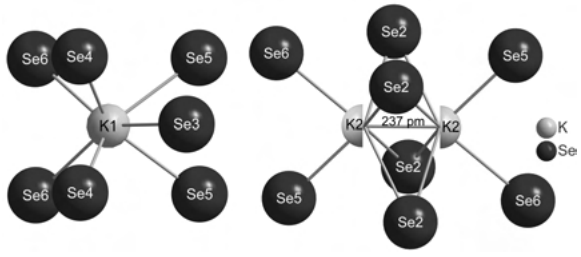

Figure 2 Selenide coordination spheres of both crystallographically different K^+ cations in the crystal structure of $K_3Lu_7Se_{12}$.

Single Crystals of K2NdCl5 and K2SmCl5

F. Lissner[1], J.-L. Hoslauer[1], G. Meyer[2], T. Schleid[1]
[1] University of Stuttgart, Stuttgart, Germany
[2] Kungliga Tekniska Högskolan Stockholm, Stockholm, Sweden

Single crystals of K_2NdCl_5 and K_2SmCl_5 were furnished by the oxidation of KNd_2Cl_5 [1] and KSm_2Cl_5 [2] with sulfur along with $Nd_3S_2Cl_5$ [3] and Sm_2SCl_4 [4] as target products. Violet K_2NdCl_5 (a = 1270.86(8), b = 874.12(6), c = 797.03(5) pm) and yellow K_2SmCl_5 (a = 1267.49(8), b = 867.61(6), c = 794.52(5) pm) crystallize in the orthorhombic space group *Pnma* (no. 62) with Z = 4 adopting the K_2PrCl_5-type structure [5]. The atomic coordinates and displacement parameters were derived from 1372 unique reflections (all: 10360, R_{int} = 0.030) with R_1 = 0.032 for K_2NdCl_5 (Table 1, *top*) [6] as well as 1337 unique reflections (all: 6787, R_{int} = 0.058) with R_1 = 0.027 for K_2SmCl_5 (Table 1, *bottom*) [6] using X-ray diffraction data collected with a MoKα-source equipped Siemens-Stoe AED2 device and the program suite SHELX-76 [7] based on full-matrix least-squares refinements. The crystallographically unique Ln^{3+} cations are surrounded by seven Cl^- anions as centers of capped trigonal prisms $[LnCl_7]^{4-}$, which share two *trans*-oriented edges to form linear 1D-$\{[Ln(Cl1,2,3)_{3/1}(Cl4)_{4/2}]^{2-}\}$ chains propagating along [010] (Figure 1, *top*). Bundled as a hexagonal rod-packing, they are connected and charge-balanced by K^+ cations in ninefold Cl^- coordination (Figure 1, *bottom*). The interatomic distances of 275 – 284 pm for $d(Nd^{3+}–Cl^-)$ and 272 – 282 pm for $d(Sm^{3+}–Cl^-)$ as well as them of 315 – 335 pm *plus* 388 pm for $d(K^+–Cl^-)$ in K_2NdCl_5 and 313 – 336 pm *plus* 384 pm for $d(K^+–Cl^-)$ in K_2SmCl_5 agree well with those in the prototypic K_2PrCl_5 ($d(Pr^{3+}–Cl^-)$ = 277 – 286 pm, $d(K^+–Cl^-)$ = 314 – 335 pm *plus* 391 pm) [5,8] nicely reflecting the consequences of the lanthanoid contraction.

References

[1] G. Meyer, Th. Schleid, *Z. Anorg. Allg. Chem.*, vol. 528, pp. 55–60, 1985.
[2] Th. Schleid, G. Meyer, *Z. Anorg. Allg. Chem.*, vol. 553, pp. 231–238, 1987.
[3] F. Lissner, Th. Schleid, *Z. Anorg. Allg. Chem.*, vol. 627, pp. 507–512, 2001.
[4] F. Lissner, Th. Schleid, *Z. Anorg. Allg. Chem.*, vol. 625, pp. 1507–1511, 1999.
[5] G. Meyer, E. Hüttl, *Z. Anorg. Allg. Chem.*, vol. 497, pp. 191–198, 1983.
[6] F. Lissner, Diploma Thesis, Univ. Hannover, Germany, 1990.
[7] G. M. Sheldrick, *Program System SHELX-76*, Univ. Göttingen, 1976.
[8] G. Meyer, J. Soose, A. Moritz, V. Vitt, T. Holljes, *Z. Anorg. Allg. Chem.*, vol. 521, pp. 161–172, 1985.

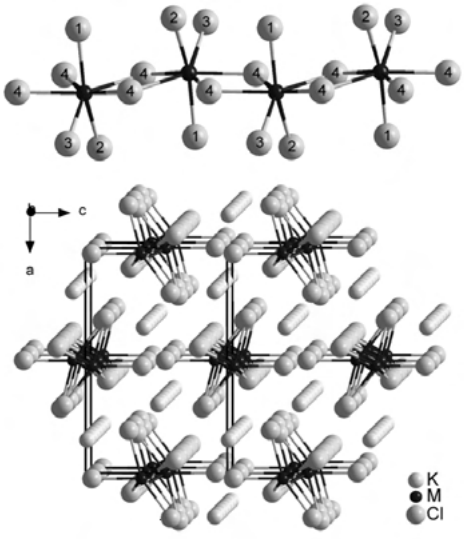

Figure 1

Table 1. Fractional atomic coordinates and coefficients of the anisotropic thermal displacement parameters for K_2NdCl_3 (*top*) and K_2SmCl_3 (*bottom*).

Atom	Site	x/a	y/b	z/c	U_{eq}*/pm²
K	8*d*	0.17079(5)	0.00572(8)	0.94769(9)	286(3)
Nd	4*c*	0.00575(1)	1/4	0.42404(3)	151(1)
Cl1	4*c*	0.18067(9)	1/4	0.62670(14)	269(5)
Cl2	4*c*	0.29458(8)	1/4	0.16321(14)	233(5)
Cl3	4*c*	0.00771(8)	1/4	0.07575(13)	211(4)
Cl4	8*d*	0.42322(6)	0.04350(8)	0.83356(11)	244(4)

* $U_{eq} = 1/3\,(U_{11} + U_{22} + U_{33})$

Atom	U_{11}	U_{22}	U_{33}	U_{23}	U_{13}	U_{12}
K	280(3)	254(3)	325(4)	−66(3)	−9(3)	11(3)
Nd	175(1)	119(1)	158(1)	0	16(1)	0
Cl1	244(5)	291(6)	271(6)	0	67(4)	0
Cl2	186(5)	265(5)	247(5)	0	15(4)	0
Cl3	225(4)	226(4)	182(4)	0	1(4)	0
Cl4	342(4)	150(3)	239(4)	21(3)	−83(3)	−27(3)

Atom	Site	x/a	y/b	z/c	U_{eq}*/pm²
K	8*d*	0.17064(6)	0.00602(8)	0.94568(12)	300(4)
Sm	4*c*	0.00556(9)	1/4	0.42449(3)	165(1)
Cl1	4*c*	0.18033(9)	1/4	0.62310(17)	278(5)
Cl2	4*c*	0.29638(8)	1/4	0.16081(16)	246(5)
Cl3	4*c*	0.00834(8)	1/4	0.07807(15)	228(5)
Cl4	8*d*	0.42514(6)	0.04389(8)	0.83349(11)	258(4)

* $U_{eq} = 1/3\,(U_{11} + U_{22} + U_{33})$

Atom	U_{11}	U_{22}	U_{33}	U_{23}	U_{13}	U_{12}
K	304(3)	269(3)	327(4)	−74(3)	−12(3)	10(3)
Sm	193(1)	133(1)	170(1)	0	16(1)	0
Cl1	258(5)	290(5)	286(6)	0	59(5)	0
Cl2	209(4)	271(5)	257(6)	0	16(4)	0
Cl3	249(4)	230(4)	204(5)	0	4(4)	0
Cl4	367(4)	168(3)	240(4)	19(3)	−74(3)	−22(3)

Figure 2

Unconnected Bromide Layers in the Crystal Structure of $DySb_2O_4Br$

R. J. C. Locke[1], F. C. Goerigk[1], T. Schleid[1]

[1] University of Stuttgart, Institute for Inorganic Chemistry, Stuttgart, Germany

Similar to the isotypic rare-earth metal(III) oxoantimonate(III) bromides $RESb_2O_4Br$ (RE = Eu - Tb) [1], almost colorless square platelets emerged during the synthesis of $DySb_2O_4Br$ [2, 3]. For this purpose, stoichiometric amounts of Dy_2O_3, $DyBr_3$ and Sb_2O_3 were mixed in a molar ratio of 1:1:3 with CsBr as flux and put into an evacuated fused silica ampoule. The mixture was heated to 750 °C for two days and cooled down to 666 °C with 5 °C/h in the furnace. This temperature was held for three days, followed by cooling with 5 °C/h to 530 °C, and this temperature was also kept for two days. Finally, the ampoule was cooled down to room temperature in the closed furnace with 150 °C/h.

$DySb_2O_4Br$ crystallizes in the monoclinic space group $P2_1/c$ with a = 895.18(6) pm, b = 783.41(5) pm, c = 782.37(5) pm and β = 91.542(3)° for Z = 4 (CSD-2051975). Eight oxygen atoms form a distorted cube around each Dy^{3+} cation and these $[DyO_8]^{13-}$ cubes are linked with each other via four edges to form 2D-$[DyO^e_{8/2}]^{5-}$ layers (Figure 1). The distances between dysprosium and oxygen range from 226 to 254 pm. Each Sb^{3+} cation is connected to three oxygen atoms resulting in $[SbO_3]^{3-}$ ψ^1-tetrahedra. The antimony-oxygen links follow a zigzag-chain motif according to 1D-$[SbO^v_{2/2}O^t_{1/1}]^{3-}$. So two of the oxygen atoms are linked to other Sb^{3+} cations and the third one is only bonded to a single one. The Sb^{3+}-O^{2-} distances are 194 - 210 pm and the bridging oxygen atoms show longer bond lengths than the terminal ones (Figure 2). There is no bonding to the layer of bromide anions, because the shortest distance between Br^- and Sb^{3+} is 320 pm and therefore no coordination is observed. The same holds for the shortest $Br^-\cdots Dy^{3+}$ distance of 425 pm.

References

[1] F. C. Goerigk, V. Paterlini, K. V. Dorn, A.-V. Mudring, Th. Schleid, *Crystals*, vol. 10, p. 1089, 2020.

[2] F. C. Goerigk, Doctoral Dissertation, Univ. Stuttgart, Germany, 2021.

[3] R. J. C. Locke, Master Thesis, Univ. Stuttgart, germany, 2021.

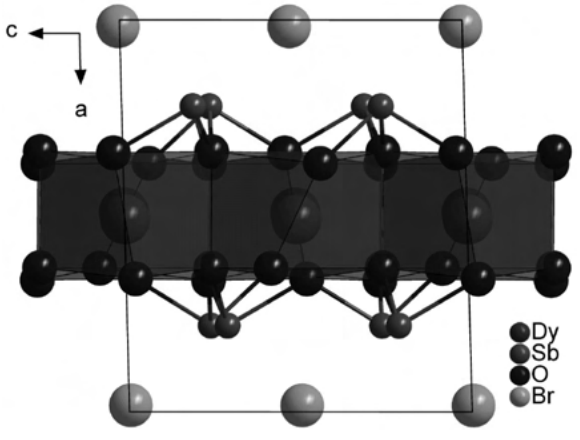

Figure 1 Extended unit cell of $DySb_2O_4Br$ in the monoclinic space group P21/c.

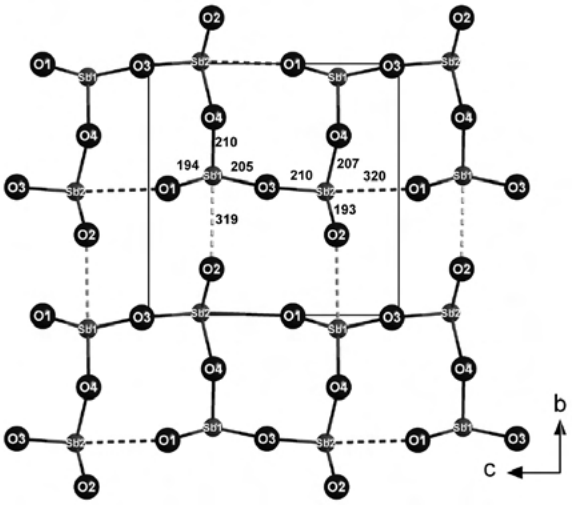

Figure 2 Meandering one-dimensional infinite chains 1D-$[SbO^{v}_{2/2}O^{t}_{1/1}]^{3-}$ of vertex-connected $[SbO_3]^{3-}$ ψ^1-tetrahedra in the monoclinic crystal structure of $DySb_2O_4Br$.

Synthesis, crystal and electronic structure of the new binary $A^I Hg_5$ mercurides KHg_5 and Rb_7Hg_{36}

C. Röhr[1], M. Wendorff[1]

[1] University of Freiburg, Institute for Inorganic and Analytical Chemistry, Freiburg, Germany

In the course of 'coloring' studies of alkali/alkaline-earth (A) mercurides AM_4 and AM_6 (M=Hg and In/Ga/Sn [1-4]) we unexpectedly obtained two new binary mercurides AHg_5 from ternary mixtures of A, Hg and the named p-block element. Later on, the two title compounds could also be prepared from nearly stoichiometric binary melts K-Hg and Rb-Hg.

KHg_5 crystallizes in a new structure type (orthorhombic, $Pmmn$, a=515.30(6), b=1756.7(2), c=1025.67(13) pm, $R1$=0.087 %, Fig. 1) which - according to its chemical composition - exhibits structure elements known from the hexamercurides AHg_6 [2,3] at one hand (planar Hg nets with 5/8-membered rings running perpendicular to the short [100] direction; $[KHg_{18}]$ cation coordination polyhedra, CCPs) and the $BaAl_4/A_5Hg_{19}$ (A=Rb,Cs [5,6]) type features on the other hand (square pyramids, $HgHg_4$ tetrahedra). The overall structure is best desribed by a space-filling arrangement of the $[KHg_x]$ (x=16-18) CCPs (yellow), squeezed $[Hg_4]$ tetrahedra (green), $[Hg_6]$ octahedra (cyan) and distorted $[Hg_8]$ cubes/trigonal double-prisms (blue). The coordination numbers of the nine crystallographically different Hg atoms vary from 4 to 7(+3) Hg (+ 2 to 5 K) with Hg-Hg distances spanning a wide range between 289 and 386 pm.

The even more complex structure of the rubidium mercuride Rb_7Hg_{36} (tetragonal, $P\bar{4}m2$, a=1061.4(2), c=2120.2(5) pm, $R1$=0.109 %) consists of 17 Hg and 6 Rb sites. Five of the six different $[RbHg_x]$ CCPs (x=16-20; yellow in Fig. 2) are fused *via* opposite pentagonal or hexagonal faces to form non-intersecting columns along [100]/[010] [Rb(5,6)] and [001] [Rb(1-3)] (= Nb positions in Nb_3Sn). A similar structural feature is observed in the cubic A_3Hg_{20} phases [6] (and the related clathrate-I type), which accordingly crystallize in the supergroup $Pm\bar{3}n$ with comparable axis lengths (Rb_3Hg_{20}: a=1073.7 pm, $\approx a \approx \frac{c}{2}$ of Rb_7Hg_{36}). The new mercuride similarly exhibits octa-capped isosahedra (icosahedra stars, IS; blue/cyan in Fig. 2), which are located at one halve of the Sn sites of the Nb_3Sn prototype. The other halve of the Sn positions are taken by $[Rb(4)Hg_{16}]$ polyhedra. Overall, Rb CCPs, IS and $[Hg_4]$ tetrahedra (green) tile the space. The latter corner-sharing tetrahedra form layers of 4- and 8-membered rings, which represent cutouts of the clathrate-I structure of melanophlogite. Comparable $[Hg_{4/2}]$ tetrahedra networks (and additional four-bonded Hg atoms) are likewise found in $K_7Hg_{28}Sn_9$ [7] and several other (pseudo)hexagonal mercurides in the 1:∼5 composition range (cf. survey in [4]), which are similarly related to dodecasil-1H.

The calculated electronic structures of the two mercurides show the expected metallic behaviour with strong Hg p-bonding inside the complex polyanions. The Bader charges of Hg (q_{BB}) vary between −0.06 for the icosahedra center (in Rb_7Hg_{36}) to −0.26 for the four-bonded Hg atoms (in both structures).

References

[1] M. Wendorff, C. Röhr, *Z. Kristallogr. Suppl.*, vol. 38, p. 86, 2018.

[2] M. Wendorff, C. Röhr, *J. Alloys Compds*, vol. 546, p. 320, 2013.

[3] F. Tamborino, C. Hoch, *J. Alloys Compds*, vol. 618, p. 299, 2015.

[4] M. Wendorff, C. Röhr, *Z. Kristallogr.*, vol. 233, p. 515, 2018.

[5] E. Biehl, H. J. Deiseroth, *Z. Anorg. Allg. Chem.*, vol. 625, p. 389, 1999.

[6] E. Todorov, S. C. Sevov, *J. Solid State Chem.*, vol. 149, p. 419, 2000.

[7] M. Wendorff, C. Röhr, in preparation.

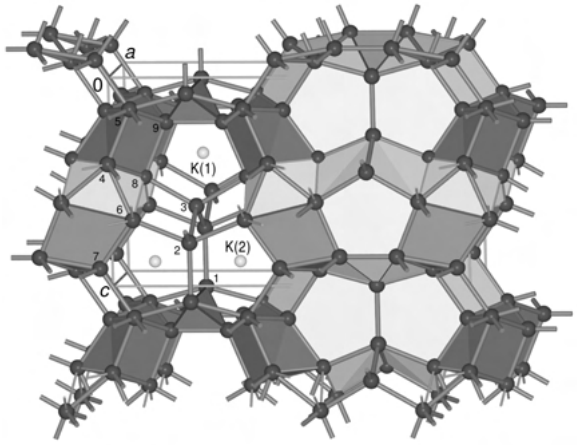

Figure 1 Crystal structure of the new binary mercuride KHg_5.

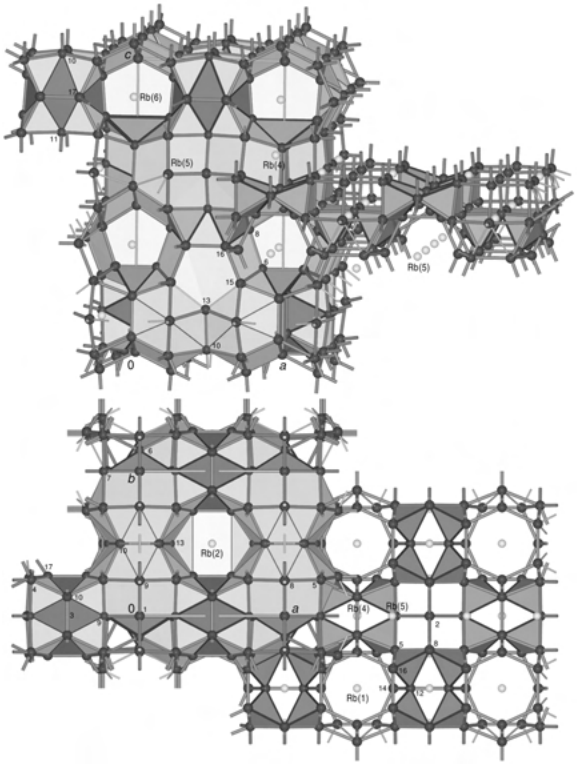

Figure 2 Different views of the tetragonal crystal structure of Rb_7Hg_{23}.

$Li_2Nd_3Cl_3[TeO_3]_4$: The First Lithium-Containing Lanthanoid Chloride Oxotellurate(IV)

P. L. Russ[1], S. Zitzer[1], T. Schleid[1]
[1] University of Stuttgart, Institute for Inorganic Chemistry, Stuttgart, Germany

Pale bluish violet single crystals of $Li_2Nd_3Cl_3[TeO_3]_4$ could be obtained as primary phase from mixtures of Nd_2O_3 and TeO_2 along with LiCl as flux and reactant in molar ratios of 2:4:3 after reactions in evacuated graphitized fused silica ampoules. Followed by 10 hours of heating up to 750 °C, this temperature was held for 5 days and then the furnace was cooled down to 500 °C within 24 h, before it was switched off.

$Li_2Nd_3Cl_3[TeO_3]_4$ crystallizes in the monoclinic space group $C\ 2/c$ with the lattice parameters a = 2354.67(13) pm, b = 564.91(3) pm, c = 1667.54(9) pm and β = 134.006(3)° for Z = 4 (CSD-2054116). Its structure is almost isotypic with that one of the $Na_2RE_3Cl_3[TeO_3]_4$ series (RE = Y, La – Nd, Sm – Lu) [1–5]. Hence there are two different Nd^{3+} cation positions just like in $Na_2Nd_3Cl_3[TeO_3]_4$ (a = 2403.29(14) pm, b = 572.35(3) pm, c = 1712.64(9) pm and β = 134.612(3)°) [2, 5]. The first one is coordinated by eight oxygen atoms as a square $[(Nd1)O_8]^{13--}$ antiprism, where two edges are bridged by ψ^1-tetrahedral bidentate $[TeO_3]^{2--}$ units and the remaining four oxide anions belong to monodentately attached $[TeO_3]^{2--}$ anions. The second Nd^{3+} cation is also surrounded by eight oxygen atoms in the shape of a square $[(Nd2)O_8]^{13--}$ antiprism, but now three edges are coordinated by bidentate $[TeO_3]^{2--}$ anions and the other two oxygen atoms are terminally bound to Te^{4+} cations. The Nd^{3+}–O^{2--} distances range from 234 to 265 pm and thus correlate well with those from 238 to 256 pm in $Na_2Nd_3Cl_3[TeO_3]_4$ showing a narrower range [2]. Via four common O···O edges all $[NdO_8]^{13--}$ polyhedra are connected to form 2D-$[NdO^e_{8/2}]^{5--}$ layers, which run parallel to the (001) plane emphasized as violet-rose bars in Figure 1. Using these layers as starting board, the two crystallographically different Te^{4+} cations dock to three oxygen atoms each, resulting in the formation of ψ^1-tetrahedral $[TeO_3]^{2--}$ anions. Their Te^{4+}–O^{2--} distances range from 187 to 191 pm and correlate well with those in $Na_2Nd_3Cl_3[TeO_3]_4$ covering an interval from 188 to 190 pm [2]. The O–Te–O angles range from 89 to 100 ° for the lithium and 89 to 102° for the sodium case [2]. For both cases almost identical 2D-$[Nd_3O_{12}Te_4]^+$ layers result, which have to be connected via A^+ cations (A = Li or Na) and Cl^{--} anions along [001]. Hence a three-dimensional network 3D-$[A_2Cl_3Nd_3O_{12}Te_4]$ is formed, due to the linkage of 2D-$[Nd_3O_{12}Te_4]^+$ layers via electrostatic interactions between two A^+ cations, certain oxygen atoms from $[TeO_3]^{2--}$ groups and three Cl^{--} anions per formula unit for charge compensation.

The unique Li^+ cation resides in an environment of three oxygen atoms, belonging to three terminal $[TeO_3]^{2--}$ anions. In addition, two Cl^{--} anions complete its coordination sphere to a square $[LiO_3Cl_2]^{7--}$ pyramid (Figure 2, *left*). The Li^+–O^{2--} distances range from 200 to 214 pm, whereas the Li+–Cl^{--} separations amount to 279 pm for Cl2 and 294 pm for Cl1. In comparison to

$Na_2Nd_3Cl_3[TeO_3]_4$, where a square $[NaO_4Cl_4]^{11--}$ antiprism is observed, the four Na^+–O^{2--} distances cover an interval from 229 to 272 pm *plus* 326 pm and the Na^+–Cl^{--} separations range from 286 to 302 pm *plus* 342 and 343 pm [2] (Figure 2, *right*).

From the two distinct Cl^{--} anions in the crystal structure, the first one (Cl1) is surrounded by two Li^+ and six Te^{4+} cations resulting in a distorted square $[ClLi_2Te_6]^{25+}$ antiprism. The second one (Cl2) receives coordination from one Li^+ and five Te^{4+} cations erecting distorted trigonal $[ClLiTe_5]^{20+}$ prism. Between the tellurium and the chlorine atoms there are σ-hole interactions [6], which also hold the three-dimensional network together. Since σ-hole interactions are known to be electrostatic and not covalent [6], the relevant $Cl^{--}\cdots Te^{4+}$ distances range from 299 to 378 pm in the lithium and from 315 to 382 pm [2] in the sodium case of the $A_2Nd_3Cl_3[TeO_3]_4$ couple with A = Li and Na.

References

[1] S. Zitzer, Doctoral Dissertation, Univ. Stuttgart, Stuttgart, Germany, 2012.
[2] S. Greiner, Doctoral Dissertation, Univ. Stuttgart, Stuttgart, Germany, 2018.
[3] S. Zitzer, F. Schleifenbaum, Th. Schleid, *Z. Naturforsch.*, vol. 69 b, pp. 150–158, 2014.
[4] D. O. Charkin, S. Zitzer, S. Greiner, S. G. Dorofeev, A. V. Olenev, P. S. Berdonosov, Th. Schleid, V. A. Dolgikh, *Z. Anorg. Allg. Chem.*, vol. 643, pp. 1654–1660, 2017.
[5] S. Greiner, S. Zitzer, S. Strobel, P. S. Berdonosov, Th. Schleid, *Z. Kristallogr.*, vol. 235, pp. 341–352, 20202.
[6] M. Beau, S. Lee, S. Kim, W.-S. Han, O. Jeannin, M. Fourmigué, E. Aubert, E. Espinosa, I.-R. Jeon, *Angew. Chem.*, vol. 133, pp. 370–374, 2021.

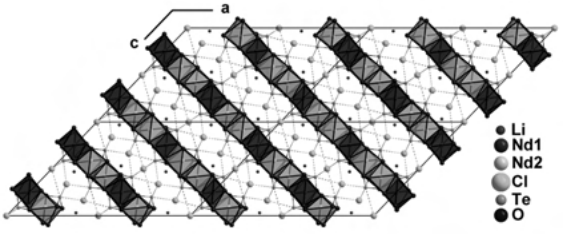

Figure 1 The three-dimensional network 3D-$[Li_2Cl_3Nd_3O_{12}Te_4]$ in the crystal structure of $Li_2Nd_3Cl_3[TeO_3]_4$ is a result of an interlink of 2D-$[Nd_3O_{12}Te_4]$ layers due to electrostatic interactions between Li^+ cations, certain oxygen atoms from $[TeO_3]^{2-}$ groups and Cl^- anions.

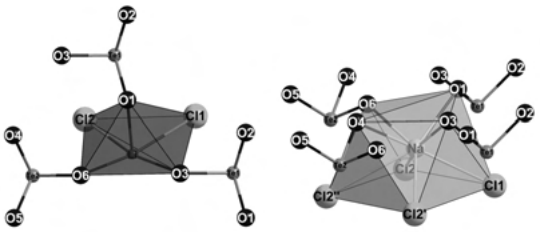

Figure 2 Square $[LiO_3Cl_2]^{7-}$ pyramid *(left)* in the crystal structure of $Li_2Nd_3Cl_3[TeO_3]_4$ and square $[NaO_4Cl_4]^{11-}$ antiprism *(right)* in the crystal structure of $Na_2Nd_3Cl_3[TeO_3]_4$.

Reconsideration of the space group symmetry of multiferroic phases TbMn2O5 and MnWO4 using neutron Renninger scans

P. Wimmer[1]
[1] LMU Munich, Munich, Germany

A precise knowledge of the crystal structure is a prerequisite to understand the mechanisms leading to the unique properties of multiferroics. Recently the well-established room temperature space groups of the multiferroics REMn2O5 (RE = rare earth, Bi, Y) and MnWO4 were questioned after the observation of weak forbidden reflections [1,2]. This thesis deals with the space group determination of TbMn2O5 and MnWO4 by focusing particularly on the influence of multiple diffraction on the intensity of such weak reflections. Therefore single crystals were studied using x-ray and neutron diffraction methods including neutron diffraction Renninger scans [3]. In both materials for the weak reflections large intensity variations of up to 600 % are observed with rotation around the azimuth angle. This indicates a strong contribution of multiple diffraction. By calculating the multiple diffraction patterns, no distinguishable differences between the different space groups are found for such small deviations in atomic positions of less than 0.03 Å. Still the results of a combined study of structural refinements from x-ray diffraction and the obtained multiple diffraction patterns of TbMn2O5 are in favor for a room temperature space group of *P2*, rather than previously stated *Pm*. In the case of MnWO4 the most likely space group is *P2*, but the results are not accurate enough to resolve the small structural changes.

References

[1] Balédent, V. et al. (2015). Evidence for Room Temperature Electric Polarization in REMn2O5 Multiferroics. Phys. Rev. Lett., 114, 117601
[2] Park, S. H. (2015). A new polar symmetry of huebnerite (MnWO4) with ferrodistortive domains. Journal of Magnetism and Magnetic Materials, Vol. 394, 160-172

[3] Renninger, M. (1937). "Umweganregung", eine bisher unbeachtete Wechselwirkungserscheinung bei Raumgitterinterferenzen. Zeitschrift für Physik, Vol. 106, 141–176

Inorganic functional materials

Controlled tuning of atomic structure in functional materials by acoustic standing waves and electric fields

C. Ludt[1], E. Ovchinnikova[2], A. Kulikov[3], D. Novikov[4], D. Meyer[1], M. Zschornak[1]

[1] TU Bergakademie Freiberg, Freiberg, Germany

[2] Physics Department of Moscow State University, Moscow, Russia

[3] A.V. Shubnikov Institute of Crystallography, Moscow, Russia

[4] Deutsches Elektronen-Synchrotron DESY, Hamburg, Germany

Active research in the field of condensed matter and nanotechnology not only led to significant progress in understanding the mechanisms of formation of electrical polarization and magnetoelectric phenomena, but also showed the possibilities of creating new classes of devices based on a combination of magnetoelectric and piezoelectric properties. Meanwhile, macroscopic properties, such as multiferroism and piezoelectricity, are associated with local structural changes that occur under the influence of external perturbations.

In a first step chosen crystal structures are analyzed by means of density functional theory (DFT) to validate the connection of external stress and internal change of lattice symmetry as well as atomic displacements. Among them are TeO_2, Li_2B4O_7, ZnO and $SrTiO_3$. Also in focus is the influence of oxygen vacancies on our structures. The research is currently accompanied by experiments in which standing acoustic waves are encoupled in crystal samples or an electric field is applied to change the structure parameters and particularly the structures' symmetry locally. Because the displacements are expected to be in picometer scale forbidden reflection technique is used to observe the induced effects. The obtained results can significantly widen the range of functional materials and can be directly used in modern technological applications.

Structure of ferroelectric low temperature phase of yttrium manganate YMn_2O_5 revisited

T. Weigel[1], C. Richter[2], M. Nentwich[3], D. Novikov[3], M. Zschornak[1], D. C. Meyer[1]

[1] TU Bergakademie Freiberg, Freiberg, Germany

[2] Leibniz Institut für Kristallzüchtung, Berlin, Germany

[3] P23 Beamline, PETRA-III, DESY, Hamburg, Germany

The material system YMn_2O_5 has several low temperatures phases, where magnetism and ferroelectricity occur. Especially, the origin of the ferroelectricity (FE) in a phase below $T_{FE} = 39$ K is an open question. The space group *Pbam* of the paraelectric phase does not allow polarization, also structural changes during the phase transition to a lower symmetry phase have not been detected yet. This means that the ferroelectricity must originate from changes in the Mn spin configuration [1] or from small atomic displacements [2], which could not be discovered by conventional structural analysis methods, because the displacements are below the spatial resolution limit. We apply the new Resonantly Suppressed Diffraction (RSD) [3] method, which is sensitive to minuscule structural changes in the sub-pm range, to shed new light on this controversial discussion. RSD is a structural characterization method in the field of Resonant Elastic X-ray Scattering and tunes the photon energy such that certain reflections approach zero due to destructive interference.

Here, we employ RSD on carefully chosen Bragg reflections below and above T_{FE}. With the data above T_{FE} we refined the static and dynamic displacements of the paraelectric phase, to receive an improved starting model for the structural characterization of the FE phase. With this starting model we were able to characterize the FE phase consolidating the findings about the origin of ferroelectricity in YMn_2O_5.

References

[1] Kimura, H., Noda, Y. & Kohn, K. (2009). Journal of Magnetism and Magnetic Materials, 321, 854. Proceedings of the Forth Moscow International Symposium on Mag.

[2] Noda, Y., Kimura, H., Fukunaga, M., Kobayashi, S., Kagomiya, I. & Kohn, K. (2008). Journal of Physics: Condensed Matter, 20, 434206.

[3] Richter, C., Zschornak, M., Novikov, D. V., Mehner, E., Nentwich, M., Hanzig, J., Gorfman,S. & Meyer, D. C. Nature Communications, 9, 178 (2018).

In situ / in operando studies

Structural and Electronic Characterization of Doped Exsolution Perovskites

L. Lindenthal[1], R. Rameshan[1], T. Ruh[1], S. Löffler[1], C. Rameshan[1]

[1] TU Wien, Institute of Materials Chemistry, Vienna, Austria

Perovskite-type oxide materials are promising candidates as catalysts for various reactions related to chemical energy conversion (e.g. the reverse water-gas shift reaction). This is due to their ability to form finely dispersed metal nanoparticles on the surface by exsolution [1]. The result is an excellent catalytic activity, while at the same time the perovskite backbone acts as a thermally and chemically highly stable support. Four such perovskite materials with the general formula La1-xCaxFeO3-δ or Nd1-xCaxFeO3-δ were characterized with respect to their crystal structure (using powder X-ray diffraction, XRD), their morphology (with scanning electron microscopy, SEM, and energy dispersive X-ray spectroscopy, EDX) and their electronic properties (by theoretical calculations based on density functional theory, DFT) [2]. For all materials, distorted perovskite structures were found, showing an orthorhombic symmetry. They were compared regarding the extent of the distortion depending on the cation-composition. Furthermore, DFT revealed the effect of Ca-doping, in particular a partial oxidation of Fe, leading to Jahn–Teller distortions. Additionally, the exsolution behaviour of the materials was investigated with in-situ XRD measurements. The formation of Fe particles could be observed and proven with SEM. Adding a small amount of Co-doping enhanced the exsolution properties. It enabled an easier exsolution and lead to smaller, Co-containing nanoparticles, which is important for catalytic applications.

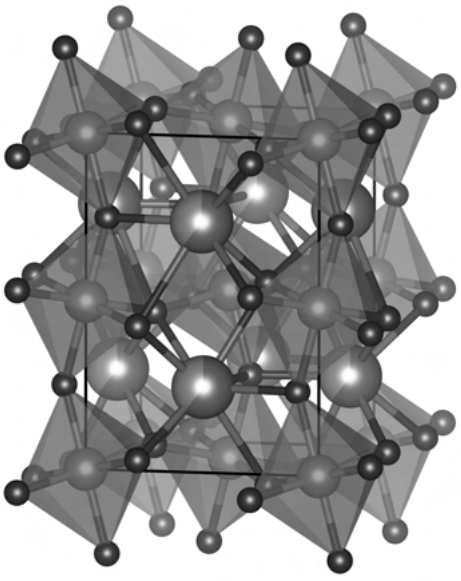

Figure 1

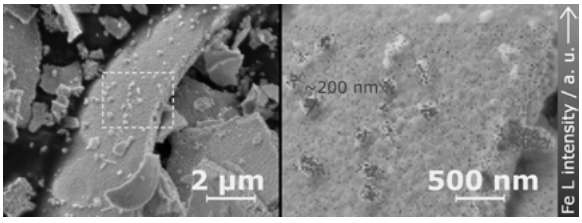

Figure 2

In situ XRPD observation of mechanochemical reactions in a ball mill

T. Rathmann[1], H. Petersen[1], S. Reichle[1], A. P. Amrute[1], W. Kersten[1], M. Etter[2], C. Weidenthaler[1]

[1] Max-Planck-Institut für Kohlenforschung , Kaiser-Wilhelm-Platz 1, 45470 Mülheim, Germany

[2] DESY, Notkestraße 85, 22607 Hamburg, Germany

Mechanochemistry has attracted a significant interest in materials synthesis and chemical reactions during the last decades. [1, 2] This applies to numerous chemical reactions, such as the synthesis of complex oxides, pharmaceuticals, or hybrid materials. [1, 3-5] Furthermore, mechanical alloying as well as the production/activation of heterogeneous catalysts or even direct mechanocatalytic reactions are pursued topics. [1, 5, 6] Mechanochemical routes meet several criteria of green chemistry and may provide unique reaction pathways and products. However, tracking what happens to a material during mechanochemical reactions is difficult. Since mechanical routes usually comprise solid-state reactants and/or products, spectroscopic and crystallographic investigations are

very interesting to understand the corresponding reaction mechanisms. Changes of structure and/or composition of crystalline compounds can be studied by *in situ* X-ray powder diffraction (XRPD) which is very promising to identify phase transitions and intermediate phases in mechanochemistry. *In situ* synchrotron diffraction has been applied successfully to study the mechanochemical synthesis of soft matter such as metal-organic frameworks or cocrystals in vibration ball mills. [1, 3, 4]

Nevertheless, the modification of commercial milling equipment turned out to be challenging for *in situ* studies of mechanochemical reactions of hard materials or mechanocatalytic reactions. In this work, we present the development of milling equipment suitable for *in situ* XRPD studies performed during the synthesis of inorganic hard materials. Several factors could be identified which turned out to be decisive for a successful reaction. Their individual contributions will be discussed and a tailor-made design of milling jars, also suitable for running catalytic reactions during ball milling, will be introduced.

References

[1] T. Friscic, C. Mottillo and H. M. Titi, *Angew. Chem. Int. Edit.*, vol. 59, pp. 1018–1029, 2020.

[2] A. P. Amrute, Z. Lodziana, H. Schreyer, C. Weidenthaler and F. Schueth, *Science*, vol. 366, p. 485, 2019.

[3] K. Uzarevic, I. Halasz and T. Friscic, *J. Phys. Chem. Lett.*, vol. 6, pp. 4129–4140, 2015.

[4] I. Halasz, S. A. J. Kimber, P. J. Beldon, A. M. Belenguer, F. Adams, V. Honkimaki, R. C. Nightingale, R. E. Dinnebier and T. Friscic, *Nat. Protoc.*, vol. 8, pp. 1718–1729, 2013.

[5] L. Takacs, *Chem. Soc. Rev.*, vol. 42, pp. 7649–7659, 2013.

[6] S. Immohr, M. Felderhoff, C. Weidenthaler and F. Schueth, *Angew. Chem. Int. Edit.*, vol. 52, pp. 12688-12691, 2013.

Micro and nano-crystalline materials

Three-dimensional coherent X-ray imaging of ferroelastic domains in $CsPbBr_3$ perovskite nanoparticles

D. Dzhigaev[1], L. Marcal[1], Z. Zhang[1], S. Sala[2], A. Björling[2], A. Mikkelsen[1], J. Wallentin[1]

[1] Lund University, Lund, Sweden

[2] MAX IV Laboratory, Lund, Sweden

Metal halide nanoparticle systems are promising candidates for the next generation of light-emitting, solar cell, and detector technologies. Characterization of their complicated crystal structures is important for tailoring their properties in a desired manner. In this work, we directly reconstruct three-dimensional twinned ferroelastic domains inside $CsPbBr_3$ (CPB) nanocrystals by Bragg coherent x-ray diffraction imaging (BCDI). An approach for phase retrieval of domain structures within twinned nanocrystals with the BCDI method is reported. A systematic study of several nanocrystals revealed a preferential double domain structure of CPB particles with sizes around 500 nm. A dislocation is also observed inside one of the reconstructed domains.

Antiphase boundaries in small iron oxide nanoparticles

T. Köhler[1], A. Feoktystov[1], E. Kentzinger[2], O. Petracic[2], T. Brückel[2]

[1] Forschungszentrum Jülich GmbH, Jülich Centre for Neutron Science JCNS at Heinz Maier-Leibnitz Zentrum MLZ, Garching, Germany

[2] Forschungszentrum Jülich GmbH, Jülich Centre for Neutron Science JCNS-2 and Peter Grünbger Institute, PGI-4, JARA-FIT, Jülich, Germany

Iron oxide nanoparticles find a wide variety of applications including targeted drug delivery and advanced cancer treatment methods. An important property of these particles is the saturation magnetization, which was shown to often be drastically reduced compared to bulk reference values. Previous studies have shown that planar lattice defects, so-called antiphase boundaries (APBs) are an important factor in this regard. Here we examine the influence of APBs on the atomic spin structure of nanoparticles with γ-Fe2O3 composition via Monte-Carlo simulations, explicitly considering dipole-dipole interactions between the magnetic moments, that have previously only been approximated. For a single APB through the particle center we find a reduction of the saturation magnetization of around 15% compared to a particle without APB due to a tilt of the net magnetic moment of both particle halves away from the applied field vector. Additionally, simulations of the Debye scattering equation are used to show the hkl-dependent line broadening effect of APBs in X-ray powder diffraction, thus providing a method of detecting APBs in nanoparticle samples.

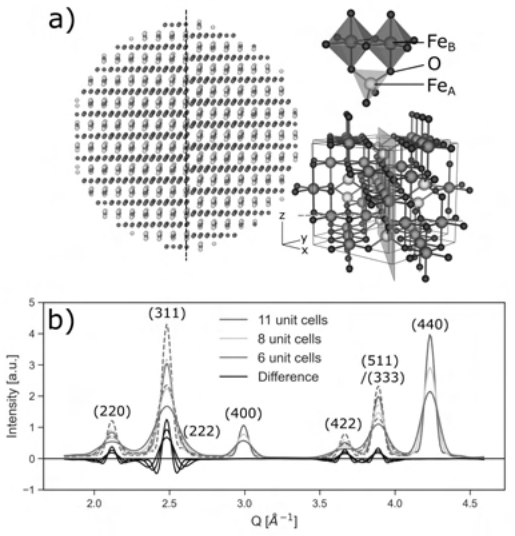

Figure 1 a) Nanoparticle structure used for Monte-Carlo and Debye scattering equation simulations. Oxygen atoms are not included for better visibility of the iron atoms. The APB is indicated with the black dashed line. The colors correspond to the lattice sites as indicated on the right. In the close-up of the unit cell the APB is drawn as a grey plane. b) Simulated X-ray powder diffraction patterns with (solid) and without (dashed) APB for different particle sizes. The difference curves highlight the hkl-dependence of the peak broadening.

Organic and metal-organic crystal structures

Experimental charge density studies on solids containing halogen bonds to pentafluoroiodobenzene

F. Busse[1], R. Wang[1], U. Englert[2], F. Otte[1], C. Strohmann[1]

[1] Anorganische Chemie, TU Dortmund, Dortmund, Deutschland

[2] RWTH Aachen University, Institute of Inorganic Chemistry, Aachen, Germany

In the last decades, significant progress has been made concerning the characterization of intermolecular interactions. Charge density studies on experimental diffraction data have been used successfully to derive information about the atom centred electron density distribution to analyse contacts such as halogen bonds. In these studies the focus was mainly on the properties of the halogen atom, whereas the effect of the halogen bond acceptor and its surrounding has not yet been systematically investigated.

We have analysed seven different structures containing pentafluoroiodobenzene either with or without a co-molecule; the co-molecules included nitrogen as the halogen acceptor in sp2 or sp3 hybridization. Based on low-temperature diffraction data collected up to high resolution, multipole refinements were used to derive information about the electron density beyond the spherical standard model.[1, 2, 3] The charge density about the iodine atoms differs largely between the structures; despite the assumed strength of the interaction, only one structure displays the typical aspheric density characteristic for a sigma-hole. Based on topological analyses according to Bader's Atoms in Molecules theory, we could evaluate the effect of different hybridizations of the halogen bond acceptor on the halogen bond.[4] In the pentafluoroiodobenzene structure without additional co-molecule, we investigated a short interhalogen contact between iodine and fluorine.

This work provides insight into specific effects of molecular structures on halogen bonds for a specific halogen donor system. As the properties of this interaction have proven to be very sensitive and variable in their outcome, further studies will be essential. They are expected to contribute to an adequate knowledge base indispensable for efficient crystal engineering.

References

[1] P. Coppens, *X-ray charge densities and chemical bonding*, Oxford, New York, USA: International Union of Crystallography/Oxford Univ. Press, 1997.

[2] N. K. Hansen, P. Coppens, *Acta Crystallographica Section A*, vol. 24, pp. 909–921, 1978.

[3] A. Volkov, P. Macchi, L. Farrugia, C. Gatti, M. PR, T. Richter, T. Koritsanszky, *XD2006*, New York, USA, 2006.

[4] R. F. W. Bader, *Atoms in molecules: A quantum theory*, reprinted, Oxford, USA: Clarendon Press, 1990 (2003).

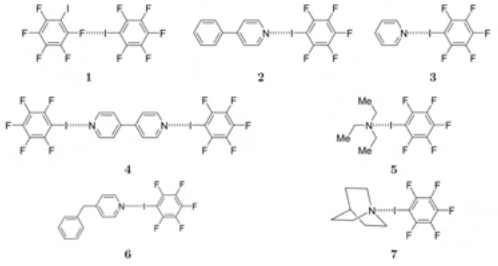

Figure 1 Presentation of the seven structures: All compositions contain pentafluoroiodobenzene, either pure (1) or with a co-molecule including nitrogen: (2) 4-Phenylpyridine, (3) Pyridine, (4) 4,4'-Bipyridine, (5) Triethylamine, (6) 4-Benzylpyridine, (7) Azabicyclo[2.2.2]octane. The horizontal dashed lines mark halogen bonds.

Exploring the Self-Assembly of Anisotropic Pillarplex Cations

A. Heidecker[1], A. Pöthig[2]

[1] Technical University of Munich, Departement of Chemistry, Chair of Inorganic and Organometal- lic Chemistry, Supramolecular Organometallics, Munich, Germany

The formation of porous molecular materials is investigated towards a possible implementation of pillarplexes as functional building blocks. The pillarplexes are supramolecular organometallic complexes (SOCs)[1] bearing tailor-made macrocyclic NHC-ligands and show exclusive shape selective encapsulation of linear molecules, tuneable solubility via anion exchange reactions and the corresponding Au(I)-pillarplexes show intrinsic photoluminescence.[2][3][4] The structural self-assembly is expected to be governed by the shape, charge and size of employed anions based on their interactions with the anisotropic pillarplex cations.

Consequently, a series of pillarplex salts with varying anions is targeted to synthesized and structurally characterized in the solid-state, with the aim to identify and understand determining interactions. Synthetically, the salts are yielded by simple anion exchange reaction or via solvothermal synthesis. The compounds are characterized by solid-state analysis (PXRD, SC-XRD, TGA) including porosity measurements (BET) and selected examples are presented and discussed.

References

[1] A. Pöthig, A. Casini, *Theranostics*, vol. 9, pp. 3150–3169, 2019.

[2] P. J. Altmann, A. Pöthig, *J. Am. Chem. Soc.*, vol. 138, pp. 13171–13174, 2016.

[3] P. J. Altmann, C. Jandl, A. Pöthig, *Dalt. Trans.*, vol. 44, pp. 11278–11281, 2015.

[4] P. J. Altmann, A. Pöthig, *Angew. Chemie - Int. Ed.*, vol. 56, pp. 15733–15736, 2017.

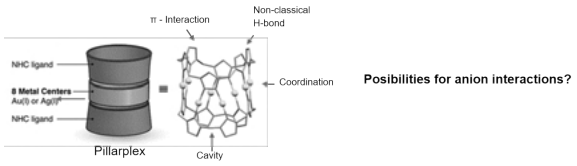

Figure 1

Application of QC Techniques to several elementorganic compounds: some reminiscences of a user

A. Nazarenko[1]

[1] SUNY College at Buffalo, Buffalo, USA

Several elementorganic compounds and macrocyclic 3d-transition metal complexes were investigated using known Hirshfeld refinement techniques (*Tonto* [1] and *NoSpherA2* [2]). These results were compared to traditional IAM refinement (*ShelXL* and *olex2.refine*) and with IAM corrected for interatomic scattering and lone pair scattering [3, 4] (these corrections were performed within *ShelXL* and/or *olex2.refine* frame). Reasonable position of hydrogen atoms is the most visible improvement over existing IAM procedures. Most of residual density in IAM solution could be removed by interatomic and lone pair scattering corrections; further application of Hirshfeld refinement techniques may result in minor r.m.s density and R-factor improvements.

An example of Cu(II) complex with 5,7,7,12,14,14-hexamethyl - 1,4,8,11-tetraazacyclotetradeca-4,11-diene (d= 0.62 Å, partially disordered) is shown on Figure 1.

References

[1] Fugel M., *et al.*, *IUCrJ*, vol. 5, pp. 32, 2018.

[2] Kleemiss F., *et al.*, *Chem.Sci.*, 2021.

[3] Franklin R. E., *Nature*, vol. 165, pp. 71, 1950.

[4] Afonine P.V, *et al., Acta Cryst*, vol. D63, pp. 1194, 2007; Nazarenko A.Y., *Z. Krist.*, vol. 38, pp. S44, 2018.

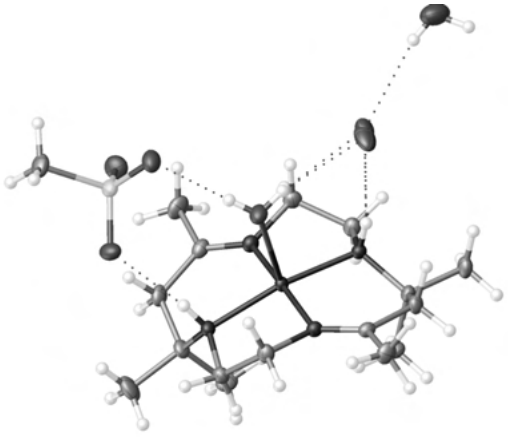

Figure 1 IAM (*ShelXL*): R=0.0404, r.m.s.$\Delta\rho$ 0.089, max/min $\Delta\rho$ 0.59/-0.34; C-C bond error 0.0017-0.0020 Å; IAM+correction *(ShelXL)*: R = 0.036, r.m.s.$\Delta\rho$ 0.081, max/min $\Delta\rho$ 0.40/-0.34; C-C bond error 0.0016-0.0017 Å; *NoSpherA2* (*ORCA, def2-TZVPD*): R = 0.036, max/min $\Delta\rho$ 0.7/-0.6, C-C bond error 0.0015-0.0018 Å.

In situ crystallization of l-menthone

M. Patzer[1], N. Nöthling[1], R. Goddard[1], C. Lehmann[1]
[1] Max-Planck-Institut für Kohlenforschung, Kaiser-Wilhelm-Platz 1, 45470 Mülheim an der Ruhr, Germany

Recently we determined the absolute configuration of a liquid product of an enantioselective Cu-catalyzed asymmetric fluorination reaction under ambient conditions by *in situ* crystallization. Establishing the absolute structure of the α-fluoroester decisively contributed to an understanding of the mechanistic course of the reaction. [1] Determination of the absolute configuration of such compounds using X-ray crystallography can be challenging. In order to explore the scope of the technique, we crystallized the natural compound, industrial feedstock and flavoring agent, (2S,5R)-trans-2-isopropyl-5-methylcyclohexanone, l-menthone, and determined its absolute configuration. This light atom structure contains just one oxygen atom as largest anomalous scattering atom (f' 0.05170, f" 0.03357, Cu-Kα radiation, λ = 1.54178 Å). Despite the importance of organic drugs in industry and nature there are a large number of liquid compounds for which their crystal structure is unknown. Knowledge about the absolute configuration of bio-organic molecules is important, since enantiomers often have different effects on an organism. Typically, the liquid sample is cooled down below its liquid-solid phase transition temperature and brought to crystallization. The crystalline powder so obtained can be used as a source for crystal growth. By translation of the capillary through the cold nitrogen gas stream a suitable single crystal can be grown at the liquid-solid phase boundary (inverse zone melting). [2] Using the example of l-menthone, we discuss the challenges and advantages of determining the absolute configuration of liquid samples using *in situ* X-ray crystallography. [3]

References

[1] M. Buchsteiner, L. Martinez-Rodriguez, P. Jerabek, I. Pozo, M. Patzer, N. Nöthling, C. W. Lehmann, A. Fürstner, *Chem. Eur. J.*, vol. 26, pp. 2509–2515, 2020.
[2] R. W. Seidel, R. Goddard, N. Nöthling, C. W. Lehmann, *Cryst. Eng. Comm.*, vol. 21, pp. 3295–3303, 2019.
[3] R. Boese, *Z. Kristallogr.*, vol. 229, pp. 595–601, 2014.

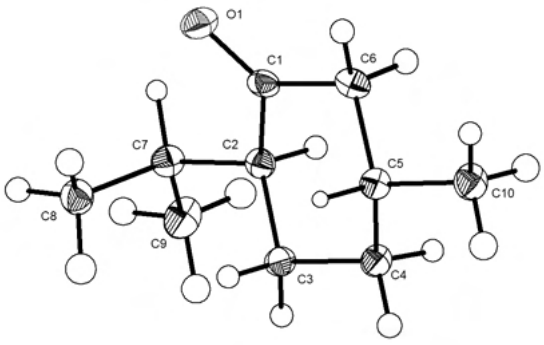

Figure 1

Expanding the Scope of Macrocyclic Poly-NHC Ligands: Bimetallic Palladium(II) and Platinum(II) Complexes

T. Pickl[1], A. Pöthig[2]
[1] Technical University of Munich, Departement of Chemistry, Chair of Inorganic and Organometallic Chemistry, Supramolecular Organometallics, Munich, Germany

Macrocyclic polyimidazolium salts are widely used in supramolecular chemistry as precursors for metal–NHC complexes. Here, we present the synthesis and structural characterization of the dinuclear palladium(II) and platinum(II)–NHC complexes Pd2L(PF6)2 and Pt2L(PF6)2 based on a macrocyclic calix[4]imidazolylidene[2]pyrazolate ligand obtained by in situ deprotonation of the tetraimidazolium salt H6L(PF6)4. Both compounds were also prepared by transmetallation from the literature-known silver(I)–NHC complex Ag8L2(PF6)4. 1H and 13C NMR spectroscopy combined with SC-XRD studies elucidated the structure of the palladium(II) and platinum(II) complexes. The d8 metal centers of both congeners are coordinated in a slightly distorted square-planar arrangement by the macrocyclic ligand. Similar to the previously reported nickel(II) complex Ni2L(PF6)2, the heavier metal homologs adopt a bent, saddle-shaped structure. In the solid state, one hexafluorophosphate ion in Pd2L(PF6)2 occupies the cavity of the cationic fragment [Pd2L]2+ with C–H···F contacts short enough to be rationalized as charge-assisted hydrogen bonds. In contrast, Pt2L(PF6)2 adopts a channel-like packing via self-assembly of the cationic [Pt2L]2+ fragments with the hexafluorophosphate counterions located outside of the cavities.

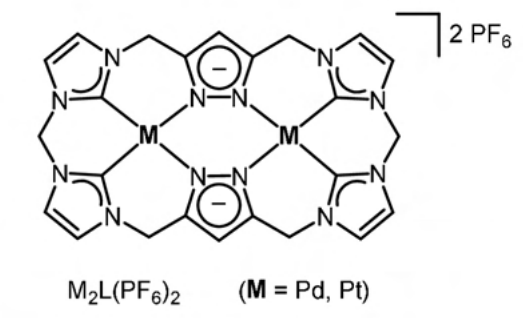

Figure 1

Spectroscopy

Soft X-ray analysis applied to crystallographic characterization of graphite

S. Matveev[1]

[1] JEOL (Germany) GmbH, Freising, Germany

There are various methods that are traditionally used for crystallographic characterization of materials, e.g. TEM, EBSD, XRD etc. JEOL recently developed a new type of wavelength dispersive spectrometer (WDS) that can be mounted on common scanning electron microscopes (SEM) or electron microprobes (EPMA). The spectrometer is sensitive to anisotropic soft X-ray emission, thus providing information about orientation of some anisotropic crystal structures. It utilizes a variable line spacing diffraction gratings, allowing the efficient and parallel collection of very low-energy X-rays (so called "soft" X-rays). This new Soft X-ray Emission Spectrometer (SXES) exhibits very high spectral resolution (0.3eV at Al L1), which allows to separately measure x-ray intensities due to sp^2-$\sigma \rightarrow$ 1s and P_z-$\pi \rightarrow$ 1s transitions in graphite. Complex structure of CKa(2) peak can be used to evaluate crystallinity of graphite, orientation, and grain size distribution at submicron scale as well as on the larger scale of tens of millimeters. Such application is relevant for development of Li batteries, in which Li concentration, distribution and chemical state can be also conveniently measured using the same SXES detector. Advantages of SXES include high sensitivity and spatial resolution, easy sample preparation and handling, as well as versatility. Since the detector can be mounted on JEOL SEM or EPMA it can be combined with other analytical methods such as EDS, WDS, CL and EBSD. Below we provide SXES spectra of C Ka(2) measured with JEOL SS-9400SXES using JS200N grating mounted on JSM-IT800HL FEG SEM at 5kV and 50nA. Graphite grains with different crystallographic orientations were analyzed. Emission intensities related to σ and π bonding exhibit maxima in parallel and perpendicular to [001] crystallographic direction respectfully. Parallel detection allows to reprocess ROI of the spectra and also plot peak ratios thus providing versatile and robust tool for investigation of carbon crystallinity.

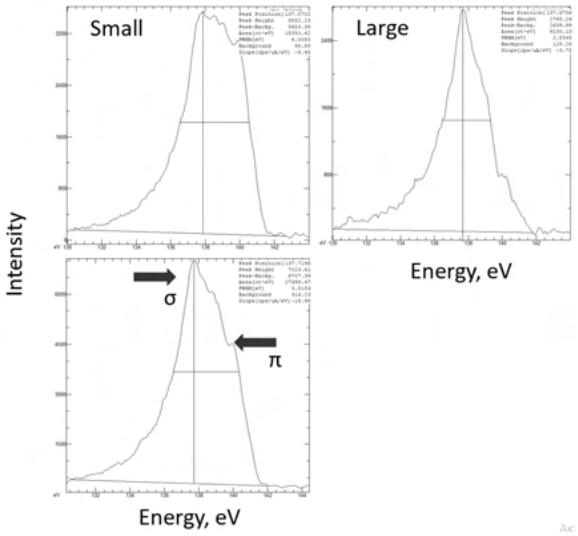

Figure 1

Author index

Table of Contents

Plenary talks

Fascinating structures of magnetic materials

M. Holynska[1]

[1] Philipps University Marburg and European Space Research and Technology Centre

Magnetic materials, in particular molecular magnets, can display remarkable, aesthetically pleasing and elegant structures, although most promising properties have been detected in simple mononuclear compounds [1]. The highly interdisciplinary field of molecular magnetism has been defined by Oliver Kahn as study of "magnetic properties of isolated molecules and/or assemblies of molecules" [2]. Applications of molecular magnets are foreseen in high-density data storage and quantum computing. The latter might be significant not only for on-ground, but also for space applications (e.g. satellite quantum communications).

Crystal structures of molecular magnets, although not fully representative of the targeted applications, play an important role in resolution of magnetostructural correlations [3]. These correlations may be retrieved via special setups, such as high-pressure crystallography [4]. For polynuclear metal complexes (Figure 1) often problems with diffraction data quality and solvent disorder are faced [5].

References

[1] A. Castro-Alvarez et al., "High performance single-molecule magnets, Orbach or Raman relaxation suppression?", *Inorg. Chem. Front.*, vol. 7, pp. 2478, 2020.

[2] O. Kahn, Molecular Magnetism, VCH, 1993.

[3] C. J. Milios et al., "Hexanuclear manganese(III) single-molecule magnets", *Angew. Chem.*, vol. 43, pp. 210, 2004.

[4] A. M. Thiel et al., "High-Pressure Crystallography as a Guide in the Design of Single-Molecule Magnets", *Inorg. Chem.*, vol. 59, pp. 1682–1691, 2020.

[5] A. J. Tasiopoulos et al., "Giant Single-Molecule Magnets: A Mn84 Torus and Its Supramolecular Nanotubes", *Angew. Chem. Int. Ed.*, vol. 43, pp. 2117 –2121, 2004.

[6] M. Holynska et al., "[MnIII6O3Ln2] single-molecule magnets: Increasing the energy barrier above 100 K", *Chem. Eur. J.*, vol. 35, pp. 9605–9610, 2011.

[7] M. Holynska et al., "A Defect Supertetrahedron Naphthoxime-Based [Mn9(III)] Single-Molecule Magnet", *Inorg. Chem.* vol. 52, no. 13, pp. 7317–7319, 2013.

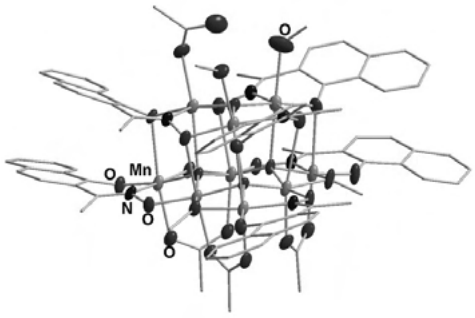

Figure 1

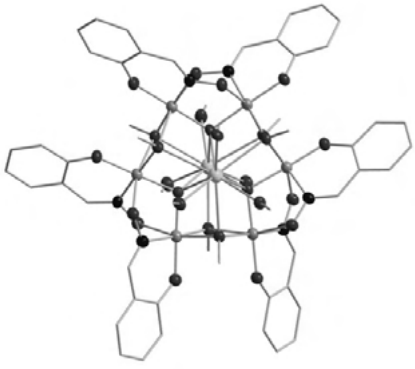

Figure 2

Exploring the Complex Structural Landscape and Potential Applications of Rare-Earth Metal–Organic Frameworks

A. J. Howarth[1], V. Quezada-Novoa[2], P. R. Donnarumma[2], H. M. Titi[3]

[1] Concordia University, Montreal

[2] Department of Chemistry and Biochemistry, Concordia University

[3] Department of Chemistry, McGill University

Metal–organic frameworks (MOFs) are structurally diverse, porous materials comprised of metal nodes bridged by organic linkers. [1] Through careful choice of nodes and linkers, the chemical and physical properties of MOFs can be elegantly tuned and materials with very high surface area and porosity can be obtained. As a consequence, MOFs have been explored for many potential applications including, but not limited to, gas storage and release, chemical separations, catalysis, drug

delivery, light harvesting and energy conversion, and the detoxification of hazardous analytes. [2] In addition to these promising potential applications, MOFs offer an interesting platform for studying fundamental concepts in inorganic materials chemistry. We are particularly interested in the study of MOFs comprised of rare-earth (RE) elements, [3] in part, because of the high and variable coordination number of these elements, which allows several unique and intricate MOF topologies to be designed and synthesized. Furthermore, RE-MOFs can be produced with diverse optical and electronic properties dictated by the 4f electron configurations of the RE-elements. In this presentation, RE-MOFs are explored from design and synthesis, to potential application.

References

[1] B. F. Hoskins and R. Robson, "Infinite polymeric frameworks consisting of three dimensionally linked rod-like segments", *J. Am. Chem. Soc.*, vol. 111, pp. 5962–5964, 1989); O. M. Yaghi and H. Li, Hydrothermal Synthesis of a Metal-Organic Framework Containing Large Rectangular Channels, *J. Am. Chem. Soc.*, vol. 117, pp. 10401–10402, 1995.

[2] A. J. Howarth, Y. Liu, P. Li, Z. Li, T. C. Wang, J. T. Hupp and O. K. Farha, "Chemical, thermal and mechanical stabilities of metal–organic frameworks", *Nat. Rev. Mater.*, vol. 1, pp. 15018, 2016.

[3] F. Saraci, V. Quezada-Novoa, P. R. Donnarumma, "Rare-earth metal–organic frameworks: from structure to applications", *Chem. Soc. Rev.*, vol. 49, pp. 7949–7977, 2020.

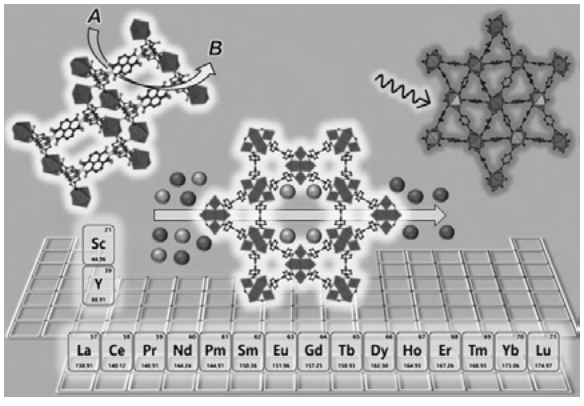

Figure 1

3D Pair Distribution Function Analysis in Materials Science

B. Iversen[1]

[1] Aarhus University, Aarhus, Denmark

X-ray diffraction from powders and single crystals has for decades been the key analytical tool in materials science. Bragg intensities provide information about the average crystals structure, but often it disorder and specific local structure that control key material properties. For 1D data there has been an immense growth in combined analysis of Bragg and diffuse scattering using the Pair Distribution Function (PDF), and in our group we frequently use 1D PDF analysis to study nanocrystal nucleation in solvothermal processes [1] or thin films [2], or to analyse materials under operating conditions [3]. For single crystals, diffuse scattering studies have a long history with elaborate analysis in reciprocal space, but direct space analysis of the 3D-PDF is still in its infancy. We have used 3D-PDF analysis to study the crystal structures of high performance thermoelectric materials Cu2Se (Fig 1) [4], PbTe [5], and 19-e half-heusler Nb1-xCoSb [6], where the true local structure is essential for understanding the unique properties. For frustrated magnetic materials direct space analysis of diffuse magnetic scattering provides a new route to magnetic structures [7].

References

[1] N. L. N. Broge et al., "Auto-catalytic formation of high entropy alloy nanoparticles", *Angew. Chem. Intl. Ed.*, vol. 59, pp. 21920-21924, 2020.

[2] M. Roelsgaard et al., "Time-Resolved Surface Pair Distribution Functions during Deposition by RF Magnetron Sputtering", *IUCrJ*, vol. 6, pp. 299–304, 2019.

[3] L. R. Jørgensen et al., "Operando X-ray scattering study of thermoelectric β-Zn4Sb3", *IUCrJ*, vol. 7, pp. 100-104, 2020.

[4] N. Roth et al., "Solving the disordered structure of β-Cu2-xSe using the three-dimensional difference pair distribution function", *Acta Crystallogr. Sect. A*, vol. 75, pp. 465–473, 2019.

[5] K. A. U. Holm et al., "Temperature Dependence of Dynamic Dipole Formation in PbTe", *Phys. Rev. B*, vol. 102, pp. 024112, 2020.

[6] N. Roth et al., "A simple model for vacancy order and disorder in defective half-Heusler systems", *IUCrJ*, vol. 7, pp. 673-680, 2020.

[7] N. Roth et al., "Model-free reconstruction of magnetic correlations in frustrated magnets", *IUCrJ*, vol. 5, pp. 410–416, 2018.

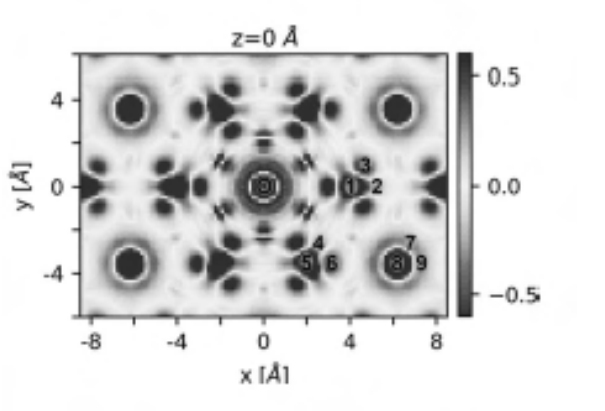

Figure 1

Massive X-ray screening against SARS-CoV-2 main protease

A. Meents[1], P. Reinke[1], S. Günther[1]

[1] Deutsches Elektronen-Synchrotron - DESY, Hamburg, Germany

As a response to the SARS-CoV-2 pandemic we have set up a large consortium of more than one hundred scientist centered at DESY in Hamburg in order to find suitable drug candidates. In contrast to common screening techniques such as biochemical activity-based assays or X-ray fragment screening, here we employed massive X-ray crystallographic screening of two drug-repurposing libraries against the SARS-CoV-2 main protease (Mpro) as initial target. In total co-crystallization experiments of 5953 individual drugs with Mpro were setup and datasets from more than 8000 crystals were collected at the PETRA III MX beamlines. Our screening effort resulted in the identification of 37 compounds binding to Mpro. Secondary screening of these hits in a cell-based viral infection assay carried out at the Bernhard Nocht-Institute revealed antiviral activity in combination with low cytotoxicity for six compounds, which have not yet been reported as inhibitors of SARS-CoV-2. While four of these inhibitors bind to the catalytic site of the enzyme, the remaining two bind to a previously undescibed allosteric site within the dimerization domain [1]. For the two most promising compounds from our screen, Calpeptin and Pelitinib, we have intiated further preclinical testing.

References

[1] S. Günther, P. Y. A. Reinke, et al., *bioRxiv*, doi:10.1101/2020.11.12.378422, 2020.

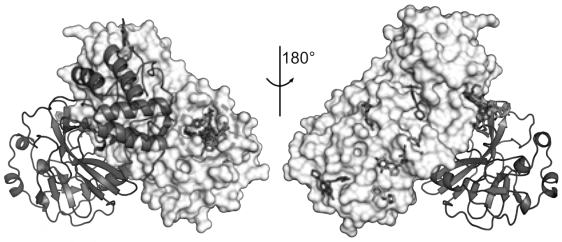

Figure 1

Time-resolved diffraction experiments at an X-ray free electron laser reveal ultrafast structural changes within a photosynthetic reaction centre

R. Neutze[1]

[1] Univ. Gothenburg, Gothenburg, Sweden

X-ray free electron lasers (XFEL) have facilitated the development of time-resolved serial femtosecond crystallography (TR-SFX) approaches to study protein structural changes [1]. This method relies upon the continuous replacement of microcrystals using micro-jet (or other) technologies and has many advantages relative to traditional time-resolved Laue diffraction methods using synchrotron radiation [2]. Photosynthetic reaction centres are integral membrane proteins which harvest the energy content of sunlight in order to power the movement of electrons. We collected TR-SFX data at the LCLS in order to observe light induced structural changes in a bacterial photosynthetic reaction centre. Our observations revealed how the light-induced movement of electrons induced a complementary structural response of the protein which stabilized the charge-separated state [3].

References

[1] Tenboer, J., et al. "Time-resolved serial crystallography captures high-resolution intermediates of photoactive yellow protein" *Science*, vol. 346, pp. 1242-1246, 2014.

[2] A. Wöhri et al., "Light-induced structural changes in a photosynthetic reaction center caught by Laue diffraction", *Science*, vol. 328, pp. 630-633, 2010.

[3] R. Dods et al., "Ultrafast structural changes within a photosynthetic reaction centre", *Nature*, vol. 589, pp. 310-314, 2021.

Atomic resolution structure determination by cryo-EM – where are the limits?

H. Stark[1], K. M. Yip[2], N. Fischer[2], E. Pakina[2], A. Chari[2]

[1] MPI Göttingen

[2] Max-Planck-Institute für biophysikalische Chemie, Göttingen

Single particle cryo electron microscopy (cryo-EM) has developed into a powerful technique to determine 3D structures of large macromolecular complexes. Due to improvements in instrumentation and computational image analysis, the number of high-resolution structures is steadily increasing. The method cannot only be used to determine high-resolution structures but also to study the dynamic behavior of macromolecular complexes and thus represents a very complementary method to X-ray crystallography. Furthermore, the maximum attainable resolution by cryo-EM has constantly improved in recent years. Most of the high-resolution structures are still in the 3 Angstrom resolution regime but some have even crossed the 2 Angstrom barrier. We have recently installed a new prototype electron microscope which is equipped with a monochromator and a next-generation spherical aberration corrector. This microscope is optically superior to the currently commercially available instruments and can therefore be used to test the resolution limits in cryo-EM. We have used the test specimen apoferritin to determine its structure at 1.25 Angstrom resolution [1] which is sufficient to visualize for the first time individual atoms clearly separated in the density map (Figure 1). Recently, we managed to use this microscope not only to improve the resolution of the very stable and rigid protein apoferritin. We also obtained significant improvement in resolution for other more dynamic macromolecular complexes for which one could have expected that the microscope itself may not be a major resolution limiting factor.

References

[1] Yip et al., "Atomic resolution protein structure determination by cryo-EM", *Nature*, vol. 587, pp. 157–161, 2020.

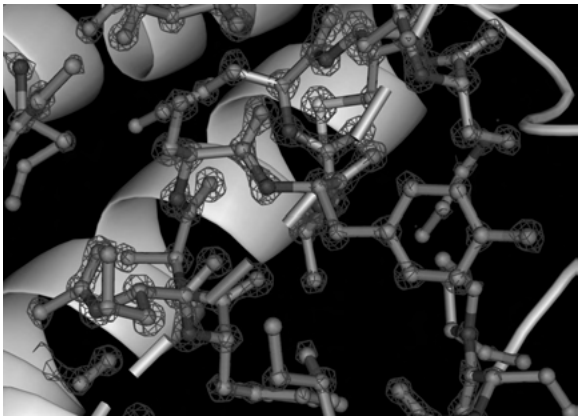

Figure 1

Research activities at the HZB-MX beamlines directed towards fighting SARS-CoV-2

M. S. Weiss[1], T. Barthel[1], C. Feiler[1], R. Foerster[1], C. Gless[1], T. Hauss[1], M. Hellmig[1], F. Lennartz[1], U. Müller[1], M. Steffien[1], H. Taberman[1], J. Wollenhaupt[1]

[1] Macromolecular Crystallography, Helmholtz-Zentrum Berlin

Since the worldwide outbreak of the Covid-19 pandemic in early 2020, researchers in many different parts of the world have started activities directed towards a better understanding of the SARS-CoV-2 virus life cycle or even towards medical treatment of Covid-19. Large-scale research facilities such as for instance synchrotron radiation facilities are playing a particularly important role in this respect by providing state-of-the-art Macromolecular crystallography (MX) facilities. MX has been instrumental in deciphering the first atomic resolution structure of the SARS-CoV-2 main protease (Figure 1) [1]. Several other viral protein structures have been determined following that [2]. Furthermore, owing to the manifold developments of MX towards automation and the concomitant increase in throughput, MX has also been employed as a primary screening technique for finding new substances, which might be active against SARS-CoV-2. In the presentation several user and in-house projects will be highlighted, which are directed towards this goal.

References

[1] L. Zhang, et al., "Crystal structure of SARS-CoV-2 main protease provides a basis for design of improved α-ketoamide inhibitors", *Science*, vol. 368, pp. 409–412, 2020.

[2] M. Scudellari, "The sprint to solve coronavirus protein structures - and disarm them with drugs", *Nature*, vol. 581, pp. 252–255, 2020.

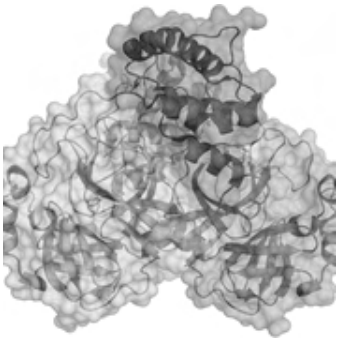

Figure 1

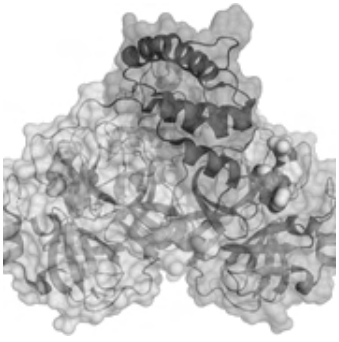

Figure 2

Max von Laue Talk:
Self-organization of biomolecular building blocks and inorganic nanoparticles into biohybrid nanomaterials

T. Beck[1,2]

[1] University of Hamburg, Institute of Physical Chemistry, Grindelallee 117, Hamburg, Germany

[2] The Hamburg Centre for Ultrafast Imaging, Hamburg, Germany

Self-organization is a key tool for the construction of functional nanomaterials. We have recently established a novel method for the self-organization of biomolecular building blocks and nanoparticles. Here, protein containers, engineered with opposite surface charge, are used as an atomically precise ligand shell for the assembly of inorganic nanoparticles.[1] The assembly of these protein-nanoparticle composites yields highly ordered nanoparticle superlattices with unprecedented precision (Fig. 1A). The structure of the protein scaffold can be tuned with external stimuli such as metal ion concentration.[2] Importantly, these composite materials show catalytic activity inside the porous material.[3] Along these lines, the protein containers used as a scaffold offer a viable route towards renewable materials.[4]

For the formation of these biohybrid materials, the inorganic cargo has to be synthesized or encapsulated into the protein containers. Here, we demonstrate that the highly specific cargo-loading mechanism of the bacterial nanocompartment encapsulin can be employed for encapsulation of artificial cargo such as inorganic nanoparticles.[5] For this purpose, gold nanoparticles were decorated with cargo-loading peptides. By lock-and-key interaction between the peptides and the peptide-binding pockets on the inner container surface, the nanoparticles are encapsulated with extremely high efficiency (Fig. 1B). Importantly, the container does not change, as shown by electron microscopy. Most notably, the supramolecular peptide binding is independent from external factors such as ionic strength.[5] Cargo-loading peptides may serve as generally applicable tool for efficient and specific encapsulation of cargo molecules into a protein compartment. Moreover, these nanoparticle protein-container composites are suitable for applications as building blocks in materials, exploiting the plasmonic properties of gold nanoparticles for light manipulation or sensing.

References

[1] M. Künzle, T. Eckert, T. Beck, *J. Am. Chem. Soc.*, vol. 138, pp. 12731-12734, 2016.

[2] M. Künzle, T. Eckert, T. Beck, *Inorg. Chem.*, vol. 57, pp. 13431-13436, 2018.

[3] M. Lach, M. Künzle, T. Beck, *Chem. Eur. J.*, vol. 23, pp. 17482-17486, 2017.

[4] a) M. Künzle, M. Lach, T. Beck, *Dalton Transactions*, vol. 47, pp. 10382-10387, 2018; b) M. Lach, M. Künzle, T. Beck, *Biochemistry*, vol. 58, pp. 140, 2019.

[5] M. Künzle, J. Mangler, M. Lach, T. Beck, *Nanoscale*, vol. 10, pp. 22917-22926, 2018.

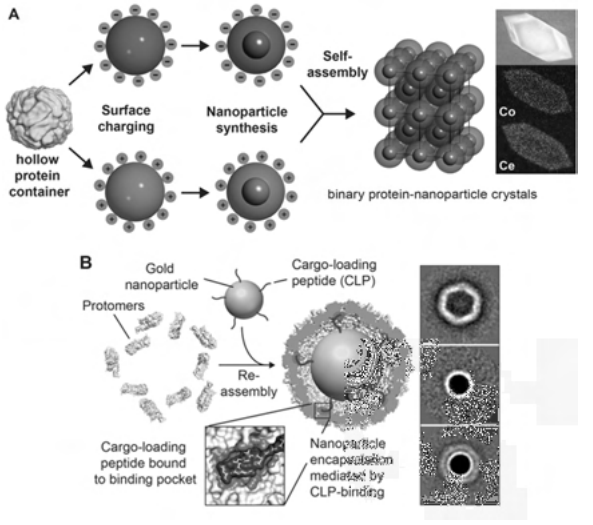

Figure 1 A) General strategy for the assembly of binary protein-nanoparticle crystals based on charged protein containers. B) Efficient encapsulation of functionalized gold nanoparticles into the encapsulin protein container. Right panel: TEM class averages of empty containers, gold nanoparticles and encapsulated gold nanoparticles.

Max von Laue Talk: From the perturbation of crystal symmetry towards functionality

M. Zschornak[1]

[1] TU Bergakademie Freiberg, Freiberg, Germany

The formation of crystals and symmetry on the atomic scale has persistently attracted scientists through the ages. The structural symmetry itself depends in this respect subtly on boundary conditions such as defects or external physical fields. In particular sensitive details in the electronic structure determine the nature of a vast diversity of symmetry-related phenomena – among them piezoelectricity, pyroelectricity, and ferroelectricity. Owing to their versatile orbital character, especially transition metal oxides span the range of ionic, covalent and metallic bonding and thus offer both local and highly dispersive degrees of freedom.

In the talk, crystalline symmetry reductions due to structural defects and external electric fields will be discussed, exemplarily for the perovskite $SrTiO_3$. To gain a thorough physical understanding of the underlying processes, interactions and dynamics, details of the local atomic and electronic structure are accessed by means of experimental Resonant X-ray Scattering methods as well as electronic structure modeling. Based on the variability of X-ray photon energy at synchrotrons, new respective approaches are presented with unique capabilities to increase the contrast for the characterization of subtle structure deviations and a positional precision below the picometer.

Talks

Advanced Instrumentation

The New PHOTON III Detector with Photon Counting in Mixed-Mode Detection

M. Adam[1], T. Stuerzer[1], M. Ruf[2], J. Kaercher[2], A. Abboud[1]
[1] MA: Bruker AXS GmbH, Karlsruhe, Germany
[2] MA: Bruker AXS, LLC; Madison WI, USA

The best crystal structures for publication require X-ray detectors with high signal-to-noise ratios and accurate intensities. The new PHOTON III detector family matches these requirements perfectly, offering mixed mode detection for the first time. Mixed mode detection simultaneously combines photon counting and integration, providing data of ultimate quality for both strong and weak reflections. Conventional photon counting detectors, like HPC or HPADs, suffer from poor linearity and count rate limitations for strong reflections, significantly degrading data quality. The mixed mode PHOTON III detector eliminates all detector noise, delivering the highest linearity and guaranteeing the highest quality data for the most challenging samples. The PHOTON III is available in three different sizes to ensure the best performance for your application needs. Users admire the detectors' ultimate sensitivity over a wide energy range (from In-Kα to Ga-Kα), low point-spread, and parallax-free diffraction data. The PHOTON III also features high-energy event discrimination (HEED) that eliminates ubiquitous cosmic radiation artefacts making it the best detector ever developed.

Details on the function principle of the PHOTON III detector and latest application examples will be discussed.

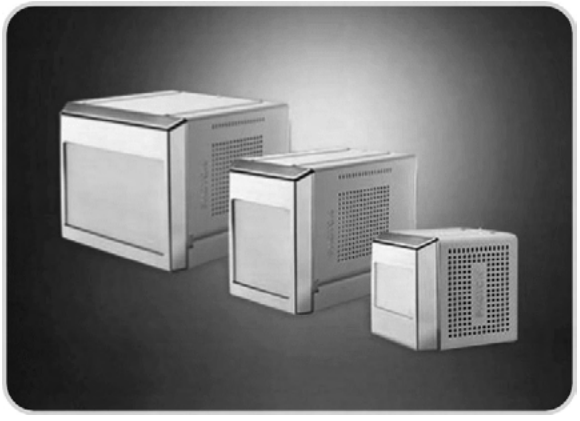

Figure 1

First user experiments of the PERCIVAL soft X-ray imager

J. Correa Magdalena[1], A. Marras[2], C. Wunderer[2], H. Graafsma[2], K. Bagschik[3], M. v. Zimmermann[4], T. Nicholls[5], H. Hyun[6], S. Rah[6], R. Pan[2], B. Keitel[2], V. Vardanyan[2], F. Krivan[2], S. Gang[2], M. Ruiz-Lopez[2], R. Battistelli[7], B. Pfau[8], F. Buettner[7], A. Dawiec[9], F. Orsini[9], K. Kharitonov[2], M. Mehrjoo[2], E. Plönjes[2], K. Kim[7], N. Tartoni[14], V. Felk[2], I. Shevyakov[2], M. Zimmer[2], N. Guerrini[5], S. Lange[2], R. Menk[11], B. Marsch[15], M. Hoesch[2], W. Nichols[10], A. Greer[10], G. Cautero[11], U. Pedersen[10]
[1] DESY, Photon Science, FS-DS (Detector Systems), Hamburg, Germany
[2] DESY, Notkestr. 85, 22607 Hamburg, Germany
[3] DESY, Photon Science, FS-PE (Experiment Support PETRY III), Hamburg, Germany
[4] DESY, HASYLAB, Hamburg, Germany
[5] STFC Rutherford Appleton Laboratory, Didcot, United Kingdom
[6] Pohang Accelerator Laboratory, Pohang, South Korea
[7] Helmholtz-Zentrum Berlin, Berlin, Germany
[8] Max-Born-Institut, Max-Born-Straße 2 A, 12489 Berlin, Germany
[9] Synchrotron SOLEIL, Saint-Aubin, France
[10] Diamond Light Source, Didcot, United Kingdom
[11] Elettra Synchrotron Trieste, Basovizza, Italy

The PERCIVAL detector, a CMOS imager specifically designed for the soft X-ray regime, has served in 2020 its two first user experiments, both at a Synchrotron Radiation source (SR) and also at a Free Electron Laser (FEL). Here, we report some preliminary results of both experiments as well as future plans.

The first experiment, in collaboration with groups at the HZB and MBI, used the P04 XUV beamline at PETRA-III to perform holography imaging of topological materials (in particular skyrmions) at an energy or 780eV. The second experiment, in collaboration used the FL24 at FLASH-2 to performed ptychography imaging of plasma treated surfaces at an energy range between 92 and 462eV. Both experiments benefited from a very large dynamic range, thanks to the PERCIVAL auto-adaptative gain switching.

With its 4 x 4 cm^2 active area, extendable to 8 x 8 cm^2 in clover-leaf like configurations, and its 2 Megapixels, 27 μm size, PERCIVAL can provide images with high spatial resolution. Moreover, its fast readout, wil be capable of speeds up to 300 frames per second. A dynamic range from 14e- to 3.5 Me- is to be expected. The development, jointly carried by 5 light sources (DESY,

PAL, Elettra, DLS and SOLEIL) and RAL/STFC, will enable increased science yield from today's FEL and synchrotron light sources in the soft X-ray regime.

Clamp cells for high pressure neutron scattering at low temperatures and high magnetic fields at the MLZ

A. Eich[1], K. Friese[1], M. Hölzle[1], Y. Su[1], T. Müller[1], V. Hutanu[1,2], M. K. B. Poli[2], R. Georgii[3], L. Beddrich[3], M. Meven[2], A. Grzechnik[2]

[1] Forschungszentrum Jülich, JCNS-MLZ, Garching, Germany

[2] RWTH Aachen University, Institute of Crystallography, Aachen, Germany

[3] Heinz Maier-Leibnitz Zentrum, Garching, Germany

To study the effect of high pressure on any sample property, suitable pressure devices are a fundamental requirement. Their design has to be tailored to the experimental demands regarding the intended pressure, the employed instrumentation and the expected scientific results. Our work presents the development of high pressure cells for neutron scattering on polycrystalline and single-crystalline samples at low temperatures and with applied magnetic fields.

One of the most common devices for high-pressure neutron experiments is the clamp cell [1], where the pressure is applied ex situ and which can be used independently in various setups. Our cell design [2] has been specifically developed for neutron scattering experiments at low temperatures in the closed-cycle cryostats on the instruments DNS (diffuse scattering neutron spectrometer), MIRA (cold three axes spectrometer), and POLI (polarized hot neutron diffractometer) at the Heinz Maier-Leibnitz Zentrum (MLZ) in Garching, Germany. The compact monobloc cell has been produced in two variants, the CuBe alloy and NiCrAl "Russian Alloy", working up to about 1.1 GPa and 1.5 GPa, respectively. The low paramagnetic moment of both alloys allows also measurements of magnetic properties.

First tests of the cell with neutron radiation were performed to calibrate the load/pressure-curve of the CuBe cell (up to 1.15 GPa), to estimate its neutron absorption and background, and to measure magnetic reflections. In addition, the thermal response in the instrument cryostat was measured and the experimental findings were complemented by simulations.

Ultimately, these cells are intended as standard cells for high pressure measurements on different instruments at MLZ suitable for all available magnets and cryostats down to 1.5 K. Further tests under various conditions (temperature, pressure, magnetic field) as well as simulations are planned for both cells. The results will help both to establish the present cells and to optimise the design of subsequent cells to achieve higher pressures, to fit into smaller cryostats and to enable neutron-independent pressure calibration.

Acknowledgement

This work was supported by the Bundesministerium für Bildung und Forschung (BMBF) [grant number 05K19PA2] and by the Deutsche Forschungsgemeinschaft (DFG) [grant number GE971/5-2].

References

[1] Klotz, S., *Techniques in High Pressure Neutron Scattering*, Boca Raton, USA: CRC Press, 2013.

[2] Eich, A. *et al.*, *High Press. Res. Advance*, 2020, doi: 10.1080/08957959.2020.1841759.

New polarized neutron diffraction setup for precise investigations of magnetic structures up to 8 T at the MLZ

V. Hutanu[1], H. Thoma[2], H. Deng[1,2], G. Brandl[2], A. Weber[2], V. Rubanskiy[2], J. Peters[3], W. Luberstetter[1,2], T. Krist[4], G. Roth[1], L. Peters[1], T. Brückel[2]

[1] RWTH Aachen University, Institute of Crystallography, Aachen, Germany

[2] Forschungszentrum Jülich, JCNS outstation @ MLZ Garching, Garching, Germany

[3] TU Munich, FRM II, Munich, Germany

[4] NOB Berlin GmbH, Berlin, Germany

Polarized neutron diffraction (PND) is a powerful method for investigating magnetic structures. It gives unique access to contributions from nuclear and magnetic scattering, their interference terms, and their magnetic chirality, and permits to distinct between them. In contrast to non-polarized neutron diffraction, where the scattered intensity depends on the square of the magnetic structure factor, PND has a linear nuclear–magnetic interference term as part of the scattered intensity. This increases the precision in the determination of the ordered magnetic moment by at least one order of magnitude. Recently, a first PND setup using a compact high Tc superconducting magnet and a 3He spin filter polarizer has been successfully implemented [1,2] on the hot neutrons single crystal diffractometer POLI at Maier-Leibnitz Zentrum (MLZ) in Garching b. München. Although this setup performs well and first scientific output from the measurements performed using it starts to appear [3], it suffers from the relatively low maximal available field of only 2.2 T. For studying many modern-topic (e.g quantum, topologic order, complex frustrated, etc.) magnetic materials with

small ordered magnetic moment, the field-limit of about 2 T is insufficient in order to produce significant measurable signal, even for PND. To overcome this limitation, a new 8 T split-coil superconducting magnet has been procured and implemented for measurements on POLI. Although, this new magnet is actively shielded, reducing the stray field by an order of magnitude compared to the classical design, its fringe fields are still too large to be used with the sensitive 3He polarizer of the previous setup. To overcome this issue, a new large-beam-cross-section solid-state supermirror bender (SB) polarizer has been developed for POLI. It was realized by a Fe/Si multilayer coating on both sides of the thin Si wafers (m=3) by the NOB company. An additional Gd oxide layer is deposited on the convex side of each wafer to absorb the neutrons with the wrong polarization. An existing shielded Mezei-type flipper is used between the magnet and SB. A dedicated guide field construction was numerically simulated, optimized and built to link the magnetic field of the SB to the flipper and to the stray field of the magnet. The neutron beam path between the monochromator drum to the sample magnet is shown in the Fig. 1. The new setup was successfully tested using a 3He spin filter as analyzer at low fields ($<$ 1 T), and a high quality Cu2MnAl single-crystal at high fields ($>$ 2T). An almost loss-free spin transport within the instrument for the complete field range of the new magnet was achieved. A high polarization efficiency of above 99% even for short wavelength neutrons could be experimentally reached using the new solid-state bender (Fig.2). The new high–field PND setup is now available for precise magnetic structure investigations on POLI for the internal and external user communities.

References

[1] H. Thoma, H. Deng, G. Roth, V. Hutanu, "Setup for polarized neutron diffraction using a high-Tc superconducting magnet on the instrument POLI at MLZ and its applications", *J. Phys.: Conf. Ser.*, vol. 1316, 2019, Art. no. 012016.

[2] H. Thoma, W. Luberstetter, J. Peters & V. Hutanu, "Polarised neutron diffraction using novel high-Tc superconducting magnet on single crystal diffractometer POLI at MLZ," *J. Appl. Cryst.*, vol. 51, pp. 17–26, 2018.

[3] J. Jeong, B. Lenz, A. Gukasov *et al.*, "Magnetization density distribution of Sr2IrO4: Deviation from a local jeff = 1/2 picture," *Phys. Rev. Lett.*, vol. 125, 2020, Art. no. 097202.

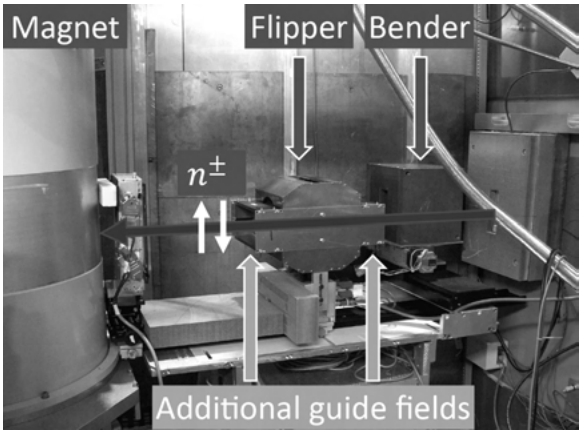

Figure 1

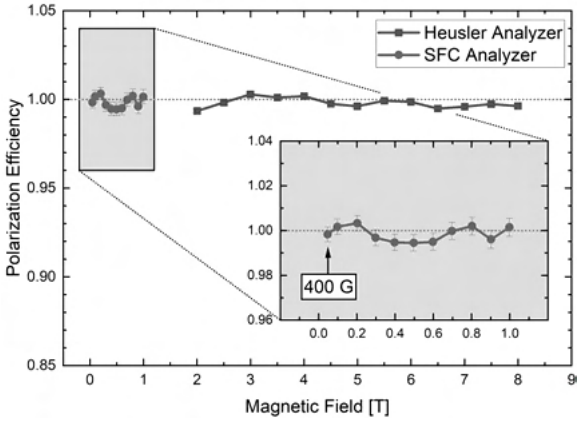

Figure 2

Single Crystal Diffraction Experiments under High Pressure with Hot Neutrons at MLZ

M. Meven[1], A. Grzechnik[1], V. Hutanu[1], K. Friese[2], A. Eich[3], G. Roth[1]

[1] Institute of Crystallography, RWTH Aachen University, Aachen, Germany

[2] Jülich Centre for Neutron Science at Heinz Maier-Leibnitz Zentrum, Forschungszentrum Jülich GmbH, Garching, Germany

[3] Jülich Centre for Neutron Science–2/Peter Grünberg-Institute–4, Forschungszentrum Jülich GmbH, 52425 Jülich, Germany

Due to their specific peculiarities neutrons are a very useful probe for structural studies on various hot topics related to physics, chemistry and mineralogy. The neutron single crystal diffractometer HEiDi at the Heinz Maier-Leibnitz Zentrum (MLZ) offers high flux, high resolution and large q range, low absorption and high sensitivity for light elements. These properties apply in a similar way to its polarized sister diffractometer POLI, which is optimized for magnetic structure determinations.

In 2016 a project was launched in order to allow studies on tiny samples < 1 mm^3 and to develop new pressure cells for HEiDi which can be combined with its existing low temperature equipment in order to study structural properties down to temperatures below 10 K, e.g. MnFe4Si3 compounds and their magnetic features [1]. As part of this project (funded by the BMBF, No. 05K16PA3), various neutron-optical components (Cu220-monochromator, solid state collimators, neutron guides) were developed and optimized in order to generate a sufficiently high flux density at the sample location at the wavelength $\lambda = 0.87$ Å. Very tiny single crystal samples (< 0.1 mm^3) were successfully studied using various newly developed diamond anvil cells up to several GPa, either with a panoramic pressure cell in combination with low temperatures [2] or in a transmission pressure cell, which allows simultaneous studies of the same sample using neutron, synchrotron as well as laboratory x-ray sources [3].

This project is now followed up by a second one (BMBF No. 05K19PA2) focusing on further improving the high pressure capabilities on HEiDi and POLI (including the installation of a 2-dimensional detector) and the development of optimized pressure cells for further instruments at the MLZ, namely POLI, DNS and MIRA (see contribution by A. Eich).

References

[1] A. Grzechnik et al., "Single-Crystal Neutron Diffraction in Diamond Anvil Cells with Hot Neutrons", *J. Appl. Cryst.*, vol. 51, pp. 351-356, 2018.

[2] A. Eich et al., "Magnetocaloric Mn_5Si_3 and $MnFe_4Si_3$ at variable pressure and temperature",*Mater. Res. Express*, vol. 6, pp. 096118, 2019.

[3] A. Grzechnik et al., "Combined X-ray and neutron single-crystal diffraction in diamond anvil cells", *J. Appl. Cryst.*, vol. 53(1), pp. 1 - 6, 2020.

Neutron protein crystallography at the Heinz Maier-Leibnitz Zentrum (MLZ): New developments and recent application examples

T. E. Schrader[1], A. Ostermann[2], M. Monkenbusch[3], B. Laatsch[4], W. Petry [2], D. Richter[3]

[1] 1Forschungszentrum Jülich GmbH, Jülich Centre for Neutron Science (JCNS) at Heinz Maier-Leibnitz Zentrum (MLZ), Lichtenbergstr.1, 85747 Garching, Germany

[2] 2Heinz Maier-Leibnitz Zentrum (MLZ), Technische Universität München

[3] Forschungszentrum Jülich GmbH, Institute for Complex Systems ICS

[4] Forschungszentrum Jülich GmbH, Engineering and Technology (ZEA-1)

The neutron single crystal diffractometer BIODIFF at the research reactor Heinz Maier-Leibnitz (FRM II) is especially designed to collect data from crystals with large unit cells. The main field of application is the structural analysis of proteins, especially the determination of hydrogen atom positions. BIODIFF is a joint project of the Jülich Centre for Neutron Science (JCNS) and the FRM II. BIODIFF is designed as a monochromatic instrument with a narrow wavelength spread of less than 3 %. To cover a large solid angle the main detector of BIODIFF consists of a neutron imaging plate in a cylindrical geometry with online read-out capability.

BIODFF is equipped with a standard Oxford Cryosystem "Cryostream 700+" which allows measurements at 100 K. A new kappa goniometer head was added recently. This allows an automated tilting of the crystal in order to increase the completeness of the data set when recording another set of frames in the tilted geometry. Typical scientific questions addressed are the determination of protonation states of amino acid side chains in proteins and the characterization of the hydrogen bonding networks between the protein active centre and an inhibitor or substrate.

Picking out some recent highlights from measurements at BIODIFF it will be shown how the method of neutron protein crystallography could be used to answer mechanistic questions in enzymatic processes or help to improve inhibitor fragment screening. New developments at the instrument will also be presented: A new collimation for the primary beam should lead to a reduction in background. It should also make it easier to align the neutron beam with the centre of the neutron imaging plate detector. Furthermore, a new single crystal x-ray diffractometer has been installed in the new MLZ lab building. It features a Molybdenum and a Copper Microfocus x-ray source and a 150° (2) x-ray detector. It also features also an Oxford Cryosystems 800 series Cryostream for sample temperatures between 80-400K. This x-ray diffractometer can be used to record an x-ray data set of the protein crystal after having been measured at the BIODIFF instrument. It may also be used to pre-scan the diffraction quality of the crystals the user brings for neutron beam times at MLZ instruments.

Diffractometer portfolio at FRM II neutron source: status and perspectives

A. Senyshyn[1]

[1] Heinz Maier-Leibnitz Zentrum (MLZ)

In the meantime the diffraction activities form the major portion of research at each large scale facility. Diffraction at neutron sources is exploring the full range of unique neutron properties (sensitivity to isotopes and magnetic subsystems, nuclear scattering form-factors independent on Q etc) and provides structural information complementary to X-ray or electron diffraction. Despite the different underlying physics supplementing the interaction of neutrons and photons with the matter, the ways of the data A wealth of neutron diffraction instrumentation as a probe of long-range atomic and magnetic orders from single crystal and powder samples at a variety of environmental conditions is available at MLZ, namely high-resolution and engineering diffractometers SPODI and STRESS-SPEC; hot, thermal and cold (macromolecular) single crystal diffractometers HEIDI, RESI and BioDIFF; diffuse instrument DNS and a pool of triple axis spectrometers. A number of new instrumental developments (POWTEX, SAPHIR, ERWIN) as well as new life project for FIREPOD (E9) are on their way to strengthen diffraction at MLZ even further.

There is a broad spectrum of structure-related scientific activities at MLZ e.g. (i) electrochemical energy storage systems and related materials; (ii) modern ferroelectrics; (iii) multiferroic materials and interrelation of the ferroic degrees of freedom; (iv) new generation engineering and shape memory alloys; (v) biological macromolecules; (vi) rock-forming minerals and glasses. In the current contribution an overview of the diffraction instrumentation at FRM II neutron source will be presented along with the future prospects and running developments.

Giant supramolecules meet synchrotron radiation: Experience with DESY P11 and P24 beamlines

A. Virovets[1], E. Peresypkina[1], M. Scheer[1]

[1] University of Regensburg, Regensburg, Germany

During last decades we have been using organometallic *cyclo*-Pn complexes (n = 4, 5) as building blocks for the rational design of giant supramolecules, up to 4.6 nm in size [1-4]. The supramolecules consisting of hundreds of atoms frequently demonstrate weak scattering power due to the severe crystallographic disorder. In many cases, the use the high-flux synchrotron sources becomes the only remedy.

The samples of organometallic supramolecules must be permanently protected from oxygen to avoid the oxidation of *cyclo*-Pn fragments. Any traces of water in the organic solvents also should be avoided. Therefore, the proper sample handling requires a vacuum-argon line (Schlenk line) that protects the sample from air during the extraction of the portion of crystals for the diffraction study. Within the long-term project II-20180597 with DESY (Hamburg, Germany) we have installed such line in the sample preparation lab of P24 beamline.

To obtain quality data at dmin $>$ 1 Å for giant supramolecules we developed optimal strategies to perform the single-crystal diffraction experiments at both P11 and P24 beamlines. For P11 beamline, the most critical is to choose radiation energy as a compromise between dmin and quantum efficiency (QE) of a PILATUS 6M detector. Higher energies improves the resolution by the cost of significantly lower QE.

The optics at the P24 beamline allows using hard X-ray radiation with E up to 44 keV. It helps in reducing the absorption and radiation damage in Ag and Ta-containing crystals. Helium open-flow cryostat provides temperature down to 10 K.

Optimization of the experimental strategy allowed us to obtain high-quality diffraction data even from weakly scattering crystals (Fig. 1) and to investigate such subtle structural effects as superstructural ordering.

This work was supported by the German Research Foundation (DFG) within the project Sche 384/44-1.

References

[1] E. Peresypkina, C. Heindl, A. Virovets, M. Scheer, *Structure and Bonding*, vol. 174, p. 321, 2016.

[2] H. Brake, E. Peresypkina, C. Heindl, *et al.*, *Chem. Sci.*, vol. 10, p. 2940, 2019.

[3] E. Peresypkina, M. Bielmeier, A. Virovets, M. Scheer, *Chem. Sci.*, vol. 11, p. 9067, 2020.

[4] J. Schiller, A.V. Virovets, E. Peresypkina, M. Scheer, *Angew. Chem. Int. Ed.*, vol. 59, p. 13647, 2020.

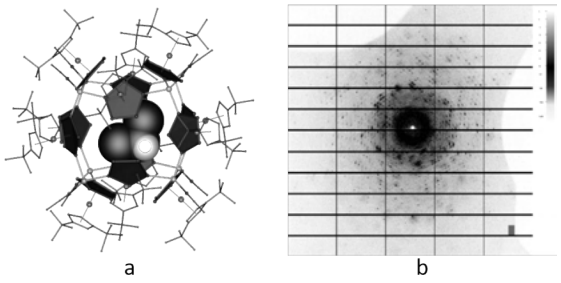

Figure 1 a) Giant cationic supramolecule [(Cp''Fe(η5-P5)12(CuNCCH3)8]8+ with an external diameter of 2.5 nm [4]. Hydrogen atoms are omitted for clarity; b) the diffraction pattern from the single crystal at P11 beamline (E = 18 keV, 0.1° scan)

Bio-crystallography

EasyAccess Frame - sliding puzzle inspired tool for eased crystal handling

T. Barthel[1], F. U. Huschmann[1], D. Wallacher[1], C. Feiler[1], G. Klebe[2], J. Wollenhaupt[1], M. Weiss[1]

[1] Helmholtz-Zentrum Berlin, Macromolecular Crystallography, Albert-Einstein-Straße 15, 12489 Berlin, Germany

[2] Philipps-University Marburg, Marburg, Germany

The experimental workflow of macromolecular crystallography has been improved enormously in the last two decades, especially regarding speed and throughput. One step of this workflow, namely the manipulation and harvesting of crystals, remains labour- and time-intense even though considerable efforts have been applied. In order to tackle this bottleneck, we developed a novel, low-cost device that acts as a lid for 96-well crystallization plates. It includes 96 movable parts that allow access to the individual experiment and simultaneously minimize the evaporation of the other experiments. Primary results show the successful evaporation minimization of many typical crystallization cocktails for up to six hours. The device, named EasyAccess Frame, avoids any sealing by foil and unsealing of individual wells in the process and thus facilitates easy crystal manipulation and harvesting. Therefore, the device increases throughput and is useful for a range of macromolecular crystallography experiments, especially screening campaigns. The device is successfully being used in crystallographic fragment screening campaigns at HZB and significantly reduces time and effort necessary for the crystal handling involved.

References

[1] Barthel T., Huschmann F. U., Wallacher D., Feiler C. G., Klebe G., Weiss M. S., Wollenhaupt J., "Facilitated crystal handling using a simple device for evaporation reduction in microtiter plates," *J. Appl. Cryst.*, accepted for publication, 2021.

Molecular mechanisms of the bacterial DEAH/RHA NTPase HrpA and its role in antibiotics susceptibility

L. Grass[1], J. Wollenhaupt[1], T. Barthel[1], B. Loll[1], M. C. Wahl[1]

[1] Laboratory of Structural Biochemistry, Freie Universität Berlin, Berlin, Germany.

Many bacteria harbor RNA-dependent nucleoside-triphosphatases of the DEAH/RHA family [1], whose molecular mechanisms and cellular functions are poorly understood [2]. Here, we show that the Escherichia coli DEAH/RHA protein, HrpA, is an ATP-dependent 3'-to-5' RNA helicase, and that the RNA helicase activity of HrpA influences bacterial survival under antibiotics treatment. Limited proteolysis, crystal structure analysis and functional assays showed that HrpA contains an N-terminal DEAH/RHA helicase cassette preceded by a unique N-terminal domain and followed by a large C-terminal region that modulates the helicase activity. Structures of an expanded HrpA helicase cassette in the apo and RNA-bound states revealed ratchet-like domain movements upon RNA engagement much more pronounced than hitherto observed in related eukaryotic DEAH/RHA enzymes (Fig. 1). Consistent with similar conformational changes supporting RNA translocation, structure-based functional analyses delineated transient inter-domain contact sites that support substrate loading and unwinding. Analogous dynamic intramolecular contacts are not possible in the related, but helicase-inactive, RNA-dependent nucleoside-triphosphatase, HrpB [3,4]. Our results indicate that HrpA may be an interesting target to interfere with bacterial tolerance toward certain antibiotics and suggest possible interfering strategies.

References

[1] Khemici, V. & Linder, P., "RNA helicases in bacteria," *Curr. Opin. Microbiol.*, vol. 30, pp. 58–66, 2016.

[2] Redder, P., Hausmann, S., Khemici, V., Yasrebi, H. & Linder, P., "Bacterial versatility requires DEAD-box RNA helicases," *FEMS Microbiol. Rev.*, vol. 39, pp. 392–412, 2015.

[3] Pietrzyk-Brzezinska, A. J. *et al.*, "Crystal Structure of the Escherichia coli DExH-Box NTPase HrpB," *Structure*, vol. 26, pp. 1462-1473.e4, 2018.

[4] Xin, B.-G., Chen, W.-F., Rety, S., Dai, Y.-X. & Xi, X.-G., "Crystal structure of Escherichia coli DEAH/RHA helicase HrpB," *Biochem. Biophys. Res. Commun.*, vol. 504, pp. 334–339, 2018.

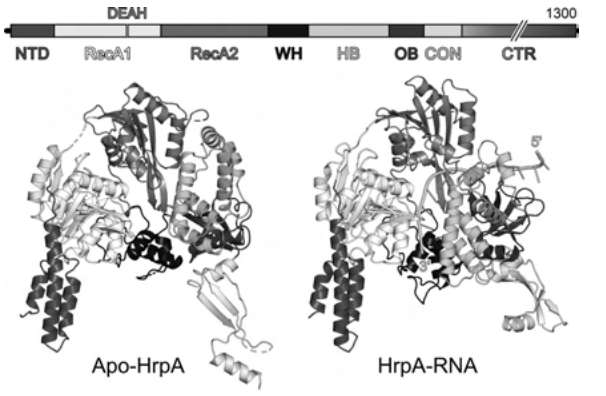

Figure 1 Top, Domain composition of the E. coli DEAH/RHA-type RNA helicase, HrpA. NTD, N-terminal domain; RecA1/2, RecA-like domains; WH, winged-helix domain; HB, helical bundle ("ratchet") domain; OB, oligonucleotide/oligosaccharide-binding domain; CON, connector domain; CTR, C-terminal region. Bottom, comparison of the crystal structures of the expanded helicase cassette of E. coli HrpA in the apo (left) and RNA-bound (right) states.

Massive X-ray screening against SARS-CoV-2 main protease

S. Guenther[1], P. Reinke[2], A. Meents[2]

[1] DESY, Photon Science, FS-BMX, Hamburg, Germany

[2] DESY, Notkestr. 85, 22607 Hamburg, Germany

Contributed on behalf of the Hamburg SARS-CoV-2 X-ray screening initiative

As a response to the current SARS-CoV-2 pandemic we have set up a large consortium of more than one hundred scientist centered around DESY in Hamburg. In contrast to common screening techniques such as biochemical activity-based assays or X-ray fragment screening, here we employed massive X-ray crystallographic screening of two drug-repurposing libraries against SARS-CoV-2 main protease (MPro) of SARS-CoV-2 as initial target. Already in March 2020 co-crystallization experiments of 5953 individual drugs with MPro were setup. In April data from more than 8000 of these crystals were collected at the PETRA III MX beamlines. In the following weeks a data analysis pipeline for fully automatic data processing and subsequent structure refinement followed by ligand identification by pan-dataset density analysis (PanDDA) was established. Our screening effort resulted in the identification of 37 compounds binding to MPro. Secondary screening of these hits in a cell-based virus-infection assay revealed antiviral activity in combination with low cytotoxicity for six compounds which have not yet been reported as inhibitors of SARS-CoV-2. While four of these inhibitors bind to the catalytic site of the enzyme, the remaining two bind to an allosteric site within the dimerization domain [1].

To our knowledge, this is the first time X-ray crystallography has been used as a primary screen for drug discovery while using drug-like molecules rather than smaller fragments. The platform developed for this project is currently being further extended and optimized and will be available for future drug discovery efforts.

References

[1] S. Günther, P. Y. A. Reinke, *et al.*, *bioRxiv*, in press, doi:10.1101/2020.11.12.378422.

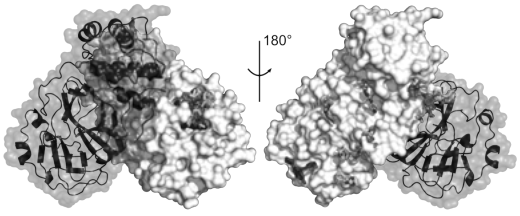

Figure 1 SARS-CoV-2 MPro dimer with hits derived from X-ray screening of drug repurposing libraries. Drug binding (stick representation) is observed across the complete MPro dimer. One MPro monomer with bound drugs is shown in white surface representation. The other monomer is shown as mixed cartoon/surface representation.

The Corona-year 2020 at Biodiffraction Beamline P11

J. Hakanpaeae[1], S. Saouane[2], E. Crosas[3], J. Meyer[3], B. Kistner[3], A. Henkel[4], S. Chatziefthymiou[5], G. Pompidor[3]

[1] DESY, Photon Science, FS-PETRA-D, P11 Beamline, Hamburg, Germany

[2] DESY, Photon Science, FS-PS (FS-Photon Science), Hamburg, Germany

[3] DESY, Notkestr. 85, 22607 Hamburg, Germany

[4] University of Lübeck, Lübeck, Germany

[5] DESY, Photon Science, FS-PE (Experiment Support PETRA III), Hamburg, Germany

Beamline P11 at PETRA III in Hamburg is a versatile instrument for macromolecular crystallography (1). During 'the Corona-year' 2020 we operated in very exceptional conditions. Here we describe DESY responses to the pandemic situation, such as the fast-track access to the beamline, exceptional user regulations and remote access.

To date, 35 PDB depositions have arisen from P11 related to Covid-19 by our fast-track, proposal and priority access users (2-5). Additionally, P11 participates to three DESY Strategic Fund projects relating to Covid-19 research: 1) Inhibitor screening and structural characterization of virulence factors from SARS-CoV-2, 2) Multidimensional serial crystallography of Sars-CoV-2 proteins to unravel structure and dynamics of function and inhibition and 3) Automated X-ray crystallography compound screening pipeline at DESY.

In spite of the restricted user operations, the beamline had a very busy user run and the scarce commissioning time was used to employ our new Eiger2 X 16M. We successfully employed the detector for serial data collections. Dedicated nodes in our central computational cluster Maxwell will be at the disposal of our users for processing (and autoprocessing) their Eiger data next year. Inspired by the properties of our new detector, we started to streamline the serial crystallography methods available at the beamline and to integrate both the data collection and the data processing more tightly into the beamline environment.

References

[1] Burkhardt *et al.*, *Eur. Phys. J. Plus*, vol. 131, 2016, Art. no. 56.

[2] Zhang *et al.*, *Science*, vol. 368, pp. 409-412, 2020.

[3] Günter *et al.*, *BioRxiv*, 2020, doi.:10.1101/2020.05.02.043554.

[4] Rut *et al.*, *Nat. Chem. Biol.*, 2020, doi:10.1038/s41589-020-00689-z.

[5] Oerlemans *et al.*, *RSC Med. Chem.*, 2021, DOI: 10.1039/D0MD00367K.

Crystal structure of bacterial cytotoxic necrotizing factor CNFy reveals molecular building blocks for intoxication

P. Chaoprasid[1], P. Lukat[2], S. Mühlen[1], T. Heidler[3], E.-M. Gazdag[2], S. Dong[2], W. Bi[4], C. Rüter[1], M. Kirchenwitz[5], A. Steffen[5], L. Jänsch[6], T. E. Stradal[5], P. Dersch[1], W. Blankenfeldt[2]

[1] University of Münster, Institute of Infectiology, Center for Molecular Biology of Inflammation (ZMBE), Münster, Germany

[2] Helmholtz Centre for Infection Research, Structure and Function of Proteins, Braunschweig, Germany

[3] Helmholtz Centre for Infection Research, Molecular Structural Biology, Braunschweig, Germany

[4] Helmholtz Centre for Infection Research, Cellular Proteomics, Braunschweig, Germany

[5] Helmholtz Centre for Infection Research, Cell Biology, Braunschweig, Germany

[6] Helmholtz Centre for Infection Research, Cellular Proteomics, Braunschweig, Germany

Cytotoxic Necrotizing Factors (CNFs) are single-chain AB-toxins and important virulence factors in pathogens such as uropathogenic *E. coli* (UPEC) or enteropathogenic *Yersinia* species. Their cytotoxic effect is based on the constitutive activation of small GTPases (Rho family) by deamidation of a glutamine residue in the switch II region, leading to cytoskeletal alterations and finally death of the host cell. Several steps are required for the toxin to fulfill its task, such as receptor binding, endocytosis and yet unknown structural changes in the B-part in order to translocate the catalytically active, toxic A-part through the endosomal membrane into the cytosol. So far, a crystal structure that could provide insight into these processes is still lacking.

Here we report on the crystal structure of full-length CNFy from *Yersinia pseudotuberculosis* at a resolution of 2.7 Å. The structure was solved by molecular replacement with the existing model of the C-terminal catalytic domain and the structure of the B-part, where the phases of the latter were obtained by single anomalous dispersion experiments in advance. The full-length AB-toxin comprises 1014 amino acid residues. While the two C-terminal domains (485 residues) are forming the A-part, the N-terminal B-part (529 residues) is consisting of 3 individual domains, of which all possess novel folds. From cell-biology experiments, the receptor-binding and translocation functions could be assigned to the first three domains although their mechanism(s) and the receptor of the host cell remain still unknown. The fourth domain shows structural similarity to ADP-ribosyl transferases but no similar function in CNFy could yet be detected.

Additionally, we also determined the structure of the two-domain A-part - as it should be released into the cytoplasm - alone (1.8 Å). The two domains show a different orientation towards each other than in the structure of the full-length toxin, which could hint towards activation of the catalytic domain upon release of the A-part.

Our first crystal structure of a full-length CNF-toxin lays the groundwork for further studies of the complex mechanism of this important bacterial virulence factor. CNF-toxins might not only be promising targets for future development of anti-infective drugs, the B-part might even have the potential to be exploited as delivery vehicle for large and complex drugs.

Facilities for Macromolecular Crystallography at the HZB

U. Müller[1], T. Barthel[2], C. Feiler[3], R. Förster[4], C. Gless[1], T. Hauß[3], M. Hellmig[4], F. Lennartz[3], M. Steffien[1], H. Taberman[1], J. Wollenhaupt[3], M. Weiss[4]

[1] Helmholtz-Zentrum Berlin für Materialien und Energie, Berlin, Germany

[2] Laboratory of Structural Biochemistry, Institute of Chemistry and Biochemistry, Freie Universität Berlin, Berlin, Germany

[3] Helmholtz-Zentrum Berlin, Berlin, Germany

[4] Helmholtz-Zentrum Berlin, Macromolecular Crystallography, Berlin, Germany

The Macromolecular Crystallography (MX) group at the Helmholtz-Zentrum Berlin (HZB) has been in operation since 2003. Since then, three state-of-the-art synchrotron beam lines (BL14.1-3) for MX have been built up on a 7T-wavelength shifter source [1-3]. Currently, the three beam lines represent the most productive MX-stations in Germany, with more than 3500 PDB depositions (Status 12/2020). BLs14.1 and 14.2 are energy tuneable in the range 5.5-15.5 keV, while beam line 14.3 is a fixed-energy side station operated at 13.8 keV. All three beam lines are equipped with state-of-the-art detectors: BL14.1 with a PILATUS3S 6M detector, BL14.2 with a PILATUS3S 2M and BL14.3 with a PILATUS 6M detector. BL14.1 and BL14.2 are in regular user operation providing close to 200 beam days per year and about 600 user shifts to approximately 100 research groups across Europe. Recently, remote beamline operation has been started successfully at BL14.1. BL14.3 is been equipped with a MD2 micro-diffractometer, a HC1 crystal dehydration device and a REX nozzle changer making it suitable for room temperature experiments. Additional user facilities include office space adjacent to the beam lines, a sample preparation laboratory, a biology laboratory (safety level 1) and high-end computing resources. Within this presentation a summary on the experimental possibilities of the beam lines and the ancillary equipment provided to the user community will be given.

References

[1] Heinemann U., Büssow K., Mueller, U. & Umbach, P., *Acc. Chem. Res.*, vol. 36, pp. 157–163, 2003.

[2] U. Mueller, N. Darowski, M. R. Fuchs, R. Förster, M. Hellmig, K. S. Paithankar, S. Pühringer, M. Steffien, G.Zocher & M. S. Weiss, *J. Synchr. Rad.*, vol. 19, pp. 442–449, 2012.

[3] Mueller, U., Forster, R., Hellmig, M., Huschmann, F. U., Kastner, A., Malecki, P., Puhringer, S., Rower, M., Sparta, K., Steffien, M., Uhlein, M. & Weiss, M. S., *Eur. Phys. J. Plus*, vol. 130, pp. 141–150, 2015.

Structure of SARS-CoV-2 papain-like protease PLpro reveals a framework for antiviral inhibitor design

V. Srinivasan[1], N. Werner[1], S. Falke[1], H. Brognaro[1], S. Günther[2], P. Y. A. Reinke[2], C. Ehrt[3], M. Rarey[3], A. Meents[2], C. Betzel[1,4]

[1] Universität Hamburg, Department of Chemistry, Institute of Biochemistry and Molecular Biology and Laboratory for Structural Biology of Infection and Inflammation, c/o DESY, 22607 Hamburg, Germany

[2] Center for Free-Electron Laser Science, DESY, Notkestrasse 85, 22607 Hamburg, Germany

[3] Universität Hamburg, Center for Bioinformatics, Bundesstr. 43, 20146 Hamburg, Germany

[4] Hamburg Centre for Ultrafast Imaging (CUI), Universität Hamburg, Luruper Chaussee 149, 22761, Hamburg, Germany.

The severe acute respiratory syndrome coronavirus 2 (SARS-CoV-2) papain-like protease (PLpro) is essential for the virus replication. PLpro has the additional function of removing ubiquitin and ISG15 (Interferon-stimulated gene 15) from host-cell proteins to aid coronaviruses in their evasion of the host innate immune responses. PLpro is thus an excellent drug target for a two-fold strategy to develop antiviral compounds that both inhibit viral replication and strengthen the immune response of the host. To provide a structural framework for efficient screening of inhibitor compounds, we expressed, purified and crystallized PLpro (Fig.1). The crystals are stable, reproducible, have a high solvent content of 66% suitable for soaking experiments and diffract to a high resolution of 1.5Å (Fig.2). Bioinformatics analysis of the active site based on the PLpro crystal structure coordinates showed interestingly high similarities to the proteasome and we screened 37 proteosome inhibitors by soaking and co-crystallization experiments. The PLpro crystals complexed with these compounds diffracted in the resolution

range of 1.5Å-2.5Å and structural efforts to identify new antiviral compounds to combat the coronavirus spread will be presented.

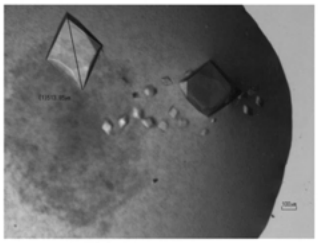

Figure 1 Trigonal PLpro crystals with cell dimensions $a = 82.03$, $b = 82.03$, $c = 134.45$, $\alpha = 90°$, $\beta = 90°$, $\gamma = 120°$.

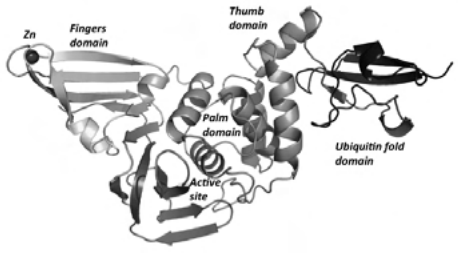

Figure 2 X-ray crystal ctructure of PLpro illustrating the four domains and the active site. The Zinc ion is represented as a magenta sphere.

The Coronavirus Structural Taskforce

A. Thorn[1]

[1] Universität Hamburg

The Coronavirus Structural Task Force [1] was an ad hoc collaboration of mostly junior researchers across nine time zones, brought together by the desire to fight the pandemic.

Most of us are crystallographic methods developers and as early as February 2020, we started evaluating the structures of macromolecules in SARS-CoV and later SARS-CoV-2 as they became available from the Protein Data Bank. We found that many could be improved. A website (www.insidecorona.net) and a database containing the evaluations and revised models were set up to aid in-silico drug discovery and other downstream research. Newly deposited structures are analysed as they come out by a bespoke structure evaluation/comparison pipeline. In addition, many individual structures were revised manually, atom-by-atom. In order to spread knowledge about the structural biology of the virus, we also reviewed the literature, putting the molecular models into a larger context for the rapidly growing community of researchers - drug developers, bioinformaticians, crystallographers - tackling the COVID-19 pandemic. We established a large network of COVID-19 related research, and forged friendships and collaborations across national boundaries.

As public outreach is so important right now, we also refine structures live on Twitch, write articles and offer a 3D printable virus model for schools.

References

[1] Croll, T., Diederichs, K., Fischer, F., Fyfe, C., Gao, Y., Horrell, S., Joseph, A. P., Kandler, L., Kippes, O., Kirsten, F., Müller, K., Nolte, K., Payne, A., Reeves, M. G., Richardson, J., Santoni, G., Stäb, S., Tronrud, D., Williams, C. & Thorn, A. *BioRxiv*, doi:10.1101/2020.10.07.307546, 2020.

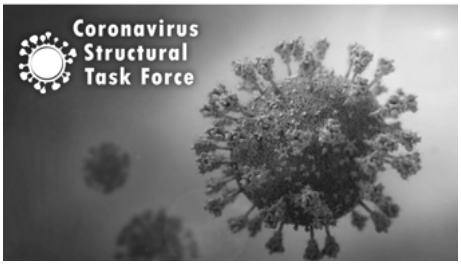

Figure 1

Disordered Materials, complex crystal structures and aperiodic crystals, diffuse scattering and 3D-PDF

Surface modifications of ion- irradiated diamonds

K. Bunk[1], W. Morgenroth[2], I. Alencar[3], F. Bertram[4], C. Schmidt[5], P. Gruszka[1], C. Trautmann[6], B. Winkler[1]

[1] Goethe University Frankfurt, Frankfurt, Germany

[2] University of Potsdam, Potsdam, Germany

[3] Federal University of Santa Catarina, Florianópolis, Brazil

[4] Deutsche Elektronen Synchrotron (DESY) (FS-PET-D Fachgruppe P08), Hamburg, Germany

[5] GFZ German Research Center for Geosciences, Potsdam, Germany

[6] GSI Helmholtz Centre for Heavy Ion Research and Technical University of Darmstadt, Darmstadt, Germany

Ion- irradiation is an established technology to change properties of diamonds in a controlled way [1] and has been studied as a function of ion species, energy and fluence for many years [2-4]. However, little is known regarding surface effects for irradiations with high energy ions which penetrate deep into the diamond. Irradiation experiments were carried out on various synthetic dia-

mond samples using 14 MeV Au6+ ions and a maximal fluence of 2.4 ×1015 ions/cm2. The penetration depth of such ions in diamond is about 1.7 μm [5]. The surface of the samples was characterized by atomic force microscopy (AFM), Raman spectroscopy and X-ray reflectometry (XRR).

Due to the irradiation, the formerly transparent samples darkened, which suggests partial amorphisation of the material. Raman spectroscopy revealed significant changes in the lattice dynamics and the formation of sp3 bonded amorphous carbon (Fig. 1). XRR experiments performed at beamline P08 @ PETRA III (Hamburg, Germany) revealed the formation of modified layers near the sample surface (Fig. 2). AFM provided information on changes of the surface topography including increased roughness and swelling. The surface roughness deduced from XRR data compared to AFM results will be discussed for the different diamond materials.

References

[1] R. Kalish, Semiconductors and Semimetals, 76, (2003), 145–181.

[2] R. Kalish and S. Prawer, Nuclear Instruments and Methods in Physics Research Section B: Beam Interactions with Materials and Atoms 106, (1995), 429.

[3] J. F. Prins, Materials Science Reports 7, (1992), 275.

[4] B. A. Fairchild, S. Rubanov, D. W. Lau, M. Robinson, I. Suarez-Martinez, N. Marks, A. D. Greentree, D. McCulloch, and S. Prawer, Advanced Materials 24, (2012), 2024.

[5] J. F. Ziegler, M. D. Ziegler, and J. P. Biersack, Nuclear Instruments and Methods in Physics Research Section B: Beam Interactions with Materials and Atoms 268, (2010), 1818-1823.

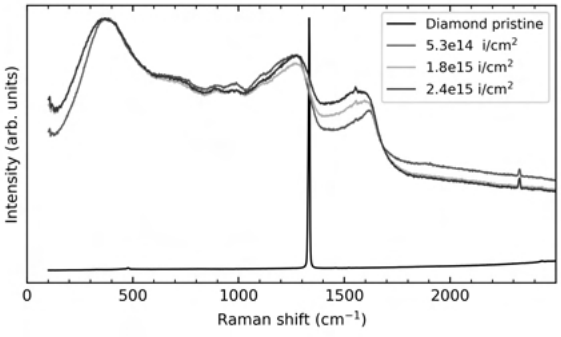

Figure 1 Raman spectra of pristine (black lines) and irradiated (colored lines) diamonds for a single crystal diamond sample irradiated with 14 MeV Au-ions of different fluences.

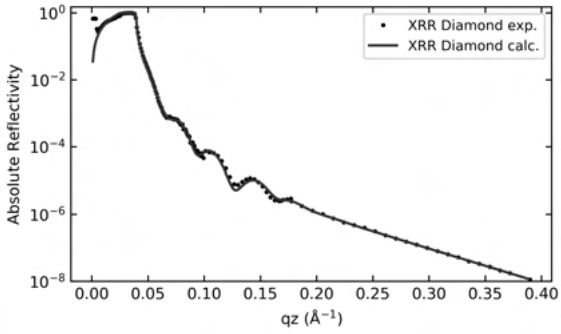

Figure 2 XRR curves for the experimental (black lines) and calculated (red lines) data of a single crystal diamond sample irradiated with 14 MeV Au-ions of fluence 2.4 × 10^{15} ions/cm^2.

Direct lock-in transition in 4-biphenylcarboxy substituted L-phenylalaninate crystals

S. Dey[1], S. Sasmal[2], D. Haldar[2]

[1] Institute of Crystallography, RWTH Aachen University, Aachen, Germany

[2] Department of Chemical Sciences, Indian Institute of Science Education and Research (IISER) Kolkata, Department of Chemical Sciences, Indian Institute of Science Education and Research (IISER) Kolkata Mohanpur, India

Protection of amino acids is an essential aspect for peptide synthesis.[1] Recently, crystals of 4-biphenylcarboxy substituted *L*-serine, *L*-tyrosine, *L*-alanine, *L*-leucine and *L*-phenylalanine methyl esters have been demonstrated to possess diverse supramolecular assembly governed by C–H···π and π···π interactions between biphenyl fragments and intermolecular N–H···O interactions between the amide O=C–N–H groups.[2,3] Amongst them, 4-biphenylcarxy-*L*-phenylalaninate is elusive because it crystallizes in monoclinic space group symmetry P21 within a pseudo-orthorhombic lattice[3] [a = 5.0748(2) Å, b = 8.7658(3) Å, c = 42.4828(13) Å, β = 90.038(3)°] at ambient conditions (phase **I**). The crystal comprises of two independent molecules (Z' = 2) with disparate molecular torsion and the monoclinic distortion is retained up to its melting temperature.

Temperature dependent single crystal X-ray diffraction experiments revealed a reversible structural phase transition at Tc ≈ 124 K upon cooling. Below Tc (phase **II**), satellite reflections in addition to main reflections were observed. **q** remains invariant as function of temperature that can be indexed with a modulation wave vector, $\mathbf{q} = (\frac{1}{2}, 0, \frac{1}{2})$ with respect to the basic monoclinic lattice. The crystal structure is described as a (3+1)D commensurately modulated structure in superspace group

P21(σ10σ3)0 ($\sigma_1 = 1/2$, $\sigma_3 = 1/2$). The equivalent 3D superstructure [space group monoclinic (b–unique) B21] comprises of four independent molecules in the asymmetric unit.

Here we present the phase relations between **I** and **II**. The phase transition at Tc is primarily characterized by evolution of torsional modulation within the biphenyl fragments that are unequal for the two independent molecules. The origin of the torsional modulation is argued to lie in the competition between possible steric hindrance between the ortho-hydrogens of the biphenyl fragment that favors torsion and intermolecular C–H$\cdots\pi$ interactions that favors planar biphenyl moiety. Stabilized by weak C–H$\cdots$O hydrogen bonds, short H–C$\cdots$C–H interactions involving the biphenyl fragment suppresses the torsion for one independent molecule while longer H–C$\cdots$C–H contacts allows larger torsional amplitude for the other.

References:

[1] Isidro-Llobet, A.; Alvarez, M. and Albericio, F. (2009) *Chem. Rev.* **109**, 2455–2504.
[2] Sasmal, S.; Podder, D.; Debnath, M.; Nandi, S. K. and Haldar, D. (2019) *ChemistrySelect* **4**, 10302–10306.
[3] Sasmal, S.; Nandi, S. K.; Kumar, S. and Haldar, D. (2019) *ChemistrySelect* **4**, 11172–11176.

Three-Dimensional Mapping of Diffuse Scattering of Perfect Si

O. Ivashko[1], A. Sarma[2], A.-C. Dippel[1], M. v. Zimmermann[3], O. Gutowski[2]
[1] DESY, FS-PETRA-D (FS-PET-D Fachgruppe P07211), Hamburg, Germany
[2] DESY, Hamburg, Germany
[3] HASYLAB at DESY, Hamburg, Germany

Single crystals often present disorder in their structure due to dopant substitution/intercalation or as an intrinsic instability of the compound. In many cases the disorder-to-order balance is responsible for key properties of the material. For example it can account for low thermal conductivity in PbTe or for the superconducting transition temperature in Sr2RuO4 where the highest Tc is obtained in disorder-free samples.

Here we present the three-dimensional mapping technique of diffuse scattering. At the Broad-Band Diffraction Swedish Material Science beamline (P21.1) at PETRA III synchrotron radiation source, total scattering measurements are possible thanks to the combination of high energy x-rays (100 keV) and large area detectors. Diffraction signal is acquired at high repetition rate allowing to operate with high incident photon flux. This is essential since the signal contains both the high intensity Bragg reflections, related to the average crystal structure, and the low intensity diffuse scattering signal accounting for the disorder. The acquired data are reconstructed in the hkl space and can be converted into the real space by Fourier transformation obtaining the three dimensional pair distribution function (3D-PDF) [1-3]. This technique is presented with the results obtained on perfect Si crystal as a standard. It is shown that 3D-PDF is sensitive to minor imperfections and/or impurities in the material.

References

[1] P. Schaub, T. Weber and W. Steurer, *Philosophical Magazine*, vol. 87, pp. 2781–2787, 2007
[2] T. Weber and A. Simonov, *Z. Kristallogr.*, vol. 227, pp. 238–247, 2012
[3] N. Roth et al., *IUCrJ*, vol. 5, pp. 410–416, 2018

Information Theory and Crystallography – a Fruitful Combination for Assessing Crystal Structure Complexity?

G. Kieslich[1]
[1] Technical University of Munich, Department of Chemistry, Munich, Germany

What is the complexity of a crystal structure? The definition of complexity is a challenging and similarly fascinating subject, touching different scientific disciplines such as economy, informatics, biology, math, and chemistry amongst others. Instead of defining complexity per sé, it is in practice easier to ask which system is more complex, showing that the challenge of defining complexity is closely related to the identification of an appropriate scale to measure complexity. In this contribution, the Shannon entropy is used as measuring system as defined by information theory, providing us with a framework to differentiate between the complexity of crystal structures as initially introduced by S. Krivovichev.[1]

In my presentation I discuss the opportunities and challenges that come with an information theory-based analysis of crystal structures as measure for complexity. I show that comparisons between Shannon entropy, crystal structure complexity and configurational entropy can be drawn,[2] opening intriguing opportunities for the systematic assessment of configurational entropy of crystal structures with implications in the areas of crystal growth and chemical bond theory.[3] Finally, and following on from recent developments in the field where theory development is in the centre, I introduce *crystIT* (crystallography & Information Theory),[4] a

python-based open-access program.[5] *crystIT* calculates various information measures based on a ∗.cif file as input, providing an easy-to-use platform for an information theory-based crystal structure analysis.

References

[1] S. Krivovichev, *Angew. Chem. Int. Ed.*, vol. 53, p. 654, 2014.
[2] S. Krivovichev, *Acta. Cryst. B*, vol. 72, p. 274, 2016.
[3] E. S. Harper, G. v. Anders, S. C. Glotzer, *Proc. Acad. Nat. Sci.*, vol. 116, p. 16703, 2019.
[4] C. Kaußler, G. Kieslich, *J. Appl. Cryst.*, accepted for publication, 2021.
[5] http://www.github.com/GKieslich/crystIT/

Tunable bonding in the incipient metal thermoelectric GeTe

S. Kimber[1], J. Zhang[2], Y. Cheng[3], D. Abernath[3], T. Ramirez-Cuesta[3], J. Hudspeth[4], Z.-Z. Luo[5], M. Kanatzidis[5], S. Billinge[6], T. Chatterji[7]
[1] University of Burgundy - Franche-Comté, Besancon, France
[2] Brookhaven National Laboratory, Upton (NY), USA
[3] Oak Ridge National Laboratory, Oak Ridge (TN), USA
[4] ESRF, Grenoble, France
[5] Northwestern University, Evanston (IL), USA
[6] Columbia University, New York (NY), USA
[7] Institut Laue-Langevin, Grenoble, France

The group IV-VI chalcogenides have important thermoelectric applications. GeTe has emerged as a promising non-toxic candidate, especially when the high-temperature cubic phase is suppressed to room temperature. However, even the mechanism of phase transition is disputed, as is the presence of disorder. Here we combine ab initio MD with synchrotron X-ray and dynamic neutron pair distribution function (PDF) analysis. We show that previous reports of disorder and symmetry breaking are entirely due to highly damped and anharmonic phonons. As predicted by metavalent bonding theories, this arises due to a softening in local bonding on heating, which strengthens long-range <100>c correlations. This picture is consistent with reported changes in resistivity and dielectric constant, and shown to be ubiquitously present in other polarisable binary chalcogenides and hR6 structured elements. Our results unify the results of local probes and spectroscopy as applied to binary chalcogenides, and should inspire a re-examination of other highly anharmonic energy materials such as hybrid perovskites and 'rattling' thermoelectrics.

The complexity of magnetic spin orders and dynamically disordered hydrogen bond networks in a hureaulite-type oxyhydroxide, Mn5[(PO4)2(PO3OH)2](HOH)4

S. Part[1]
[1] Ludwig-Maximilians-Universität München, the Department of Earth and Environmental Sciences, München, Germany

Pentamers of transition metal octahedra and double semi-helical chains of hydrogen bonds frame hureaulite-type oxyhydroxides (C2/c; a = 11.5 Å, b = 9.1 Å, c = 9.5 Å, beta = 96.4°) highly interesting for rich magnetic spin orders and polaron-dependent charge transport phenomena. Neutron powder diffraction data of its manganese end-member agree with that the magnetic lattice retains the (1a x 1b x1c) unit cell below the Curie temperature 7.2 K down up to 2 K, but magnetic moments of Mn2+ within MnO6 pentamers oriented predominantly parallel to the crystallographic b axis vividly change on to the (a-c) plane at lowered temperatures. The respective ferrimagnetic order corresponds to the magnetic space group C2/c at 6.5 K (Figure 1a) and C2'/c' at 3.4 K (Figure 1b). This reflects complicated discontinuity curves of AC magnetic susceptibility. Another phase transition occurs around at 2 K, where the magnetic spins are incommensurately modulated with a propagation vector (0.545(2), 0, 0). We present here subtle details of a complex evolution of magnetic spin orders of the title compound along with briefing quasi- and inelastic neutron scattering studies to demonstrate mechanism for the ease with protonic superconductivity.

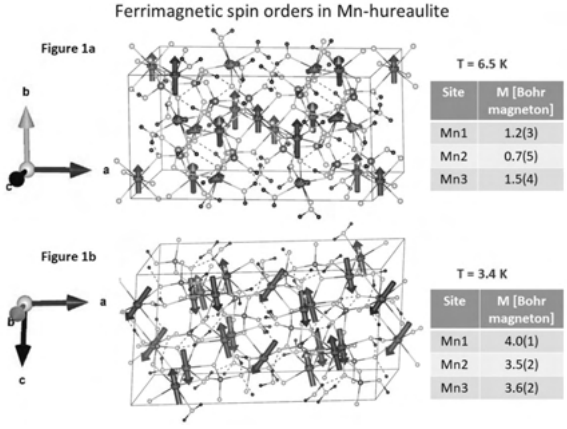

Figure 1

Single-crystal-to-single-crystal phase transitions of commensurately modulated sodium saccharinate 1.875-hydrate

T. Rekis[1], A. M. Schaller[1], S. R. Kotla[1], A. Schönleber[1], L. Noohinejad[2], M. Tolkiehn[2], C. Paulmann[2], S. van Smaalen[1]
[1] University of Bayreuth, Bayreuth, Germany
[2] DESY, Notkestr. 85, 22607 Hamburg, Germany

This contribution reports reversible, single-crystal-to-single-crystal phase transitions of commensurately modulated sodium saccharinate 1.875-hydrate [Na(sac)(15/8)H_2O]. The phases were studied in the temperature range 298 to 20 K. They exhibit complex disordered states. An unusual reentrant disorder has been discovered upon cooling through a phase transition at 120 K. The disordered region involves three sodium cations, four water molecules and one saccharinate anion. At room temperature, the structure is an eightfold superstructure that can be described by the superspace group $C2/c(0b0)s0$ with $\mathbf{q} = (0, 3/4, 0)$. It demonstrates maximum disorder with the disordered chemical entities having slightly different but close to 0.50:0.50 disorder component ratios. Upon cooling, the crystal tends to an ordered state, smoothly reaching a unified disorder component ratio of around 0.90:0.10 for each of the entities. Between 130 and 120 K a phase transition occurs involving a sudden increase of the disorder towards the disorder component ratio 0.65:0.35. Meanwhile, the space group and general organization of the structure are retained. Between 60 and 40 K there is another phase transition leading to a twinned triclinic phase. After heating the crystal back to room temperature its structure is the same as before cooling, indicating a complete reversibility of the phase transitions.

The application of mean field theory to single crystal diffuse scattering

E. Schmidt[1], A. L. Goodwin[1], J. Bulled[1]
[1] University of Oxford

Correlated disorder in crystalline materials gives rise to single crystal diffuse scattering. While the average structure determination via Bragg data analysis is considered a standard procedure, disorder analysis is thought of as a lengthy and complicated process. We present a mean field approximation to model single crystal diffuse scattering in molecular materials from a simple pair-interaction Hamiltonian.

Mean filed theory is a self-consistent field theory, which is widely used in statistical physics to model high-dimensional random systems. It has proven a valuable tool in the analysis of magnetic diffuse scattering data [1]. Here, the formalism is applied to describe orientationally disordered molecular crystals.

We present a computational study based on the mean field model suggested by Naya [2] and proof its applicability to strongly correlated disorder, where the local building block geometry dictates allowed and prohibited local configurations. The system that will be analysed in detail is a two-dimensional analogue the mercury diammonium halide $Hg(NH_3)_2Cl_2$ as depicted in the Figure [3].

We compare the results of the diffuse scattering analysis using the mean field model as introduced by Naya [2] to the results of RMC modelling and ΔPDF models based on a Warren-Cowley short range order parameter refinement (see Figure). Finally, the stability of the mean field analysis on limited data availability is demonstrated: Diffraction experiments under pressure or electric field yield a limited reciprocal space coverage. Here, we demonstrate the robustness of the proposed method against incomplete data sets.

References

[1] Paddison, J. A. textitet al., *Phys. Rev. Lett.*, vol. 11, no. 26, Jun. 2013, Art. no. 267207.
[2] Naya, S., *J. Phys. Soc. Jpn.*, vol. 37, no. 2, pp. 340–347, Aug. 1974.
[3] Lipscomb, W., *Anal. Chem.*, vol. 25, no. 5, pp. 737–739, May 1953.

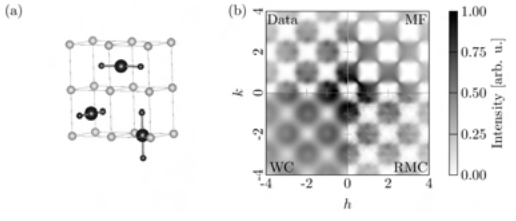

Figure 1 (a) Disordered structure of mercury diammonium halide $Hg(NH_3)_2Cl_2$ [3]. Hg in black, N in blue, Cl in light green. H atoms were omitted for clarity. The Hg is disordered over the face centres of the cubic unit cell. The ammonia groups occupy the centre of the shown cell, while the Cl is placed on the corner of the unit cell.
(b) X-ray diffuse scattering for the two-dimensional model system. Due to the fourfold symmetry of the average structure, one quadrant of the hk-layer is sufficient to represent the full data. Upper left corner: data as calculated from a model structure that fulfils the local rules; upper right corner: mean field refinement; bottom right corner: RMC refinement; bottom left corner: Warren-Cowley short range order analysis.

First order CDW phase transitions in R2Ir3Si5 (R = Ho, Er, Lu)

S. van Smaalen[1], S. Ramakrishnan[1], A. Schönleber[1], J. Bao[1], C. Eisele[1], S. R. Kotla[1], A. M. Schaller[1], T. Rekis[1], N. van Well[2], B. Bag[3], A. Thamizhavel[3], S. Ramakrishnan[3], D. Pal[4], N. S. Sangeetha[4], L. Noohinejad[5], M. Tolkiehn[5], C. Paulmann[5]

[1] University of Bayreuth, Laboratory of Crystallography, Bayreuth, Germany

[2] Ludwig Maximilians University of Munich, Department for Earth- and Environmental Sciences, Crystallography Section, Munich, Germany

[3] Tata Institute of Fundamental Research, Department of Condensed Matter Physics and Materials Science, Mumbai, India

[4] Indian Institute of Technology, Department of Physics, Indian Institute of Technology, Guwahati, India

[5] DESY, Notkestr. 85, 22607 Hamburg, Germany

$R_2Ir_3Si_5$ (R = Ho, Er, Lu) crystallize in the $U_2Co_3Si_5$ structure type at room temperature (orthorhombic space group Ibam) [1]. Upon cooling they undergo first-order charge-density-wave (CDW) phase transitions, as evidenced by anomalies with hysteresis in the temperature dependencies of the electrical resistivity (ρ), specific heat (C_p), magnetic susceptibility (χ), Seebeck coefficient (S) and thermal conductivity (κ) [1-4]. The CDW character of the low-temperature phases is corroborated by the appearance of satellite reflections at q = (0.2495, 0.4973, 0.2483) in diffraction experiments [4,5]. Single-crystal x-ray diffraction has revealed that the incommensurate CDW is accompanied by a strong monoclinic lattice distortion, while the symmetry of the CDW phase is reduced to triclinic. Here, we discuss the microscopic mechanism of CDW formation on the basis of a superspace analysis of single-crystal x-ray diffraction data [4].

Acknowledgement

Single-crystal X-ray diffraction data were collected at Beamline P24 of PETRA-III at DESY, Hamburg, Germany.

References

[1] Y. Singh, D. Pal, S. Ramakrishnan, A. M. Awasthi and S. K. Malik, *Phys. Rev. B*, vol. 71, 2005, Art. no. 045109.

[2] Y. K. Kuo, K. M. Sivakumar, T. H. Su and C. S. Lue, *Phys. Rev. B*, vol. 74, 2006, Art. no. 045115.

[3] N. S. Sangeetha, A. Thamizhavel, C. V. Tomy, S. Basu, A. M. Awasthi, P. Rajak, S. Bhattacharyya, S. Ramakrishnan and D. Pal, *Phys. Rev. B*, vol. 91, 2015, Art. no. 205131.

[4] S. Ramakrishnan, A. Schonleber, T. Rekis, N. van Well, L. Noohinejad, S. van Smaalen, M. Tolkiehn, C. Paulmann, B. Bag, A. Thamizhavel, D. Pal and S. Ramakrishnan, *Phys. Rev. B*, vol. 101, 2020, Art. no. 060101(R).

[5] M. H. Lee, C. H. Chen, M. -W. Chu, C. S. Lue and Y. K. Kuo, *Phys. Rev. B*, vol. 83, 2011, Art. no. 155121.

Electron diffraction and electron microscopy

Three-dimensional electron diffraction for structure and property analysis of metal-organic framework nanocrystals

Z. Huang[1]

[1] Stockholm University, Stockholm, Sweden

Metal-organic frameworks (MOFs) or porous coordination polymers (PCPs) are known for their versatile combination of inorganic building units and organic linkers, which offers immerse opportunities in a wide range of applications. Such applications are often designed by considering the inherent properties of MOFs, which in turn are governed by the crystal structures. Therefore, development of new structural characterization techniques parallels discovery of new materials.

Although single crystal X-ray diffraction (SCXRD) is the most practiced and routine method for structure determination, the acquisition of adequate data quality from weakly scattering nano- and submicro-sized crystals remains a challenge for this technique. While powder X-ray diffraction (PXRD) is more suitable technique for handling small crystals, structure determination of MOFs in particular can be challenging due to severe peak overlap as a consequence of large unit cell parameters, complexity of the structures themselves, as well as phase mixtures.

Three-dimensional electron diffraction (3DED) techniques have shown to be powerful for structural determination of 'intractable' crystals that are too small for SCXRD analysis. These techniques benefit from the strong Coulomb interaction between electrons and matter. Compared to X-ray, electrons generate much higher signal-to-noise ratios, even when the volume of the crystals are 6 or 7 orders of magnitude smaller. I will discuss applying 3DED in revealing the unique properties of MOFs for photo- and electrocatalysis. I will first present it on investigating heteroatom distribution in a photoactive MOF1. Further example will be given by applying 3DED on the study of the electrocatalyst PCN-226, where the spacing between active-sites are found crucial for its activity2. Last, I will demonstrate

3DED as a high throughput single crystal approach that can accelerate the discovery of new materials, especially in a phase mixture of nanocrystals, which makes the structure determination inaccessible to other characterization techniques. I believe 3DED as a significant development for the community of MOFs, where it allows to obtain accurate atomic information from nanocrystals, and can thus avoid the slow and arduous process of crystal growth.

References

[1] Yuan, S.; Qin, J.-S.; Xu, H.-Q.; Su, J.; Rossi, D.; Chen, Y.; Zhang, L.; Lollar, C.; Wang, Q.; Jiang, H.-L.; Son, D. H.; Xu, H.; Huang, Z.; Zou, X.; Zhou, H.-C. ACS Cent. Sci. 2018, 4 (1), 105–111.

[2] Cichocka, M. O.; Liang, Z.; Feng, D.; Back, S.; Siahrostami, S.; Wang, X.; Samperisi, L.; Sun, Y.; Xu, H.; Hedin, N.; Zheng, H.; Zou, X.; Zhou, H.-C.; Huang, Z. J. Am. Chem. Soc. 2020, 142, 15386-15395.

Exomorphism of jacobsite precipitates in bixbyite single crystals from the Thomas Range in Utah

J. Peter[1], M. Trapp[1], S. Lauterbach[1], P. Gollé-Leidreiter[1], U. Kolb[2], H.-J. Kleebe[1]

[1] Technical University of Darmstadt, Institute of Applied Geosciences, Working Group: Geomaterialscience, Schnittspahnstr. 9, 64287 Darmstadt, Germany

[2] Johannes Gutenberg University Mainz, Institute of Physical Chemistry, Centre for High Resolution Electron Microscopy (EMC-M), Duesbergweg 10-14, 55128 Mainz, Germany

Naturally occurring single crystals of bixbyite, (Fe,Mn)2O3, from the Thomas Mountain Range in Utah, USA were studied via (scanning) transmission electron microscopy (S)TEM. With up to 5 cm edge length, these mineral specimens are the largest bixbyite crystals found worldwide. Their hexahedral shapes are often modified by 211 facets at the corners and small 211 truncations along their cube edges. Characteristic lamellar defects running parallel to the 100 planes can be observed via TEM imaging, which are, according to EDS analyses, attributed to the tetragonal manganese silicate braunite, Mn7[SiO12]. In the present study, electron nano-diffraction and atomic resolution (S)TEM were employed to verify the presence of braunite lamellae and to investigate their orientation relationship with bixbyite. The analysis confirmed an epitaxial intergrowth of both phases, with their main axes being parallel and the unique c axis of braunite always aligned perpendicularly to the lamellar plane. Moreover, small rectangular shaped precipitates, which had been, due to their almost identical chemical composition, previously interpreted as small bixbyite inclusions within the host crystal, were often observed in contact with the braunite lamellae. Electron nano-diffraction and atomic resolution (S)TEM imaging revealed these crystallites not to be bixbyite but jacobsite, a cubic iron-manganese spinel with the stoichiometric formula MnFe2O4, whose occurrence in this unique context had not been reported before. Moreover, due to the higher temperatures needed for spinel crystallization, the occurrence of jacobsite may serve as a geo-thermometer. (S)TEM in conjunction with automated crystal orientation mapping (ACOM)-TEM showed that no orientation relationship exists between the jacobsite inclusions and the bixbyite/braunite matrix. Nevertheless, their characteristic rectangular shape is typically aligned concordantly with the (001) plane of the braunite lamellae. The resulting crystal shape of jacobsite is determined by the presence of the braunite lamellae, while the respective crystallites maintain their freedom of rotation. To the authors' knowledge, this is a novel observation of exomorphosis of jacobsite, i.e. the change in habitus of the spinel crystallites due to external conditions. Note that the term exomorphosis is used here in the mineralogical sense in contrast to the often used petrological aspect. Based on the TEM results, the formation of the jacobsite precipitates is discussed and a growth model suggested.

Electron diffraction and nanocrystallography: A device dedicated to the crystallography community

G. Santiso-Quinones[1], G. Steinfeld[1], E. Hovestreydt[1]

[1] Eldico Scientific AG, Villigen, Switzerland

After the Science nomination for "Breakthrough of the year 2018"[1,2], 3D-Electron Diffraction (3D-ED) using the continuous rotation method and X-ray crystallographic software, is gaining a lot of attention. In the past years many achievements using electron diffraction techniques have been made in the fields of organic and inorganic molecules, polymorphism, material sciences, geological sciences, natural products, energetic materials, bio-molecules and many others [2,3]. Such experiments are done in a (modified)-Electron Microscope. Though the realization of such experiments still requires plenty of expertise and efforts and it cannot be applied on daily bases by everyone. Pioneers in the field of Electron Diffraction [4], all agree that a dedicated device for the realization of such experiments would be of great advantage to the crystallographic community. Though such a device doesn't exists (up to now) at all. Therefore, it is a necessity that such a device could be made available for the realization

of this exciting field of nano-crystallography. Here will present a new device which is dedicated exclusively for such purposes. The device, an Electron Diffractometer, is built and optimized for electron diffraction experiments. Furthermore, it uses exclusively the crystallographic approach (continuous rotation method) and crystallographic software. Experimental examples carried out in this device will be showcased too.

References

[1] R. F. Service. "Molecular structures made simple." sciencemag.com.
https://vis.sciencemag.org/breakthrough2018/finalists/#rapid-structure
[2] a) T. Gruene *et al.*, *Angew. Chem. Int. Ed.*, vol. 57, pp. 16313–16317, 2018. b) C. G. Jones *et al.*, *ACS Cent. Sci.*, vol. 4, pp. 1587–1592, 2018.
[3] a) P. Brázda *et al.*, *Science*, vol. 364, pp. 667–669, 2019. **b)** R. Bücker *et al.*, *Nat. Commun.*, vol. 11, p. 996, 2020. c) E. T. Broadhurst *et al.*, *IUCrJ*, vol. 7, pp. 5–9, 2020.
[4] S. Parsons, T. Grüne, M. Gemmi, U. Kolb, among others, private communication.

Energy materials: batteries, photovoltaics, etc.

Solid-solution modelling using first-principles methods: Case studies for $(Cu,Ag)_2ZnSnSe_4$ and (FA,Cs)PbI_3

D. Fritsch[1], S. Schorr[1]
[1] Helmholtz-Zentrum Berlin, Berlin, Germany

Our quest to find new materials to be utilised in technological applications leads us more and more towards solid solutions between different materials. These solid solutions allow for the fine-tuning of desired material properties, but also pose additional problems in experimental characterisation and theoretical modelling. While we're able to deal with fractional occupancies of Wyckoff positions in experimental investigations, this is not the case for theoretical materials modelling based on density functional theory, and we have to resort to additional methods to properly model the structural, electronic, and optical properties of solid solutions.

Here, we're using first-principles calculations based on density functional theory to shed some light into the structure-property relations in the $(Cu,Ag)_2ZnSnSe_4$ and (FA,Cs)PbI_3 solid solutions (FA: formamidinium). While $(Cu,Ag)_2ZnSnSe_4$ only requires the mixing over different Wyckoff positions, in (FA,Cs)PbI_3 we additionally have to account for the rotations of the FA cation. For both systems, in order to simulate the different concentrations within the solid solution, we're employing a supercell approach. All our structure models are geometry optimised employing the recently developed SCAN exchange and correlation functional. In order to obtain more reliable electronic and optical properties, selected optimised structures are subjected to one-shot calculations employing the more accurate hybrid functional HSE06.

Acknowledgement
This work made use of computational resources provided by the North-German Supercomputing Alliance (HLRN).

Tuning the structural and electronic properties of strontium titanite thin films by Ni doping

Z. Jansa[1], P. Šutta[1], F. Alarab[1,2], L. Prušáková[1], B. Leikert[3], R. Claessen[3], C. Richter[2], K. Hricoviny[2], J. Minár[1]
[1] New Technologies Research Centre, University of West Bohemia, Pilsen, Czech Republic
[2] LPMS, CY Cergy Paris Université, Neuville-sur-Oise, France
[3] Physikalisches Institut und Röntgen Center for Complex Materials (RCCM), Universität Würzburg, Germany

We report the fabrication of SrTiO3 thin films doped by Ni and its influence on the electronic structure. The SrTiO3 thin films were deposited by magnetron sputtering which is suitable for mass-production of samples adapted for nanoelectronic applications. The structure of the STO:Ni was investigated by XRD phase analysis. We evaluated the influence of Ni on crystallinity, the size of coherent diffract areas, and micro-stress in the lattice of STO as a function of Ni concentration[1]. The second part of the presentation deals with the study of the electronic band structure of STO films doped with Ni, high-quality ordered pristine and SrTiO3:Nix films with x=0.06 and 0.12 were prepared by pulsed laser deposition. Electronic band structure calculations for the ground state, as well as one-step model photoemission calculations performed by using the Korringa-Kohn-Rostoker Greens's function method, predicted the formation of localized 3d-impurity bands in the bandgap of SrTiO3 close to the valence band maxima. The measured valence bands at the resonance Ni2p excitation and band dispersion are in agreement with theory [2].

References

[1] Z. Jansa, L. Prusakova, F. Alarab, P. Sutta; Structural analysis of Ni-doped SrTiO3: XRD study, AIP Conference Proceedings 2131(1):020022, July 2019

[2] F. Alarab, K. Hricovini, B. Leikert, L. Nicolai, M. Fanciulli, O. Heckmann, Ch. Richter, L. Prušáková, Z. Jansa, P. Šutta, J. Rault, P. Lefevre, M. Muntwiller, R. Claessen, and J. Minár; Photoemission study on pristine and Ni-doped SrTiO3 thin films, Materials Science, arXiv:2011.12684, November 2020

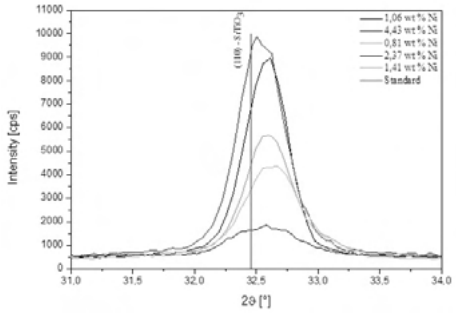

Figure 1

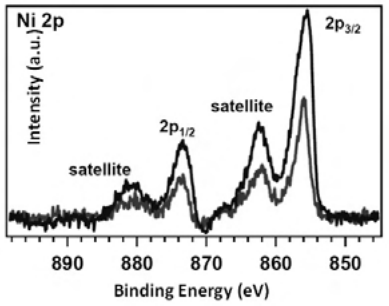

Figure 2

2D layered perovskite micro-crystalline films as efficient X-Ray dosimeters

F. Lédée[1], M. Verdi[1], L. Basiricò[1], C. Andrea[1], B. Fraboni[1]
[1] University of Bologna, Department of Physics and Astronomy (DIFA), Bologna, Italy

Hybrid halide perovskites are a new class of solution-processed semiconductors that combine low-temperature (<100 °C) synthesis, high charge carrier diffusion length and low defect density. The past few years, hybrid halide perovskites such as $CH_3NH_3PbI_3$ have shown promising results for the detection of high-energy ionizing radiation (X- and Gamma-rays).[1] Their large-scale commercialization is however hindered by their poor stability, owing to the volatility of the small organic cation $CH_3NH_3^+$.

2D layered hybrid halide perovskites ($R - NH_3)_2PbX_4$ (R = organic chain, X = Cl^-, Br^-, I^-) have recently shown an increasing interest in the fields of solar cells and LEDs. This sub-class of perovskite crystallizes in a natural, self-assembled quantum well structure and possess several interesting features, among which a much better stability than their 3D counterparts.[2,3] We will present in this work the first solid-state ionizing radiation detector based on a 2D layered hybrid perovskite. This material can be deposited from solution in the form of micro-crystalline thin films that display a single crystalline orientation. We will expose the direct integration of this material onto a pre-patterned flexible substrate and demonstrate the effective detection of X-Rays with sensitivity values as high as 757 uC.Gy-1.cm-2 and a Limit of Detection (LoD) of 8 nGy.s-1, which is among the lowest reported value for solid-state detectors. 2D perovskites offers the prospects of flexible solid-state detectors capable of working at low radiation flux for real-time X-Ray dosimetry.

References

[1] L. Basiricò, S. P. Senanayak, A. Ciavatti, M. Abdi-Jalebi, B. Fraboni and H. Sirringhaus, Adv. Funct. Mater., 2019, 9.
[2] D. B. Mitzi, Journal of the Chemical Society, Dalton Transactions, 2001, 0, 1–12.
[3] J. V. Passarelli, D. J. Fairfield, N. A. Sather, M. P. Hendricks, H. Sai, C. L. Stern and S. I. Stupp, J. Am. Chem. Soc., 2018, 140, 7313–7323.

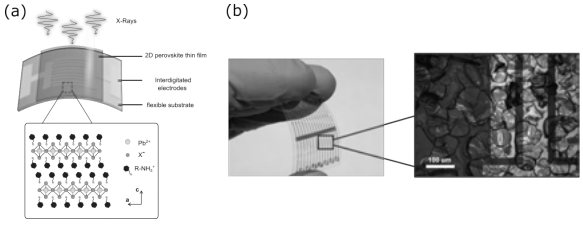

Figure 1 (a) Schematic of the device structure. Bottom: graphical representation of the $(R - NH_3)_2PbX_4$ crystal structure projected along the direction ⟨010⟩ showing the stacking of the 2D layers. (b) Photograph (left) and microscope image (right) showing the crystal grains morphology close to the pixel area.

Oxygen release from nanoporous perovskite oxides and its effect on thermal catalysis applications

S. Mascotto[1], E. Poffe[1], H. Kaper[2], B. Ehrhardt[1], L. Gigli[3], L. Nodari[4], S. Gross[5]
[1] University of Hamburg, Hamburg, Germany
[2] CNRS/Saint-Gobain CREE, Cavaillon, France
[3] Elettra-Sincrotrone, Trieste, Italy
[4] ICMATE-CNR, Padua, Italy
[5] University of Padua, Italy

The oxygen mobility and exchange are fundamental properties of perovskite oxides which regulate their application in catalysis, sensing, energy conversion and information technology [1]. The increasing need of sustainable catalytic materials has driven the development of nanoporous perovskite structures with improved surface reactivity [2,3]. Although it is intuitive that enhanced specific surface area (SSA) might improve the catalytic activity, it is not clear yet how this increase influences oxygen release and mobility in nanostructured grains and what is its effect on catalysis.

In the present paper, we investigate the role of porosity on the oxygen release of mesoporous perovskite oxides and demonstrate how the combination of these two parameters affects methane and carbon monoxide oxidation. We prepared mesoporous SrTi0.65Fe0.35O3-δ perovksites with SSA ranging from 45 to 80 m2/g via a template-free approach [2]. Combining thermal analyses with in situ synchrotron X-ray diffraction under Ar-atmosphere we showed that the material with least porosity does not release surficial oxygen species as the more porous counterparts. Instead much larger desorption of lattice oxygen is observed, as result of the larger lattice strain and higher Fe(IV) concentration.

This had significant effects on the catalytic performance of the materials. For low-temperature reactions as the CO oxidation the highly porous perovskite shows better performance due to the higher SSA and larger surface defect concentration. In case of high temperature reactions as methane combustion, the contribution of lattice oxygen is more relevant and the least porous material achieves the same performance as the high porous systems.

Hence, even though nanoporosity is usually considered beneficial for catalysis applications, mere maximization of the SSA is not necessarily of help and oxygen defect location (surface, bulk) and concentration need to be taken into account for the design of nanostructured catalysts.

References

[1] Y. Cao, M. J. Gadre, A. T. Ngo, S. B. Adler, Dane D. Morgan, *Nat. Commun.*, vol. 10, p. 1346, 2019.

[2] B. Kayaalp, S. Lee, K. Klauke, S. Jongsu, L. Nodari, A. Kornowski, W. Jung, S. Mascotto, *Appl. Catal. B Environ.*, vol. 245, pp. 536–545, 2019.

[3] B. Kayaalp, S. Lee, L. Nodari, J. Seo, S. Kim, W. Jung, S. Mascotto, *ACS Appl. Nano Mater.*, vol. 3, pp. 11352–11362, 2020, doi: 10.1021/acsanm.0c02456.

Study on the anharmonicity of the lead-halide bond and effective pair potentials of chlorine-substituted $CH_3NH_3PbI_3$

G. Schuck[1], D. M. Többens[1], D. Wallacher[1], N. Grimm[1], S. Schorr[1,2]

[1] Helmholtz-Zentrum Berlin für Materialien und Energie, Hahn-Meitner-Platz 1, 14109 Berlin, Germany

[2] Institut für Geologische Wissenschaften, Freie Universität Berlin, Malteserstr. 74, 12249 Berlin, Germany

Research interest has increasingly focused on hybrid perovskites $MABX_3$ like $[CH_3NH_3]^+$ (MA), B = Pb and X = I or Cl as a future photovoltaic material. There is a strong demand to better understand the possible impact of various entropy contributions (stochastic structural fluctuations, anharmonicity and lattice softness) on the optoelectronic properties of halide perovskite materials and devices [1]. There are essentially two sources of dynamic disorder in halide perovskites. One is the motion of the organic cations. FTIR [2] and quasi-elastic neutron scattering (QENS) [2] studies showed that chlorine substitution has a large influence on the rotational dynamics of the MA molecule in $MAPbI_{3-x}Cl_x$ perovskites [3] since the chlorine substitution leads to a weakening of the hydrogen bridge bonds (these bonds connect the MA molecules with the $[PbX_6]^-$ octahedra host structure) [3]. Another source of dynamic disorder is the anharmonic motion of the halide atom. The analysis of the Pb L3-edge EXAFS Debye-Waller factor of chlorine-substituted $MAPbI_3$ allows a direct determination of the influence of chlorine substitution on the anharmonicity of the lead-halide bond. This allows quantitative statements to be made about the effective pair potentials of the bond. The experimentally determined potential parameters can then be compared with computational results obtained, for example, from ab initio molecular dynamics simulations.

References

[1] Katan, C. et al, *Nature Materials*, vol. 17, pp. 377, 2018.

[2] G. Schuck, et. al., *J. Phys. Chem. C*, vol. 122, pp. 5227, 2018.

[3] G. Schuck, et. al., *J. Phys. Chem. C*, vol. 123, pp. 11436, 2019.

A solid-state chemistry approach for bulk $ZnSnN_2$ at ambient pressure

Z. Wang[1,2], J. Breternitz[1], S. Schorr[1,2]

[1] Helmholtz-Zentrum Berlin für Materialien und Energie, Hahn-Meitner-Platz 1, 14109 Berlin, Germany

[2] Free University of Berlin, Department Geosciences, Malteserstraße 74-100, 12249 Berlin, Germany

$ZnSnN_2$ is an earth-abundant semiconductor with a predicted direct bandgap between 1.12-2.09 eV, based on DFT calculations.[1] Thus, it has been considered as a potential absorber material for solar cells. Recently, a numerical device simulation based on reported experimental material properties found a theoretical maximum efficiency of $\eta \approx 22\%$ of for a $ZnSnN_2$ based solar cell.[2]

Still, the fundamental study of structural properties of $ZnSnN_2$ is essential to facilitate the development of high-efficiency solar cells. Well crystallised bulk $ZnSnN_2$ is key to an in-depth study on its material properties, while thin-film $ZnSnN_2$ may hinder advanced studies due to preferred orientation and low crystallinity. However, the narrow stability region of $ZnSnN_2$ due to the small decomposition energy,[3] and the low decomposition temperature of $ZnSnN_2$ [4] hamper the preparation of bulk $ZnSnN_2$.

In this work, we report a convenient pathway to obtain well-crystallised bulk zinc tin oxide nitrides as approximant towards $ZnSnN_2$ at ambient pressure and open the door to investigate structure-property relationships based on bulk samples. We achieved zinc tin oxide nitrides ($Zn_{1+x}Sn_{1-x}N_{2-2x}O_{2x}$) in the form of well-crystallised powder through a solid-state reaction route. This method further allows advanced characterisations that require bulk material and/or well-crystallised samples. We performed XRD experiments and interconnected it with a chemical analysis (XRF) to investigate the chemical composition and structural properties of the synthesised material. Using Raman spectroscopy, we compared the synthesised compound with reported $ZnSnN_2$ thin films.[5] The optical bandgap value of our powder material is in the range of the values reported by thin-film $ZnSnN_2$.[6] By correlating the synthesis conditions with the structural properties of the synthesised $Zn_{1+x}Sn_{1-x}N_{2-2x}O_{2x}$, we are now able to optimise the synthesis route. This will allow us to reduce the oxygen content in the material in a controlled way to obtain bulk $ZnSnN_2$ and tailor the materials properties.

References

[1] N. Feldberg, J. Aldous, W. Linhart, L. Phillips, K. Durose, P. Stampe, R. Kennedy, D. Scanlon, G. Vardar and R. Field III, *Appl. Phys. Lett.*, vol. 103, 2013, Art. no. 042109.

[2] A. Laidouci, A. Aissat and J. Vilcot, *Sol Energy*, vol. 211, pp. 237–243, 2020.

[3] S. Chen, P. Narang, H. A. Atwater and L. W. Wang, *Adv. Mater.*, vol. 26, pp. 311–315, 2014.

[4] F. Kawamura, N. Yamada, M. Imai and T. Taniguchi, *Cryst. Res. Technol.*, vol. 51, pp. 220–224, 2016.

[5] P. C. Quayle, G. T. Junno, K. He, E. W. Blanton, J. Shan and K. Kash, *Phys. Status Solidi B*, vol. 254, 2017, Art. no. 1600718.

[6] T. D. Veal, N. Feldberg, N. F. Quackenbush, W. M. Linhart, D. O. Scanlon, L. F. Piper and S. M. Durbin, *Adv. Energy Mater.*, vol. 5, 2015, Art. no. 1501462.

Extreme/non-ambient conditions

Amorphous–amorphous transition in SnI_4 reexamined

K. Fuchizaki[1]

[1] Ehime University, Matsuyama 790-8577, Japan

The pressure-induced solid-state amorphization found in 1985 [1] set off a series of subsequent researches on polyamorphism in SnI_4. The discovery of another amorphous state [2], called Am-II to Am-I previously identified, on decompression became a breakthrough in solving the puzzle.

Later, a consistent thermodynamic argument has been given for the observed polyamorphic behaviors [3]. However, the following questions remain unanswered: The ambient crystalline phase CP-I never transforms into Am-II, which appears only on Am-I decompression. Nonetheless, CP-I can directly transform to Am-I on *recompression* skipping CP-II [4], the high-pressure modification of CP-I.

We reexamined the Am-I-to-Am-II process conducting high-pressure synchrotron x-ray diffraction studies with a diamond anvil cell [5]. Detailed analysis of the structural evolution revealed that the association of molecules, which are entirely dissociated, starts at around 14 GPa on decompression. About 30% of isolated Sn atoms suddenly complete the molecular formation at the Am-I-to-Am-II transition at 3.3 GPa, associated with an abrupt drop of

density. Thus, the molecules formed recover their original symmetry of T_d at the transition, implying the strong coupling between the global order parameter of density and the local symmetry.

Because the centers (Sn atoms) were distributed everywhere in Am-I, formed molecules' resulting location is not necessarily energetically optimized, leaving uniform distribution of shorter (2.64 Å) van der Waals I_2 bonds, which play as *defects*. The open questions are then understandable in terms of the defects. Crystallization of Am-II to CP-I could be a defect extinction process, but the reverse process would hardly occur. It seems impossible to remove the whole defects in recovering CP-I, and the residual defects prevent defective CP-I from reordering to CP-II, which may require highly ordered stacking of Sn layers [6].

References

[1] Y. Fujii *et al.*, *J. Phys. C*, vol. 18, p. 789, 1985.
[2] N. Hamaya *et al.*, *Phys. Rev. Lett.*, vol. 79, p. 4597, 1997.
[3] K. Fuchizaki *et al.*, *J. Chem. Phys.*, vol. 135, 2011, Art. no. 091101.
[4] B. Grocholski *et al.*, *Phys. Rev. B*, vol. 81, 2010, Art. no. 094101.
[5] K. Fuchizaki *et al.*, *J. Phys.: Condens. Matter*, submitted for publication.
[6] H. Naruta *et al.*, *J. Phys.: Condens. Matter*, vol. 32, 2019, Art. no. 055401.

Probing ultrafast laser plasma processes inside solids with resonant small-angle X-ray scattering

L. Gaus[1]
[1] HZDR, Drezden, Germany

The development of second-generation short-pulse laser-driven radiation sources requires a mature understanding of the relativistic laser-plasma processes such as heating and transport of relativistic electrons as well as the development of plasma instabilities. Accessing these dynamic effects occurring on femtosecond and nanometer scales experimentally is very difficult but it is crucial to understand the behavior of matter under the extreme conditions, which follow the interaction of solids with ultra-intense laser irradiation.

In a first experiment in 2014 at the Matter of Extreme Conditions facility at LCLS we demonstrated that Small Angle X-ray Scattering (SAXS) of femtosecond x-ray free electron laser pulses is able to make these fundamental processes accessible on the relevant time and length scales in direct in-situ pump-probe experiments [Kluge et al., Phys. Rev. X 8, 031068 (2018)]. Here we report on a follow-up experiment with significantly higher pump intensity reaching the relativistic intensity domain, improved targetry, XFEL shaping, and particle diagnostics. We give an overview of the new capabilities in combining a full suite of particle and radiation diagnostics and SAXS. In particular, probing at resonant x-ray energies has shown to give new insight into the ionization process, plasma opacity and density by studying asymmetries in SAXS patterns from nanostructured grating targets [Gaus et al., arXiv: 2012.07922 (under review)].

High Pressure Single-Crystal X-Ray Diffraction Investigation of Nitrosonium Nitrate: Solving a 55 Years Old Enigma

D. Laniel[1], B. Winkler[2], E. Koemets[1], T. Fedotenko[1], S. Chariton[3], V. Milman[4], K. Glazyrin[5], V. Prakapenka[3], L. Dubrovinsky[1], N. Dubrovinskaia[1]
[1] University of Bayreuth, Bayreuth, Germany
[2] Goethe-University Frankfurt, Frankfurt, Germany
[3] University of Chicago, Chicago, USA
[4] Dassault Systèmes BIOVIA
[5] DESY, Photon Science, FS-PE (Experiment Support PETRA III), Hamburg, Germany

The study of the behavior of matter at extreme pressure conditions is essential to deepen our understanding of the pressure dependence of interatomic interactions and to benchmark theoretical models. Simple molecular systems at high densities are well known to exhibit a transformation towards polymeric (*e.g.* N_2,[1,2] CO,[3] CO_2,[4,5] C_2H_2[6]) or metallic (*e.g.* O_2,[7] H_2[8,9]) states as a mechanism to redistribute their electron density. In contrast, nitrogen-oxygen systems (N_2O, N_2O_4, N_2-O_2 mixtures) are hypothesized to instead exploit a third avenue, ionization, and are presumed to form nitrosonium nitrate ($NO^+NO_3^-$).[10,11] Despite its first solid state synthesis in 1965[12] and an impressive number of subsequent in-situ high pressure powder X-ray diffraction studies as well as theoretical calculations,[10,11,13−−19] the crystal structure of nitrosonium nitrate remains controversial.

Here, we present experimental investigations on nitrosonium nitrate between 3 and 55 GPa employing synchrotron single-crystal X-ray diffraction applied to polycrystalline samples (sc-XRDp)—a novel technique developed by our group. Through these measurements, a full structural solution of $NO^+NO_3^-$ was obtained. Its structure is shown in Fig. 1. Chemical peculiarities of this compound were unveiled, namely the striking presence of a positively charged oxygen atom in the NO^+ ion deduced from crystal-chemical principles. Accompanying

theoretical calculations validated the positively charged nature of the oxygen atom in the NO^+ ion and established the experimentally determined structure as the most thermodynamically stable among those previously proposed.

This study unambiguously authenticates the unorthodox preference of nitrogen and oxygen to form an ionic compound to redistribute its pressure-induced increase in electron density. Moreover, it highlights the importance of a high accuracy characterization techniques, such as sc-XRDp, as an essential method that is key to expose the crystal chemical and physico-chemical singularities indigenous to high pressure research.

References

[1] M. I. Eremets, A. G. Gavriliuk, I. A. Trojan, D. A. Dzivenko, R. Boehler, *Nat. Mater.*, vol. 3, pp. 558–563, 2004.

[2] D. Laniel, B. Winkler, T. Fedotenko, A. Pakhomova, S. Chariton, V. Milman, V. Prakapenka, L. Dubrovinsky, N. Dubrovinskaia, *Phys. Rev. Lett.*, vol. 124, 2020, Art. no. 216001.

[3] W. J. Evans, M. J. Lipp, C. S. Yoo, H. Cynn, J. L. Herberg, R. S. Maxwell, M. F. Nicol, *Chem. Mater.*, vol. 18, pp. 2520–2531, 2006.

[4] K. F. Dziubek, M. Ende, D. Scelta, R. Bini, M. Mezouar, G. Garbarino, R. Miletich, *Nat. Commun.*, vol. 9, pp. 5–10, 2018.

[5] F. Datchi, V. M. Giordano, P. Munsch, A. M. Saitta, *Phys. Rev. Lett.*, vol. 103, 2009, Art. No. 185701.

[6] C. C. Trout, J. V. Badding, *J. Phys. Chem. A*, vol. 104, pp. 8142–8145, 2000.

[7] G. Weck, P. Loubeyre, R. LeToullec, *Phys. Rev. Lett.*, vol. 88, 2002, Art. no. 035504.

[8] P. Loubeyre, F. Occelli, P. Dumas, *Nature*, vol. 577, pp. 631–635, 2020.

[9] E. Wigner, H. B. Huntington, *J. Chem. Phys.*, vol. 3, pp. 764–770, 1935.

[10] M. Somayazulu, A. Madduri, A. F. Goncharov, O. Tschauner, P. F. McMillan, H. Mao, R. J. Hemley, *Phys. Rev. Lett.*, vol. 87, 2001, Art. no. 135504.

[11] S. F. Agnew, B. I. Swanson, L. H. Jones, R. L. Mills, D. Schiferl, *J. Phys. Chem.*, vol. 87, pp. 5065–5068, 1983.

[12] L. Parts, J. T. Miller, *J. Chem. Phys.*, vol. 43, pp. 136–139, 1965.

[13] S. F. Agnew, B. I. Swanson, L. H. Jones, R. L. Mills, *J. Phys. Chem.*, vol. 89, pp. 1678–1682, 1985.

[14] Y. Meng, R. B. Von Dreele, B. H. Toby, P. Chow, M. Y. Hu, G. Shen, H. K. Mao, *Phys. Rev. B - Condens. Matter Mater. Phys.*, vol. 74, 2006, Art. no. 214107.

[15] C. S. Yoo, V. Iota, H. Cynn, M. Nicol, J. H. Park, T. Le Bihan, M. Mezouar, *J. Phys. Chem. B*, vol. 107, pp. 5922–5925, 2003.

[16] A. Y. Kuznetsov, L. Dubrovinsky, A. Kurnosov, M. M. Lucchese, W. Crichton, C. A. Achete, *Adv. Phys. Chem.*, vol. 2009, pp. 1–11, 2008.

[17] Y. Song, M. Somayazulu, H. Mao, R. J. Hemley, D. R. Herschbach, *J. Chem. Phys.*, vol. 118, pp. 8350–8356, 2003.

[18] Y. Song, R. J. Hemley, Z. Liu, M. Somayazulu, H. Mao, D. R. Herschbach, *J. Chem. Phys.*, vol. 119, pp. 2232–2240, 2003.

[19] D. Sihachakr, P. Loubeyre, *Phys. Rev. B*, vol. 74, 2006, Art. no. 064113.

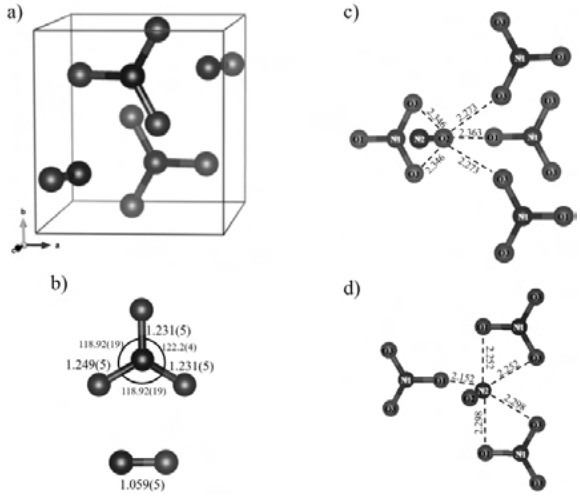

Figure 1 a) Monoclinic unit cell of $NO^+NO_3^-$ at 37 GPa. b) Representation of the trigonal planar nitrate (top) and linear nitrosonium (bottom) ions. c-d) Environment of the O2 and N2 atoms forming the NO^+ cation: both N2 and O2 atoms are five-fold coordinated by negatively-charged oxygen atoms from the $NO^+NO_3^-$ anions. When shown, bond lengths and bond angles are given in Angstroms (Å) and degrees (°), respectively.

Dedicated X-ray diffraction setup for diamond anvil cell studies at European X-ray free electron laser

C. Prescher[1], H.-P. Liermann[2], Z. Konopkova[3], K. Appel[3], R. Husband[4], J. Mainberger[5], H. Damker[6], P. Talkovski[6], M. Röper[4], A. Berghäuser[7], C. Strohm[5], C. Baehtz[7], U. Zastrau[3], . EuXFEL Community Proposal #2292

[1] Universität Freiburg, Freiberg, Germany

[2] DESY, FS-PE (Experimentebetreuung PETRA III), Hamburg, Germany

[3] European XFEL, HED, Schenefeld, Germany

[4] DESY-HiBEF, Hamburg, Germany

[5] DESY, Hamburg, Germany

[6] DESY-ZM1, Hamburg, Germany

[7] Helmholtz-Zentrum Dresden-Rossendorf, Germany

Scientific advances are often enabled by either new emerging techniques or a previously unconsidered combination of existing methods. Particularly synchrotron X-ray diffraction (XRD) has led to large advances in our understanding of materials under high pressure and temperature conditions. Especially its combination with diamond anvil cells (DAC) has been very fruitful and, therefore, almost every 3rd generation synchrotron source in the world has now one or several beamlines dedicated to high pressure DAC research.

On the other hand, in the regime of X-ray free-electron lasers (XFEL), which provide previously unprecedented brightness in a single X-ray pulse, high-pressure and temperature XRD experiments as of today are mainly conducted with a combination of laser driven shock. The absence of DAC research at these facilities is mainly due to a combination of two factors: either the XFEL sources provide only a relatively low photon energy (<11 keV) leading to strong absorption of the X-rays in the diamond anvils as well as a small angular XRD coverage; or if the pulse energy is high enough (e.g. SACLA up to 25 keV on the fundamental) repetition rate on the order of only 10 to 120 Hz is not fast enough to provide significant advantage over 3rd generation synchrotron sources for time-resolved studies, such as the dynamic piezo-driven DAC.

The European XFEL (EuXFEL) in Schenefeld, Germany, is now capable of providing X-ray photons with energies up to 25 keV and a repetition rate of 4.5 Mhz and thus, facilitates the opportunity of combining DAC-XRD experiments with the unique properties of XFEL radiation sources.

Here we want to present the new DAC setup dedicated to XRD studies at the high energy density (HED) instrument of the EuXFEL. This setup has been provided through the Helmholtz International Beamline for Extreme Fields (HiBEF) user consortium and is situated in the interaction chamber 2 of the HED instrument. Currently, two sample platforms are available in the vacuum chamber: the first is a combination of standard or membrane DACs, for use with time resolved optical spectroscopy as well as pulsed laser heating, and the second provides capabilities and space for dynamic DACs with ultrafast piezo driven compression drivers.

The primary goal of both setups is to utilize the high brightness of the EuXFEL source, which permits good quality XRD images, comparable to several seconds of exposure in a 3rd generation synchrotron, even from a single X-ray pulse. The EuXFEL provides bursts of X-ray pulses within a so-called pulse-train with a frequency of 4.5 MHz, equating to 220 ns between each pulse. In combination with an AGIPD detector currently commissioned at the instrument, images will be collected with 4.5 MHz, facilitating the study of physical phenomena by XRD with a unique time resolution.

In the standard DAC setup, the thermal response due to single laser heating pulses or heating by intense X-ray pulses can be investigated by a combination of spectroradiometric measurements (utilizing a streak camera) and XRD on a submicrosecond timescale without the need of collecting multiple iterations in a pump-probe experiment, as performed previously at 3rd generation synchrotron facilities. The dynamic DAC setup enables the study of materials under fast compression and closes the strain rate gap between these type of experiments at synchrotron facilities and shock compression experiments further.

First experiments utilizing the standard DAC setup have been conducted during a community assisted commissioning beamtime in October 2019 (Proposal number 2292, PI R.S. McWilliams). Many exciting new results have been obtained, but also challenges arising from the nature of an XFEL source have been identified.

We will present the setup, its capabilities and some of the first interesting results in this contribution.

Acknowledgment

The authors are indebted to the HiBEF UC for the provision of instrumentation and Staff that enabled this experiment. We acknowledge European XFEL in Schenefeld, Germany, for provision of X-ray free-electron laser beamtime at Scientific Instrument HED (High Energy Density Science) and would like to thank the staff for their assistance.

The low-dimensional magnetic van der Waals compound FeOCl at extreme conditions: pressure and temperature induced phase transitions and structural evolution

A. M. Schaller[1], M. Bykov[2], E. Bykova[2], K. Glazyrin[3], S. van Smaalen[1]

[1] University of Bayreuth, Laboratory of Crystallography, Bayreuth, Germany

[2] Carnegie Institution for Science, Earth & Planets Laboratory, Washington DC, USA

[3] DESY, Photon Science, FS-PE (Experiment Support PETRA III), Hamburg, Germany

FeOCl features a simple structure built from Fe-O double layers stacked along the c-axis and separated through bi-layers of chlorine; the latter are bonded through weak van der Waals forces. On cooling, an orthorhombic-to-monoclinic lattice distortion occurs at $T_N = 81$ K [1] which removes the geometric frustration of magnetic order of Fe^{3+} moments, as it exists on the orthorhombic lattice [1,2]. This allows antiferromagnetic order to develop [1,2]. The quasi-two-dimensional magnetic character of FeOCl stems from the unpaired 3d electrons (Fe^{3+} with $3d^5$ electronic state), which results in strong intra- and interchain exchange interactions in the ab-plane of the structure [2,3]. (Quasi-)hydrostatic pressure, applied within a diamond anvil cell (DAC) up to ≈ 38 GPa, provides a way of modifying the interlayer van der Waals gap and more importantly, through geometrical modifications of the $FeCl_2O_4$ octahedra, a way to modify and tune the magnetic exchange interactions. These experiments have been carried out above and below the Néel temperature, which allows us to investigate the interplay of magnetic order and pressure-induced structural changes in FeOCl. Here we present one of the essential steps in this project: a detailed analysis of the pressure and temperature dependent structural evolution of FeOCl, as investigated by high-pressure low-temperature single crystal X-ray diffraction at beamline P02.2/PETRA III (Hamburg, Germany). This includes the phase transitions and an in-depth analysis of bond lengths and -angles, which sheds light on the magneto-elastic interplay in this compound. This may further contribute to the understanding of the mechanisms in exotic strongly correlated systems in general and low dimensional magnetic compounds in particular.

References

[1] Zhang *et al.*, *Phys. Rev. B*, vol. 86, no. 13, Oct. 2012, Art. no. 134428.

[2] Angelkort *et al.*, *Phys. Rev. B*, vol. 80, no. 14, Oct. 2009, Art. no. 144416.

[3] Glawion *et al.*., *Phys. Rev. B*, vol. 80, no. 15, Oct. 2009, Art. no. 155119.

Experimental Charge Densities of Minerals under Pressure

K. Wozniak[1]

[1] University of Warsaw, Warsaw, Poland

This is quite a paradox that a century after introduction of the spherical Independent Atom Model (IAM, 1914 [1]), 99.7% of all ca. 1.5mln known crystal structures, including almost all structures of minerals, have been refined using IAM which suffers from severe methodological deficiencies. Far better results can be obtained when new approaches of quantum crystallography ustilising aspherical atomic factors are applied.

A short beam wavelength (0.4Å) and a special type of Diamond Anvil Cell (DAC) with large opening angle allow us to collect data with extremaly high resolution and 100% completeness up to as high resolution as ca. 0.4 Å.

We will present details of aspherical Hansen-Coppens pseudoatom refinement of electron density which we applied in multipole modeling [2] of electron density in crystals of minerals including minerals under pressure. We have successfully refined quantitative experimental electron densities for crystals of several minerals such as fluorite, grossular and hsianghualite and others. We will present the most interesting results such as onset of F...F interactions (charge-shift bonding) in fluorite [3] and flow of charge among ions in the structure of hsianghualite, Ca3Li2(Be3Si3O12)F2, under pressure. Up to our best knowledge, these are the very first successful experimental determinations of quantitative charge density distributions in mineral crystals under high pressure. They allow for quantitative characterisation of electron density in crystals of minerals including studies of changes of electron density under pressure.

Such studies open a new field of mineralogical subatomic investigations (at the level of changes of electron density properties) of different mineralogical processes in the Earth mantle by simulating them in DAC in laboratory conditions.

Acknowledgement

KW acknowledges a financial support within the Polish National Science Centre (NCN) OPUS17 grant number DEC-2019/33/ B/ST10/02671.

References

[1] Compton, A.H., *Nature.*, vol. 95, pp. 343–344, 1915.

[2] Hansen, N. K., & Coppens, P., *Acta Cryst. A*, vol. 34, pp. 909–921, 1978.

[3] Stachowicz, M., Malinska, M., Parafiniuk, J., &Woźniak, K., *Acta Cryst. B*, vol. 73, pp. 643–653, 2017.

[4] Gajda, R., Stachowicz, M., Makal, A., Sutuła, S., Parafiniuk, J., Fertey, P., & Wozniak, K., *IUCRJ*, vol. 7, no. 3, pp. 383–392, 2020.

Framework structures: MOFs, COFs, etc.

High-Throughput Electron Diffraction Reveals a Hidden Novel Metal-Organic Framework

M. Ge[1], X. Zou[1], Z. Huang[1]

[1] Stockholm University, Stockholm, Sweden

Metal-organic frameworks (MOFs) are known for their versatile combination of inorganic building units and organic linkers, which offers immense opportunities in a wide range of applications. However, many MOFs are typically synthesized as multiphasic polycrystalline powders, which are challenging for studies by X-ray diffraction. Therefore, developing new structural characterization techniques is highly desired in order to accelerate discoveries of new materials. Here, we report a high-throughput approach for structural analysis of MOF nano- and sub-microcrystals by three-dimensional electron diffraction (3DED). A new zeolitic-imidazolate framework (ZIF), denoted ZIF-EC1, was first discovered in a trace amount during the study of a known ZIF-CO3-1 material by 3DED. The structures of both ZIFs were solved and refined using 3DED data. ZIF-EC1 has a dense 3D framework structure, which is built by linking mono- and bi-nuclear Zn clusters and 2-methylimidazolates (mIm-). The discovery of this new MOF highlights the power of 3DED in developing new materials and their applications.

Water cluster structure in the MOF CAU-10-H: A powder diffraction perspective

G. Nenert[1], S. Canossa[2], D. Rega[3], M. van der Veen[3]

[1] Malvern Panalytical, Malvern, United Kingdom

[2] University of Antwerpen, Department of Physics, Groenenborgerlaan 171, 2020 Antwerpen, Belgium

[3] TU Delft, Catalysis Engineering, Department of Chemical Engineering, Delft, the Netherlands

Several metal-organic frameworks (MOF) excel in harvesting water from the air or as heat pumps as they show a steep step in the water isotherm at 10-30 RH%c [1]. Yet, a precise understanding of the water structure within the confined space of such MOF is still lacking. Here, we unravel the structural properties of CAU-10-H under various water content. We show that the water content can be tuned using the relative humidity, temperature and history of the sample. Previous studies have shown a structural phase transition from hydrated (non-centrosymmetric structure) to dry (centrosymmetric structure) [2]. Here in this contribution, we show that high resolution powder diffraction can allow to locate water molecules and the existence of various states of hydrated phases including centrosymmetric one.

This study besides bringing further insight into the water clusters present in this MOF enlights also the powerfulness of powder diffraction in the study of MOF materials.

References

[1] Wentao Xu, Omar M. Yaghi, *ACS Cent. Sci.*, vol. 6, no. 8, pp. 1348–1354, 2020.

[2] Dominik Fröhlich *et al.*, *J. Mater. Chem. A*, vol. 4, pp. 11859–11869, 2016.

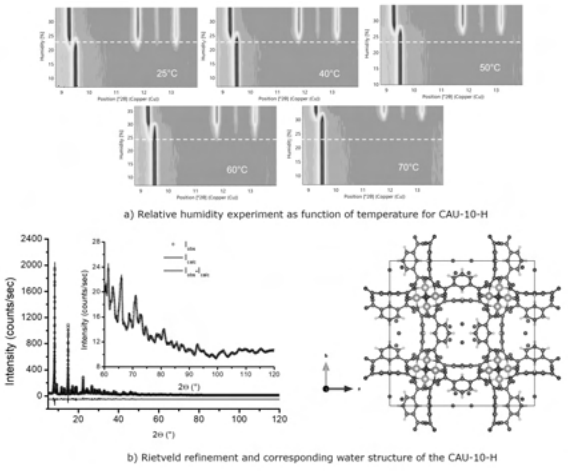

Figure 1

Discontinuous three-component self-assembly: A leap from simple polymers to 3D networks of spherical host-guest assemblies

E. Peresypkina[1], K. Grill[1], B. Hiltl[1], A. Virovets[1], M. Scheer[1]
[1] University of Regensburg, Regensburg, Germany

In the artificial self-assembling systems based on metal atoms and spacing ligands small variations of reagents, stoichiometry, solvents or concentration may cause drastic changes in the structure of the resulting supramolecular architectures [1,2]. Methodologically based rational supramolecular design requires the systematic study of the effects of variation of one of the parameters when other controllable synthetic conditions are kept as close as possible.

Having experience in using pentaphosphaferrocenes [CpRFe(η5-P5)] (CpR = η5-C5R5, R = Me, CH2Ph) as building blocks to construct coordination polymers and giant supramolecules via coordination of the cyclo-P5 ligand to coinage metal cations [3,4], we systematically investigated how the direction of one-pot self-assembly reaction of [Cp*Fe(η5-P5)] (A) with AgSbF6 and flexible aliphatic dinitriles NC(CH2)xCN (DNx) [5] depends on the length of the aliphatic chains in a range x = 1 – 10. We found that this reaction can lead to two distinct types of the products, namely, 1D–3D simple coordination polymers (CPs), or 3D supramolecular coordination polymers (SCPs), where huge polycationic nano-sized supramolecules are linked by the DNx spacers into 3D networks (Fig.). The value of x = 7 marks the borderline: for x < 7 the self-assembly leads to various 1D–3D CPs, while at x = 7 the system discontinuously switches to 3D SCP (SbF6)@[(A)9Ag11(DN7)6](SbF6)10 with huge, supramolecules of ø2.21 nm in size as nodes. For x = 8 – 10 the self-assembly leads to 3D SCPs (A)@[(A)12Ag12(DNx)6](SbF6)12 with spherical cationic supramolecules of 2.40 – 2.44 nm in size acting as nodes. The SCPs specifically encapsulate guests, SbF6- anion or A, inside the nodes, while the voids between the nodes in the 3D network are filled with solvent molecules and SbF6- counterions. All products are characterized by NMR spectroscopy, MS spectrometry and single-crystal X-ray diffraction at 10-90 K.

The research was partly performed at P11 and P24 beamlines on PETRA III at DESY. This work was supported by the German Research Foundation (DFG) within the project Sche 384/44-1.

References

[1] T. Schnitzer, G. Vantomme, *ACS Cent. Sci.*, vol. 6, p. 2060, 2020.
[2] Y. Sun, C. Chen, P. J. Stang, *Acc. Chem. Res.*, vol. 52, p. 802, 2019.
[3] E. Peresypkina, C. Heindl, A. Virovets, M. Scheer, *Structure and Bonding*, vol. 174, p. 321, 2016.
[4] J. Schiller, A. V. Virovets, E. Peresypkina, M. Scheer, *Angew. Chem. Int. Ed.*, vol. 59, p. 13647, 2020.
[5] E. Peresypkina, M. Bielmeier, A. Virovets, M. Scheer, *Chem. Sci.*, vol. 11, pp. 9067–9071, 2020.

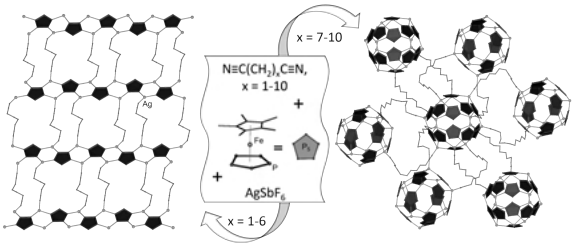

Figure 1

Tracking nerve-agent simulant decomposition in UiO-67 using in situ total scattering pair distribution function analysis

M. Terban[1], S. Ghose[2], A. Plonka[3], D. Troya[4], P. Juhás[5], R. Dinnebier[1], J. Mahle[6], W. Gordon[6], A. Frenkel[3,7]
[1] Max Planck Institute for Solid State Research, Heisenbergstr. 1, 70569 Stuttgart, Germany
[2] Brookhaven National Laboratory, National Synchrotron Light Source II, Upton, New York, NY 11973, USA
[3] Stony Brook University, Department of Materials Science and Chemical Engineering, Stony Brook, New York, NY 11794, USA
[4] Virginia Tech, Department of Chemistry, Blacksburg, VA 24061, USA
[5] Brookhaven National Laboratory, Computational Science Initiative, Upton, New York, NY 11973, USA
[6] Aberdeen Proving Ground, U.S. Army Combat Capabilities Development Command Chemical Biological Center, Aberdeen, Maryland, MD 21010, USA
[7] Brookhaven National Laboratory, Chemistry Division, Upton, New York, NY 11973, USA

The ability to selectively take up and store gases is one of the promising properties of metal–organic frameworks (MOFs) already implemented for industrial applications. Judicious choice of secondary building units can allow for further catalyzing reactions with stored content; for example, much research is currently pursuing their use for fil-

tration of chemical warfare agents. Recently, the Zr-based MOF UiO-67 was shown to effectively adsorb and decompose the nerve-agent simulant, dimethyl methylphosphonate (DMMP).

Various methods are available for probing the gas sorption and reaction pathway, but quantitative structural information on the localized binding is difficult to obtain. A better understanding of the binding behavior is necessary to improve the performance of these MOFs for chemical agent neutralization. Here, we demonstrate the quantitative tracking of both framework and binding component structures using in situ X-ray total scattering measurements of UiO-67 under DMMP exposure, pair distribution function analysis, and theoretical calculations. The adsorption and desorption of DMMP within the pores, association with linker-deficient Zr6 cores, and decomposition to irreversibly bound methyl methylphosphonate were directly observed and analyzed with atomic resolution.

Going forward, wider access to powerful synchrotron beamlines and robust in situ capabilities will allow for comprehensive investigations into the structural implications of the full processing procedure from activation to adsorption, reaction, and re-activation. The procedures developed in this study could help guide further investigations into processes in other MOF/functional systems.

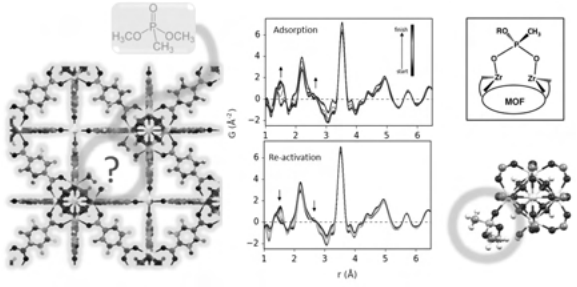

Figure 1

Inorganic crystal structures

High-pressure synthesis of novel yttrium nitride, Y5N14, at 50 GPa

A. Aslandukov[1], A. Aslandukova[1], D. Laniel[1], T. Fedotenko[1], L. Yuan[2], G. Steinle-Neumann[2], K. Glazyrin[3], L. Dubrovinsky[2], N. Dubrovinskaia[1]

[1] University of Bayreuth, Bayreuth, Germany

[2] University of Bayreuth, Bayerisches Geoinstitut, Bayreuth, Germany

[3] DESY, Photon Science, FS-PE (PETRA III Experiment Support), Hamburg, Germany

Homonuclear dinitrogen anions are common intermediates in biological and organometallic synthetic chemistry, and play an important role in the processes of nitrogen reduction to ammonia. In extended solid-state compounds, nitrogen is typically present in the form of a nitride anion N3- and does not form catenated polyanions. However at high-pressure conditions MN2 dinitride compounds of alkali-earth metals (M = Ca, Sr, Ba), transition metals (M=Ti, Cr, Fe, Co, Ni, Cu, Ru, Rh, Pd, Re, Os, Ir, Pt) and rare earth metal (M = La) were obtained. In MN2 compounds, metals usually possess their common oxidation states, while the dinitrogen anion formally accommodates from 1 to 4 electrons. The degree of charge transfer from the metal to the nitrogen dimers significantly affects the properties of the materials (e.g. MN2 (M = Pt, Ir, Os, Ti) pernitrides with [N2]4- units are much less compressible than MN2 (M = Cr, Fe, Co, Ni, Ru, Rh) with [N2]3- units). In this study yttrium and molecular nitrogen were compressed to 50 GPa and laser heated above 2000 K. Under these conditions, synchrotron single-crystal X-ray diffraction from multigrain samples revealed the formation of a new tetragonal yttrium nitride phase with the unusual Y5N14 composition (Fig. 1a). All nitrogen atoms form dimers, but strikingly there are three different types of nitrogen dimers in the structure with 1.24 Å, 1.28 Å and 1.36 Å nitrogen-nitrogen bond length (Fig. 1b). The bond length correlates with the multiplicity of the nitrogen-nitrogen bond and charge state of the nitrogen dimers. Our detailed analysis shows that there are six [N=N]2- dimers and one [N- N]3- dimer per Y5N14 formula unit, which corresponds to the typical Y3+ oxidation state for all yttrium atoms. Ab-initio calculations confirm that this structure is dynamically stable at such pressure. Although [N2]2- and [N2]3- ions are known in the structures of other dinitrides, Y5N14 is the first example of the presence of two different types

of charged nitrogen dimers in the same structure, which indicates more complex chemical processes of dense dinitrides formation under high pressure.

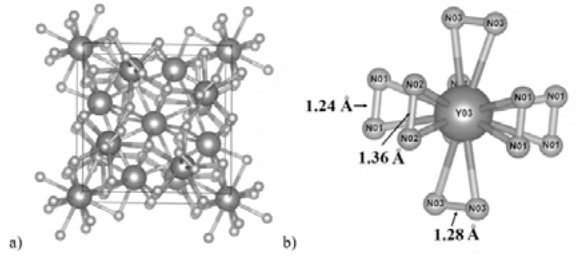

Figure 1 a) Structure of the novel Y5N14 phase and b) different dinitrogen anions in the Y03 atom coordination environment.

Novel high-pressure yttrium carbide, HP-Y4C5.

A. Aslandukova[1], L. Yuan[1], D. Laniel[1], A. Aslandukov[1], S. Khandarkhaeva[2], T. Fedotenko[1], G. Steinle-Neumann[3], N. Dubrovinskaia[1], L. Dubrovinsky[3], K. Glazyrin[4]

[1] University of Bayreuth, Bayreuth, Germany

[2] DESY, Photon Science, FS-PS (FS-Photon Science), Hamburg, Germany

[3] University of Bayreuth, Bayerisches Geoinstitut, Bayreuth, Germany

[4] DESY, Photon Science, FS-PE (PETRA III Experiment Support), Hamburg, Germany

Transition-metal carbides exhibit high melting points, high hardness, and metallic conductivity that make these materials attractive candidates for different technological applications and for material science studies. Carbon has the capability of forming various bonding states affecting the structures and properties of transition metal carbides. High pressure can be used to alter bonding patterns, leading to new compounds with unusual bonding states and properties. The yttrium carbide family shows a large variety of possible phases at ambient pressure with different stoichiometry (e.g., Y2C, Y4C5, Y3C4, Y2C3, Y4C7, YC2). Here, we report results on the synthesis and characterization of a previously unknown high-pressure yttrium carbide, HP-Y4C5, which displays very unusual crystal chemistry. The HP-Y4C5 phase was synthesized by the chemical reaction of pure metallic yttrium and paraffin oil at P 44 GPa and T 1500 K in a laser-heated diamond anvil cell, and was characterized by synchrotron single-crystal X-ray diffraction and Raman spectroscopy. On decompression, diffraction lines of HP-Y4C5 were traced down to at least 16(2) GPa, and the characteristic Raman modes of the phase were observed to 2 GPa. The HP-Y4C5 phase crystallizes in the orthorhombic system (space group Cmce, Z = 16) with the unit cell parameters a = 12.1834(8) Å, b = 7.6592(4) Å and c = 8.8584(11) Å at 44 GPa (Fig. 1). Notable structural elements of HP-Y4C5 are [C2] dumbbells and [C3] trimers. While the first coordination sphere Y-C distances (2.24-2.69 Å) are typical for yttrium carbides, the C-C distances in the [C2] dimers (1.40(2) Å) and the [C3] trimers (1.43(1) Å) are unusual: they are significantly larger than expected for double-bonded carbon atoms (1.33 Å) and much shorter than for single-bonded (1.54 Å). Phonon dispersion calculations show that HP-Y4C5 is dynamically stable at 44 GPa. The electron localization function (ELF) demonstrates strong covalent bonding between carbon atoms within the carbon dumbbells and trimers, and covalent bonds between Y and C. According to our analysis of the charge distribution in the ionic approximation, the HP-Y4C5 phase contains the anions [C2]5- and [C3]6-, with a bond order of 1.5 in both cases. The calculated electronic density of states shows that yttrium carbide HP-Y4C5 is metallic and that the main contribution at the Fermi level comes from Y 4d and C 2p states.

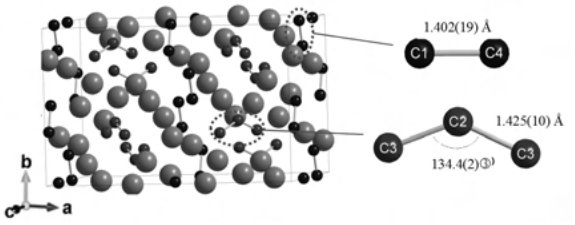

Figure 1 Crystal structure of Y4C5 at 44 GPa. The grey, blue and red spheres represent yttrium and carbon atoms in dimers and trimers, respectively. The [C2]5- and [C3]6- species with their bond lengths and angles are indicated on the right side.

Charge density wave order in Pr2Ru3Ge5

J.-K. Bao[1], Y. Li[2], S. Ramakrishnan[1], S. R. Kotla[1], C. Eisele[1], D. Y. Chung[3], C. Paulmann[4], L. Noohinejad[4], M. Tolkiehn[4], Z.-A. Xu[2], M. Kanatzidis[5], S. van Smaalen[1]

[1] University of Bayreuth, Laboratory of Crystallography, Bayreuth, Germany

[2] Zhejiang University, Department of Physics, Zhejiang Province Key Laboratory of Quantum Technology and Device, Hangzhou, China

[3] Argonne National Laboratory, Materials Science Division, Lemont, IL 60439, USA

[4] DESY, Notkestr. 85, 22607, Hamburg, Germany

[5] Northwestern University, Evanston, IL 60208, USA

The charge density wave (CDW) is a collective phenomenon where electrons at the Fermi level form a density wave with an additional periodicity as compared to the atomic lattice. $RE_2Ru_3Ge_5$ (RE = Pr, Sm, Dy) crystallize in the $Sc_2Fe_3Si_5$-type structure (space group $P4/nmc$). They show peculiar CDW-induced lattice modulations in a certain temperature range below which those modulations disappear.[1] Compared to $Sm_2Ru_3Ge_5$, $Pr_2Ru_3Ge_5$ has a higher transition temperature and no detailed structure refinements have been reported for the modulated phase for this compound. In this presentation, we will show that $Pr_2Ru_3Ge_5$ exhibits phase transitions at around 200 K from specific heat and transport property measurements. Satellite peaks have been observed in x-ray diffraction with a modulation wave vector q = (0.18,±0.18, 0). Unanticipatedly, satellite peaks disappear below 180 K. The modulated crystal structure of the CDW phase of $Pr_2Ru_3Ge_5$ will be presented on the basis of the superspace method.

References

[1] Bugaris, D. E *et al.*, "Charge Density Wave in the New Polymorphs of $RE_2Ru_3Ge_5$ (RE = Pr, Sm, Dy)," *J. Am. Chem. Soc.*, vol. 139, no. 11, pp. 4130–4143, 2017.

Structural investigations of mixed anionic rare-earth and transition metals selenide oxides using synchrotron radiation

D. C. Benndorf[1]

[1] Leipzig University, Leipzig, Germany

The simultaneous reaction of oxygen, its heavier homologs, and metals usually lead to the formation of substances characterized by the presence of covalent O-Ch (Ch = S, Se) bonds within complex anions like sulfates or selenides. Examples for compounds containing both, O^{2-} and Ch^{2-} without any attractive interaction between these species are far less known. Only a few examples for chalcogenide oxides of transition (T) and rare-earth metals (RE) are described in the literature so far, though exhibiting a relatively high variety in composition and crystal structures.

Salt-flux assisted reactions of rare-earth metals and their oxides, transition metals and selenium lead to the discovery of the mixed anionic selenide oxides $RE_2ZrSe_2O_3$ (RE = Ce-Nd, Sm) and $Ce_7TiSe_5O_7$. All these substances appear as thin needle-like crystals with diameters of 5 μm and less which are extraordinarily sensitive to mechanical stress. Consequently, structure determination had to be realized using synchrotron radiation. First investigations of $Ce_7TiSe_5O_7$ were carried out at the ESRF, beamline ID11, using micro-focused synchrotron radiation. Small crystals were pre-selected and pre-characterized using transmission electron microscopy including EDX spectroscopy [1]. The substance crystallizes with the $La_7VSe_5O_7$ structure type [2], space group $Cmcm$, suggesting the presence of Ti^{3+} cations.

The first Zr containing selenide oxides $RE_2ZrSe_2O_3$ (= 2 $RE^{3+}Zr^{4+}2Se^{2-}3O^{2-}$) were investigated at PETRA III, beamline P24, and the ESRF, beamline ID11. The compounds were found to crystallize with their own structure type, space group $C\ 2/m$, characterized by the presence of large cavities extended along [010] formed by Se atoms (see Fig. 1).

References

[1] F. Fahrnbauer, T. Rosenthal, T. Schmutzler, G. Wagner, G. B. M. Vaughan, J. P. Wright, O. Oeckler, *Angew. Chem. Int. Ed.*, vol. 54, pp. 10020–10023, 2015.

[2] S. Peschke, L. Gamperl, V. Weippert, D. Johrendt, *Dalton Trans.*, vol. 46, pp. 6230–6243, 2017.

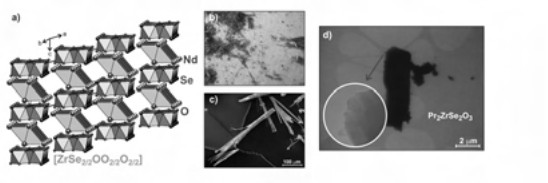

Figure 1 a-c) Crystal structure, bulk material, and SEM-SE image of $Nd_2ZrSe_2O_3$. d) TEM-BF image of the $Pr_2ZrSe_2O_3$ single-crystal investigated at ERSF, beamline ID11. The crystal part used for structure determination is emphasized.

Crystal Structures and Anisotropic Expansion of Coordination Compounds from the Mg(SCN)2 · x H2O/THF System

S. Bette[1], M. Joos[1], M. Conrad[2], R. Merkle[1], T. Schleid[2], J. Maier[1], R. Dinnebier[1]

[1] Max Planck Institute for Solid State Research, Germany

[2] University of Stuttgart, Institute for Inorganic Chemistry, Stuttgart, Germany

Magnesium halides and pseudo-halides are essential compounds for many applications ranging from biochemistry to construction and building materials. These phases exhibit a great variety of chemical and structural properties and hence, were extensively studied. However, in the row of magnesium pseudo-halides, i.e. cyanides, cyanates etc., the thiocyanates were often overseen and are therefore still only poorly characterized.

Mg(SCN)2 · x H2O/THF coordination compounds were synthesized, characterized, their crystal structures solved ab initio from X-ray powder diffraction (XRPD) data and their thermal expansion properties investigated by temperature dependent in situ XRPD.

The recrystallization of Mg(SCN)2 · 4 H2O in THF yields the novel compounds Mg(SCN)2 · 2 (H2O, THF) and α-Mg(SCN)2 · 4 THF. By heating, α-Mg(SCN)2 · 4 THF undergoes a phase transition into β-Mg(SCN)2 · 4 THF that is associated with an increasing disorder of the THF molecules. Finally, two THF molecules are released, which leads to the formation of Mg(SCN)2 · 2 THF. The investigated compounds show a remarkable anisotropic thermal expansion and the growing disorder of THF molecules has a major impact on the expansion properties.

The coordination chemistry of Mg(SCN)2 turned out to be rich and has the potential to go beyond H2O and THF as ligands. An expansion towards other metals like nickel, cobalt or iron appears to be very feasible.

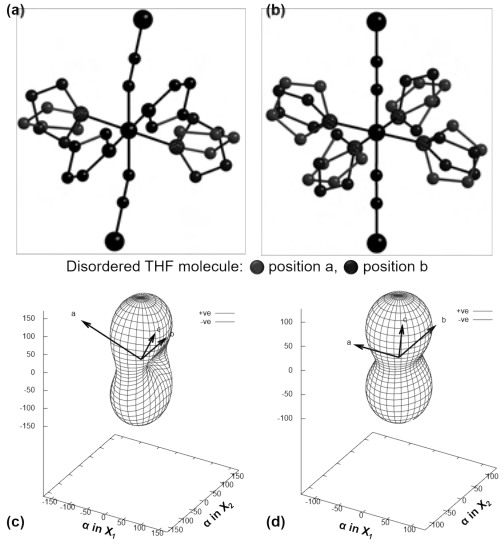

Figure 1 Octahedral coordination of Mg2+ with SCN- and THF for a) α-Mg(SCN)2 · 4 THF; b); β-Mg(SCN)2 · 4 THF, Plots showing the variation of the thermal expansion coefficient α with the principal directions X1, X2 and X3 of c) α-Mg(SCN)2 · 4 THF, d) β-Mg(SCN)2 · 4 THF.

The lanthanoid olxoantimonate(III) bromides $Ln\mathbf{Sb_2O_4Br}$ (Ln = Eu – Tb): Synthesis, crystal structure and luminescence

F. C. Goerigk[1], T. Schleid[1], V. Paterlini[2], A.-V. Mudring[2]

[1] University of Stuttgart, Institute for Inorganic Chemistry, Pfaffenwaldring 55, 70569 Stuttgart, Germany

[2] Stockholm University, Department of Materials and Environmental Chemistry, Arrhenius Laboratory, Stockholm, Sweden

Pale yellow crystals of $Ln\mathrm{Sb_2O_4Br}$ (Ln = Eu – Tb) were synthesized via high temperature solid-state reactions from antimony sesquioxide, the respective lanthanoid sesquioxides and tribromides. Single-crystal X-ray diffraction studies revealed a layered structure in the monoclinic space group $P2_1/c$. In contrast to hitherto reported quaternary lanthanoid(III) halide oxoantimonates(III) [1], in $Ln\mathrm{Sb_2O_4Br}$ the lanthanoid(III) cations are exclusively coordinated by oxygen atoms in the shape of square hemiprisms. These $[Ln\mathrm{O_8}]^{13-}$ polyhedra form layers parallel to the (100) plane by sharing common edges as shown in Figure 1. All antimony(III) cations are coordinated by three oxygen atoms forming ψ^1-tetrahedral $[\mathrm{SbO_3}]^{3-}$ units, which have oxygen atoms in common building up meandering strands along [001] (Figure 2) according to 1D-$[\mathrm{SbO}^{v}_{2/2}\mathrm{O}^{t}_{1/1}]^{-}$– ($v$ = vertex-sharing, t = terminal). The bromide anions are located between two layers of these parallel running oxoantimonate(III) strands and have no bonding contacts with the Ln^{3+} cations. Since Sb^{3+} is known to be an efficient sensitizer for Ln^{3+} emission, photoluminescence studies were carried out to characterize the optical properties and assess their suitability as light phosphors. Indeed, for both, $\mathrm{GdSb_2O_4Br}$ and $\mathrm{TbSb_2O_4Br}$ doped with about 1.0 – 1.5 at-% Eu^{3+} efficient sensitization of the Eu^{3+} emission could be detected. The resulting luminescence properties of both doped and undoped $\mathrm{GdSb_2O_4Br}$ and $\mathrm{TbSb_2O_4Br}$ are summarized in Figure 3. For $\mathrm{TbSb_2O_4Br}$, in addition, a remarkably high energy transfer from Tb^{3+} to Eu^{3+} could be detected that leads to a substantially increased Eu^{3+} emission intensity, rendering it an efficient red light emitting material [2].

References

[1] F. C. Goerigk, Th. Schleid, *Z. Anorg. Allg. Chem.*, vol. 645, pp. 1079–1084, 2019.

[2] F. C. Goerigk, V. Paterlini, K. V. Dorn, A.-V. Mudring, Th. Schleid, *Crystals*, vol. 10, pp. 1089–1111, 2020.

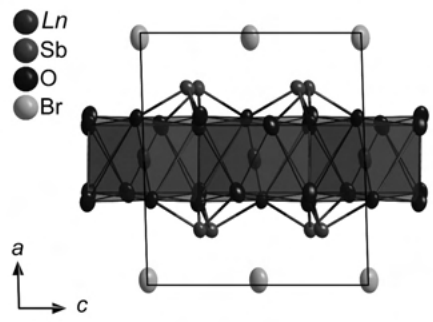

Figure 1 Section of the crystal structure of the $Ln Sb_2O_4Br$ series (*Ln*=Eu-Tb) viewed along [010] emphasizing the unit-cell edges and $[LnO_8]^{13-}$ polyhedra (dark red) utilizing the refined anisotropic displacement parameters with an ellipsoidal probability of 95%.

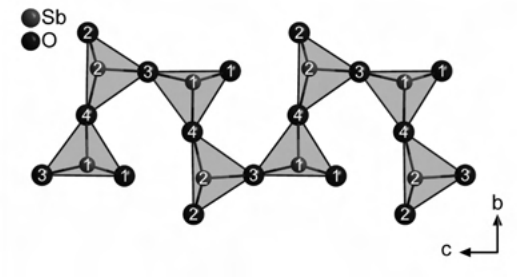

Figure 2 Meandering 1D-$[SbO^{v}_{2/2}O^{t}_{1/1}]^{-}$ chain of vertex-connected $[SbO_3]^{3-}$ ψ^1 - tetrahedra running along [001] in the crystal structure of the $LnSb_2O_4Br$ series (*Ln*=Eu-Tb).

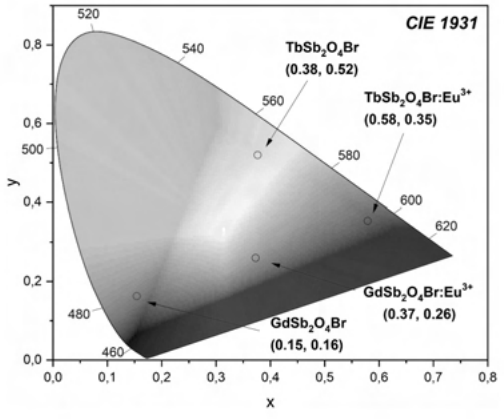

Figure 3 Commission internationale de l'éclairage (CIE) diagram (CIE 1931) for $TbSb_3O_4Br:Eu^{3+}$, $GdSb_3O_4Br$ and $GdSb_3O_4Br:Eu^{3+}$ at λ_{ex} = 257 nm.

A mineral with new loop-branched sechser single chains Khurayyimite Ca7Zn4(Si2O7)2(OH)10·4H2O

B. Krüger[1], I. O. Galuskina[2], E. Galuskin[2], Y. Vapnik[3], M. Murashko[4]

[1] University of Innsbruck, Institute of Mineralogy and Petrography, Innsbruck, Austria

[2] University of Silesia, Faculty of Earth Sciences, Będzińska 60, 41-200 Sosnowiec, Poland

[3] Ben-Gurion University of the Negev, POB 653, Beer-Sheva 84105, Israel

[4] Saint Petersburg State University, Faculty of Geology, 7-9sp Universitetskaya nab., 199034 St Petersburg, Russia

The mineral khurayyimite Caenter code here $Zn_4(Si_2O_7)_2(OH)_{10}·4H_2O$, (IMA 2018-140) was found in small cavities in altered spurrite marbles, in the northern part of the Siwaqa pyrometamorphic rock area, Central Jordan. It is a low-temperature, hydrothermal mineral and it forms at a temperature of ca. 100 °C. It builds nearly 50 μm white or colourless, platy crystals arranged in up to 200-300 μm big spherulitic aggregates.

Single-crystal X-ray diffraction experiments at ambient conditions were performed at the X06DA beamline at the Swiss Light Source (Paul Scherrer Institute, Villigen, Switzerland). Khurayyimite crystallises in space group P21/*c*, with unit cell parameters (a=11.2450(8), b=9.0963(5), c=14.0679(10)Å, β = 113.237(8)°, V = 1322.25(17)Å^3 and Z = 2. The average structure was solved using direct methods. All H-sites are located by difference Fourier analysis. The resulting structure model was refined up to R1= 0.02. The crystal structure of khurayyimite consists of sheets perpendicular to a. Each sheet is built by very unusual loop-branched sechser single chains $\{1B,1^1_\infty\}[^6Zn_4Si_4O_{21}]$. Voids between chains are filled by blocks of five Ca-octahedra and two CaO_7 polyhedra with additional OH groups and water molecules.

The loop-branched *sechser* single chains $\{1B,1^1_\infty\}[^6Zn_4Si_4O_{21}]$ are made of dimers of Si_2O_7 and two types of $ZnO_2(OH)_2$ tetrahedra connected by corners. Loops of the chain contain three tetrahedra, analogous to *dreier* ring. Strong repulsive forces between the tetrahedra in *dreier* ring are pressing connecting O atoms as far as possible forming equilateral triangle with longer ZnO_4 edge (≈ 3.176 Å) and two shorter two SiO_4 edges (≈ 2.67). These repulsive forces are, according to [1], a possible reason for why such loops have not been observed more frequent.

Different combinations of chains and frameworks made of ZnO_4 and SiO_4 tetrahedra are known. In $ZnSiO_3$ [2], with Zn atoms in six and four-fold coordination, two pyroxene-like chains running along the c-direction are branched with two ZnO_4 tetrahedra forming four-membered loops. The crystal structure of the LT and HT forms of $BaZn_2Si_2O_7$ [3] exhibit a disilicate group Si_2O_7 linked via corners with ZnO_4 tetrahedra in a three-dimensional framework. In such a manner are created six member rings ($2\times Si_2O_7$, $2\times ZnO_4$), four member-rings ($2\times SiO_4$, $2\times ZnO_4$) and three-membered rings ($1\times SiO_4$, $2\times ZnO_4$). Still, three-membered loops, made of Si_2O_7 and ZnO_4, like in khurayyimite, have not been observed yet.

References

[1] Libau, F., *Structural Chemistry of Silicates*. Berlin, Heidelberg, Germany: Springer-Verlag Berlin Heidelberg, 1985.

[2] Morimoto, N., Nakajima, Y., Syono, S., Akimoto, S. and Matsui, Y., "Crystal structure of pyroxene-type $ZnSiO_3$ and $ZnMgSi_2O_6$," *Acta Cryst. B*, vol. 31, pp. 1041–1049, 1975.

[3] Lin, J.H., Lu, G.X., Du, J., Su, M.Z., Loong, C.-K. and Richardson, J.W., "Phase transition and crystal structures of $BaZn_2Si_2O7$," *J. Phys. Chem. Solids*, vol. 60, no. 7, pp. 975–983, 1999.

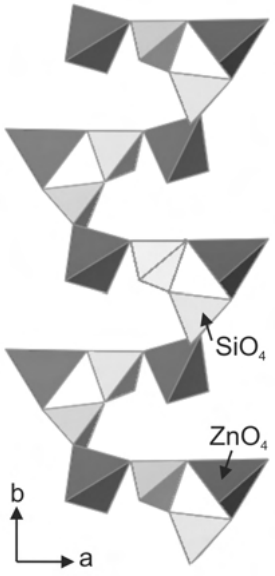

Figure 1

The telluridogallates REGaTe2 (RE = La – Nd)

T. Lindemann[1], O. Oeckler[1]

[1] Leipzig University, Faculty of Chemistry and Mineralogy, Institute of Mineralogy, Crystallography and Materials Science, Leipzig, Germany

New telluridogallates(I) $REGaTe_2$ (RE = La – Nd, space group $Pmc2_1$) were obtained from the elements. Chemical bonding and charge distribution are not trivial. Bond valence sums suggest an electron-precise description according to $RE^{III}Ga^{I}Te_2^{-II}$, and the coordination of gallium(I) is pyramidal as expected for a lone-pair atom. In contrast, known telluridogallates(III) such as $CuGaTe_2$ [1] and $AgGaTe_2$ [2] typically contain $[GaTe_4]$ tetrahedra. $REGaTe_2$ are a rare example of compounds with exclusively monovalent Ga atoms, probably the first one without organic residues. A short Nd-Ga distance of 3.13 Å is a possible indication of an interaction of the lone pair of Ga(I) with the Nd atoms. This is stronger than, for example, $NdGaSb_2$ (Nd-Ga distance 3.35 Å),[3] which has a different structure and bonding situation. Similar Nd-Ga distances are observed in intermetallic phases such as NdGa [4] or NdGaRh [5], so that a description as an oxidized intermetallic phase may also be considered. A formal consideration in the framework of the Zintl concept would assume a mixed chain-like $[Ga^{(-2)}Te^{(0)}Te^{(-1)}]^{3-}$-polyanion. It is consistent with all descriptions that the distances of 2.67 Å to the terminal Te atom are shorter than those to Te atoms bridging along the chain (2.95 Å). Interactions between the polyanionic chains appear negligible. The Nd atoms are located in single-capped trigonal prisms of Te atoms, with Ga atoms forming two additional caps.

References

[1] T. Plirdpring, K. Kurosaki, A. Kosuga, T. Day, S. Firdosy, V. Ravi, G. J. Snyder, A. Harnwunggmoung, T. Sugahara, Y. Ohishi, *Adv. Mater.*, vol. 24, pp. 3622, 2012.

[2] S. Chatraphorn, T. Panmatarite, S. Pramatus, A. Prichavudhi, R. Kritayakirana, J.-O. Berananda, V. Sayakanit, J. C. Woolley, *J. Appl. Phys.*, vol. 57, pp. 1791, 1985.

[3] A. M. Mills, A. Mar, *J. Am. Chem. Soc.*, vol. 123, pp. 1151, 2001.

[4] S.P. Yatsenko, A. A. Semyannikov, B. G. Semenov, K. A. Chuntonov, *J. Less-Common Met.*, vol. 64, pp. 185, 1979.

[5] F. Hulliger, *J. Alloys Compd.*, vol. 239, pp. 131, 1996.

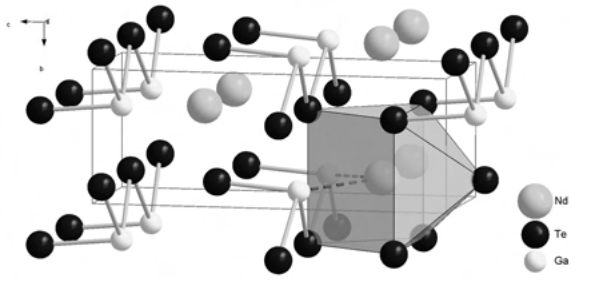

Figure 1 Unit cell of $NdGaTe_2$ in which the polyanionic substructure has been highlighted. The Nd-Ga contacts are shown by dashed "bonds".

Structural variations in RETe1.875–δ – distorted Te nets and chemical bonding

H. Poddig[1], T. Doert[1]
[1] Technical University of Dresden, Helmholtzstr. 10, 01069 Dresden, Germany

The structures of the rare earth metal polychalcogenides $REX_{2-\delta}$ (X = S, Se, Te; $0 \leq \delta \leq 0.2$) share a common motive of alternating stacks of a puckered [REX] double layer and planar [X] layer, which are structurally related to the ZrSSi type. This class of compounds adopts different (super)structures, according to the chalcogen defects in their planar layers. The deficient sulfides and selenides are dominated by X^{2-} and X_2^{2-}-anions, whereas a tendency to form larger anionic entities has been observed for the tellurides.[1–3] Crystals of $RE\mathrm{Te}_{1.875-\delta}$ (RE = Ce, Pr, Sm, Gd; $0.005 \leq \delta \leq 0.02$) have been grown by chemical transport reactions utilizing iodine and alkali halide flux reactions. All compounds crystallize in an orthorhombic unit cell, resembling a 3×4×2 supercell of the basic ZrSSi cell, with cell dimensions of about $a \approx 13.2(2)$, $b \approx 17.6(2)$ and $c \approx 18.0(2)$. Structure solution and subsequent refinement has been performed in space group *Amm2* (No. 38), in accordance with the structures of the related sulfides and selenides.[1] The generalized motif of all compounds resembles well the motif of the $GdSe_{1.875}$ type structure, as two stacks of a puckered [RE Te] and a planar [Te] layer are observed for all structures. Minor structural variations, i.e. slightly shifted atoms or additional vacancies, are observed for individual compounds within the planar [Te] layer, hinting towards marginally different ordered motifs, which can be understood as a result of structural frustration. The structural variety of the planar layer also manifests itself in a growing number of reflections violating the A-centering condition. Quantum mechanical calculations based on DFT theory have been performed to investigate the bonding situation inside the planar [Te] layer by using the real space indicator ELI-D. The results justify the description of small anionic fragments constituting the [Te] layers, but also indicate long range order within a characteristic eight-membered Te ring. Unlike for the sulfides and selenides, these calculations suggest formally a Te_8^{8-} anion, as bonding interactions are expected between all neighboring atoms of the ring.

References

[1] T. Doert, C. J. Müller, in *Reference Module in Chemistry, Molecular Sciences and Chemical Engineering*, Elsevier, 2016.
[2] H. Poddig, T. Donath, P. Gebauer, K. Finzel, M. Kohout, Y. Wu, P. Schmidt, T. Doert, *Z. Anorg. Allg. Chem.*, vol. 644, pp. 1886–1896, 2018.
[3] K. Stöwe, *Z. Kristallogr. - Cryst. Mater.*, vol. 216, pp. 215–224, 2001.

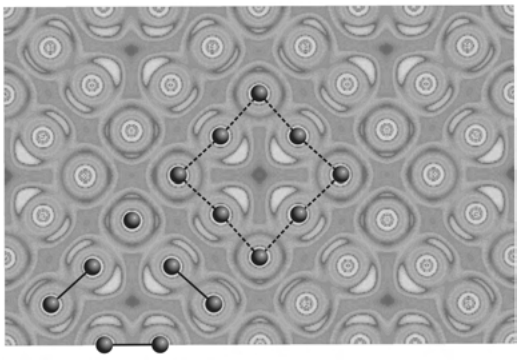

Figure 1

Luminescent nitridoalumooxophosphates by high-pressure/high-temperature synthesis

M. Pointner[1], O. Oeckler[2], W. Schnick[1]
[1] Ludwig Maximilian University of Munich, Munich, Germany
[2] Leipzig University, Leipzig, Germany

Intriguing properties of mixed nitride networks have led to a range of viable applications. Nitrido(litho)aluminates, e.g. $Sr[LiAl_3N_4]:Eu^{2+}$ and $Sr_2[MgAl_5N_7]:Eu^{2+}$, are an important part of developments in the lightening industry due to their chemical and thermal stability and luminescence.[1, 2] Likewise, nitridosilicophosphates and nitridophosphates contain rare structural motifs.[3, 4, 5] Dense frameworks and luminescence properties that may improve the quality of specialized light-emitting diodes (LEDs) are highly sensitive to the valence state, coordination spheres, site symmetry of atoms and the concentration of activator ions. Therefore, understanding relationships between luminescent properties and crystal structures is crucial. In investigating the nitride

network of nitridoalumo(oxo)phosphates, we combine these characteristics and properties and aimed at luminescent properties like low thermal quenching and a narrow emission due to the structural relationship to nitrido(litho)aluminates. $Sr_2Al_{10}P_8N_{20}O_{4.034}F_{5.094}:Eu^{2+}$ was obtained from $Sr(N_3)_2$, $SrCO_3$, P_3N_5, AlN, EuF_3 and the mineralizer NH_4F by mineralizer-assisted high-temperature high-pressure (HT/HP) synthesis (1400 °C, 5 GPa) with a Walker-type module.[6] The structure was elucidated by SCXRD (single-crystal X-ray diffraction, R1 = 0.0142, wR2 = 0.0327). BVS (bond valence sum) and CHARDI (charge-distribution) calculations indicate mixed anionic positions. The new nitridoalumofluoridooxophosphate crystallizes in space group I-4m2 [a = 11.17902(8), c = 5.1484(1) Å]. TEM SAED (transmission electron microscopy selected area electron diffraction) patterns confirmed the metric and TEM and SEM (scanning transmission electron) EDX (energy dispersive X-ray) coincide with the element ratio obtained by SCXRD. $Sr_2Al_{10}P_8N_{20}O_{4.034}F_{5.094}:Eu^{2+}$ shows a broadband emission with a maximum at 450 nm and a fwhm (full width at half maximum) of 108 nm (5315.0 cm^{-1}). It contains chains of face-sharing $Sr(N/O/F)_{12}$ cuboctahedra, supertetrahedra-like elements composed of ten edge-sharing $Al(N/O/F)_6$ octahedra where Al is positioned on three different crystallographic sites. A three-dimensional network is built by twofold and threefold vertex-sharing PN_4 tetrahedra.

References

[1] M. Zeuner, S. Pagano, W. Schnick, *Angew. Chem.-Int. Ed.*, vol. 50, p. 7754, 2011.
[2] P. Wagatha, V. Weiler, P. J. Schmidt, W. Schnick, *Chem. Mater.*, vol. 30, p. 1755, 2018.
[3] S. Vogel, A. T. Buda, W. Schnick, *Angew. Chem.-Int. Ed.*, vol. 58, p. 3398, 2019.
[4] S. Vogel, M. Bykov, E. Bykova, S. Wendl, S. D. Kloß, A. Pakhomova, S. Chariton, E. Koemets, N.Dubrovinskaia, L. Dubrovinsky, W. Schnick, *Angew. Chem.-Int. Ed.*, vol. 58, p. 9060, 2019.
[5] S. D. Kloß, W. Schnick, *Angew. Chem.-Int. Ed.*, vol. 58, p. 7933, 2019.
[6] S. Merlino, C. Biagioni, E. Bonaccorsi, N. V. Chukanov, I. V. Pekov, S. V. Krivovichev, V. N. Yakovenchuk, T. Armbruster, *Mineral. Mag.*, vol. 79, p. 145, 2015.

Crystal structure, complex phase diagram and re-entrant phase transition in NaSrPO4

M. Schreyer[1], G. Nenert[1]
[1] Malvern Panalytical, Malvern, United Kingdom

The crystal chemistry of AIBIIXO4 (AI = Alkali ion, BII = alkali-earth ion, X = P, V, As) is very rich and has been widely investigated, particularly the phosphate family [1]. In recent years, we have been investigated the crystal structures [2,3] and magnetic properties of some compositions within the AIBIIXO4 series [4]. However, despite its simple chemistry NaSrPO4 has never been reported so far. Here, we present the synthesis, crystal structure and phase transitions of this phosphate. Surprisingly, this material exhibits a complex structure (31 atoms in the asymmetric unit-cell, Z = 10) at room temperature characterized by a strongly under bonded Na atom. This under-bonded atom is responsible for the complex and rich phase diagram as function of temperature as illustrated in Figure 1. NaSrPO4 exhibits 4 phase transitions between room temperature and 750°C. Besides its rich phase diagram, NaSrPO4 exhibits a re-entrant phase transition slightly below 600°C before to reach a hexagonal paraelastic phase at high temperature. In addition, we show that the sequence of phase transitions is strongly driven by the history of the sample and several phases can be quenched at room temperature.

References

[1] V. A. Isupov, Ferroelectrics, 274(1), 203–283 (2002)
[2] G. Nénert, P. O'Meara, T. Degen, Phys Chem Minerals 44, 455–463 (2017)
[3] G. Nénert, Z. Kristallogr.; 232(10), 669–674 (2017)
[4] G. Nénert, et al., Inorg. Chem., 52, 9627-9635 (2013).

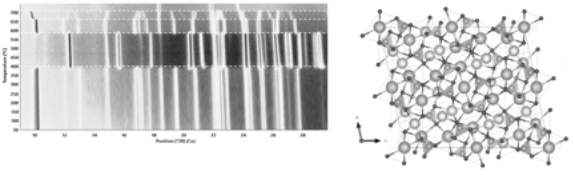

Figure 1 (Left) Temperature phase diagram of NaSrPO4and (right) the crystal structure of the α re-entrant polymorph.

Disorder in layered tellurides Tt1Pn2Te4 (Tt = Ge, Sn, Pb; Pn = As, Sb, Bi)

L. Staab[1], L. Eisenburger[2], S. Geisler[1], O. Oeckler[1]
[1] Universität Leipzig, Leipzig, Germany
[2] LMU München, Munich, Germany

The crystal structure of the mineral tetradymite Bi2S2Te has inspired discussions about its details for a long time.[1,2] Variations of this structure led to a large family of chalcogenides composed of slabs with alternating cation and anion layers stacked in rocksalt-type fashion, which show characteristic van der Waals gaps between anion layers.[3] These compounds are of interest not only for their exact crystal structures but also for their thermoelectric properties and their high likelihood of being topologically non-trivial systems insulators.[4,5] The rhombohedral compounds Tt1Pn2Te4 (*Tt* = Ge, Sn, Pb; *Pn* = As, Sb, Bi) feature septuple layers, in which the multiplicity of Wyckoff positions would allow complete cation ordering, which has been postulated in some cases.[6] However, more detailed studies based on single-crystal diffraction data almost always revealed cation disorder.[7] In the case of small scattering contrast, resonant X-ray diffraction corroborated the disorder.[8] Here we present a systematic investigation of these compounds with high-quality single crystal diffraction data collected with synchrotron radiation in order to establish exact site occupancy factors. As diffraction data cannot exclude short-range ordering, Z-contrast imaging by STEM-HAADF was used as a local probe, complemented by EDX spectroscopy with atomic resolution. All of these data confirm the cation disorder and could not even demonstrate short-range ordering. The disorder observed might be explained as an interplay between charge balance at the vdW-gap and octahedron size mismatch in the layer.

References

[1] Harker, D. *Z. Kristallogr.*, vol. 89, pp. 175-181, 1934.
[2] Pauling, L. *Am. Mineral.*, vol. 60, pp. 994-997, 1975.
[3] Cook, N. J.; Ciobanu, C. L.; Stanley, C. J.; Paar, W. H.; Sundbald, K. *Can. Mineral.*, vol. 45, pp. 417-435, 2007.
[4] Grauer, D. C.; Hor, Y. S.; Williams, A. J.; Cava, R. J. *Mater. Res. Bull.*, vol. 44, pp. 1926–1929, 2009.
[5] Silkin, I. V.; Menshchikova, T. V.; Otrokov, M. M.; Eremeev, S. V.; Koroteev, Yu. M.; Vergniory, M. G.; Kuznetsov, V. M.; Chulkov, E. V. *JETP Letters.*, vol. 96, pp. 322-325, 2012.
[6] Shu, H. W.; Jauilmes, S.; Flahaut, *J. Solid State Chem.*, vol. 74, pp. 277-28, 1988.
[7] Karpinsky, O. G.; Shelimova, L. E.; Kretova, M. A.; Fleurial. J. P. *J. Alloys Compd.*, vol. 268, pp. 112-117, 1998.
[8] Oeckler, O.; Schneider, M. M.; Fahrnbauer, F.; Vaughan, G. *Solid State Sci.*, vol. 13, pp. 1157-1161, 2011.

Inorganic functional materials

Bandgap tuning in ZnGeN2: Effective cation disorder control through oxygen incorporation.

Z. Wang[1], J. Breternitz[1], S. Schorr[1]
[1] Helmholtz-Zentrum Berlin für Materialien und Energie, Hahn-Meitner Platz 1, 14109 Berlin, Germany

Growing concern over resource availability and toxicity are leading to a paradigm shift towards truly sustainable materials for photovoltaics. Zn-group IV-nitrides are one potential class of materials fulfilling these criteria, which adopt a wurtzite-type derived structure. The ternary nitrides were postulated to allow a unique bandgap tuning mechanism through cation disorder [1] in addition to cation alloying. Fully ordered structure $ZnGeN_2$ crystallises in a ß-$NaFeO_2$ type structure in a subgroup of the wurtzite type. Interestingly, incorporating oxygen into $ZnGeN_2$ also introduces an increased degree of disorder in the material [2].

We present a detailed study of the degree of cation disorder in oxygen containing $Zn_{1-x}GeN_2O_x$ that is revealed through neutron powder diffraction. Studying samples with a variable degree of oxygen allows us to conclude on the role of oxygen and further comparing different samples of nominally similar composition allows to decorrelate the oxygen effect from intrinsic cation disorder. We will combine our results with optoelectronic and chemical properties of the materials and finally aim to answer the question, whether cation disorder exists independently of oxygen incorporation or is fundamentally linked to it.

References

[1] A.D. Martinez, A.N. Fioretti, E.S. Toberer, A.C. Tamboli, *J. Mater. Chem. A*, vol. 5, p. 11418, 2017.
[2] J. Breternitz, Z.Y. Wang, A. Glibo, A. Franz, M. Tovar, S. Berendts, M. Lerch, S. Schorr, *Phys. Status Solidi A*, vol. 216, 2019, Art. no. 1800885.

Structure-ammonia sensing property correlation in Sn1-xVxO2 mesoporous nanoparticles

N. Chakraborty[1], A. Sanyal[1], S. Das[1], D. Saha[1], S. K. Medda[1], S. Mondal[1]

[1] CSIR Central Glass & Ceramic Research Institute, Kolkata, India

Doping is a well-known method for improving gas sensing responses by metal oxide based functional materials.[1] And the plausible explanations provided in justification of using a specific dopant have been changes in material crystallinity, particle size, morphology and so on; but these ideas alone aren't able to clearly highlight the fundamental changes and intricacies of a system that exhibits improved performance by virtue of doping.[2] In this context, we have tried to analyze improved ammonia sensing responses by vanadium doped tin oxide nano-particles of formula Sn1-xVxO2 with respect to crystal structure and surface structural aspects.[3] While the doped samples showed a nearly four-fold improved response as compared to pure SnO2, the sample Sn0.696V0.304O2 showed 1.2 times improved response than Sn0.857V0.343O2. Structural analyses by Rietveld refinement[4] revealed reduction of unit cell volume in doped samples, leading to generation of surface active sites up to 1019/mm3 of doped sample, explaining improved response by increase in surface interaction. Surface structure analyses by XPS reveal presence of 1.2 times excess surface positive charge in Sn0.857V0.343O2 as compared to Sn0.696V0.304O2. Considering the concept of charge immobilization by surface electronic states in the former, the variable sensing responses amidst the doped samples can be explained. The specific role of vanadium ion in improving ammonia sensing responses by pure SnO2 has been delineated.

References

[1] Morrison, S. R., "Mechanism of Semiconductor Gas Sensor Operation," *Sensors and Actuators*, vol. 11, pp. 283–287, 1987.

[2] Mirzaei, A., Lee, J. H., Majhi, S. M., Weber, M., Bechelany, M., Kim, H. W., Kim, S. S., "Resistive gas sensors based on metal-oxide nanowires," *J. Appl. Phys.*, vol. 126, 2019, Art. no. 241102.

[3] Rietveld, M. H., "A profile refinement method for nuclear and magnetic structures," *J. Appl. Crystallogr.*, vol. 2, pp. 65–71, 1969.

[4] N. Chakraborty, A. Sanyal, S. Das, D. Saha, S. K. Medda and S. Mondal, "Ammonia Sensing by Sn1-xVxO2 Mesoporous Nanoparticles," *ACS Appl. Nano Mater.*, vol. 3, no. 8, pp. 7572–7579, 2020.

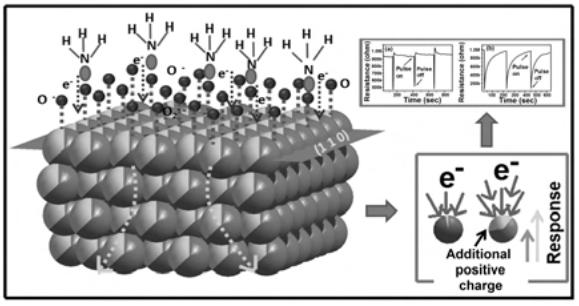

Figure 1

Dynamic disorder of fluoride anions in all-silica zeolites: Enhancing understanding with DFT-based molecular dynamics simulations

M. Fischer[1]

[1] University of Bremen, Faculty of Geosciences, Klagenfurter Straße 2-4, 28359 Bremen, germany

The "fluoride route", synthesis in the presence of fluoride anions, has been established as a versatile strategy for the synthesis of all-silica zeolites. Experimental investigations of as-synthesised zeolites using diffraction and NMR methods have shown that the fluoride anions are often located in small cages and bonded to one Si atom at a cage corner, with dynamic or static disorder occurring in some, but not all systems.[1] It has also been observed that the dynamic disorder can be modulated through a variation of the organic structure-directing agent (OSDA) used in the zeolite synthesis.[2] As relatively little is known about the underlying factors determining the preferred fluoride location(s) in a given cage and the dynamic behaviour, the present work employs a combination of density functional theory (DFT) calculations and DFT-based ab-initio molecular dynamics (AIMD) simulations to contribute to the understanding of these systems.

A systematic comparison of different fluoride positions in four all-silica zeolites with different topologies (IFR, NON, STF, STT) shows excellent agreement with experiment for all systems except STF. A remarkable result is obtained for STT, where the DFT calculations predict three distinct sites to be very close in energy, in perfect correspondence with the experimentally observed disorder over these sites. The AIMD simulations do not only reproduce the dynamic disorder of fluoride anions in IFR and STT, and its absence at room temperature in NON and STF, but also allow to develop an explanation for the qualitative differences between these systems. The role of the OSDA in influencing the dynamics of the fluoride anions is investigated for MFI-type Silicalite-1. AIMD simulations for Silicalite-1 models containing

different alkylammonium OSDAs show that the introduction of asymmetric organic cations with one short alkyl chain leads to a strong reduction of the fluoride mobility, agreeing with experimental observations. Further analysis shows that the heterogeneous charge distribution of these OSDAs, together with their restricted freedom of movement in the channels, enhances electrostatic interactions with the fluoride anions, reducing the dynamic motion.[3] While the primary aim of the present work is an improved fundamental understanding, similar computational approaches may, in the future, be exploited to aid the targeted synthesis of zeolites in fluoride-containing media.

Acknowledgement
Funding by the Deutsche Forschungsgemeinschaft (DFG project no. 389577027) is gratefully acknowledged.

References

[1] D. S. Wragg, R. E. Morris, A. W. Burton, *Chem. Mater.*, vol. 20, no. 4, pp. 1561–1570, Feb. 2008.
[2] S. L. Brace, P. Wormald, R. J. Darton, *Phys. Chem. Chem. Phys.*, vol. 17, no. 18, pp. 11950–11953, May 2015.
[3] M. Fischer, *J. Phys. Chem. C*, vol. 124, no. 10, pp. 5690–5701, Mar. 2020.

Ab initio structure determination of two new titanium phosphates synthesized via molten salt synthesis.

H. Petersen[1], N. Stegmann[1], M. Fischer[2], B. Zibrowius[1], W. Schmidt[1], M. Etter[3], C. Weidenthaler[1]
[1] Max-Planck-Institut für Kohlenforschung, Heterogeneous Catalysis , Kaiser-Wilhelm-Platz 1, 45470 Mülheim, Germany
[2] University of Bremen, Crystallography/Geosciences, Klagenfurter Straße, 28359 Bremen, Germany
[3] DESY, Notkestraße 85, 22607 Hamburg, Germany

The class of transition metal phosphates (TMPs) shows a wide range of chemical compositions, variations of valence states and respective crystal structures. Among TMPs, $VO(P_2O_7)$ and $LiFePO_4$ are of special interest as the only commercially used heterogeneous catalyst for the selective oxidation of butane to maleic anhydride [1] and cathode material in rechargeable batteries [2]. Due to their structural features, TMP are considered as proton exchange-membranes in fuels cells, working in the intermediate-temperature range [2, 3]. We report on the successful ab initio structure determination of two novel titanium pyrophosphates, $NH_4Ti(III)P_2O_7$ and $Ti(IV)P_2O_7$, from X-ray powder diffraction data. Both compounds were synthesized via a new molten salt synthesis route. The low symmetry space groups $P2_1/c$ ($NH_4TiP_2O_7$) and $P\bar{1}$ (TiP_2O_7) complicate the structure determination, making the combination of spectroscopic, diffraction and computation techniques mandatory. In $NH_4TiP_2O_7$, titanium ions (Ti^{3+}) occupy the TiO_6 polyhedron, coordinated by five pyrophosphate groups, one as a bi-dentate ligand. This secondary coordination causes the formation of one-dimensional six-membered ring channels with a diameter d_{max} of 514(2) pm, stabilized by ammonium ions. Annealing $NH_4TiP_2O_7$ in inert atmospheres results in the formation of the new TiP_2O_7, showing a similar framework consisting of $[P_2O_7]^{4-}$ units and TiO_6 octahedra as well as an empty one-dimensional channel (d_{max} = 628(1) pm). The *in situ* X-ray diffraction study of the transformation of $NH_4TiP_2O_7$ to TiP_2O_7 reveals a two-step mechanism, the decomposition of ammonium ions coupled with the oxidation of Ti^{3+} to Ti^{4+} and a subsequent structural relaxation.

References

[1] Hutchings, G.J., "Vanadium phosphate: a new look at the active components of catalysts for the oxidation of butane to maliec anhydirde," *J. Mater. Chem.*, vol. 14, pp. 3385–3395, 2014.
[2] Jin, Y., Y. Shen, and T. Hibino, "Proton conduction in metal pyrophosphates (MP_2O_7) at intermediate temperatures," *J. Mater. Chem.*, vol. 20, pp. 6214–6217, 2010.
[3] Nalini, V., M.H. Sørby, K. Amezawa, R. Haugsrud, H. Fjellvåg, and T. Norby, "Structure, Water Uptake, and Electrical Conductivity of TiP_2O_7," *J. Am. Ceram. Soc.*, vol. 94, no. 5, pp. 1514–1522, 2011.

Termo- and Photo-induced Spin Crossover in a novel 2x2 iron (II) Grid. Crystallography and Photocrystallography studies

J. Velazquez Garcia[1], K. Basuroy[1], J. Wong[2], D. Storozhuk[1], S. Saouane[3], R. Henning[4], S. Techert[1]
[1] DESY, Photon Science, Structural Dynamics in Chemical Systems, Notkestraße 85, Hamburg, 22607, Germany
[2] Georg-August University of Göttingen, Institut for Inorganic Chemistry, Tammannstraße 4, Göttingen, 37077, Germany
[3] DESY, Photon Science, PETRA III, P11 Beamline, Notkestraße 85, Hamburg, 22607, Germany
[4] University of Chicago, Argonne National Laboratory, Center for Advanced Radiation Sources, 9700 South Cass Ave, Lemont, Illinois 90439, USA

We studied the thermo- and photo-induced phase transition between low spin (LS) and high spin (HS) states of the 2x2 grid-like iron complex: [Fe4L4](BF4)4·C2H3N (FE4), L=4-methyl-3,5-Bis6(2,2′-dipyridyl)pyrazole in

solid state, by using X-ray diffraction techniques. The structural analysis of the coordination geometry of the two crystallographically independent metal atoms at different temperatures demonstrates that the formation of the thermo-induced HS in one atom affects the coordination geometry of the other. The analysis of the photo-induced HS over time do not only exhibit similar structural reorganization as the thermo-induced HS state but also a relaxation from HS to LS in less than one nanosecond. The understanding of photo-switching dynamics and its relation with the thermo-induced HS under systems with strong short-range elastic coupling between small set of metal ions, such as the FE4 system, could allow for new mechanism of energy redistribution after photoexcitation and therefore, the design of new storage and processing devices.

Analyzing Order of Light Anions in LiLa2NH2O by Neutron and X-Ray Powder Diffraction and Spectroscopy

N. Zapp[1], D. Sheptyakov[2], M. Bertmer[1], H. Kohlmann[1]
[1] Leipzig University, Leipzig, Germany
[2] Paul Scherrer Institute, Villigen, Switzerland

Heteroanionic hydrides are an emerging class of compounds with representatives showing hydride ion conductivity [1] or catalytic activity [2]. Their properties are fundamentally linked to their anionic substructure; for example, might a difference between ordered and disordered anions change their behavior from a conducting to an isolating behavior [3].

From the solid-state reaction of Li_2O, LaN and LaH_3, we obtained the new nitride hydride oxide $LiLa_2NH_2O$ as a black powder. It crystallizes in the K_2NiF_4 structure type ($I4/mmm$, a = 3.65431(6) Å, c = 13.3570(3) Å) and can be described as an aliovalent substitution product ($2\ O^{2-} \rightarrow N^{3-} + H^-$) of the hydride ion conductor $LiLa_2HO_3$ [1]. The analysis of the anion substructure demanded the combination of different methods. We therefore performed neutron powder diffraction measurements on both hydride $LiLa_2NH_2O$ and deuteride $LiLa_2ND_2O$ (coherent scattering lengths b_c(H) = -3.7 fm, b_c(D) = 6.7 fm) in addition to powder X-ray diffraction and nuclear magnetic resonance spectroscopic analysis.

H/D and N/O show a separation on two crystallographic sites 4*d* and 4*e* with only slight but significant mixing. Additionally, both sites are significantly underoccupied, resulting in a charge imbalanced composition. H/D occupies favorably the Li-rich site 4*d*, while N and O share the La-rich 4*e* position (Figure 1). Both sites are coordinated in a distorted octahedral fashion with Li situated on opposite vertices of the H-rich polyhedron with short Li-H distances (1.83 Å; LiH: 2.04 Å).

References

[1] G. Kobayashi *et al.*, *Science* **2016**, *351*, 1314-7.
[2] M. Kitano *et al.*, *J. Am. Chem. Soc.* **2019**, *141*, 20344-53.
[3] H. Nawaz *et al.*, *Chem. Commun.* **2020**, *56*, 10373-6.

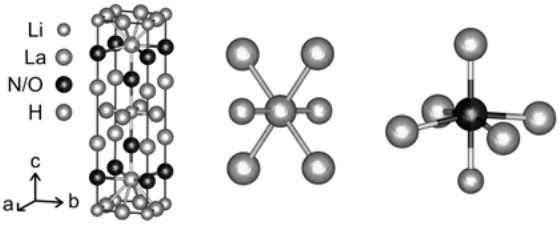

Figure 1

In situ / in operando studies

Insitu X-ray analysis of misfit strain and curvature of bent polytypic InxGa1-xAs/GaAs core/shell nanowires

M. Al-Humaidi[1], J. Feigl[2], J. Jakob[2], P. Schroth[2], A. AlHassan[1], A. Davtyan[1], J. Herranz[3], A. Tahraoui[3], D. Novikov[4], T. Baumbach[2], L. Geelhaar[3], U. Pietsch[1]
[1] Solid State Physics, University of Siegen, Siegen, Germany
[2] Institute for Photon Science and Synchrotron Radiation, Karlsruhe Institute of Technology, Karlsruhe, Germany
[3] Paul Drude Institut für Festkorperelektronik, Leibniz Institut im Forschungsverbund Berlin, Berlin, Germany
[4] DESY, HASYLAB, Hamburg, Germany

Misfit strain in crystalline core-shell nanowires can be elastically released by nanowire curvature in case of inhomogeneous shell growth around the nanowires [1]. In this work, we performed time-resolved in-situ XRD investigations of the evolution of GaAs nanowires bending during the asymmetric growth of InxGa1-xAs shell without substrate rotation. By means of micro X-ray beam at beamline P23 and P09 at PETRA-III at DESY and a portable molecular beam epitaxy chamber (pMBE) [2], this study gives insight into the temporal development of the bending as well as the strain in the core-shell nanowire. In particular, different bending directions of nanowires grown on Si with native oxide and thermal oxide were observed and the demonstration of the nanowire curvature as function of shell thickness showed nonlinear dependency.

References
[1] Lewis R B, Corfdir P, Küpers H, Flissikowski T, Brandt O and Geelhaar L 2018, Nano Lett. 18 2343–50
[2] Slobodskyy T, Schroth P, Grigoriev D, Minkevich A A, Hu D Z, Schaadt D M and Baumbach T 2012, Review of Scientific Instruments vol 83

Observing the oxidation of platinum under operando electrochemical conditions

L. Jacobse[1], R. Schuster[2], X. Deng[1], S. Dolling[1], T. Weber[3], H. Over[3], J. Libuda[2], V. Vonk[1], A. Stierle[1]
[1] Deutsches Elektronen-Synchrotron (DESY), FS-NL (Nanolab), Hamburg, Germany
[2] Interface Research and Catalysis, Friedrich-Alexander-Universität Erlangen-Nürnberg, Erlangen, Germany
[3] Physikalisch-Chemisches Institut and Zentrum für Materialforschung, Justus Liebig University, Giessen, Germany

Platinum electrocatalyst degradation forms a large barrier for the wide-spread application of electrolysers and fuel cells, which are crucial for a sustainable energy society. A detailed understanding of the catalyst surface structure during the chemical reaction is required to design more stable catalysts. We have developed a Rotating Disk Electrode (RDE) setup that enables a structural characterization by synchrotron High-Energy Surface X-Ray Diffraction (HE-SXRD) experiments while maintaining well-defined diffusion conditions and high catalytic reaction rates (current densities). With this setup we followed the oxidation of Pt(111) and Pt(100) model electrodes, from the Place-Exchange surface oxidation occurring around 1.1 V until the formation of a (bulk) oxide at potentials relevant for the oxygen evolution reaction. In contrast with heterogenous oxidation experiments, no ordered oxide structures are observed.

Tracking the facet-resolved strain state of a PtRh nanoparticle under catalytic reaction conditions

Y. Y. Kim[1], T. F. Keller[1], T. J. Goncalves[3], M. Abuin[1], H. Runge[1], L. Gelisio[1], J. Carnis[1], V. Vonk[1], P. N. Plessow[2], I. Vartaniants[1], A. Stierle[1]
[1] Deutsches Elektronen-Synchrotron (DESY), Hamburg, Germany
[2] Institute of Catalysis Research and Technology, Karlsruhe Institute of Technology, D-76344 Eggenstein-Leopoldshafen, Germany

Oxide-supported nanoparticles are important heterogeneous catalysts. The nanoparticles shapes and type of facets are decisive for the catalyst activity and lifetime. During a catalytic reaction, the nanoparticle may be subject to shape changes, and segregation in alloys may adjust the termination of the surface to a changing gas environment.

Here we report on the evolution of the 3D strain state in a single alloy PtRh nanoparticle operando followed by coherent X-ray diffraction imaging (CXDI). At a temperature of T=700 K the nanoparticle environment was switched between the gas compositions (I) inert Ar, (II) CO+Ar, (III) CO+O_2+Ar and (IV) CO+Ar resembling different adsorption and catalytic reaction scenarios on the nanoparticle surface.

$SrTiO_3$ supported nanoparticles were grown by co-deposition of Pt and Rh and annealed in UHV to induce the equilibrium shape. A single nanoparticle was pre-selected in an SEM and subsequently, hierarchical Pt fiducial markers were deposited in the vicinity of the selected nanoparticle and used to re-locate the same particle in the X-ray beam.

The nanoparticle exhibited solely low index <100> and <111> type facet surfaces, intriguingly showing distinct, facet-family specific strain states. Under the catalytic reaction condition (III) we observed significant strain relaxations for all facets accompanied with a preferential segregation of Rh to the nanoparticle surface, in line with density functional theory calculations (DFT). The Rh enrichment on the facets turned out to be non-reversible under the subsequent CO reduction condition (IV) as compared to the identical previous gas condition (II).

Tracking the dynamics of facet-specific structural reorganizations of the nanoparticle is one key for the future design of heterogeneous catalysts with optimized efficiency and selectivity.

Crystallization pathway control of $Bi_2Fe_4O_9$ studied by in situ Pair Distribution Function analysis

A. Kirsch[1], N. Lefeld[2], M. Gogolin[2], S. Banerjee[3], K. Jensen[1]
[1] University of Copenhagen, 2100 Copenhagen, Denmark
[2] Universität Bremen, Bremen, Germany
[3] PETRA III, Deutsches Elektronen-Synchrotron (DESY), Hamburg, Germany

The targeted control of particle/crystallite size, crystallinity, and polymorphism is of crucial importance for many functional materials, in particular quantum materials[1]. They are frequently synthesized by the facile sol-gel method which in a broader sense can be described as the conversion of molecular precursors in solution into inorganic solids via hydrolysis, condensation, and aggregation[2]. The synthesis of pure nanocrystalline samples, however, can be very difficult if various stable and metastable phases exist often leading to co-crystallization. In this study, we use *in situ* total scattering and Pair Distribution Function (PDF) analysis to follow the

transformation of molecular precursors into multiferroic $Bi_2Fe_4O_9$ with a second-scale time resolution. The precursors were synthesized by the sol-gel process using the respective metal nitrates and meso-erythritol as the complexing agent. We show how the crystallization pathways and kinetics of the target compound can dramatically be changed by variation of the synthesis medium and ratio of metal nitrate to the complexing agent and relate this to the precursor structure. As an example, using small amounts of complexing agent leads to a crystalline precursor which first gets amorphous at 613 K, crystallizes into $BiFeO_3$ at 706 K, and subsequently transforms into $Bi_2Fe_4O_9$ at 815 K. On the other hand, bigger amounts of complexing agent produce an amorphous precursor which directly crystallizes into $Bi_2Fe_4O_9$ at 762 K. Using PDF we reveal the importance of the initial gel structure in the overall crystallization behaviour of the system.

References

[1] Samarth, N. *Nat. Mater.*, 2017, 16, 1068.
[2] Niederberger, *M. Acc. Chem. Res.*, 2007, 40, 793.

Stabilization mechanisms of pure tetragonal zirconia nanocrystallites using an original supercritical-based synthesis route

G. Philippot[1], A. Auxemery[2], D. Testemale[3], B. Iversen[4], C. Aymonier[2]

[1] University of Bordeaux, Bordeaux, France

[2] CNRS, ICMCB, Pessac, France

[3] Institut Neel, Grenoble, France

[4] Aarhus University, Aarhus, Denmark

Zirconium dioxide (ZrO2) has been of major industrial and scientific interest over the past decades for its wide range of applications, in particular thanks to its catalytic properties. Regardless the multiple synthesis routes employed, undoped bulk ZrO2 is stabilized in the monoclinic structure (m-ZrO2) at ambient temperature and atmospheric pressure. However, these last years, studies showed that it was also possible to stabilize pure t-ZrO2 without cationic substitution. To do so, three main effects are identified in the literature: (i) the presence of oxygen vacancies, (ii) the existence of structural similarities, and (iii) the size effect, with the existence of a critical size below which pure t-ZrO2 is formed.

In this presentation we will introduce the synthesis of quasi pure t-ZrO2 nanocrystals in supercritical fluids using borderline nonhydrolytic sol-gel (B.N.H.S.G.) conditions. The term borderline is used to express the nuance from nonhydrolytic sol-gel (N.H.S.G.) reactions when small amounts of water molecules are generated in situ from solvent (alcohols) decomposition to trigger hydrolysis/condensation. This amount of water being controlled, the reaction kinetics can be tuned and slow down. This enabled us to performed in situ total scattering measurements in order to catch the various stages of the nanocrystal formation upon various conditions (temperature, nature of the alcohols and presence of surfactants). These observations where combined to various ex situ characterizations (Raman, PDF, EXAFS, HR-TEM, XRD, etc.) to discuss the existence of a critical size below which pure t-ZrO2 is formed, as reported in literature and propose a formation mechanism in this specific synthesis route.

Selective in-situ exsolution of catalytically active metals from doped perovskites during methane dry reforming

F. Schrenk[1], L. Lindenthal[1], D. Hedda[1], R. Rameshan[1], C. Rameshan[1]

[1] TU Wien, Institute of Materials Chemistry, Vienna, Austria

Perovskite type oxides, doped with catalytically active metals, have shown great potential to catalyse MDR (Methane Dry Reforming) [1]. These materials can undergo exsolution, the formation of metallic nanoparticles on the surface, of B-site elements if reducing conditions are applied [2]. These exsolved nanoparticles are leading to an increase in catalytic activity. A Ni-doped perovskite (Nd0.6Ca0.4Fe0.97Ni0.03O3) and a Co-doped perovskite (Nd0.6Ca0.4Fe0.9Co0.1O3) were investigated in MDR conditions with a CH4 excess of 2:1 over CO2. To investigate the changes the catalyst undergoes during the reaction *in situ* NAP XPS (Near Ambient Pressure X-ray Photoelectron Spectroscopy) as well as *in situ* XRD (X-Ray Diffraction) experiments were performed. The XRD data showed the formation of a bcc phase at higher temperatures which cannot be assigned to Fe or the dopant (Ni/Co) due to the bad signal to noise ratio (Figure 1). The XPS data reveals that Ni is exsolving before Fe, as the Ni2p signal is shifting from the oxidized state into a metallic state between 600 °C and 650 °C and the Fe2p signal does not show a metallic component even at 700 °C, as seen in Figure 2. For the Co-doped catalyst, the formation of a metallic Co component was observed while no metallic Fe was detected.

References

[1] D. Pakhare and J. Spivey, "A review of dry (CO2) reforming of methane over noble metal catalysts," *Chem. Soc. Rev.*, vol. 43, no. 22, pp. 7813-7837, Nov. 2014, doi: 10.1039/c3cs60395d.

[2] L. Lindenthal et al., "Modifying the Surface Structure of Perovskite-Based Catalysts by Nanoparticle Exsolution," *Catalysts*, vol. 10, no. 3, Mar. 2020, Art no. 268, doi: 10.3390/catal10030268.

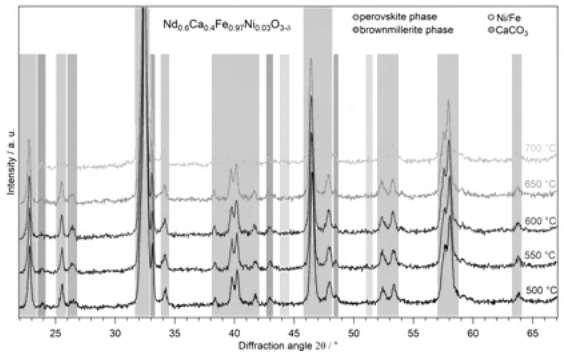

Figure 1 In-situ XRD diffractograms of the Ni-doped catalyst with a CH4:CO2 ratio of 2:1 and temperature steps from 500 °C to 700 °C. The phases observed could be assigned to a perovskite phase (blue) as well as a brownmillerite phase with ordered oxygen vacancies (grey) during all temperatures. Forming at higher temperatures a CaCO3 (violet) and a bcc Phase, stemming ether from Ni or Fe (green), could be detected.

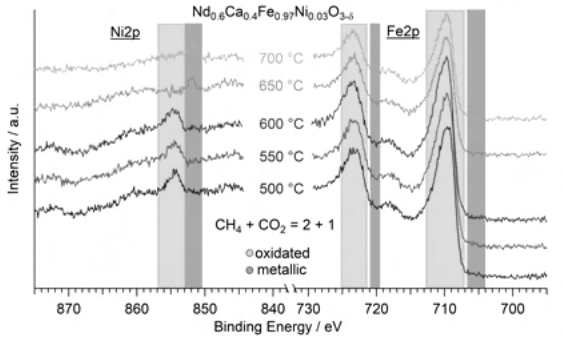

Figure 2 Comparison of the Fe2p and Ni2p transitions in the in-situ NAP XPS experiment of the Ni-doped catalyst. The sample was oxidized at 1 mbar O2 before the reaction, afterwards an atmosphere of 1 mbar CH4 and CO2 in a ratio of 2:1 was set and temperature steps between 500 °C and 700 °C were performed. A metallic component (blue) is forming between 600°C and 650 °C for Ni, whereas the Fe transition does not so such a component even at 700 °C.

Homoepitaxial growth of magnetite (Fe_3O_4) (001)

S. Tober[1], M. Creutzburg[1], B. Arndt[2], S. Chung[1], L. Jacobse[1], A. Vlad[3], A. Resta[3], H. Noei[1], V. Vonk[1], A. Stierle[1]
[1] Deutsches Elektronen-Synchrotron (DESY), FS-NL (Nanolab), Hamburg, Germany
[2] DESY, Hamburg, Germany
[3] Synchrotron SOLEIL, Synchrotron SOLEIL, Saint-Aubin, Essonne, France

The performance of magnetite-based devices and catalysts crucially depends on their surface structure and stoichiometry [1]. While annealing in ultra high vacuum and the adsorption of small molecules (partially) lift the subsurface cation vacancy reconstruction on Fe_3O_4 (001) surfaces [3,4,5], annealing under oxidising conditions results in the growth of new Fe_3O_4 layers involving near-surface cation transport [6].

To study the influence of O_2 pressure on cation transport in the Fe_3O_4 near-surface region, the homoepitaxial growth of Fe_3O_4 by molecular beam epitaxy was observed in-situ by surface X-ray diffraction (SXRD) at different pressures and growth rates.

Details about the grown structures and the growth process obtained from crystal truncation rods and X-ray intensity growth oscillations will be complemented by low energy electron diffraction and X-ray reflectivity data. These results will be presented in relation with their implications for cation transport in Fe_3O_4 [7].

References

[1] Parkinson, G., Surf. Sc. Rep. 71, 272 (2016)
[2] Bliem, R. et al., Science 346, 1215 (2014)
[3] Arndt, B. et al., Chem. Comm. 1, 92 (2019)
[4] Arndt, B. et al., Surf. Sci. 653, 76 (2016)
[5] Arndt, B. et al., PCCP 22, 8336 (2020);
[6] Nie, S. et al., J. Am. Chem. Soc. 135, 10091 (2013),
[7] Dieckmann, R. et al., Ber. Bunsenges. Phys. Chem. 81, 344 (1977)

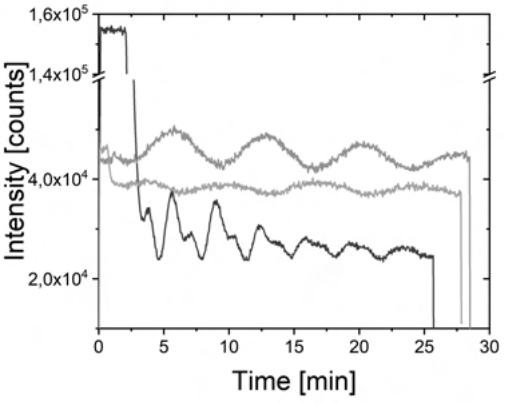

Figure 1. Growth oscillations observed by SXRD at (4 0 1.97) (blue), (4 0 1) (green) and (2 2 0.97) (yellow) indicating a layer by layer growth of half unit cells. Growth at 4×10^{-6} mbar O_2 and a flux of 30 nA.

Understanding thermal exfoliation of h-BN using in situ X-ray diffraction

Z. Yan[1], A. Abdelkader[2], W. Mirihanage[1]

[1] University of Manchester, Manchester M13 9PL, United Kingdom

[2] Bournemouth University, Poole BH12 5BB, United Kingdom

2D materials are considered as unique class of modern materials. Understanding the mechanisms behind the exfoliation processes enables us to significantly enhance processing potential of 2D materials. In-situ synchrotron X-ray characterization is employed to study the temporal changes of hexagonal-boron nitride (h-BN) while its initial processing from bulk 3D crystalline material towards its 2D counterpart. In situ X-ray powder diffraction (XPDF) experiment is conducted with thermal cycle that heating bulk h-BN up to 1273 K and subsequent cooling. The results show a linear expansion in c-axis direction of h-BN crystals as commonly understanding, however a contraction behaviour in a-axis direction is observed up to around 750 K during heating process, followed by an expansion behaviour when temperature over 750 K. Characterization particularly indicates structural changes of long-range order favourable for exfoliation between the range of 750 K to 950 K. With the consideration of thermal oxidation studies also, a hypothesis of thermal assisted exfoliation with oxygen interstitial and substitution of nitrogen at high temperature is proposed through our studies to drive the exfoliation mechanisms.

Micro and nano-crystalline materials

Morphology and growth behavior of Cu nanoparticles on the vicinal ZnO(10-14) surface

R. Gleissner[1], H. Noei[1], V. Vonk[1], S. Chung[1], G. Semione Dalla Lana[1], E. E. Beck[1], G. Gizer[2], A. Stierle[1]

[1] DESY, Photon Science, FS-NL (Nanolab), Hamburg, Germany

[2] Helmholtz-Zentrum Geesthacht, Hamburg, Germany

The ZnO(10-14) surface raised recent scientific interest for its outstanding stability despite its high indexed orientation, which results in a stepped mixed-terminated surface.[1] In this study, copper nanoparticles were grown via physical vapor deposition onto a ZnO(10-14) single crystalline surface and the structure and morphology was investigated using low energy electron diffraction, high energy grazing incidence x-ray diffraction, scanning electron microscopy and scanning tunneling microscopy.

Caused by anisotropic diffusion, elongated Cu particles are formed parallel to the surface steps of the substrate. They show a unique tilt of their (111) planes parallel to the (0001) terraces of the vicinal surface. This causes the generation of large, high indexed Cu facets in which their atomic steps could act as reaction sites in catalytic reactions such as methanol synthesis and CO2 activation.

Self assembled monolayer of silica nanoparticles with improved order by drop casting

A. Qdemat[1], E. Kentzinger[2], J. Buitenhuis[2], U. Rücker[2], M. Ganeva[3], T. Brückel[2]

[1] Forschungszentrum Jülich, Jülich Centre for Neutron Science JCNS and Peter Grünberg Institut PGI Quantum Materials and Collective Phenomena, Jülich, Germany

[2] Forschungszentrum Jülich, Institute of Biomacromolecular Systems and Processes (IBI-4), Jülich, Germany

[3] Forschungszentrum Jülich, JCNS outstation @ MLZ Garching, Garching, Germany

Assembly of NPs into large-area monolayers on a solid substrate is fundamentallyinteresting due to their unique optical and electronic properties. Furthermore, they have an impact on the creation of next-generation materials design [1] and for new devices that require monolayers with ordered structure over large areas formed with a simple method at low cost to meet the growing industrial needs. But controlling the deposition on a substrate to obtain two-dimensional and three-dimensional nanoparticle arrays is a complex process, and it occurs under specific conditions.

In this contribution, we report on the formation of large area, self assembled, highly ordered monolayers of stearyl alcohol grafted silica nanospheres of 50 nm diameter on a silicon substrate based on the drop-casting method. Our novel approach to achieve improved order uses stearyl alcohol as an assistant by adding it to the colloidal NanoParticle (NP) dispersion from which the monolayers are formed. Additionally, a heat treatment step is added, to melt the stearyl alcohol in the monolayer and thereby give the particles more time to further selfassemble, leading to additional improvement in the monolayer quality. The formation of the monolayers is significantly affected by the concentration of the NPs and the stearyl alcohol, the volume of the drop as well as the time of the heat treatment. A high surface coverage and uniform monolayer film of SiO2 NPs is achieved by appropriate control of the abovementioned preparation parameters. Structural characterization of the obtained SiO2 NP monolayer was done locally by Scanning Elec-

tron Microscopy (SEM), and globally by X-ray reflectivity (XRR) and grazing incidence small-angle X-ray scattering (GISAXS), where the data was reproduced by simulation within the Distorted Wave Born Approximation (DWBA) [2]. In conclusion, our modified drop-casting method is a simple, inexpensive method, which provides highly ordered self-assembled monolayers of silica particles, if combined with a compatible additive and a heat treatment step. This method might be more general and applicable to improve the ordering between different particles in monolayers as well as multilayers after finding an appropriate additive [3].

References

[1] M. A. Boles, M. Engel and D. V. Talapin, *Chem. Rev.*, vol. 116, pp. 11220–11289, 2016.
[2] G. Pospelov, W. Van Herck, J. Burle, J. M. Carmona Loaiza, C. Durniak, J. M. Fisher, M. Ganeva, D. Yurov and J. Wuttke, *J. Appl. Crystallogr.*, vol. 53, pp. 1600–5767, 2020.
[3] A. Qdemat, E. Kentzinger, J. Buitenhuis, U. Rücker, M. Ganeva and T. Brückel, *RSC Adv.*, vol. 10, pp. 18339–18347, 2020.

Crystal structure and lattice dynamics of endotaxial $FeSi_2$ nanowires

J. Kalt[1], M. Sternik[2], B. Krause[1], I. Sergueev[3], M. Mikolasek[4], D. G. Merkel[5], D. Bessas[4], O. Sikora[2], T. Vitova[1], J. Göttlicher[1], R. Steininger[1], P. Jochym[2], A. Ptok[2], O. Leupold[3], H.-C. Wille[6], A. Chumakov[4], P. Piekarz[2], K. Parlinski[2], T. Baumbach[1], S. Stankov[1]
[1] Karlsruhe Institute of Technology, Karlsruhe Germany
[2] Polish Academy of Sciences, Poland
[3] Deutsches Elektronen-Synchrotron, Hamburg Germany
[4] ESRF – The European Synchrotron, Grenoble France
[5] Hungarian Academy of Sciences, Hungary
[6] XFEL-User (XFEL-User), Hamburg,Germany

Metallic silicides constitute an important part of current microelectronics, serving as Schottky barriers and ohmic contacts, gate electrodes, local interconnects, and diffusion barriers [1–3]. Silicide nanowires, self-organized on the Si(110) surface, are considered as building blocks of future nanoelectronics and have been intensively investigated [4]. However, the reports about their crystal structure remain contradictory, spanning cubic (s or γ) [5–7] and tetragonal (α) [8] phases. Furthermore, in nanostructures the lattice vibrational waves (phonons) deviate drastically from those in bulk crystals, giving rise to anomalies in thermodynamic, elastic, electronic, and magnetic properties. Hence, a thorough understanding of the physical properties of these materials requires a comprehensive investigation of the crystal structure and lattice dynamics as a function of the nanowire size.

Using extended x-ray absorption fine structure (EXAFS) spectroscopy and nuclear inelastic scattering (NIS) we performed a systematic study of the crystal structure and the lattice dynamics of endotaxial $FeSi_2$ nanowires, which are in-plane embedded into the Si(110) surface. The EXAFS results unveiled the formation of the metastable, surface-stabilized α phase. The Fe-partial phonon density of states, obtained by the NIS experiment, exhibits a broadening of the spectral features with decreasing nanowire width and a pronounced vibrational anisotropy that originates from the specific orientation of the tetragonal α-$FeSi_2$ unit cell on the Si(110) surface. The results from first-principles calculations are fully consistent with the experimental observations [9].

References

[1] S.P. Murarka, Intermetallics 3, 173 (1995).
[2] L. J. Chen, Silicide Technology for Integrated Circuits (Institution of Electrical Engineers, London, 2004).
[3] L.J. Chen, JOM 57, 24 (2005).
[4] P.A. Bennett et al., Thin Solid Films 519, 8434 (2011).
[5] S. Liang et al., Appl. Phys. Lett. 88, 113111 (2006).
[6] S. Liang et al., J. Cryst. Growth 295, 166 (2006).
[7] D. Das et al., Appl. Phys. Lett. 105, 191606 (2014).
[8] Z.-Q. Zou et al., Appl. Surf. Sci. 399, 200 (2017).
[9] J. Kalt et al., Phys. Rev. B 102, 195414 (2020).

Scattering is a powerful tool to follow nucleation and growth of minerals from solutions

T. Stawski[1], A. E. S. Van Driessche[2]
[1] Federeal Institute for Material Research and Testing, Berlin, Germany
[2] Grenoble Alpes University, University Savoie Mont Blanc, CNRS, IRD, IFSTTAR, ISTerre, 38000 Grenoble, France

In recent years, we have come to appreciate the astounding intricacy of the formation process of minerals from ions in aqueous solutions. The original 'textbook' image of these phenomena, stemming from the adaptation of classical nucleation and growth theories, has increased in complexity due to the discovery of a variety of precursor and intermediate species [e.g. 1], including solute clusters (e.g. prenucleation clusters, PNCs), liquid(-like) phases, as well as amorphous and nanocrystalline solids etc. In general, these precursor or intermediate species constitute different, often short-lived, points along the pathway from dissolved ions to the final solids (typically crystals in

this context). In this regard synchrotron-based scattering (SAXS/WAXS/HEXD) appears to be the perfect tool to follow in situ and in a time-resolved manner the crystallization pathways because of the temporal and spatial length scales that can be directly accessed with these techniques. Here, we show how we used scattering to probe the crystallization mechanisms of calcium sulfate. CaSO4 minerals (i.e. gypsum, anhydrite and bassanite) are widespread in natural and industrial environments. During the last several years, a number of studies have revealed indeed that nucleation in the CaSO4-H2O system is non-classical. Our SAXS data demonstrate that gypsum precipitation, involves formation and aggregation of sub-3 nm primary species. These species constitute building blocks of an amorphous precursor phase [2]. Further, we show how in situ high-energy X-ray diffraction experiments and molecular dynamics (MD) simulations can be combined to derive the atomic structure of the primary CaSO4 clusters seen at small-angles [3]. We fitted several plausible structures to the derived pair distribution functions and explored their dynamic properties using unbiased MD simulations based on polarizable force fields. Finally, based on combined SAXS/WAXS, broad-q-range measurements, we show that the process of formation of bassanite, a less hydrated form of CaSO4, is very similar to the formation of gypsum: it also involves the aggregation of small primary species into larger disordered aggregates [4]. Based on these recent insights we formulated a tentative general model for calcium sulfate precipitation from solution. This model involves primary species that are formed through the assembly of multiple Ca2+ and SO42- ions into nanoclusters. These nanoclusters assemble into poorly ordered (i.e. amorphous) hydrated aggregates, which in turn undergo ordering into coherent crystalline units of either gypsum or bassanite (and possibly anhydrite). Determination of the structure and (meta)stability of the primary species is important from both a fundamental, e.g. establishing a general non-classical nucleation model, and applied perspective; e.g. allow for an improved design of additives for greater control of the nucleation pathway.

References

[1] J.J. De Yoreo, P.U.P.A. Gilbert, N.A.J.M. Sommerdijk, R. L. Penn, S. Whitelam, D. Joester, H. Zhang, J. D. Rimer, A. Navrotsky, J. F. Banfield *et al.*, *Science*, vol. 349, 2015, Art. no. aaa6760.

[2] T.M. Stawski, A.E.S. van Driessche, M. Ossorio, J. Diego Rodriguez-Blanco, R. Besselink, L.G. Benning, *Nat. Commun.*, vol. 7, p. 11177, 2016.

[3] T.M. Stawski, A.E.S. Van Driessche, R. Besselink, E.H. Byrne, P. Raiteri, J.D. Gale, L.G. Benning, *J. Phys. Chem. C*, vol. 123, no. 37, 2019.

[4] T.M. Stawski, R. Besselink, K. Chatzipanagis, J. Ho¨velmann, L.G. Benning, A.E.S. Van Driessche, *J. Phys. Chem. C*, vol. 124, no. 15, 2020.

Organic and metal-organic crystal structures

Lattice energies of all known Crystal Structures

D. W. Hofmann[1], L. Kuleshova[1]

[1] CRS4, Pula, Italy

We calculated the Gibb's energy of all known organic and organometallic crystal structures at ambient conditions with FlexCryst [1]. Firstly, the implemented data mining force field was validated for the experimental lattice energies of the reference structures. Secondly, the force field was used for the minimization of 100 structures and the error in density and energy was examined. Finally, the Gibb's energy was calculated for all structures. After applying different filters and cleanser did remain 247 344 crystal structures.

In our analysis of the results we concentrated on crystal structures with a Gibbs energy above zero. Obviously these structures violates the second law of thermodynamics. A visualization of the intermolecular interactions did allow us to indicate poor intermolecular potentials and faulty crystal structures. The condition is fulfilled in 96.7 % of structures.

The data mining force field is integrated in the FlexCryst program suite and we tested it crystal structure prediction and in combination with XPRD for crystal structure determination. Since the obtained energies are Gibb's energies, the energies can be used to predict reactions at ambient conditions, for instance solubility [2], co-crystal formation [3], or polymorphism.

References

[1] Hofmann, Detlef WM., "Data mining in organic crystallography," in *Data Mining in Crystallography*, Berlin, Heidelberg, Germany: Springer, 2009, pp. 89–134.

[2] Hofmann, Detlef Walter Maria, and Ludmila Kuleshova, "New similarity index for crystal structure determination from X-ray powder diagrams," *J. Appl. Crystallogr*, vol. 38, no. 6, pp. 861–866, 2005.

[3] Stepanovs, Dmitrijs *et al.*, "Cocrystals of pentoxifylline: In silico and experimental screening," *Cryst. Growth Des.*, vol. 15, no. 8, pp. 3652–3660, 2015.

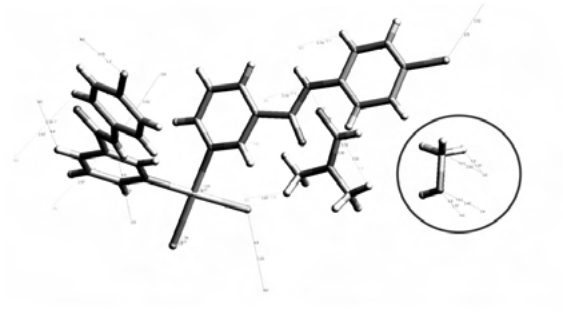

Figure 1 The hydrate of the ruthenium complex (CSD reference code: AMUPUU) show strong repulsive interactions between two water molecules. It indicates that water should be placed different in the correct structure.

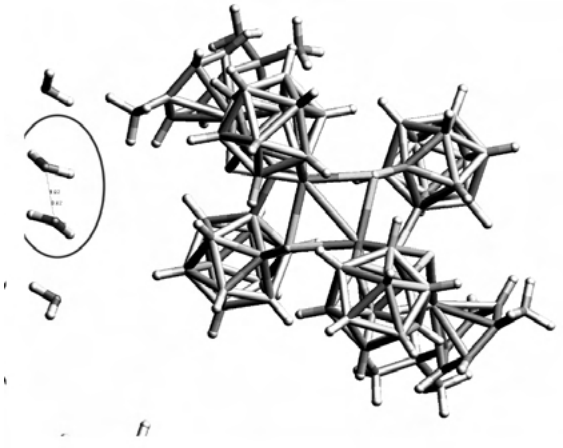

Figure 2 The co-crystal (CSD reference code: ALARAH) of a platinum complex with methanol show strong repulsive interactions between methanol and it image. It indicates that methanol should be placed different in the correct structure.

Chaperone Compounds for Co-crystallization of Organics

T. Stuerzer[1], M. Adam[1], W. Frey[1], F. Krupp[1], F. Rami[1], C. Richert[1]

[1] MA: Bruker AXS GmbH, Karlsruhe, Germany

Modern instrumentation and processing techniques for single crystal X-ray diffraction enable high-quality 3D structure analysis – including absolute structure determination – often in less than an hour, faster and more comprehensively than many spectroscopic methods can even start to achieve. However, large numbers of small or highly flexible organic molecules remain intractable to even the most sophisticated crystallization methods. Our new set of chemical chaperones for co-crystallization [1] offers a new alternative to other methods, such as the crystal-sponge approach [2], [3], can significantly increase the probability of successful crystallization and provides faster access to the absolute 3D structure of an organic analyte:

- The chaperone method is fast and easy to use
- Structures in hours rather than weeks
- Small quantities of analyte required
- Excellent quality crystals
- 88% diffraction-quality crystals from a 52 organic compounds test screen
- The chaperone compounds are highly stable
- 100% analyte occupancy in the crystal guarantees reliable determination of the absolute configuration.

We will discuss and demonstrate the features in detail along the diastereomers of Limonene including a demonstration of the crystal growth.

References

[1] Richert *et al.*, *Angew. Chem. Int. Ed.*, vol. 59, pp. 15875–15879, 2020, doi: 10.1002/anie.202004992.

[2] Fujita *et al.*, *IUCrJ*, vol. 3, pp. 139–151, 2016, doi: 10.1107/S2052252515024379.

[3] Clardy *et al.*, *Acta Cryst. A*, vol. 71, pp. 46–58, 2015, doi: 10.1107/S2053273314019573.

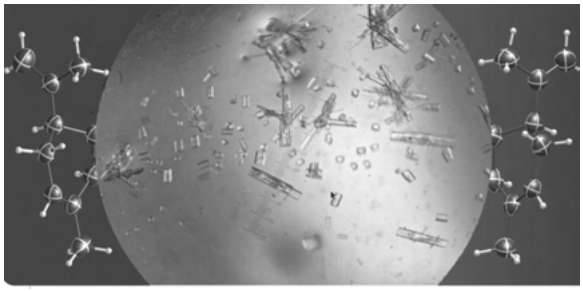

Figure 1

Quantum crystallography

Relativistic Hirshfeld atom refinement of an organo-gold(I) compound

S. Pawlędzio[1], M. Malinska[1], M. Woińska[1], J. Wojciechowski[2], L. A. Malaspina[3], F. Kleemiss[3], S. Grabowsky[3], K. Woźniak[1]

[1] Biological and Chemical Research Centre, Department of Chemistry, University of Warsaw, Warsaw, Poland

[2] Rigaku Europe SE, Neu-Isenburg, Germany
[3] University of Bern, Department of Chemistry and Biochemistry, Bern, Switzerland

During the last 50 years, relativistic quantum chemistry has undergone significant developments and methodological progress. Nowadays, it is well-known that a relativistic quantum formalism is necessary for the study of compounds with heavy elements [1-3].

Within last years it has appeared that quantum crystallography is a very prospective method of refinement of crystal structures. It relies on the high-resolution and high-quality XRD data to describe crystal structure in unprecedented details [4-5]. Intensities of the diffracted beam are affected not only by relativistic effects but also by many other effects such as absorption [6], anharmonic motion [7], anomalous dispersion [8], and others effects which significantly influence electron density distribution in the crystal and, in consequence, derived properties.

In this study, we validated relativistic Hirshfeld atom refinement (HAR) [9] as implemented in Tonto [10] by performing refinement of experimental high-resolution X-ray diffraction data for an organo-gold(I) compound. The influence of relativistic effects on statistical parameters, geometries and electron density properties was analyzed and compared to the influence of electron correlation and anharmonic atomic motions.

Acknowledgement
Support of this work by the National Science Centre, Poland through grant PRELUDIUM no. UMO-2018/31/N/ST4/02141 is gratefully acknowledged. The experiment was carried out at the Spring-8 with the approval of the Japan Synchrotron Radiation research Institute (Proposal Number 2019A1069).

References

[1] I. P. Grant, Advances in Physics, 1970, 19, 747–811.
[2] J. P. Desclaux, Atomic Data and Nuclear Data Tables, 1973, 12, 311–406.
[3] T. Ziegler, J. G. Snijders and E. J. Baerends, The Journal of Chemical Physics, 1998, 74, 1271.
[4] L. J. Farrugia, C. Evans, D. Lentz and M. Roemer, Journal of the American Chemical Society, 2009, 131, 1251–1268.
[5] T. S. Koritsanszky and P. Coppens, Chem. Rev., 2001, 101, 1583–1628.
[6] J. Als-Nielsen and D. McMorrow, in Elements of Modern X-ray Physics, John Wiley & Sons, Ltd, 2011, pp. 1–28.
[7] R. Herbst-Irmer, J. Henn, J. J. Holstein, C. B. Hübschle, B. Dittrich, D. Stern, D. Kratzert and D. Stalke, The Journal of Physical Chemistry A, 2013, 117, 633–641.
[8] S. Caticha-Ellis, Anomalous dispersion of x-rays in crystallography, University College Cardiff Press, Cardiff, Wales, 1981.
[9] L. Bučinský, D. Jayatilaka and S. Grabowsky, The Journal of Physical Chemistry A, 2016, 120, 6650–6669.
[10] D. Jayatilaka and D. J. Grimwood, Acta Crystallographica Section A, 2001, 57, 76–86.

Spectroscopy

MagStREXS: A crystallograhic software for magnetic structure determination from resonant magnetic X-ray diffraction data

P. J. Bereciartua[1], J. Rodríguez-Carvajal[2], S. Francoual[1]
[1] DESY, Photon Science, FS-PETRA-S, Beamline P09, Hamburg, Germany
[2] Institut Laue-Langevin, Grenoble, France

Resonant X-ray elastic scattering (REXS) is a unique element, site, and valence specific probe to study the charge, spin and orbital degrees of freedom and multipole orders in solids and thin films [1,2]. This technique, which combines X-ray diffraction with X-ray absorption spectroscopy, has been successful in unraveling different order parameters and solving magnetic structures.

REXS is complementary to neutron techniques for magnetic structure determination. Several situations make it essential: when the magnetic species involved present a neutron absorption cross-section too large, like Eu, Dy, Gd... [3], when the magnetic moments cannot be determined unambiguously with neutron experiments [4], or when more than one magnetic species is involved.

Different types of data can be collected during a REXS experiments: intensities of a set of magnetic reflections, full linear polarization analysis of a specific magnetic reflection, or its azimuthal dependence. The analysis of these data is highly complex and no crystallographic software has been developed yet to enable users to solve magnetic structures from a REXS experiment.

MagStREXS is a crystallographic software dedicated to the determination of **Mag**-netic **St**-ructures through **R**-esonant **E**-lastic **X**-ray **S**-cattering and the preparation of magnetic diffraction experiments. It is under development since mid-2017 at beamline P09 [5] at PETRA III

at DESY and based on CrysFML, a library developed to facilitate the creation of crystallographic software that includes some resources especially oriented to deal with magnetic structures.

Hereby, we will present an overview of MagStREXS, its current status and some of the magnetic structures which have already been solved with it in the field of highly correlated systems.

References

[1] J. P. Hill and D. F. Mc Morrow, *Acta Cryst. A*, vol. 52, pp. 236–244, 1996.

[2] Y. Murakami and S. Ishihara, *Resonant X-Ray Scattering in Correlated Systems* in Springer Tracts in Modern Physics, vol. 269, Berlin, Heidelberg, Germany: Springer, 2017.

[3] T. Kurumaji *et al.*, "Skyrmion lattice with a giant topological Hall effect in a frustrated triangular-lattice magnet," *Science*, vol. 365, pp. 914–918, 2019.

[4] J. Sears *et al.*, "Ferromagnetic Kitaev interaction and the origin of large magnetic anisotropy in α-$RuCl_3$," *Nature Physics*, vol. 16, pp. 837–840, 2020.

[5] J. Strempfer, S. Francoual, *et al.*, *Synchrotron Rad.*, vol. 20, pp. 541–549, 2013.

An Anomalous Diffraction study of $Cu_2Zn(Ge,Si)Se_4$

D. M. Többens[1], G. Gurieva[1], S. Niedenzu[1], S. Schorr[1]

[1] Helmholtz-Zentrum Berlin (HZB), Hahn-Meitner-Platz 1, 14109 Berlin, Germany

While the silicon-rich members of the series $Cu_2Zn(Ge,Si)Se_4$ crystallize in wurtz-kesterite type structure [1], germanium-rich samples adopt a tetrahedral structure of the kesterite type [2]. Identification of the silicon site is straightforward from regular X-ray diffraction, as Si^{4+} is a light element and has less electrons than the other cations. However, Cu^{1+}, Zn^{2+}, and Ge^{4+} are all isoelectronic and have very similar form factors. The kesterite type of the cation distribution has been established by neutron diffraction [2].

We now applied anomalous X-ray diffraction to this system, using Rietveld refinement and Multiple Edge Anomalous Diffraction (MEAD) [1] with data taken at the K-absorption edges of Cu, Zn, and Ge. These energies are accessible at beamline KMC-2, BESSY II, Berlin [3]. In contrast to previous studies, where Sn^{4+} was the M(IV) species in the structure [1], in $Cu_2ZnGeSe_4$ all cations have very similar scattering power under normal conditions. This results in superstructure peaks (with respect to the cubic ZnS parent structure) that are very weak. For Rietveld analysis this is a drawback, as the optimization will be dominated by the main peaks of the parent structure. In MEAD, however, it increases the effect of the changing scattering power close the absorption edges. As a result, not only are Kesterite and Stannite types clearly distinguishable at the Cu-K edge (figure 1), also the Cu/Zn ordering within the Kesterite structure is clearly detectable and quantifiable at the Zn-K edge. The structure of the MEAD spectrum at the Ge-K edge was found to be very sensitive to the presence of vacancies at the Ge 2*b* site of the structure at the Si-free composition. Within the compositional range, Si^{4+} has very similar influence.

References

[1] D. M. Többens *et al.*, "Cation distribution in $Cu_2ZnSnSe_4$, Cu_2FeSnS_4 and $Cu_2ZnSiSe_4$ by multiple-edge anomalous diffraction," *Acta Crystallographica B*, vol. 76, pp. 1027–1035, 2020.

[2] G. Gurieva *et al.*, "Cu-Zn disorder in $Cu_2ZnGeSe_4$. A complementary neutron diffraction and Raman spectroscopy study," *Journal of Physics and Chemistry of Solids*, vol. 99, pp. 100–104, 2016.

[3] Helmholtz-Zentrum Berlin für Materialien und Energie, "KMC-2: an X-ray beamline with dedicated diffraction and XAS endstations at BESSY II," *Journal of large-scale research facilities*, vol. 2, 2016, Art. no. A49.

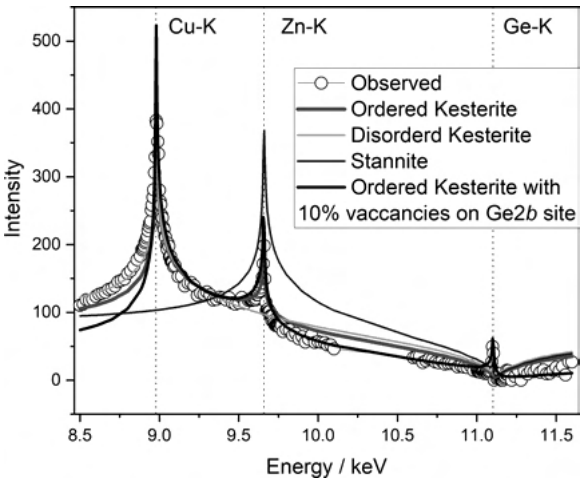

Figure 1 Observed and simulated MEAD spectra of Bragg peak 011 of $Cu_{2.03}Zn_{1.060}Ge_{0.947}Se_4$. The structure is highly ordered Kesterite. The peak at the Ge-edge indicates $\leq$10% vacancies at the Ge 2b site.

Analysis of potentially Ferroelectric Strontium Titanate Thin Films with Resonant X-ray Diffraction and Density Functional Theory

M. Nentwich[1], C. Richter[2], M. Zschornak[3], T. Weigel[2], D. C. Meyer[3], D. Novikov[1]
[1] P23 Beamline, PETRA-III, DESY, Hamburg, Germany
[2] Leibniz Institut für Kristallzüchtung, Berlin, Germany
[3] TU Bergakademie Freiberg

Ferroelectric materials possess a spontaneous polarisation that can be electrically switched between different orientations. Compared to ferromagnetics, the domain walls are small, allowing memory cells of higher storage density. Thin films of ferroelectric materials allow to increase the storage density even further. Exemplarily, incipient ferroelectricity is found in strontium titanate SrTiO3 (STO) at a low transition temperature. This ferroelectricity can be stabilized by a variety of external factors such as doping, strain, electric field, isotope substitution etc., even up to room temperature.

Recently, we studied the effect of the electroformation of STO and the accompanied creation of the *migration-induced field-stabilized polar* (MFP) phase [1] extensively, *i.e.* with the newly developed approach of *Resonantly Suppressed Diffraction* (RSD) [2] at Beamline P23 of PETRA III. Because of the breakdown of Friedel's law under resonant conditions, RSD can be used to obtain information about the polarization state of polar materials, namely by monitoring the Bragg intensity while scanning the energy of the incident beam through the absorption edge of strontium.

Here, we transferred this methodology to ferroelectric STO thin films and measured the energy dependent intensities for different Bragg reflections. As underlying structure model, we combined the structure of the low temperature antiferrodistortive (AFD) phase and of a generalized MFP phase. The resulting structure is ferroelectric and rather unknown within the perovskites. The energy dependent intensities of the chosen reflections of simulated data were fitted against the experimental values. Additionally, we performed *Density Functional Theory* (DFT) calculations to determine the atomic displacements from the lattice parameters at the different low temperatures. The results show that the major structural components within those STO thin films are the AFD displacements, while the MFP displacements are negligible.

References

[1] J. Hanzig, M. Zschornak, F. Hanzig, E. Mehner, H. Stöcker, B. Abendroth, C. Röder, A. Talkenberger, G. Schreiber, D. Rafaja, S. Gemming, D. C. Meyer: Migration-induced field-stabilized polar phase in strontium titanate single crystals at room temperature, Physical Review B 88, 024104 (2013).
[2] C. Richter, M. Zschornak, D. Novikov, E. Mehner, M. Nentwich, J. Hanzig, S. Gorfman, D. C. Meyer: Picometer polar displacements in strontium titanate determined by a new approach of resonant x-ray diffraction, Nature Communications 9, 178 (2018).

Young crystallographers: Lightning talks

A Crystallographic and Spectroscopic Investigation of Photo-Induced Electron Transfer in Pyrene-(CH2)2-N,N'-Dimethylaniline: Time-Resolved Studies in Solutions and Polymorphic Crystals.

K. Basuroy[1], J. D. J. Velazquez-Garcia[1], D. Storozhuk[1], D. Gosztola[1], S. Thekku Veedu[1], S. Techert[1]
[1] DESY, Hamburg, Germany

Photo-induced electron transfer reactions are crucial for many of the biological and chemical reactions that occur in nature. According to Marcus and others, electronic coupling between an electron donor and acceptor must be nonzero, for a successful electron transfer reaction. [1] Several studies are performed in order to have a better understanding of the photoinduced intramolecular electron transfer, in terms of the rate of transfer and the overall geometry of the donor-bridge-acceptor (D-B-A) system.[2] Pyrene and its derivatives, owing to their high quantum efficiency, high fluorescence lifetimes, prone to form excimers or exciplex in high concentrations and highly sensitive nature of their photophysical properties to microenvironmental changes, are considered extremely useful for photoinduced electron transfer studies.[3] We have designed a mono-substituted pyrene derivative, pyrene-(CH2)2-N, N'-dimethylaniline, where dimethylaniline (DMA) (electron donor) is connected to pyrene (electron acceptor, in this case) through alkane chain. The distance between the donor and acceptor in this molecule is expected to be suitable for electron transfer by tunneling mechanism. A serendipitous occurrence of two polymorphic crystals from two separate batches of crystallization setup, while dissolved in ethanol, provided us a unique opportunity to study these two conformational polymorphs, A and B. While, in A crystal

structure pyrene and dimethylaniline are in axial orientation (P-1) with respect to each other, in B they are equatorial (P21/n). Studies on photo-induced intramolecular electron transfer has revealed the importance of conformational parameters of the molecules such as rotation around bonds that affects the distance and relative orientation of donor and acceptor which in turn can proved to be quite decisive in the photo-physical properties of charge transfer states. [4] We have performed time-resolved Laue diffraction experiments with these two polymorphic crystal forms in the ns time domain. Apart from steady-state spectroscopy, we have also measured ultrafast transient absorption with the solution, at different concentrations. A thorough crystallographic and spectroscopic investigation of this particular system, especially with the polymorphic crystals have allowed us to understand the important aspects of photo-induced electron transfer.

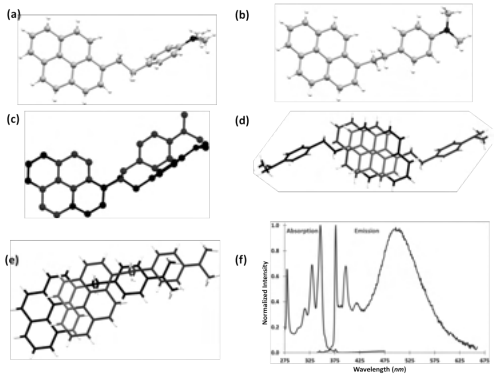

Figure 1 Conformation of molecules in single crystals, a) PyDMA1 and b) PyDMA2. c) Molecular superposition of PyDMA1 (black) and PyDMA2 (red) on pyrene ring with RMSD=0.0427Å. The extent of overlap between the pyrene rings belong to the symmetry related/unit translated molecules in PyDMA1/PyDMA2 in single crystals are 67% and 17%, respectively. f) Absorption (blue) and emission (red) spectra of PyDMA1, in toluene, at 0.1mM concentration.

References

[1] Jortner, J; Bixon, M. Electron Transfer-From Isolated Molecules to Biomolecules, Part 1 and Part 2; John Wiley & Sons, Inc: New York, 1999.

[2] a) Paddon-Row, M. N. Acc. Chem. Res. 1994, 27, 18. b) M. D. Newton, Chem. Rev., 1991, 91, 767.

[3] Stockmann,A; Kurzawa, J.; Fritz, N.; Acar, N.; Schneider, S.; Daub, J.; Engl, R. and Clark. T. J. Phys. Chem. A 2002, 106, 7958.

[4] a) Bleisteiner, B.; Marian, Th.; Schneider, S.; Brouwer, A. M.; Verhoeven, J. W. Phys. Chem. Chem. Phys. 2001, 3, 2070.

b) Verhoeven, J. W.; Wegewijs, B.; Scherer, T.; Rettschnik, R. P. H.; Warman, J. M.; Jäger, W.; Schneider, S. J. Phys. Org. Chem. 1996, 9, 387.

(c) Wegewijs, B.; Ng, A. K. F.; Verhoeven, J. W. Recl. TraV. Chim. Pays-Bas 1995, 114, 6. (d) Jäger, W.; Schneider, S.; Lauteslager, X. Y.; Verhoeven, J. W. J. Phys. Chem. 1996, 100, 8118.

(e) Lauteslager, X. Y.; van Stokkum, I. H. M.; van Ramesdonk, H. J.; Brouwer, A. M.; Verhoeven, J. W. J. Phys. Chem. 1999, 103, 653. (f) Jäger, W.; Schneider, S.; Verhoeven, J. W. Chem. Phys. Lett. 1997, 270, 50.

How Occupancy Disorder Impacts Magnetism in Topological Insulators

L. Folkers[1], A. Isaeva[1]

[1] Technische Universität Dresden, Dresden, Germany

Magnetic topological insulators (MTIs) are a hot topic of materials science, promising future availability of spintronics with low energy consumption, quantum computing and phenomena like the Quantized Anomalous Hall Effect (QAHE) [1-2]. MTIs are chemically and structurally akin to the original non-magnetic topological insulators. Of those, the tetradymites Bi2Te3 and Sb2Te3 have recently proven to allow the introduction of a third magnetic element resulting in magnetically active, topologically non-trivial compounds. A magnetic element can be incorporated either via substitution on the Bi/Sb position in (Bi, Sb)2Te3, or by adding a third element which introduces a new crystallographic site, resulting for example in (MnBi2Te4)(Bi2Te3)m (m = 0, 1, 2). (Bi, Sb)2Te3 itself and all members of its family exhibit the rhombohedral R -3 m 1 space group (No. 166) [2]. Therein interchanging sheets of (Bi, Sb) and Te build (Bi, Sb)2Te3 quintuple layers and Mn, (Bi, Sb) and Te build septuple layers with the central sheet being Mn (Wyckoff position 3a). Situated between the respective layers is a Van der Waals gap (Fig. 1) and depending on m, various stacking orders can be observed. Our group was the first to successfully grow single crystals, and conduct an in depth study of the physical properties of MnBi2Te4, the m = 0 member of the above discussed MTI family [4-5]. Single crystal diffraction experiments reported in

that study showed intermixing of Mn and Bi and since then several studies have reported intermixing of the two elements (MnBi2.14Te3.96 [6], Mn1.01Bi1.99Te4 and Mn0.98Bi2.05Te4 [7]). While a lot of attention has been given to MnBi2Te4 and its higher order relatives, MnSb2Te4 proved to be synthetically achievable too. Similar to MnBi2Te4, MnSb2Te4 features intermixing of Mn and Sb (Mn0.852Sb2.296Te4 [8]). For MnSb2Te4, a recent study by Murakami et al. uncovers the impact of finding a certain amount of the magnetic Mn on the position of the non-magnetic Sb [9]. According to their discoveries, this changes the magnetic order from antiferromagnetic to ferrimagnetic. These compounds are known to react sensitively to synthesis procedure and tempering history. Hence, our studies aim at understanding the greater connection between synthesis aspects and the resulting structural and physical properties. More precisely we studied MnBi2Te4 and MnSb2Te4 containing various amounts of Mn and other analogues of these systems.

References

[1] Y. Ando, *Journal of the Physical Society of Japan*, (2013), *82*, 102001.
[2] I. I. Klimovskikh, M. M. Otrokov, D. Estyunin, et al., *Quantum Materials*, (2020), *54*.
[3] Y. Feutelais, B. Legendre, N. Rodier, V. Agafonov, *Materials Research Bulletin*, (1993), *28*, 591-596
[4] A. Zeugner, F. Nietschke, A. U. B. Wolter, et al., *Chemistry of Materials*, (2019), *31*, 2795-2806.
[5] M. M. Otrokov, I. I. Klimovskikh, H. Bentmann, et al., *Nature*, (2019), *576*, 416-422.
[6] H. Li, S. Liu, C. Liu, et al., *Physical Chemistry Chemical Physics*, (2020), *22*, 556-563.
[7] M.-H. Du, J. Yan, V. R. Cooper, M. Eisenbach, *Advanced Functional Materials*, (2020), 2006516.
[8] L. Zhou, Z. Tan, D. Yan, et al., *Physical Review B*, (2020), *102*, 85114.
[9] T. Murakami, Y. Nambu, T. Koretsune, et al., *Physical Review B*, (2019), *100*, 195103.

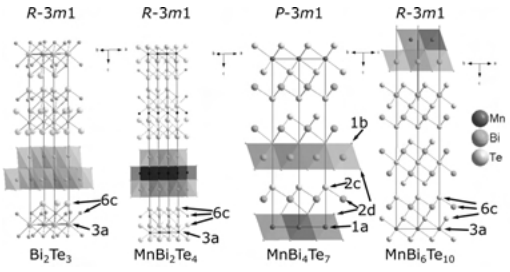

Figure 1 The structure of Bi2Te3 [3] and the stacking variants (MnBi2Te4)(Bi2Te3)m (m = 0 - 2). For clarity, only 1/3 of the unit cell of MnBi6Te10 is displayed.

MOFs of a O,P,N heterotritopic Ligand – One reaction, two networks – A topological analysis

H. Gildenast[1], U. Englert[1]
[1] RWTH Aachen University, Institute of Inorganic Chemistry, Aachen, Germany

The field of metal-organic frameworks (MOFs) is dominated by the chemistry of oxygen and nitrogen donor based ligands [1]. Next to no work revolves around polytopic ligands containing phosphorus donors.

The usage of phosphorus widens the horizon of MOF chemistry. It may broaden the structural variety, enable new applications and stabilize metal cations in low oxidation states that were previously inaccessible to MOF chemists.

The ligand 4-(3-(4-(diphenylphosphino)phenyl)-3-oxopropanoyl)benzonitrile is a prototype for the combination of the three donor atoms O, P and N. It combines a chelating beta-diketone as the oxygen donor, a nitrile representing the nitrogen donors and a triarylphosphine as a phosphorus based ligand functionality.

Using a stepwise approach we were able to synthesize a cationic heterobimetallic Fe^{III}/Ag^{I} MOF with Fe^{III} bound to the oxygen donors and Ag^{I} bound to the P and N donors. The network can emerge in 2 different topologies while the chemical connectivity remains unchanged. Type **A** corresponds to the rtl network type [2], Type **B** has not been observed yet. Both have a three dimensional pore system. The pores are large enough so a sphere with a diameter of 4 Å could move through them along all low-indexed directions.

References

[1] F. Almeida Paz, *Chem. Soc. Rev.*, vol. 41, p. 1088, 2012.
[2] M. O'Keeffe *et al.*, *Acc. Chem. Res.*, vol. 41, p. 1782, 2008.

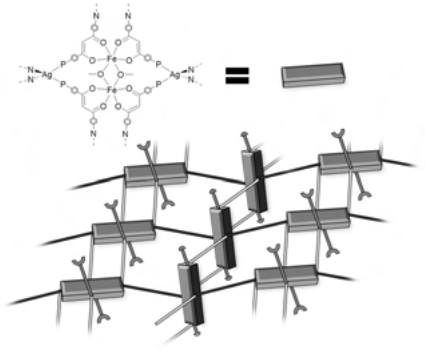

Figure 1

Coordination Polymers featuring Dibenzoyltartaric and Ditoluoyltartaric Acid: A different approach to a popular compound.

M. Kremer[1], U. Englert[1]

[1] RWTH Aachen University, Institute of Inorganic Chemistry, Aachen, Germany

The two tartaric acid derivatives dibenzoyltartaric acid (DBTA) and di-*para*-toluoyltartaric acid (DPTTA) are common compounds in organic chemistry and pharmaceutical science, where they mostly function as derivatisation agents or as chiral templates. There are currently about 250 crystal structures featuring either of the acids deposited in the CCDC [1]. While the compounds are decent chelating ligands with the ability to extend bridges to neighbouring metal centres to form coordination polymers, they are hardly used in this capacity. Less than 40 structures featuring both carboxylato groups connected to a metal are deposited in the CCDC currently.

Our work focusses on the synthesis of coordination polymers with dicarboxylic acids, including tartaric acid and the titular derivatives thereof [2,3]. During these experiments, several new compounds featuring DBTA or DPTTA were synthesised, crystallized, and characterized. In this presentation we showcase several of these compounds, discuss structural similarities and differences as well as the influence of different metals, coligands or stereoisomers on the resulting structures.

References

[1] C. R. Groom, I. J. Bruno, M. P. Lightfoot and S. C. Ward, *Acta Cryst. B*, vol. 72, pp. 171-179, 2016, DOI: 10.1107/S2052520616003954.

[2] M. Kremer, J. van Leusen, U. Englert, *Crystals*, vol. 10, 2020, DOI: 10.3390/cryst10060485.

[3] M. Kremer, Dissertation, RWTH Aachen, Germany, 2020.

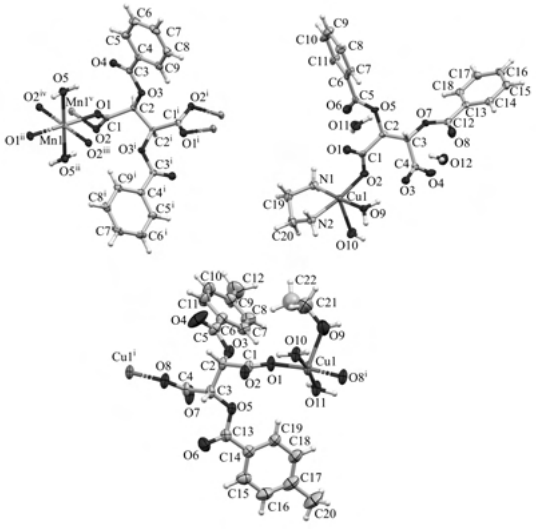

Figure 1

Encapsulation of inorganic nanoparticles into novel T. maritima encapsulin variants

M. Rütten[1], T. Beck[1]

[1] University of Hamburg, Department of Chemistry, Institute of Physical Chemistry, Hamburg, Germany

Supported by an established synthetic strategy towards optical materials protein containers and nanoparticles are used. With protein containers as building blocks, nanoparticles will be assembled with high precision into mesoscale materials with optical properties that emerge from interactions between the components. Along the recent advances in computational redesign of protein containers, it is now possible to combine these results with nanoparticle synthesis and protein crystallography. An innovative design approach with two oppositely charged protein containers as building blocks, a new type of protein-based material will be realized (Figure 1). Surface charged protein containers can be combined with inorganic compounds to unite biological features with the chemical and physical properties of abiotic materials. In particular, protein containers, with their inherent ability to encapsulate cargo molecules, are perfect platforms for the generation of multifunctional assemblies.[1, 2] Gold nanoparticles can be decorated with a small number of encapsulin cargo-loading peptides to fill protein containers. By lock-and-key interaction between the peptides and the peptide-binding pockets on the inner container surface (Figure 2), the nanoparticles will be encapsulated with high efficiency.[3] Typically encapsulin bears a flavin that is attached to the outer surface. The flavin leads to a yellow coloured solution and its presence on the protein surface might be problematic

for future applications or in crystallization. Based on the latest cryo-EM data it was possible to remove the flavin.[4] Crystalline materials are produced, which is crucial for future applications. Because the protein scaffold is independent of the nanoparticle cargo, this modular approach will enable tuning of the optical properties by choice of nanoparticle content, assembly type and protein container type. For further future applications, surface charged protein containers will be used as sustainable building blocks for bioinorganic nanomaterials.[5]

References

[1] M. Künzle, T. Eckert, T. Beck, *J. Am. Chem. Soc.*, vol. 138, p. 12731, 2016.
[2] M. Lach, M. Künzle, T. Beck, *Chem. Eur. J.*, vol. 23, p. 17482, 2017.
[3] M. Künzle, J. Mangler, M. Lach, T. Beck, *Nanoscale*, vol. 10, pp. 22917–22926, 2018.
[4] D. Diaz *et al.*, *bioRxiv*, preprint, 2020.
[5] M. Lach, M. Künzle, T. Beck, *Biochemistry*, vol. 58, pp. 140–141, 2019.

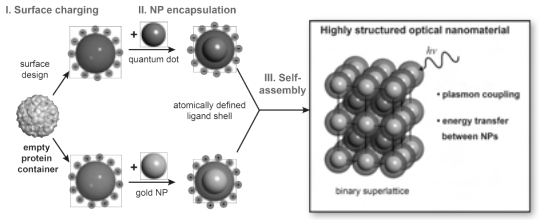

Figure 1 Strategy overview for the synthesis of highly structured optical nanomaterial.

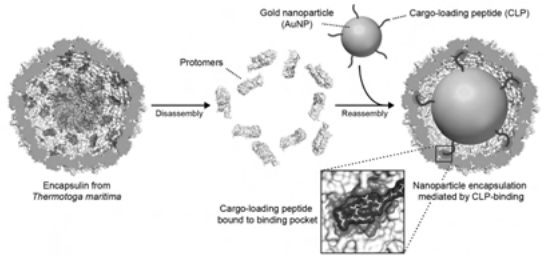

Figure 2 Gold nanoparticle encapsulation via cargo-loading peptide into T. maritima encapsulin.

A One-Dimensional Heterobimetallic Fe(III)/Hg(II) Coordination Polymer Linked by a Ditopic Pyrazole Substituted Acetylacetone

S. van Terwingen[1], B. Ebel[1], U. Englert[1]
[1] RWTH Aachen University, Institute of Inorganic Chemistry, Aachen, Germany

Due to their vast applications monometallic coordination polymers (CPs) have increasingly attracted the interest of various fields over the last years.[1] We focus on using heterofunctional ligands to synthesize heterobimetallic CPs, combining the properties of two metals in one homogenous material.[2] Our stepwise approach includes the synthesis of a metalloligand and, afterwards, its crosslinking using a second metal cation. Herein we present this approach for the ligand (3-(1,3,5-trimethyl-4-1H-pyrazolyl)acetylacetone (HacacMePz) with its heterobimetallic coordination polymer containing Fe(III) and Hg(II).

The CP crystallizes as an acetonitrile solvate in the triclinic space group $P\bar{1}$ with $Z = 2$. The [Fe(acacMePz)$_3$] metalloligands are linked by $Hg_2(\mu_2\text{-}Cl)Cl_3$ moieties. While the coordination sphere around the Fe(III) ion is a rather regular octahedron, the two symmetry inequivalent Hg(II) ions adopt distorted tetrahedral coordination environments (τ_4 = 0.82, 0.76).[3] Interestingly, only one chlorido ligand is bridging and the other three are bound to one Hg(II) ion. This connectivity leads to an one-dimensional CP with a ladder-like structure as seen in Figure 1. The polymer expands in [1 -1 1] direction without any meaningful interactions between adjacent chains.

References

[1] S. R. Batten, S. M. Neville, D. R. Turner, *Coordination Polymers: Design, Analysis and Application*, Cambridge: RSC Publishing, 2009.
[2] M. Kremer, U. Englert, *Z. Kristallogr.*, vol. 233, pp. 437-452, 2018.
[3] A. W. Addison, T. N. Rao, *J. Chem. Soc., Dalton Trans.*, vol. 1984, pp. 1349-1356, 1984.

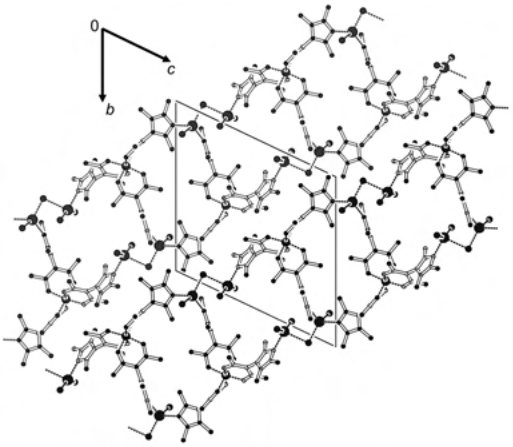

Figure 1

Poster

Bio-crystallography

High-resolution crystal structure and biochemical characterization of a GH11 endoxylanase from Nectria haematococca

H. Andaleeb[1], C. Betzel[1], H. Brognaro[1], S. Falke[1], N. Ullah[1], M. Perbandt[1]

[1] Institute of Biochemistry and Molecular Biology, Laboratory for Structural Biology of Infection and Inflammation, University of Hamburg,, DESY, Hamburg, Germany

Biofuels are one of the important and renewable energy sources, obtained from lignocellulosic waste materials by utilizing special enzymatic cocktails (1). Biofuels can replace fossil fuels to a large extend and in parallel reduce carbon dioxide emission and global warming. Xylanases play crucial role in the hemicellulose biodegradation within the industrial biofuel preparation processes and are in focus of structure-function analyses for many years (2). In this context we anlaysed a xylanase from *Nectria haematococca* (NhGH11) and solved the three-dimensional structure to atomic 1.0 Å resolution. At this resolution the positions of hydrogen atoms in the active site cleft could be identified. Data obtained highlight the potential of NhGH11 to be applied in industrial biomass degradation processes, in which the catalysis of xylan biopolymers can produce sustainable chemicals and bio-based commercial eco-friendly materials. Functional and structural details will be presented.

References

[1] Raud, M., Kikas, T., Sippula, O., & Shurpali, N. J. (2019). Renewable and Sustainable Energy Reviews, 111, 44-56.

[2] Paës, G., Berrin, J. G., & Beaugrand, J. (2012). Biotechnology advances, 30(3), 564-592.

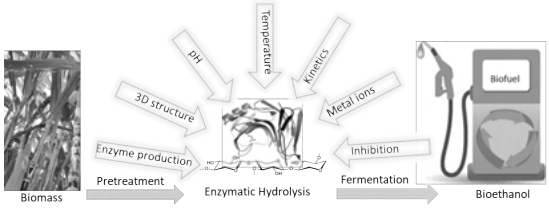

Figure 1 Graphical abstract, presenting a summary of the structural and biochemical analysis of NhGH11.

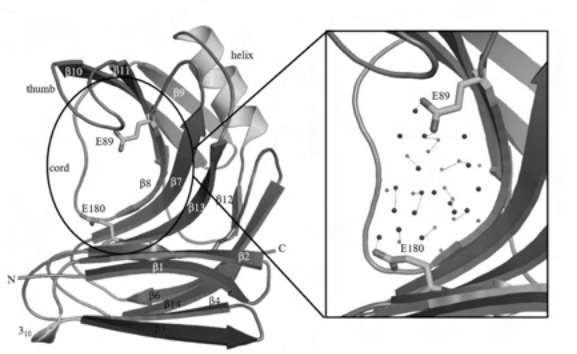

Figure 2 Cartoon plot of NhGH11 with catalytic active residues are shown in sticks. A zoom of the active site region is shown (right figure), with catalytic residues surrounded by solvent molecules in the active site cavity.

XDSAPP3 – the new graphical user interface for the convenient processing of diffraction data using XDS

T. Hauß[1], K. Röwer[1], U. Mueller[1], M. S. Weiss[1]

[1] Helmholtz-Zentrum Berlin, Macromolecular Crystallography, Berlin, Germany

For many years, XDSAPP [1] is a well-known program to (semi-) automatically process diffraction data using XDS [2]. Here, the new version XDSAPP3 is presented, with improvements in the graphical user interface (GUI) as well as in the underlying Python code. The main motivations for the upgrade of XDSAPP were the nowadays widespread use of Dectris EIGER detectors and the phasing out of the Qt 4 framework, with the last release already in 2011, and Python 2.7, its end-of life was finally reached in 2020. XDSAPP3 is written in Python 3 and utilizes the PyQt 5 framework for the GUI and the matplotlib library. EIGER detectors are now supported by using the generate_XDS.INP script [3] in combination with the XDS plugins dectris-neggia [4] from Dectris or durin-plugin [5] from Diamond. Various important statistics generated from the XDS output files are presented in 2-D plots for the convenient inspection of the results. In the command-line version, a multi-dataset mode is implemented for batch processing of multiple datasets. If used on the beam-line, it will process new incoming data as soon as available. XDSAPP3 has been tested on various Linux distributions, like RHEL 6,7 , openSUSE 15, centOS 6, and Kubuntu 20, as well as macOS 10.13 High Sierra through 11.1 Big Sur. The development team may be contacted at xdsapp@helmholtz-berlin.de.

References

[1] Sparta, K., Krug, M., Heinemann, U., Mueller, U., Weiss, M. S., *J. Appl. Cryst.*, vol. 49, pp. 1085-1092, 2016.
[2] Kabsch, W., *Acta Cryst. D*, vol. 66, pp. 125-132, 2010.
[3] Diederichs, K.,
https://strucbio.biologie.uni-konstanz.de/xdswiki/
/index.php/Generate_XDS.INP
[4] https://www.dectris.com
[5] https://github.com/DiamondLightSource/durin

Low dose measurements for spatially resolved anomalous dispersion refinement

F. Lennartz[1], J.-H. Jeoung[2], H. Dobbek[2], M. Weiss[1]

[1] Helmholtz-Zentrum Berlin, Departement of Photon Science, Macromolecular Crystallography, Albert-Einstein-Straße 15, 12489 Berlin, Germany

[2] Humboldt University of Berlin, Berlin, Germany

Spatially resolved anomalous dispersion (SpReAD) refinement is a method to analyse the oxidation states of individual protein-bound metals and is based on collecting several x-ray diffraction datasets across an x-ray absorption edge. Such an approach can expose crystals to relatively high total dose of radiation. This can result in radiation damage, including reduction of metals.

Here, we have conducted experiments for SpReAD analysis on HZB MX beamline 14.1. To analyse the effect of dose on the result of the experiments, we have tested different transmission settings to vary the total dose per experiment and test whether data collected at low transmission are suitable for SpReAD refinement.

High-pressure macromolecular crystallography

J. Lieske[1], S. Saouane[2], S. Guenther[3], P. Reinke[4], T. Pakendorf[2], B. Reime[2], E. Crosas[4], J. Hakanpaeae[2], H. Chapman[1], A. Meents[3]

[1] FS-CFEL-1 (CFEL-Coherent X-Ray Imaging), Hamburg, Germany

[2] FS-PETRA-D (FS-PET-D Fachgruppe P11), Hamburg, Germany

[3] FS-BMX (FS-CFEL-1 Fachgruppe BMX), Hamburg, Germany

Pressure and temperature are physical parameters that define the free energy landscape of proteins and hence their conformational space. Studying the influence of these thermodynamic parameters on the structure and function of proteins provides the basis for understanding fundamental principles of biological processes, ranging from enzymatic reaction mechanisms to protein folding. Whereas experiments performed at varying temperatures using diverse methods are straight-forward and well-established, experiments at elevated or changing pressures are still technically challenging. Current crystallographic methods to obtain high-resolution structural data of proteins at high pressure involve the usage of diamond anvil cells (DAC) that were originally designed for geological science purposes and are suboptimal for fragile protein crystals. In order to overcome practical challenges of the DAC, we developed a new cell for high-pressure macromolecular crystallography using a fixed target-approach combined with the application of thin-walled sapphire and gaseous helium as pressurizing medium. Pressure levels can be freely adjusted between 0.1 and 120 MPa. We will present the experimental setup and first results obtained at beamline P11 of the PETRA III storage ring at DESY.

Structure based identification of Bortezomib and Ixazomib as new lead compounds for the development of novel boron-based ß-lactamase inhibitors

A. Prester[1], N. Werner[2], H. Rohde[1], M. Perbandt[3], C. Betzel[2]

[1] Universitätsklinikum Hamburg-Eppendorf, Institut für Mikrobiologie, Hamburg, Germany

[2] Universität Hamburg, Institut für Biochemie und Molekularbiologie, Hamburg, Germany

[3] UNI/CUI (The Hamburg Centre for Ultrafast Imaging), Hamburg, Germany

In recent years the efficacy of traditional ß-lactam antibiotics against Gram-negative bacteria has declined dramatically, mainly due to their ability to express multiple ß-lactamases that are not inhibited anymore by first-generation ß-lactam inhibitors (BLIs), such as clavulanic acid, tazobactam, and sulbactam [1]. Substantial efforts have been made to develop new families of BLIs that are also effective against many medical problematic β-lactamases. Diazabicyclooctane derivatives (DBOs), such as Avibactam and Relebactam, were the first group of these new non-ß-lactam BLIs, which form a relatively hydrolytically stable acyl enzyme-type complex [2]. However, a novel approach for the development of BLIs is represented by boronate-based compounds, such as Vaborbactam and Taniborbactam [3]. The ability of boron to adopt a tetrahedral geometry allows to effectively mimic tetrahedral transition state analogs during hydrolytic reactions, making it one of the most useful elements in synthetic organic chemistry. In the field of protease inhibitors, boronate-based inhibitors, such as Bortezomib and Ixazomib were already designed and developed with applications in cancer therapy and are ap-

proved drugs for approx. 10 years. As serine β-lactamases and serine proteases share similarities in their mechanism of action, we analysed structural and biochemical features of β-lactamase inhibition, by utilizing these protease inhibitors in terms of a repurposing approach and targeted the ß-lactamase enzyme CTX-M-14 from K. pneumoniae, the most widely distributed extended-spectrum ß-lactamase (ESBL). We will describe and present details for the crystal structures in complex with Bortezomib and Ixazomib, shown on the left. β-lactamase CTX-M-14, in green with covalently bound protease inhibitor Ixazomib in purple. Results obtained prove that both can be not only utilized as proteasome inhibitors, but moreover as ß-lactamase-inhibitors. The dual inhibition mode provides new insights into the catalytic mechanism of inhibition and may guide new strategies for repurposing of known boron-based proteasome inhibitors to antibiotic active drugs.

References

[1] Vena, A., N. Castaldo, and M. Bassetti, The role of new beta-lactamase inhibitors in gram-negative infections. Curr Opin Infect Dis, 2019. 32(6): p. 638-646.
[2] Ehmann, D.E., et al., Avibactam is a covalent, reversible, non-beta-lactam beta-lactamase inhibitor. Proc Natl Acad Sci U S A, 2012. 109(29): p. 11663-8.
[3] Hamrick, J.C., et al., VNRX-5133 (Taniborbactam), a broad-spectrum inhibitor of serine- and metallo-beta-lactamases, restores activity of cefepime in Enterobacterales and Pseudomonas aeruginosa. Antimicrob Agents Chemother, 2019.

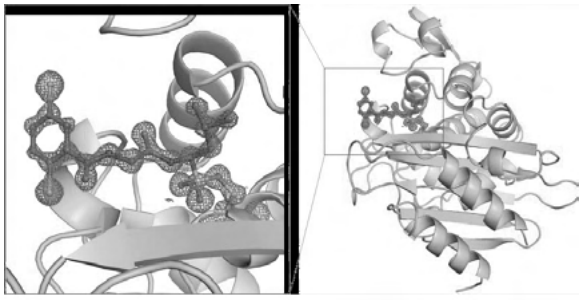

Figure 1

Structural characterization of ClpP and PBPs from Staphylococcus epidermidis - central and vital enzymes in bacterial virulence, stress survival and antibiotic resistance

M. Schwinzer[1], B. Alves França[1], M. Perbandt[1], C. Betzel[1]
[1] University of Hamburg, Institute of Biochemistry and Molecular Biology, Hamburg, Germany

Staphylococcus epidermidis (*Se*) is known to be a highly abundant bacterium on human skin. Although *Se* is usually not pathogenic under normal conditions, immunocompromised patients are at risk of acquiring persistent nosocomial infections caused by the aforementioned organism [1]. In this context, we performed structure-function analysis of two key bacterial enzymes, in terms of drug discovery investigations, known as penicillin-binding proteins (PBPs) and a distinct caseinolytic protease P (ClpP). PBPs are essential for the synthesis and the integrity of the bacterial cell wall. They exhibit a transpeptidase domain, a C-terminal head sub-domain and a N-terminal domain, including a membrane-anchor [2]. Moreover, ClpP is a barrel-like tetradecameric hydrolase composed by two-stacked heptameric rings and 14 identical proteolytic sites. That protein is one of the major intracellular enzymatic gears in protein turnover, in heat and oxidative stress control, and in the transcription of virulence factors [3]. Thus, meticulous studies on PBP and ClpP structures and their non-enzymatic modulators are relevant for the development of novel strategies that aim to reduce bacterial virulence. Further details about initial structural and functional investigations, including structures solved and refined so far to 2.2 Å and 1.9 Å for PBP and ClpP respectively, will be reported.

References

[1] Büttner H, Mack D, Rohde H., et al. Structural basis of Staphylococcus epidermidis biofilm formation: mechanisms and molecular interactions. Front Cell Infect Microbiol., 5, 5(14), pp. 1-14, 2015.
[2] H. Yoshida, F. Kawai, E. Obayashi, S., et al. Crystal Structures of Penicillin-Binding Protein 3 (PBP3) from Methicillin-Resistant Staphylococcus aureus in the Apo and Cefotaxime-Bound Forms, Journal of Molecular Biology, 423(3), pp. 351-364 2012.
[3] Bhandari, V.; Wong, K. S.; Zhou, J. L.; et al. The Role of ClpP Protease in Bacterial Pathogenesis and Human Dieases. ACS Chem, Biol., 13, pp. 1413-1425, 2018.

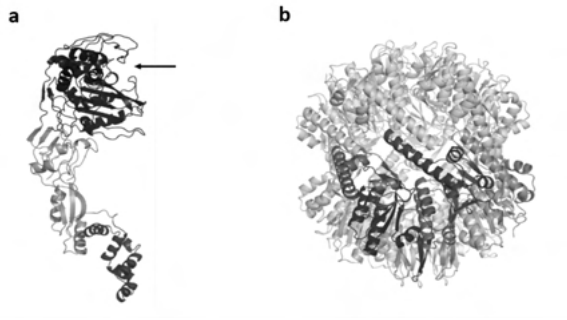

Figure 1 Initial structure of a. PBP: N-terminal domain (orange), head sub-domain (red) and the catalytic center indicated (black arrow) within the transpeptidase domain (blue); and b. ClpP: two-stacked heptameric rings (green and multi colored). Monomeric subunits are displayed in different colors (lower ring). Each domain contains the same internalized proteolytic site with a Ser-His-Asp triad.

Crystallographic fragment screening workflow at HZB

J. Wollenhaupt[1], T. Barthel[1], G. Lima[2], A. Metz[3], D. Wallacher[1], E. Jagudin[2], T. Hauß[1], C. Feiler[1], A. Heine[3], G. Klebe[3], M. Weiss[1]

[1] Helmholtz-Zentrum Berlin, Berlin, Germany

[2] MAX IV Laboratory, Lund, Sweden

[3] Philipps-University Marburg, Marburg, Germany

The only method utilized routinely to discover starting points for ligand development that at the same time delivers detailed 3D-information for downstream ligand optimization is macromolecular crystallography. Typically, small organic compounds, called fragments, are screened against an optimized crystal system of a target protein, and detected by electron density differences compared to the apo protein, i.e. the protein structure without fragments present. This technique, crystallographic fragment screening (CFS), is widely established now in academia and indispensable in the pharmaceutic industry. However, its routine use requires specialized workflows including suitable fragment libraries, dedicated beamlines able to handle large amounts of samples and largely automated software solutions for concise analysis of the results.

At Helmholtz-Zentrum Berlin, we provide the full workflow as well as practical guidance for our users conducting CFS campaigns. We prepared the 96-membered F2X-Entry Screen, an efficient and CFS-focused fragment library, as ready-to-use plates with dried-in compounds that can be used with or without DMSO present in the soaking experiment. In addition, special tools like the EasyAccess Frame, an evaporation protection device for crystallization plates, speed up the crystal handling. The HZB beamlines BL 14.1 and BL 14.2 are both equipped with state-of-the-art photon-counting detectors as well as with robotic sample changers, enabling enhanced throughput. Processing of the data is achieved via FragMAXapp, a user friendly, browser-controlled tool employed at several CFS facilities that manages in and output of many processing, refinement and hit identification software pipelines that are routinely used for CFS nowadays.

Taken together, HZB provides a workflow for routine crystallographic screening experiments via fragments. The intertwined workflow components and gathered expertise increase the chances for successful identification of fragments as starting points for the development of potent ligand molecules.

References

[1] Wollenhaupt, J. *et al.*, "F2X-Universal and F2X-Entry: Structurally Diverse Compound Libraries for Crystallographic Fragment Screening," *Structure*, vol. 28, pp. 694–706.e5, 2020.

[2] Barthel, T. *et al.*, "Facilitated crystal handling using a simple device for evaporation reduction in microtiter plates," *J. Appl. Cryst.*, accepted for publication, 2021.

[3] Lima, G. M. A. *et al.*, "FragMAXapp: Crystallographic Fragment Screening Data Analysis and Project Management System," article in revision, 2021.

[4] Schiebel, J. *et al.*, "High-Throughput Crystallography: Reliable and Efficient Identification of Fragment Hits," *Structure*, vol. 24, pp. 1398–1409, 2016.

Disordered Materials, complex crystal structures and aperiodic crystals, diffuse scattering and 3D-PDF

The incommensurate structure of the binary thallides A_4Tl_{13} (A = Rb, Cs).The solution of an old problem.

B. Lehmann[1], C. Röhr[1]

[1] Institut für Anorganische und Analytische Chemie, Universität Freiburg, Freiburg

In the course of our studies on alkali trielides with mixed triel positions (Ga/In) [1] and (In/Tl), analysis of the binary phase diagrams Rb-Tl and Cs-Tl [2] show incongruent melting behaviour at the composition A Tl $_3$ (A = Rb, Cs). A complete structural description of those phases has not been published to this day, even though *Corbett* and *Dong* [3] were able to determine the composition 'A_4Tl_{13}', as well as one of the structural elements of

those phases. In our work, due to the incongruent melting behaviour, the alkali poorer composition A Tl_4 was chosen for the synthesis of the two isotypic title compounds. X-Ray single crystal data were used to solve the structure.

The main reflections of the modulated structure were indexed with a C-centered orthorhombic lattice. The basic structure was solved in the space group *Cmca* using the *charge-flipping* method (Basic structure of Rb_4Tl_{13}: *Cmca*, $Z = 1$, $a = 545.75(3)$, $b = 3909.95(20)$, $c = 2148.90(11)$ pm). All satellite reflections could be indexed with a primitive orthorhombic lattice and the q-vector $\boldsymbol{q}$ = (0 0 0.2996(1)), allowing the refinement of the (3+1) D modulated structure. The model was obtained by $k2$ symmetry reduction from *Cmca* to *Pbcm* (Rb_4Tl_{13}: *Pbcm*(0 0 γ)s00, $\boldsymbol{q}$ =(0 0 0.2996(1)), $Z = 1$, $a = 3907.80(20)$, $b = 2147.61(11)$, $c = 545.63(3)$ pm, $R1$=0.083, $R1_{\mathrm{mr}}$=0.063, $R1_{\mathrm{sr}+-(1)} = 0.168$). The structure exhibits as one structural element isolated chains of interpenetrating icosahedra

(Fig. 1b). These chains are coordinated by cations only. They are embedded between complex 2D thallide layers (Fig. 1a), similar to those observed in the structure of K_6Tl_{17} [4]. Both positions in the centre of the chains as well as two atoms in the layer exhibit a strong positional modulation, which is refined using the *saw-tooth* function (Fig. 2). The positions of the remaining atoms affected by this modulation can be refined using harmonic modulation functions. The modulation is probably caused by the size of the thallium atoms, which are too large to fit into the structure in a way compatible with the periodicity of the lattice.

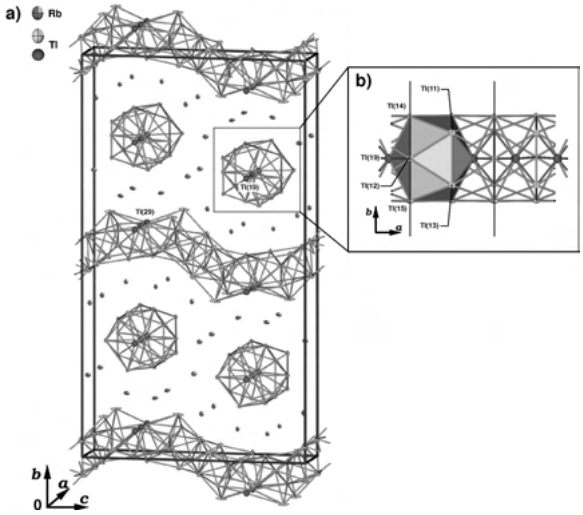

Figure 1 a) Unit cell of the basic structre of Rb_4Tl_{13}. The thallium atoms refined with a saw-tooth function in the final model (Tl(19) and Tl(29)) are represented as blue spheres. All remaining atomic positions are shown as red (Rubidium) resp. green (Thallium) ellipsoids (Probability: 90%). b) Detailed view of one chain of interpenetrating icosahedra with 90% probability ellipsoids and atomic labels from the model of the basic structure (projection along [001]).

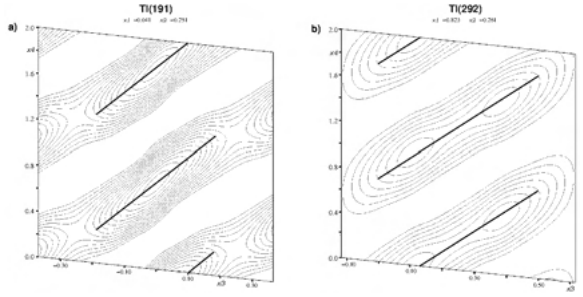

Figure 2 De Wolff's sections from the final structure of Rb_4Tl_{13}. a) $x3$-$x4$-section at the Tl(191) site. b) $x3$-$x4$-section at the Tl(292) site (Contour lines at intervals of 30 e^- x $10^{-6}pm^{-3}$).The difference between the atomic labels of the final and the basic structure (Fig.1) results from the symmetry reduction from *Cmca* to *Pbcm*. The Tl(19) site splits up to Tl(191) and Tl(192) and the Tl(29) site splits up to Tl(291) and Tl(292).

References

[1] M. Falk, C. Röhr, *Z. Kristallogr.* **234**, 623-646 (2019).
[2] T. Massalski, H. Okamoto, and P. R. Subramanian, editors. *Binary Alloy Phases Diagramms*, 2nd Edition, ASM International (1990).
[3] Z. Dong, J. D. Corbett, *Inorg. Chem.* **35**, 1444-1450 (1996).
[4] S. Kaskel, Z. Dong, M. T. Klem, J. D. Corbett, *Inorg. Chem.* **42**, 1835-1841 (2003).

Energy materials: batteries, photovoltaics, etc.

Evaluation of oxygen delivery from nanoporous perovskite solid solutions with in situ XRD and TG-MS

B. Ehrhardt[1], S. Mascotto[1], L. Gigli[2], N.-F. Meyer[1]

[1] University of Hamburg, Department of Chemistry, Hamburg, Germany

[2] Elettra-Sincrotrone Trieste S.C.p.A.„ Strada Statale 14, 34149 Basovizza, Trieste, Italy

Perovskite solid solutions are versatile materials, which are widely used especially in heterogeneous catalysis [1]. Their performance is determined by the materials'defect chemistry, charge charrier transport properties and surface area. Hence, nanoporous perovskites, due to their large surface and thus higher reactive area, are well suited for the use in Solid Oxide Fuel Cells (SOFC), solar-to-fuel processes, the oxidation of n-alkanes and the soot combustion in diesel exhaust gases. All these applications need oxygen as reactive species, so they are all strongly influenced by the oxygen release and transport property of a catalyst or substrate material [1-4].

In order to be able to tailor the perovskites for the above applications, we wanted to understand the influence of the porosity and surface area on oxygen delivery and transport in nanoporous perovskite solid solutions of cubic SrTiO3 with lanthanum and manganese which partly replaced strontium and titanium, respectively (space group $Pm\bar{3}m$). Samples were prepared using a modified Pechini synthesis with surface areas ranging from 5 m^2/g to 150 m^2/g [5]. Structural and morphological characterization of the samples were carried out via x-ray diffraction (XRD), electron microscopy and nitrogen physisorption. Oxygen delivery was quantified via thermogravimetric (TG) measurements coupled with mass spectrometry (MS) as well as in situ high temperature synchrotron radiation x-ray diffraction with temperatures up to 1223 K. Subsequent Rietveld refinement was used to determine the site occupation of oxygen at varying temperatures.

The highest oxygen release rates were found in the perovskite sample with higher porosity. All TG measurement showed three gradients at different temperatures during heating under low oxygen partial pressure, which we contribute to different oxygen species that where released from different sites of the perovskite lattice [6]. The measurements from the in situ x-ray diffraction supported the results from the TG-MS experiments well.

References

[1] Zhou X. *et al.*, *RSC Advances.*, pp. 118–131, 2014.

[2] A. H. McDaniel *et al.*, *Energy Environ. Sci.*, pp. 2424–2428, 2013.

[3] B. Kayaalp *et al.*, *Applied Catalysis B: Environmental.*, pp. 536-545, 2019.

[4] A. Kotarba *et al.*, *Applied Catalysis B: Environmental.*, pp. 169-175, 2011.

[5] B. E. Kayaalp *et al.*, *RSC Advances.*, pp. 90401–90409, 2016.

[6] N. A. Merino *et al.*, *Journal of Catalysis.*, pp. 232–244, 2005.

Cu/Zn disorder in Cu2ZnSn(SxSe1-x)4 monograins: the result of "ordering" procedure

G. Gurieva[1], A. Franz[2], S. Levcenko[2], K. Muska[2], K. Ernits[2], S. Schorr[3]

[1] Helmholtz Zentrum Berlin, Berlin, Germany

[2] Freie Universität Berlin, Department Geosciences, Berlin, Germany

[3] Helmholtz-Zentrum Berlin für Materialien und Energie, Berlin, Germany

Kesterite-type based thin film solar cell technologies are mainly based on polycrystalline absorber layers. A promising low cost alternative technology uses Cu2ZnSn(S,Se)4 (CZTSSe) monograins (single crystals of 50-100 μm size) which are fixed in a polymer matrix to form a flexible solar cell [1]. It is agreed in literature that large band tailing observed in Cu-based kesterite-type semiconductors causes voltage losses limiting the efficiency of kesterite-based devices. The Cu/Zn disorder (CuZn and ZnCu anti-sites in Cu-Zn planes at z=$\frac{1}{4}$ and $\frac{3}{4}$), which is always present in these compounds [2], is discussed as a possible reason for band tailing. The experimental determination of the order parameter Q which is a quantitative measure of the degree of Cu/Zn disorder [3] requires a differentiation between the isoelectronic cations Cu+ and Zn2+. An in depth analysis of neutron diffraction data provides information on the cation distribution in the crystal structure allowing the determination of type and concentration of intrinsic point defects including a distinction between Cu and Zn [2]. On the other hand neutron diffraction requires large sample volumes, thus kesterite monograins offer the unique possibility to correlate structural disorder in kesterite-type absorbers with device performance parameters. We will present a detailed structural investigation of the effect of the disordering procedure and the long low temperature – "ordering" annealing on the Cu/Zn disorder and optical properties of the CZTSSe monograins will be presented.

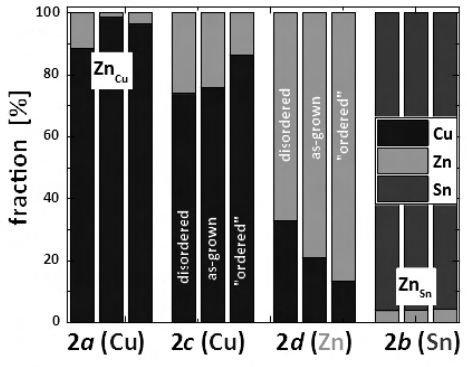

Figure 1

Proton motions in hydrogen bonds of hureaulite-type phosphatic oxyhydroxides

A. Hartl[1], S. Park[1], F. Juranyi[2], M. Krack[2], D. Cheptiakov[2], M. Appel[3], C. Paulmann[4], A. Arauzo[5], P. Lunkenheimer[6]
[1] Ludwig-Maximilians-Universität München, Germany
[2] Paul Scherrer Institut, Villigen, Switzerland
[3] Institut Laue-Langevin, Grenoble, France
[4] DESY, Hamburg, Germany
[5] Universidad de Zaragoza, Zaragoza, Spain
[6] Universität Augsburg, Augsburg, Germany

The peculiar hydrogen arrangement in the hureaulite-type manganese endmember $(Mn_5[(PO_4)_2(PO_3OH)_2](HOH)_4)$ comprises semihelical hydrogen bond chains along porous channels as well as framework HOH ligands in small cages. Results from extensive, complementary studies are presented to show (1) the time and length scales of local and long-range proton dynamics in the title compound and (2) contribute to the basic understanding of proton transport in confinement.

Diffuse difference Fourier maps around those hydrogen bond chains evaluated with X-ray single crystal and high-resolution neutron powder diffraction data adumbrate strong protonic disorder above 250 K together with fast rotating framework polyhedra. This temperature coincides with the onset of DC conductivity as probed by broadband dielectric spectroscopy. Neutron time-of-flight and backscattering spectroscopy revealed proton motions above room temperature with an activation energy of 0.39(1) eV and relaxation time of 11(2) ps. With a combined quasielastic neutron scattering data treatment, alongside geometrical considerations and ab initio molecular dynamics studies, these local motions were assigned to the rotations of HOH groups within the hydrogen bond chains. The vibrational density of states, collected with inelastic neutron scattering, was compared with experimentally obtained infrared and Raman spectra as well as simulated spectra based on electronic structure calculations.

As a result, we could elucidate lattice-dynamic-induced proton motions over the hydrogen bond network in this phosphatic oxyhydroxide. Such proton-phonon coupling is of great interest in the search for superprotonic conductors.

Dynamics of the Lithium-Distribution in commercial LFP|C lithium-ion batteries under charge/discharge

D. Petz[1], V. Baran[2], M. Mühlbauer[3], A. Schökel[4], M. Hofmann[5], P. Müller-Buschbaum[1], A. Senyshyn[5]
[1] Technical University of Munich, Munich, Germany
[2] DESY, Photon Science, FS-PS (FS-Photon Science), Hamburg, Germany
[3] Karlsruhe Institute of Technology (KIT), Karslruhe, Germany
[4] DESY, Notkestr. 85, 22607 Hamburg, Germany
[5] Heinz Maier-Leibnitz Zentrum (MLZ), Garching, Germany

Operation of typical lithium-ion battery is supplemented by the continuous mass transfer, which affects the ionic transport through the electrodes and electrolyte. Ionic transfer is defined by different factors like electrode dimensions and geometry, current density, temperature, pressure, reaction rate etc. All these properties are not necessarily uniformly distributed and, therefore, can affect heterogeneities in lithium concentrations in the cell electrodes [1, 2].

Typically, the lithium distribution in the graphite anode was probed at cells in fully charged and well equilibrated state, leaving the evolution of lithium distribution under real cell charging unclear.

In the current work, the lithium-ion distribution in a graphite anode and a lithium-iron-phosphate cathode were studied using a combination of spatially-resolved neutron-powder diffraction (anode) and X-ray powder diffraction (cathode) during the cell charge/discharge. It will be shown, that different inhomogeneities occur on different length scale still complementing each other.

References

[1] Senyshyn, A. *et al.*, "Homogeneity of lithium distribution in cylinder-type Li-ion batteries," *Scientific Reports*, vol. 5, no. 1, p. 18380, 2015.

[2] Petz, D. *et al.*, "Heterogeneity of Graphite Lithiation in State-of-the-Art Cylinder-Type Li-Ion Cells," *Batteries & Supercaps*, in print.

Extreme/non-ambient conditions

Squeezing the most data out of your high-pressure experiment

J. Graf[1], T. Stürzer[2], P. Dera[3], M. Ruf[4]

[1] Incoatec GmbH, Geesthacht, Germany

[2] Bruker AXS GmbH, Karlsruhe, Germany

[3] University of Hawaii, 2500 Campus Rd, Honolulu, HI 96822, USA

[4] Bruker AXS Inc, Madison, WI, USA

Within the last decade high pressure studies have received significant increase of interest. Present typical applications range from the investigation of high-pressure polymorphism of solid-state organics as part of the pharmaceutical drug development to the study of rocks and minerals with an applied pressure of up to 50 GPa.

A major challenge in the field of high pressure crystallography is the acquisition of data of sufficient quality and completeness for a successful structure determination. This presentation will be reviewing recent advances in hardware development, such as X-ray sources with radiation harder than Mo-Kα, and highlight the latest improvements in software, which help in tackling the problems with data acquisitions in high-pressure experiments.

Using a Bruker D8 VENTURE system, we will be demonstrating the advanced hardware capabilities and processing methods based on selected data, including data from the Indium METALJET X-ray source. Further, we will be showing how to increase the completeness of high-pressure experiments by mounting multiple samples in a diamond anvil cell and measuring and processing data concurrently.

The high flexibility of the D8 VENTURE can be further expanded by adding enhanced features typically only available at synchrotron facilities, e.g. for studying tiny mineral crystals enclosed in diamond anvil cells. These features include highly accurate, motorized sample positioning and the ability to monitor the intensity of the X-ray beam passing through the diamond anvil cell, as well as an extension for online pressure measurements based on ruby fluorescence. This makes the D8 VENTURE system "a little synchrotron at home".

Framework structures: MOFs, COFs, etc.

Elucidating the structural evolution of a highly porous responsive metal-organic framework (DUT-49(M)) upon guests desorption by time-resolved in-situ powder X-ray diffraction

V. Bon[1], B. Garai[1], F. Walenszus[1], A. Khadiev[2], D. Novikov[2], S. Kaskel[1]

[1] Technical University of Dresden, Dresden, Germany

[2] DESY, Photon Science, PETRA III, P23 Beamline, Hamburg, Germany

Metal-organic frameworks (MOFs) are 3-dimensional architectures constructed via the coordination of metal ions or cluster as nodes and organic linkers as struts, resulting in crystallographically well-defined porosity.[1] After removing the guest molecules from the pores, record values of surface area and pore volumes can be reached.

A unique type of adsorption-induced phenomenon has been discovered in the hierarchical mesoporous Cu2(BBCDC) framework, further denoted as DUT-49(Cu).[2] The MOF is constructed from the coordination of tetratropic carbazole-based linker with Cu-Cu paddlewheel, forming three distinct types of pores: cuboctahedral MOPs with 10 Å in diameter, interconnected by edges via biphenyl moieties and form additional tetrahedral (17 Å) and octahedral (24 Å) cages.[3] The framework can be desolvated by exchange with supercritical CO2 without losing crystallinity. Variation in the metal centres of M-M paddle-wheel SBU results in the formation of isostructural DUT-49(M) [DUT-49(M); M= Ni, Mn, Fe, Co, Zn, Cd] frameworks. However, the porosity of the framework was found to be different for each of the structures. All attempts to regain the structure by resolvation at elevated temperatures were unsuccessful and only only DUT-49(Cu) and DUT-49(Ni) retain the structural integrity after the supercritical drying procedure. Thus, herein, we aimed to study the detailed structural transformations that are possibly occurring during the removal of the subcritical fluid from the framework by time-resolved synchrotron PXRD at P23 beamline aiming to access the structural pathways of the framework collapse [4].

References

[1] a) S. Kitagawa, R. Kitaura, S.-i. Noro, *Angew. Chem., Int. Ed.* vol. 43, pp. 2334-2375, 2004; b) M. Eddaoudi, D. B. Moler, H. Li, B. Chen, T. M. Reineke, M. O'Keeffe, O. M. Yaghi, *Acc. Chem. Res.*, vol. 34, pp. 319-330, 2001; c) S. R. Batten, N. R. Champness, X.-M. Chen, J. Garcia-

Martinez, S. Kitagawa, L. Öhrström, M. O'Keeffe, M. P. Suh, J. Reedijk, *Cryst. Eng. Comm.*, vol. 14, pp. 3001-3004, 2012; d) H. Furukawa, N. Ko, Y. B. Go, N. Aratani, S. B. Choi, E. Choi, A. Ö. Yazaydin, R. Q. Snurr, M. O'Keeffe, J. Kim, O. M. Yaghi, *Science*, vol. 329, pp. 424, 2010.

[2] S. Krause, V. Bon, I. Senkovska, U. Stoeck, D. Wallacher, D. M. Többens, S. Zander, R. S. Pillai, G. Maurin, F.-X. Coudert, S. Kaskel, *Nature*, vol. 532, pp. 532, 348-352, 2016.

[3] U. Stoeck, S. Krause, V. Bon, I. Senkovska, S. Kaskel, *Chem. Commun.*, vol. 48, pp. 10841-10843, 2012.

[4] B. Garai, V. Bon, F. Walenszus, A. Khadiev, D. V. Novikov, S. Kaskel, *Cryst. Growth Des.*, vol. 21, 2020, DOI: 10.1021/acs.cgd.0c01080.

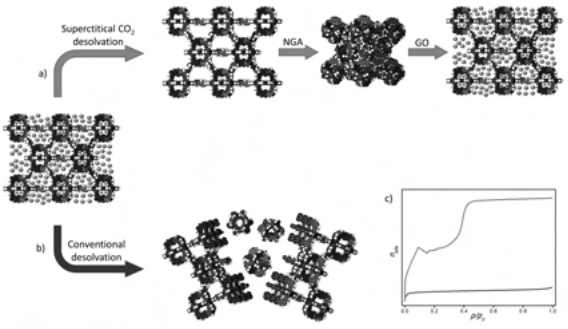

Figure 1 Strucutral transformation of DUT-49(Cu) MOF during solvent removal through (a) supercritical CO2 activation approach to retain the highly porous (op) phase that can undergo further structural transition during gas adsorption process; and (b) conventional activation approach. (c) Typical adsorption isotherm from op phase of the framework (green line) and amorphous phase (red line).

A new type of hydrous layer silicates and zeolites obtained by 3D electron diffraction

Y. Krysiak[1], B. Marler[2], L. Palatinus[3], U. Kolb[4]

[1] Institute of Inorganic Chemistry, Leibniz University Hannover, Hannover, Germany

[2] Departure of Geology, Mineralogy and Geophysics, Ruhr University Bochum, Bochum Germany

[3] Department of Structure Analysis, Institute of Physics of the Czech Academy of Sciences, Prague, Czech Republic

[4] Centre for High Resolution Electron Microscopy, Johannes Gutenberg University Mainz, Mainz Germany

The structure elucidation of zeolites and their related hydrous layer silicates (HLS) is an important aspect in the extensive investigation of structure, synthesis and function of these materials to identify potential applications. The hydrothermal synthesis usually results in crystals that are too small for conventional single crystal X-ray diffraction experiments. Furthermore, the structure determination is even more complicated due to the presence of diffuse scattering, which originates from stacking disorder of the weakly bonded silica layers.

Complete structural models based on the real and average structure of different HLS resp. zeolite samples (RUB-5, RUB-6 and RUB-11) were developed with high-resolution transmission electron microscopy (HRTEM) and 3D electron diffraction (3D ED).

The complex structures of RUB-5, RUB-6 and RUB-11 could be solved ab initio even though strong diffuse scattering with pseudo-tetragonal symmetry was present. The structures of RUB-5 and layer silicate RUB-6 contain the same dense layer-like building units (LLBU). In the case of RUB-5, these building units are interconnected via additional SiO4/2 tetrahedra, giving rise to a framework structure with a two-dimensional pore system consisting of intersecting 8-ring channels. RUB-5 and RUB-11 which are structurally related can be described as pure silica "zeolites" with high framework densities of 22.0 and 21.2 silicon atoms per 1000 $Å^3$.[1]

The frameworks of RUB-5 and RUB-11 are unique and represent two new silica polymorphs. In addition to the comprehensive structural descriptions, the extracted diffuse scattering was used to show that the formation of RUB-5 and RUB-6 occurs through a similar intermediate step.

Acknowledgement

This research was supported by the Czech Science Foundation (project No. 19-08032S).

References

[1] Y. Krysiak, B. Marler, B. Barton, S. Plana-Ruiz, H. Gies, R. B. Neder, U. Kolb, *IUCrJ*, vol. 7, 2020, DOI 10.1107/S2052252520003991.

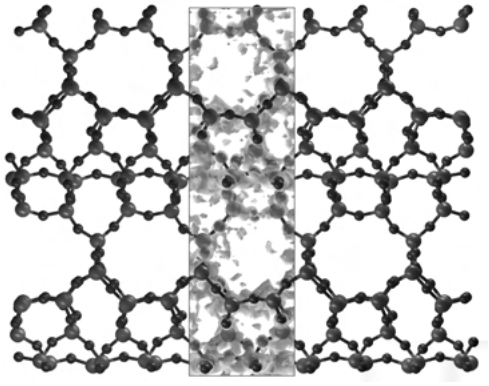

Figure 1 Potential map of structure solution of RUB-11 combined with structure model projected down [100].

Tuning the high-pressure phase behaviour of ultra-compressible zeolitic imidazolate frameworks – From discontinuous to continuous pore closure by linker substitution

J. Song[1], R. Pallach[1], S. Henke[1]

[1] Technical University of Dortmund, Faculty of Chemistry and Chemical Biology, Anorganic Chemistry, Otto-Hahn-Straße 6, 44227 Dortmund, Germany

Zeolitic imidazolate frameworks (ZIFs), a very important subfamily of metal-organic frameworks (MOFs), are constructed from tetrahedrally coordinated M2+ (Zn2+ or Co2+) ions, which are interlinked by imidazolate linkers[1]. Recently, we discovered that the prototypical ZIF-4 (chemical composition M(im)2, im– = imidazolate) undergoes a phase transition from an open pore (op) to a closed pore (cp) phase under hydrostatic pressure[2]. Here we further present the high-pressure (HP) behaviour of a series of isostructural ZIF-4 derivatives, named ZIF-62, with the general chemical composition M(im)2-x(bim)x (bim– = benzimidazolate, $0.02 < x < 0.35$). The ZIF-62 materials crystallize in the space group Pbca and feature the same network topology (cag) as the original ZIF-4, however, some of the im– linkers are substituted by the bulkier bim– linkers. HP-PXRD experiments were performed at beamline I15 of Diamond Light Source in the pressure range from ambient up to 4000 bar using silicon oil as a non-penetrating pressure transmitting medium and a hydraulic pressure cell[3]. Under hydrostatic pressure, all ZIF-62 derivatives reversibly contract from the op to the cp phase only by rotations about the imidazolate-metal bonds (Fig. 1). Crystal symmetry and network topology are preserved. With increasing bim— concentration, the threshold pressure for the op-cp phase transition increases from 700 bar to 1300 bar and the overall volume contraction across the transition decreases from 25% to 17% of the initial volume. Most importantly, the 1st order (discontinuous) transition transfers to a 2nd order (continuous) transition for $x > 0.30$. Thus, the void space and pore openings of ZIF-62 can be tuned continuously by the application of mechanical pressure – a unique feature which might be useful for adjusting and enhancing the gas separation performance of these flexible MOFs.

References

[1] a) J. H. Lee, S. Jeoung, Y. G. Chung, H. R. Moon, *Coord. Chem. Rev.*, vol. 389, p. 161, June 2019. b) J.-P. Zhang, Y.-B. Zhang, J.-B. Lin, X.-M. Chen, *Chem. Rev.*, vol. 112. p. 1001, Feb. 2012.

[2] S. Henke, M. T. Wharmby, G. Kieslich, I. Hante, A. Schneemann, Y. Wu, D. Daisenberger, A. K. Cheetham, *Chem. Sci.*, vol. 9, p. 1654, Feb. 2018.

[3] N. J. Brooks, B. L. L. E. Gauthe, N. J. Terrill, S. E. Rogers, R. H. Templer, O. Ces, J. M. Seddon, *Rev. Sci. Instrum.*, vol. 81, no. 6, May 2010, Art. no. 64103.

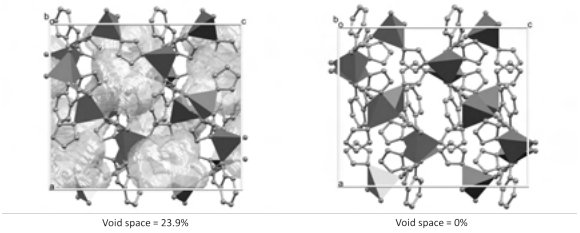

Figure 1 Structural models of ZIF-62 with the composition Zn(im)1.65(bim)0.35 at ambient pressure (left) and 4000 bar (right). The void space available for CO2 molecules (kinetic diameter = 3.30 Å) is shown in gold.

Inorganic crystal structures

$Mn(H_2O)_6[B_{10}Cl_{10}] \cdot 2.5\ H_2O$: Synthesis and Crystal Structure

K. U. Bareiß[1], F. B. Goerigk[1], T. Schleid[1]

[1] University of Stuttgart, Institute for Inorganic Chemistry, Pfaffenwaldring 55, 70569 Stuttgart, Germany

The previously reported crystal structure of $Tl_2[B_{10}Cl_{10}] \cdot 2\ H_2O$ [1] led to the preparation of further hydrated salts with perchlorinated B_{10}-cluster analogues, such as $Mg(H_2O)_6[B_{10}Cl_{10}] \cdot 2.5\ H_2O$ [2]. We now present the synthesis and structural characterization of $Mn(H_2O)_6[B_{10}Cl_{10}] \cdot 2.5\ H_2O$ (CSD-2052005) crystallizing isotypically with $Mg(H_2O)_6[B_{10}Cl_{10}] \cdot 2.5\ H_2O$ and $Co(H_2O)_6[B_{10}Cl_{10}] \cdot 2.5\ H_2O$ [2] in the triclinic space group $P\bar{1}$ with $a = 1172.06(3)$ pm, $b = 1237.42(3)$ pm, $c = 1752.73(4)$ pm, $\alpha = 84.409(2)^\circ$, $\beta = 88.942(2)^\circ$ and $\gamma = 88.694(2)^\circ$ for $Z = 4$. The $[B_{10}Cl_{10}]^{2-}$-cluster anions feature typical B−−B bond lengths of 167 – 169 pm to the caps and 181 – 185 pm inside the square antiprisms as well as B−−Cl distances from 178 to 181 pm. The four crystallographically different Mn^{2+} cations at special sites (1*a*, 1*b*, 1*e* and 1*h*) are coordinated by six water molecules each, of which always three are crystal-

lographically unique. The Mn−−O distances within the $[Mn(H_2O)_6]^{2+}$ octahedra reach from 213 to 222 pm and therefore are significantly longer than in the Mg- and Co-analogues, which show average distances of 207 (Mg) and 209 pm (Co) [2]. These distances perfectly fit the M−−O distance trends in the $M(H_2O)_6[B_{10}H_{10}] \cdot 2\ H_2O$ series (M = Mn – Ni and Zn) crystallizing in the monoclinic space group $C2/c$ [3]. The $[Mn(H_2O)_6]^{2+}$ octahedra in $Mn(H_2O)_6[B_{10}Cl_{10}] \cdot 2.5\ H_2O$ are connected through five crystallographically different interstitial water molecules, revealing O···O distances from 274 to 285 pm, which may be discussed as O−−H···O hydrogen bridges. The water bridged $[Mn(H_2O)_6]^{2+}$ octahedra build up a three-dimensional network of linked chains along [110], [1$\bar{1}$0] and [001] with interstices filled up with the bicapped square antiprismatic $[B_{10}Cl_{10}]^{2-}$ anions.

In order to prepare $Mn(H_2O)_6[B_{10}Cl_{10}] \cdot 2.5\ H_2O$ solid manganese(II) carbonate ($Mn[CO_3]$) was neutralized by an aqueous acidic solution of $(H_3O)_2[B_{10}Cl_{10}]$. The reaction mixture was filtrated and the pale pink solution slowly evaporated isothermally to obtain almost colorless crystals of $Mn(H_2O)_6[B_{10}Cl_{10}] \cdot 2.5\ H_2O$ from the mother liquor.

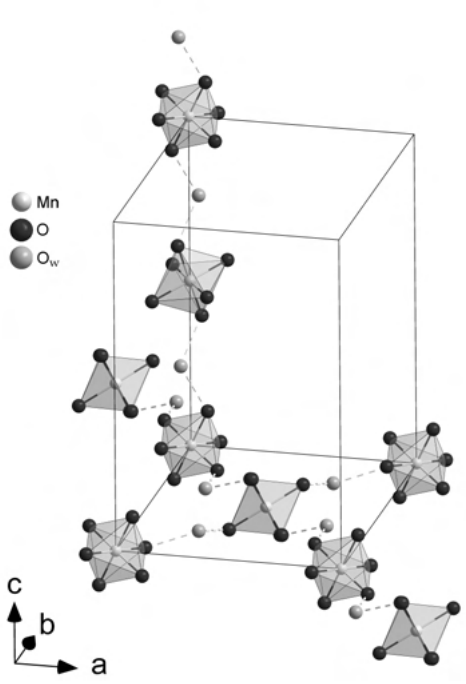

Figure 1 Extended unit cell of $Mn(H_2O)_6[B_{10}Cl_{10}] \cdot 2.5\ H_2O$ as viewed along [001] (*left*) and [100] (*right*).

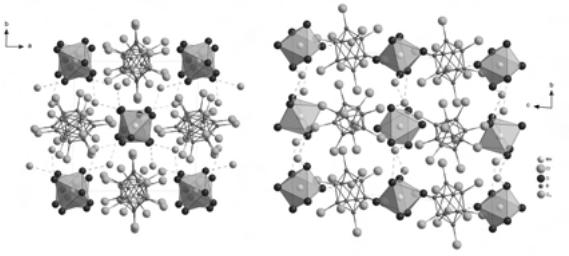

Figure 2 Simplified network $^3_\infty[[Mn(H_2O)_6](H_2O)_{6/2}]^{2+}$ of water-bridged $[Mn(H_2O)_6]^{2+}$ octahedra in $Mn(H_2O)_6[B_{10}Cl_{10}] \cdot 2.5\ H_2O$.

References

[1] K. U. Bareiß, Th. Schleid, in *Joint Polish-German Crytallographic Meeting, February 24–27, 2020, Wroclaw, Poland,* Berlin, Germany, Boston, USA: De Gruyter, 2020, pp. 64–64.

[2] F. M. Kleeberg, Doctoral Dissertation, University of Stuttgart, Germany, 2017.

[3] L. W. Zimmermann, Th. Schleid, *Z. Kristallogr.*, vol. 228, no. 10, pp. 558–564, Oct. 2013.

Group-Subgroup Relationships in Wurtzite-related Nitrides

J. Breternitz[1,2], S. Schorr[1]

[1] Helmholtz-Zentrum Berlin für Materialien und Energie, Hahn-Meitner Platz 1, 14109 Berlin, Germany

[2] University of Potsdam, Potsdam, Germany

A vast number of materials crystallise in the wurtzite-type structure or one of its subgroups. A prominent class of materials that crystallises in this structural family are wurtzite- and wurzite-related nitrides, some of which are, for instance, hopeful solar absorber materials. The different cation orderings and structural distortions in this class of materials open a rich variety of different crystal

structures in subgroups of the wurtzite-type structure. We establish a structural-systematic to this class of materials, which culminates in the establishment of a Bärnighausen tree. [1]

In a second part, we illustrate the practical use of this structural-systematic work on the example of $Zn(IV)N_2$ materials (IV = Ge, Sn). Those materials crystallise either in the wurtzite aristotype structure [2] where the Zn^{2+} and IV^{4+} cations are disordered, or in the ß-$NaFeO_2$-type structure, where the cations are ordered.[3] Furthermore, a third potential structure in the wurtzite subgroup $Pmc2_1$ was proposed that has a nominally higher symmetry than the ß-$NaFeO_2$-type structuer in space group $Pna2_1$.[4] We demonstrate why this alternative in space group $Pmc2_1$ is unlikely to form, due to the symmetry arrangement in this space group.

References

[1] J. Breternitz, S. Schorr, *Acta Crystallogr. A*, to be published.
[2] J. Breternitz, Z. Y. Wang, A. Glibo, A. Franz, M. Tovar, S. Berendts, M. Lerch and S. Schorr, *Phys. Status Solidi (a)*, vol. 216, 2019, Art. no. 1800885.
[3] E. W. Blanton, K. He, J. Shan, K. Kash, *J. Cryst. Growth*, vol. 461, pp. 38–45, 2017.
[4] P. C. Quayle, *Acta Crystallogr. A*, vol. 76, pp. 410–420, 2020.

Crystal-structure determination of hydrothermally produced nanocrystalline synthetic bastnaesite-type NdF[CO_3]

C. Buyer[1], T. Schleid[1]
[1] University of Stuttgart, Institute for Inorganic Chemistry, Stuttgart, Germany

In 1930 *Oftedal* reported the crystal structure of the mineral bastnaesite $REF[CO_3]$ (RE = La – Nd) in the hexagonal space group $P\bar{6}2m$ with a = 709.4(7) pm, c = 485.9(4) pm for Z = 3 [1]. In 1931 he did a correction of his 1930s result and found the space group $P\bar{6}2c$ with a = 709.4(7) pm, c = 971.8(8) pm for Z = 6 [2]. The most abundant rare-earth metal ore mineral is bastnaesite [3]. An Eu^{3+}-doped version of $LaF[CO_3]$ shows luminescence and after thermal decomposition trimorphic LaFO (or LaFO:Eu^{3+}) is obtained [4, 5]. While *Jansen et al.* [6] synthesized bastnaesites by adding aqueous HF to a dispersion of $Ce_2O[CO_3]_2 \cdot 4\,H_2O$ in water under a CO_2 atmosphere, *Janka* and *Schleid* [4] added a solution of $Na[HCO_3]$ and NaF dropwisely to a stirred solution of $La[NO_3]_3 \cdot 6\,H_2O$. Now we synthesized $NdF[CO_3]$ by adding a hot solution of NaF and $Na_2[CO_3]$ fast to a hot solution of $Nd[NO_3]_3 \cdot 6\,H_2O$. After that, we washed the resulting pale bluish violet, insoluble fine powder to remove the soluble by-products with water and dried it at 110 °C. About 150 mg of that powder was heated up to 200 °C for 5 days with about 5 ml water in a teflon autoclave. An X-ray diffraction powder pattern (Figure 1, top) was measured with Cu-Kα radiation on a STADI-P device and Rietveld refinement with the Fullprof program was used for the crystal structure refinement. Our obtained compound $NdF[CO_3]$ (CSD-2053207) crystallizes in the hexagonal space group $P\bar{6}2c$ (no. 190) with a = 707.48(1) pm, c = 973.45(2) pm for Z = 6. The atomic parameters are given in Figure 1 (bottom). The average crystallite size was calculated to be about 30 nm by using *Scherrer* equation. Figure 2 is showing a unit cell of $NdF[CO_3]$ with alternating layers of Nd^{3+}/F^- and $[CO_3]^{2-}$ ions (d(Nd—F) = 239 – 248 pm (3×), d(Nd—O) = 249 – 268 pm (6×) + 304 pm (2×), C.N.(Nd^{3+}) = 9 + 2, d(C—O) = 139 – 152 pm).

References

[1] I. Oftedal, *Z. Kristallogr.*, vol. 72, pp. 239–248, 1930.
[2] I. Oftedal, *Z. Kristallogr.*, vol. 78, pp. 462–469, 1931.
[3] Y. Ni, J. M. Hughes, A. N. Mariano, *Am. Mineral.*, vol. 78, pp. 415–418, 1993.
[4] O. Janka, Th. Schleid, *Eur. J. Inorg. Chem.*, vol. 2009, pp. 357–362, 2009.
[5] C. Buyer, J. Cybinska, E. Zych, Th. Schleid, *in preparation*, 2021
[6] G. J. Jansen, G. B. Magin, B. Levin, *Am. Mineral.*, vol. 44, pp. 180–181, 1959.

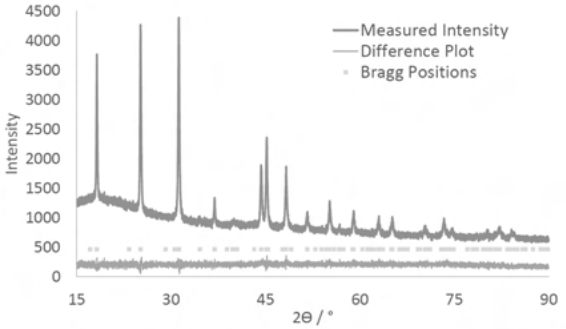

Atom	Wyckoff Site	Symmetry	x/a	y/b	z/c
Nd	6g	.2.	0.3375(9)	0	0
F1	2a	32.	0	0	0
F2	4f	3..	1/3	2/3	0.082(3)
C	6h	m..	0.201(6)	0.267(7)	1/4
O1	6h	m..	0.250(5)	0.005(7)	1/4
O2	12i	1	0.371(6)	0.311(7)	0.1405(11)

Figure 1 Rietveld structure refinement of $NdF[CO_3]$ with bastnaesite-type structure (top) and atomic parameters (bottom).

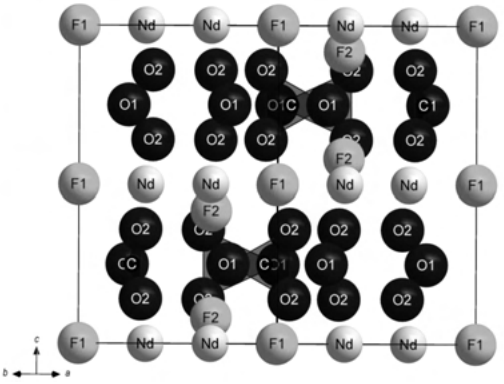

Figure 2 Hexagonal unit cell of $NdF[CO_3]$ as viewed along [110].

Single crystals of orthorhombic BaTa2O6: Serendipitous formation and rational structure determination

M. Conrad[1], T. Schleid[1]

[1] University of Stuttgart, Institute for Inorganic Chemistry, Stuttgart, Germany

The trimorphism of $BaTa_2O_6$ was first described in 1967 by Layden, who grew crystals of an orthorhombic low-temperature and a hexagonal high-temperature modification, along with powder samples of tetragonal $BaTa_2O_6$, which is stable in between [1]. However, he was just able to propose a structure model for hexagonal $BaTa_2O_6$ based on powder X-ray diffraction data in 1968 [2]. Almost half a decade later, in 2007 *Mumme* et al. [3] could collect single-crystal data and determined the structure of hexagonal $BaTa_2O_6$. The structures of the other polymorphs remained elusive until today, which is why the synthesis and characterization of orthorhombic $BaTa_2O_6$ is described here and now.

During an attempt to prepare mixed-anionic barium meta-perrhenates by arc melting equimolar amounts of barium fluoride (BaF_2) and anhydrous barium meta-perrhenate ($Ba[ReO_4]_2$) in an open tantalum crucible using a high-frequency furnace, few single crystals of orthorhombic $BaTa_2O_6$ were obtained after cooling the reaction mixture from roughly 2600 K to room temperature.

Orthorhombic $BaTa_2O_6$ crystallizes in the space group *Cmcm* with lattice parameters of a = 768.96(4) pm, b = 1233.25(7) pm and c = 1032.98(6) pm for Z = 8 (CSD 1897796) matching well with the cell parameters previously reported by *Layden* in 1967 (a = 767 pm, b = 1026 pm, c = 1233 pm) [1].

The crystal structure contains crystallographically unique Ta^{5+} cations octahedrally surrounded by six oxygen atoms (d(Ta–O) = 194 – 204 pm) along with two distinct Ba^{2+} cations in tenfold and twelvefold coordination of oxygen atoms (d(Ba–O) = 275 – 318 pm). Strands of alternatively corner- and edge-sharing $[TaO_6]^{7--}$ octahedra propagate along [010] (Figure 1, *left*), becoming interconnected by a single common oxygen vertex per polyhedron to form corrugated layers parallel to the (001) plane (Figure 1, *right*). These layers are connected in the [001] direction at every second octahedron leading to a three-dimensional network 3D-$[Ta_2O_6]^{2--}$ with Ba^{2+} cations in its voids (Figure 2).

References

[1] G. K. Layden, *Mater. Res. Bull.*, vol. 2, no. 5, pp. 533–539, May 1967.

[2] G. K. Layden, *Mater. Res. Bull.*, vol. 3, no. 4, pp. 349–359, Apr. 1968.

[3] W. G. Mumme, I. E. Grey, R. S. Roth, T. A. Vanderah, *J. Solid State Chem.*, vol. 180, no. 9, pp. 2429–2436, Sep. 2007.

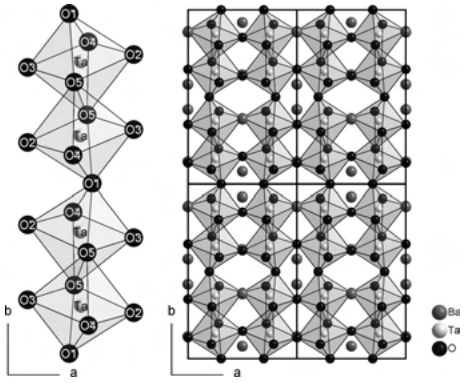

Figure 1 Chains of corner- and edge-sharing $[TaO_6]^{7--}$ octahedra running along [010] (*left*) and corrugated layers of these vertex-connected chains parallel to the (001) plane (*right*) in $BaTa_2O_6$.

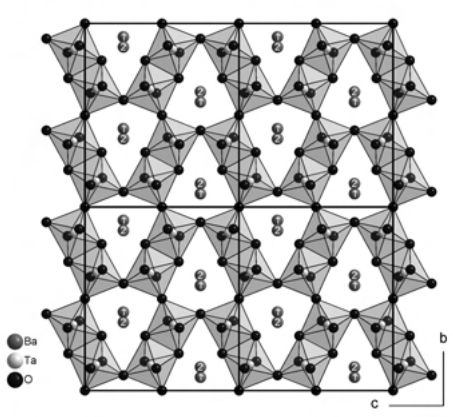

Figure 2 View at the network of interconnected $[TaO_6]^{7--}$ octahedra in $BaTa_2O_6$ along [100] with two kinds of Ba^{2+} cations in the voids.

Synthesis, Crystal Structure and Magnetic Properties of $Gd_2Se[SiO_4]$

P. Djendjur[1], B. Blaschkowski[1], T. Schleid[1]

[1] University of Stuttgart, Institute for Inorganic Chemistry, Stuttgart, Germany

Solid-state syntheses in glassy silica ampoules including elemental rare-earth metals sometimes yield unwanted by-products, such as multinary oxosilicates due to uncontrolled reactions with the container material. An attempt to synthesize Gd_2O_2Se in fused silica vessels furnished colorless, plate-shaped crystals of the title compound, which has structurally not yet been described based on single-crystal X-ray diffraction data in literature. Many other representatives of this substance class of lanthanoid selenide oxosilicates $Ln_2Se[SiO_4]$ (Ln = La, Ce, Nd, Sm, Eu, Tb – Er) have been well characterized throughout the years, however [1–7].

The oxidation of gadolinium metal with selenium dioxide in a molar ratio of 2:1 designed to produce Gd_2O_2Se with caesium chloride as flux led to the formation of $Gd_2Se[SiO_4]$ after some reaction with the SiO_2 container material. This gadolinium selenide *ortho*-oxosilicate crystallizes orthorhombically in the space group *Pbcm* (no. 57) with the lattice parameters a = 607.48(5) pm, b = 702.85(6) pm and c = 1086.74(9) pm for Z = 4 (CSD-2053795).

This structure exhibits two crystallographically distinct Gd^{3+} cations, which feature an (8+1)-membered coordination sphere for $(Gd1)^{3+}$ (6 O and 2+1 Se, d(Gd–O) = 242 – 254 pm, d(Gd–Se) = 291 – 352 pm) and an (8+2)-membered coordination sphere for $(Gd2)^{3+}$ (6 O and 2+2 Se, d(Gd–O) = 239 – 243 pm, d(Gd–Se) = 308 – 376 pm), respectively (Figure 1). Thereby, this structure exhibits Se^{2--} centered $(Gd^{3+})_7$ polyhedra (capped trigonal prisms) connected via corners, edges and faces to form a three-dimensional network $^3_\infty\{[Se(Gd1)_{3/3}(Gd2)_{4/4}]^{4+}\}$ with empty voids apt to be filled with tetrahedral $[SiO_4]^{4--}$ anions (d(Si–O) = 163 – 165 pm) for charge compensation (Figure 2).

Magnetic susceptibility measurements for a bunch of selected crystals of $Gd_2Se[SiO_4]$ show a magnetic moment of μ_{exp} = 7.92 μ_B, which corresponds well to the expected value of μ_{eff} = 7.94 μ_B [8]. The θ value of –7.2 K in the *Curie-Weiss* equation suggests a certain tendency to antiferromagnetic ordering at very low temperatures (Figure 3).

References

[1] T. D. Brennan, J. A. Ibers, *Acta Crystallogr. C*, vol. 47, pp. 1062–1064, 1991.

[2] B. Deng, J. Yao, J. A. Ibers, *Acta Crystallogr. C*, vol. 60, pp. i110–i112, 2004.

[3] M. Grupe, W. Urland, *Z. Naturforsch.*, vol. 45 b, pp. 465–468, 1990.

[4] H. Person, M. Grupe, W. Urland, *Z. Anorg. Allg. Chem.*, vol. 626, pp. 280–283, 2000.

[5] D. D. Zimmermann, Th. Schleid, *Z. Kristallogr./Suppl.*, vol. 36, pp. 88–88, 2016.

[6] I. Ijjaali, K. Mitchell, J. A. Ibers, *Z. Kristallogr. – NCS*, vol. 217, pp. 157–158, 2002.

[7] K. Stöwe, *Z. Naturforsch.*, vol. 49 b, pp. 733–740, 1994.

[8] A. Weiss, H. Witte, *Magnetochemie*, 1. ed, Weinheim, Germany: Verlag Chemie GmbH, 1973, pp. 187–189.

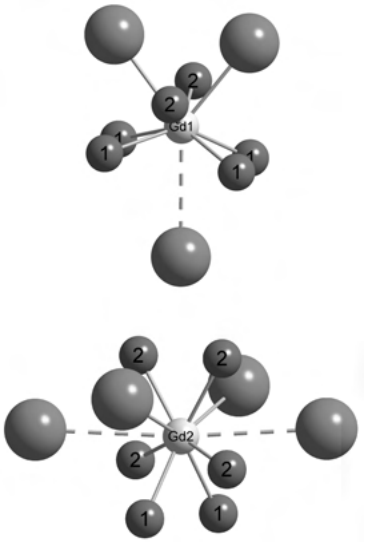

Figure 1 Coordination polyhedra of $(Gd1)^{3+}$ *(top)* and $(Gd2)^{3+}$ *(bottom)* in $Gd_2Se[SiO_4]$.

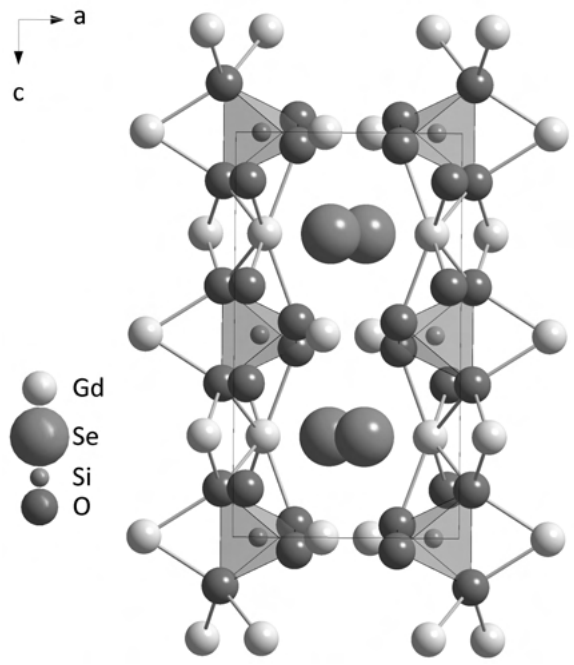

Figure 2 Extended unit cell of $Gd_2Se[SiO_4]$ as viewed along [010].

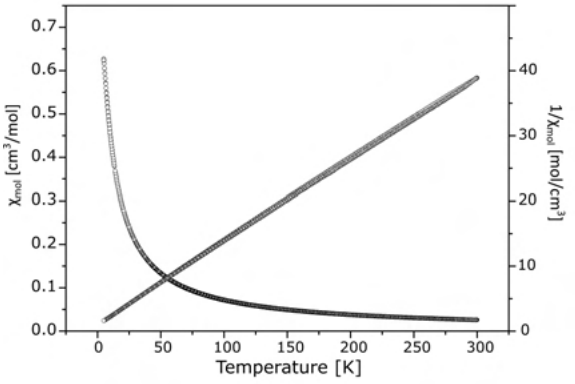

Figure 3 Molar *(black)* and inverse molar susceptibility (red) of $Gd_2Se[SiO_4]$

.

High-Pressure Hydrothermal Synthesis and Single Crystal X-Ray Structure Determination of K_2TmF_5

F. C. Goerigk[1], T. Schleid[1]

[1] University of Stuttgart, Institute of Inorganic Chemistry, Stuttgart, Germany

Prism-shaped single crystals of K_2TmF_5 could be obtained via hydrothermal synthesis from Tm_2O_3, TmF_3 and KF performed in a gold capsule filled with about 20 vol-% H_2O to provide suitable conditions for aiming at TmOF as target product. The sealed capsule was placed in a water-filled autoclave and kept at 300 °C and 75 bar pressure four five days. Single crystal X-ray diffraction revealed an orthorhombic unit cell (a = 1080.58(9) pm, b = 723.45(6) pm, c = 660.12(5) pm) for K_2TmF_5 in the space group *Pnma*.

The crystal structure of K_2TmF_5 features a crystallographically unique position for the Tm^{3+} cations with a coordination number of seven and interatomic $Tm^{3+} - -F^-$ distances of 218 – 227 pm. The edge-connected $[TmF_7]^{4--}$ polyhedra build up strands along the b-axis according to 1D-$[Tm(F1,2,3)^t_{3/1}(F4)^e_{4/2}]^{2--}$, which are bundled like a hexagonal rod packing (Figure 1). The potassium cations also occupy only one single position with a coordination number of eight *plus* one and bond lenghts of $d(K^+ - -F^- -)$ = 264 – 289 pm *plus* 334 pm. The $[KF_{8+1}]^{8--}$ polyhedra are – in contrast – connected via common edges in all spatial dimensions, but link the 1D-$[Tm(F1,2,3)^t_{3/1}(F4)^e_{4/2}]^{2--}$ chains as shown in Figure 2.

In hitherto research, the hydrothermal synthesis of K_2TmF_5 was published for the first time in 1990, but no crystallographic details such as a possible space group or atomic positions were given [1]. Other compounds concerning the K–Ln–F systems, such as K_2SmF_5 (1973) or K_2ErF_5 (1982), have been described using the non-centrosymmetric space group $Pna2_1$ [2, 3]. Single crystal structure solution and refinement calculations in this space group led to a *Flack-x* parameter of 0.45(7), so furthermore no obvious reason resulting in a loss of inversion symmetry could be identified. Hence, the centrosymmetric crystal structure description in space group *Pnma* was concluded to be the most appropriate one for the representatives of the K_2LnF_5 series, just like already described correctly by *Güde* and *Hebecker* for K_2GdF_5 in 1985 [4].

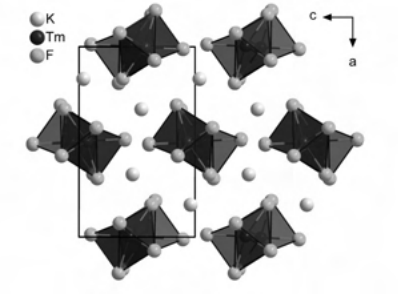

Figure 1 Section of the crystal structure in the centrosymmetric space group *Pmma* showing chains of edge-connected $[TmF_7]^{4-}$ polyhedra bundled like a hexagonal rod packing. The unit cell edges are emphasized as black lines.

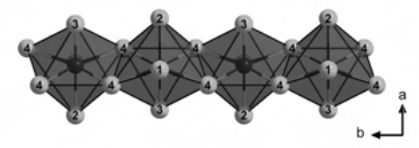

Figure 2 Strands of edge-connected $[TmF_7]^{4-}$ polyhedra according to 1D-$[Tm(F1,2,3)^{t}_{3/1}(F4)^{e}_{4/2}]^{2-}$ propagating along the *b*-axis in the crystal structure of K_2TmF_5.

Li2EuGd4O8: A New Lithium Lanthanoid Oxide with Orange-Yellow Luminescence

J.-L. Hoslauer[1], T. Schleid[1]

[1] University of Stuttgart, Institute for Inorganic Chemistry, Stuttgart, Germany

Orange-red needles of monoclinic $Li_2EuGd_4O_8$ were found in synthesis experiments using Gd_2O_3, $EuBr_2$ and LiH in silica-jacketed, arc-welded niobium capsules at 750 °C. These air- and water-stable crystals show a strong orange-yellow luminescence under ultraviolet light. The novel compound may further exhibit interesting magnetic properties, such as ferromagnetism like already reported for the analogous all-europium derivative $Li_2Eu_5O_8$ [1].

In 1973 *Bärnighausen*, *Schuster* and *Vogt* presented the lithium europium oxides $Li_2Eu_5O_8$, as well as $Li_2SrEu_4O_8$ and $Li_2BaEu_4O_8$ [2]. While their synthesis for the mixed-valent europium representative $Li_2Eu_5O_8$ used a combination of EuO, EuOCl and LiH, we could find similar dark red crystals using Eu_2O_3, $EuBr_3$ and LiH. Although $Li_2Eu_5O_8$ does not exhibit any luminescence under UV light, it shows an interesting ferromagnetic behavior that can described using a linear *Heisenberg* chain model, as reported by *Nyokong* and *Greedan* in 1981 [1].

It was therefore of particular interest to also synthesize the corresponding compound $Li_2EuGd_4O_8$ with an increased overall magnetic moment due to the presence of now five 4 f^7 configurated lanthanoid cations (one Eu^{2+} and four Gd^{3+}). Much to our surprise orange-red needles of $Li_2EuGd_4O_8$ showed a strong orange-yellow luminescence under UV light ($\lambda = 254$ nm). The Eu:Gd ratio was further confirmed by *EDXS* measurements, using three needles that gave Eu:Gd compositions around 1:3.8. An analogous *in-situ* reduction of $EuBr_3$ to $EuBr_2$ using an excess of LiH however did not lead to the formation of the title compound.

$Li_2EuGd_4O_8$ crystallizes in the monoclinic space group $C2/m$ and its crystal structure was refined from powder X-ray diffraction data ($\lambda = 71.07$ pm, Mo-Kα_1) using the *Rietveld* method (Tables 1 and 2). In this structure (Figure 1), the Eu^{2+} cations reside in a cubic arrangement $[EuO_8]^{14-}$ of eight oxide anions (d(Eu-O) = 275 – 284 pm). Both crystallographically distinguishable Gd^{3+} cations are surrounded by seven oxide anions capped trigonal prisms $[GdO_7]^{11-}$ d(Gd-O) = 223 – 250 pm). The Li^+ cations serve as centers of $[LiO_4]^{7-}$ tetrahedra (d(Li-O) = 187 – 207 pm) , while the oxide anions find themselves in three different octahedra $[(O1)Gd_3Eu_2Li]^{12+}$,$[(O2)Gd_4Li_2]^{12+}$ and $[(O3)Gd_3Eu_2Li]^{12+}$ as well as in a $[(O4)Gd_4]^{10+}$ tetrahedron. The $Eu^{2+}\cdots Eu^{2+}$ distances of 353 pm resemble those found for other europium(II) oxides that show ferromagnetic coupling like EuO (364 pm) [4] or Eu_3O_4 (350 pm) [5].

References

[1] T. Nyokong, J. E. Greedan, *Inorg. Chem.*, vol. 21, pp. 398–401, 1982.

[2] H. Bärnighausen, R. Schuster, K. Vogt, in *Proceedings of the 10th Rare Earth Research Conference*, Carefree (AZ), USA, 1973.

[3] H. Bommer, *Z. Anorg. Allg. Chem.*, vol. 241, pp. 273–280, 1939.

[4] H. A. Eick, N. C. Bänzinger, L. Eyring, *J. Am. Chem. Soc.*, vol.78, pp. 5147–5149, 1956.

[5] R. C. Rau, in *Proceedings of the 3rd Conference on Rare Earth Research*, Clearwater (FL), USA, 1963.

Table 1. Crystallographic data and structure refinement for $Li_2EuGd_4O_8$ from powder X-ray diffraction data.

Empirical formula	$Li_2EuGd_4O_8$
Space group	$C2/m$ (no. 12)
a / pm	1333.64(6)
b / pm	352.62(2)
c / pm	963.28(4)
β / °	119.648(1)
Z	2
ρ_{calc} / g·cm^{-3}	7.782
V_m / cm^3·mol^{-1}	118.55(2)
Diffractometer	Stadi-P (STOE & Cie), Mo-Kα_1
F(000)	778
Range in h,k,l	0–26, 0–7, ±19
R_p, R_{wp}	0.089, 0.121
R_{exp}	0.064
Goodness of Fit	1.876

Table 2. Atomic positions and *Wyckoff* sites in the asymmetric unit of $Li_2EuGd_4O_8$.

Atom	Site	x/a	y/b	z/c
Li	4*i*	0.309*	0	0.738*
Eu	2*a*	0	0	0
Gd1	4*i*	0.1102(2)	0	0.4392(2)
Gd2	4*i*	0.3377(2)	0	0.1870(2)
O1	4*i*	0.458*	0	0.758*
O2	4*i*	0.264*	0	0.381*
O3	4*i*	0.315*	0	0.936*
O4	4*i*	0.082*	0	0.656*

* The positions of the lithium and oxide ions are taken from the published data of $Li_2Eu_2O_5$ [2] and were not further refined.

Figure 1

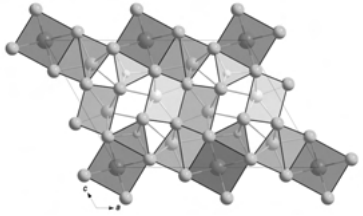

Figure 2 Unit cell of $Li_2EuGd_4O_8$ as viewed along [010] with emphasized oxygen polyhedra around Eu^{2+}, Gd^{3+} and Li^+. The Eu^{2+} cations are displayed in orange, the Gd^{3+} cations in grey, the Li^+ cations in yellow and the O^{2-} anions in blue.

Hydrothermal crystallization in phosphate systems with alkaline and transition metals

E. Kochetkova[1]

[1] Lomonosov Moscow State University, Moscow, Russia

The synthesis was carried out in multicomponent phosphate systems in hydrothermal conditions (T = 280 ° C and P = 100 bar) containing transition metal ions (Mn2+, Ni2+, Co2+), alkali ions (Li+, K+), aluminum ion (Al3+).

The crystallization products were examined under a binocular microscope and separated into phases according to morphological features. To determine the chemical composition of the synthesized phases, a semi-quantitative X-ray spectral analysis was performed on a scanning electron microscope. X-ray diffraction of powder and single-crystal samples was used to determine the symmetry and the unit cell parameters of the compounds. Based on the achieved data, the phases were identified using the ICSD crystal structure database.

As a result of 9 experiments, analogs of minerals such as the Co-analogue of the triphilin-lithiophilite series LiCoPO4, synthetic lithiophosphate Li3PO4, pechkaite Mn5(PO4)3Cl and berlinite AlPO4 were identified. Also in the experiments were obtained KNiPO4·H2O, a phase of mixed composition Mn2(PxV1-x)(VyP1-y)O7, as well as (Mn, Co)6(PO4)4·H2O and KAlPO4OH (Al-analog of KTP).

In one of the experiments in a system containing manganese(II) chloride, potassium pyrophosphate, aluminum oxide and water, two new compounds KMnAl2(PO4)3(H2O)2 and K2Mn3(H2O)2[P2O7] were obtained. Their crystal structures were established as a result of an X-ray diffraction (Xcalibur-S-CCD diffractometer) study based on a single-crystal experimental material. The crystal structures was solved by direct methods and refined by full-matrix leastsquares method using the program SHELX [1,2]. These results were published [3].

References

[1] Sheldrick G.M., "SHELXT – Integrated space-group and crystal structure determination," *Acta Crystallogr. Sect. A*, vol. 71, pp. 3–8, 2015.

[2] Sheldrick G.M., "Crystal structure refinement with SHELXL," *Acta Crystallogr. Sect. C*, vol. 71, pp. 3–8, 2015.

[3] Kiriukhina G. V., Yakubovich O. V., Shvanskaya L. V., Kochetkova E. M., Dimitrova O. V.,. Volkov A. S and Simonov S. V., "Novel K/Mn phosphate hydrates, K2Mn3(H2O)2[P2O7]2 and KMn(H2O)2[Al2(PO4)3]: hydrothermal synthesis and crystal chemistry," *Acta Crystallogr. Sect. C*, vol. 76, pp. 302–310, 2020.

Crystal Structure of a new ternary phase in the system Ba-Mg-Zn

K. Köhler[1], C. Röhr[1]

[1] Albert-Ludwigs-Universität Freiburg, Institut für Anorganische und Analytische Chemie, Freiburg, Germany

Magnesium-containing alloys of the heavier alkaline earth metals Ca and Sr with Zn have been investigated for their mechanical stability combined with low weight and toxicological safety, among other applications, as biodegradable materials [1-3]. The obtained ternary phases exhibit a variety of different crystal structures [1,2,4]. Now the Ba-Mg-Zn ternary system has also been systematically investigated for the presence of analogous phases.

The synthesis was carried out by melting reaction from the elements, which were weighed under argon and sealed in a tantalum tube. The sample was heated up to 900°C and cooled with a rate of 20 K/h. The crystal structure of the new ternary phase was determined by means of single-crystal X-ray data. The intermetallic phase $Ba_6Mg_xZn_{11-x}$ [$x = 2.80(1)$, $R\bar{3}m$, $a = 1011.96(8)$ pm, $c = 1703.6(2)$ pm, $Z = 3$] crystallizes in a new $AM_{\sim 2}$ type structure (s. Fig. 1). The structure consists of one A and three M layers. Six A atoms join, to form an empty octahedral cluster, and the M atoms form corner-linked [M_{11}] dumbbells. The complete structure can be described by a string of these polyhedra along [001] direction (s. Fig. 2). Ba occupies the A positions, $M(1)$ is a pure zinc layer. The remaining atomic positions $M(2)$ and $M(3)$ are occupied by zinc and magnesium satistically (49 at.-% and 67 at.-% Mg at $M(2)$ and $M(3)$, respectively).

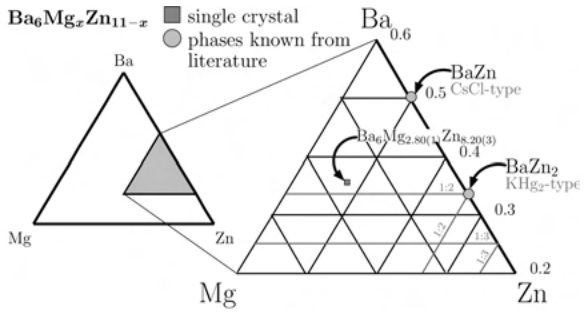

Figure 1 Section of the ternary composition chart of the Ba-Mg-Zn system (the compounds known from literature marked in gray, the composition of the single crystal is in dark blue).

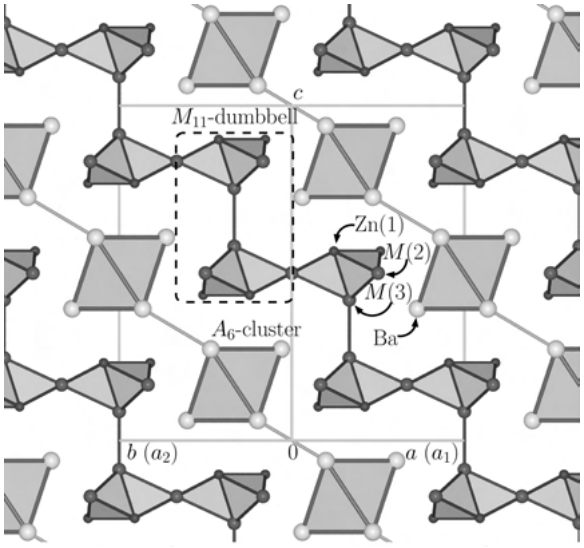

Figure 2 Section [polyhedral layer of the (110) plane] of the crystal structure of $Ba_6Mg_{2.80(1)}Zn_{8.20(3)}$ (red/magenta/gold spheres: Zn/M/Ba atoms , | :A_6 - M_{11} : | along [001] direction).

$K_3Lu_7Se_{12}$: The first potassium lanthanoid selenide with $Cs_3Y_7Se_{12}$-type crystal structure

P. L. Lange[1], A. Friedly[1], B. M. Schulz[1], T. Schleid[1]

[1] University Stuttgart, Institute of Inorganic Chemistry, Solid-State Chemistry, Stuttgart, Germany

In the late 1990s years the first ternary compounds with the composition $A_3RE_7Ch_{12}$ were identified (A = Rb and Cs, RE = Y and Yb) for the examples of $Rb_3Yb_7Se_{12}$ [1] and $Cs_3Y_7Se_{12}$ [2, 3]. Today selenides with the formula $Cs_3RE_7Se_{12}$ are known for RE = Sm, Gd – Tm [4–7] and tellurides $Cs_3Ln_7Te_{12}$ with Ln = Sm, Gd, Tb [8]. Other examples are $K_3Er_7S_{12}$ and $Rb_3Er_7S_{12}$ [9] among the sulfides as well as $Rb_3Dy_7Se_{12}$ [10]. They all crystallize in the orthorhombic space group *Pnnm* in a channel-providing defect Z-type structure of the sesquiselenides (*e.g.* Lu_2Se_3: orthorhombic, *Fddd*; $d(Lu^{3+}–Se^{2--}) = 279 – 286$ pm [11]) according to 3D-$[Lu_7Se_{12}]^{3--}$ filled with A^+ cations. As easily can be seen there is no combination with K^+, Ln^{3+} and Se^{2--} ions so far.

Single crystals of $K_3Lu_7Se_{12}$ were now obtained from the reaction of lutetium powder (Lu), red phosphorus (P), selenium (Se) and potassium chloride (KCl) mixed in a molar ratio of 1:1:4:1 designed to yield $KLu[P_2Se_6]$ in analogy to $KDy[P_2Se_6]$ [12]. The mixture was filled into an evacuated silica glass ampoule and heated to 950 °C for 48 h. The temperature was held for 144 h and subsequently the ampoule was cooled down to 350 °C within 36 h. $K_3Lu_7Se_{12}$ occurs as orange-colored needle-shaped single crystals and crystallizes with the lattice parameters a = 1227.96(8) pm, b = 2561.03(17) pm and c = 407.82(3) pm for Z = 2. Its crystal structure (CSD-2052785) displays a three-dimensional network of vertex- and edge-sharing $[LuSe_6]^{9-}$ octahedra ($d(Lu^{3+}–Se^{2--}) = 277 – 294$ pm). In this way channels along [001] are created and occupied by K^+ cations (Figure 1). To ensure electroneutrality and a reasonable distance between two $(K2)^+$ cations (d(K2···K2) = 237 pm) the K2 position must be half occupied, which is confirmed by the results of the structure refinement.The $K^+–Se^{2--}$ distances within the resulting (capped) trigonal prisms (Figure 2) range from 322 to 372 pm and agree well with those in *anti*-CaF_2-type K_2Se ($d(K^+–Se^{2--})$ = 333 pm for C.N. = 4) [13].

References

[1] S.-J. Kim, S.-J. Park, H. Yun, J. Do, *Inorg. Chem.*, vol. 35, no. 18, pp. 5283–5289, Aug. 1996.

[2] M. Folchnandt, Th. Schleid, *Z. Kristallogr./Suppl.*, vol. 11, p. 80, 1996.

[3] M. Folchnandt, Th. Schleid, *Z. Anorg. Allg. Chem.*, vol. 623, no. 10, pp. 1501–1502, Oct. 1997.

[4] M. Folchnandt, Th. Schleid, *Z. Kristallogr./Suppl.*, vol. 12, p. 125, 1997.

[5] M. Folchnandt, Th. Schleid, *Z. Anorg. Allg. Chem.*, vol. 624, no. 10, pp. 1595–1600, Oct. 1998.

[6] C. Schneck, A. Elbe, C. M. Schurz, Th. Schleid, *Acta Crystallogr. E*, vol. 68, no. 1, i2 , Jan. 2012.

[7] A. H. Geyer, A. Elbe, Th. Schleid, in *26th Annual Conference of the German Crystallographic Society, March 5–8, 2018, Essen, Germany*, Berlin, Germany, Boston, USA: De Gruyter, 2018, p. 99.

[8] O. Tougaît, H. Noël, J. A. Ibers, *Solid State Sci.*, vol. 3, no. 4, pp. 513-518, May 2001.

[9] F. Lissner, I. Hartenbach, Th. Schleid, *Z. Anorg. Allg. Chem.*, vol. 628, no. 7, pp. 1552–1555, Jul. 2002.

[10] M. Folchnandt, Th. Schleid, *Z. Kristallogr. NCS*, vol. 215, no. 1, p. 9, 2000.
[11] M. Folchnandt, C. Schneck, Th. Schleid, *Z. Anorg. Allg. Chem.*, vol. 630, no. 1, pp. 149–155, Jan. 2004.
[12] B. M. Schulz, Doctoral Dissertation, University Stuttgart, Germany, 2021.
[13] E. Zintl, A. Harder, B. Dauth, *Z. Elektrochem.*, vol. 40, no. 8, pp. 588–593, Aug. 1934.

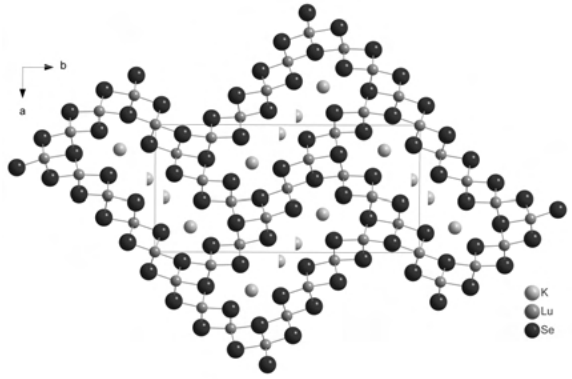

Figure 1 Extended unit cell of $K_3Lu_7Se_{12}$ as viewed along [001]. The lutetium-selenium sublattice consists of vertex- and edge-shared $[LuSe_6]^{9-}$ octahedra, while the empty channels are occupied with potassium cations.

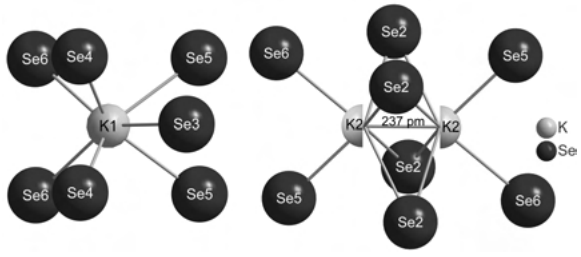

Figure 2 Selenide coordination spheres of both crystallographically different K^+ cations in the crystal structure of $K_3Lu_7Se_{12}$.

Single Crystals of K2NdCl5 and K2SmCl5

F. Lissner[1], J.-L. Hoslauer[1], G. Meyer[2], T. Schleid[1]
[1] University of Stuttgart, Stuttgart, Germany
[2] Kungliga Tekniska Högskolan Stockholm, Stockholm, Sweden

Single crystals of K_2NdCl_5 and K_2SmCl_5 were furnished by the oxidation of KNd_2Cl_5 [1] and KSm_2Cl_5 [2] with sulfur along with $Nd_3S_2Cl_5$ [3] and Sm_2SCl_4 [4] as target products. Violet K_2NdCl_5 (a = 1270.86(8), b = 874.12(6), c = 797.03(5) pm) and yellow K_2SmCl_5 (a = 1267.49(8), b = 867.61(6), c = 794.52(5) pm) crystallize in the orthorhombic space group *Pnma* (no. 62) with Z = 4 adopting the K_2PrCl_5-type structure [5]. The atomic coordinates and displacement parameters were derived from 1372 unique reflections (all: 10360, R_{int} = 0.030) with R_1 = 0.032 for K_2NdCl_5 (Table 1, *top*) [6] as well as 1337 unique reflections (all: 6787, R_{int} = 0.058) with R_1 = 0.027 for K_2SmCl_5 (Table 1, *bottom*) [6] using X-ray diffraction data collected with a MoKα-source equipped Siemens-Stoe AED2 device and the program suite SHELX-76 [7] based on full-matrix least-squares refinements. The crystallographically unique Ln^{3+} cations are surrounded by seven Cl^- anions as centers of capped trigonal prisms $[LnCl_7]^{4-}$, which share two *trans*-oriented edges to form linear 1D-$\{[Ln(Cl1,2,3)_{3/1}(Cl4)_{4/2}]^{2-}\}$ chains propagating along [010] (Figure 1, *top*). Bundled as a hexagonal rod-packing, they are connected and charge-balanced by K^+ cations in ninefold Cl^- coordination (Figure 1, *bottom*). The interatomic distances of 275 – 284 pm for $d(Nd^{3+}–Cl^-)$ and 272 – 282 pm for $d(Sm^{3+}–Cl^-)$ as well as them of 315 – 335 pm *plus* 388 pm for $d(K^+–Cl^-)$ in K_2NdCl_5 and 313 – 336 pm *plus* 384 pm for $d(K^+–Cl^-)$ in K_2SmCl_5 agree well with those in the prototypic K_2PrCl_5 ($d(Pr^{3+}–Cl^-)$ = 277 – 286 pm, $d(K^+–Cl^-)$ = 314 – 335 pm *plus* 391 pm) [5,8] nicely reflecting the consequences of the lanthanoid contraction.

References

[1] G. Meyer, Th. Schleid, *Z. Anorg. Allg. Chem.*, vol. 528, pp. 55–60, 1985.
[2] Th. Schleid, G. Meyer, *Z. Anorg. Allg. Chem.*, vol. 553, pp. 231–238, 1987.
[3] F. Lissner, Th. Schleid, *Z. Anorg. Allg. Chem.*, vol. 627, pp. 507–512, 2001.
[4] F. Lissner, Th. Schleid, *Z. Anorg. Allg. Chem.*, vol. 625, pp. 1507–1511, 1999.
[5] G. Meyer, E. Hüttl, *Z. Anorg. Allg. Chem.*, vol. 497, pp. 191–198, 1983.
[6] F. Lissner, Diploma Thesis, Univ. Hannover, Germany, 1990.
[7] G. M. Sheldrick, *Program System SHELX-76*, Univ. Göttingen, 1976.
[8] G. Meyer, J. Soose, A. Moritz, V. Vitt, T. Holljes, *Z. Anorg. Allg. Chem.*, vol. 521, pp. 161–172, 1985.

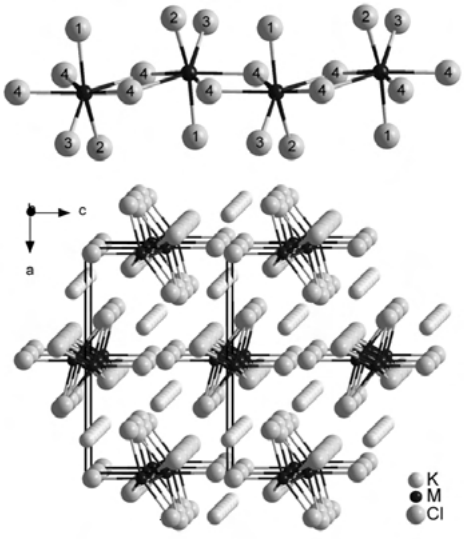

Figure 1

Table 1. Fractional atomic coordinates and coefficients of the anisotropic thermal displacement parameters for K_2NdCl_3 (*top*) and K_2SmCl_3 (*bottom*).

Atom	Site	x/a	y/b	z/c	U_{eq}*/pm²
K	8*d*	0.17079(5)	0.00572(8)	0.94769(9)	286(3)
Nd	4*c*	0.00575(1)	1/4	0.42404(3)	151(1)
Cl1	4*c*	0.18067(9)	1/4	0.62670(14)	269(5)
Cl2	4*c*	0.29458(8)	1/4	0.16321(14)	233(5)
Cl3	4*c*	0.00771(8)	1/4	0.07575(13)	211(4)
Cl4	8*d*	0.42322(6)	0.04350(8)	0.83356(11)	244(4)

* $U_{eq} = 1/3\,(U_{11} + U_{22} + U_{33})$

Atom	U_{11}	U_{22}	U_{33}	U_{23}	U_{13}	U_{12}
K	280(3)	254(3)	325(4)	−66(3)	−9(3)	11(3)
Nd	175(1)	119(1)	158(1)	0	16(1)	0
Cl1	244(5)	291(6)	271(6)	0	67(4)	0
Cl2	186(5)	265(5)	247(5)	0	15(4)	0
Cl3	225(4)	226(4)	182(4)	0	1(4)	0
Cl4	342(4)	150(3)	239(4)	21(3)	−83(3)	−27(3)

Atom	Site	x/a	y/b	z/c	U_{eq}*/pm²
K	8*d*	0.17064(6)	0.00602(8)	0.94568(12)	300(4)
Sm	4*c*	0.00556(9)	1/4	0.42449(3)	165(1)
Cl1	4*c*	0.18033(9)	1/4	0.62310(17)	278(5)
Cl2	4*c*	0.29638(8)	1/4	0.16081(16)	246(5)
Cl3	4*c*	0.00834(8)	1/4	0.07807(15)	228(5)
Cl4	8*d*	0.42514(6)	0.04389(8)	0.83349(11)	258(4)

* $U_{eq} = 1/3\,(U_{11} + U_{22} + U_{33})$

Atom	U_{11}	U_{22}	U_{33}	U_{23}	U_{13}	U_{12}
K	304(3)	269(3)	327(4)	−74(3)	−12(3)	10(3)
Sm	193(1)	133(1)	170(1)	0	16(1)	0
Cl1	258(5)	290(5)	286(6)	0	59(5)	0
Cl2	209(4)	271(5)	257(6)	0	16(4)	0
Cl3	249(4)	230(4)	204(5)	0	4(4)	0
Cl4	367(4)	168(3)	240(4)	19(3)	−74(3)	−22(3)

Figure 2

Unconnected Bromide Layers in the Crystal Structure of $DySb_2O_4Br$

R. J. C. Locke[1], F. C. Goerigk[1], T. Schleid[1]

[1] University of Stuttgart, Institute for Inorganic Chemistry, Stuttgart, Germany

Similar to the isotypic rare-earth metal(III) oxoantimonate(III) bromides $RESb_2O_4Br$ (RE = Eu - Tb) [1], almost colorless square platelets emerged during the synthesis of $DySb_2O_4Br$ [2, 3]. For this purpose, stoichiometric amounts of Dy_2O_3, $DyBr_3$ and Sb_2O_3 were mixed in a molar ratio of 1:1:3 with CsBr as flux and put into an evacuated fused silica ampoule. The mixture was heated to 750 °C for two days and cooled down to 666 °C with 5 °C/h in the furnace. This temperature was held for three days, followed by cooling with 5 °C/h to 530 °C, and this temperature was also kept for two days. Finally, the ampoule was cooled down to room temperature in the closed furnace with 150 °C/h.

$DySb_2O_4Br$ crystallizes in the monoclinic space group $P2_1/c$ with a = 895.18(6) pm, b = 783.41(5) pm, c = 782.37(5) pm and β = 91.542(3)° for Z = 4 (CSD-2051975). Eight oxygen atoms form a distorted cube around each Dy^{3+} cation and these $[DyO_8]^{13-}$ cubes are linked with each other via four edges to form 2D-$[DyO^e_{8/2}]^{5-}$ layers (Figure 1). The distances between dysprosium and oxygen range from 226 to 254 pm. Each Sb^{3+} cation is connected to three oxygen atoms resulting in $[SbO_3]^{3-}$ ψ^1-tetrahedra. The antimony-oxygen links follow a zigzag-chain motif according to 1D-$[SbO^v_{2/2}O^t_{1/1}]^{3-}$. So two of the oxygen atoms are linked to other Sb^{3+} cations and the third one is only bonded to a single one. The Sb^{3+}-O^{2-} distances are 194 - 210 pm and the bridging oxygen atoms show longer bond lengths than the terminal ones (Figure 2). There is no bonding to the layer of bromide anions, because the shortest distance between Br^- and Sb^{3+} is 320 pm and therefore no coordination is observed. The same holds for the shortest $Br^-\cdots Dy^{3+}$ distance of 425 pm.

References

[1] F. C. Goerigk, V. Paterlini, K. V. Dorn, A.-V. Mudring, Th. Schleid, *Crystals*, vol. 10, p. 1089, 2020.

[2] F. C. Goerigk, Doctoral Dissertation, Univ. Stuttgart, Germany, 2021.

[3] R. J. C. Locke, Master Thesis, Univ. Stuttgart, germany, 2021.

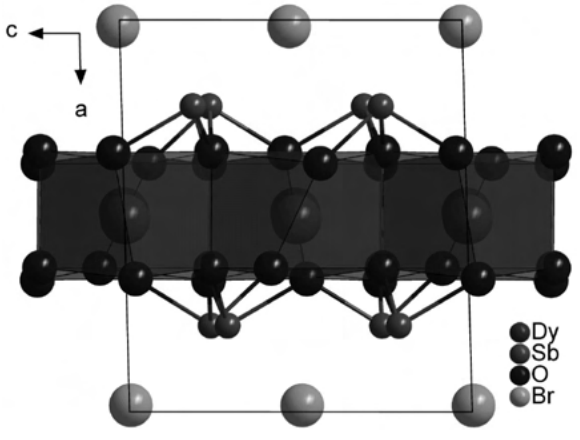

Figure 1 Extended unit cell of $DySb_2O_4Br$ in the monoclinic space group P21/c.

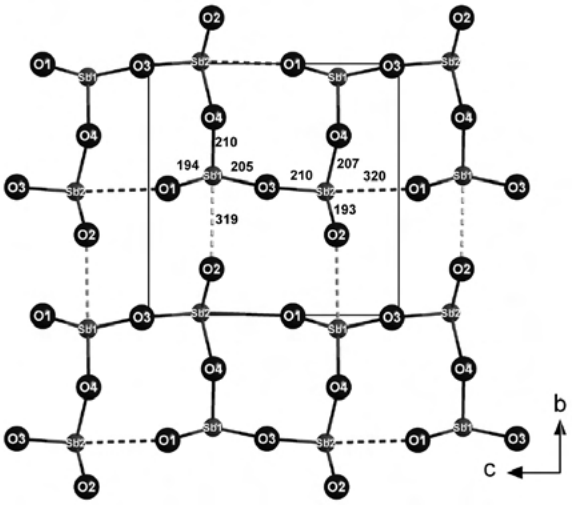

Figure 2 Meandering one-dimensional infinite chains 1D-$[SbO^{v}_{2/2}O^{t}_{1/1}]^{3-}$ of vertex-connected $[SbO_3]^{3-}$ ψ^1-tetrahedra in the monoclinic crystal structure of $DySb_2O_4Br$.

Synthesis, crystal and electronic structure of the new binary $A^I Hg_5$ mercurides KHg_5 and Rb_7Hg_{36}

C. Röhr[1], M. Wendorff[1]

[1] University of Freiburg, Institute for Inorganic and Analytical Chemistry, Freiburg, Germany

In the course of 'coloring' studies of alkali/alkaline-earth (A) mercurides AM_4 and AM_6 (M=Hg and In/Ga/Sn [1-4]) we unexpectedly obtained two new binary mercurides AHg_5 from ternary mixtures of A, Hg and the named p-block element. Later on, the two title compounds could also be prepared from nearly stoichiometric binary melts K-Hg and Rb-Hg.

KHg_5 crystallizes in a new structure type (orthorhombic, $Pmmn$, a=515.30(6), b=1756.7(2), c=1025.67(13) pm, $R1$=0.087 %, Fig. 1) which - according to its chemical composition - exhibits structure elements known from the hexamercurides AHg_6 [2,3] at one hand (planar Hg nets with 5/8-membered rings running perpendicular to the short [100] direction; $[KHg_{18}]$ cation coordination polyhedra, CCPs) and the $BaAl_4/A_5Hg_{19}$ (A=Rb,Cs [5,6]) type features on the other hand (square pyramids, $HgHg_4$ tetrahedra). The overall structure is best desribed by a space-filling arrangement of the $[KHg_x]$ (x=16-18) CCPs (yellow), squeezed $[Hg_4]$ tetrahedra (green), $[Hg_6]$ octahedra (cyan) and distorted $[Hg_8]$ cubes/trigonal double-prisms (blue). The coordination numbers of the nine crystallographically different Hg atoms vary from 4 to 7(+3) Hg (+ 2 to 5 K) with Hg-Hg distances spanning a wide range between 289 and 386 pm.

The even more complex structure of the rubidium mercuride Rb_7Hg_{36} (tetragonal, $P\bar{4}m2$, a=1061.4(2), c=2120.2(5) pm, $R1$=0.109 %) consists of 17 Hg and 6 Rb sites. Five of the six different $[RbHg_x]$ CCPs (x=16-20; yellow in Fig. 2) are fused *via* opposite pentagonal or hexagonal faces to form non-intersecting columns along [100]/[010] [Rb(5,6)] and [001] [Rb(1-3)] (= Nb positions in Nb_3Sn). A similar structural feature is observed in the cubic A_3Hg_{20} phases [6] (and the related clathrate-I type), which accordingly crystallize in the supergroup $Pm\bar{3}n$ with comparable axis lengths (Rb_3Hg_{20}: a=1073.7 pm, $\approx a \approx \frac{c}{2}$ of Rb_7Hg_{36}). The new mercuride similarly exhibits octa-capped isosahedra (icosahedra stars, IS; blue/cyan in Fig. 2), which are located at one halve of the Sn sites of the Nb_3Sn prototype. The other halve of the Sn positions are taken by $[Rb(4)Hg_{16}]$ polyhedra. Overall, Rb CCPs, IS and $[Hg_4]$ tetrahedra (green) tile the space. The latter corner-sharing tetrahedra form layers of 4- and 8-membered rings, which represent cutouts of the clathrate-I structure of melanophlogite. Comparable $[Hg_{4/2}]$ tetrahedra networks (and additional four-bonded Hg atoms) are likewise found in $K_7Hg_{28}Sn_9$ [7] and several other (pseudo)hexagonal mercurides in the 1:∼5 composition range (cf. survey in [4]), which are similarly related to dodecasil-1H.

The calculated electronic structures of the two mercurides show the expected metallic behaviour with strong Hg p-bonding inside the complex polyanions. The Bader charges of Hg (q_{BB}) vary between −0.06 for the icosahedra center (in Rb_7Hg_{36}) to −0.26 for the four-bonded Hg atoms (in both structures).

References

[1] M. Wendorff, C. Röhr, *Z. Kristallogr. Suppl.*, vol. 38, p. 86, 2018.

[2] M. Wendorff, C. Röhr, *J. Alloys Compds*, vol. 546, p. 320, 2013.

[3] F. Tamborino, C. Hoch, *J. Alloys Compds*, vol. 618, p. 299, 2015.

[4] M. Wendorff, C. Röhr, *Z. Kristallogr.*, vol. 233, p. 515, 2018.

[5] E. Biehl, H. J. Deiseroth, *Z. Anorg. Allg. Chem.*, vol. 625, p. 389, 1999.

[6] E. Todorov, S. C. Sevov, *J. Solid State Chem.*, vol. 149, p. 419, 2000.

[7] M. Wendorff, C. Röhr, in preparation.

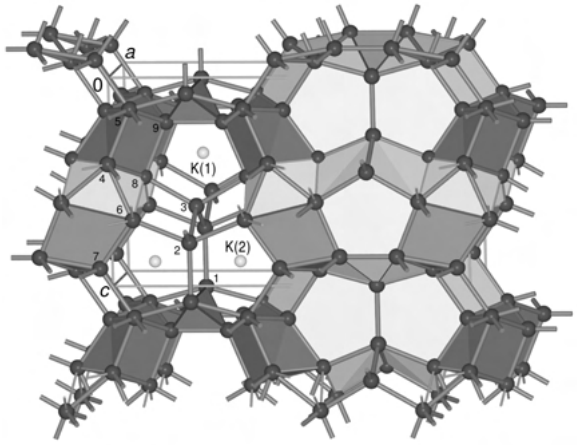

Figure 1 Crystal structure of the new binary mercuride KHg_5.

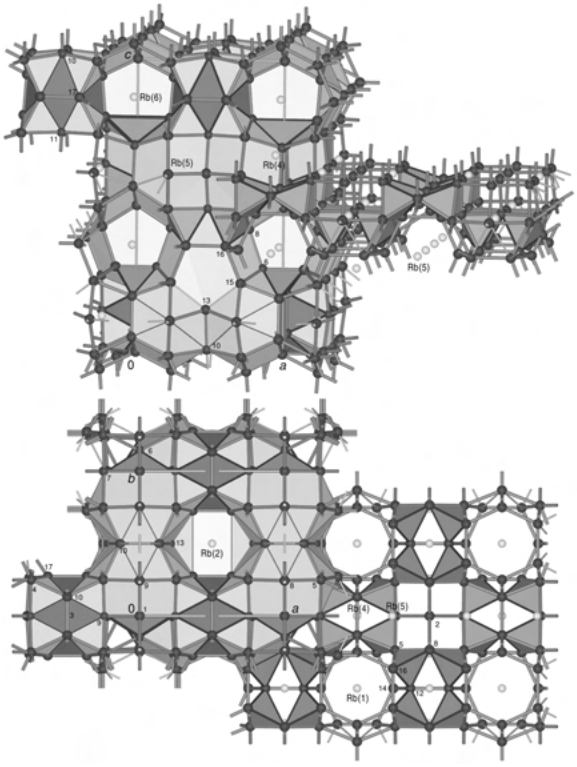

Figure 2 Different views of the tetragonal crystal structure of Rb_7Hg_{23}.

$Li_2Nd_3Cl_3[TeO_3]_4$: The First Lithium-Containing Lanthanoid Chloride Oxotellurate(IV)

P. L. Russ[1], S. Zitzer[1], T. Schleid[1]
[1] University of Stuttgart, Institute for Inorganic Chemistry, Stuttgart, Germany

Pale bluish violet single crystals of $Li_2Nd_3Cl_3[TeO_3]_4$ could be obtained as primary phase from mixtures of Nd_2O_3 and TeO_2 along with LiCl as flux and reactant in molar ratios of 2:4:3 after reactions in evacuated graphitized fused silica ampoules. Followed by 10 hours of heating up to 750 °C, this temperature was held for 5 days and then the furnace was cooled down to 500 °C within 24 h, before it was switched off.

$Li_2Nd_3Cl_3[TeO_3]_4$ crystallizes in the monoclinic space group $C\ 2/c$ with the lattice parameters a = 2354.67(13) pm, b = 564.91(3) pm, c = 1667.54(9) pm and β = 134.006(3)° for Z = 4 (CSD-2054116). Its structure is almost isotypic with that one of the $Na_2RE_3Cl_3[TeO_3]_4$ series (RE = Y, La – Nd, Sm – Lu) [1–5]. Hence there are two different Nd^{3+} cation positions just like in $Na_2Nd_3Cl_3[TeO_3]_4$ (a = 2403.29(14) pm, b = 572.35(3) pm, c = 1712.64(9) pm and β = 134.612(3)°) [2, 5]. The first one is coordinated by eight oxygen atoms as a square $[(Nd1)O_8]^{13--}$ antiprism, where two edges are bridged by ψ^1-tetrahedral bidentate $[TeO_3]^{2--}$ units and the remaining four oxide anions belong to monodentately attached $[TeO_3]^{2--}$ anions. The second Nd^{3+} cation is also surrounded by eight oxygen atoms in the shape of a square $[(Nd2)O_8]^{13--}$ antiprism, but now three edges are coordinated by bidentate $[TeO_3]^{2--}$ anions and the other two oxygen atoms are terminally bound to Te^{4+} cations. The Nd^{3+}–O^{2--} distances range from 234 to 265 pm and thus correlate well with those from 238 to 256 pm in $Na_2Nd_3Cl_3[TeO_3]_4$ showing a narrower range [2]. Via four common O···O edges all $[NdO_8]^{13--}$ polyhedra are connected to form 2D-$[NdO^e_{8/2}]^{5--}$ layers, which run parallel to the (001) plane emphasized as violet-rose bars in Figure 1. Using these layers as starting board, the two crystallographically different Te^{4+} cations dock to three oxygen atoms each, resulting in the formation of ψ^1-tetrahedral $[TeO_3]^{2--}$ anions. Their Te^{4+}–O^{2--} distances range from 187 to 191 pm and correlate well with those in $Na_2Nd_3Cl_3[TeO_3]_4$ covering an interval from 188 to 190 pm [2]. The O–Te–O angles range from 89 to 100 ° for the lithium and 89 to 102° for the sodium case [2]. For both cases almost identical 2D-$[Nd_3O_{12}Te_4]^+$ layers result, which have to be connected via A^+ cations (A = Li or Na) and Cl^{--} anions along [001]. Hence a three-dimensional network 3D-$[A_2Cl_3Nd_3O_{12}Te_4]$ is formed, due to the linkage of 2D-$[Nd_3O_{12}Te_4]^+$ layers via electrostatic interactions between two A^+ cations, certain oxygen atoms from $[TeO_3]^{2--}$ groups and three Cl^{--} anions per formula unit for charge compensation.

The unique Li^+ cation resides in an environment of three oxygen atoms, belonging to three terminal $[TeO_3]^{2--}$ anions. In addition, two Cl^{--} anions complete its coordination sphere to a square $[LiO_3Cl_2]^{7--}$ pyramid (Figure 2, *left*). The Li^+–O^{2--} distances range from 200 to 214 pm, whereas the Li+–Cl^{--} separations amount to 279 pm for Cl2 and 294 pm for Cl1. In comparison to

$Na_2Nd_3Cl_3[TeO_3]_4$, where a square $[NaO_4Cl_4]^{11--}$ antiprism is observed, the four Na^+–O^{2--} distances cover an interval from 229 to 272 pm *plus* 326 pm and the Na^+–Cl^{--} separations range from 286 to 302 pm *plus* 342 and 343 pm [2] (Figure 2, *right*).

From the two distinct Cl^{--} anions in the crystal structure, the first one (Cl1) is surrounded by two Li^+ and six Te^{4+} cations resulting in a distorted square $[ClLi_2Te_6]^{25+}$ antiprism. The second one (Cl2) receives coordination from one Li^+ and five Te^{4+} cations erecting distorted trigonal $[ClLiTe_5]^{20+}$ prism. Between the tellurium and the chlorine atoms there are σ-hole interactions [6], which also hold the three-dimensional network together. Since σ-hole interactions are known to be electrostatic and not covalent [6], the relevant $Cl^{--}\cdots Te^{4+}$ distances range from 299 to 378 pm in the lithium and from 315 to 382 pm [2] in the sodium case of the $A_2Nd_3Cl_3[TeO_3]_4$ couple with A = Li and Na.

References

[1] S. Zitzer, Doctoral Dissertation, Univ. Stuttgart, Stuttgart, Germany, 2012.
[2] S. Greiner, Doctoral Dissertation, Univ. Stuttgart, Stuttgart, Germany, 2018.
[3] S. Zitzer, F. Schleifenbaum, Th. Schleid, *Z. Naturforsch.*, vol. 69 b, pp. 150–158, 2014.
[4] D. O. Charkin, S. Zitzer, S. Greiner, S. G. Dorofeev, A. V. Olenev, P. S. Berdonosov, Th. Schleid, V. A. Dolgikh, *Z. Anorg. Allg. Chem.*, vol. 643, pp. 1654–1660, 2017.
[5] S. Greiner, S. Zitzer, S. Strobel, P. S. Berdonosov, Th. Schleid, *Z. Kristallogr.*, vol. 235, pp. 341–352, 20202.
[6] M. Beau, S. Lee, S. Kim, W.-S. Han, O. Jeannin, M. Fourmigué, E. Aubert, E. Espinosa, I.-R. Jeon, *Angew. Chem.*, vol. 133, pp. 370–374, 2021.

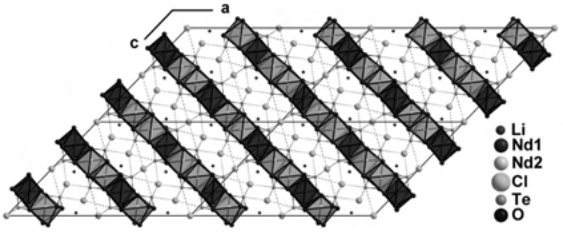

Figure 1 The three-dimensional network 3D-$[Li_2Cl_3Nd_3O_{12}Te_4]$ in the crystal structure of $Li_2Nd_3Cl_3[TeO_3]_4$ is a result of an interlink of 2D-$[Nd_3O_{12}Te_4]$ layers due to electrostatic interactions between Li^+ cations, certain oxygen atoms from $[TeO_3]^{2-}$ groups and Cl^- anions.

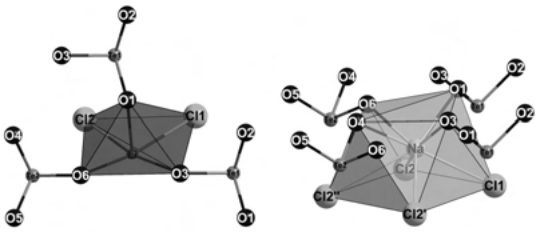

Figure 2 Square $[LiO_3Cl_2]^{7-}$ pyramid *(left)* in the crystal structure of $Li_2Nd_3Cl_3[TeO_3]_4$ and square $[NaO_4Cl_4]^{11-}$ antiprism *(right)* in the crystal structure of $Na_2Nd_3Cl_3[TeO_3]_4$.

Reconsideration of the space group symmetry of multiferroic phases TbMn2O5 and MnWO4 using neutron Renninger scans

P. Wimmer[1]
[1] LMU Munich, Munich, Germany

A precise knowledge of the crystal structure is a prerequisite to understand the mechanisms leading to the unique properties of multiferroics. Recently the well-established room temperature space groups of the multiferroics REMn2O5 (RE = rare earth, Bi, Y) and MnWO4 were questioned after the observation of weak forbidden reflections [1,2]. This thesis deals with the space group determination of TbMn2O5 and MnWO4 by focusing particularly on the influence of multiple diffraction on the intensity of such weak reflections. Therefore single crystals were studied using x-ray and neutron diffraction methods including neutron diffraction Renninger scans [3]. In both materials for the weak reflections large intensity variations of up to 600 % are observed with rotation around the azimuth angle. This indicates a strong contribution of multiple diffraction. By calculating the multiple diffraction patterns, no distinguishable differences between the different space groups are found for such small deviations in atomic positions of less than 0.03 Å. Still the results of a combined study of structural refinements from x-ray diffraction and the obtained multiple diffraction patterns of TbMn2O5 are in favor for a room temperature space group of *P2*, rather than previously stated *Pm*. In the case of MnWO4 the most likely space group is *P2*, but the results are not accurate enough to resolve the small structural changes.

References

[1] Balédent, V. et al. (2015). Evidence for Room Temperature Electric Polarization in REMn2O5 Multiferroics. Phys. Rev. Lett., 114, 117601
[2] Park, S. H. (2015). A new polar symmetry of huebnerite (MnWO4) with ferrodistortive domains. Journal of Magnetism and Magnetic Materials, Vol. 394, 160-172

[3] Renninger, M. (1937). "Umweganregung", eine bisher unbeachtete Wechselwirkungserscheinung bei Raumgitterinterferenzen. Zeitschrift für Physik, Vol. 106, 141–176

Inorganic functional materials

Controlled tuning of atomic structure in functional materials by acoustic standing waves and electric fields

C. Ludt[1], E. Ovchinnikova[2], A. Kulikov[3], D. Novikov[4], D. Meyer[1], M. Zschornak[1]

[1] TU Bergakademie Freiberg, Freiberg, Germany

[2] Physics Department of Moscow State University, Moscow, Russia

[3] A.V. Shubnikov Institute of Crystallography, Moscow, Russia

[4] Deutsches Elektronen-Synchrotron DESY, Hamburg, Germany

Active research in the field of condensed matter and nanotechnology not only led to significant progress in understanding the mechanisms of formation of electrical polarization and magnetoelectric phenomena, but also showed the possibilities of creating new classes of devices based on a combination of magnetoelectric and piezoelectric properties. Meanwhile, macroscopic properties, such as multiferroism and piezoelectricity, are associated with local structural changes that occur under the influence of external perturbations.

In a first step chosen crystal structures are analyzed by means of density functional theory (DFT) to validate the connection of external stress and internal change of lattice symmetry as well as atomic displacements. Among them are TeO_2, Li_2B4O_7, ZnO and $SrTiO_3$. Also in focus is the influence of oxygen vacancies on our structures. The research is currently accompanied by experiments in which standing acoustic waves are encoupled in crystal samples or an electric field is applied to change the structure parameters and particularly the structures' symmetry locally. Because the displacements are expected to be in picometer scale forbidden reflection technique is used to observe the induced effects. The obtained results can significantly widen the range of functional materials and can be directly used in modern technological applications.

Structure of ferroelectric low temperature phase of yttrium manganate YMn_2O_5 revisited

T. Weigel[1], C. Richter[2], M. Nentwich[3], D. Novikov[3], M. Zschornak[1], D. C. Meyer[1]

[1] TU Bergakademie Freiberg, Freiberg, Germany

[2] Leibniz Institut für Kristallzüchtung, Berlin, Germany

[3] P23 Beamline, PETRA-III, DESY, Hamburg, Germany

The material system YMn_2O_5 has several low temperatures phases, where magnetism and ferroelectricity occur. Especially, the origin of the ferroelectricity (FE) in a phase below $T_{FE} = 39$ K is an open question. The space group *Pbam* of the paraelectric phase does not allow polarization, also structural changes during the phase transition to a lower symmetry phase have not been detected yet. This means that the ferroelectricity must originate from changes in the Mn spin configuration [1] or from small atomic displacements [2], which could not be discovered by conventional structural analysis methods, because the displacements are below the spatial resolution limit. We apply the new Resonantly Suppressed Diffraction (RSD) [3] method, which is sensitive to minuscule structural changes in the sub-pm range, to shed new light on this controversial discussion. RSD is a structural characterization method in the field of Resonant Elastic X-ray Scattering and tunes the photon energy such that certain reflections approach zero due to destructive interference.

Here, we employ RSD on carefully chosen Bragg reflections below and above T_{FE}. With the data above T_{FE} we refined the static and dynamic displacements of the paraelectric phase, to receive an improved starting model for the structural characterization of the FE phase. With this starting model we were able to characterize the FE phase consolidating the findings about the origin of ferroelectricity in YMn_2O_5.

References

[1] Kimura, H., Noda, Y. & Kohn, K. (2009). Journal of Magnetism and Magnetic Materials, 321, 854. Proceedings of the Forth Moscow International Symposium on Mag.

[2] Noda, Y., Kimura, H., Fukunaga, M., Kobayashi, S., Kagomiya, I. & Kohn, K. (2008). Journal of Physics: Condensed Matter, 20, 434206.

[3] Richter, C., Zschornak, M., Novikov, D. V., Mehner, E., Nentwich, M., Hanzig, J., Gorfman,S. & Meyer, D. C. Nature Communications, 9, 178 (2018).

In situ / in operando studies

Structural and Electronic Characterization of Doped Exsolution Perovskites

L. Lindenthal[1], R. Rameshan[1], T. Ruh[1], S. Löffler[1], C. Rameshan[1]

[1] TU Wien, Institute of Materials Chemistry, Vienna, Austria

Perovskite-type oxide materials are promising candidates as catalysts for various reactions related to chemical energy conversion (e.g. the reverse water-gas shift reaction). This is due to their ability to form finely dispersed metal nanoparticles on the surface by exsolution [1]. The result is an excellent catalytic activity, while at the same time the perovskite backbone acts as a thermally and chemically highly stable support. Four such perovskite materials with the general formula La1-xCaxFeO3-δ or Nd1-xCaxFeO3-δ were characterized with respect to their crystal structure (using powder X-ray diffraction, XRD), their morphology (with scanning electron microscopy, SEM, and energy dispersive X-ray spectroscopy, EDX) and their electronic properties (by theoretical calculations based on density functional theory, DFT) [2]. For all materials, distorted perovskite structures were found, showing an orthorhombic symmetry. They were compared regarding the extent of the distortion depending on the cation-composition. Furthermore, DFT revealed the effect of Ca-doping, in particular a partial oxidation of Fe, leading to Jahn–Teller distortions. Additionally, the exsolution behaviour of the materials was investigated with in-situ XRD measurements. The formation of Fe particles could be observed and proven with SEM. Adding a small amount of Co-doping enhanced the exsolution properties. It enabled an easier exsolution and lead to smaller, Co-containing nanoparticles, which is important for catalytic applications.

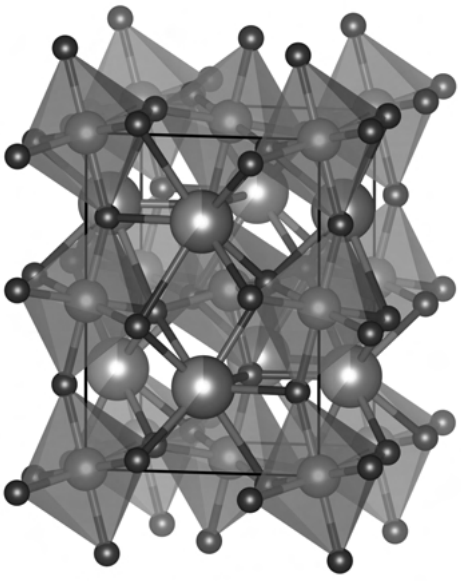

Figure 1

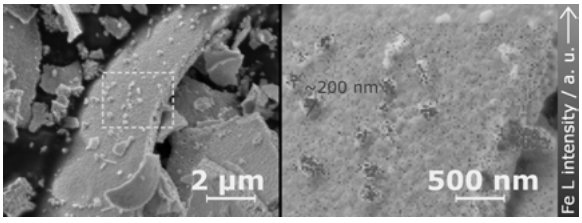

Figure 2

In situ XRPD observation of mechanochemical reactions in a ball mill

T. Rathmann[1], H. Petersen[1], S. Reichle[1], A. P. Amrute[1], W. Kersten[1], M. Etter[2], C. Weidenthaler[1]

[1] Max-Planck-Institut für Kohlenforschung , Kaiser-Wilhelm-Platz 1, 45470 Mülheim, Germany

[2] DESY, Notkestraße 85, 22607 Hamburg, Germany

Mechanochemistry has attracted a significant interest in materials synthesis and chemical reactions during the last decades. [1, 2] This applies to numerous chemical reactions, such as the synthesis of complex oxides, pharmaceuticals, or hybrid materials. [1, 3-5] Furthermore, mechanical alloying as well as the production/activation of heterogeneous catalysts or even direct mechanocatalytic reactions are pursued topics. [1, 5, 6] Mechanochemical routes meet several criteria of green chemistry and may provide unique reaction pathways and products. However, tracking what happens to a material during mechanochemical reactions is difficult. Since mechanical routes usually comprise solid-state reactants and/or products, spectroscopic and crystallographic investigations are

very interesting to understand the corresponding reaction mechanisms. Changes of structure and/or composition of crystalline compounds can be studied by *in situ* X-ray powder diffraction (XRPD) which is very promising to identify phase transitions and intermediate phases in mechanochemistry. *In situ* synchrotron diffraction has been applied successfully to study the mechanochemical synthesis of soft matter such as metal-organic frameworks or cocrystals in vibration ball mills. [1, 3, 4]

Nevertheless, the modification of commercial milling equipment turned out to be challenging for *in situ* studies of mechanochemical reactions of hard materials or mechanocatalytic reactions. In this work, we present the development of milling equipment suitable for *in situ* XRPD studies performed during the synthesis of inorganic hard materials. Several factors could be identified which turned out to be decisive for a successful reaction. Their individual contributions will be discussed and a tailor-made design of milling jars, also suitable for running catalytic reactions during ball milling, will be introduced.

References

[1] T. Friscic, C. Mottillo and H. M. Titi, *Angew. Chem. Int. Edit.*, vol. 59, pp. 1018–1029, 2020.

[2] A. P. Amrute, Z. Lodziana, H. Schreyer, C. Weidenthaler and F. Schueth, *Science*, vol. 366, p. 485, 2019.

[3] K. Uzarevic, I. Halasz and T. Friscic, *J. Phys. Chem. Lett.*, vol. 6, pp. 4129–4140, 2015.

[4] I. Halasz, S. A. J. Kimber, P. J. Beldon, A. M. Belenguer, F. Adams, V. Honkimaki, R. C. Nightingale, R. E. Dinnebier and T. Friscic, *Nat. Protoc.*, vol. 8, pp. 1718–1729, 2013.

[5] L. Takacs, *Chem. Soc. Rev.*, vol. 42, pp. 7649–7659, 2013.

[6] S. Immohr, M. Felderhoff, C. Weidenthaler and F. Schueth, *Angew. Chem. Int. Edit.*, vol. 52, pp. 12688-12691, 2013.

Micro and nano-crystalline materials

Three-dimensional coherent X-ray imaging of ferroelastic domains in $CsPbBr_3$ perovskite nanoparticles

D. Dzhigaev[1], L. Marcal[1], Z. Zhang[1], S. Sala[2], A. Björling[2], A. Mikkelsen[1], J. Wallentin[1]

[1] Lund University, Lund, Sweden

[2] MAX IV Laboratory, Lund, Sweden

Metal halide nanoparticle systems are promising candidates for the next generation of light-emitting, solar cell, and detector technologies. Characterization of their complicated crystal structures is important for tailoring their properties in a desired manner. In this work, we directly reconstruct three-dimensional twinned ferroelastic domains inside $CsPbBr_3$ (CPB) nanocrystals by Bragg coherent x-ray diffraction imaging (BCDI). An approach for phase retrieval of domain structures within twinned nanocrystals with the BCDI method is reported. A systematic study of several nanocrystals revealed a preferential double domain structure of CPB particles with sizes around 500 nm. A dislocation is also observed inside one of the reconstructed domains.

Antiphase boundaries in small iron oxide nanoparticles

T. Köhler[1], A. Feoktystov[1], E. Kentzinger[2], O. Petracic[2], T. Brückel[2]

[1] Forschungszentrum Jülich GmbH, Jülich Centre for Neutron Science JCNS at Heinz Maier-Leibnitz Zentrum MLZ, Garching, Germany

[2] Forschungszentrum Jülich GmbH, Jülich Centre for Neutron Science JCNS-2 and Peter Grünbger Institute, PGI-4, JARA-FIT, Jülich, Germany

Iron oxide nanoparticles find a wide variety of applications including targeted drug delivery and advanced cancer treatment methods. An important property of these particles is the saturation magnetization, which was shown to often be drastically reduced compared to bulk reference values. Previous studies have shown that planar lattice defects, so-called antiphase boundaries (APBs) are an important factor in this regard. Here we examine the influence of APBs on the atomic spin structure of nanoparticles with γ-Fe2O3 composition via Monte-Carlo simulations, explicitly considering dipole-dipole interactions between the magnetic moments, that have previously only been approximated. For a single APB through the particle center we find a reduction of the saturation magnetization of around 15% compared to a particle without APB due to a tilt of the net magnetic moment of both particle halves away from the applied field vector. Additionally, simulations of the Debye scattering equation are used to show the hkl-dependent line broadening effect of APBs in X-ray powder diffraction, thus providing a method of detecting APBs in nanoparticle samples.

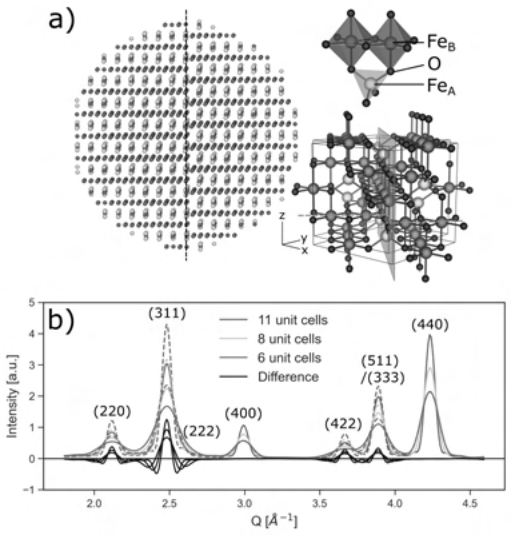

Figure 1 a) Nanoparticle structure used for Monte-Carlo and Debye scattering equation simulations. Oxygen atoms are not included for better visibility of the iron atoms. The APB is indicated with the black dashed line. The colors correspond to the lattice sites as indicated on the right. In the close-up of the unit cell the APB is drawn as a grey plane. b) Simulated X-ray powder diffraction patterns with (solid) and without (dashed) APB for different particle sizes. The difference curves highlight the hkl-dependence of the peak broadening.

Organic and metal-organic crystal structures

Experimental charge density studies on solids containing halogen bonds to pentafluoroiodobenzene

F. Busse[1], R. Wang[1], U. Englert[2], F. Otte[1], C. Strohmann[1]

[1] Anorganische Chemie, TU Dortmund, Dortmund, Deutschland

[2] RWTH Aachen University, Institute of Inorganic Chemistry, Aachen, Germany

In the last decades, significant progress has been made concerning the characterization of intermolecular interactions. Charge density studies on experimental diffraction data have been used successfully to derive information about the atom centred electron density distribution to analyse contacts such as halogen bonds. In these studies the focus was mainly on the properties of the halogen atom, whereas the effect of the halogen bond acceptor and its surrounding has not yet been systematically investigated.

We have analysed seven different structures containing pentafluoroiodobenzene either with or without a co-molecule; the co-molecules included nitrogen as the halogen acceptor in sp2 or sp3 hybridization. Based on low-temperature diffraction data collected up to high resolution, multipole refinements were used to derive information about the electron density beyond the spherical standard model.[1, 2, 3] The charge density about the iodine atoms differs largely between the structures; despite the assumed strength of the interaction, only one structure displays the typical aspheric density characteristic for a sigma-hole. Based on topological analyses according to Bader's Atoms in Molecules theory, we could evaluate the effect of different hybridizations of the halogen bond acceptor on the halogen bond.[4] In the pentafluoroiodobenzene structure without additional co-molecule, we investigated a short interhalogen contact between iodine and fluorine.

This work provides insight into specific effects of molecular structures on halogen bonds for a specific halogen donor system. As the properties of this interaction have proven to be very sensitive and variable in their outcome, further studies will be essential. They are expected to contribute to an adequate knowledge base indispensable for efficient crystal engineering.

References

[1] P. Coppens, *X-ray charge densities and chemical bonding*, Oxford, New York, USA: International Union of Crystallography/Oxford Univ. Press, 1997.

[2] N. K. Hansen, P. Coppens, *Acta Crystallographica Section A*, vol. 24, pp. 909–921, 1978.

[3] A. Volkov, P. Macchi, L. Farrugia, C. Gatti, M. PR, T. Richter, T. Koritsanszky, *XD2006*, New York, USA, 2006.

[4] R. F. W. Bader, *Atoms in molecules: A quantum theory*, reprinted, Oxford, USA: Clarendon Press, 1990 (2003).

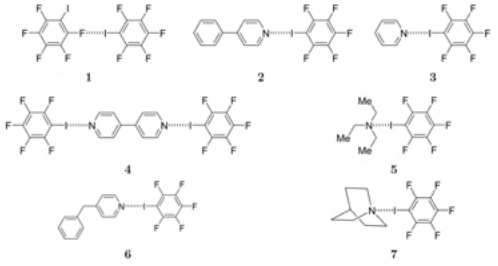

Figure 1 Presentation of the seven structures: All compositions contain pentafluoroiodobenzene, either pure (1) or with a co-molecule including nitrogen: (2) 4-Phenylpyridine, (3) Pyridine, (4) 4,4'-Bipyridine, (5) Triethylamine, (6) 4-Benzylpyridine, (7) Azabicyclo[2.2.2]octane. The horizontal dashed lines mark halogen bonds.

Exploring the Self-Assembly of Anisotropic Pillarplex Cations

A. Heidecker[1], A. Pöthig[2]

[1] Technical University of Munich, Departement of Chemistry, Chair of Inorganic and Organometal- lic Chemistry, Supramolecular Organometallics, Munich, Germany

The formation of porous molecular materials is investigated towards a possible implementation of pillarplexes as functional building blocks. The pillarplexes are supramolecular organometallic complexes (SOCs)[1] bearing tailor-made macrocyclic NHC-ligands and show exclusive shape selective encapsulation of linear molecules, tuneable solubility via anion exchange reactions and the corresponding Au(I)-pillarplexes show intrinsic photoluminescence.[2][3][4] The structural self-assembly is expected to be governed by the shape, charge and size of employed anions based on their interactions with the anisotropic pillarplex cations.

Consequently, a series of pillarplex salts with varying anions is targeted to synthesized and structurally characterized in the solid-state, with the aim to identify and understand determining interactions. Synthetically, the salts are yielded by simple anion exchange reaction or via solvothermal synthesis. The compounds are characterized by solid-state analysis (PXRD, SC-XRD, TGA) including porosity measurements (BET) and selected examples are presented and discussed.

References

[1] A. Pöthig, A. Casini, *Theranostics*, vol. 9, pp. 3150–3169, 2019.

[2] P. J. Altmann, A. Pöthig, *J. Am. Chem. Soc.*, vol. 138, pp. 13171–13174, 2016.

[3] P. J. Altmann, C. Jandl, A. Pöthig, *Dalt. Trans.*, vol. 44, pp. 11278–11281, 2015.

[4] P. J. Altmann, A. Pöthig, *Angew. Chemie - Int. Ed.*, vol. 56, pp. 15733–15736, 2017.

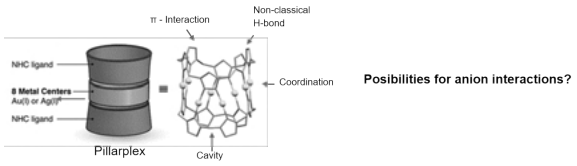

Figure 1

Application of QC Techniques to several elementorganic compounds: some reminiscences of a user

A. Nazarenko[1]

[1] SUNY College at Buffalo, Buffalo, USA

Several elementorganic compounds and macrocyclic 3d-transition metal complexes were investigated using known Hirshfeld refinement techniques (*Tonto* [1] and *NoSpherA2* [2]). These results were compared to traditional IAM refinement (*ShelXL* and *olex2.refine*) and with IAM corrected for interatomic scattering and lone pair scattering [3, 4] (these corrections were performed within *ShelXL* and/or *olex2.refine* frame). Reasonable position of hydrogen atoms is the most visible improvement over existing IAM procedures. Most of residual density in IAM solution could be removed by interatomic and lone pair scattering corrections; further application of Hirshfeld refinement techniques may result in minor r.m.s density and R-factor improvements.

An example of Cu(II) complex with 5,7,7,12,14,14-hexamethyl - 1,4,8,11-tetraazacyclotetradeca-4,11-diene (d= 0.62 Å, partially disordered) is shown on Figure 1.

References

[1] Fugel M., *et al.*, *IUCrJ*, vol. 5, pp. 32, 2018.

[2] Kleemiss F., *et al.*, *Chem.Sci.*, 2021.

[3] Franklin R. E., *Nature*, vol. 165, pp. 71, 1950.

[4] Afonine P.V, *et al., Acta Cryst*, vol. D63, pp. 1194, 2007; Nazarenko A.Y., *Z. Krist.*, vol. 38, pp. S44, 2018.

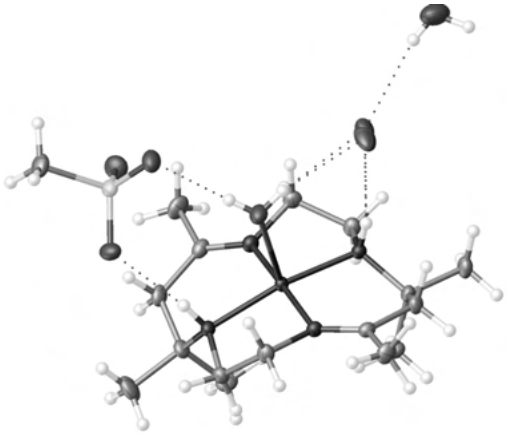

Figure 1 IAM (*ShelXL*): R=0.0404, r.m.s.$\Delta\rho$ 0.089, max/min $\Delta\rho$ 0.59/-0.34; C-C bond error 0.0017-0.0020 Å; IAM+correction *(ShelXL)*: R = 0.036, r.m.s.$\Delta\rho$ 0.081, max/min $\Delta\rho$ 0.40/-0.34; C-C bond error 0.0016-0.0017 Å; *NoSpherA2* (*ORCA, def2-TZVPD*): R = 0.036, max/min $\Delta\rho$ 0.7/-0.6, C-C bond error 0.0015-0.0018 Å.

In situ crystallization of l-menthone

M. Patzer[1], N. Nöthling[1], R. Goddard[1], C. Lehmann[1]
[1] Max-Planck-Institut für Kohlenforschung, Kaiser-Wilhelm-Platz 1, 45470 Mülheim an der Ruhr, Germany

Recently we determined the absolute configuration of a liquid product of an enantioselective Cu-catalyzed asymmetric fluorination reaction under ambient conditions by *in situ* crystallization. Establishing the absolute structure of the α-fluoroester decisively contributed to an understanding of the mechanistic course of the reaction. [1] Determination of the absolute configuration of such compounds using X-ray crystallography can be challenging. In order to explore the scope of the technique, we crystallized the natural compound, industrial feedstock and flavoring agent, (2S,5R)-trans-2-isopropyl-5-methylcyclohexanone, l-menthone, and determined its absolute configuration. This light atom structure contains just one oxygen atom as largest anomalous scattering atom (f' 0.05170, f" 0.03357, Cu-Kα radiation, λ = 1.54178 Å). Despite the importance of organic drugs in industry and nature there are a large number of liquid compounds for which their crystal structure is unknown. Knowledge about the absolute configuration of bio-organic molecules is important, since enantiomers often have different effects on an organism. Typically, the liquid sample is cooled down below its liquid-solid phase transition temperature and brought to crystallization. The crystalline powder so obtained can be used as a source for crystal growth. By translation of the capillary through the cold nitrogen gas stream a suitable single crystal can be grown at the liquid-solid phase boundary (inverse zone melting). [2] Using the example of l-menthone, we discuss the challenges and advantages of determining the absolute configuration of liquid samples using *in situ* X-ray crystallography. [3]

References

[1] M. Buchsteiner, L. Martinez-Rodriguez, P. Jerabek, I. Pozo, M. Patzer, N. Nöthling, C. W. Lehmann, A. Fürstner, *Chem. Eur. J.*, vol. 26, pp. 2509–2515, 2020.
[2] R. W. Seidel, R. Goddard, N. Nöthling, C. W. Lehmann, *Cryst. Eng. Comm.*, vol. 21, pp. 3295–3303, 2019.
[3] R. Boese, *Z. Kristallogr.*, vol. 229, pp. 595–601, 2014.

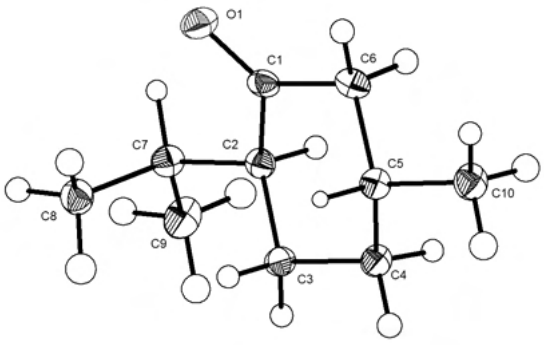

Figure 1

Expanding the Scope of Macrocyclic Poly-NHC Ligands: Bimetallic Palladium(II) and Platinum(II) Complexes

T. Pickl[1], A. Pöthig[2]
[1] Technical University of Munich, Departement of Chemistry, Chair of Inorganic and Organometallic Chemistry, Supramolecular Organometallics, Munich, Germany

Macrocyclic polyimidazolium salts are widely used in supramolecular chemistry as precursors for metal–NHC complexes. Here, we present the synthesis and structural characterization of the dinuclear palladium(II) and platinum(II)–NHC complexes Pd2L(PF6)2 and Pt2L(PF6)2 based on a macrocyclic calix[4]imidazolylidene[2]pyrazolate ligand obtained by in situ deprotonation of the tetraimidazolium salt H6L(PF6)4. Both compounds were also prepared by transmetallation from the literature-known silver(I)–NHC complex Ag8L2(PF6)4. 1H and 13C NMR spectroscopy combined with SC-XRD studies elucidated the structure of the palladium(II) and platinum(II) complexes. The d8 metal centers of both congeners are coordinated in a slightly distorted square-planar arrangement by the macrocyclic ligand. Similar to the previously reported nickel(II) complex Ni2L(PF6)2, the heavier metal homologs adopt a bent, saddle-shaped structure. In the solid state, one hexafluorophosphate ion in Pd2L(PF6)2 occupies the cavity of the cationic fragment [Pd2L]2+ with C–H···F contacts short enough to be rationalized as charge-assisted hydrogen bonds. In contrast, Pt2L(PF6)2 adopts a channel-like packing via self-assembly of the cationic [Pt2L]2+ fragments with the hexafluorophosphate counterions located outside of the cavities.

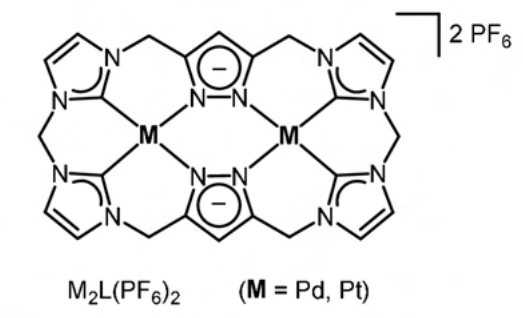

Figure 1

Spectroscopy

Soft X-ray analysis applied to crystallographic characterization of graphite

S. Matveev[1]

[1] JEOL (Germany) GmbH, Freising, Germany

There are various methods that are traditionally used for crystallographic characterization of materials, e.g. TEM, EBSD, XRD etc. JEOL recently developed a new type of wavelength dispersive spectrometer (WDS) that can be mounted on common scanning electron microscopes (SEM) or electron microprobes (EPMA). The spectrometer is sensitive to anisotropic soft X-ray emission, thus providing information about orientation of some anisotropic crystal structures. It utilizes a variable line spacing diffraction gratings, allowing the efficient and parallel collection of very low-energy X-rays (so called "soft" X-rays). This new Soft X-ray Emission Spectrometer (SXES) exhibits very high spectral resolution (0.3eV at Al L1), which allows to separately measure x-ray intensities due to sp^2-$\sigma \rightarrow$ 1s and P_z-$\pi \rightarrow$ 1s transitions in graphite. Complex structure of CKa(2) peak can be used to evaluate crystallinity of graphite, orientation, and grain size distribution at submicron scale as well as on the larger scale of tens of millimeters. Such application is relevant for development of Li batteries, in which Li concentration, distribution and chemical state can be also conveniently measured using the same SXES detector. Advantages of SXES include high sensitivity and spatial resolution, easy sample preparation and handling, as well as versatility. Since the detector can be mounted on JEOL SEM or EPMA it can be combined with other analytical methods such as EDS, WDS, CL and EBSD. Below we provide SXES spectra of C Ka(2) measured with JEOL SS-9400SXES using JS200N grating mounted on JSM-IT800HL FEG SEM at 5kV and 50nA. Graphite grains with different crystallographic orientations were analyzed. Emission intensities related to σ and π bonding exhibit maxima in parallel and perpendicular to [001] crystallographic direction respectfully. Parallel detection allows to reprocess ROI of the spectra and also plot peak ratios thus providing versatile and robust tool for investigation of carbon crystallinity.

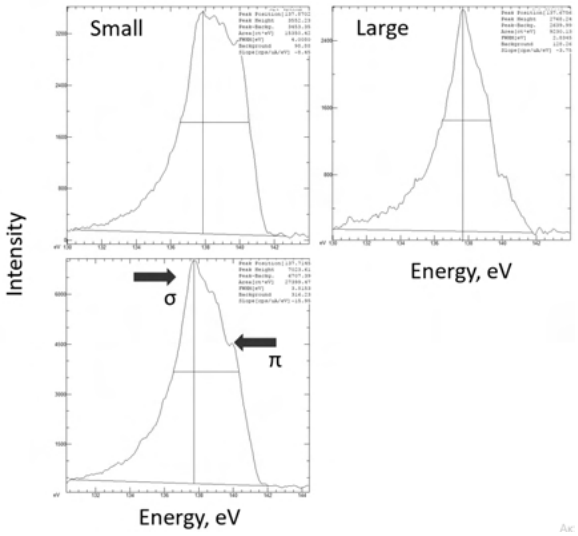

Figure 1

Author index